

3-6

FLUIDIZATION AND RELATED PROCESSES

A Symposium



**COUNCIL OF SCIENTIFIC & INDUSTRIAL RESEARCH
NEW DELHI**

FLUIDIZATION AND RELATED PROCESSES

Fluidization is a novel technique of fluid-solid contacting which found commercial application first in Germany after the First World War, and later in U.S.A. during the Second World War. This study of interaction of fluid-solid systems and its application to industry has been engaging the attention of chemical engineers in the country during the last decade.

Realizing the need for coordinating and consolidating the researches in the field in various laboratories of the country, the Chemical Research Committee of CSIR organized a symposium on 'Fluidization and Related Processes' at the Indian Institute of Technology, Kharagpur in January 1964.

This publication brings together under one cover as many as twenty-seven papers presented and discussed at the symposium. The papers cover a broad spectrum of studies on such different aspects as: (i) Fundamental measurements, (ii) Physical interpretation and momentum transfer, (iii) Mass transfer, (iv) Heat transfer, and (v) Chemical reactions in fluidized beds.

The publication is bound to be useful to research workers in research institutions and industry. It is also hoped that the book would stimulate research work in fields hitherto uncovered, particularly for the designing of fluidized bed units.

Rs 24.00

Sh. 48-/

\$ 8.00

FLUIDIZATION AND
RELATED PROCESSES

FLUIDIZATION AND RELATED PROCESSES

A SYMPOSIUM

held under the auspices of the
Chemical Research Committee, CSIR

AT THE INDIAN INSTITUTE OF TECHNOLOGY
KHARAGPUR

January 6-7, 1964



PUBLICATIONS & INFORMATION DIRECTORATE
NEW DELHI

© 1966
Publications & Information Directorate, CSIR
Hillside Road, New Delhi 12, India

Editorial & Production Staff

S. A. Chari

V. N. Chhibber

S. K. Das Gupta

P. S. Shankar

S. N. Saxena

P. N. M. Menon

Printed by S. N. Guha Ray at Sree Saraswaty Press Ltd
32 Acharya Prafulla Chandra Road, Calcutta 9

FOREWORD

The application of fluidization as a novel technique of fluid-solid contacting was started first on a commercial scale when BASF in Germany developed Winkler gas generator in 1921 to manufacture water and producer gas. The first large scale application of fluidization in USA dates back to about 1940 and pertains to catalytic cracking of petroleum oil vapours. Since then, this technique has successfully been applied in petroleum, petrochemical, chemical and metallurgical industries because of very good fluid-solid contact, high turbulence at the solid surface and high heat transfer coefficient. All these have been possible due to massive research efforts made by scientists and engineers.

It is hoped that this publication which brings together the work done in the field of fluidization and related processes in various laboratories of our country will be helpful to industry as well as research workers, and will stimulate further research in hitherto uncovered areas like rigorous mixing model where the temperature gradients are not negligible.

S. HUSAIN ZAHEER

Director-General

Scientific and Industrial Research

New Delhi

Aug. 28, 1965

ORGANIZING COMMITTEE

Patron

DR S. R. SEN GUPTA
Director, Indian Institute of Technology
Kharagpur

Members

PROF. S. K. NANDI
PROF. A. N. ROY
PROF. S. G. MUKHERJEE
DR P. SEN
DR D. K. GUHA
DR J. V. S. MANI
DR N. K. ROY

DR N. C. ROY
DR N. K. ROY CHOUDHURI
PROF. V. N. PRASAD
PROF. S. C. MITRA
SHRI K. C. CHAKRAVARTY
SHRI B. B. MUKHERJEE
PROF. M. N. RAO (*Convener*)

EDITORIAL COMMITTEE

DR N. C. ROY
DR D. K. GUHA
SHRI A. K. MITRA

P R E F A C E

Since the early forties of this century chemical engineers have been taking an active interest in the study of interaction of fluid-solid systems and its application to industry. In our country, work in this area was started in the early fifties and considerable work has been done.

The Chemical Research Committee of CSIR realized the need for consolidating and coordinating the work already done and being carried out in the different laboratories of the country and hence made a proposal to hold a symposium on 'Fluidization and Related Processes' at the Department of Chemical Engineering, Indian Institute of Technology, Kharagpur in January 1964.

In spite of short notice, the symposium was fairly successful. A number of delegates from various industrial units and research laboratories participated in the symposium by contributing papers and taking part in discussions.

Of the thirty-eight papers read at the symposium, twenty-seven have been included in this publication. The papers have been grouped under the following heads: (i) Fundamental measurements, (ii) Physical interpretation and momentum transfer, (iii) Mass transfer, (iv) Heat transfer, and (v) Chemical reactions in fluidized beds.

It is hoped that this publication would contribute at least to the extent of pointing out the areas, for example rigorous mixing model where the temperature gradients are not negligible, in which further active work has to be carried out to bring out detailed designs of bed units.

Thanks are expressed to Dr S. Husain Zaheer, Director-General, Scientific and Industrial Research, Chairman and Members of the Chemical Research Committee, all the participants in the symposium and the members of the Organizing Committee, Editorial Committee, and the authorities of the Indian Institute of Technology, Kharagpur, for making the symposium a great success.

M. N. RAO
Convener

CONTENTS

Section One : Fundamental Measurements

| | |
|---|---|
| Size Determination of Particulate Material by Microscope Method .. | 1 |
| S. GURUSWAMY & S. K. BAGAI | |
| Specific Surface Determination of Particulate Material by Permeability Method | 9 |
| S. GURUSWAMY & V. S. NARASIMHACHAR | |

Section Two : Physical Interpretation and Momentum Transfer

| | |
|--|-----|
| A Mechanism of Incipient Bubble Destruction and Particulate Fluidization | 17 |
| FREDERICK A. ZENZ | |
| Gravity Flow of Granular Solids through Vertical and Inclined Tubes | 33 |
| K. D. MANCHANDA & N. GOPAL KRISHNA | |
| Flow Characteristics of Counter-current Gas-Solid Fluidized Beds: Part II—Studies on Elimination of Bubbles and Slugs .. | 46 |
| M. S. MAHALINGAM & R. SATAPATHY | |
| Closed-circuit Hydraulic Sand Stowing in Mines | 51 |
| G. B. MISRA | |
| Correlation of Gaseous Fluidized Bed Expansion Data | 65 |
| (Miss) C. R. SRIMATHI & G. N. BHAT | |
| Fluidization of Dissimilar Materials | 72 |
| G. R. VENKITAKRISHNAN & G. N. BHAT | |
| Performance Characteristics of Two-Fluid Atomizer | 83 |
| N. N. KAURA, S. K. VARMA & M. N. RAO | |
| Dispersed Phase Hold-up in a Pulsed Sieve Plate Extraction Column .. | 98 |
| P. C. DEB & D. K. DUTT | |
| Studies on Fluidization of Pyrites | 110 |
| A. K. MITRA & S. K. NANDI | |

Section Three : Mass Transfer in Fluidized Beds

- Mass Transfer Study in Fluidized Bed for Hydrogen Sulphide-Iron
Oxide System 117
S. BANERJEE, R. K. CHAKRAVARTI
B. K. BHATTACHARYA & A. LAHIRI
- Drying in Fluidized Beds 125
P. SEN GUPTA, K. J. R. SARMA & M. N. RAO
- Inter-phase Mass Transfer during Drop or Bubble Formation: A
Re-evaluation 143
D. VIR & F. H. GARNER

Section Four : Heat Transfer in Fluidized Beds

- Heat Transfer and Pressure Drop in Continuous Fluidization ..
P. S. LELE 153
- Heat Transfer to Flowing Gas-Solid Suspensions in Circular Tubes .. 164
V. R. K. RAO & P. S. MURTI
- Heat Transfer to Flowing Gas-Solid Suspensions in Circular Conduits
Containing Turbulence Promoters 179
V. R. K. RAO & P. S. MURTI
- Heat Transfer Studies in Batch-Fluidized Beds: Liquid-Solid Systems 189
G. J. V. JAGANNADHA RAJU
M. S. KRISHNA & C. VENKATA RAO
- Heat Transfer Studies in Continuous Fluidized Beds: Part III—
Prediction of Heat Transfer Coefficients from Simple Fluid Flow
Considerations applying Momentum Heat-Transfer Analogies .. 200
P. SEN GUPTA, K. J. R. SARMA & M. N. RAO

Section Five : Chemical Reactions in Fluidized Beds

- Scaling up of Fluidized Bed Process for Production of Fertilizers
by Reaction of Ammonia-Air Mixture on Coal 207
S. BANERJEE, R. K. CHAKRAVARTI, B. K. BHATTACHARYA
D. K. BANERJEE & N. G. BASAK
- Fluidization Studies in an Operating Fluidized Bed Reactor .. 217
C. M. LAKSHMANAN, B. CHENNAKESAVAN
& H. E. HOELSCHER

| | |
|--|-----|
| Kinetics of Fluidized Bed Vapour Phase Oxidation of Toluene .. | 227 |
| R. N. KUMAR, G. N. BHAT & N. R. KULLOOR | |
| Studies on Some Catalytic Reactions of Industrial Importance in Fixed as well as Fluidized Bed | 241 |
| S. K. BHATTACHARYYA, N. D. GANGULY B. N. AVASTHI, A. K. KAR & VIJAY SHANKAR | |
| Particle Distribution of a Heterogeneous Mixture of Ilmenite and Carbon in Fluidized Bed Reactors | 248 |
| M. N. KRISHNAMURTHI | |
| Catalytic Upgrading of Water Gas in Fluidized Bed | 253 |
| R. K. S. MEHTA | |
| Reactivation of Clays in Fluidized Beds | 265 |
| D. K. GUPTA, R. SATAPATHY & B. C. BANERJEE | |
| Conversion of Barytes to Barium Chloride in Fluidized Bed .. | 269 |
| M. V. CHANDORIKAR, D. J. MEHTA & B. K. SHUKLA | |
| AUTHOR INDEX | 272 |

SECTION ONE

Fundamental Measurements

Size Determination of Particulate Material by Microscope Method

S. GURUSWAMY & S. K. BAGAI

Central Mining Research Station
Dhanbad, Bihar

Two microscope methods of particle size determination and analysis have been discussed in detail: (i) count method to obtain average size, and (ii) direct measurement method to obtain data on particle size-number distribution. Brief reference has been made to apparatuses that have been developed commercially during the last ten years to count and size particles in an automatic or semi-automatic way so that size analysis can be carried out rapidly.

The authors' experience of experimental work on the development of standard procedures and a new graticule for direct measurement method has been discussed.

The subject of particle size studies has developed enormously during the last two or three decades mainly from the fact that modern technology is using materials in a powdered form in enormous quantities. Broadly speaking, particle size measurement is needed for (i) controlling the fineness of powdered material, e. g. cement, and the performance of crushers, pulverizers and grinders in industrial processes, (ii) for dealing quantitatively with the dust problems in mines and industry, (iii) for progress in technological research and development work¹, and (iv) for improving the quality of finished product in several industries, especially when the finished product is in a powdered form.

Several methods for particle size measurements were presented and discussed at the ASTM symposium on the subject². In this paper, however, only the microscope method has been dealt with in detail. One of the convenient methods for particle size measurement is sieving. The apertures of standard sieves are determined with the help of a projection microscope. The microscope method is generally useful for size measurement of

powders that pass through the finest woven wire sieve (opening* *c.* 70 μ , 70×10^{-4} cm.). The lower limit of size that can be determined by the microscope method is limited by the optical resolution of the objective of the microscope; for ordinary light, this is generally taken as 0.2 μ . The lower limit can be decreased by the use of ultraviolet microscope and ultra-microscope³. The latter is useful for detecting particles as small as about 0.01 μ . However, both these types of microscopes have generally been superseded by the electron microscope⁴ for determining the sizes of particles less than 0.2 μ in diameter.

There are two general microscope methods available for the determination of particle size: (i) the count method, in which particles in suspension are counted through microscope to obtain average size, and (ii) the direct measurement method, by which data on particle size-number distribution are obtained from slides prepared from powder samples.

During the last ten years apparatuses have been developed to count and size particles in automatic and semi-automatic ways so that size analysis can be carried out rapidly. The automatic equipment are of the electronic type, and are useful when the volume of work is sufficiently large to justify their cost. Excepting for brief references to them, they will not be considered further in this paper.

Two different types of automatic apparatus and one semi-automatic apparatus have been described in literature and are commercially available. The Casella automatic counter⁵ has been specifically developed to size and count particles from dust deposits from sampling instruments like thermal precipitator. Berg² has described an electronic size analyser for subsieve particles based on the application of the Coulter principle, that is, change of conductivity of an electrolyte in an aperture when a particle momentarily passes through it. A semi-automatic apparatus⁶ has been developed in Germany for precise particle size work from photomicrographs.

Count Method

The principle underlying the determination of average particle size by the count method is simple. A suspension containing a known concentration (by weight) of the given sample is prepared, and the number of particles present in unit volume is estimated by count through the microscope. To obtain reliable results, however, it is necessary that the individual particles in the sample be as uniform in size as possible, and be of suitable size so that they do not settle too rapidly. The rate of settling of the particles can be controlled to some extent by a proper choice of liquids for preparing the suspensions. However, very viscous liquids are not suitable on account of easy air bubble formation and drainage errors. It is also necessary to make a precise estimate of the volume of the suspension from which

*The recently available micromesh sieves extend the range of sieving¹ to as low as 10 μ .

the particles are counted. For such an estimate, a depth measurement along the axis of the microscope has to be made, as the depth of focus of the microscope especially at higher magnification is much smaller than the depth (*c.* 1mm.) of commercially available counting cells.

In practice, the count method consists in estimating in an efficient manner the average number of particles present per square in a grid of squares, as the particles are counted from standard circular/rectangular counting cells of uniform depth (*c.* 1mm.) through the microscope.

If the size of the particle is large enough so that it settles in the counting cell, an estimate of the number per square is obtained by counting the settled particles at the bottom of the cell. In such a case, on account of the finite depth of the cell, the counting cannot be carried out at higher magnification.

If the particles are fine in size, counting of particles lying in one plane becomes difficult at higher magnification due to Brownian motion. In such a case, a snap count method is adopted. In this method, the suspension is diluted sufficiently well so that by instantaneous observation it can be noted whether there are none, 1, 2, 3, etc. particles per square. The results of several snap observations are used to arrive at an estimate of the average number of particles per square. Since few observers can estimate at a glance a number of more than three particles, the mean per square has to be kept so low, that very few squares will have more than three. It is common to work with a mean of 0.5 particles per square. With such a low mean as this, a count of as many as 1000 squares only reduces⁷ the standard error of the mean to 4.5 per cent. There could be a gain in accuracy (or for constant accuracy, an economy of labour) if the technical difficulties of counting at higher densities of particle could be surmounted.

Tippet⁷ proposed a most useful modification of the snap count method. The modification consists in making counts only of squares with a few particles, those squares with more than a certain number of particles being classed together. The mean is estimated from the modified frequency distribution so formed. By the use of nomographs that he provides, it is possible to identify the exact distribution applicable and hence the average number of particles per square. This procedure is so much faster than the usual count method that many more particles can be counted in equal time and, since the accuracy is proportional to the square root of the number counted, greater accuracy is obtained in equal time. Further advantages in this method are that (i) greater range of particle densities can be investigated than might otherwise be possible, and (ii) the number of squares with only a few particles are counted at a glance, and hence very quickly.

To obtain reliable results by the count method, a precise estimate has to be made of the volume of the suspension from which the particles are counted. For such an estimate, a depth measurement along the axis of the microscope is necessary. To avoid this measurement the coating

method has been employed by some workers² in this field. The principle of this method consists in coating a definite volume of the suspension over a definite area of a glass slide. Only the area under the microscope need be determined, the depth factor being dropped out. This method is successful when a skilled coating technique is used. The special factors involved are (i) thorough cleaning of the slides, (ii) skill in coating, and (iii) correct formula for coating solution that shows on spreading and drying less tendency to withdraw from the edges.

A valuable contribution to the count method can be made if it is possible in practice to count by electronic devices through a microscope eyepiece fitted with photocells, from a well diluted suspension flowing through a thin-walled flat counting cell kept on the stage of the microscope. It is necessary to keep the depth of the cell below the microscope objective to the depth of focus. Such a device will reduce the time for a determination of average size of a sample to a few minutes, and will be of help in repeating the experiments several times.

Direct Measurement Method

The characteristics of powders are often governed by the size distribution of individual particles rather than the average size of the powder, and in such cases experimental results on particle size analysis become important. Microscope sizing enables one to obtain such data on the number-size distribution of the particles in the powder.

While using microscope for particle size work, it is necessary to take into account the fact that the size of single particle in a powder is of very limited practical importance. What is needed in practice is a rapid method for direct and convenient classification of a sufficient number of particles according to their sizes. This is generally done by a comparison (on a simple inspection basis) of the projected area of the particles with standard areas that may be a series of circles engraved on a reticule which can be fitted into the eyepiece of a microscope.

Graticules of different designs are available². However, the one described by May⁸ in which the circles increase in diameter by a factor of $\sqrt{2}$ has been widely used by workers in this field. With the above graticule (Fig. 1), using a set of 9 circles and 4 lines, it is possible to classify particles of ratio of sizes 1:64 into 13 size groups; the actual size in microns of the graticule circles is obtained by calibration against a stage micrometer (1 division = 10 μ).

A new graticule, recently developed⁹ by one of the authors (S. G.) in this laboratory, is designed to reduce to a minimum the labour involved in the calculation of (i) suitable size parameters for a comparative study of particle size-number distribution data, and (ii) projected specific surface from experimental data on particle size-number distribution. In this graticule, reference circles increase by a factor of 1.2589 instead of $\sqrt{2}$ (=1.414)

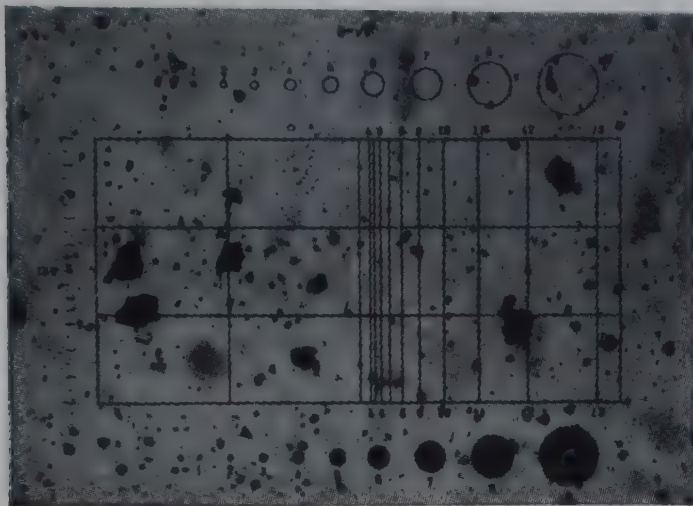


FIG. 1—GRATICULE IN WHICH THE DIAMETER OF THE CIRCLES INCREASES BY $\sqrt{2}$

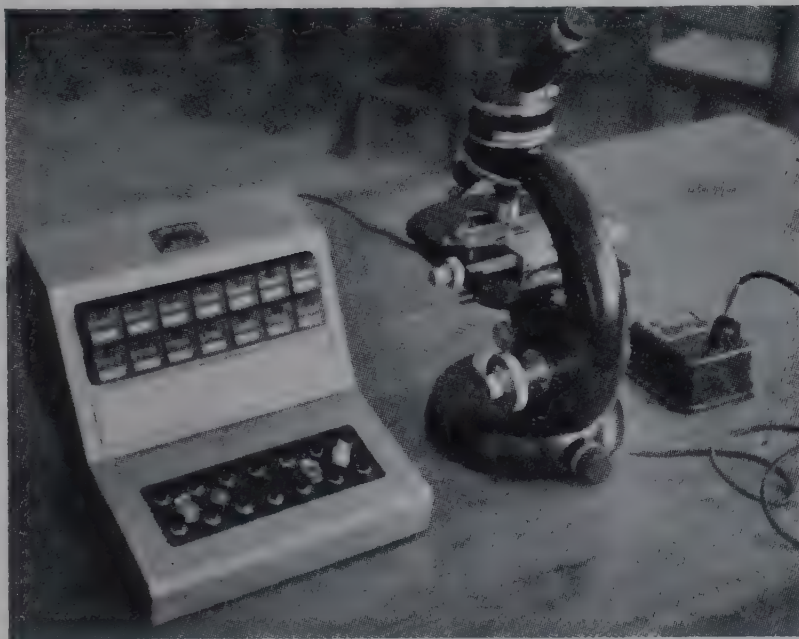


FIG. 2—MICROSCOPE COUNTING UNIT

as in the graticule shown in Fig. 1. The advantage of the new graticule is due to the fact that $\log 1.2589$ is 0.1. This helps in the rapid calculation of values of $\sum fx$, $\sum fx^2$, $\sum fx^3$ and $\sum fx^4$ from experimental results. The values are needed in statistical analysis of microscope data for research purposes, and also in the rapid estimation of the projected specific surface from microscope size data.

Next to the graticule, a good research microscope and a counting unit are needed for sizing work by the microscope method. In Fig. 2 is shown a photograph of the microscope counting unit employed by the authors in their recent investigation to develop a standard procedure¹⁰

for particle size determination of sub-sieve size mine dust by the microscope. The microscope has the following features: (i) built-in illumination, (ii) centrabale and movable substage condenser, (iii) rectangular graduated mechanical stage, and (iv) facility for tube length variation. The latter one is an essential facility, since sizing in general has to be done at more than one magnification in view of the fact that a wide range of particle sizes is encountered in powders. It is of advantage, however, to adjust the tube length-objective-eyepiece combination so that (i) the magnification increases in regular steps, and (ii) the value of 1 unit of the graticule used in the experimental set-up is a whole number of microns at the lowest available magnification. An arrangement in which the magnification of the microscope increases by the same factor as the graticule circles ($\sqrt{2}$ for graticule⁸, and 1.2589 for the new graticule) introduces simplification in combining particle counts of more than one magnification¹⁰.

The counting unit (Fig. 2) employed by the authors has 14 individual counters so that the results of counting 14 different size groups at one magnification can be recorded. In practice, an observer sizes the particles under the microscope by finding the number of the graticule circle (Fig. 1) that has the same area as the projected image of the particle. The circle numbers are entered into the counting unit by a recorder who presses the appropriate individual counter when the observer gives the equivalent graticule circle numbers.

The preparation of suitable slides of the given powder sample is an essential step in the work of direct size measurement by the microscope method. Care in preparing the slides to ensure that the individual particles of the different sizes are uniformly distributed in the slides greatly reduces the work of counting and sizing. As the slides are used for size distribution studies, it is important to avoid (i) aggregation of the particles, and (ii) the removal of either coarse or fine sizes from the sample. Preliminary experiments to disperse the powder in liquids and to prepare slides out of the suspension showed that it is difficult to avoid the separation of sizes that takes place in the suspension. Hence, slides were prepared by dispersing a small quantity of the powder on the slide itself, care being taken to avoid any breakage of the material. Several dispersion media were tried; each one was found to have its own limitations. However, a solution of collodion in butyl acetate was found to be a suitable dispersion medium for mineral dusts and powders. This particular medium has the following advantages: (i) it gives more or less permanent slide mount of the sample, and (ii) the concentration of the powder sample in the mount is easily controlled by using the solvent butyl acetate. This is of particular advantage to obtain an optimum density of particle concentration in the slide to facilitate the sizing of particles.

Loveland² has described a laboratory mill in which a wooden rod in a precision glass tube is used for dispersion of powders of friable material

by viscous shear forces. The clearance between the rod and glass tube is kept considerably larger than any individual particle in the given powder sample to avoid the breakage of material. Such a mill is extremely useful as a standard laboratory equipment when the volume of work on particle size determination is large, or when powders of friable material have to be sized.

Size evaluation by the direct microscope method, although simple in theory, needs a standard procedure, in order to obtain reliable results, for the following reasons: (i) size evaluation varies from person to person, more so when the particles are widely different in size and shape, (ii) the sample may not be uniformly dispersed on the slides, and (iii) the counting work should be carried out efficiently to a predetermined standard of accuracy.

Bagai, Das Gupta and Guruswamy¹⁰ have developed a procedure based on the application of chi-squared (χ^2) test to determine the 'significance' of the difference between two particle size counts. The particle size distribution is obtained from a minimum of 2 and a maximum of 8 slides; the number of particles counted depends on the nonuniformity of dispersion of particles on the slides. The procedure for particle size determination of a powder is discussed in detail by them.

Rapid Calculation of Size Parameters from Microscope Size-Number Distribution Data

The results of microscope count are generally expressed graphically, and the graph shows the percentage number particles of the different particle sizes. For practical purposes, however, it is necessary to calculate suitable averages of particle sizes. Any contribution to simplify and reduce the work involved in calculation of suitable averages is valuable in making the direct measurement method sufficiently rapid for practical application.

Recently, one of the authors (S. G.) has described⁹ a method for calculating rapidly the different averages that are useful in the analysis of experimental results of microscope sizing. The method is illustrated with an example of size analysis by an eyepiece graticule in which the reference circles increase in diameter by a factor of $\sqrt{2}$.

It is possible to further reduce the arithmetical work by designing a graticule on the basis of 1.2589 instead of $\sqrt{2}$ ($=1.414$). The advantage in the former case is due to the fact that $\log (1.2589)^n$, $\log (1.2589)^{2n}$ and $\log (1.2589)^{3n}$ are $0.1n$, $0.2n$ and $0.3n$ respectively. Details of the new graticule will be published elsewhere.

REFERENCES

1. IRANI, R. R. & CALLIS, C. F., *Particle Size Measurement, Interpretation and Application* (John Wiley & Sons Inc., New York), 1963, 1, 107.
2. *ASTM Symposium on Particle Size Measurement. Spec. Tech. Pub.*, No. 234, 1959.

3. CADLE, R. D., *Particle Size Determination* (Interscience Publishers, Inc., New York), 1955, 105.
4. CARTWRIGHT, J., *Brit. J. appl. Phys.*, Suppl. No. 3, (1954).
5. *Automatic Particle Counter and Sizer*, Leaflet No. 872 [Casella (Electronics Ltd)].
6. *Particle Size Analyzer after Endter*, *Zeiss Werkzeitschrift*, No. 33, 1959, 68.
7. TIPPET, L. C. H., *Proc. roy. Soc.*, **137A** (1932), 434.
8. MAY, K. R., *J. sci. Instrum.*, **22** (1945), 194.
9. GURUSWAMY, S., *Indian J. Technol.*, **2** (1964), 211.
10. BAGAI, S. K., DAS GUPTA, A. & GURUSWAMY, S., *Indian J. Technol.*, **1** (1963), 69.

Specific Surface Determination of Particulate Material by Permeability Method

S. GURUSWAMY & V. S. NARASIMHACHAR

Central Mining Research Station
Dhanbad, Bihar

Liquid and gas permeability methods of determining specific surface of powders in the sieve and sub-sieve range of sizes are described. The importance of permeability surface in shape investigations, and in the control of the fineness of powdered material in industrial processes is discussed. The relevant equations for calculation of specific surface from experimental data are given. The authors' experience of experimental work in this field is reviewed.

Specific surface, i.e. surface per unit volume or weight, increases enormously as particle size decreases, and hence data on specific surface are useful in quantitative investigations of the dust problems in mines, and also in the solution of certain problems in powder technology in which the control of the fineness of powdered material and quantitative knowledge of shape of particles in the powder are of importance.

Several methods for the experimental determination of specific surface are available¹. The permeability method², however, has the following advantages: (i) it gives the 'skin' surface, which is of interest in shape investigations³, and (ii) it is possible to obtain an average value for particle size of powders containing a wide size range of particles.

Liquid Permeability Method

The rate of flow of a fluid through a bed of particles depends on the area of the cross-section of the bed, the fractional pore space (voidage) available for its flow, the pressure drop across the bed, the kinematic vis-

cosity of the fluid, and the specific surface of the material. An apparatus suitable for using liquids is described by Carman².

The equation for determining the surface area³ from liquid permeability data is

$$S_o = \sqrt{\frac{g}{C} \frac{1}{Pv} \frac{\epsilon^3}{(1-\epsilon)^2}} \quad (1)$$

For coal particles (sieve size range) employed in earlier studies³, the value of C used was 4.5 and the specific surface measured was in the range 40–840 cm.²/g. There are, however, difficulties in extending the method to finer particles of size 100 μ and less due to (i) lack of suitable material to retain and support the particles as a bed; (ii) extremely slow rate of flow of liquids through beds of fine particles; and (iii) uncertainty in using the value of 4.5 for C in Eq. (1) for all conditions of porosity of packing of the bed, size and shape of the particle.

The results of some liquid permeability experiments using samples of closely graded sizes of coal, sand, and also samples of coal containing a continuous range of particle sizes are given in Table 1. A retainer made from 320 mesh cloth (opening about 50 μ) was used. For particles less than about 50 μ , a method was developed by finding the overall and individual permeability of two beds of particles built one above the other. The permeability of the top bed containing small particles was calculated from the experimental values of permeability of the bottom and that of the combined bed. The porosity of packing of the bed was changed over a limited range by preparing beds from a mixture of two different sizes of particles.

In all cases, the specific surface of mixed sizes of particle was less than that estimated from the specific surface of individual sizes. The specific surfaces were calculated using a value of 4.5 for the constant C in Eq. (1). The percentage reduction in specific surface in Table 1 varies over a wide range (1.9–22.4%).

It can be anticipated that the bed prepared from particles of widely different particle size and shape, such as sand and coal (Sl. No. 13, Table 1) will not be homogeneous in void space along the length of the bed. As the latter (nonhomogeneity of void space) is difficult to define, determine and control in a bed of particles, it is perhaps not possible to determine surface area accurately from a single experiment. In practice, an average value of specific surface may have to be obtained from a number of independent experiments with a given sample. The largest specific surface of coal particle so far measured by the authors by the liquid permeability method is about 0.89 m.²/g. This value of specific surface gives an average size of about 10 μ for the coal particle, assuming that the sphericity of the coal particle is 0.5.

The specific surface, 0.89 m.²/g, would represent generally the largest value that can be measured satisfactorily by the liquid permeability method.

TABLE 1—SPECIFIC SURFACE VALUES FOR DIFFERENT MATERIALS AND THEIR MIXTURES DETERMINED BY LIQUID PERMEABILITY METHOD

| SL. MATERIAL No. | SIZE B.S.S. SIEVE NUMBERS | SIEVE OPENING μ | FRACTIONAL POROSITY OF PACKING OF BED | SP. GR. | S_o , cm. ² /cm. ³ | | REDUC- TION IN S_o % |
|---------------------|--------------------------------------|---------------------------|--|------------|--|--|---------------------------------|
| | | | | | Using Eq. (1) (av. values) | Using S_o values of Sl. No. 1 to 3 | |
| 1. Sand | 52 to 60 | 295 to 251 | 0.4334 0.4356 0.4348 | 2.658 | 321 | .. | .. |
| 2. Coal | 36 to 44 | 422 to 353 | 0.5581 0.5432 0.5335 0.5519 0.5621 0.5431 | 1.297 | 294 | .. | .. |
| 3. Coal | 60 to 72 | 251 to 211 | 0.4714 0.4661 0.4863 0.4842 | 1.304 | 409 | .. | .. |
| 4. Coal | 8 to 14 | 2057 to 1204 | 0.5291 | 1.867 | 66.5 | .. | .. |
| 5. Coal | 14 to 36 | 1204 to 422 | 0.5196 | 1.874 | 154 | .. | .. |
| 6. Coal | 36 to 72 | 422 to 211 | 0.5455 0.5328 | 1.858 | 499 | .. | .. |
| 7. Coal | 72 to 120 | 211 to 124 | 0.5056 | 1.954 | 1020 | .. | .. |
| 8. Coal | 120 to 200 | 124 to 76 | 0.5423 | 1.734 | 1831 | .. | .. |
| 9. Coal | -200 | 75 | 0.5778 0.6001 0.6010 | 1.760 | 10870 | .. | .. |
| 10. Coal | -300 | 53 | 0.5554 | 1.405 | 12460 | .. | .. |
| 11. Coal | 36 to 44 & 60 to 72; 50: 50 by wt | .. | 0.5025 | .. | 339 | 350 | 3.1 |
| 12. Coal | 36 to 44 & 60 to 72; 70: 30 by wt | .. | 0.5211 | .. | 298 | 327 | 8.9 |
| 13. Sand: Coal | 52 to 60 & 36 to 44; 69: 31 by wt | .. | 0.5100 | .. | 239 | 308 | 22.4 |
| 14. Coal | 60 to 72 & 36 to 44; 70: 30 by wt | .. | 0.4898 | .. | 365 | 372 | 1.9 |
| 15. Coal | 60 to 72 & 36 to 44; 1: 5 by wt | .. | 0.5458 | .. | 272 | 312 | 12.8 |
| 16. Sand: Coal | 52 to 60 & 36 to 44; 50: 50 by wt | .. | 0.5236 | .. | 265 | 303 | 12.5 |

Beds prepared with particles smaller than an average size of about 10μ offer enormous resistance to the flow of liquids, and hence measurement of rate of liquid flow becomes tedious. To overcome this difficulty, efforts were made to increase the rate of flow by applying a positive, and a negative pressure on the top and bottom of the bed respectively. However, it was found difficult to maintain the pressures steady. Further, there was a limit to the pressure difference that could be safely applied across the bed without producing local fissures.

Gas Permeability Method

The use of air or gas instead of liquid for permeability studies is of advantage from the experimental point of view, when working with particles of large specific surface. This, along with the fact that fine powders can be compressed to form self-supporting beds in glass or metal tubes has helped considerably in developing the air permeability method for specific surface of fine powders. Further, the self-supporting beds of fine powders in tubes are capable of withstanding large pressure differences across them. This is of practical importance in permeability studies as the flow of air or gas can be increased appreciably by applying a large pressure difference across the bed.

The apparatus employed by the authors is shown in Fig. 1 and is a modification of the one used by Rigden⁴.

The sample whose specific surface is required is compressed in a glass tube with the help of two steel plungers having a minimum of clearance between the tube and the plungers. The experimental procedure for determining the permeability of the bed is as follows:

The pressure of air in the system is reduced to any desired level by connecting a vacuum pump to stopcock (a). The liquid level (high vacuum oil with a minimum of vapour pressure) in the left limb of U-tube is brought to a higher level by introducing air on the right-hand side, stopcocks (b) and (c) being closed. Then, stopcock (b) is opened. The level of liquid in the left limb of the U-tube falls as air flows through the bed. The liquid is allowed to fall through a good height to attain steady conditions. Then the time (t) taken by the liquid to fall through a definite height, h_o to h , is measured.

The heights are measured from the equilibrium line of the oil, which point is quickly reached by opening stopcock (c). Finally, the pressure (p_o) when the levels at the two limbs are in equilibrium is measured in the mercury manometer. The permeability (G) and the mean pressure (p) are calculated using the following equations, derived by the authors using the P - V relationship for gases flowing across the bed in a closed system.

$$G = \left(\frac{La}{2A} \right) \left(\frac{2.303}{t} \right) \left(\log_{10} \frac{h_o}{h} \right) \left[p_o \frac{\rho_m}{\rho_o} + \frac{2H_1H_2}{H_1+H_2} - h_m \frac{4(H_1-H_2)+6\bar{h}}{H_1+H_2} \right] \quad (2)$$

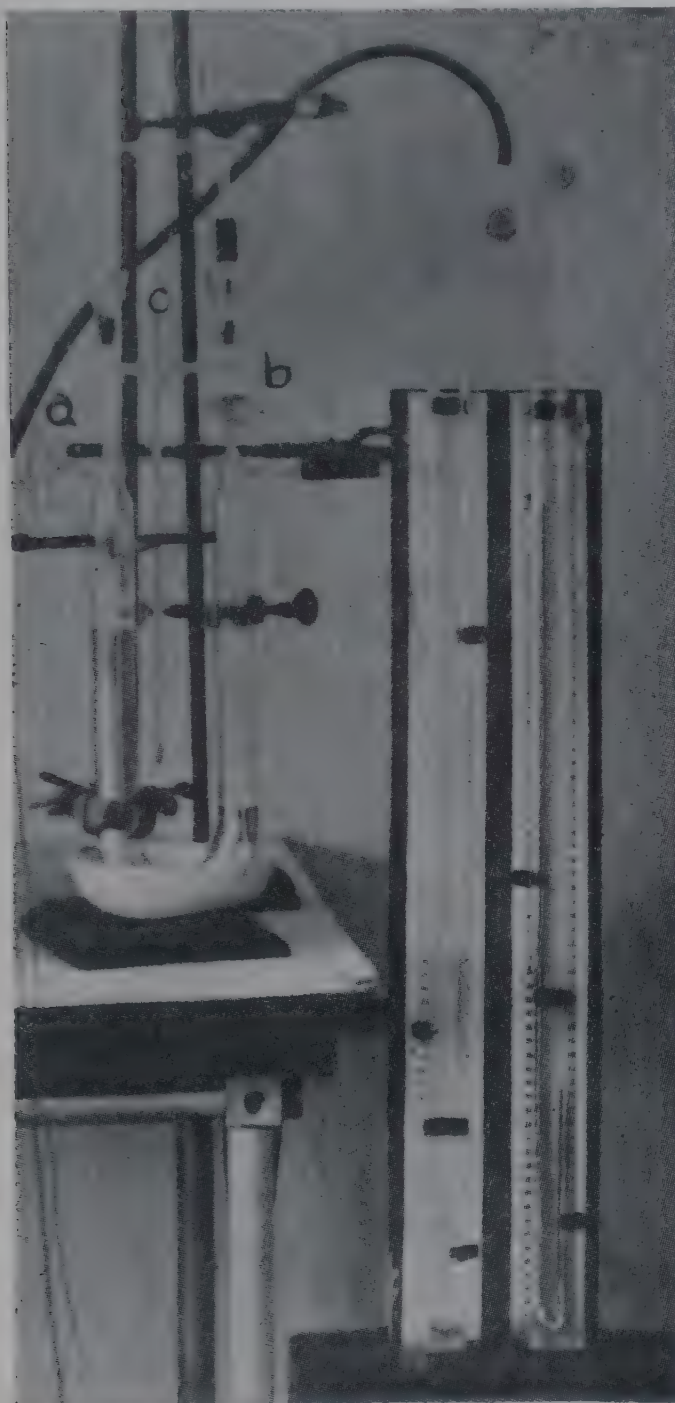


FIG. 1—APPARATUS FOR DETERMINING SURFACE AREA BY GAS PERMEABILITY METHOD

$$p = \left[p_o - \left(\frac{H_1 - H_2}{H_1 + H_2} \right) \left(\frac{\rho_o}{\rho_m} \right) h \right] - \left[\left(\frac{2}{H_1 + H_2} \right) \left(\frac{\rho_o}{\rho_m} \right) \left(\frac{h_o^2 + h^2}{2} \right) \right] \quad (3)$$

It has been found by Carman⁵ and other workers⁶ that the permeability versus mean pressure is a straight line giving a positive value of intercept; in other words, there is a definite flow of air at zero pressure. This has been explained by them as due to 'molecular' flow. The surface area can be calculated from the slope of the straight line, that is, when the permeability is governed by the viscosity of the flowing gas.

When S_o is large, that is, when dealing with fine particles, the slope will be small and hence estimation of specific surface from the slope will be difficult. Under such conditions the surface area has to be worked out from the intercept of the straight line on the basis that permeability is governed by diffusion (a molecular) phenomenon.

To obtain an accurate plot of permeability versus mean pressure, several experiments have to be carried out using elaborate apparatus. Such a procedure is unsuitable for practical purposes, where it is always preferable² to make a single measurement with the simplest possible apparatus, and to determine S_o from two calculated values, S_k and S_m . S_k and S_m are defined as the specific surface area, calculated from experimental results on the assumption¹ that observed flow is completely governed by viscous and molecular forces respectively. The relevant equations² are

$$S_k^2 = \frac{F_1 \bar{p}}{5\eta G} \quad (4)$$

$$S_m = 0.6 \left(\frac{F_2 \bar{v}}{G} \right) \quad (5)$$

$$S_o = \frac{S_m}{2} + \sqrt{\frac{S_m^2}{4} + S_k^2} \quad (6)$$

The simplest apparatus for routine purposes is described by Carman². The authors have made a comparative experimental study of permeability by the apparatus described by Carman and that devised by them, and conclude that the former gives satisfactory permeability values for a bed prepared from a given sample of powder as long as the experiments are conducted at pressures very near that of the atmosphere.

DISCUSSION

Although it is easy to determine the permeability of a given bed experimentally, it is rather difficult to obtain reliable values of specific surface of a powder for the following reasons:

- (i) The self-supporting beds of powders used in air permeability experiments are seldom homogeneous in void space along the length of the bed.
- (ii) There is uncertainty in the estimation of fractional void space on the basis of the true and apparent volume of the bed, due to lack of reliable data on true density of fine powders or the non-availability of a suitable direct method for the estimation of void space in a bed.
- (iii) The constants in Eq. (4) and (5) are empirical, although attempts have been made to determine their values on theoretical grounds^{5,7}.

The authors' experience with several powders and mine dusts (whose average sizes are widely different) has shown that: (i) the calculated values of specific surface using Eq. (4), (5) and (6) depend on the actual value of the porosity of the bed; the dependence of the value of surface area on porosity is much larger in the case of coal dust than in the case of quartz; surface activity of coal may have an influence on the result; (ii) it is difficult to control the porosity of the bed to within 0.4 to 0.5, as recommended by Carman²; keeping porosity within limits will minimize the effect of porosity functions F_1 and F_2 in Eq. (4) and (5).

Some experiments were conducted to see if the permeability specific surface could be calculated for comparative purposes at two or more specific values of porosity like 0.4 or 0.5. For this purpose, permeability of air flow of the bed was determined at the maximum and minimum voidage of the bed, i.e. using loose and compact beds of the dry powder. The permeability at the specific values of porosity was obtained by interpolation and extrapolation as required from experimentally determined values. The results, however, were not encouraging. Using several powders (of different size ranges) which can be compressed over a wide range of porosities, it was found that no dependable unique set of average values could be obtained for permeability specific surface.

CONCLUSION

On account of the various assumptions involved in determining surface area of subsieve fine powders by the gas permeability method, the permeability surface area, though not very accurately determined, is still useful for comparative purposes to control the fineness of powdered material in industrial processes⁸.

NOMENCLATURE

| | |
|------------|--|
| S_0 | = specific surface of material, $cm.^2/cm.^3$ |
| g | = acceleration due to gravity, $cm./sec.^2$ |
| ϵ | = fractional voidage or porosity of bed (calculated from the apparent volume of bed, weight, and density of sample) |
| C | = Kozeny's constant |
| P | = permeability under laminar conditions of liquid flow through the bed = volume rate of liquid flowing across unit cube of the bed under unit pressure difference of liquid |
| ν | = kinematic viscosity of liquid |
| G | = permeability of air flow through bed = quantity (product of pressure and volume) rate of air flowing across unit cube of bed under unit pressure difference |
| L | = length of bed, $cm.$ |
| A | = area of cross-section of bed, $cm.^2$ |
| a | = area of cross-section of left limb of U-tube, $cm.^2$ |

| | |
|------------|--|
| h_o, h | = height of liquid in left limb of U-tube, above equilibrium line at time o and time t , <i>cm.</i> |
| p_o | = pressure of air when the levels in U-tube are in equilibrium position, <i>cm.</i> of mercury |
| ρ_m | = density of mercury |
| ρ_o | = density of oil |
| \bar{h} | = $(h_o + h)/2$ |
| h_m | = $(h_o - h)/2 \cdot 303 \log_{10} (h_o/h)$ |
| H_1, H_2 | = equivalent heights of dead space over equilibrium line on right and left limbs of U-tube, based on area of cross-section of U-tube |
| p | = mean pressure of air in bed when liquid level in U-tube changes from h_o to h , <i>cm.</i> of mercury |
| F_1 | = $\epsilon^3/(1-\epsilon)^2$ = porosity function |
| F_2 | = $\epsilon^2/(1-\epsilon)$ = porosity function |
| \bar{p} | = mean pressure of air/gas in bed |
| \bar{v} | = mean thermal molecular velocity of air/gas = $\sqrt{8 RT/\pi M}$ |
| R | = gas constant |
| T | = absolute temperature |
| M | = molecular weight of gas |

REFERENCES

1. ROSE, H. E., *The Measurement of Particle Size in very Fine Powders* (Constable Co. Ltd, London), 1953, 86.
2. CARMAN, P. C., *Flow of Gases through Porous Media* (Butterworths Scientific Publications Ltd, London), 1956, Chapter 4.
3. GURUSWAMY, S. & SRINIVASAN, S. R., *J. sci. industr. Res.*, **12B** (1953), 101; **13B** (1954), 368.
4. RIGDEN, P. J., *J. Soc. chem. Ind., Lond.*, **62** (1943), 1T.
5. CARMAN, P. C., *Proc. roy. Soc.*, **203A** (1950), 55.
6. BARRER, R. M. & GROVE, D. M., *Trans. Faraday Soc.*, **47** (1951), 826; ROSS, J. W. & GIRIFALCO, L. A., *J. phys. Chem.*, **57** (1953), 330.
7. CARMAN, P. C., *Trans. Instn chem. Engrs, Lond.*, **15** (1937), 150.
8. *Standard method of test for fineness of portland cement by air permeability apparatus*, ASTM: C204-55.

SECTION TWO

Physical Interpretation and
Momentum Transfer

A Mechanism of Incipient Bubble Destruction and Particulate Fluidization

FREDERICK A. ZENZ

Squires International Inc.
Roslyn Harbor, N. Y.

The 'dispersive pressure' or bed dilation phenomenon occurring under the influence of a bed-penetrating velocity gradient (accompanying the horizontal flow of fluid over a surface of particulate solids) can be combined with single particle saltation velocities and bubble-gas recirculation rates to indicate the relative magnitude of forces leading to either bubble stability or bubble destruction in any fluid bed system. If the dilating forces are large, there is little probability that a distinguishable bubble will ever appear and the system will exhibit the so-called particulate fluidization characteristics. This picturization of a fundamental mechanism leading to destruction of a bubble, or rather the thwarting of any tendency for bubbles ever to form, is in qualitative agreement with observations and can be shown to justify such empirical approximations as have been proposed in the past.

Bubbles in gas fluidized beds of solids are visual evidence of the passage of gas through the bed with a minimum of contact with the solid particles incurring a process inefficiency whether in transfer of heat or of mass. Attempts have been made to suppress bubbles, or to increase their residence time, by the design of intricate reactor internals¹⁻³ and their inefficiency has been empirically studied in terms of bubble frequency² and bubble size⁴⁻⁶ to permit correction of theoretical reactor design calculations⁷. Since no generally satisfactory bubble suppressor has yet been devised attention has been focused on the hydrodynamics of bubbles in beds of solids.

To date, it has been shown that, once formed, the upper surface of a gas bubble in a fluidized bed of solids is stable⁸; solids do not shower down

into the bubble⁹; its stability is a fundamental phenomenon associated with particle drag and can be so demonstrated experimentally. Gas flow streamlines into and through bubbles have also been observed by introducing coloured tracer gas through jets into thin sections of air fluidized beds¹⁰. These observations, coupled with a theoretical model assuming the bubble to be a spherical void within a porous body have permitted definition of the fluid flow patterns from the interstices of surrounding solids into and out of a bubble¹¹; this allows calculation of the gas circulation within, or rather through, the bubble and suggests the limits of proximity of bubbles which will lead to their merger into larger bubbles. Though this formidable body of knowledge is developing around the hydrodynamics of an existing bubble, there has been very little offered in the way of a fundamentally sound and simple mechanism for the mode of formation or destruction of a bubble in the first place. Such a simple mechanism is developed here on

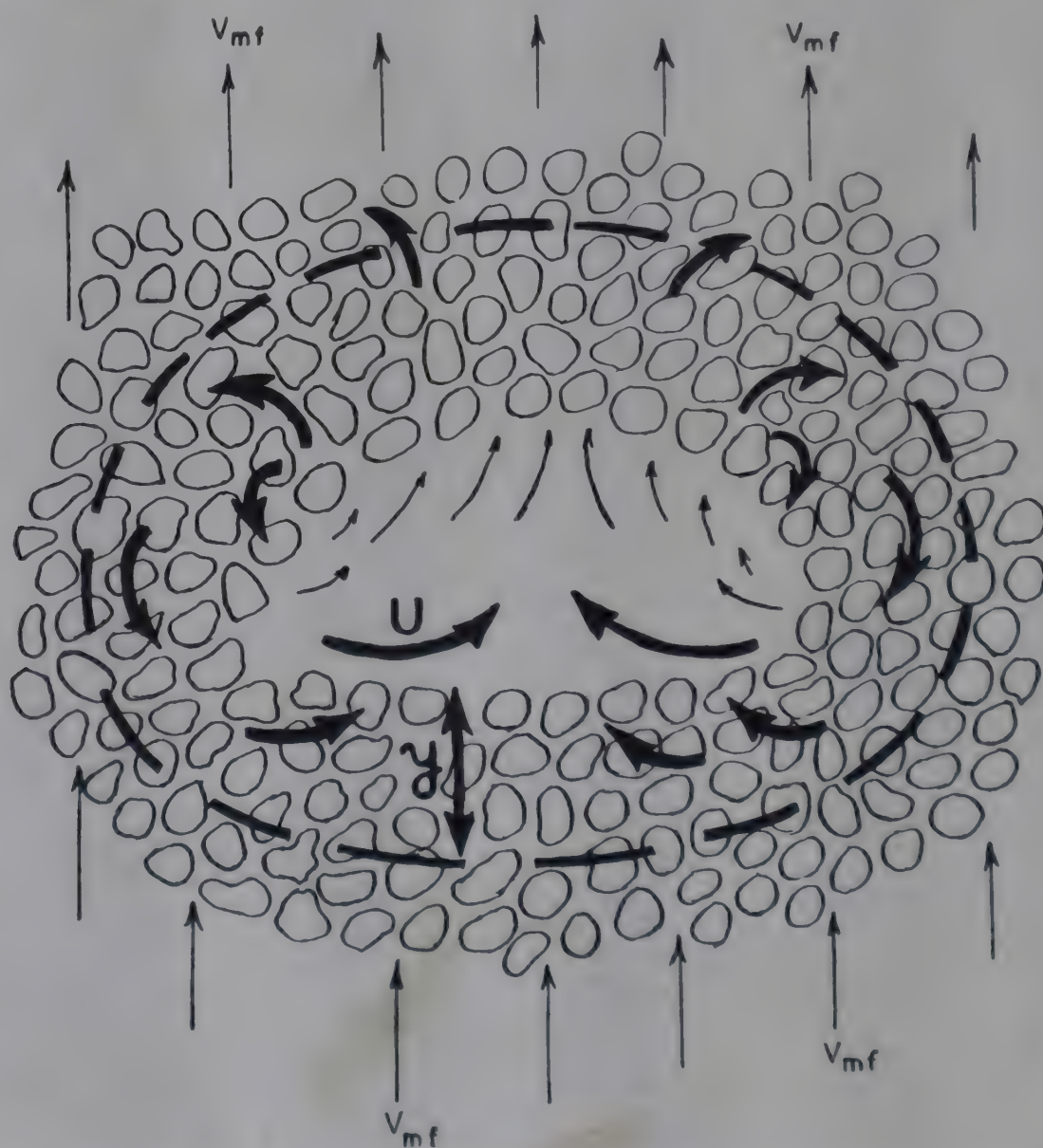


FIG. 1 —MODEL OF FLUID VELOCITY PATTERNS IN THE AREA OF INFLUENCE OF A BUBBLE RISING THROUGH A FLUIDIZED BED OF PARTICLES

the basis of recent studies of single-particle drag¹² and of bed-shearing forces in horizontal flow¹³.

A Model of Incipient Bubble Destruction

Fig. 1 schematically illustrates the well demonstrated flow patterns in and around a rising bubble¹¹. The interstitial fluidizing velocity field is designated by V_{mf} ; the shell of dense bed surrounding the bubble, through which there exist the streams of recirculating fluid, is outlined by the dashed lines and its thickness designated by y ; the horizontally directed surface velocity of the circulating fluid along the bottom of the bubble is denoted by U . Over the major portion of the bubble's lower surface there exists a velocity gradient penetrating the 'shell' which in terms of Fig. 1 can be denoted by dU/dy . This velocity gradient creates a shearing stress tending to dilate the bed within the depth y . If this dilation is sufficient in magnitude to swell the bottom surface to within a few particle diameters of the upper surface then the bubble is destroyed or rather its incipient formation is thwarted. This is true not only because it becomes 'flooded' by the swelling bottom surface but also because the upper surface particles will collapse on to the particles approaching from beneath when their distance of separation is small enough to disturb the drag forces on the upper particles⁸.

To evaluate this mechanism of bubble formation, even if qualitatively, requires means of calculating U , y , and the bed-dilating 'dispersive grain pressures' resulting from dU/dy .

Velocity Gradient and Dispersive Grain Pressure

A unique measurement of 'dispersive grain pressures', a measure of bed dilation forces, was reported by Bagnold¹³ in 1954. His apparatus, the essentials of which are illustrated in Fig. 2, consisted of a pair of concentric drums. The solid outer drum could be rotated at various speeds. The periphery of the stationary inner drum was made of sheet rubber sealed to the drum flanges. The inside of the inner drum communicated through a hollow spindle, with a manometer. Both the inner and outer drums were filled with water. On rotating the outer drum the manometer indicated the excess pressure in the annular space, exerted on the rubber sheathed inner drum, due to the centrifugal force on the rotating fluid between the drum flanges from the axis to the radius of the inner drum periphery. These pressures were recorded at various speeds of rotation. A measured volume of granular solids was then added to the annular space between the drums and again pressures were recorded at various speeds of rotation. The difference in recorded pressure with grains in the annular space and with plain fluid in the space was taken as representative of a so-called 'dispersive grain pressure'. The grains used in these tests were spherical particles made of nearly 50 per cent mixture of paraffin wax and lead stearate with a very constant

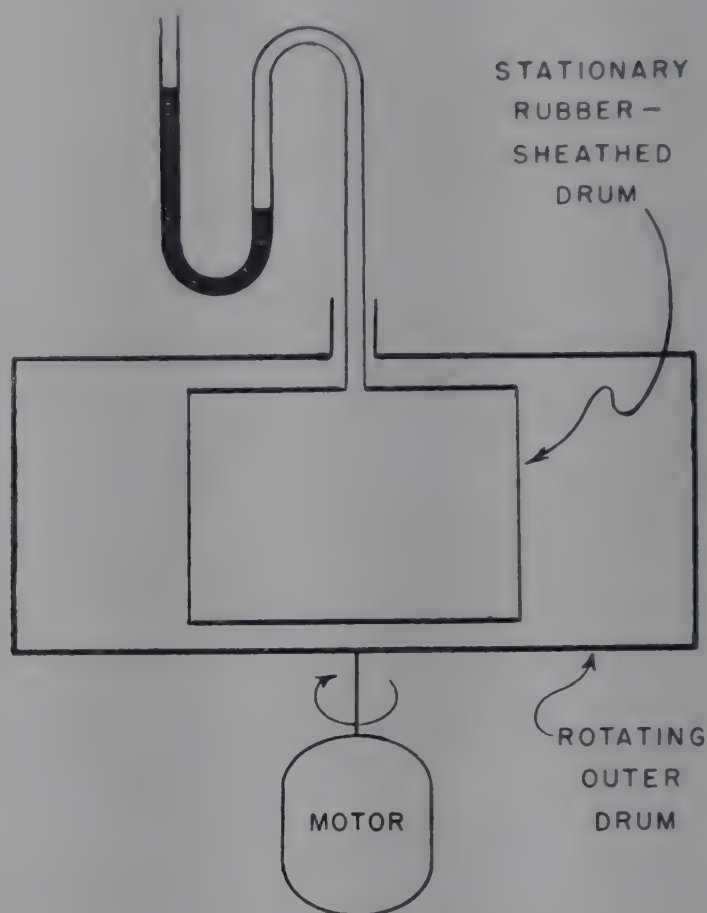


FIG. 2- SCHEMATIC ILLUSTRATION OF BASIC ELEMENTS OF BAGNOLD'S EXPERIMENTAL APPARATUS

diameter of 0.132 cm. Their density differed from that of water by less than 0.1 per cent.

Stated in the simplest terms, Bagnold measured the force on the wall of a container caused by the random impaction of particles against each other as they moved past the wall all in the same net direction but at relatively different velocities. The velocity gradient in the annulus of his apparatus caused certain particles or layers of particles to move more rapidly than others. This means that some particles would catch up with others and bounce them aside. In a dense liquid medium the side thrust on particle B (Fig. 3), upon being hit by particle A will be felt as a pressure pulse on the wall C. Greater the number of particles and greater the velocity difference, $U_2 - U_1$, or velocity ratio, U_2/U_1 , the greater is the sustained pressure on C. The process might be viewed as a multitude of continuous grazing billiard shots occurring within an incompressible fluid medium, or as random molecular collisions in an ideal gas where the drum rotational speed is replaced by temperature level. One might expect that in such an annular apparatus the resulting pressure would depend on the square of the speed of rotation since doubling the speed would double the relative particle velocities and also double the frequency of impacts. This is in accord with Bagnold's results illustrated schematically in Fig. 4. The dispersive grain pressure is proportional to (r.p.m.)² since the lines of constant

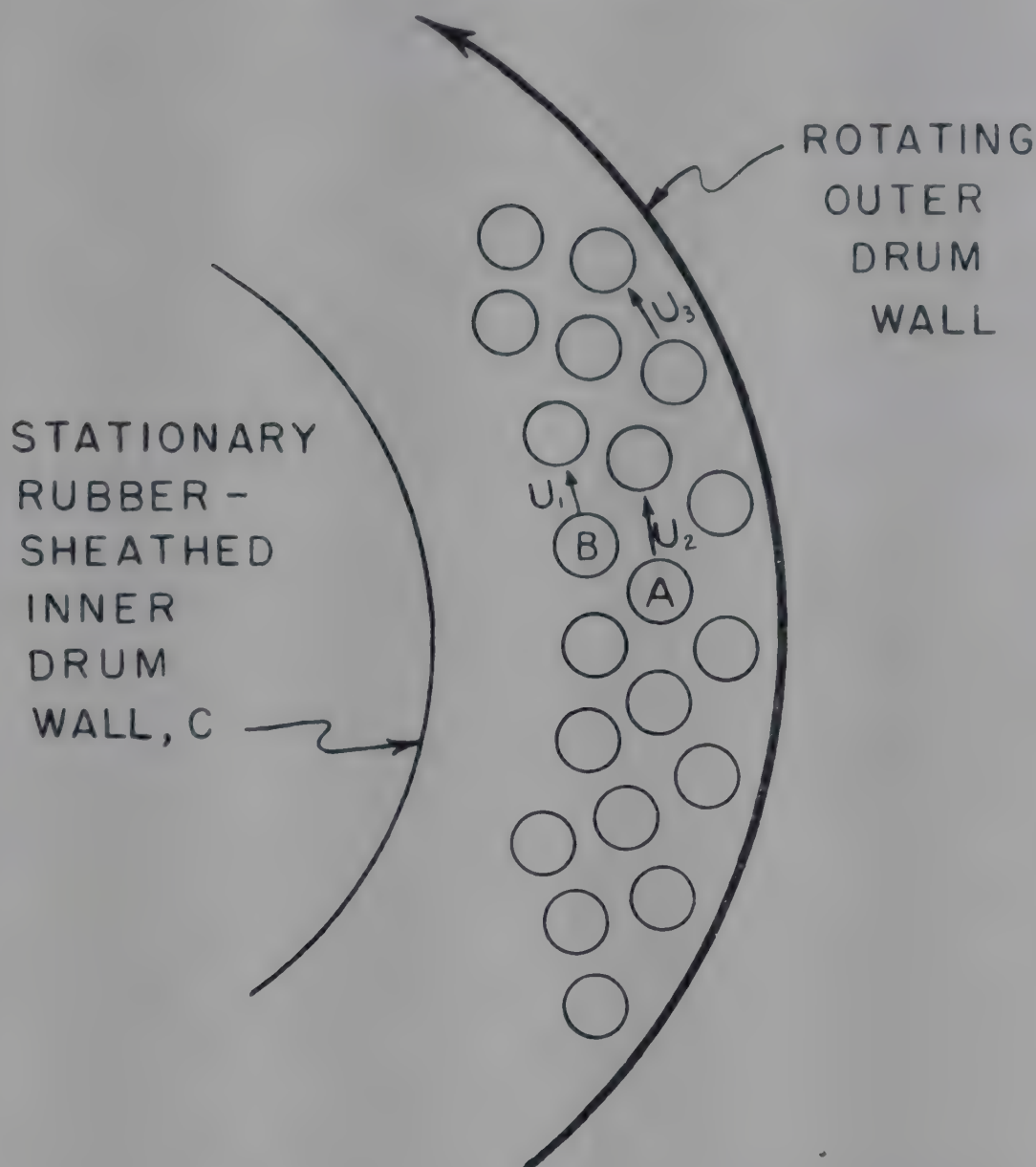


FIG. 3—SCHEMATIC CROSS-SECTION OF A PORTION OF BAGNOLD'S APPARATUS ILLUSTRATING PARTICLE FLOW MECHANISM

voidage, or solids concentration, are straight and parallel with a slope of unity.

Fig. 5 represents a cross plot of Fig. 4 to illustrate the effect of voidage or change in solids concentration. Bagnold chose to characterize his suspensions in terms of an effective particle-diameter to particle-spacing ratio, D_p/s , where an s equal to zero would correspond to rhombohedral or closest packing. For convenience in referring back to his original work this convention has been maintained in Fig. 4 and 5 with voidage values superimposed.

Of immediate interest in the physical interpretation of dispersive grain pressure is the appearance of a decided change in slope of the curves at a voidage in the neighbourhood of 48 per cent. This voidage corresponds to that in a square or cubic array of spheres. As long as the concentration of particles is such that they can exist in the loosest packing form (square

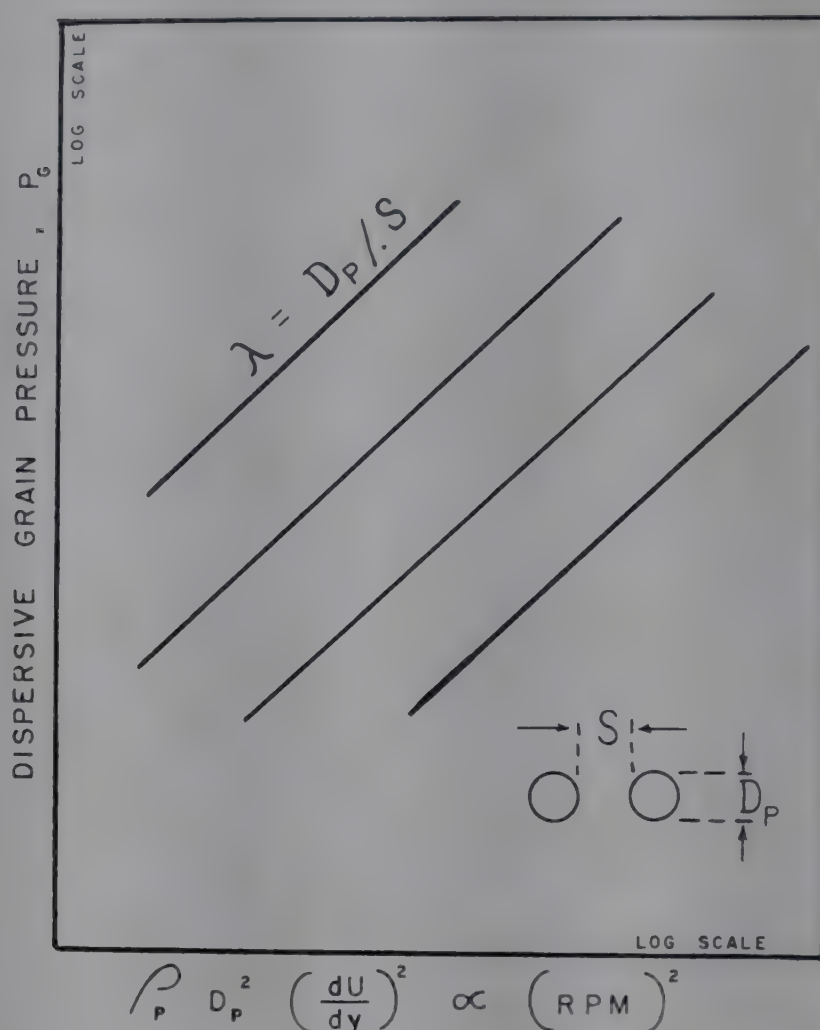


FIG. 4—BAGNOLD'S CORRELATION OF EXPERIMENTAL RESULTS

or cubic) the measured dispersive pressure P_G should simply be a reflection of the number of random inter-particle impacts. If we assume that the number of impacts would be proportional to the reciprocal of the distance between particles and then take this distance to be the log mean between the extremes for cubic and rhombohedral particle orientations, we can generate the dashed curve in Fig. 5. Something other than the log mean might be a better 'average' for the random structure and might even be chosen to match the experimental curve with greater precision than the data probably justify. When ϵ is less than 0.477 the dispersive pressure, P_G , must begin to rise more rapidly since the 'congestion' of particles due to the overlapping configurations which must now exist adds exponentially to the number of collisions. At ϵ less than 0.477, the particles cannot orient themselves in such a way that the number of collisions could theoretically be zero. At the extreme or lowest possible voidage of 26 per cent ($\epsilon=0.26$), corresponding to closest or rhombohedral packing, the dispersive pressure would be a reflection of the force necessary to shear a restrained bed of spheres and would have as an upper limit the tensile strength of the material making up the spheres.

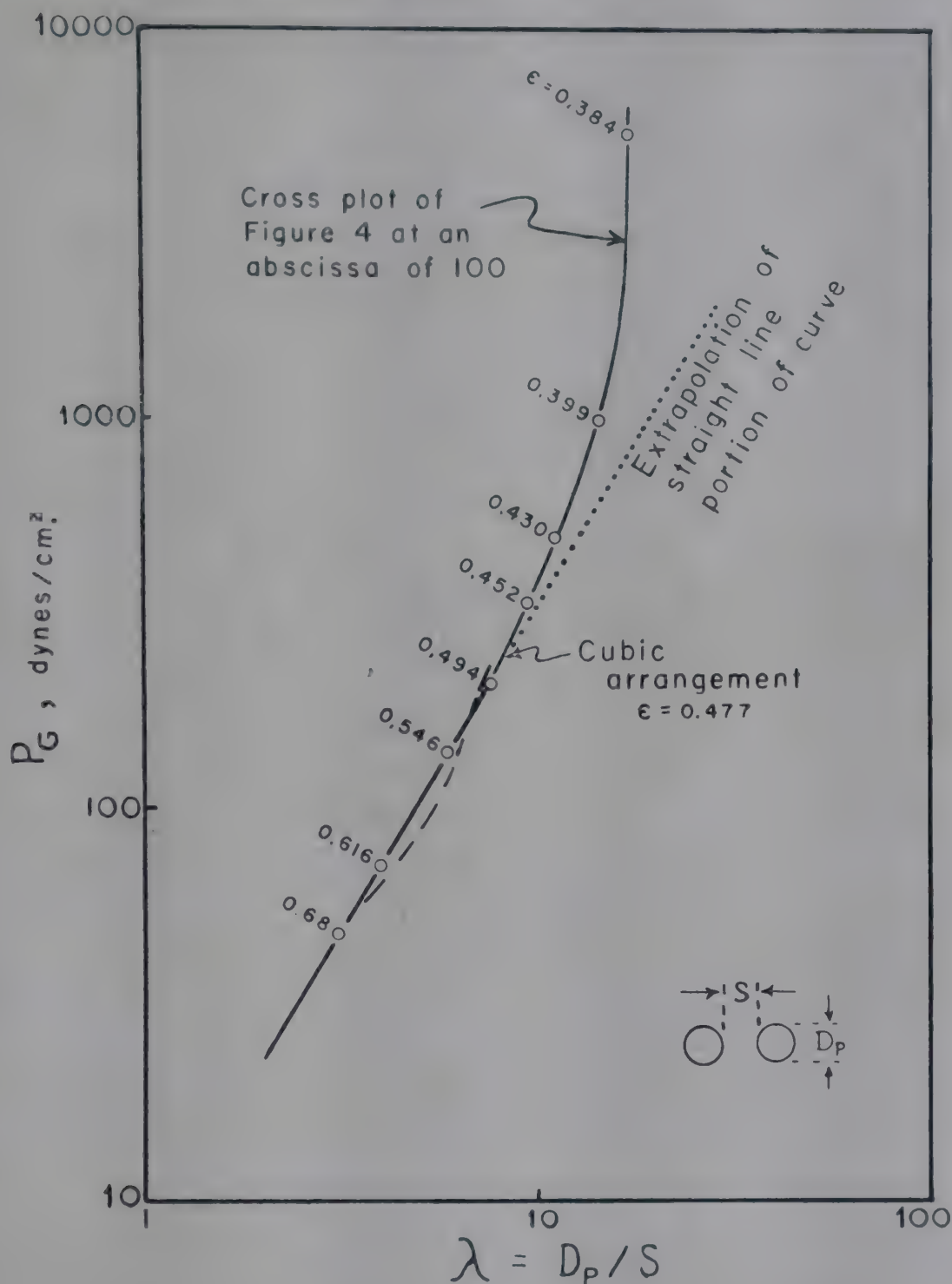


FIG. 5—EFFECT OF SOLID CONCENTRATION ON DISPERSIVE GRAIN PRESSURE

With Fig. 5 as a measure of the forces tending to dilate or disperse a bed of solids (subjected to the shearing force of a horizontal fluid velocity gradient) we need to determine the value of dU/dy for the bubble model of Fig. 1 in order to make some relative quantitative comparisons.

Velocity Gradient within a Bubble

The experimental measurement of gas circulation within a bubble rising through a fluid bed poses extraordinary difficulties. Even the relatively

simpler questions of bubble size, velocity and frequency have not as yet been fully resolved. Nevertheless reasonable inferences can be drawn from the existing data and theoretical studies, to arrive at credible quantitative values for nearly all such bubble-associated phenomena. Let us first consider the studies of bubble size which will lead to the internal gas velocity, U , in Fig. 1, and then the studies of gas flow patterns in the vicinity of bubbles which will lead to the depth or thickness of the dense phase shell surrounding the bubble and penetrated by the circulating gas.

Harrison *et al.*⁴ presented a theory defining the maximum stable bubble size in a powder maintained fluid by aeration at just the minimum fluidizing velocity. This bubble size is found by setting bubble velocity equal to the terminal velocity of an individual particle in free fall. Bubble diameter D_B is computed as the diameter of a sphere having a volume equal to the bubble, and is related to bubble velocity V_B as $V_B = 0.711 \sqrt{g D_B}$, where g is the gravitational constant. Harrison *et al.* postulate that the intensity of gas circulation within a bubble is proportional to the bubble's velocity of rise. Large, rapidly rising bubbles display greater internal circulating gas velocities than small slowly rising bubbles. A large bubble may have such intense internal circulation that particles injected into it, by whatever mechanism, will be entrained by the circulating gas. These particles will therefore remain in the bubble, and the bubble will therefore tend to become smaller. A small bubble, on the other hand, will not have sufficient internal circulation to retain a particle injected into it. Thus they conclude that a stable maximum bubble size must exist, and that the factors which determine its size are the intensity of internal circulation and the settling velocity of an individual particle in free fall. Their assumption that maximum bubble velocity equals settling velocity is an arbitrary one and they emphasize that the size calculated from this assumption is probably only a rough approximation of the maximum. They also cite the work of Bagnold¹⁴ on horizontal transport velocity of small particles as an indication that perhaps the terminal free-fall velocity might also not be the relevant parameter for computing bubble sizes in beds of very fine particles.

Squires⁵ illustrated the magnitude of bubble sizes calculated by the theory of Harrison *et al.* for typical fluid-particle systems in which bubble characteristics have been observed and reported by many investigators. His results showed that the calculated bubble sizes for particle sizes below *c.* 0.01 in. are certainly much below observed sizes. Squires proposed that in place of terminal velocity one might more realistically assume that single particle saltation velocity¹² would apply since the particles would be entrained in the bubble void by the recirculating gas flow sweeping across the particle surface making up the bottom of the bubble. Bubble sizes recalculated on this assumption showed excellent agreement with observations. Thus one can conclude that in an existing bubble the horizontal sweeping gas velocity designated by U in Fig. 1 must at least be

approximated by single particle saltation velocities, V_{s_0} , for which correlations have already been proposed¹².

The question of how deep an internal circulating gas flow might penetrate into the shell of dense phase powder surrounding the bubble void can be answered to a good first approximation from the experiments of Wace and Burnett¹⁰ and the theoretical studies of Rowe¹¹. Wace and Burnett observed the gas flow in a 'two-dimensional' bed fluidized with air. By admitting dark brown nitrogen dioxide through small holes drilled into the face wall of the bed near the grid plate they were able to observe the gas flow streamlines up through the bed. The photographs presented in their paper and subsequently elaborated upon by Rowe demonstrated unmistakably the pattern of the flow into the bottom of the bubble and out through the sides and the top. The gas flow appeared to be strictly streamline in spite of the violent solids movement caused by the passing bubbles. Rowe drew an analogy of these results to the ideal case of two and three dimensional flow through a body of infinite extent containing a circular hole. In the two dimensional case all the fluid in a zone having a width of two radii on either side of the centre line through the hole (or bubble) passes through the hole so that the velocity therein is twice that of the remote fluid. In the three dimensional case the gas velocity in the spherical void is three times that in the remote fluid (where the remote fluid is analogous to the dense particle mass in the fluidized bed). This means that gas is drawn from a shell of thickness equal to $D_B (\sqrt{3}-1)/2$ surrounding the bubble.

Dispersive Pressure with a Bubble

From the work of Rowe and Squires a first approximation of the velocity gradient within the bottom surface of a bubble can simply be shown proportional to V_{s_0} and D_B in the form

$$\frac{dU}{dy} \sim \frac{V_{s_0}}{D_B(\sqrt{3}-1)/2} \quad (1)$$

From the work of Harrison *et al.*

$$D_B = \left(\frac{V_B}{0.711 \sqrt{g}} \right)^2 \quad (2)$$

and since Squires has shown that to a better approximation V_B is proportional to V_{s_0} we may write

$$D_B \sim \frac{V_{s_0}^2}{(4.03)^2} \quad (3)$$

so that

$$\frac{dU}{dy} \sim \frac{1}{V_{s_0}} \quad \text{and} \quad \left(\frac{dU}{dy} \right)^2 \sim \left(\frac{1}{V_{s_0}} \right)^2 \quad (4)$$

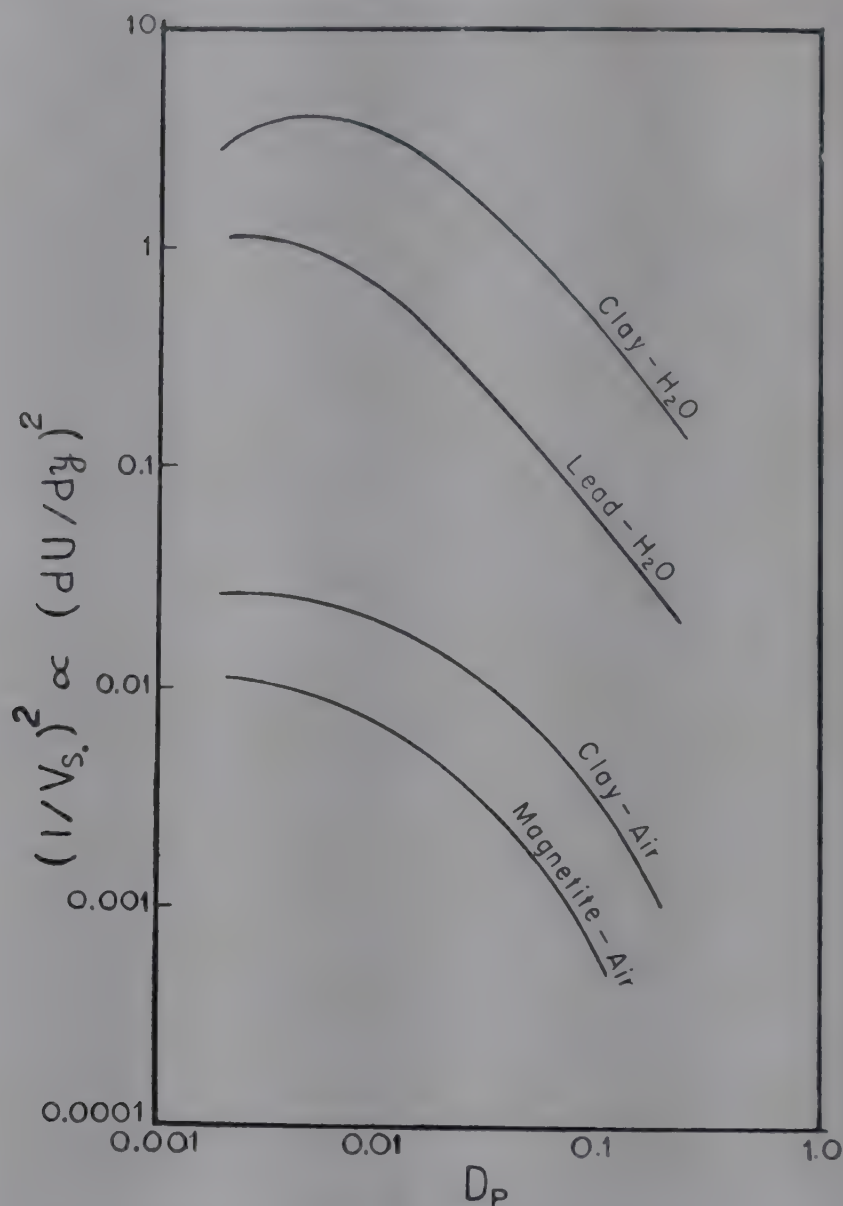


FIG. 6—VELOCITY GRADIENT OR DISPERSIVE PRESSURES FOR VARIOUS FLUID PARTICLE SYSTEMS

The dispersive grain pressure measurements of Bagnold, illustrated in Fig. 4 and 5, have as a correlant the square of velocity gradient which is thus proportional to $1/V_{s_0}^2$.

The theoretical stable bubble sizes calculated by Squires can now be compared with the magnitude of the velocity gradient, or rather the dispersive pressure. A high velocity gradient corresponds to a high dispersive pressure and certainly a high dispersive pressure coupled with a small theoretically 'stable' bubble size would lead to bubble disappearance or at any rate small probability of bubble formation ever fully occurring.

From correlations¹² of V_{s_0} it is possible to calculate relative values of the gradient $(dU/dy)^2$ within the bubble as a function of particle diameter. The results of such calculations are shown in Fig. 6 for a few typical systems. Since Bagnold showed dispersive pressure to be directly proportional to velocity gradient, the ordinate of Fig. 6 could be relabelled P_G ; however, Bagnold showed (as in Fig. 4 and 5) that dispersive pressure is also a function

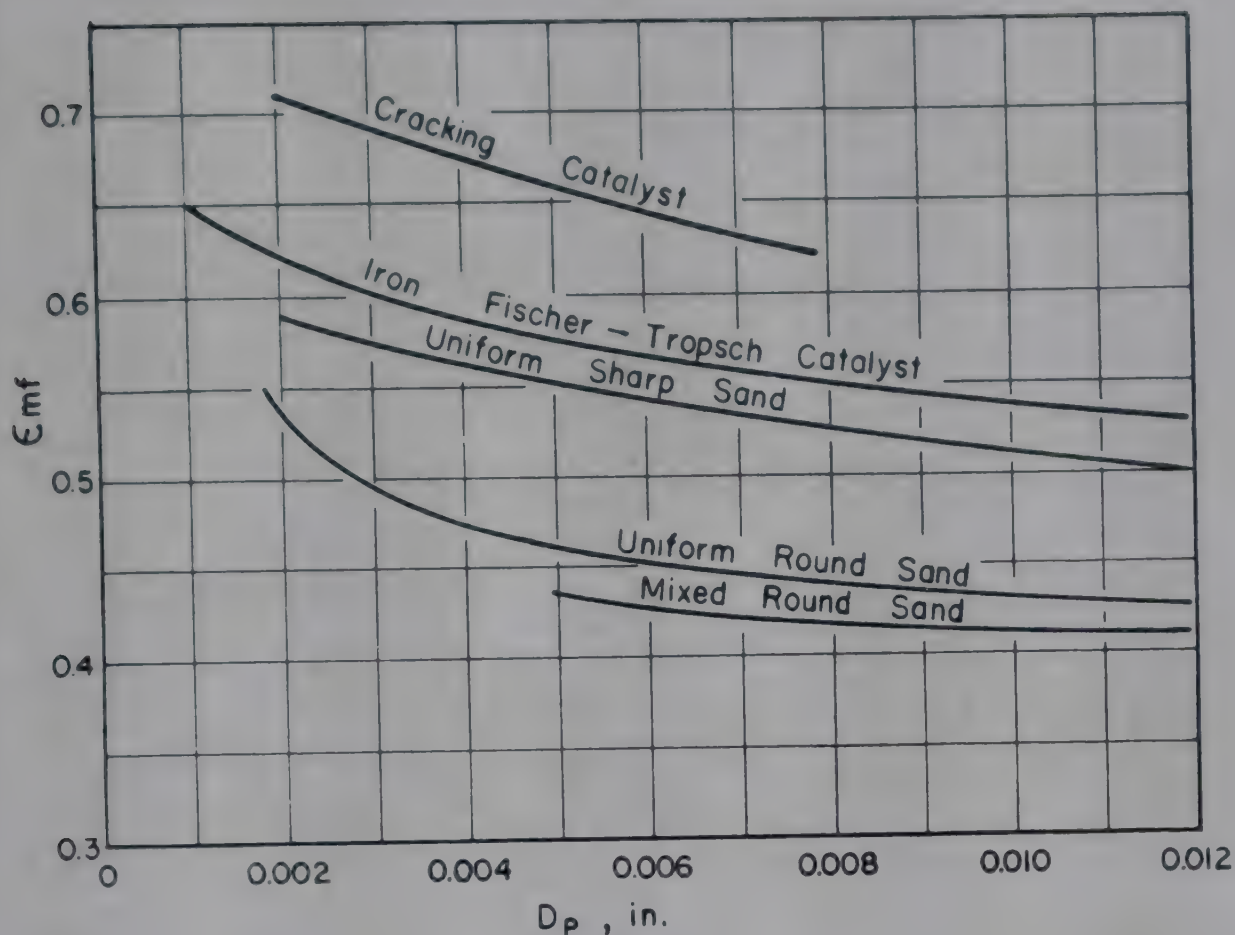


FIG. 7—VOID FRACTIONS IN VARIOUS PARTICULATE SOLIDS AT INCIPIENT FLUIDIZATION

of voidage. Since the loosest static bed density of powders is a function of particle size (finer powders exhibiting high bulk voidages) the curves of Fig. 6 can be corrected for voidage by means of Fig. 5. In making this correction it is assumed that the curves of Fig. 6 are based on 40 per cent voids for all particle sizes and that the actual voidage as a function of particle size is given by curves¹⁵ such as in Fig. 7. This voidage correction to Fig. 5 bends the curves downward to a greater and greater extent as particle diameter decreases and effectively flattens them to the results shown in Fig. 8 in which the ordinate is now labelled P_G . The degree of displacement due to the voidage correction is illustrated for the clay-water system in Fig. 8 by the dashed curve which is taken from Fig. 6. Unfortunately there is no direct quantitative means for matching the P_G scale to the abscissa. Quantitatively the coordinates of Fig. 8 are reasonable and probably near the proper magnitude since Bagnold's measurements went up to 2 lb./sq. ft at a voidage of 40 per cent.

Before carrying this reasoning to the next logical step let us reflect on what Fig. 8 physically implies. The ordinate is a measure of the force tending to dilate the solids making up the bottom surface of the largest calculable stable bubble in a fluidized bed of particles of the size given in the abscissa. Since the gradient and hence dispersive pressure is related to a calculated maximum bubble size it is not to be implied that bubbles will or do exist

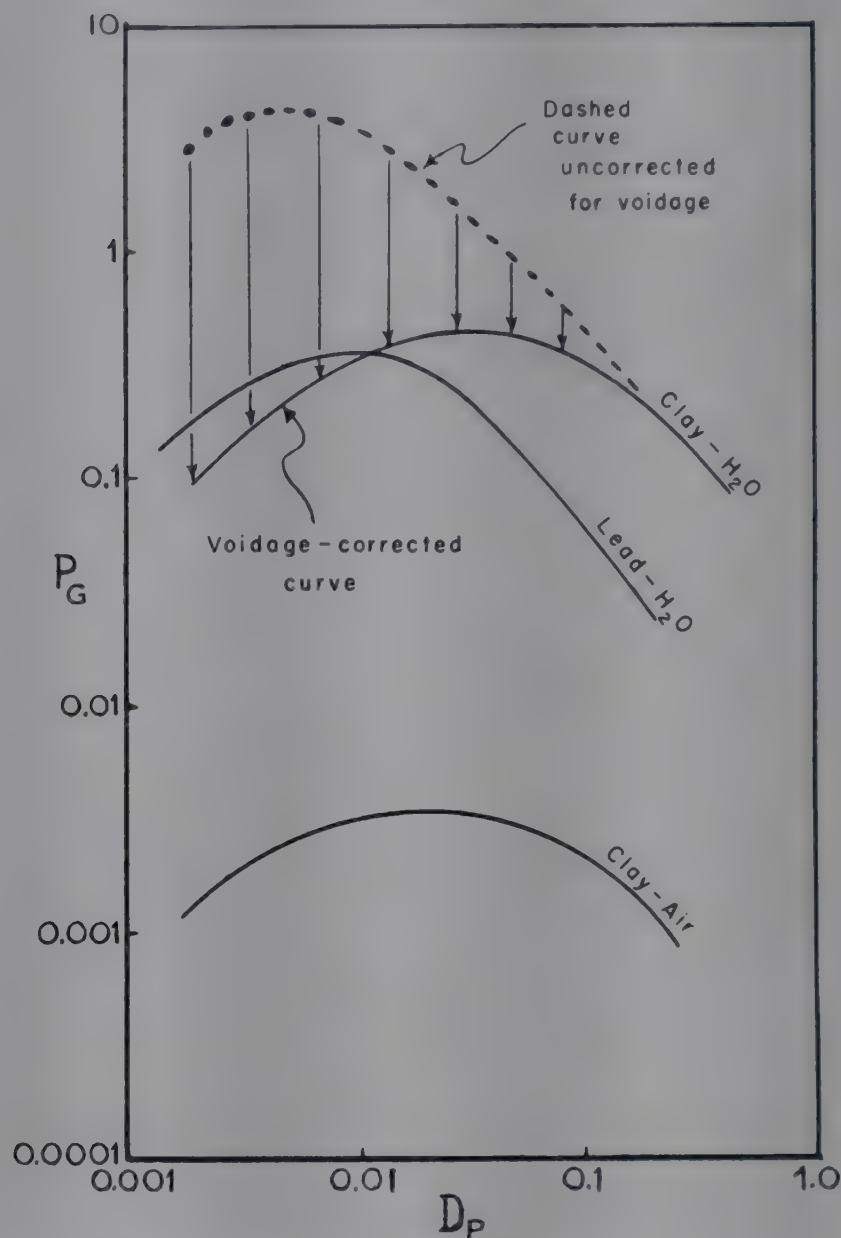


FIG. 8—DISPERSIVE PRESSURE CURVES OF FIG. 6, CORRECTED FOR PARTICLE SIZE EFFECT ON VOIDAGE

under all conditions, but merely that *if* they did exist they would have a dispersive pressure within their bottom surface of the magnitude given in Fig. 8.

The existence of a dispersive pressure begs the question, why it does not simply exert its influence and dilate the solids to the eventual destruction of any bubble. Since this does not happen in all cases it is obvious that the magnitude of the dispersive pressure must be compared with the magnitude of whatever force it must move against to effect the dispersion. The first force against which the dispersive pressure must act is the weight of the uppermost layer of particles on the bottom surface of the bubble. The weight of this layer is simply $\rho_p (1 - \epsilon) D_p / 12$ in units of lb./sq. ft, if ρ_p is expressed in lb./cu. ft and D_p in inches. The voidage ϵ is again taken from curves such as in Fig. 7 corresponding therefore to the conditions on which the curves of Fig. 8 are based. Fig. 9 is a reproduction of Fig. 8 with curves

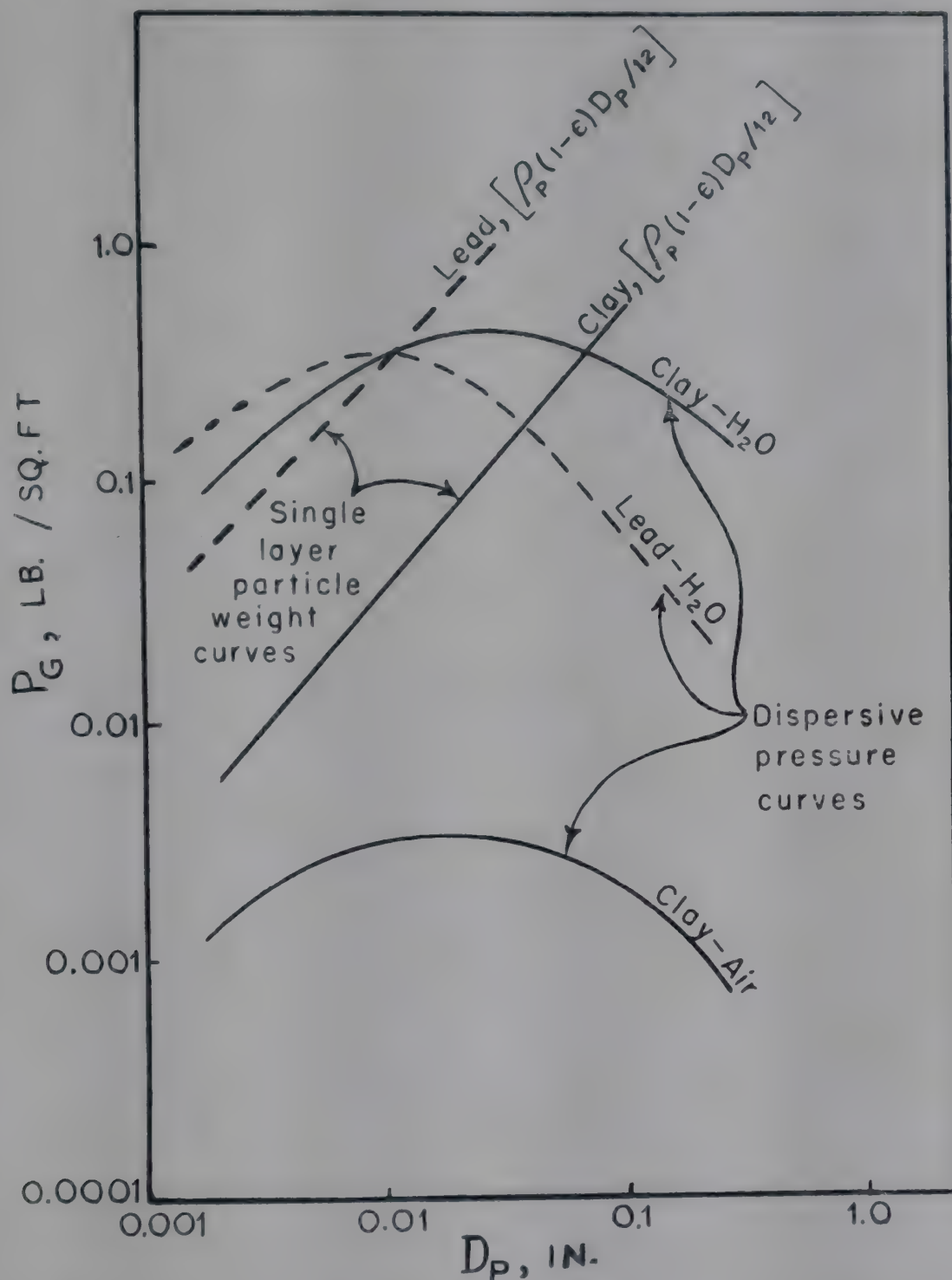


FIG. 9—RELATIVE MAGNITUDE OF DISPERSIVE PRESSURE AND WEIGHT OF SINGLE LAYER OF PARTICLES

of $\rho_P (1-\epsilon) D_P/12$ corresponding to clay catalyst and lead shot superimposed.

We now note in Fig. 9 that for the water-clay catalyst system the dispersive pressure curve intersects the single-particle-layer-weight curve and that to the left of this intersection the dispersive pressure exceeds the layer weight. We may therefore expect that to the left of this point of intersection the beds will dilate and no bubbles will be able to persist whereas in beds

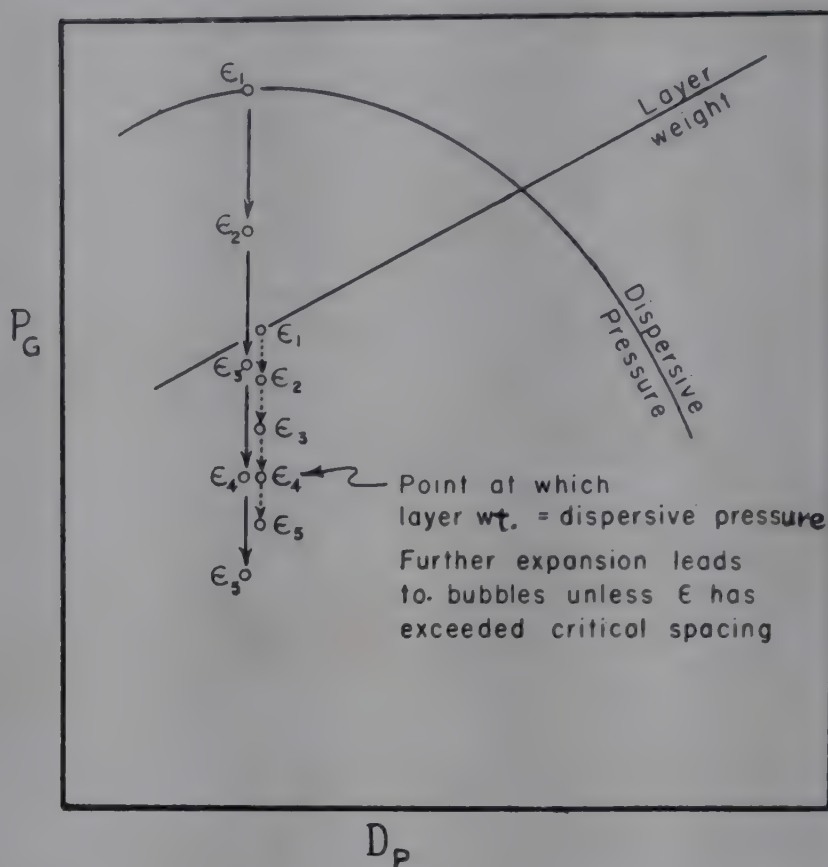


FIG. 10—SCHEMATIC ILLUSTRATION OF CHANGE IN DISPERSIVE PRESSURE AND PARTICLE LAYER WEIGHT WITH BED EXPANSION DURING FLUIDIZATION

of larger particle size the dispersive pressure cannot overcome the particle weight and hence bubbles will persist. It is to be noted that in accord with reported observations, the air-clay system dispersive pressure is always below the particle-layer weight curve and thus this system always exhibits bubbles, whereas in water medium only very large clay catalyst particles will allow bubbles to persist. Also in accord with reported observations, lead particles would exhibit bubbles in water medium for all but the very smallest particle sizes.

The above reasoning would appear plausible only for a point condition and raises the question, what happens in beds of small particle size after the solids have dilated (and thereby thwarted the bubble) since then the bed exhibits a higher voidage and hence a lower dispersive pressure. Note, however, that if the voidage increases the particle layer weight also decreases. This raises the question, which decreases more rapidly with increased voidage—the particle layer weight or the dispersive pressure? As illustrated in Fig. 10 for a bed of constant particle size exhibiting no bubbles at an incipient fluidization voidage of ϵ_1 the bed may expand without distinct bubbles to a voidage of say ϵ_4 at which point its unit layer weight will equal the dispersive pressure. Further expansion would be accompanied by bubble formation because the dispersive pressure could no longer counteract the weight of the bottom surface of a forming bubble. The change in dispersive pressure with voidage is again obtainable from Fig. 4 or 5,

and the particle layer weight from the expression $\rho_p (1-\epsilon) D_p/12$. Such particulate (non-bubble) fluidization to bed expansions of rather high voidage prior to the observation of distinct bubbles has been reported by Simpson and Rodger¹⁶ who carried out extensive experiments with light solids fluidized in dense pressured gases as well as heavy solids fluidized in water. For most of their data they arrived at an empirical correlation for predicting the degree of particulate fluidization or bed expansion obtainable prior to the onset of distinct bubbling; however, their correlation did not fit all of the data. With their original data in hand it should be possible to derive the dispersive pressure curves necessary to match their observations to the bubble destruction theory presented here. Such a procedure might be of considerable help in establishing Fig. 8 on a firmer quantitative basis.

There are also systems in which particulate fluidization is observable over the entire range of voidages from the static bed to a single suspended particle. Fig. 4 and 5 would ordinarily indicate such rapid decrease in P_G with increased voidage that the particle layer weight curve would always be passed (as illustrated in Fig. 10) well before ϵ neared 1.0, the value for expansion to the single suspended particle. However, the possibility of bubble formation is overcome as soon as bed expansion has reached the point where the particles are far enough apart so that the wake behind one particle will not touch or sufficiently influence the flow field facing the next nearest downstream particle to cause it to fall down onto its upstream neighbour¹⁷. Once the particles are that far apart there is also no longer a mechanism for stabilizing the roof of the bubble and thus the entire question of bubbles vanishes. If, as illustrated in Fig. 10, the particle separation at ϵ_4 or at lower voidages already exceeds wake length then the bed will expand further to $\epsilon=1.0$ without bubble formation even if the dispersive pressure is zero. Observations of dilute phase fluidization, even for systems exhibiting violent bubbling at low voidages, are in accord with this viewpoint. Further work on the influence of neighbouring particles on drag, such as reported by Rowe, should help in establishing the critical particle separation.

The mechanisms proposed here as leading to natural destruction, or persistence of bubbles, suggest a broad spectrum of experimentation to provide the necessary tools for a quantitative treatment. A few selected systems, chosen specifically to explore the region around the intersection of dispersive pressure and single layer weight curves, have been observed¹⁸ to be in accord with curves such as shown in Fig. 9 and 10.

NOMENCLATURE

| | |
|-------|-----------------------------|
| D_B | = bubble diameter |
| D_P | = particle diameter |
| g | = gravitational constant |
| P_G | = dispersive grain pressure |

- s = particle spacing parameter ($s=0$ corresponds to rhombohedral or closest spacing)
 U = horizontally directed surface velocity of the circulating fluidizing medium along the inside bottom of the bubble
 V_B = velocity of bubble rise through a fluidized bed
 V_{s_u} = minimum horizontal fluid velocity required to prevent a particle from settling out along the bottom of a horizontal line
 V_{mf} = superficial fluidization velocity
 γ = thickness of recirculating gas shell surrounding a bubble
 ϵ = void fraction
 ϵ_{mf} = void fraction at incipient fluidization
 λ = D_P/s
 ρ_P = particle density

REFERENCES

1. HEBDEN, D., *Trans. Instn chem. Engrs, Lond.*, **39** (1961), 225.
2. ROMERO, J. B. & JOHANSON, L. N., *Chem. Engng Progr., (Symp. Ser.)*, **58**(38) (1962), 28.
3. VOLK, W., JOHNSON, C. A. & STOTLER, H. H., *Chem. Engng Progr., (Symp. Ser.)*, **58**(38) (1962), 38.
4. HARRISON, D., DAVIDSON, J. F. & DEKOCK, J. W., *Trans. Instn chem. Engrs, Lond.*, **39** (1961), 39.
5. SQUIRES, A. M., *Chem. Engng Progr., (Symp. Ser.)*, **58**(38) (1962), 57.
6. YASUI, G. & JOHANSON, L. N., *J. Ass. Inst. chem. Engrs*, **4** (1958), 445.
7. ROWE, P. N., AERE—R 4383, Harwell, July 1963.
8. ROWE, P. N. & HENWOOD, G. A., *Trans. Instn chem. Engrs, Lond.*, **39** (1961), 43.
9. ROWE, P. N., PARTRIDGE, B. A., LYALL, E. & ARDRAN, G. M., *Nature, Lond.*, **193** (1962), 278.
10. WACE, P. F. & BURNETT, S. J., *Trans. Instn chem. Engrs, Lond.*, **39** (1961), 168.
11. ROWE, P. N., *Chem. Engng Progr., (Symp. Ser.)*, **58**(38) (1962), 42.
12. ZENZ, F. A., *Modern Chemical Engineering*, edited by Alrivos, A. (Reinhold Publishing Corp., New York), 1963, Chapter 6.
13. BAGNOLD, R. A., *Proc. roy. Soc.*, **225A** (1954), 49.
14. BAGNOLD, R. A., *The Physics of Blown Sand and Desert Dunes* (Methuen & Co., London), (1941), 88.
15. ZENZ, F. A. & OTHMER, D. F., *Fluidization and Fluid Particle Systems* (Reinhold Publishing Corp., New York), 1960, 234.
16. SIMPSON, H. C. & RODGER, B. W., *Chem. Engng Sci.*, **16** (1961), 153.
17. ZENZ, F. A. & OTHMER, D. F., *Fluidization and Fluid Particle Systems* (Reinhold Publishing Corp., New York), 1960, 257.
18. JAKOVAC, J., M. S. Thesis, Polytechnic Inst. of Brooklyn, 1965.

Gravity Flow of Granular Solids through Vertical and Inclined Tubes

K. D. MANCHANDA* & N. GOPAL KRISHNA†

Indian Institute of Technology
New Delhi 16

The gravity flow of granular solids through vertical and inclined tubes of conical funnels has been determined for spherical glass and plastic beads and crushed material like sandstone and coal. Data have been obtained both under constant and varying head conditions. Keeping a constant inclination of the leg, flow rates have been observed with varying discharge openings. Flow rate data have also been obtained at different inclinations of the leg from 90° to 30° maintaining a constant discharge opening of the funnels. The effect of solid properties like diameter, angle of repose and density upon flow rates has been studied.

A knowledge of the various factors affecting the gravity flow of granular solids is very important in the design of feeding mechanism of the solids into reactors and other equipment. Several workers¹⁻³ have reported on gravity flow of solids through orifices and vertical pipes, and correlated the data in the form of an empirical equation.

Newton, Dunham and Simpson⁴ observed the flow rate of cylindrical clay cracking catalyst particles through horizontal orifices of a flat-bottomed container. The empirical equation proposed by them is as follows:

$$W = 8.5 D_o^{2.96} \times H^{0.04} \quad (1)$$

This equation is specific and gives no information on the influence of particle diameter, angle of repose and other fundamental variables.

*Present address: Chemical Engineering Department, McMaster University, Canada.

†Present address: Regional Engineering College, Srinagar, Kashmir.

Deming and Mehring⁵ investigated the flow of solids through an inverted truncated cone orifice and obtained

$$t = \frac{\mu_1}{D_o^{2.5} \times D_p} [0.21 + (39.21 + 2.58 \sin \phi/2)]$$

where t is the time of flow and μ_1 , the static angle of the cone angle.

Takahasi⁶ studied flow rates of sand, lean coal, and a mixture of sand and sulphur, and sand and talc, and correlated the results by the empirical equation

$$t = \sqrt{\frac{b}{g}} D_o^{2.5} [f(\mu_2) - a (D_p/D_o)]$$

where a and b are constants depending only on the material, $f(\mu_2)$ is a power function of the tangent of the surface angle.

Rose and Tanaka⁷ considered the rate of flow of solids from storage bins and hoppers through a circular orifice. They gave a correlation based on their original data and the data of Mehring⁵. The correlation of Rose and Tanaka includes the funnel angle as an explicit factor, and reads

$$\frac{W}{D_o^{2.5} \cdot \rho_p \cdot g^{0.5}} = 0.16 (D_o/D_p - 3)^{0.3} \phi_6 (\phi) \times (\mathcal{Z} - 5)^{0.3}$$

The value of $(\tan \frac{\phi}{2})$ is to be used for

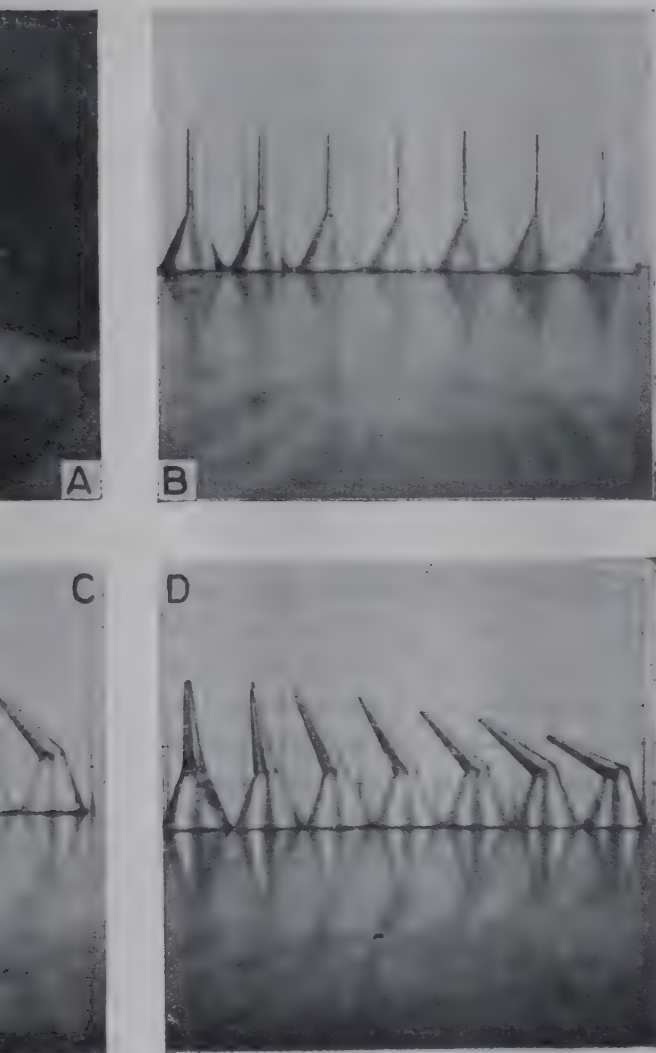
$\frac{\phi}{2} < (90 - \alpha)$. For $\frac{\phi}{2} \geq (90 - \alpha)$, the value

used. Their correlation holds good for particles of all sizes but does not find extensive application.

Harmens⁸ presented a correlation for the flow of solids through a horizontal orifice and extended it to flow from funnel-shaped hoppers.

$$W = \rho_p \cdot A \cdot \sqrt{g D_o} [0.505 - 0.16 f - F_1 (\phi)]$$

with $F_1 = f(\phi) = 0.35 \sin \phi$



, (B) VERTICAL FUNNELS WITH VARYING DISCHARGE OPEN-
 INCLINATION BUT VARYING DISCHARGE OPENINGS; (D) FUNNELS
 INCLINATION BUT CONSTANT DISCHARGE OPENINGS

EXPERIMENTAL SET-UP

consisted essentially of a funnel positioned in
 on stand and a bottom receiver to collect the
 A. Before charging the material, the top surface
 horizontal by means of a spirit level. The discharge

Materials employed were close-cut fractions of spherical glass and plastic beads and crushed substances like sandstone and coal. Various types of funnels employed in the study include: (i) vertical funnels with different discharge openings (Fig. 1B); (ii) funnels with constant inclination but different discharge openings (Fig. 1C); and (iii) funnels with varying inclination but constant discharge openings (Fig. 1D).

RESULTS AND DISCUSSION

Head effect. The effect of head on gravity flow of solids was studied both under constant and varying head conditions. The results expressed as mass flow rates are shown in Table 1. The flow rate values under constant and varying head conditions are almost identical indicating that the flow rate is independent of head, of size ($-5+7$ mesh to $-40+60$ mesh), shape (crushed material and spherical) and the density (1–2.65 g./cc.) of the solids.

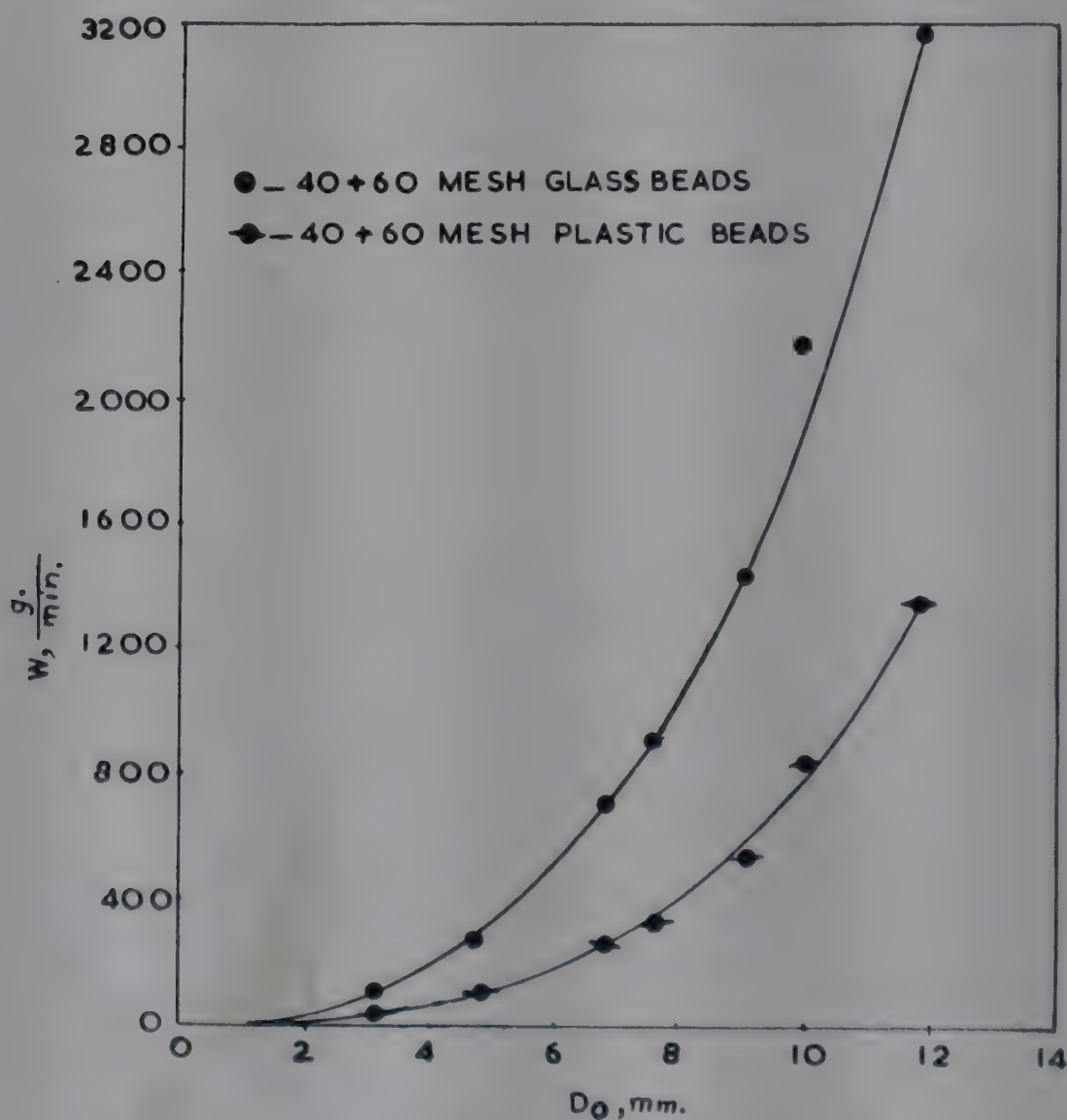


FIG. 2—EFFECT OF DISCHARGE OPENING ON GRAVITY FLOW OF SOLIDS IN VERTICAL FUNNELS ($-40+60$ mesh glass & plastic beads)

TABLE 1—COMPARISON OF MASS FLOW RATES UNDER CONSTANT AND VARYING HEAD CONDITIONS

(Variation of head of solids, 15–25 cm.)

| MATERIAL | MESH SIZE | FUNNEL SURFACE | DISCHARGE OPENING <i>mm.</i> | MASS FLOW RATE <i>G</i> <i>g./min. cm.²</i> | |
|-------------------------|--------------|-------------------|------------------------------------|---|-----------------|
| | | | | Constant head | Varying head |
| <i>Vertical funnels</i> | | | | | |
| Sandstone | —40+60 | Glass | 7.28 | 1635 | 1605 |
| do | do | do | 3.50 | 1100 | 1080 |
| do | do | Polythene | 5.89 | 1010 | 1000 |
| do | do | do | 4.75 | 635 | 630 |
| Coal | do | Glass | 7.28 | 1325 | 1330 |
| do | do | do | 3.50 | 838 | 840 |
| do | do | Polythene | 5.89 | 700 | 700 |
| do | do | do | 4.75 | 461 | 465 |
| <i>Inclined funnels</i> | | | | | |
| Glass beads | — 5+ 7 | Sheet metal | 12.7 | 2166 | 2154 |
| do | — 7+ 8 | do | do | 2472 | 2508 |
| do | — 8+10 | do | do | 2604 | 2706 |
| Sandstone | —10+14 | do | do | 1392 | 1410 |
| do | —20+28 | do | do | 1830 | 1848 |
| do | —28+35 | do | do | 2292 | 2292 |
| Shellac | — 8+10 | do | do | 1002 | 1005 |
| do | —10+14 | do | do | 1170 | 1188 |
| Coal | —10+14 | do | do | 1140 | 1143 |
| do | —14+20 | do | do | 1230 | 1212 |
| do | —20+28 | do | do | 1308 | 1308 |
| do | —28+35 | do | do | 1392 | 1392 |

Vertical funnels. The effects of discharge opening, size of the feed and the density of the solids were studied in vertical funnels with different discharge openings and the flow rate data are shown in Fig. 2–6. It was observed that (i) the flow rate increases with the increase in discharge opening and decrease in particle diameter as shown in Fig. 2 and 3. With the increase in particle density, delivery rate increased correspondingly; and (ii) a minimum ratio of D_o/D_p (5–7) has to be maintained if the flow rate is to take place, as can be seen in Fig. 4.

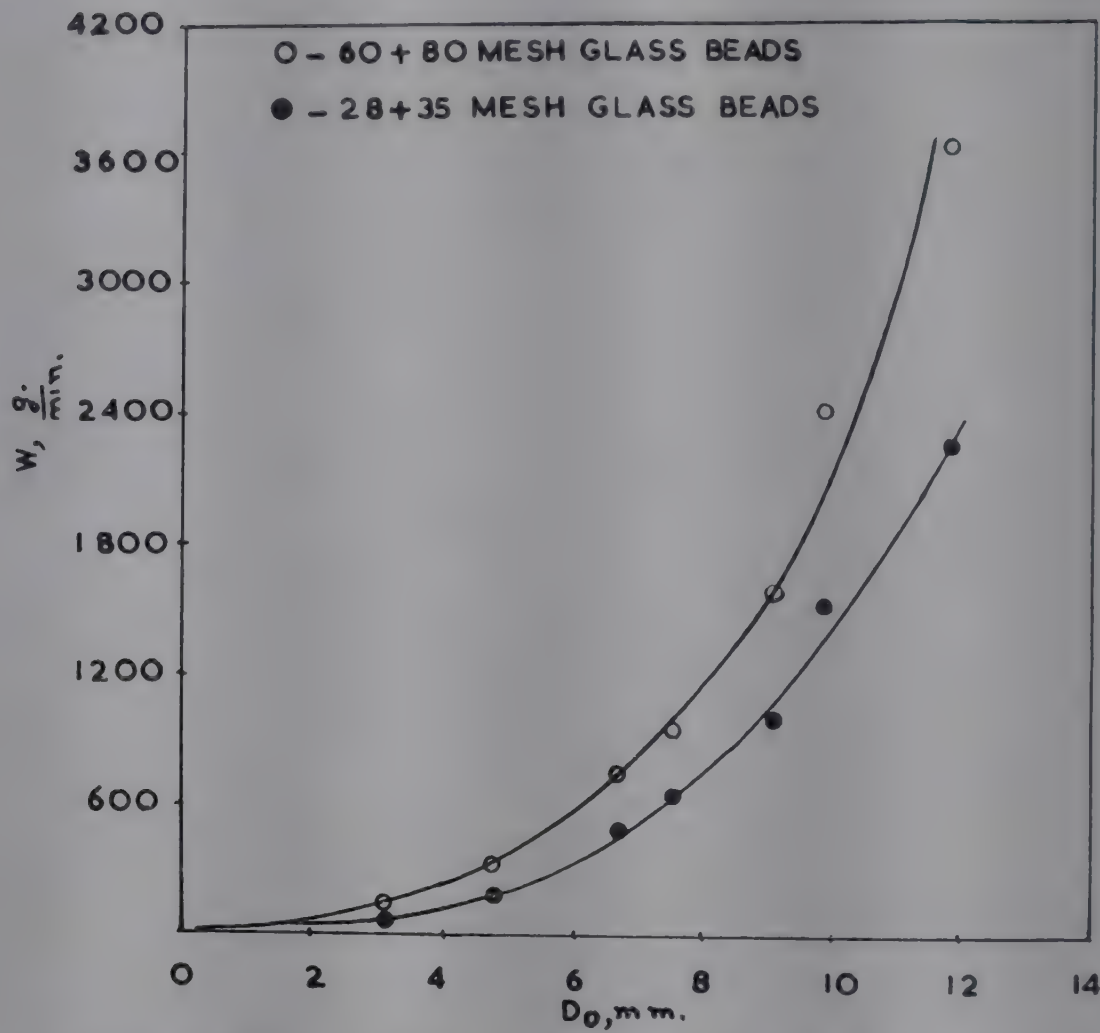


FIG. 3—EFFECT OF DISCHARGE OPENING ON GRAVITY FLOW OF SOLIDS IN VERTICAL FUNNELS (—60+80 & —28+35 mesh glass beads)

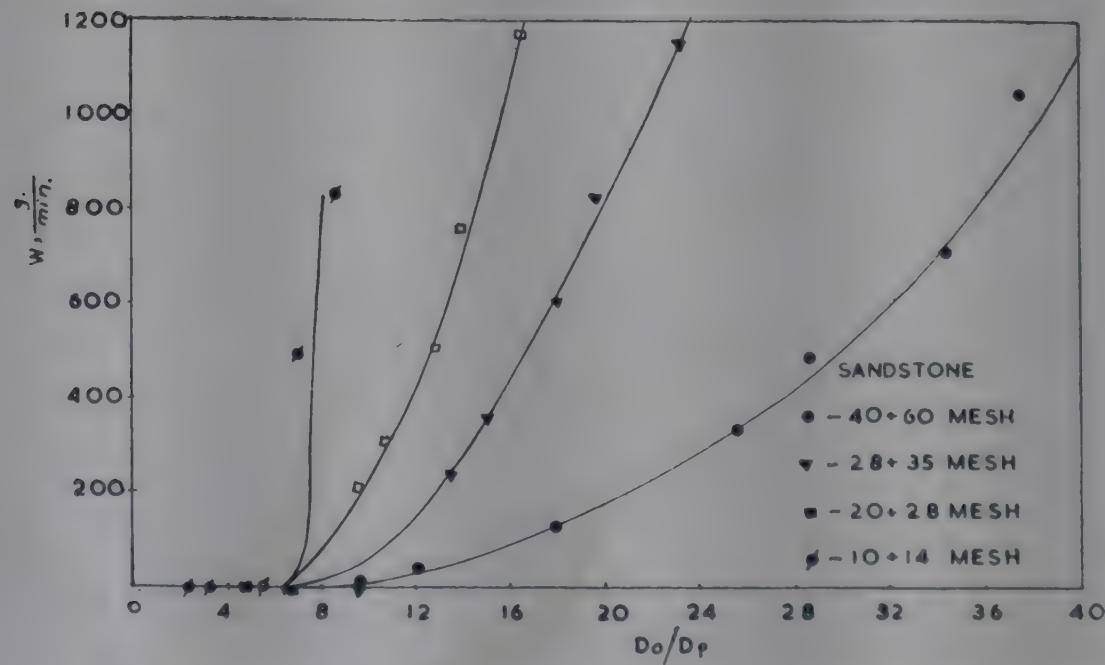


FIG. 4—EFFECT OF PARTICLE SIZE AND DISCHARGE OPENING ON GRAVITY FLOW OF SOLIDS IN VERTICAL FUNNELS [Sandstone: —40+60; —28+35; —20+28; —10+14 mesh]

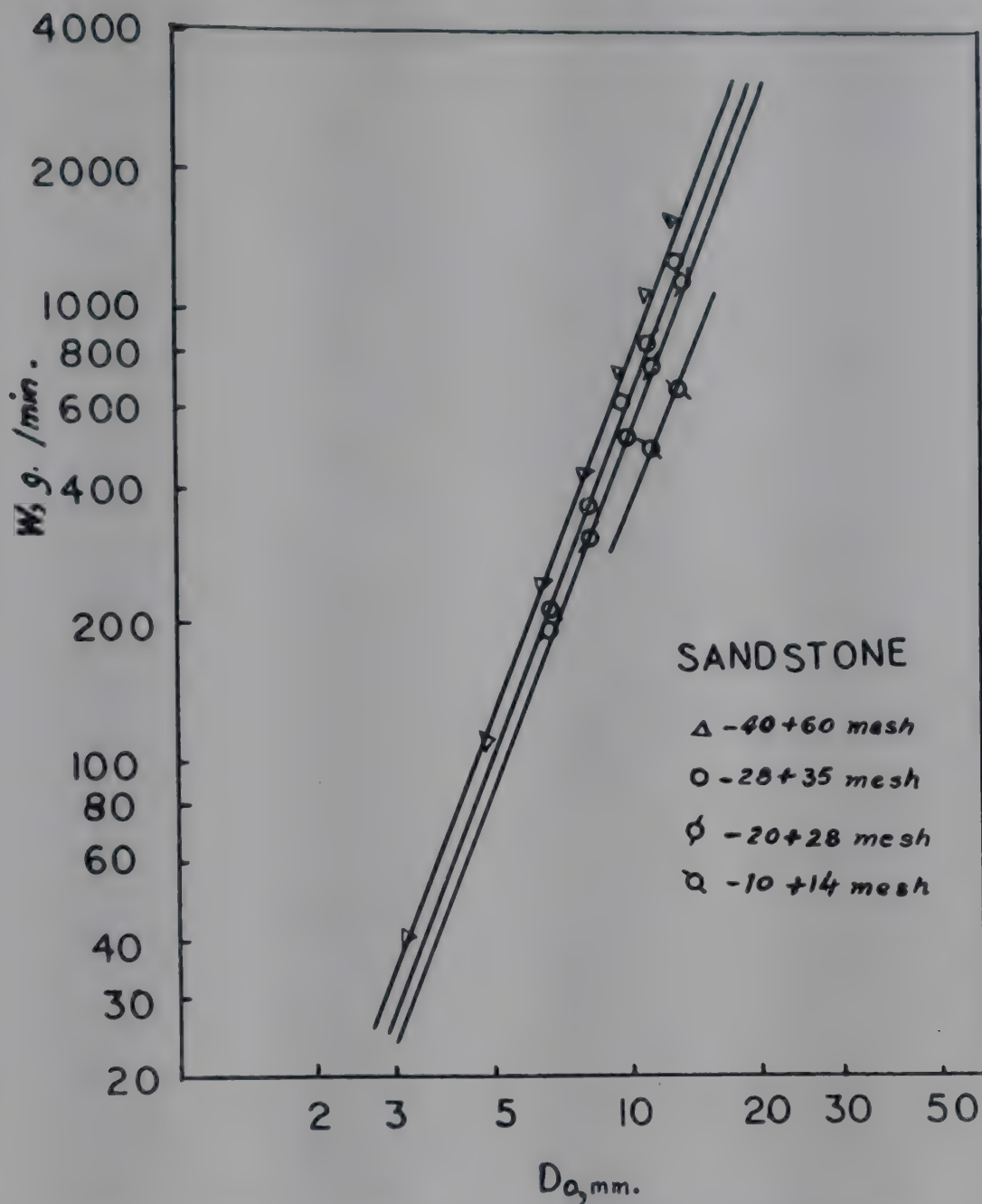


FIG. 5—EFFECT OF DISCHARGE OPENING ON GRAVITY FLOW OF SOLIDS IN VERTICAL FUNNELS
[Sandstone: -40+60; -28+35; -20+28; -10+14 mesh]

Fig. 5 shows W plotted against D_o on log-log scale. The experimental data are represented by a straight line. For these conditions,

$$W = 2.43 D_o^{2.53} \quad (6)$$

where W is in g./min. and the discharge opening in mm. This is similar to the equation proposed by Gregory¹ for gravity flow of solids through vertical pipes.

The relationship between G/ρ_p and D_o/D_p is indicated in Fig. 6. For materials with sphericity of 1, i.e. glass and plastic beads, all the points fall on one line, while those for coal and sandstone cluster on another straight line having the same slope. The two straight lines can be represented by

$$G/\rho_p = 168 (D_o/D_p)^{0.44}, \text{ for spherical beads} \quad (7)$$

$$G/\rho_p = 88 (D_o/D_p)^{0.44}, \text{ for crushed material} \quad (8)$$

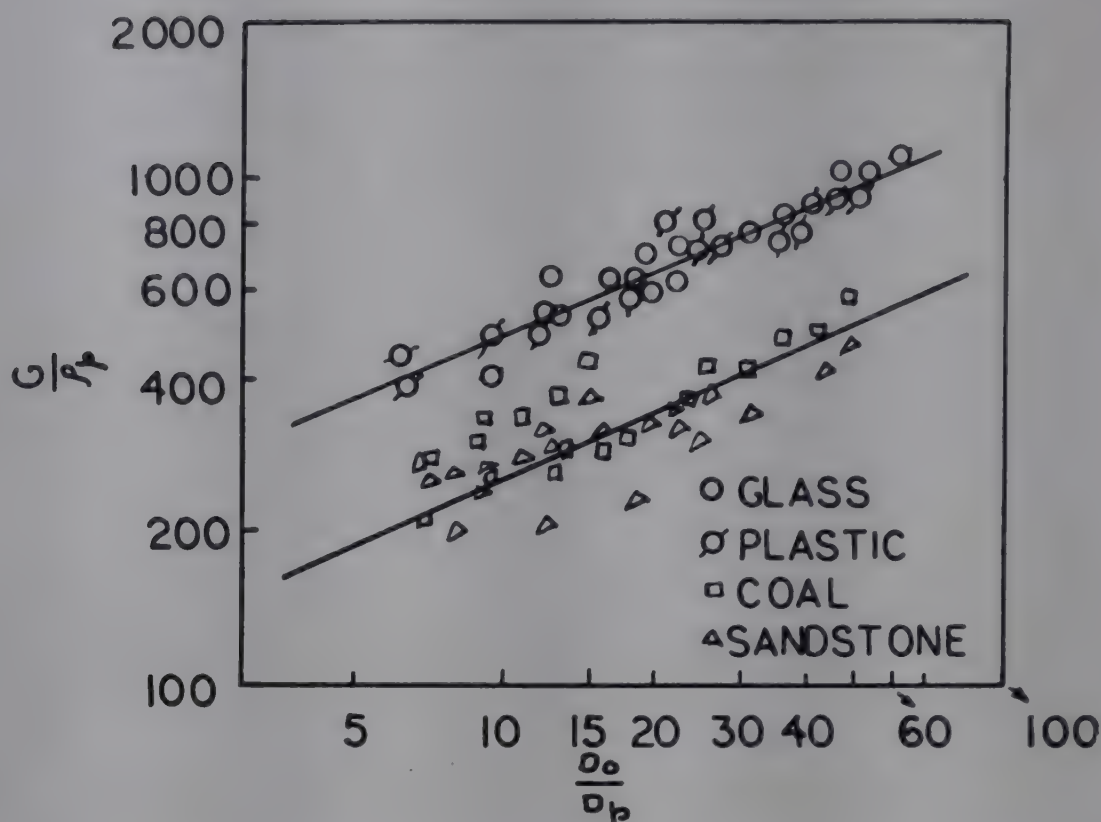


FIG. 6—CORRELATION FOR FLOW RATE OF SOLIDS IN VERTICAL FLOW FUNNELS

Funnels with inclined legs. The same tendency is observed in inclined funnels as in the case of vertical funnels, viz. the effect of particle diameter, discharge opening and particle density on the flow rate. A comparison of the flow rates between vertical and inclined funnels reveals that the flow rate is higher in the case of inclined funnels (Fig. 7). To investigate the effect of inclination on flow rate, funnels with same discharge opening but of varying inclinations ranging from 90° to 30° were employed.

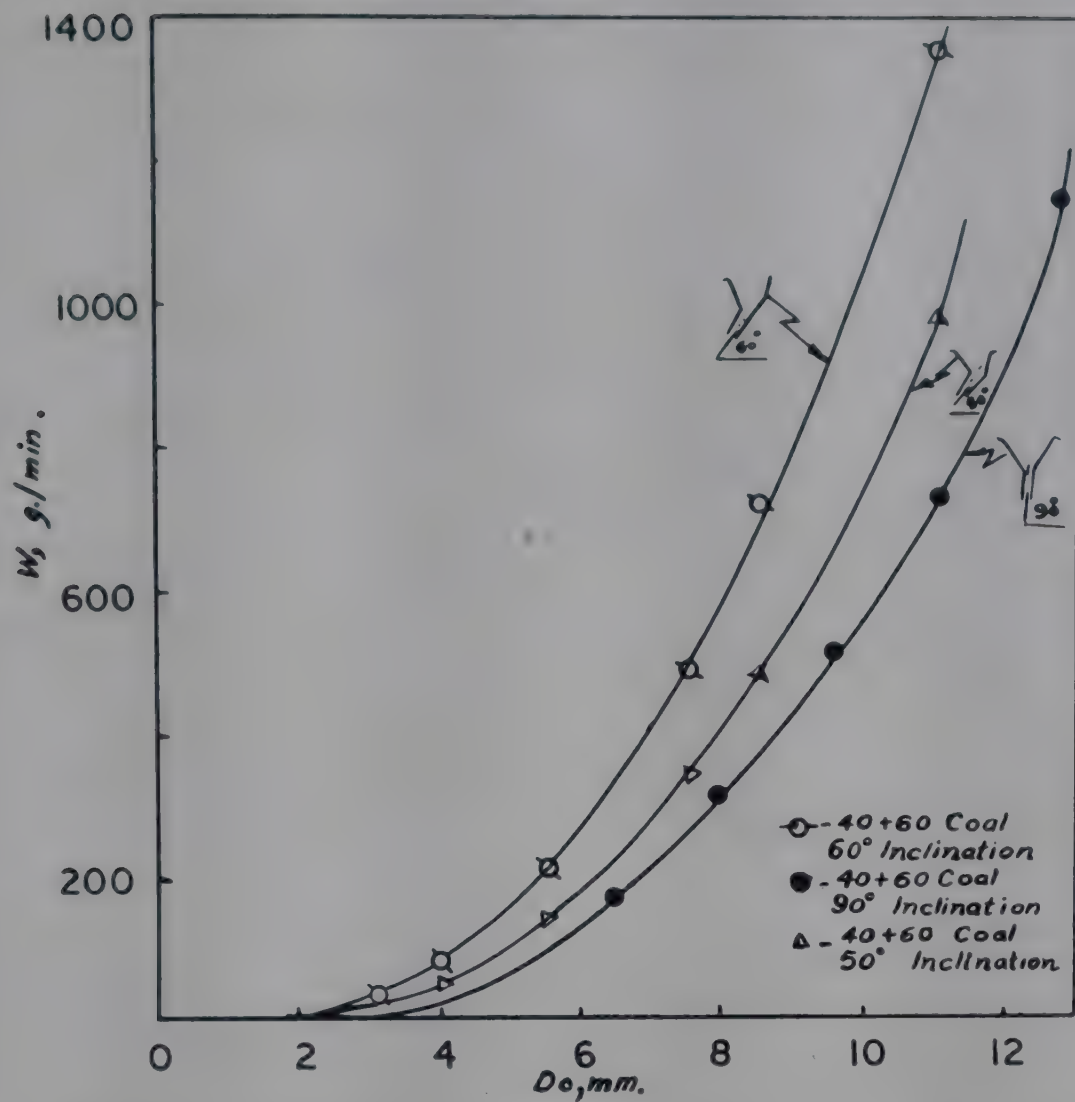
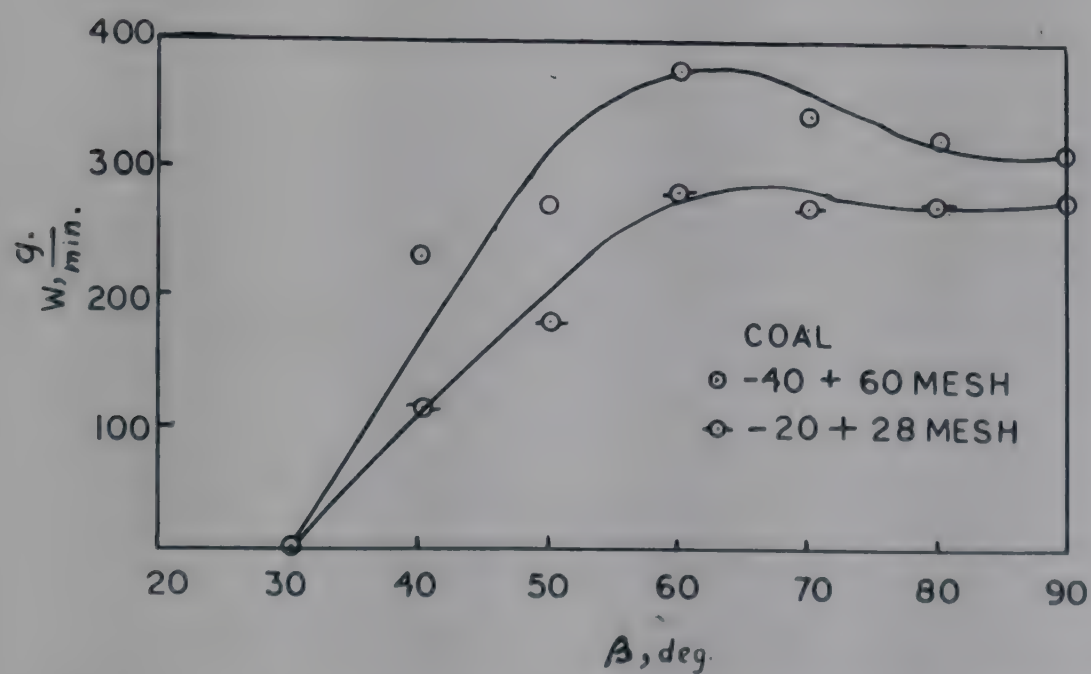
Fig. 8–11 show the effect of inclination of the leg of the funnel on the flow rate of solids. It is observed that the flow rate increases gradually from 90° inclination up to 60° and then decreases rapidly tending to become zero at 30° inclination, which is very nearly equal to the angle of repose for the solids employed.

The relationship between $G/\rho_p \cdot f$, the angle of inclination of the funnel, β , and the ratio, D_o/D_p is shown in Fig. 12. The data for spherical glass and plastic beads, and close-cut fractions of sandstone and coal in vertical and inclined funnels can be represented by the equation

$$G/\rho_p \cdot f = 362 \left[\frac{\sin \beta - \sin \alpha}{1 - \sin \alpha} (D_o/D_p) \right]^{0.545} \quad (9)$$

where f is the tangent of the poured angle of repose, α .

Effect of surface. To study the effect of the surface, funnels of sheet metal, polythene and glass were used. G/ρ_p values for glass beads, plastic beads, sandstone and coal in these funnels are shown in Table 2.

FIG. 7—EFFECT OF TUBE INCLINATION ON GRAVITY FLOW OF SOLIDS [$-40+60$ mesh coal]FIG. 8—EFFECT OF TUBE INCLINATION ON GRAVITY FLOW OF SOLIDS [$-40+60$; $-20+28$ mesh]

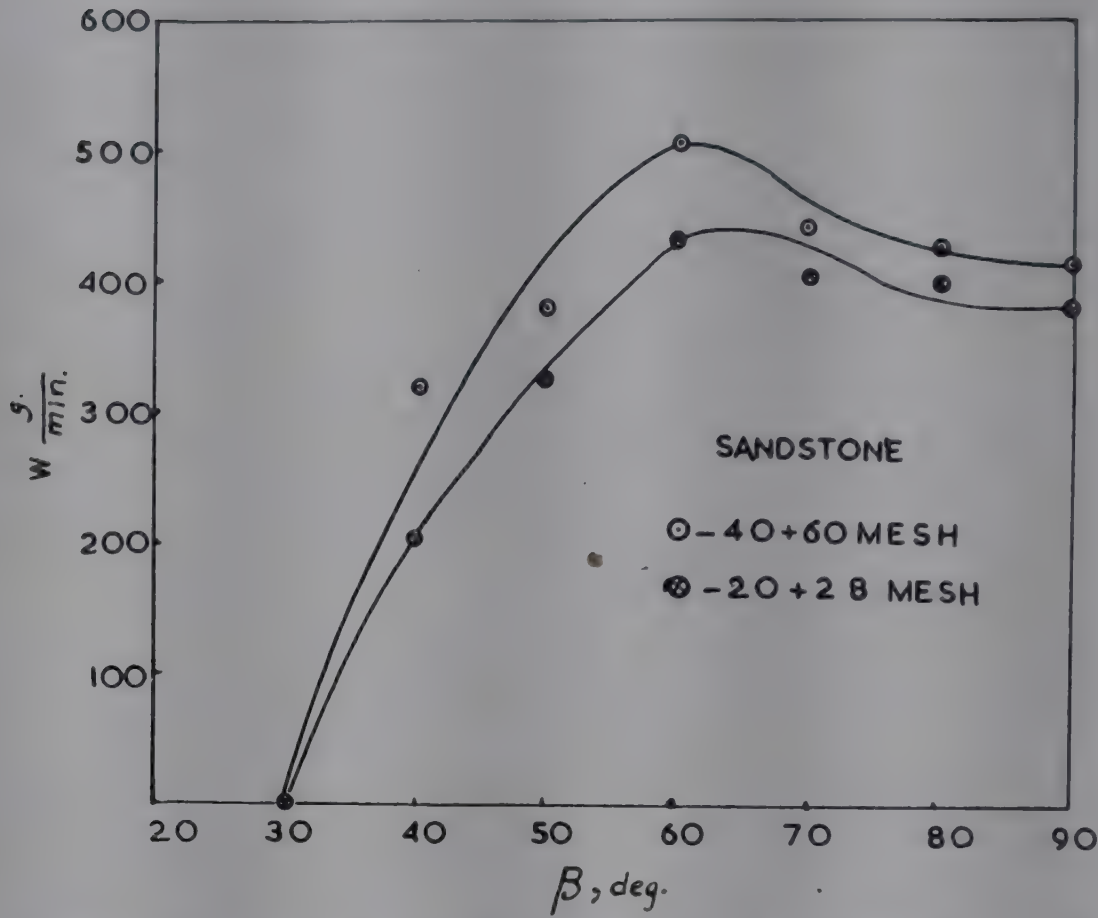


FIG. 9—EFFECT OF TUBE INCLINATION ON GRAVITY FLOW OF SOLIDS [Sandstone: -40+60; -20+28 mesh]

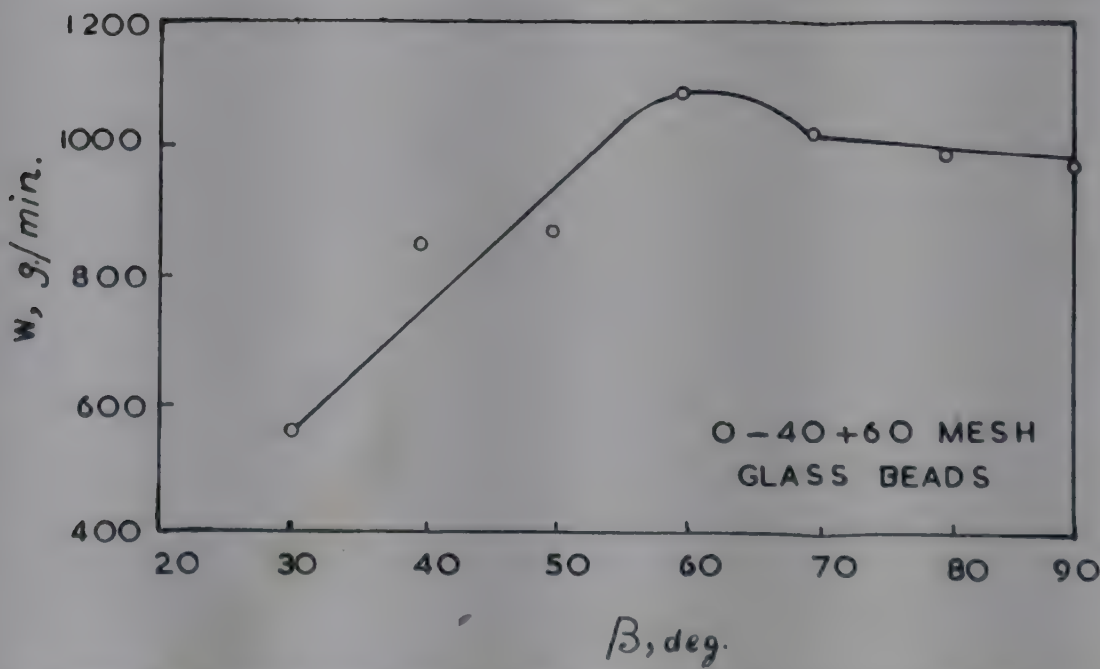


FIG. 10—EFFECT OF TUBE INCLINATION ON GRAVITY FLOW OF SOLIDS [-40+60 mesh glass beads]

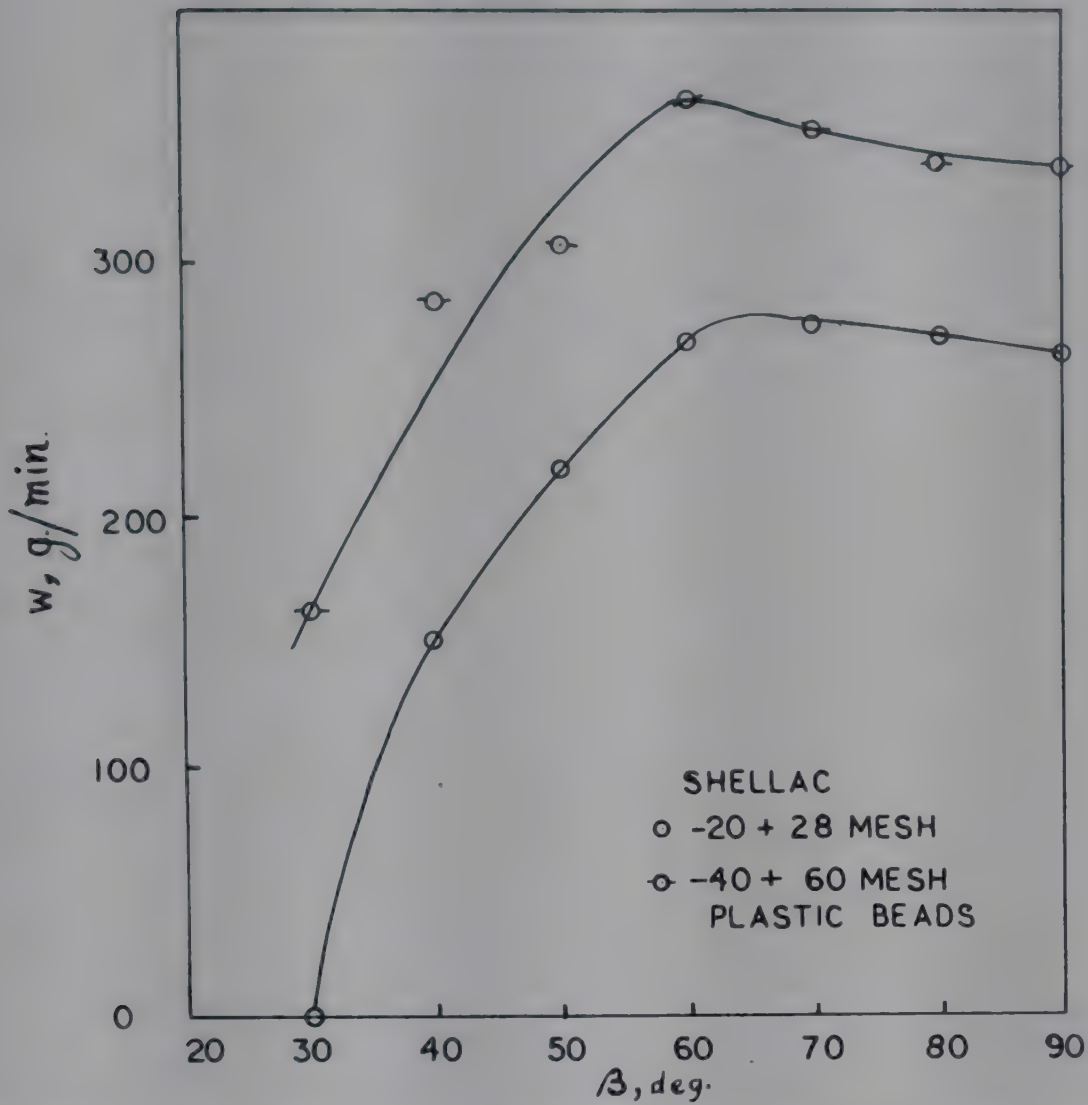


FIG. 11—EFFECT OF TUBE INCLINATION ON GRAVITY FLOW OF SOLIDS [—20+28 mesh shellac; —40+60 mesh plastic beads]

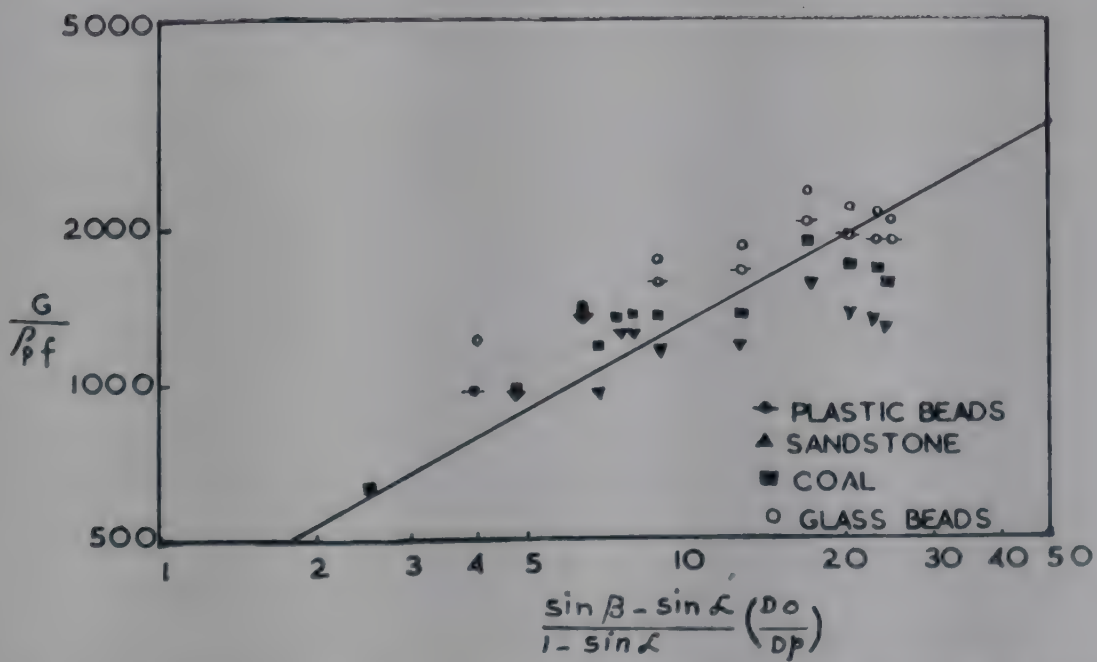


FIG. 12—FINAL CORRELATION FOR FLOW RATE OF SOLIDS THROUGH VERTICAL AND INCLINED FUNNELS

TABLE 2—EFFECT OF SURFACE ON THE MASS FLOW RATE OF SOLIDS IN VERTICAL FUNNELS

(Particle size, —40+60 mesh)

| MATERIAL | G/ρ_p IN | | |
|---------------|---------------|-------------|-------|
| | Polythene | Sheet metal | Glass |
| Coal | 453 | 627 | 857 |
| Sandstone | 394 | 460 | 515 |
| Plastic beads | 835 | 1320 | 1635 |
| Glass beads | 1050 | 1400 | 1475 |

From Table 2 it is seen that while there is no appreciable difference between the value of G/ρ_p for the plastic and the glass beads in a sheet metal funnel, the G/ρ_p value for the plastic beads is lower than that for the glass beads in a polythene funnel, but is more in a glass funnel. This is probably due to the fact that the sheet metal offers a neutral surface for both the plastic and the glass beads giving almost the same flow rates. In the case of glass funnels, the flow rate of the plastic beads is higher than that of the glass beads because of the electrostatic forces developed during the flow of glass beads in a glass funnel, thus retarding the flow rate of glass beads in a glass funnel. Similarly, due to the electrostatic forces between plastic beads and plastic funnels, the flow is retarded.

NOMENCLATURE

| | |
|------------|--|
| A | = surface area |
| C | = constant |
| D_o | = discharge opening |
| D_p | = particle diameter |
| G | = mass flow rate |
| H | = head |
| W | = flow rate of the solids |
| a, b | = constants |
| f | = $\tan \alpha$ |
| $f(\mu_2)$ | = power function of the tangent of the surface kinetic angle of repose |
| g | = acceleration due to gravity |
| t | = time of flow |
| ρ_p | = particle density |
| α | = angle of repose |
| ϕ | = cone angle |
| μ_1 | = static angle of repose |
| β | = angle of inclination of funnel |

REFERENCES

1. GREGORY, S. S., *J. appl. Chem., Lond.*, **2** (1952) (Suppl. to No. 1), 51.

2. SHIRAI, T., *Chem. Engng (Japan)*, **16** (1952), 86.
3. RAUSCH, J. M., Ph.D. Thesis, Princeton University, 1948.
4. NEWTON, R. H., DUNHAM, G. S. & SIMPSON, T. P., *Trans. Amer. Inst. chem. Engrs*, **41** (1945), 215.
5. DEMING, W. E. & MEHRING, A. L., *Industr. Engng Chem.*, **21** (1929), 666.
6. TAKAHASI, K., *Bull. Inst. phys. Chem. Res., Tokyo*, **12** (1933), 984.
7. ROSE, H. E. & TANAKA, T., *Engineer, Lond.*, **208** (1959), 465.
8. HARMENS, A., *Chem. Engng Sci.*, **18** (1963), 297.
9. FRANKLIN, F. C. & JOHANSON, L. N., *Chem. Engng Sci.*, **4** (1955), 119.

Flow Characteristics of Counter-current Gas-Solid Fluidized Beds : Part II—Studies on Elimination of Bubbles and Slugs

M. S. MAHALINGAM & R. SATAPATHY*

Shri Ram Institute for Industrial Research

Delhi 6

The potential value of fluidized beds in petroleum, chemical and nuclear industries is well known. However, the application of gas fluidized beds for drying and heat treatment of textiles and paper is limited because of slug formation. It is shown that slugging is a direct consequence of formation of bubbles, their growth motion and coalescence in fluidized beds. The success of fluidized beds as driers in textile and paper industries depends mainly on elimination of bubbles and attainment of uniformity in fluidization.

The close similarity of motion of liquid drops and gas bubbles in liquids with that of gas bubbles in fluidized beds is discussed and the effect of obstructions such as fins protruding from the inner wall of the bed on the rupture and disintegration of gas bubbles in counter-current fluidized beds is studied. The results of experimental investigations are presented in a sequence of photographic plates.

Commercial fluidized bed operations began with applications in the petroleum industry and have been extended to the chemical, nuclear, metallurgical and other industries¹ during the last two decades. The application of fluidized beds in drying and other heat treatment of textile fabrics

*Present address: Indian Organic Chemicals Ltd, Khopoli, Dist. Kolaba, Maharashtra

and paper^{2,3} is the outcome of research and development work in this field. Although the potential value of this technique in textile and paper industry is realized, many engineering difficulties must be overcome before successful commercial exploitation can be achieved. Several aspects including heat transfer and scaling up of models have been well developed. However, the intriguing problem of elimination of bubbles and slugs in all kinds of beds remains unsolved. The formation of bubbles and slugs in fluidized bed equipments employed in drying and processing of textiles results in uneven tension in the fabric, and the nonuniformity of particle dispersion adversely affects enthalpy distribution. Several modified equipments¹⁻⁶ to eliminate bubbles and slugs and to attain uniformity of fluidization have been introduced; examples of such equipment are the sieve plate columns, packed beds and stirred bed columns. These have limited applications: for example, the sieve plate columns are not applicable to particle systems of varying sizes, the packed bed columns are applicable to solids of free flowing nature, while the stirred bed columns are limited to small size operations. None of these modified equipments is of any use for drying textiles and paper, particularly of long lengths of these materials in a continuous manner.

The formation of bubbles and slugs is inherent in aggregative fluidization⁷ and in particular in gas-solid systems where the ratio of particle to fluid density is generally high. An ideal state of fluidization with reference to uniformity would occur when the bubble size^{2,8} is nearly equal to that of the fluidized particles or when the ratio of densities of the solid to fluid tends to unity⁹. It is rather impractical to have gas-solid systems wherein the ratio of the densities can be minimized in order to achieve uniformity in fluidization. Alternatively, it is possible to achieve uniformity in fluidization by rupturing and disintegrating the bubbles within practical limits by various means. One such method which is employed for achieving uniformity of fluidization, in counter-current solid-gas contacting systems as applied to sheet material drying and heat treatment is presented in this paper.

Theory of bubbles. The main theoretical interest of motion of bubbles in fluidized beds has always been associated with the motion of solid spheres, liquid drops and gas bubbles in liquids. In 1851, Stokes¹⁰ analysed the free motion of a solid spherical body in an incompressible fluid of infinite extent. As distinct from solid spheres and liquid drops moving in inviscid liquids, the velocity of a gas bubble moving inside fluidized beds is a function of its volume. The experimental work of Davidson and coworkers¹¹ on the rate of rise of bubbles in fluid beds has shown close agreement with the semi-empirical relation of Davies and Taylor¹² developed for the motion of gas bubbles in liquids, and several attempts have since been made to study the formation¹³, growth⁵ and coalescence^{14,15} of air bubbles in fluidized beds.

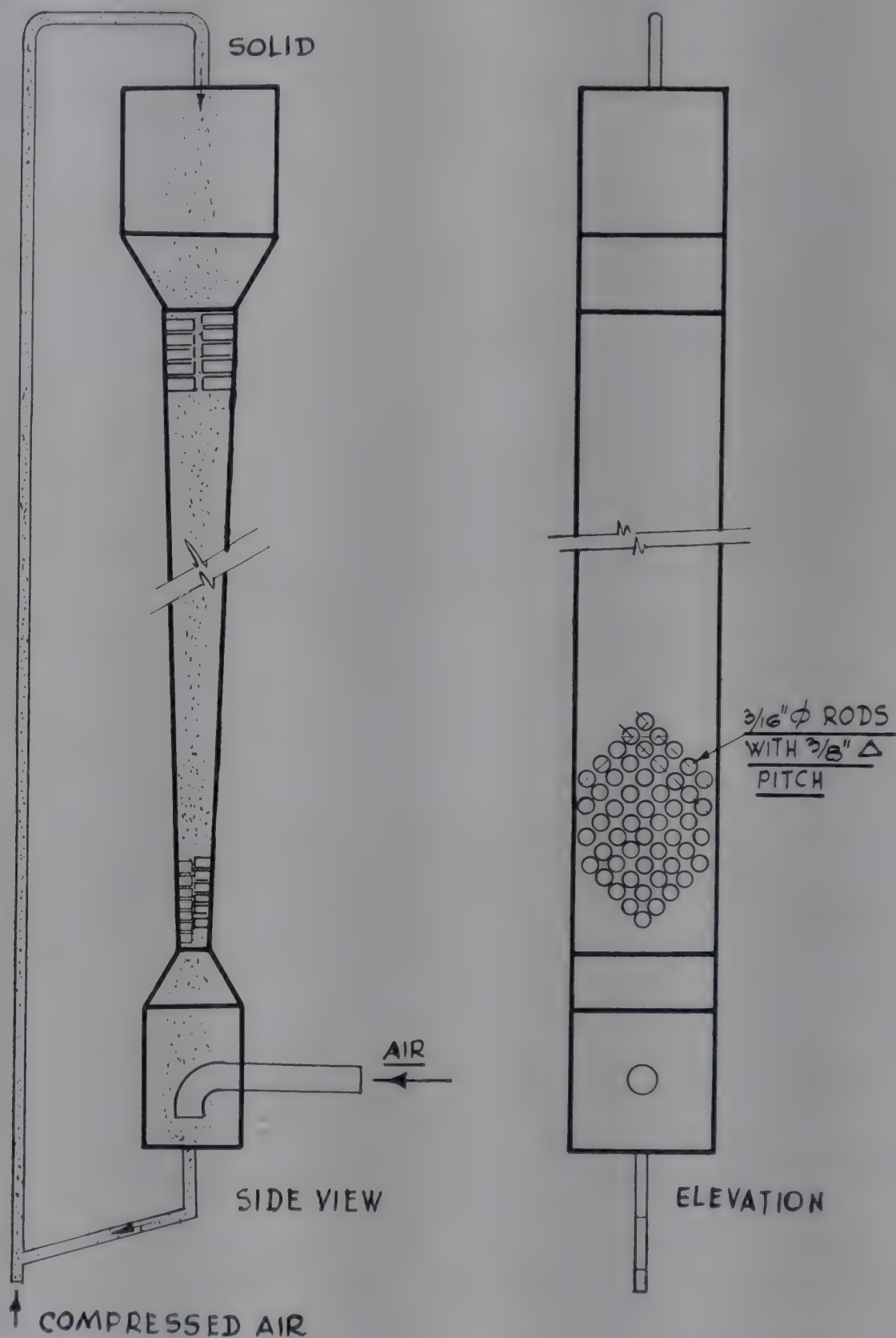
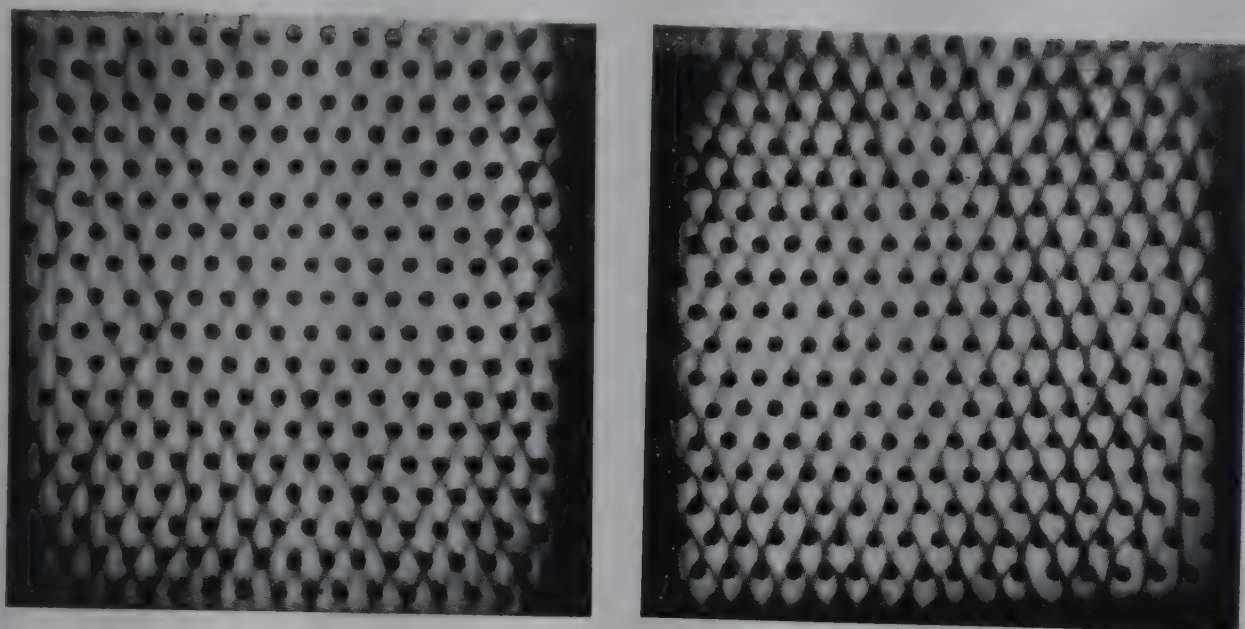


FIG. 1—EXPERIMENTAL SET-UP FOR MEASURING FLOW CHARACTERISTICS OF COUNTER-CURRENT GAS-SOLID FLUIDIZED BED



A

B

FIG. 2—PHOTOGRAPH SHOWING UNIFORMITY OF FLUIDIZATION WITH 30 PER CENT SOLID PARTICLE HOLD-UP IN FIN SURFACE FLUID BED COLUMN : A, BOTTOM SECTION; B, TOP SECTION

EXPERIMENTAL WORK AND RESULTS

The experimental work consisted in visual observation and photographic study of fluidization by having fins on the internal surface of the fluidized bed column (Fig. 1). The fins were of rod-like nature and the columns were of square and rectangular cross-section having different aspect ratios and tapered walls, the tapering being limited to about 3° to the normal. Most of the columns in which studies were carried out consisted of perspex sheet material, while the fins were of steel, fixed in triangular pitch horizontally to the walls, the pitch distance varying between $3/8$ in. and $1/2$ in. Other types of extended surfaces were also employed.

Sand particles and glass beads of 20–40, 40–60 and 60–80 B.S. mesh size were allowed to flow from the top counter-current to the air flow in the columns at various solid and gas mass flow rates within and beyond the choking velocity ranges. The uniformity of fluidization in the rare phase (3–7% hold-up) region was found to be 100 per cent with or without finned surfaces, although this could not be recorded photographically.

However, as the gas flow rate was increased for a fixed mass flow rate of solid particles, the hold-up of the bed increased progressively in the case of column containing rod-like fins only without affecting the uniformity of fluidization. This has been shown in Fig. 2. Measurements showed that the hold-up can be maintained between 3 and 30 per cent without slug formation and choking of the column. The effective pressure drop due to the fins provided on the walls of the column was negligible. It was also possible to pass from the counter-current to the co-current phase by gradual increase of the gas flow rate from $U_{cc} < U_t < U_{coc}$.

CONCLUSION

1. The choking phenomenon¹⁶ is a result of bubble and slug formation.
2. Uniformity of fluidization in counter-current as well as co-current gas-solid systems can be achieved within practical limits by insertion of fins in the manner described earlier without causing excessive pressure drop in the column.
3. Rate of heat transfer from wall to bed in such systems can be increased in accordance with the finned surface in use and the overall heat transfer coefficient would in such cases be far higher than available in conventional types of fluid bed equipment.
4. It is possible to attain very nearly ideal state of fluidization by bringing down the pitch distance of the fins within practical limits of design.
5. Fin surface counter-current fluidized beds of high aspect ratios (as high as 1: 20) can be operated smoothly irrespective of shape and size of the equipment.
6. With particular reference to processing of sheet materials like textiles and paper, these can be passed through the bed at high speeds (up to 200 yd/min.) with little tension exerted on these materials.

NOMENCLATURE

- U_{cc} = counter-current gas velocity, ft/sec.
 U_{coc} = co-current gas velocity, ft/sec.
 U_t = terminal velocity of particle in use, ft/sec.

REFERENCES

1. ZENZ, A. & OTHMER, D. F., *Fluidization and Fluid Particle Systems* (Reinhold Publishing Corp., New York), 1959.
2. DOLEMAN, J. & MORGAN, M. U., *Brit. Pat.* 849,329, Feb. 1956.
3. SATAPATHY, R., *Indian Pat.*, 76,418, April 1961.
4. MATHESON, G. L., *U. S. Pat.*, 2,533,026, Dec. 1950.
5. SENSEL & BECK, *U. S. Pat.* 2, 562, 993, Aug. 1951.
6. WASTON, F., *U. S. Pat.* 2, 463, 729, Nov. 1952.
7. LEVA, M., WEINTRAUB, M., GRUMMER, M., POLLCHICK, M. & STORCH, H. H., *U. S. Bur. Mines Bull.* No. 504 (1951).
8. GROHSE, E. W., *Amer. Inst. chem. Engrs J.*, **1** (1955), 358.
9. LEVA, M., *Fluidization* (McGraw Hill Book Co. Inc., New York), 1959.
10. STOKES, G. G., *Trans. Camb. phil. Soc.*, **9** (1851), 55.
11. DAVIDSON, J. F., PAUL, R. C., SMITH, M. J. S. & DUSBURY, H. A., *Trans. Instn chem. Engrs, Lond.*, **37** (1959), 323.
12. DAVIES, R. N. & TAYLOR, G. G., *Proc. roy. Soc.*, **A-200** (1950), 375.
13. TOOMEY, R. D. & JOHNSTONE, H. F., *Chem. Engng Progr.*, **48** (1952), 220.
14. HARRISON, D. & LEUNG, L. S., *Trans. Instn chem. Engrs, Lond.*, **40** (1962), 146.
15. HARRISON, D. & LEUNG, L. S., *Trans. Instn chem. Engrs, Lond.*, **39** (1961), 409.
16. MAHALINGAM, M. S., SATAPATHY, R. & CHIPALKATTI, V. B., *Indian chem. Engr*, **6**(2) (1964), 31.

Closed-circuit Hydraulic Sand Stowing in Mines

G. B. MISRA

Department of Mining, Indian Institute of Technology
Kharagpur

Hydraulic stowing of river sand and mill tailings finds wide use in coal and metal mines. In hydraulic transportation of solids, particles below $30\ \mu$ diameter form homogeneous mixtures, while those above $50\ \mu$ form heterogeneous mixtures. Several empirical relations have been developed for determining the pressure gradient in hydraulic transport systems. Analysis of data on the hydraulic transportation of mixed size Damodar river sand shows that any of these relations, with slight modifications, can be used.

The closed-circuit hydraulic stowing system can be adopted in both coal and metal mines provided the goaf or stope to be filled can be made watertight against high head. The system will result in the saving of the pumping cost amounting to about 7 per cent of the total stowing cost in the normal open-circuit stowing system, though some extra expenditure has to be incurred on making the seals watertight. In any case, the system would minimize the water nuisance underground.

Hydraulic stowing of river sand is now widely practised in the coal mines of this country. The Nundidrug gold mine, Kolar Gold Fields (K.G.F.), has also successfully introduced hydraulic stope filling with classified mill tailings in the intermediate levels (down to a depth of 1500 m.). With the availability of sufficient river sand near our coalfields and the concerted drive for conserving good quality metallurgical coal, hydraulic stowing will be more widely adopted in our coal mines in the near future. Hydraulic filling of tailings in stopes has also a great possibility at the Mosabani copper mine where the workings have now reached a depth requiring stope filling. Hydraulic filling not only gives a more compact fill than many other methods, but involves easier and cheaper transportation and distribution of the fill material in the goaf or stope. However, it poses the problem of handling and pumping out the drained water underground. With a view to tackling

this problem it was contemplated to investigate the possibility of adopting a closed-circuit stowing system in which the solids transported with water would separate out by gravitational settling underground and the clear water would return to the surface without involving any additional pumping. This would not only reduce the nuisance of handling stowing water underground, but eliminate or minimize the cost of pumping the drained water to the surface.

Transportation of Solid Particles in Water

Before examining the feasibility of a stowing system, it is essential to study the transportation properties of the fill material in water. Extensive work by Durand¹ using sharp-cut particles up to 25 mm. in size and of different densities travelling in water at true volume concentrations of up to 22 per cent in horizontal and vertical pipes of 35–500 mm. diam., has shown that the nature of flow is governed by the particle size. Particles of sand below 30 μ in size form homogeneous mixtures with water, while particles greater than 50 μ in size travel as heterogeneous mixtures. An intermediate mixture is formed by the particles 30–50 μ in size.

Flow of Homogeneous Mixtures

Homogeneous mixtures such as mud behave as Bingham plastics. They solidify when at rest, behave as liquids in the turbulent flow regime and have an intermediate behaviour in the laminar flow regime. In the turbulent flow regime, the hydraulic gradient can be given by the Fanning equation

$$i_m = \frac{f_m V^2}{2 g D} \quad (1)$$

The equation is not the same as for Newtonian fluids. Wilhelm *et al.*², studying the hydraulic transportation of boiler ash, found that at high velocities, the correlation between f_m and Re was the same for a slurry as for a homogeneous liquid when the density used in the calculation of Re was that of the slurry and the viscosity, that of water. However, as the velocity was decreased below a critical value, f_m increased rapidly with decreasing velocity, ultimately reaching a value many times greater than that for the homogeneous liquid.

Expressing i_m in terms of head of water, Eq. (1) becomes

$$i = \frac{i_m \rho_m}{\rho_w} = i_w \{1 + C (S - 1)\} \text{ assuming } f_m = f_w$$

$$\text{or} \quad \frac{i - i_w}{C i_w (S - 1)} = 1 \quad (2)$$

Eq. (2) can be modified as

$$\frac{i - i_w}{C i_w (S - 1)} = K \quad (3)$$

to take into account the inequality of f and f_m . Work on the flow of homogeneous mixtures of very fine sand (0.02 mm. diam.) in water by Newitt *et al.*³ as well as of minute (—174 mesh) particles of solids of various densities in water and kerosene by Bhattacharya and Roy⁴ confirms the validity of Eq. (3) at high velocities greater than 0.8 m./sec. At lower velocities, K no longer remains constant, but increases rapidly with decreasing velocity. As has been shown by Bhattacharya and Roy⁴, the flow of homogeneous mixtures of very fine particles exhibiting plastic behaviour can be more appropriately represented by Eq. (4) which was developed by Vogt and White⁵ from theoretical considerations for pneumatic transportation of solids:

$$\frac{i - i_w}{i_w} = K \left(\frac{D}{d} \right)^2 \left(\frac{\rho_w}{\rho_s} \right) \left(\frac{r}{Re} \right) \quad (4)$$

K in Eq. (4) is a function of the dimensionless group

$$Re \sqrt{C_D} = \frac{\sqrt{\frac{1}{3}} (\rho_s - \rho_w) \rho_w g d^3}{\mu_w}$$

Newitt *et al.*³ have shown that even coarser particles form homogeneous mixtures at high velocities. For example, sand particles of 0.097 mm. diam. formed a homogeneous mixture with water at velocities exceeding 1.5 m./sec. However, such homogeneous mixtures show no plasticity and follow Eq. (2) rather than Eq. (3).

Flow of Heterogeneous Mixtures

Heterogeneous mixtures of particles between 50 μ and 0.2 mm. size are usually transported in suspension while those with particles greater than 2 mm. in size are transported by saltation (successive jumps), the intermediate size forming a transition category. Heterogeneous suspensions however differ from homogeneous suspensions in that there is in the former a fall in the solid concentration from the bottom to the top of horizontal pipes.

The work of Durand, Worster⁶ and others shows that the hydraulic gradient with heterogeneous mixtures, whether transported in suspension or by saltation, has a minimum value at a critical velocity termed by Durand as limit deposit velocity which is given by the equation

$$\frac{V_L}{\sqrt{2 g D (S-1)}} = K \quad (5)$$

where K is a constant depending on the particle diameter and the concentration. For sizes between 0.05 and 1 mm., K varies widely with concentration, though the variation is considerably reduced at relatively high concentrations ($>15\%$). With particles greater than 2 mm. in size, K becomes independent of both particle size and concentration and has a constant value of 1.34. Spells⁷, analysing the data of Howard, Blatch, Yufin, Smith

and Carruthers as well as Settle and Parkins, gave the following relation for V_L over a range of particle size, 0.05–0.5 mm.:

$$V_L^{1.225} = 0.0251 \ gd \left(\frac{D\rho_m}{\mu} \right)^{0.775} (S-1) \quad (6)^*$$

The actual mechanics of hydraulic transportation of solids is not yet fully understood. Durand found that there is a striking resemblance between his classification of particles according to their hydraulic conveyance characteristics and the grouping of particles according to the various laws of gravitational settling. This led him to suggest that the relative velocity of water to the solids in a mixture is approximately equal to the free terminal settling velocity of the solids in water.

Newitt *et al.*³, equating the work done on the particles to keep them afloat with that causing the hydraulic gradient due to the solids alone, developed the following equation for heterogeneous suspensions of sand in water:

$$\frac{i - i_w}{Ci_w} = 1100 (S-1) \frac{W}{V} \cdot \frac{gD}{V^2} \quad (7)$$

Eq. (7) holds good for medium size particles. With gravel of size greater than 2 mm., however, the particles no longer remain in suspension, but settle down to the bottom of the pipe. The movement of the particles is then by saltation or in a sliding bed, but there is no deposited bed of solids. Newitt *et al.*³ contended that with such a type of flow, the hydraulic gradient due to solids is primarily due to solid-solid friction. From energy balance, they developed the following equation for heterogeneous mixtures travelling by saltation or in sliding bed:

$$\frac{i - i_w}{Ci_w} = 66(S-1)gD/V^2 \quad (8)$$

It is to be noted that Eq. (8) has no term depending on particle size and hence holds good for all particles travelling by saltation. This is also well borne out by the work of Durand, and Worster⁶.

Though Eq. (7) and (8) developed by Newitt *et al.*³ have a simple theoretical basis and agree well with their own experimental results, they fail to correlate the data of Durand which are better collated by the empirical relation

$$\frac{i - i_w}{Ci_w} = 121 \left\{ \frac{gD(S-1)}{V^2} \cdot \frac{W}{\sqrt{g d (S-1)}} \right\}^{1.5} \quad (9)$$

Eq. (9) holds good for the flow of all heterogeneous mixtures, whether in suspension or by saltation. The discrepancy between the equations developed

*Values in this equation are in C.G.S. units.

by Newitt *et al.* and by Durand may partly be due to the material of the pipe. While Newitt's work was carried out in a 25 mm. bore brass pipe, Durand used cast iron and steel pipes of various diameters.

Though Eq. (4) was developed by Vogt and White⁵ from theoretical considerations for pneumatic conveying of solids, it failed to correlate their own experimental data which agreed better with the empirical modification:

$$\frac{i - i_a}{i_a} = A \left(\frac{D}{d} \right)^2 \left(\frac{\rho_a}{\rho_s} \cdot \frac{r}{Re} \right)^K \quad (10)$$

where A and K are functions of $\frac{\sqrt{\frac{1}{3}(\rho_s - \rho_a)\rho_a g d^3}}{\mu_a}$

No attempt has, however, been made to use Eq. (10) for correlating data on the hydraulic transportation of solids.

Flow in Vertical Pipes

So far, flow in horizontal pipes has been considered. Flow of fine particles in homogeneous suspension in vertical pipes has been found by Durand to be similar to that in horizontal pipes where the frictional pressure loss is equal to that due to the flow of a liquid having the same density as the mixture. Newitt *et al.*⁸ also show that for fine particles (0.1 mm.), the flow in vertical pipes is almost identical with that in horizontal pipes. However, they give the following equation for correlating their experimental data on the flow of homogeneous suspensions in vertical pipes:

$$\frac{i - i_w}{C i_w} = 0.0037 \left(\frac{gD}{V^2} \right)^{\frac{1}{2}} \left(\frac{D}{d} \right) S^2 \quad (11)$$

Eq. (4) has been shown by Bhattacharya and Roy to hold good for slurries of very fine particles travelling in vertical pipes.

Particles of larger size, which form heterogeneous mixtures, have been found by Durand¹, Worster⁶ and Newitt *et al.*⁸ to cause no extra pressure loss when travelling in vertical pipes, i.e. the pressure loss due to the slurry is the same as that with pure water without taking into account the density of the slurry as in the case of flow in horizontal pipes. This has been suggested by Durand and Worster to be due to there being no slip between the water and the particles, while Newitt explains it as due to the magnus effect that large particles when travelling in suspension in a vertical pipe tend to flock to the centre leaving an annulus of clear water between the pipe wall and the core of suspended particles.

Flow of Particles of Mixed Sizes

So far we have considered the flow characteristics of sharp-cut particles. Though only limited work has been done on the flow of mixed particles, it is logical to think that the presence of very fine particles in a slurry of

mixed particle sizes would help in the conveying of the coarser particles by forming a homogeneous heavy medium suspension.

Newitt *et al.*³ have shown from theoretical considerations that Eq. (7) could be used for a two-component (one coarse and one fine) mixture of particles if W in the equation is replaced by

$$B = (1-X) K_f W_f + X [1-(1-X)C] K_c W_c,$$

where X is the fraction of the coarse component. However, the constants K_f and K_c are not predictable and hence Newitt's modification of Eq. (7) is hardly of any practical value. Most of the data on the flow of particles of mixed sizes can be correlated by the existing equations for sharp-cut particles, if a suitable average particle diameter could be used.

Bhattacharya and Roy⁴ used very fine particles of mixed sizes, the average particle size (effective diameter) being determined either from microscopic study or from data on hindered sedimentation of suspensions of known consistency. Durand (discussion to Worster⁶) has shown that in a mixture of particles of all sizes above 50μ , the mean diameter is that which corresponds to the drag coefficient of the entirety of the grains. Such mixtures follow Eq. (9) if the above mean diameter is taken into consideration. On the other hand, if the mixture contains some particles smaller than 50μ in size, plastic phenomena come into play. In any case, fine particles have always a favourable effect on the head loss for the mixture.

Smith⁹ tried to correlate his experimental data on the hydraulic transportation of sands of mixed sizes by Eq. (9) by adopting an equivalent

diameter $= \frac{\sum X}{\sum (X/d)}$ but the agreement was poor except for coarse sand of

an equivalent diameter of 0.85 mm. Fine sands of an equivalent diameter of 0.19 mm. form homogeneous suspensions obeying Eq. (2) rather than Eq. (9).

The author tried to correlate the experimental data of Khanna¹⁰ on the hydraulic transportation of Damodar river sand in 123 mm. and 152 mm. inner diameter cast iron and steel pipes. The data on flow in vertical pipe ranges were unreliable since rarely did the pipes run to their full capacity. Khanna's results on the flow in horizontal pipe ranges as given in Tables 5 and 6 of his paper have been analysed. While the results in Table 6 are for the same pipe range and hence plot well, those in Table 5 include observations in several pipe ranges of the same diameter. Naturally, they show a wide scatter.

Table 1 shows a typical size analysis of Damodar river sand as given by Khanna¹⁰. The sand has a mean volume-surface diameter (as calculated by the method of statistical averaging given by Dallavalle¹¹) of 0.72 mm. and this diameter has been used in all the calculations of the author. The free settling velocity W for this size of sand is 0.08 m./sec. (cf. graph of Budyck in Ref. 1). The limit deposit velocity as calculated from Eq. (5)

TABLE 1—SIZE ANALYSIS OF DAMODAR RIVER SAND

| SCREEN SIZE (I.M.M. STANDARD SCREEN) MESH | ARITHMETIC MEAN PARTICLE DIAM. mm. | WEIGHT % |
|---|--|-------------|
| +10 | 3.175 | 20* |
| —10+30 | 0.846 | 64 |
| —30+60 | 0.318 | 14 |
| —60+90 | 0.175 | 2 |

*Maximum size of grains is assumed to be 5 mm.

assuming $K=1.45$ for particles of 0.7 mm. size and concentrations greater than 15 per cent, is 2.9 m./sec. for 123 mm. diam. pipes and 3.2 m./sec. for 152 mm. diam. pipes.

An attempt was made to collate the data of Khanna by equations similar to those of Newitt, Durand and Vogt and White. Fig. 1 shows a log-log plot of

$$\frac{i - i_w}{C i_w} \text{ versus } \frac{V^2}{gD(S-1)} \cdot \frac{\sqrt{gd(S-1)}}{W}$$

A straight line with a slope of -1.5 can be drawn through all the points in the non-deposit flow regime thus suggesting a relationship similar to that in Eq. (9). The actual equation as given below is, however, slightly different from that of Durand:

$$\frac{i - i_w}{C i_w} = 60 \left[\frac{gD(S-1)}{V^2} \cdot \frac{W}{\sqrt{gd(S-1)}} \right]^{1.5} \quad (12)$$

A log-log plot of $\frac{i - i_w}{C i_w}$ versus $\left\{ \frac{V^2}{gD(S-1)} \right\} \left(\frac{V}{W} \right)$ (Fig. 2) gives a straight line with a slope of -1 , the equation to the curve being

$$\frac{i - i_w}{C i_w} = 850 \frac{gD}{V^2} \cdot \frac{W(S-1)}{V} \quad (13)$$

Eq. (13) differs from Eq. (7) of Newitt only in the value of the multiplying constant. Fig. 3 shows a log-log plot of $\frac{i - i_w}{C i_w}$ versus $\left(\frac{\rho_s}{\rho_w} \cdot \frac{Re}{r} \right)$.

The curves for the two pipe diameters are parallel straight lines with a slope of -2 thus suggesting an equation similar to Eq. (10) of Vogt and White, but with the value of $K=2$.

It thus appears that all the three equations of Newitt, Durand and Vogt and White, when suitably modified, correlate the data of Khanna on the flow of particles of mixed size. However, a more detailed study

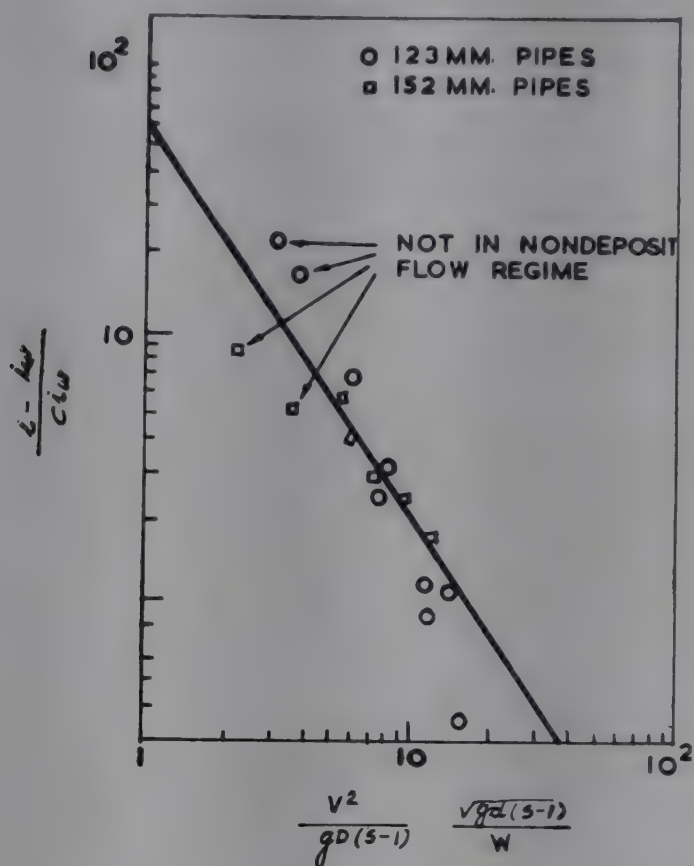


FIG. 1—PLOT OF $(i - i_w) / C i_w$ VERSUS $\frac{V^2}{g D (S-1)}$ $\frac{\sqrt{g d (S-1)}}{W}$

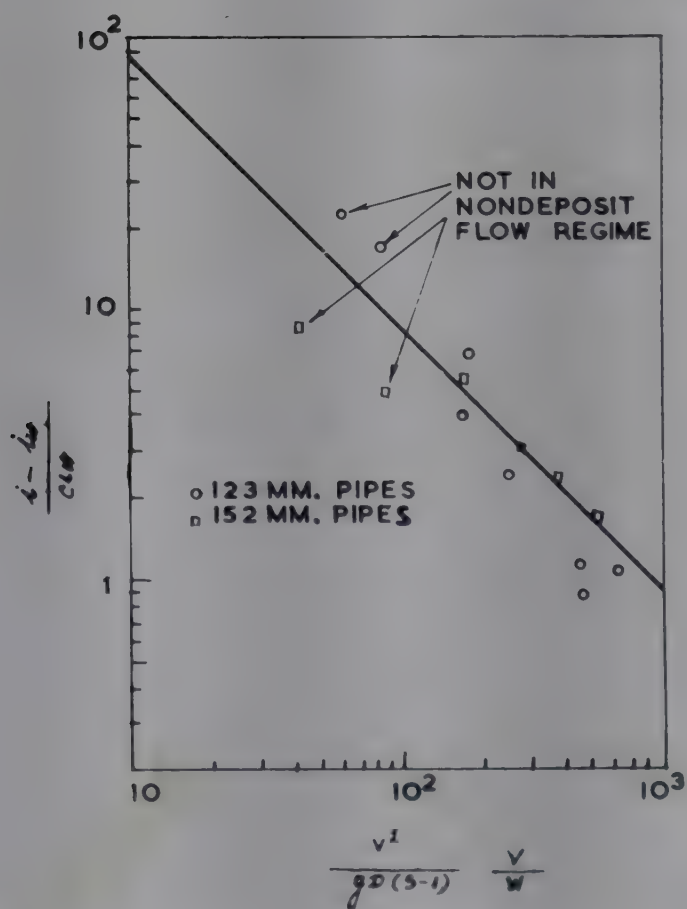


FIG. 2—PLOT OF $(i - i_w) / C i_w$ VERSUS $\frac{V^2}{g D (S-1)}$ $\frac{V}{W}$

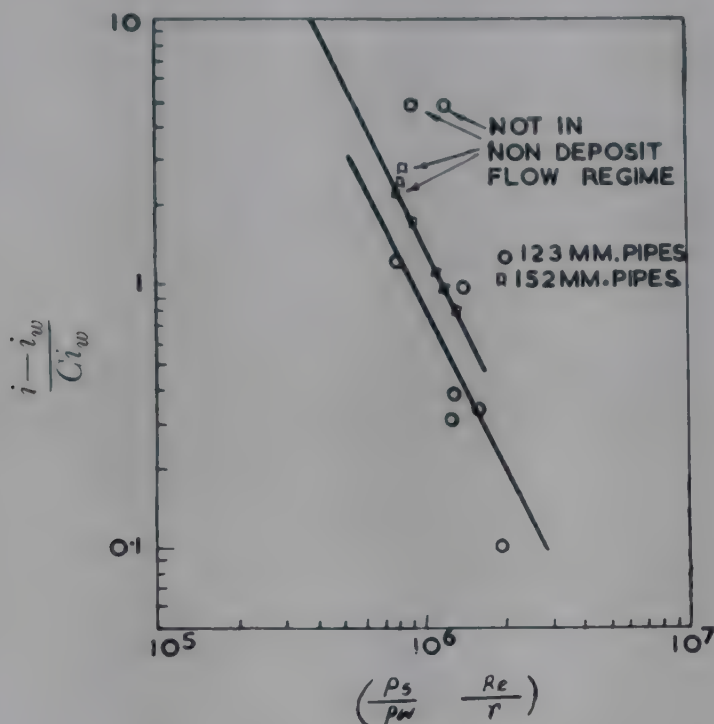


FIG. 3—PLOT OF $(i - i_w) / C i_w$ VERSUS $\left(\frac{\rho_s}{\rho_w} \cdot \frac{Re}{\tau} \right)$

covering a wider field is needed to bring out the subtle difference in the accuracy of the above equations.

So far we have considered the flow of mixed particles travelling in homogeneous or heterogeneous suspension. When all the particles in the mixture are above 2 mm. in diameter, i.e. the flow is by saltation, the particle diameter has no effect on the hydraulic gradient. This is obvious from Eq. (8).

Closed-circuit Stowing Method

In the proposed closed-circuit stowing method, the sand-water mixture will travel down the shaft and along the roadways to the goaf or stope to be filled. The space to be stowed should be sealed watertight and have an inlet for the stowing mixture at one end and an outlet for clear water at the opposite end. A return pipe range should carry the clear water from the outlet to the surface. The sand from the slurry will then separate out by gravitational settling in the goaf or stope owing to the reduction in the transportation velocity there and the clear water will return to the surface.

The method is not likely to fill the goaf completely since, as the goaf gets progressively filled up with sand, the transportation velocity in the goaf will go on rising, until there is no more settling in the goaf. This, in the usual dip-rise layout of long-wall faces, will leave a small gap near the roof which would be impossible to pack up subsequently. Besides, dip-rise long-wall faces in inclined seams may get packed on the dip side, thus choking the passage of the slurry through the goaf. That is why long-wall

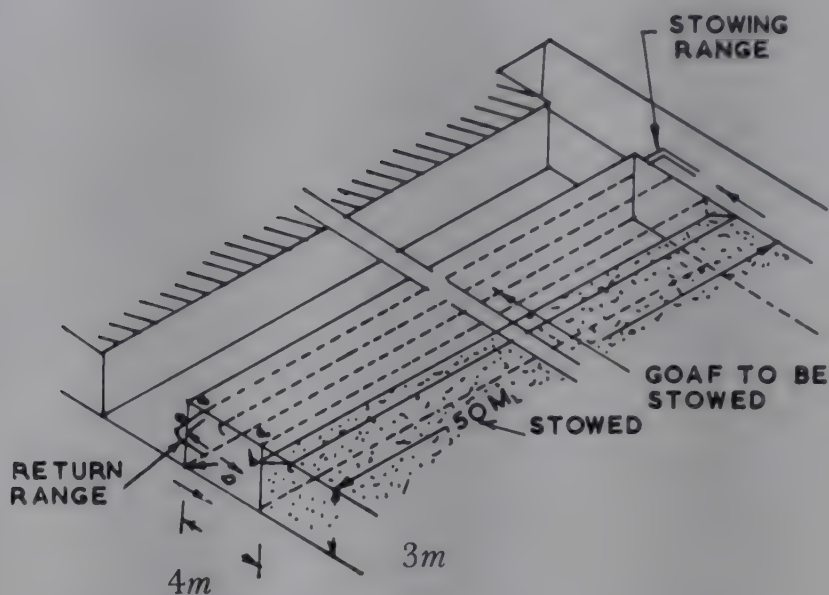


FIG. 4—LAY-OUT OF CLOSED-CIRCUIT STOWING METHOD

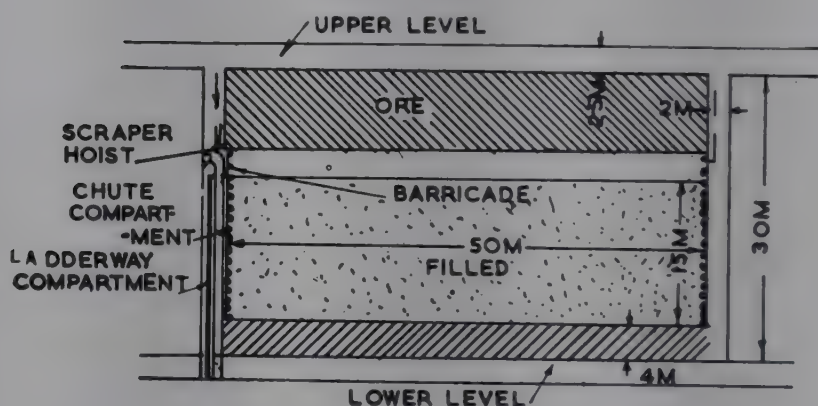


FIG. 5—CLOSED-CIRCUIT STOWING IN STOPES IN STEEP LODES

faces have to be laid out along the strike with the face advancing to the rise for the successful application of this method. With this layout (Fig. 4) almost the whole of the goaf except a small wedge, a b c, at the roof on the face side will get filled by gravitational settling. This wedge will, however, get filled in the subsequent stowing of the adjacent goaf.

The method can be successfully adopted in stopes in steep lodes as illustrated in Fig. 5. The filling can be so adjusted as to leave a small gap below the ore face in order to provide an additional free face for blasting. Ore has to be broken by breasting starting from the rise. Ore should be broken on planks laid on the fill and scraped into a chute compartment in the rise.

There are however two apparent difficulties with this method: (i) the barricade or boxing has to be absolutely watertight, and (ii) it should be able to withstand the high head of slurry which may be of the order of 80–90 atm. at a 600 m. deep working face. The former could be overcome by using waterproof lining of plastic, jutex or tar paper inside the boxing.

It may be difficult to obtain a watertight seal against the rough roof and floor in a mine, but once an initial seal is established, for example by mud plastering at the junction of the lining and the rock, the water pressure would hold the seal tight.

It would be impossible for the common boxing material such as bamboo or coir matting backed by timber support to withstand the high pressure. This could be overcome by backing the boxing with hydraulically operated steel sheets of required strength. These sheets could be removed after filling and used repeatedly. In stopes, only the end barricades have to be designed to withstand a heavy pressure, the walls providing the necessary support on the other sides.

Economics of Closed-circuit Stowing of River Sand

The success of the method of closed-circuit stowing will depend on two conditions: (i) the head developed by the slurry in the down-going pipe range is the maximum, and (ii) the pressure loss in the pipe range is the minimum. While the maximum possible concentration has to be transported to achieve the former, the latter can be achieved by transporting the slurry at the limit deposit velocity.

Assuming a transportation velocity of 3 m./sec. in a 123 mm. diam. pipe (this size of pipe is more than sufficient for carrying the amount of sand commonly needed in Indian mines; the velocity is slightly more than the limit deposit velocity of 2.9 m./sec., but has been adopted to absolutely ensure nondeposit regime of flow),

$$i_w = 0.067 \text{ m./m.}, \text{ taking } f_w = 0.018.$$

For horizontal pipes,

$$i = 0.281 \text{ m./m.}, \text{ using Eq. (9)}$$

$$\text{and } i = 0.174 \text{ m./m.}, \text{ using Eq. (12)}$$

However, the former value of i has been used in the following calculations in order to get a more conservative estimate. For vertical pipes,

$$i = i_w = 0.067 \text{ m./m.}$$

Assuming $C=0.4$, a figure commonly used in this country, head developed by the slurry $= [1 + C(S-1)] h = 1.65 h$. Equating this head with that consumed in the whole pipe range in the closed-circuit method, we have

$$\frac{l}{h} = 1.5$$

When l/h exceeds 1.5, some additional pumping has to be done to lift the water to the surface.

On the other hand, with the usual open-circuit stowing practice, the maximum possible $l/h=5.63$. If we now assume the maximum l/h in a deep mine to be 5, we have the head to be developed by the pump, $h'=1.224 h$. Head required for pumping the water from the settling sump in the normal stowing method, $h''=1.47 h$. Saving in head at the maximum

stowing distance (i.e. $l/h=5$) $=h''-h'=0.246 h$. At a stage of working where $l/h=1.5$, the head saved $=1.106 h$; and in the beginning where $l/h=0$, the head saved $=1.067 h$. Therefore, the average head saved throughout the life of the mine $=0.8 h$, assuming the mine to have a life of 30 years and the progress of working to be uniform throughout the life of the mine.

Assuming an annual production of 0.5 million tonnes of coal and the sand required to be 1 tonne per tonne of coal raised, the stowing water requirement is 280,000 m.³/annum, the water flow rate being 0.0214 m.³/sec.

$$\text{The water horsepower saved} = \frac{0.8h \times 0.0214 \times 1000}{75} \text{ PS.}$$

$$\text{Saving in electrical power} = \frac{0.8h \times 0.0214 \times 1000 \times 0.736}{0.5 \times 75} \text{ kW.}$$

assuming the combined pump and motor efficiency to be 50 per cent. Total annual saving in electrical energy is

$$\frac{0.8h \times 0.0214 \times 1000 \times 0.736 \times 280,000}{0.0214 \times 3600 \times 0.5 \times 75} = 1220h \text{ kW.hr.}$$

Total annual saving in power cost $= 1220h \times 0.09 = \text{Rs } 110h$, assuming power cost to be 9P/kW.hr.

$$\begin{aligned} \text{Cost saved per tonne stowed} &= \frac{110h}{500,000} = 0.022h \text{ P} \\ &= 11 \text{ P for a 500 m. deep mine} \\ &= 7 \text{ per cent of the stowing cost} \end{aligned}$$

assuming the normal stowing cost to be Rs 1.50 per tonne of coal raised.

This figure seems to be too small and may well be offset by the extra cost involved in making the boxing watertight and pressure-proof. It must be noted here that a 4 m. \times 3 m. \times 60 m. goaf requires a boxing area of 204 m². and the saving in pumping cost works out to hardly 50 P per m.² of boxing area which may be easily consumed up in making the boxing watertight and pressure-proof.

However, in calculating the above, a highly conservative estimate has been made of the pressure loss in the pipes. In practice, this pressure loss may be much less as suggested by Eq. (12). This would eventually increase the saving in the pumping cost. Besides, the value of C could be increased to 0.5 when the head developed by the slurry would be more. This would, of course, increase the pressure loss in the horizontal pipes, but to a lesser extent than the increase in the head developed. Addition of a small amount of fine clay to sand-water mixture may result in considerable reduction in the frictional pressure loss by rendering the flow to be in homogeneous suspension. Even coarse sand has been reported by Durand to form homogeneous mixtures at high concentrations.

TABLE 2—SIZE ANALYSIS OF K.G.F. CLASSIFIED MILL RESIDUE

| SIZE | $\frac{\%}{\text{BY WT}}$ |
|--------|---------------------------|
| +66 | 52.2 |
| —66+53 | 13.2 |
| —53+20 | 30.4 |
| —20 | 4.3 |

Economics of Closed-circuit Filling of Tailing Sand

The K.G.F. classified tailing sand has a size analysis as given in Table 2.

The weighted average diameter of this sand $\left[= \frac{\sum X}{\sum (\frac{X}{d})} \right]$ is 47μ . Obviously,

the sand is likely to travel in homogeneous suspension obeying Eq. (2). For flow in a 100 mm. diam. pipe, the limit deposit velocity = 1.8 m./sec., taking K in Eq. (5) to be equal to 1 for 47μ particles.

Proceeding as before,

$$i_w = 0.033 \text{ m./sec. assuming a stowing concentration of 0.5.}$$

For both vertical and horizontal pipes,

$$i = i_w [1 + C(S-1)] = 0.06 \text{ m./m.}$$

Equating head developed with that consumed in the pipe ranges, we have $l/h=8.6$ for closed-circuit filling. Pumping head saved = $1.297h$, assuming a limiting l/h ratio of 8. The average pumping head saved = $1.165h$. The rate of pumping water with the normal method of stowing = $0.071 \text{ m.}^3/\text{sec.}$

Therefore, the saving in pumping cost = $0.0217h \text{ kW. hr/tonne of sand filled}$, assuming 50 per cent efficiency for pump and motor and the cost of power at 9P/kW. hr. This amounts to 21.7 P or about 7 per cent of the total stowing cost of Rs 3.00 per tonne of sand stowed in case of a 1000 m. deep mine.

CONCLUSION

The closed-circuit method of hydraulic stowing can be successfully applied in both coal and metal mines, if the goaf or stope to be filled can be sealed watertight and the seal made strong enough to withstand high pressure. Though there is a definite saving in the pumping cost of the order of 7 per cent of the total cost of stowing, this may well be consumed up in making the boxing or barricade watertight and pressure-proof, particularly in coal mines. However, the above figure is based on conservative estimates of pressure loss in the pipes and transportation concentrations.

With proper care, the saving can be increased. In any case, the closed-circuit method of stowing will minimize the water nuisance underground.

ACKNOWLEDGEMENT

The author is thankful to Prof. M. N. Rao, Head of the Department of Chemical Engineering, Indian Institute of Technology, Kharagpur for the suggestion of the problem and encouragement.

NOMENCLATURE

| | |
|--------|--|
| C | = true volume concentration of solids |
| C_D | = drag coefficient |
| D | = diameter of pipe |
| d | = particle diameter |
| f | = coefficient of friction |
| g | = acceleration due to gravity |
| h | = height of vertical pipe range |
| i | = hydraulic gradient in head of water |
| i_m | = hydraulic gradient in head of mixture |
| K | = constant |
| l | = length of horizontal pipe range |
| r | = weight ratio of solid to liquid |
| Re | = Reynolds number |
| S | = density ratio of solid to water |
| V | = velocity of flow of mixture |
| V_L | = limit deposit velocity |
| W | = free settling velocity of particles in water |
| X | = weight fraction |
| ρ | = density |
| μ | = viscosity |

Subscripts

| | |
|-----|--------------------|
| a | = air |
| c | = coarse particles |
| f | = fine particles |
| m | = mixture |
| s | = solid |
| w | = water |

REFERENCES

1. DURAND, R., *Proc. Minn. Hydraul. Convention*, (1953), 89.
2. WILHELM *et al.*, *Industr. Engng Chem.*, **31** (1939), 622.
3. NEWITT *et al.*, *Trans. Instn chem. Engrs, Lond.*, **33** (1955), 93.
4. BHATTACHARYA, A. & ROY, A. N., *Industr. Engng Chem.*, **47** (1955), 268.
5. VOGT, E. G. & WHITE, R. R., *Industr. Engng Chem.*, **40** (1948), 1731.
6. WORSTER, R. C. & DENNY, D. F., *Proc. Inst. mech. Engrs*, **169** (1955), 563.
7. SPELLS, K. E., *Trans. Instn chem. Engrs, Lond.*, **33** (1955), 79.
8. NEWITT *et al.*, *Trans. Instn chem. Engrs, Lond.*, **39** (1961), 93.
9. SMITH, R. A., *Trans. Instn chem. Engrs, Lond.*, **33** (1955), 85.
10. KHANNA, R. R., *Trans. Min. geol. Inst. India*, **50** (1954), 127.
11. DALLAVALLE, J. M., *Micromeritics*, (1948), 116.

Correlation of Gaseous Fluidized Bed Expansion Data

(MISS) C. R. SRIMATHI & G. N. BHAT

Department of Chemical Engineering, Indian Institute of Science
Bangalore 12

Gaseous fluidization of solid materials is accompanied by the expansion of the bed, which is a function of air velocity, particle size and tube diameter. The influence of these parameters on bed expansion has been presented in the form of an empirical correlation on the basis of the data collected with four solids (charcoal, fullers' earth, sand and hematite) in 3.3 cm. and 4.6 cm. glass columns. On the basis of this correlation a method has been suggested for estimating the free-fall terminal velocities of solid particles of irregular shapes. The shape factors of such solids have also been evaluated.

In the early days of development of the fluidized solids technique, the physical flow phenomena noticed in fluidized beds were divided into two distinct categories, viz. particulate fluidization associated with liquids as fluidizing media, and aggregative fluidization associated with gaseous fluidized systems. Different characteristics were ascribed to these two categories of fluidized systems. For instance, while correlating data governing fluid-bed expansion and fluidizing velocities, it was observed that the following relationships¹⁻⁴ hold good in the case of liquid-solids systems.

$$V \propto \epsilon^a \quad (1)$$

$$V \propto \frac{\epsilon^5}{\{1 + 0.5 (1 - \epsilon)\}} \quad (2)$$

$$V \propto \frac{\epsilon^3}{1 - \epsilon} \quad (3)$$

$$V \propto \epsilon^2 \exp \left[\frac{-2.5 (1 - \epsilon)}{1 - \{39/64 (1 - \epsilon)\}} \right] \quad (4)$$

With regard to gas-solids systems, the following relationships^{5,3,2}, in which m is a function of particle size, have been proposed:

$$V \propto \epsilon^p \quad (5)$$

$$\frac{V}{(1-\epsilon)} \propto \left\{ \frac{\epsilon^3}{(1-\epsilon)^2} \right\}^m \quad (6)$$

$$V \propto \left[\frac{\epsilon^{15}}{(1-\epsilon)^{10} \{1+0.5(1-\epsilon)\}} \right]^{\frac{1}{3}} \quad (7)$$

However, Bhat, Rao and Weingaertner⁶, Jackson⁷, Harrison *et al.*⁸ and Zenz⁹ have pointed out that the particulate and aggregative fluidized-bed conditions cannot be respectively restricted to liquid-solid and gas-solid systems, and all fluidized systems may be considered basically alike. This would, however, be the case with regard to gas-solid systems at bed voidages lower than about 0.8, when the top of the beds would show a sharp boundary. Further, it has been shown¹⁰ that the voidage function of Eq. (3) can be represented as an equivalent voidage function of the exponential form.

In view of these considerations, an attempt has been made in this paper to elucidate how far the fluid-bed expansion data can be satisfactorily represented as an exponential function of bed voidage in relation to the corresponding superficial fluid velocities, and to obtain empirical correlations for such relationships.

DATA

Experimental results^{11,12} obtained on fluid-bed expansion at different superficial air velocities, with hematite, sand, charcoal and fullers' earth, of size fractions $-28+35$, $-35+48$, $-48+65$, and $-65+100$ Tyler mesh, in glass columns of inner diameter 3.3 cm. and 4.6 cm. were presented as log-log plots. A set of representative plots is shown in Fig. 1.

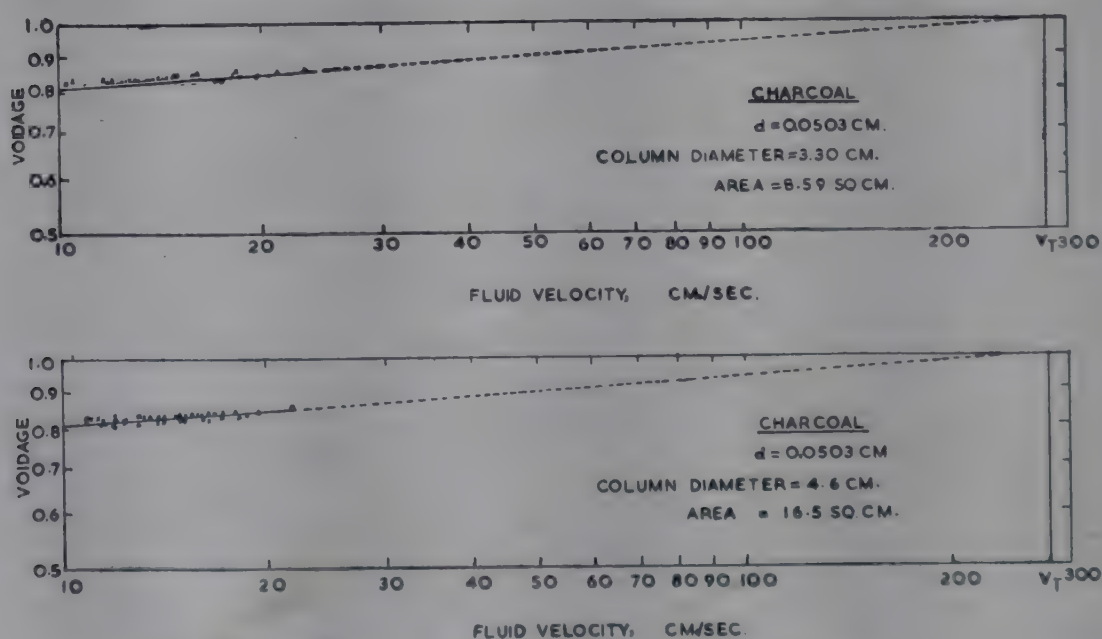


FIG. 1—PLOTS OF BED VOIDAGE VERSUS FLUID VELOCITY

The bed expansion data reported by Krunija Guconic¹¹ and Vasudev (unpublished results) were such that under the operating conditions of particle size, bed height and material density, in the columns used, the top surfaces of beds were clearly discernible, and channeling and slugging tendencies were not exhibited as indicated by $\log \Delta \rho$ versus $\log V$ plots.

CORRELATION AND DISCUSSION

From the log-log plots similar to the ones shown in Fig. 1, it is considered satisfactory to represent bed voidage versus superficial fluid velocity relationships as log-log plots, up to 2–5 times the minimum fluidization velocity, depending on the system and operating conditions in the case of the air-solids systems presently investigated:

$$\epsilon \propto V^n \quad (8)$$

The values of n obtained in the case of different systems considered are given in Table 1. It was found possible to correlate n with ratio D/d , as shown in Fig. 2, by the equation

$$n = K (D/d)^a \quad (9)$$

where a and K were found to be functions of ρ_s , as shown in Fig. 3 and 4, and given by the following expressions:

$$a = 0.026 \rho_s^2 - 0.271 \rho_s + 0.188 \quad (10)$$

$$K = -0.04667 \rho_s^2 + 0.9234 \rho_s - 1.1601 \quad (11)$$

These correlations, together with the empirical correlation for minimum fluidization velocity and data on bed-voidage at incipient fluidization conditions for these systems as reported by Bhat¹², are helpful in estimating the terminal free-fall velocity in air, for the solids referred to, by extrapolating the log-log plots of ϵ versus V to $\epsilon = 1$. Such an extrapolation is satisfactory when particulate type of fluidization continuously occurs at all velocities up to the voidage condition, $\epsilon = 1$. However, in practice, with respect to gas-solids systems such a tendency is not exhibited and slugging sets in at a certain intermediate velocity. As such, only the experimental data on bed expansion obtained with the present systems under conditions of particulate type of fluidization have been extrapolated to the voidage condition, $\epsilon = 1$. Such terminal free-fall velocities for the solids considered are given in Table 1, and are found to be independent of column diameter, with regard to a particular size fraction of a solids material. This observation seems to be a satisfactory feature of the applicability of the proposed method of representing fluid-bed expansion data of laboratory-scale gaseous fluidized systems. The free-fall velocity data, as obtained by the graphical procedure presented, agreed with the calculated results using Eq. (9), (10) and (11) and the results of Bhat¹², within an average deviation of ± 10 per cent.

On the basis of the free-fall terminal velocities obtained graphically for the different solids studied, the corresponding diameters, d_s , of equivalent

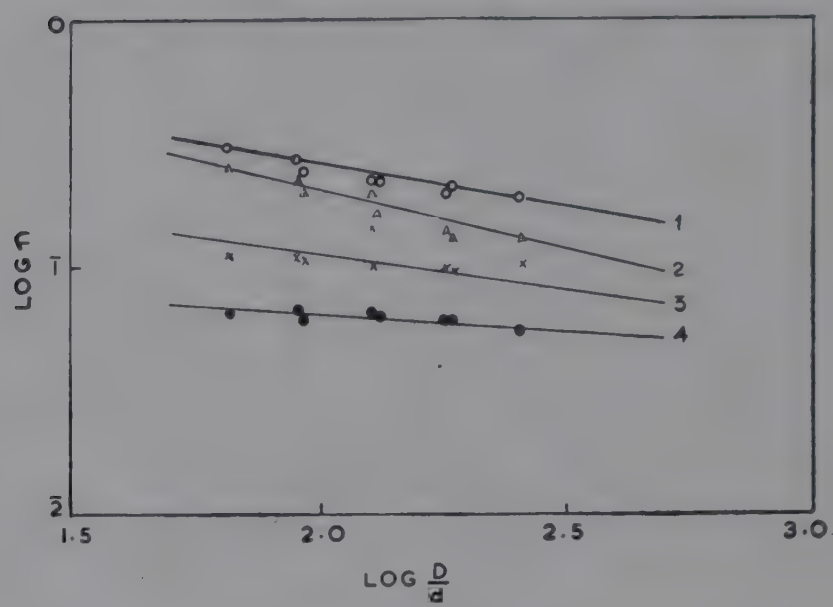


FIG. 2—PLOTS OF $\log n$ VERSUS $\log D/d$ [(1) Sand; (2) Hematite; (3) Fullers' Earth; (4) Charcoal]

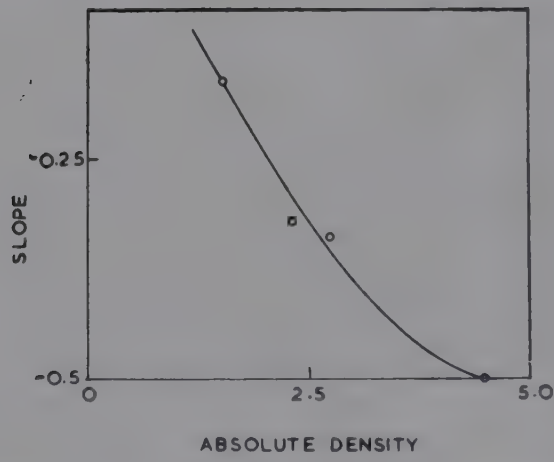


FIG. 3—PLOT OF SLOPE VERSUS ABSOLUTE DENSITY OF MATERIAL

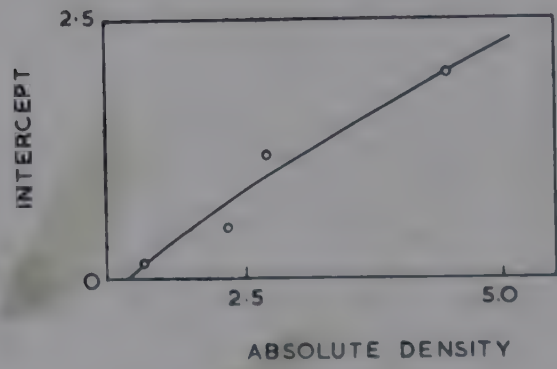


FIG. 4—PLOT OF INTERCEPT VERSUS ABSOLUTE DENSITY OF MATERIAL

TABLE 1—BED EXPANSION DATA FOR CHARCOAL, FULLERS' EARTH, SAND AND HEMATITE

| COLUMN DIAM. (<i>D</i>) <i>cm.</i> | AV. PARTICLE SIZE (<i>d</i>) <i>cm.</i> | $\frac{D}{d}$ | SLOPE (<i>n</i>) cf. Eq. (8) | V_T <i>cm./sec.</i> | <i>d_s</i> <i>cm.</i> | $\phi = \frac{d}{d_s}$ | V_{mf} <i>cm./sec.</i> | V_p <i>cm./sec.</i> | V_g/V_{mf} |
|---|---|---------------|-----------------------------------|--------------------------|------------------------------------|------------------------|-----------------------------|--------------------------|--------------|
| CHARCOAL: Absolute density = 1.48 g./cm. ³ ; <i>K</i> of Eq. (9) = 0.15; <i>a</i> of Eq. (9) = -0.16 | | | | | | | | | |
| 4.60 | 0.0503 | 91.45 | 0.067 | 280 | 0.0787 | 0.64 | 10.0 | 20.0 | 2.00 |
| | 0.0356 | 129.2 | 0.064 | 190 | 0.0577 | 0.62 | 5.3 | 14.0 | 2.64 |
| | 0.0252 | 182.6 | 0.060 | 135 | 0.0371 | 0.68 | 3.5 | 12.0 | 3.42 |
| | 0.0178 | 258.4 | 0.055 | 110 | 0.0277 | 0.64 | 2.1 | 6.4 | 3.05 |
| 3.30 | 0.0503 | 65.8 | 0.065 | 280 | 0.0787 | 0.64 | 11.0 | 23.0 | 2.09 |
| | 0.0356 | 93.0 | 0.062 | 190 | 0.0577 | 0.62 | 5.4 | 15.0 | 2.78 |
| | 0.0252 | 131.3 | 0.063 | 135 | 0.0371 | 0.68 | 4.0 | 13.5 | 3.38 |
| | 0.0178 | 186.0 | 0.060 | 110 | 0.0277 | 0.64 | 2.1 | 6.8 | 3.24 |
| FULLERS' EARTH: Absolute density = 2.33 g./cm. ³ ; <i>K</i> of Eq. (9) = 0.50; <i>a</i> of Eq. (9) = -0.32 | | | | | | | | | |
| 4.60 | 0.0503 | 91.45 | 0.111 | 290 | 0.0690 | 0.73 | 6.0 | 25.0 | 4.17 |
| | 0.0356 | 129.2 | 0.140 | 240 | 0.0520 | 0.69 | 6.0 | 17.0 | 2.83 |
| | 0.0252 | 182.6 | 0.097 | 200 | 0.0388 | 0.65 | 3.3 | 12.0 | 3.64 |
| | 0.0178 | 258.4 | 0.098 | 130 | 0.0280 | 0.64 | 3.2 | 10.5 | 3.28 |
| 3.30 | 0.0503 | 65.8 | 0.111 | 290 | 0.0690 | 0.73 | 7.6 | 26.0 | 3.42 |
| | 0.0356 | 93.0 | 0.105 | 240 | 0.0520 | 0.69 | 5.5 | 16.0 | 2.91 |
| | 0.0252 | 131.3 | 0.102 | 200 | 0.0388 | 0.65 | 4.3 | 16.0 | 3.72 |
| | 0.0178 | 186.0 | 0.095 | 130 | 0.0280 | 0.64 | 1.8 | 9.3 | 5.16 |

TABLE 1 —BED EXPANSION DATA FOR CHARCOAL, FULLERS' EARTH, SAND AND HEMATITE (Contd.)

| COLUMN DIAM. (D) cm. | AV. PARTICLE SIZE (d) cm. | $\frac{D}{d}$ | SLOPE (n) cf. Eq. (8) | V_p cm./sec. | d_s cm. | $\phi = \frac{d}{d_s}$ | V_{mf} cm./sec. | V_p cm./sec. | V_p/V_{mf} |
|--|-------------------------------------|---------------|------------------------------|-------------------|--------------|------------------------|----------------------|-------------------|--------------|
| SAND: Absolute density = 2.66 g./cm. ³ ; K of Eq. (9) = 1.2; a of Eq. (9) = -0.34 | | | | | | | | | |
| 4.60 | 0.0503 | 91.45 | 0.277 | 260 | 0.0535 | 0.94 | 13.0 | 26.0 | 2.00 |
| | 0.0356 | 129.2 | 0.226 | 220 | 0.0378 | 0.94 | 7.6 | 18.0 | 2.36 |
| | 0.0252 | 182.6 | 0.202 | 160 | 0.0256 | 0.99 | 5.0 | 16.0 | 3.20 |
| | 0.0178 | 258.4 | 0.188 | 120 | 0.0183 | 0.98 | 3.2 | 16.0 | 5.00 |
| 3.30 | 0.0503 | 91.45 | 0.302 | 260 | 0.0535 | 0.94 | 20.0 | 26.0 | 1.30 |
| | 0.0356 | 93.0 | 0.244 | 220 | 0.0378 | 0.94 | 8.8 | 17.0 | 1.93 |
| | 0.0252 | 131.3 | 0.226 | 160 | 0.0256 | 0.99 | 6.4 | 11.0 | 1.72 |
| | 0.0178 | 186.0 | 0.203 | 120 | 0.0183 | 0.98 | 4.0 | 8.4 | 2.10 |
| HEMATITE: Absolute density = 4.45 g./cm. ³ ; K of Eq. (9) = 2.05; a of Eq. (9) = -0.5 | | | | | | | | | |
| 4.60 | 0.0503 | 91.45 | 0.227 | 350 | 0.0555 | 0.91 | 16.0 | 32.0 | 2.00 |
| | 0.0356 | 129.2 | 0.195 | 320 | 0.0470 | 0.76 | 14.0 | 32.0 | 2.28 |
| | 0.0252 | 182.6 | 0.143 | 300 | 0.0425 | 0.59 | 3.2 | 15.0 | 4.69 |
| | 0.0178 | 258.4 | 0.130 | 270 | 0.0357 | 0.50 | 4.6 | 10.5 | 2.28 |
| 3.30 | 0.0503 | 65.8 | 0.253 | 350 | 0.0555 | 0.91 | 18.0 | 32.0 | 1.80 |
| | 0.0356 | 93.0 | 0.199 | 320 | 0.0470 | 0.76 | 11.0 | 22.0 | 2.00 |
| | 0.0252 | 131.3 | 0.164 | 300 | 0.0425 | 0.59 | 5.8 | 20.0 | 3.45 |
| | 0.0178 | 186.0 | 0.133 | 270 | 0.0357 | 0.50 | 3.0 | 7.8 | 2.60 |

spheres were calculated using Rubey's expression¹³ for free-fall velocities of spherical particles. The ratio d/d_s was considered as a shape factor for the material of average size d , whose equivalent diameter as determined above was d_s . Such shape factors tended to unity, as the particle shapes approached spheres. It is interesting to note that the shape factors evaluated in the manner suggested for crushed charcoal were about 0.6, the same as given by Van Heerden *et al.*¹⁴ for such porous materials.

NOMENCLATURE

| | |
|--------------|---|
| a | = exponent (slope) |
| d | = particle size |
| d_s | = diameter of an equivalent sphere |
| D | = inner diameter of column |
| K | = constant (intercept) |
| m, n, p, q | = exponents |
| V | = fluid velocity |
| V_{mf} | = minimum fluidization velocity |
| V_s | = fluidizing velocity up to the range of validity of Eq. 8. |
| V_T | = terminal free-fall velocity |
| ϵ | = bed-voidage, dimensionless |
| ρ_s | = absolute density of material |

REFERENCES

1. LEWIS, E. W. & BOWERMAN, W., *Chem. Engng Progr.*, **48** (1952), 603.
2. JOHNSON, E., *Res. Fellowship Rep. Inst. Gas Engrs, Lond.*, 1949-50, 304.
3. LEVA, M., *Canad. J. chem. Engng*, **35**(8) (1957), 71.
4. HANRATTY, T. J. & BANDUKWALA, A., *Amer. Inst. chem. Engrs, J.*, **3** (1957), 293.
5. LEWIS, W. K. *et al.*, *Industr. Engng Chem.*, **41** (1949), 1104.
6. RAO, M. G., BHAT, G. N. & WIENGAERTNER, E., *Trans. Indian Inst. chem. Engrs*, **8** (1955-56), Part II, 137.
7. JACKSON, R., *Trans. Instn chem. Engrs, Lond.*, **41** (1963), 13.
8. HARRISON, D. *et al.*, *Trans. Instn chem. Engrs, Lond.*, **39** (1961), 202.
9. ZENZ, F. A., *Encyclopedia of Chemical Technology*, edited by Othmer, D. F. & Zenz, F. A. (Interscience Encyclopedia Inc., New York), 1957, 374.
10. RICHARDSON, J. F. & MEIKLE, R. A., *Trans. Instn chem. Engrs, Lond.*, **39** (1961), 348.
11. KRUNIJA GUCONIC, Ph.D. Thesis, Indian Institute of Science, Bangalore, 1959.
12. BHAT, G. N., Ph.D. Thesis, University of Bombay, 1961.
13. RUBEY, W. W., *Amer. J. Sci.*, **25** (1933), 325.
14. VAN HEERDEN, C. *et al.*, *Chem. Engng Sci.*, **1** (1951), 37.

Fluidization of Dissimilar Materials

G. R. VENKITAKRISHNAN & G. N. BHAT

Department of Chemical Engineering, Indian Institute of Science
Bangalore 12

Experimental studies on the gaseous fluidization of mixtures of solids having different particle sizes and densities are reported. Hematite and coal have been taken for initial studies and have been fluidized in glass columns of 4.6 cm. and 7.1 cm. internal diameter during which partial segregation of the components of the mixture was observed. The factors influencing segregation, viz. duration of fluidization, fluid velocity, bed height and column diameter have been discussed and the extents of segregation have been assessed as deviations from the original composition of the mixture. A mechanism of segregation has been proposed on the basis of the transfer of momentum between the two kinds of particles in the bed, which satisfactorily explains the observed results.

Fluidized solids technique is being widely used for gas/vapour-solids and solid-catalysed gas/vapour reactions. There are certain systems wherein reactions between two solids of dissimilar physical characteristics and chemical properties, or reactions between such solids mixtures and a gas/vapour phase, may occur. Examples of such systems are: chlorination of ilmenite in the presence of coke, reduction of anhydrite of calcium with coke, chlorination of bauxite, and reduction of hematite with coal. Since fluidized beds offer facilities for high heat and mass transfer rates, uniformity of bed temperature and surface area, they may prove advantageous to carry out the heterogeneous reactions mentioned above. However, flow data on fluidized systems are primarily restricted to systems wherein particles are of uniform size and density^{1,2} or mixtures of particle sizes of same density³⁻⁵. Meagre information⁶ is available with regard to systems constituted of particles of different sizes and densities.

When fluidization of solids mixtures is carried out, it is essential that during the course of fluidization, the mixtures retain their homogeneity

of composition over the entire bed height under the operating conditions such as gas velocity, particle size, column diameter, etc. It is the aim of this paper to present data collected with a view to investigating the factors that would influence the homogeneity of certain solids mixtures and assess qualitatively such influences under various operating conditions.

MATERIALS, EXPERIMENTAL SET-UP AND PROCEDURE

Hematite and coal having the following physical properties were used for the present studies:

| | Absolute density <i>g./cc.</i> | Bulk density <i>g./cc.</i> | Particle size (Tyler mesh) |
|----------|-----------------------------------|-------------------------------|-------------------------------|
| Hematite | 4.40 | 2.04 | —65+100 |
| Coal | 1.47 | 0.76 | —28+ 35 |

Fluidization experiments were carried out in glass columns of 4.6 cm. and 7.1 cm. internal diameter. Air for fluidization entered the column from the bottom. A packed bed of —10+14 Tyler mesh hematite filled up to a height of 10 cm. from the bottom served as distributor for 4.6 cm. diam. column. Such an air distribution arrangement was found unsatisfactory in the case of 7.1 cm. diam. column, and a 250-mesh stainless steel wire gauze served the purpose better. During pressure drop measurements, a U-tube water manometer was used with one of its ends open to atmosphere and the other end connected to a movable pressure tap immersed in the bed. A scoop with a long handle (Fig. 1) was used for taking out samples from the bed.

Definite amounts of hematite and coal were separately weighed out and mixed thoroughly such that a sample of about one-tenth of the weight of the mixture contained the two components in the same proportion as originally taken. Such a mixture was considered to be a 'homogeneous' mixture. Compressed air from a constant pressure tank (15 p.s.i.g.) dried by passing through a calcium chloride tower was metered through a set of rotameters and was allowed to flow into the fluidizing column at such a rate that the desired fluidization was obtained. The fluidization of the mixture was carried out over a definite interval of time after which the air supply to the system was suddenly stopped. The solids settled to yield a packed bed. The material contained over each unit of length of the packed bed thus obtained was removed by scooping, using the scoop introduced from the top of column. Withdrawal of samples through outlets at sides used by Sutherland⁷, Talmor and Benenati⁸ and Vakhrushev and Erokhin⁹ was considered unsuitable in the present studies since flow properties of the two

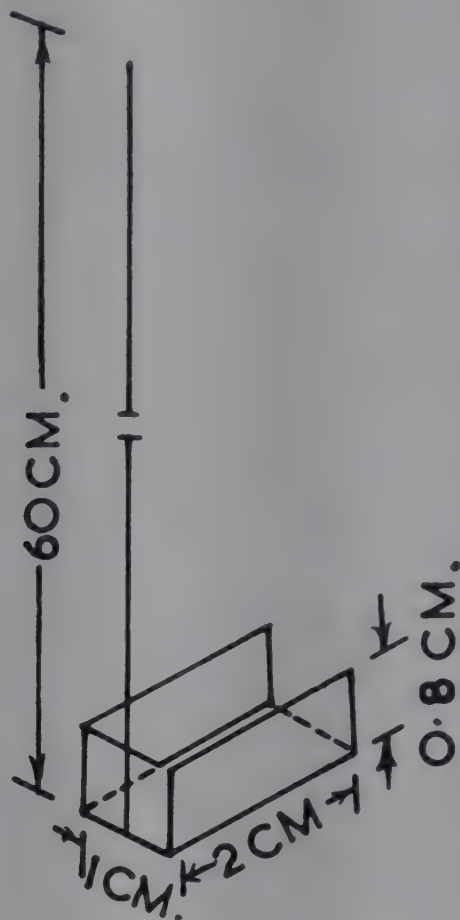


FIG. 1—SCOOP USED FOR REMOVING SOLIDS

solids constituting the bed were not identical. Solids mixtures removed from the bed were sieve analysed and the compositions of the mixture by weight per cent of hematite were determined. Results from two similar experimental runs were found to be consistent within ± 5 per cent. Experiments were carried out under the various operating conditions given below:

| | |
|--|--|
| Duration of fluidization, min. | 0.25, 0.50, 0.75, 1.0, 2, 3, 5, 10, 15 |
| Composition of the initial mixture fed to the column, % hematite by weight | 10, 30, 50, 70, 90 |
| Fluidizing air velocity, cm./sec. | 6-16 |
| Bed height, cm. | 6, 9, 12, 18 |
| Column diam., cm. | 4.6, 7.1 |

For the determination of minimum fluidizing velocity, the homogeneous mixture of known composition was fed to the column and the mixture fluidized with air. After fluidization for 15 min., flow of compressed air was stopped. Then the air velocity to the system was gradually increased stepwise from zero, the pressure drop being observed at each step, until the bed fluidized and expanded. The minimum fluidizing velocity was determined from a graph of pressure drop per unit length versus superficial linear velocity of air. The results are given in Table 1.

TABLE 1—MINIMUM FLUIDIZING VELOCITY OF THE MIXTURES

[Column diam., 7.1 cm.; Initial bed height, 12.0 cm.; Minimum fluidizing velocity of sand (—65+100) Tyler mesh, 4.0 cm./sec.]

| INITIAL COMPOSITION OF MIXTURE WT % HEMATITE | MINIMUM FLUIDIZING VELOCITY cm./sec. |
|--|--|
| 0 | 12.5 |
| 10 | 11.5 |
| 30 | 10.5 |
| 50 | 9.2 |
| 70 | 8.4 |
| 90 | 6.4 |
| 100 | 5.8 |

TABLE 2—VARIATION OF HEMATITE COMPOSITION AT DIFFERENT LEVELS OF BED

(Wt of hematite, 110 g.; Wt of coal, 110 g.; Column diam., 4.6 cm.; Duration of fluidization, 3.0 min.; Initial bed height, 12.0 cm.; Air velocity, 14.0 cm./sec.)

| HEIGHT FROM TOP cm. | COMPOSITION OF MIXTURE WT % HEMATITE | | |
|------------------------|---|--------|------|
| | Run I | Run II | Mean |
| 2.0 | 20.0 | 22.0 | 21.0 |
| 4.0 | 23.0 | 24.0 | 23.5 |
| 6.0 | 25.0 | 26.0 | 25.5 |
| 8.0 | 31.0 | 32.0 | 31.5 |
| 10.0 | 50.0 | 54.0 | 52.0 |
| 12.0 | 95.0 | 90.0 | 92.5 |

RESULTS AND DISCUSSION

General Observations on Segregation

When a homogeneous mixture of two components with different particle sizes and densities is fluidized, the bed tends to segregate into its individual components. In order to avoid segregation, particle sizes and compositions of the mixture are to be suitably selected. During the investigation, it was observed that in most cases the bed did not segregate with a distinct plane of demarcation between the particles of the two materials in each case, but there was a continuous change in composition of the mixture along the length of the column. The results obtained in a representative set of runs are given in Table 2.

The results are consistent under identical operating conditions and the concentration of hematite increases downwards and that of coal increases upwards in the bed. Such a behaviour was observed in all the experiments with all the systems. However, the observed phenomenon of continuous variation in solids composition over the bed length may not be of a general nature obtainable in all particle size combinations of materials of different density. In other words, depending on the differences in particle sizes and/or the differences in densities of solids used, a complete segregation of materials constituting the bed into two distinct phases may become possible.

Factors Influencing Segregation

Duration of fluidization. At the onset of fluidization (i.e. at time equal to zero), the composition of the solids mixture is the same over the entire length of the bed. However, as the fluidization is continued, the composition at a particular plane of the bed may become a function of time.

The data for a typical set of runs are presented in Fig. 2, from which it is seen that (i) only partial segregation of the mixture occurs in the bed; (ii) for the first few minutes, composition is a function of both the interval of fluidization and bed level; and (iii) after certain initial period of fluidization, the composition is a function of bed level only and is independent of time.

These observations indicate that at any bed level the solids experience two opposing tendencies, viz. one that would tend to segregate the mixtures and the other that would tend to mix them. It is under conditions of imbalance of these two tendencies that segregation becomes time-dependent.

It is further seen from Fig. 2 that at a height of about 8 cm. from the top, the composition of the bed remained the same as the initial composition and did not change with time.

Fluid velocity. The effect of fluid velocity on the segregation is shown in Fig. 3 from which it is seen that the extent of segregation is reduced on increasing gas velocity.

Bed height. The influence of bed height on the segregation of solids in the bed is shown in Fig. 4. It is seen that for the same height from the top, the composition is different for each initial bed height.

The effect, however, has been compared as percentage distance from the top of the bed and has been presented in Table 3.

It is evident from the table that at any percentage height, the composition of the mixture remains nearly the same irrespective of the initial height of the bed. The slight differences can be due to variation in the quality of fluidization with height to diameter ratio, and also due to the fact that the samples were taken over the same thickness of the bed.

Column diameter. The effect of column diameter was studied under nearly the same bed height to column diameter ratio 2 with a mixture of initial composition of 50 per cent by weight of hematite. Table 4 shows that

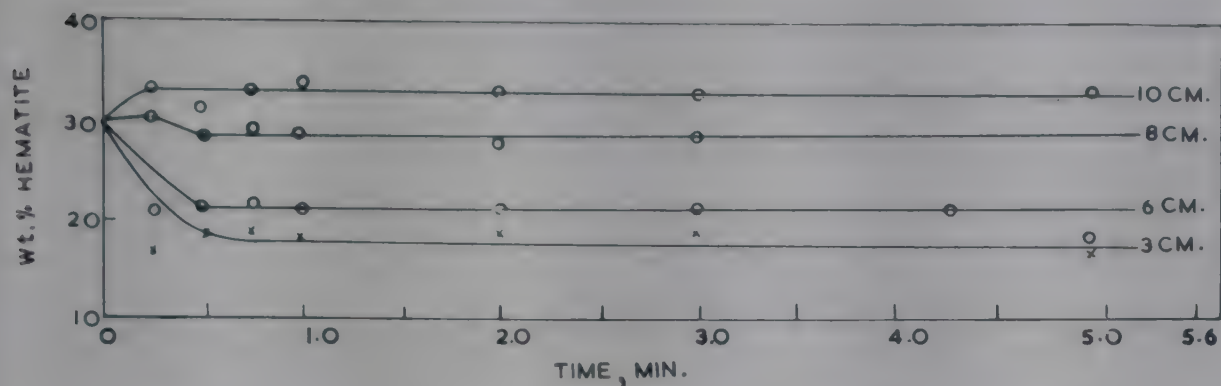


FIG. 2—VARIATION OF MIXTURE COMPOSITIONS AT VARIOUS LEVELS OF BED

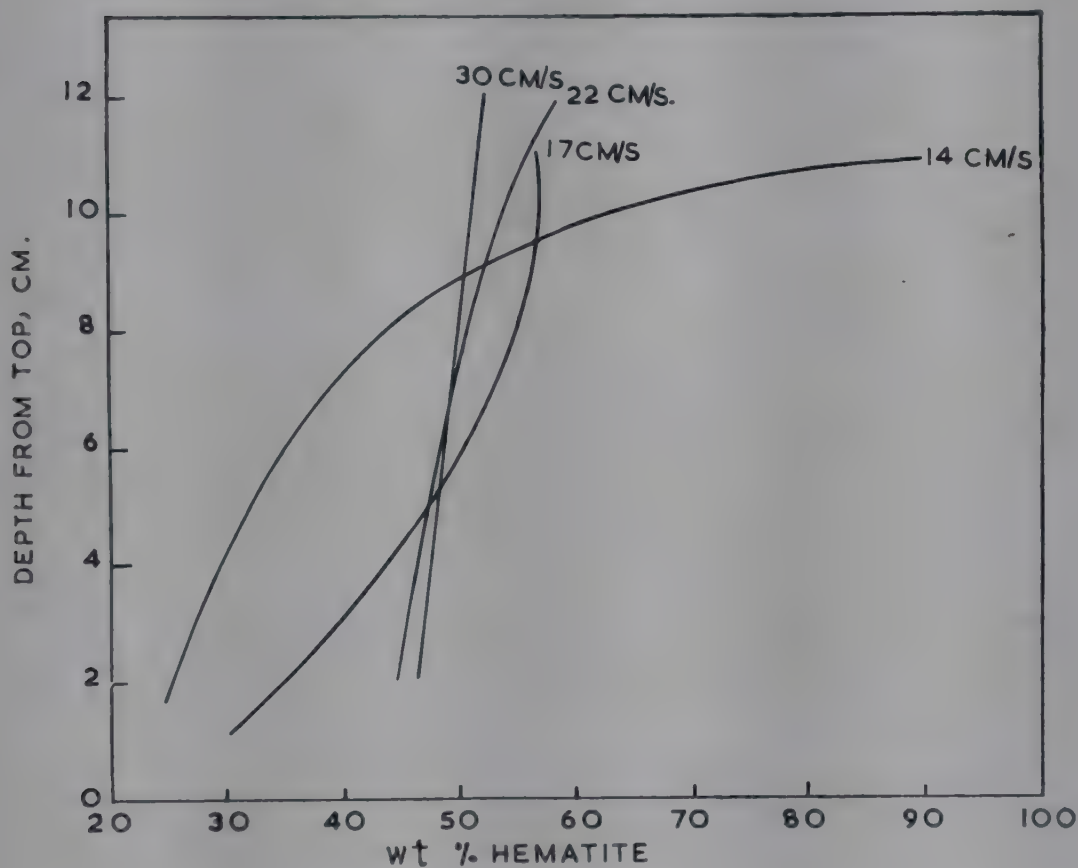


FIG. 3—VARIATION IN COMPOSITION OF SOLIDS MIXTURE WITH BED LEVEL FOR DIFFERENT FLUIDIZING VELOCITIES

the column diameter does not have any influence on segregation as long as the bed nature is unaltered, i.e. as long as it does not exhibit slugging tendencies.

Assessment of Segregation

The desired criterion to express segregation should be a comparison between the composition of the material initially fed to the bed and that

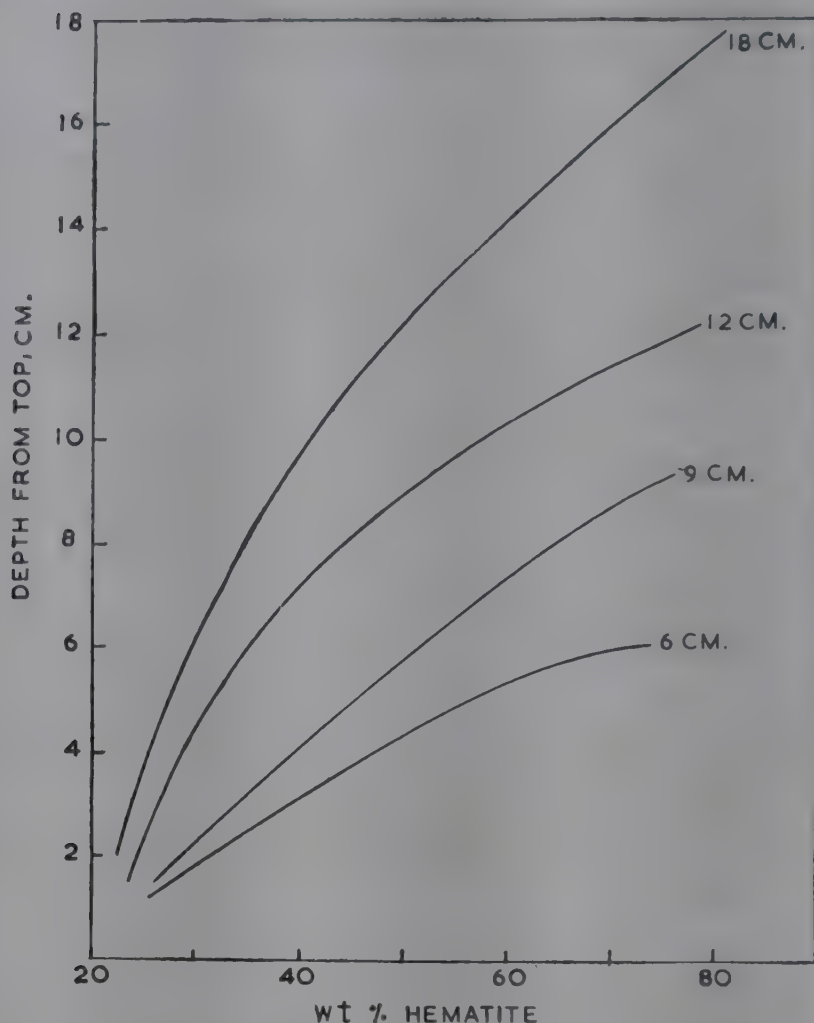


FIG. 4—VARIATION IN COMPOSITIONS OF SOLIDS MIXTURE WITH BED LEVEL FOR DIFFERENT INITIAL BED HEIGHTS

obtained when steady-stage conditions are attained. Fig. 2 shows that the bed under steady-state conditions can be divided into two sections, considering the bed level, at which the composition is the same as that of the feed mixture, to be the datum level. The sections above and below the datum level can be called the enriching and stripping section respectively as in the case of conventional separation processes. In the enriching section, the composition of the mixture is higher than that of the feed, whereas the composition of mixture is lower in the stripping section. The deviation of the composition at any bed level from that of the feed gives the extent of segregation, and the nature of deviation (mathematically, positive or negative) gives information whether enrichment or depletion has taken place. Thus, this method of assessing the extent of segregation has been employed in the present case. It is similar to the separation factor employed in the case of other separation processes, but is not identical with it, as it takes into account only the feed composition rather than the compositions of the mixture in equilibrium with the separated material, in evaluating the segregation tendency.

TABLE 3—HEMATITE CONCENTRATION AT DIFFERENT PERCENTAGES OF TOTAL INITIAL BED HEIGHT

(Feed composition, 50% hematite by wt; Duration of fluidization, 15 min.; Column diam., 4.6 cm.)

| INITIAL BED HEIGHT <i>cm.</i> | HEMATITE CONC. AT DIFFERENT PERCENTAGES OF TOTAL INITIAL BED HEIGHT | | | |
|-------------------------------------|--|-------|-------|-------|
| | 25% | 50% | 75% | 100% |
| 6 | 27.5 | 38.5 | 51.0 | 71.0 |
| 9 | 30.0 | 42.0 | 55.0 | 72.5 |
| 12 | 26.5 | 35.0 | 50.0 | 75.0 |
| 18 | 26.5 | 37.5 | 51.0 | 75.0 |
| Range of compo- sition variation | 25-30 | 35-45 | 50-55 | 70-75 |

TABLE 4—HEMATITE CONCENTRATION AT DIFFERENT PERCENTAGES OF TOTAL INITIAL BED HEIGHT FOR NEARLY THE SAME HEIGHT TO DIAMETER RATIO

(Feed composition, 50% hematite by wt; Initial bed height for 4.6 cm. internal diam. column, 9 cm.; Initial bed height for 7.1 cm. internal diam. column, 12 cm.; Air velocity, 14 cm./sec.)

| PERCENTAGE OF TOTAL INITIAL BED HEIGHT | HEMATITE CONC. IN COLUMNS OF | |
|--|---------------------------------|--------------|
| | 4.6 cm. i.d. | 7.1 cm. i.d. |
| 25 | 30 | 26 |
| 50 | 42 | 40 |
| 75 | 55 | 54 |
| 100 | 73 | 60 |

The percentage deviations as calculated above are presented in Fig. 5, for all the five initial compositions of the mixture studied. The percentage deviation has been plotted against bed level (measured from top) with initial composition of the mixture as parameter. The point of intersection of these curves with the vertical line corresponds to the plane of zero deviation (i.e. the datum line, having the same composition as the feed composition) and gives the height at which the datum level is obtained. The present data show that such a level (measured from top) increases with feed composition up to about 50 per cent feed composition by weight but is at a lower height (measured from top), with further increase in compositions.

The actual compositions (weight per cent hematite) have also been plotted in Fig. 6 for all the five initial compositions. It is seen that for mixtures

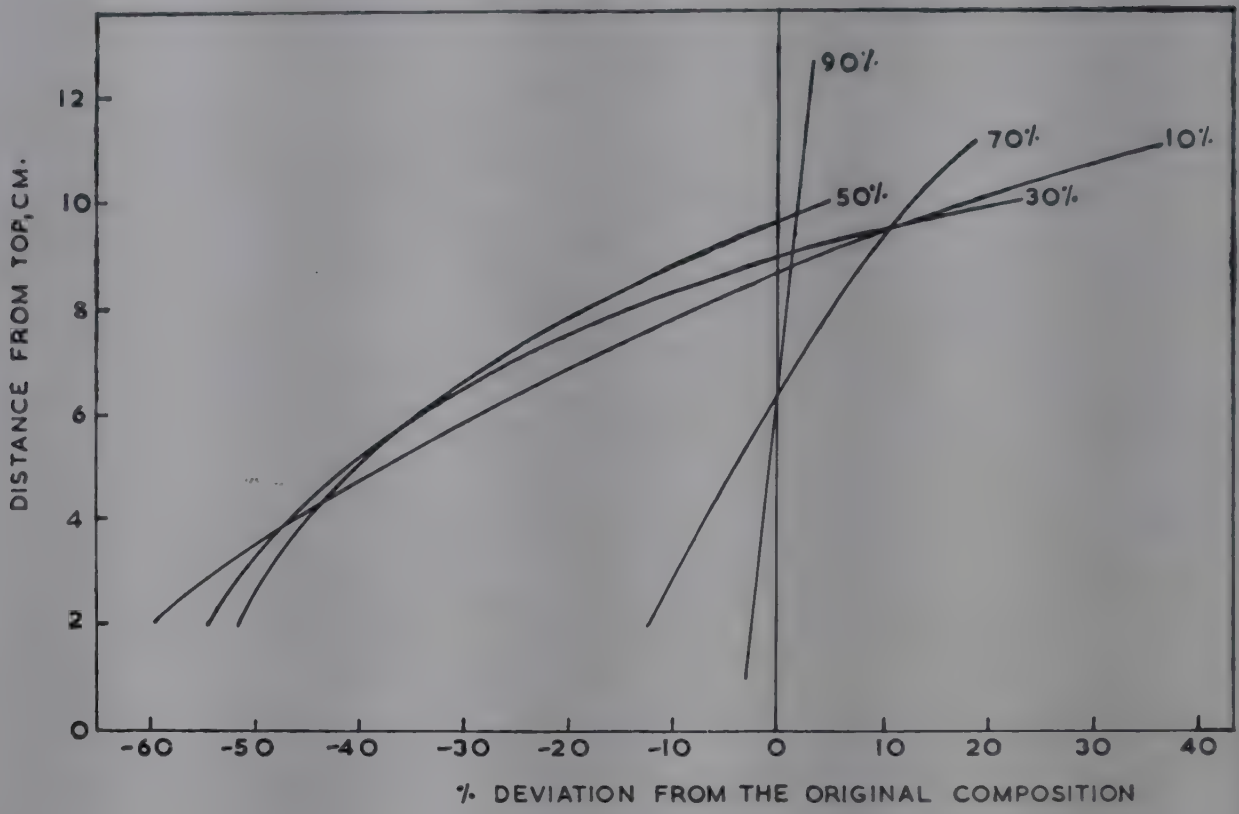


FIG. 5—PERCENTAGE DEVIATION FROM ORIGINAL COMPOSITION VERSUS BED LEVEL FOR DIFFERENT INITIAL COMPOSITIONS OF MIXTURE

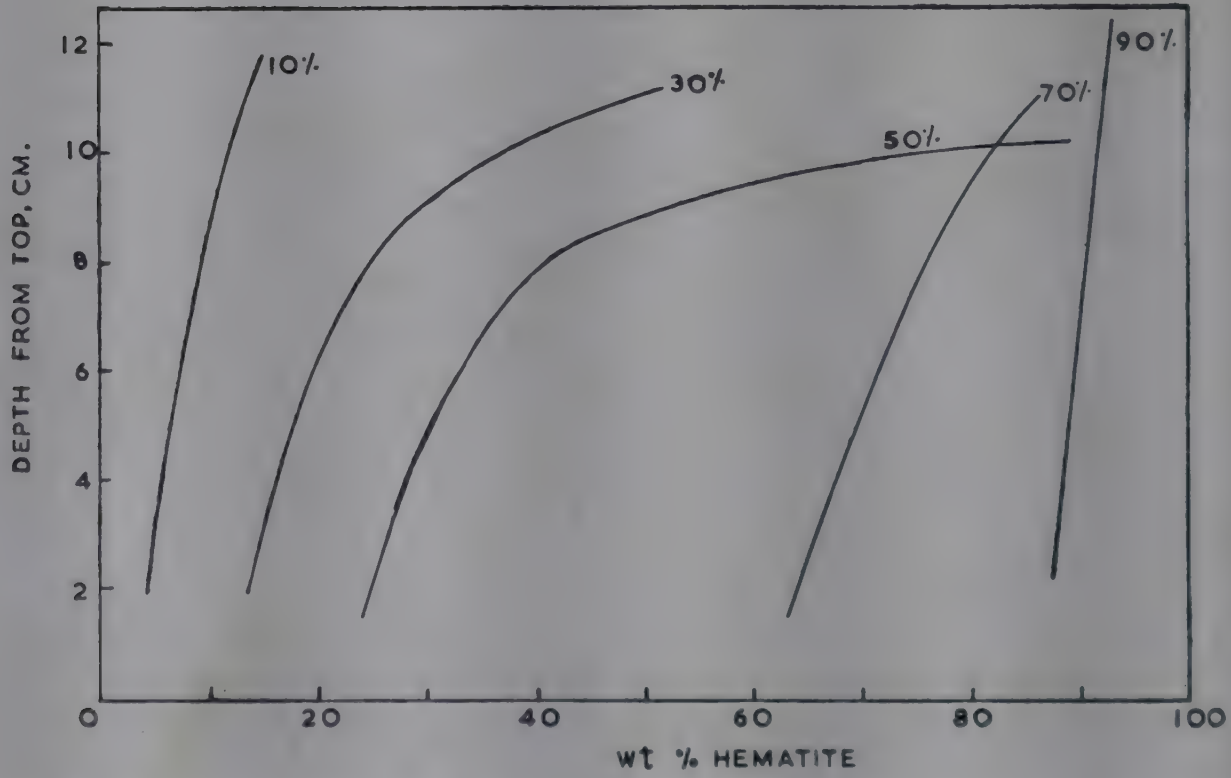


FIG. 6—VARIATION IN COMPOSITION OF SOLIDS MIXTURE AT DIFFERENT LEVELS FOR VARIOUS INITIAL COMPOSITIONS OF MIXTURE

of 10, 70 and 90 per cent initial hematite content, the percentage of hematite in the column changes approximately linearly with height, whereas for 30 and 50 per cent, the change is not linear. In these cases, the rate of change of composition is slower at the bottom of the bed but becomes faster as the top of the bed is approached.

Possible Mechanism of Segregation

It is seen that the coal concentration builds up at the top of the column. Data presented in Table 2 indicate that the fluidizing velocity employed is higher than the minimum fluidizing velocity of hematite and lower than that of coal used. Therefore, it may normally be anticipated that the coal particles would settle to the bottom leaving the hematite particles at the top. However, it is seen from Table 1 that the concentration of coal builds up at the top and that of hematite builds up at the bottom levels in the bed.

Generally, during the fluidization phenomena, particle mobility is considered to be a function of exchange of momentum between the fluidizing medium and the particles constituting the bed and also due to the exchange of momentum among the particles of the bed. However, in the case of solids mixtures, the mobility of all the particles may not entirely be due to such a phenomenon. In fact, if the fluidizing velocity used is such that only one of the constituents can be fluidized, the momentum associated with such fluidized particles may actually be exchanged with the other set of particles which themselves may not be fluidized at the fluid velocity employed. Such an exchange of momentum between the fluidized solids and the other solids component mixed with it may actually cause movement of the latter particles and the overall extent of particle movement is the resultant of such momentum transfer phenomena and the gravitational forces acting on the system.

The observed results reveal that the exchange of momentum has taken place in such a way as to keep the coal particles at the top. Should this be the situation that is responsible for the enrichment of coal towards the top of the bed, it may be anticipated that under conditions of lower momentum transfer facility, coal would get enriched towards the bottom of the beds. Experiments carried out with sand-coal beds in the place of hematite-coal beds show tendencies for enrichment of coal towards the lower section of the beds. This effect may be due to the fact that the momentum of a sand particle is relatively less than that of a hematite particle of the same size and moving at the same velocity. However, while momentum level of a set of fast-moving hematite particles is a governing factor in the transfer of momentum to the slow-moving coal particles, there may be additional factors that may influence the transfer of this momentum. These factors may be the number of fast-moving particles for every slow-moving particle (i.e. feed composition), the facility for the movement of slower-moving particles (i.e. voidage), etc. Further work is in progress to evaluate

the influence of all these factors on the fluidization characteristics of mixtures of dissimilar solids.

CONCLUSION

A mixture of solids constituted of differently sized materials of different densities can be fluidized without complete segregation of the two components. The factors influencing the segregation are the initial composition of the mixture, the relative weights of the particles of solids constituting the mixture and the velocity used for fluidization. The observed phenomena can be satisfactorily explained on the basis of the transfer of momentum between the two kinds of particles in the bed.

ACKNOWLEDGEMENT

The authors wish to express their sincere thanks to Prof. N. R. Kuloor for his keen interest and kind encouragement in the work. One of the authors (G.R.V.) is grateful to the Council of Scientific & Industrial Research, New Delhi, for the award of a fellowship during the period of the investigation.

REFERENCES

1. ZENZ, F. A. & OTHMER, D. F. *Fluidization and Fluid Particle Systems* (Reinhold Publishing Corp., New York), 1960.
2. LEVA, M., *Fluidization* (McGraw-Hill Book Co. Inc., New York), 1959.
3. JACOBS, J. K. & MINET, R. G., *Fluidization of Non-uniform Particles*, Paper presented at the meeting of *Amer. Inst. chem. Engrs*, held at New Orleans, U.S.A., 6-9 May, 1956.
4. HOFFMAN, R. F., LAPIDUS, L. & ELGIN, J. C., *Amer. Inst. chem. Engrs J.*, **6** (1960), 321.
5. GOPALAKRISHNA, N. & RAO, M. N., *Indian chem. Engr*, **5** (1963), 6.
6. LEVA, M., Doctor of Engng Thesis, Tokyo Inst. Technol., Tokyo, 1961; referred by Talmor & Benenati (cf. below).
7. SUTHERLAND, K. S., *Trans. Instn chem. Engrs, Lond.*, **39** (1961), 188.
8. TALMOR, E. & BENENATI, R. F., *Amer. Inst. chem. Engrs J.*, **9** (1963), 536.
9. VAKHRUSHEV, I. A. & EROKHIN, G. S., *Int. chem. Engng*, **3** (1963), 333.

Performance Characteristics of Two-Fluid Atomizer

N. N. KAURA*, S. K. VARMA & M. N. RAO

Indian Institute of Technology
Kharagpur

Experimental results for the atomization of a water jet by air and an immiscible liquid (kerosene) have been presented. A dependable correlation,

$$\frac{X_{sm}}{d_o} = 1953 \left(\frac{\sigma d_o}{M_{ar}} \right)^{0.7} \left[1 - 0.12 \left(\frac{M_{tr}}{\sigma d_o} \right)^{0.12} \right]^{0.7} \left(\frac{M_d}{M_c} \right)^{0.23} \left(\frac{v_a}{v_o} \right)^{0.46}$$

for the prediction of Sauter mean diameter of atomized drops in both the systems has been proposed.

Atomization of a jet of liquid by high-velocity gas streams has been studied by a number of workers¹⁻⁷.

The atomization in this case has been postulated by Castleman⁴ to be a two-step process. The liquid jet is first torn up into ligaments, and then the ligaments collapse to form drops in accordance with Rayleigh's theory. High-speed motion pictures by Wetzel and Marshall⁷ show that, at low liquid rates, the impact of the gas stream on the liquid jet plays an important part in the mechanism of jet break-up. They observed that the air blows out a bag from the main mass of the liquid which collapses to give the droplets. Lane⁸ observed a similar phenomenon in the study of the break-up of a single drop suddenly exposed to a high-velocity gas stream. The actual atomization process in a two-fluid atomizer can be visualized to be taking place in two steps: (i) break-up of liquid jet due to fluid friction and impaction between the two streams, and (ii) secondary break-up of the large-sized drops formed in the first step.

Nukiyama and Tanasawa⁵ on the basis of their experimental results

*Present address: Department of Chemical Engineering, Indian Institute of Technology, Kanpur.

developed the following empirical expression for the mean dropsize to be expected from small air-atomizing venturi type nozzles:

$$X_{sm} = \frac{585}{v_r} \sqrt{\frac{\sigma}{\rho_d}} + 597 \left(\frac{\mu_d}{\sqrt{\sigma \rho_d}} \right)^{0.45} \left(\frac{1000 Q_d}{Q_c} \right)^{1.5} \quad (1)$$

where v_r is the relative velocity between the two streams, ρ_d is the density of dispersed phase, μ_d is the viscosity of dispersed phase, σ is the interfacial tension, and Q_d and Q_c are the volumetric flow rates of dispersed and continuous phase respectively.

Wetzel and Marshall⁷, and Marshall⁹ studied the effect of relative velocity and the jet (central tube) diameter for dispersed phase on the mean diameter of the spray with industrial sized air-atomizing nozzles. They came to the conclusion that the jet diameter of dispersed phase is an important parameter and should be taken into account for scale-up purposes. On comparing their results with the Nukiyama and Tanasawa equation, they found that there was good agreement only in the case of runs where the relative velocity was more than 400 ft/sec.

The break-up of a drop of a liquid in a turbulent stream of another immiscible fluid has been studied by a number of workers¹⁰⁻¹³.

Hinze¹⁰ presented a mathematical analysis of the conditions of break-up of a liquid drop by an air stream. A distinction was made between the freely falling drop and the one suddenly subjected to an air blast, and the effect of viscosity was taken into account.

Sleicher¹² experimentally studied the maximum stable droplet size for two immiscible liquids flowing through a pipe. He came to the conclusion that the dispersed phase viscosity, interfacial tension, properties of the continuous phase and its velocity are the main factors controlling break-up.

In the present study the characteristics of atomization of water jet by air and of water by another immiscible liquid, kerosene, have been evaluated.

EXPERIMENTAL SET-UP AND PROCEDURE

The experimental set-up is shown in Fig. 1. The nozzle (Fig. 2) used in the study was such that the continuous phase could be given a swirl also. The tangential entry to swirl chamber as well as the orific diameter for the continuous phase and the central tube (or jet) diameter of dispersed phase could be changed.

The sampling technique consisted in the collection of drops into a transparent bottomed cell filled up with a suitable immiscible liquid. The drop liquid was coloured and photographs of the sample were prepared within 5 min. of sampling.

The assembly used for sampling is shown in Fig. 3A. The cell was of 1 in. diam. and was fitted with a transparent bottom of optically flat

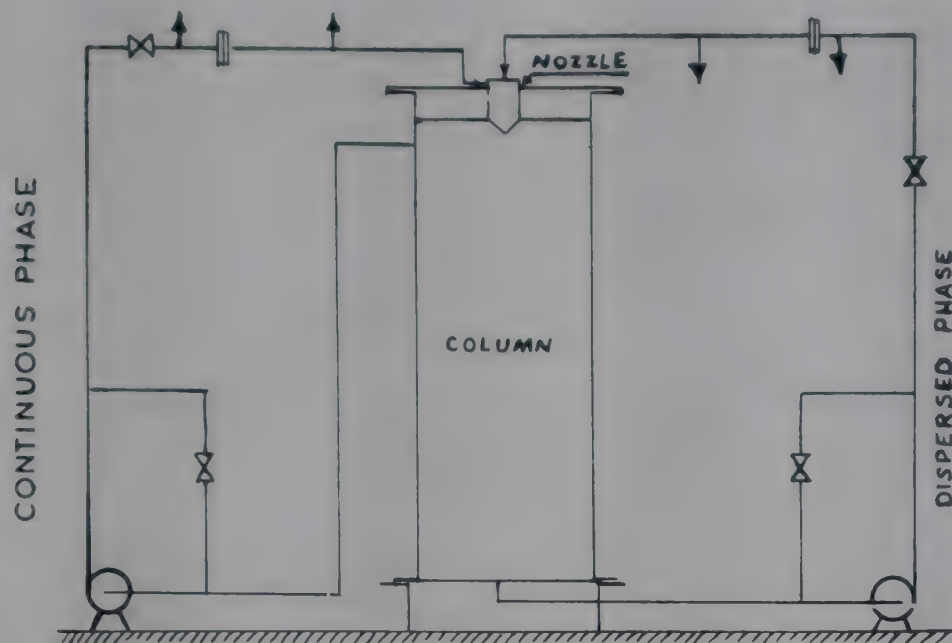


FIG. 1—EXPERIMENTAL SET-UP FOR TWO-FLUID ATOMIZER

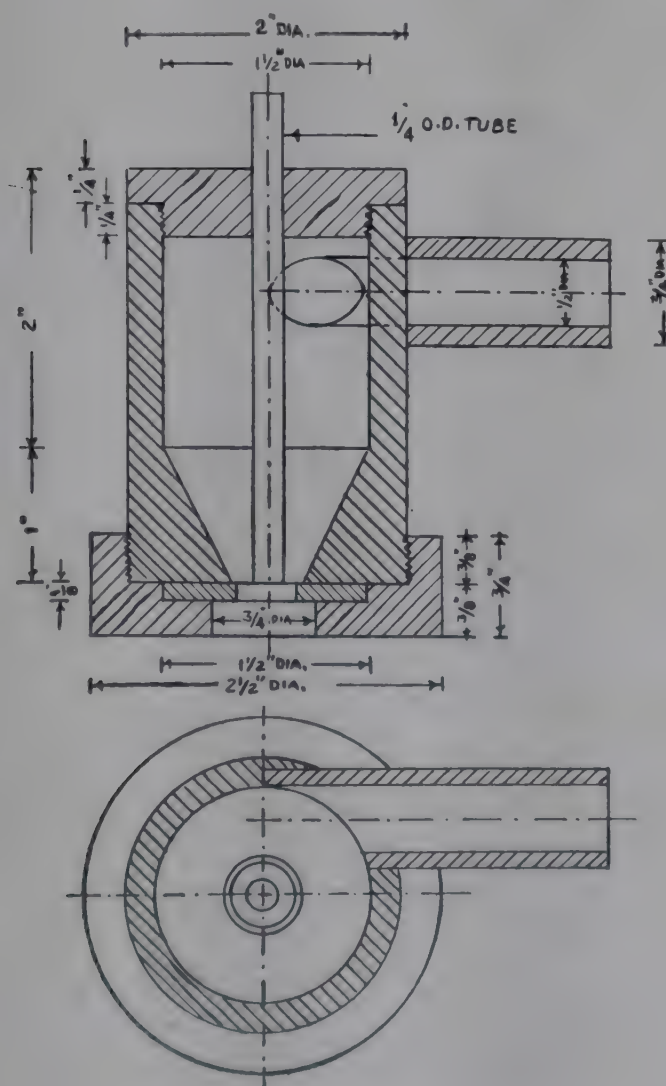
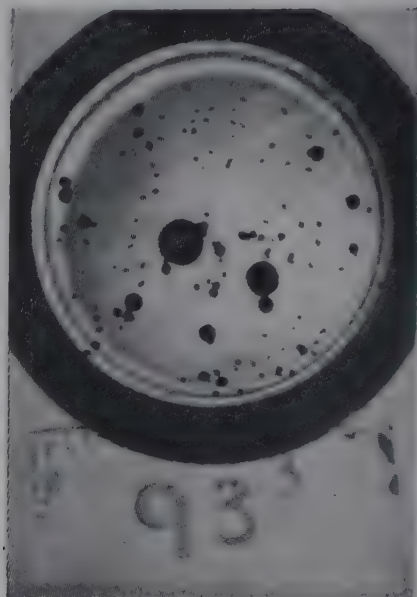


FIG. 2—TWO-FLUID NOZZLE



A



B

FIG. 3(A)—ASSEMBLY FOR SAMPLING; (B)—SPRAY SAMPLE

glass. The cell was filled with a high viscosity oil in case of runs with water as the dispersed phase and sugar syrup of a predetermined density and viscosity in case of other systems. The cell was then placed in a chamber (diam., 3 in.) with a camera shutter acting as lid. The assembly was mounted on a metallic frame and lowered into the column such that the total depth of the sampling point from the nozzle orifice was 3 ft. To avoid the accumulation of liquid on the camera shutter it was initially kept covered with a metallic flap. While sampling, the flap was removed from over the shutter and the shutter operated. To reduce the target effect of the bottom of the cylindrical chamber the cell was supported in its centre by three radial ribs. The position of the nozzle with respect to the sampling point could be varied such that the radial distance of sampling point from the axis of the nozzle varied from 0 to 5. in.

The analysis for dropsizes distribution of the spray was carried out by projecting the photographic negatives, through a microfilm reading equipment, on to a graph sheet. The total number of drops sampled for any one run varied from 500 to 7000, and the results were reproducible within ± 10 per cent. The photograph of the spray sample is shown in Fig. 3B.

The systems used in the studies, along with their physical properties, are listed in Table 1. The physical properties of pure liquids are given in Table 2.

RESULTS

Effect of mass ratio. Using the kerosene-water system, the latter as the dispersed phase, the variation of Sauter mean diameter of the spray with mass ratio was studied at different axial velocities of the continuous

TABLE 1—PHYSICAL PROPERTIES OF SYSTEMS USED IN THE STUDIES

(Proportions of the components of the mixture were so adjusted as to get the required viscosity and interfacial tension.)

| SYSTEM | CONTINUOUS PHASE | DISPERSED PHASE | μ_o cP. | ρ_c lb./ft ³ | μ_d cP. | ρ_d lb./ft ³ | σ dynes/cm. |
|----------------|------------------|---|----------------|---------------------------------|----------------|---------------------------------|-----------------------|
| A | Air | Water | 0.018 | 0.0735 | 0.800 | 62.24 | 70.0 |
| B | Kerosene | Water | 1.800 | 48.82 | do | do | 21.6 |
| C ₁ | Water | Ethylene dibromide-carbon tetrachloride | 0.800 | 62.24 | 2.00 | 120.2 | 19.00 |
| C ₂ | do | Ethylene dibromide | do | do | do | 136.0 | do |
| C ₃ | do | Ethylene dibromide-bromoform | do | do | do | 149.8 | do |
| C ₄ | do | Bromoform | do | do | do | 180.3 | do |
| D ₁ | do | Ethylene dibromide | do | do | do | 136.0 | 13.0 |
| D ₂ | do | Ethylene dibromide | do | do | do | do | 6.0 |

TABLE 2—PHYSICAL PROPERTIES OF PURE LIQUIDS

| | DENSITY lb./ft ³ | INTERFACIAL TENSION dynes/cm. | VISCOSITY cP. |
|----------------------|--------------------------------|----------------------------------|------------------|
| Bromoform | 177.8 | 40.60 | 2.10 |
| Ethylene dibromide | 135.4 | 36.58 | 1.78 |
| Carbon tetrachloride | 98.9 | 44.60 | 1.10 |

phase. Sample plots of drop size distribution are shown in Fig. 4, and the effect of mass ratio on Sauter mean diameter is shown in Fig. 5. Sauter mean diameter of the spray increases with increase in the mass ratio.

Effect of axial velocity of continuous phase. These studies were made with the kerosene-water system. Keeping all other conditions of operation fixed, the axial velocity for the continuous phase was varied by changing the continuous phase orifice diameter and hence the annular area of flow. The effect of continuous phase axial velocity on Sauter mean diameter of the spray is shown in Fig. 6. Sauter mean diameter decreases with increase in the axial velocity.

Effect of tangential velocity of continuous phase. The effect of tangential velocity of continuous phase on Sauter mean diameter was studied by changing the tangential entry diameter, under other constant conditions of operation. The results are shown in Fig. 7. Sauter mean diameter decreases with increase in tangential velocity.

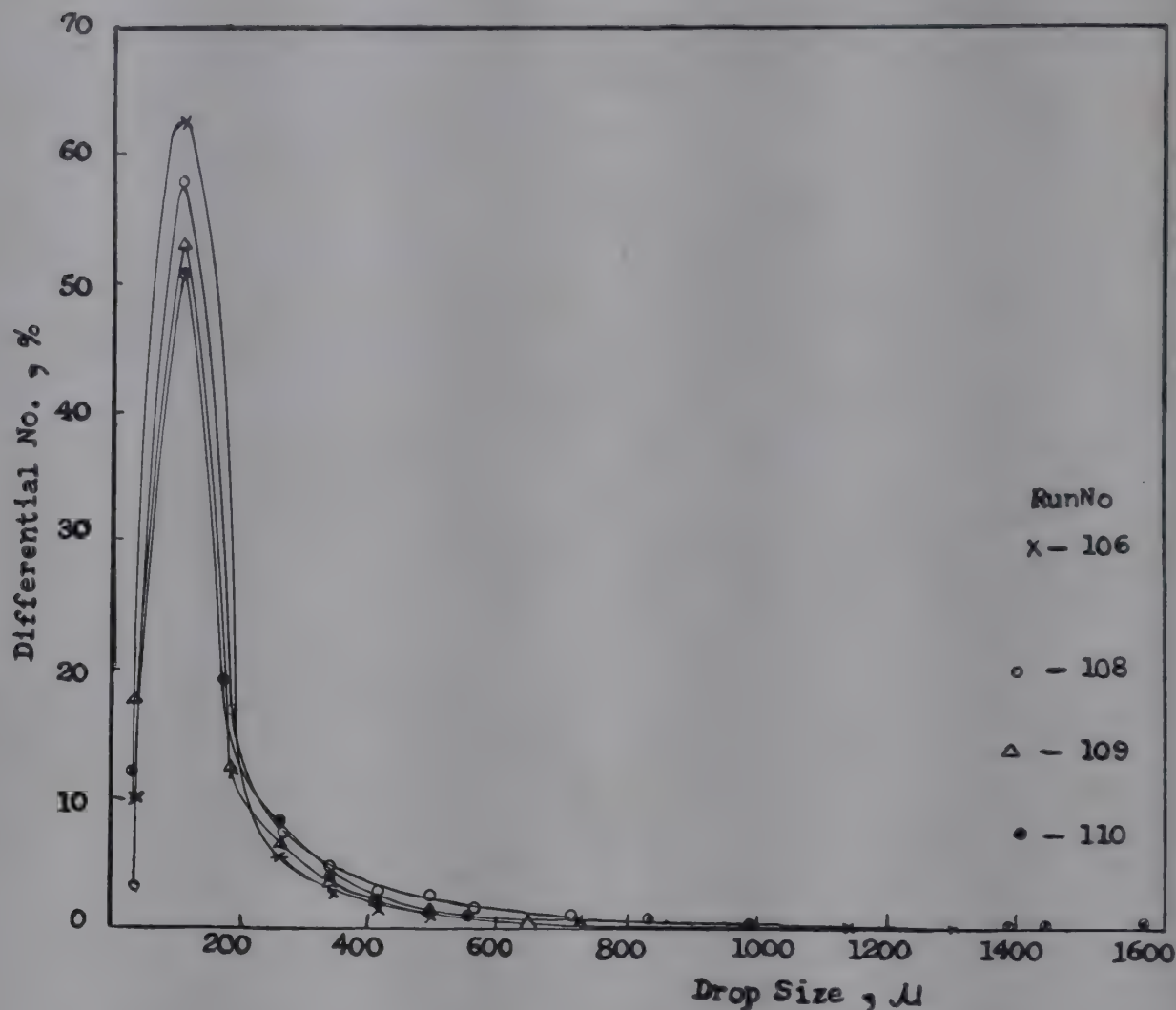


FIG. 4—EFFECT OF AXIAL VELOCITY OF CONTINUOUS PHASE ON DROP SIZE DISTRIBUTION

Effect of jet diameter. At other fixed conditions of operation, the effect of jet (or central tube) diameter of dispersed phase on Sauter mean diameter of spray was studied by varying the inside diameter of the central tube. The results are shown in Fig. 8. Sauter mean diameter of the spray increases with increase in jet diameter.

Effect of dispersed phase flow rate. The effect of dispersed phase momentum flow rate on Sauter mean diameter of the spray was studied with both kerosene-water and air-water systems. The results are shown in Fig. 9. Sauter mean diameter of spray increases with increase in momentum flow rate of dispersed phase.

Effect of liquid properties. The effects of the density of the dispersed phase and the interfacial tension on Sauter mean diameter of spray have been studied.

To study the effect of dispersed phase density, studies were carried out with water as the continuous phase, and mixtures of ethylene dibromide-bromoform and ethylene dibromide-carbon tetrachloride as the dispersed phase. The results are shown in Fig. 10. Sauter mean diameter of the spray decreases with increase in the density of the dispersed phase.

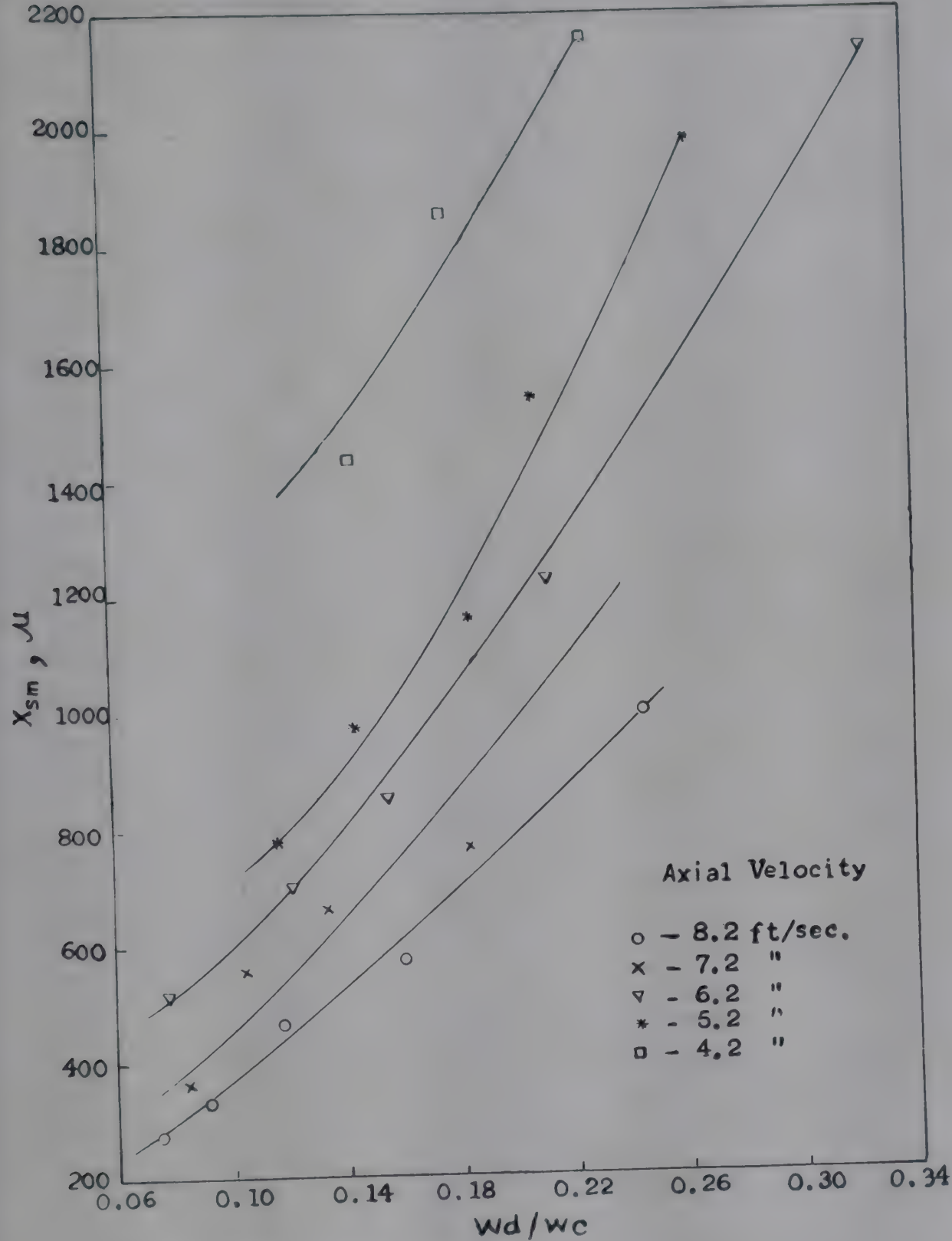


FIG. 5—EFFECT OF MASS RATIO ON SÄUTER MEAN DIAMETER OF SPRAY

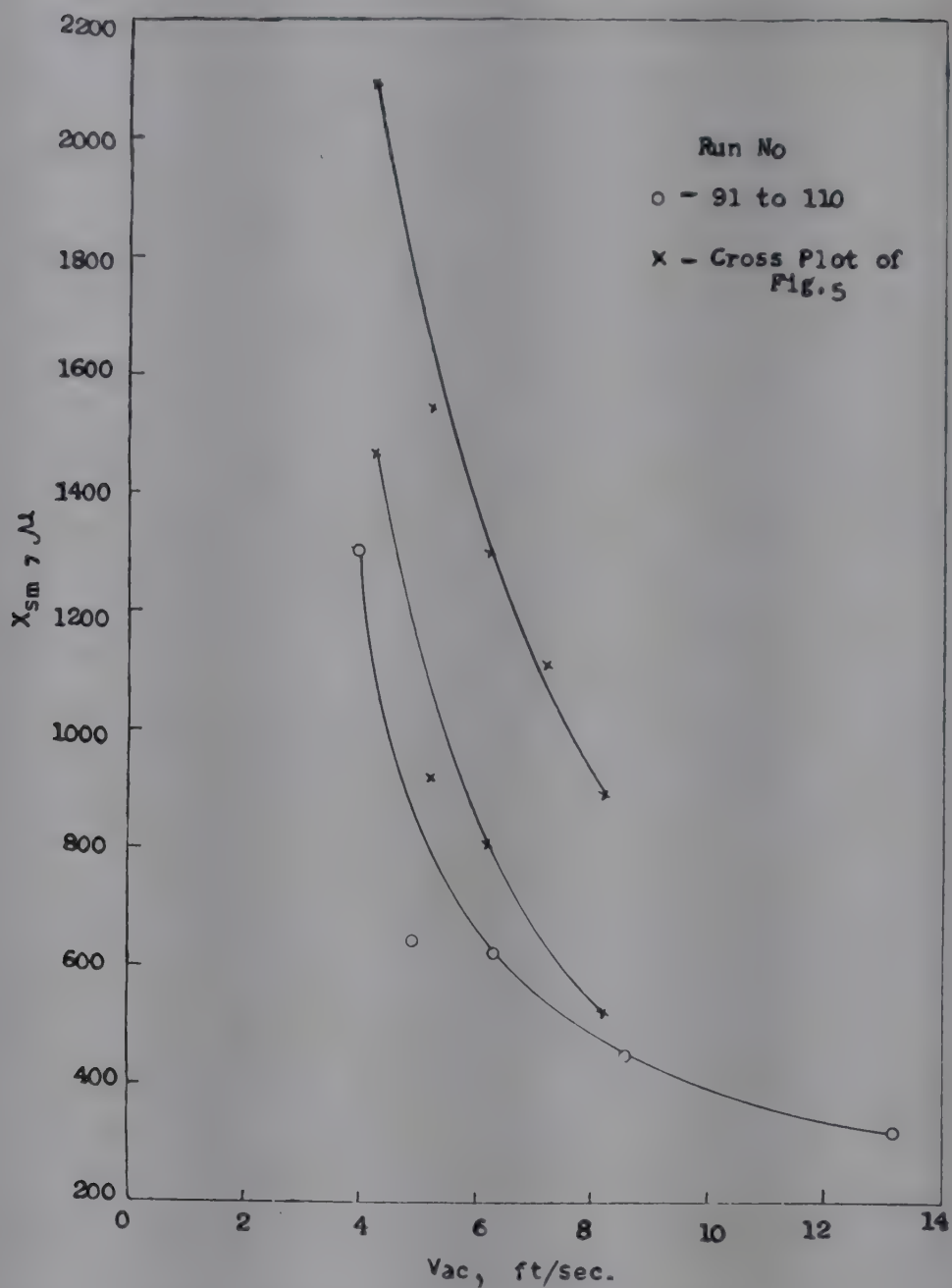


FIG. 6—EFFECT OF AXIAL VELOCITY OF CONTINUOUS PHASE ON SÄUTER MEAN DIAMETER OF SPRAY

The effect of interfacial tension on Sauter mean diameter of the spray was studied using water as continuous phase and ethylene dibromide as dispersed phase. The interfacial tension was reduced by adding a surface active agent to the dispersed phase. The results are shown in Fig. 11. Sauter mean diameter decreases with decrease in interfacial tension.

CORRELATIONS

Sauter mean diameter of the spray can be taken to be a function of the following variables:

$$X_{sm} = \Phi (M_c, M_d, d_o, \sigma, \rho_c, \rho_d, \mu_c, \mu_d) \quad (2)$$

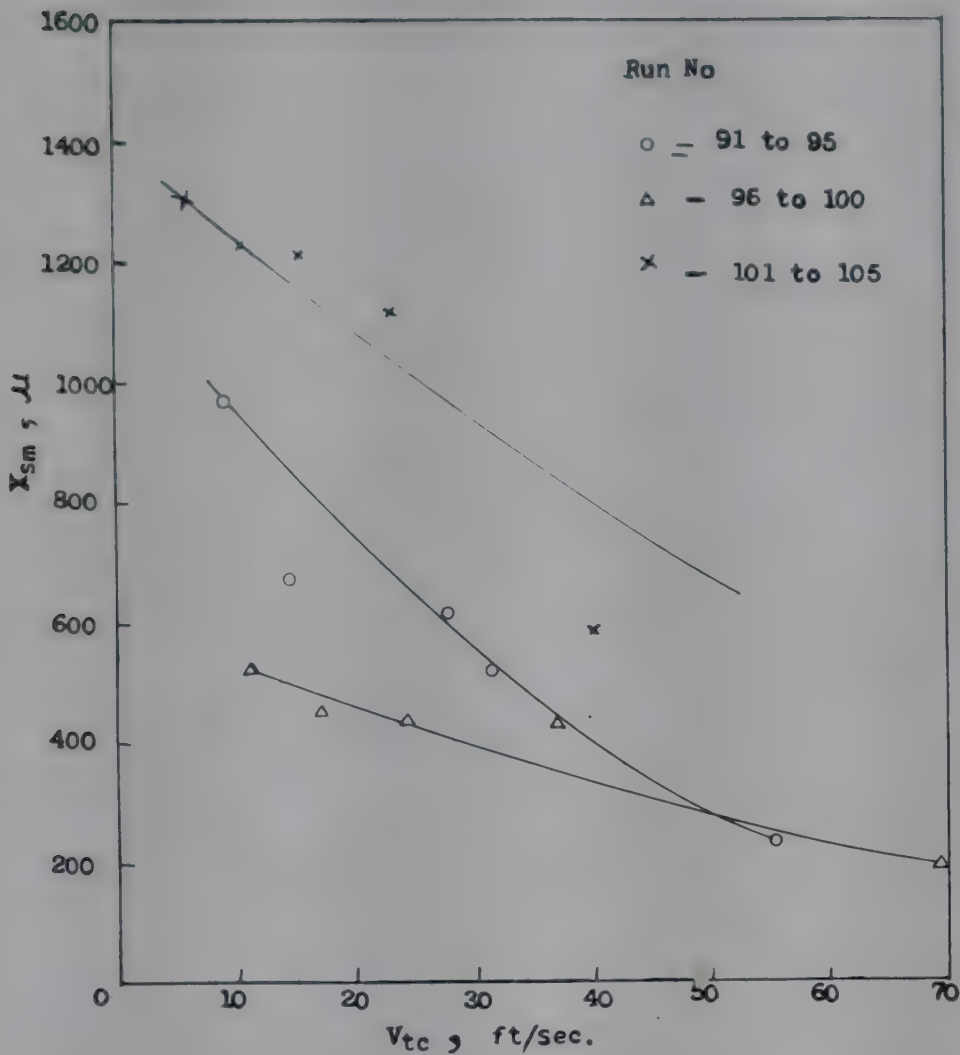


FIG. 7—EFFECT OF TANGENTIAL VELOCITY OF CONTINUOUS PHASE ON SÄUTER MEAN DIAMETER OF SPRAY

The choice of M_c and M_d , the momentum flow rates of the two phases, as the fundamental variables has been based on the following considerations:

(i) The process of atomization in the present case is one of impaction and friction due to relative velocity between the two streams. The forces involved in an impact are proportional to the rate of change of momentum, hence the momentum flow rate is the proper choice to account for the disruptive forces acting on the jet.

(ii) The mass ratio has been found to effect the atomization. Since it can only be the mass in motion which can effect atomization it is reasonable to account for the disintegrating force on the jet by taking into account the product of mass and velocity, namely momentum.

It follows by dimensional analysis from Eq. (2) that

$$\frac{X_{sm}}{d_o} = \Psi \left(\frac{\sigma d_o}{M_c}, \frac{M_d}{M_c}, \frac{\mu_d}{\sqrt{M_d \rho_d}}, \frac{\mu_c}{\sqrt{M_c \rho_c}}, \frac{\rho_d}{\rho_c} \right) \quad (3)$$

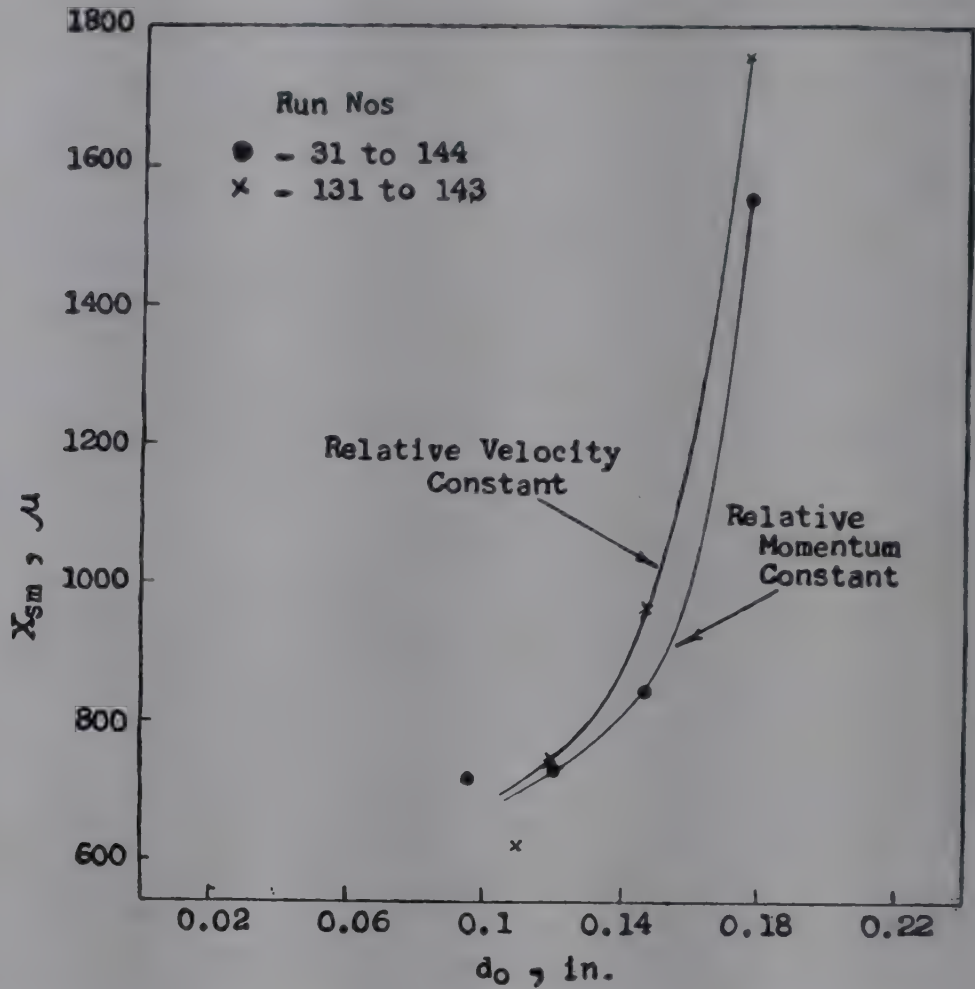


FIG. 8—EFFECT OF CENTRAL TUBE (JET) DIAMETER ON SÄUTER MEAN DIAMETER OF SPRAY

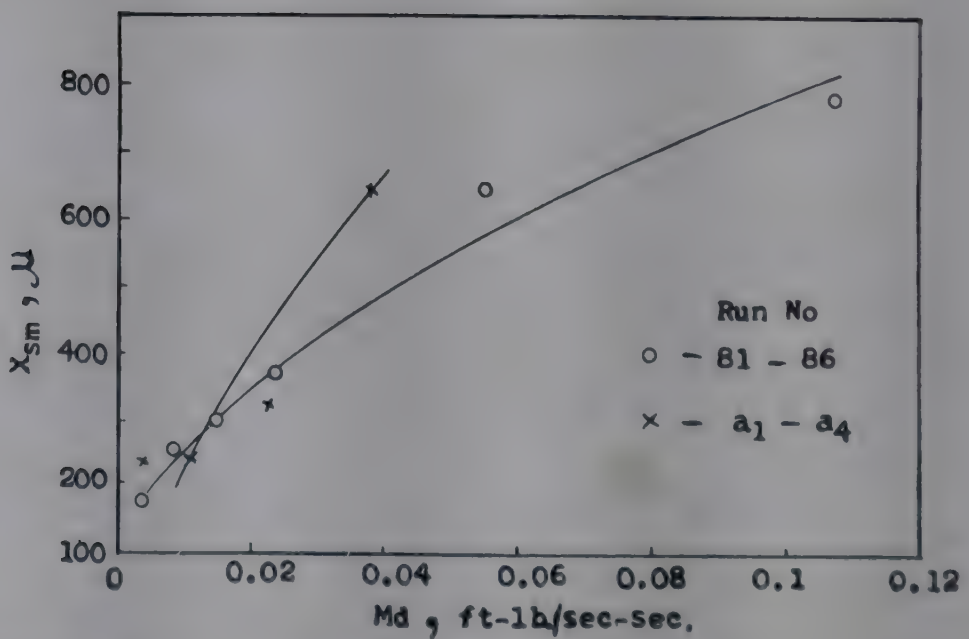


FIG. 9—EFFECT OF DISPERSED PHASE MOMENTUM FLOW ON SÄUTER MEAN DIAMETER OF SPRAY

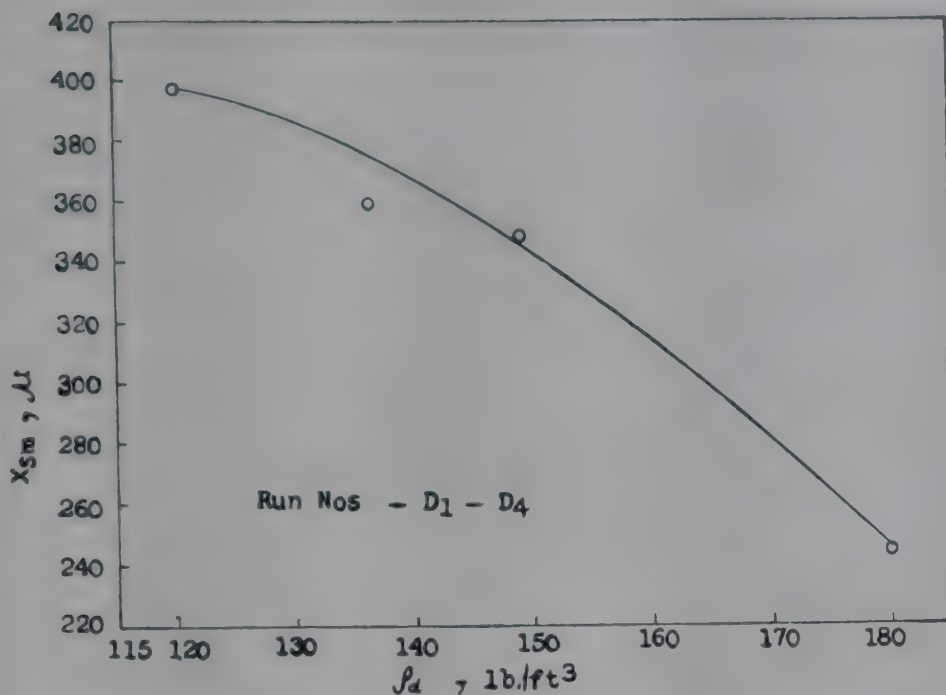


FIG. 10—EFFECT OF DISPERSED PHASE DENSITY ON SÄUTER MEAN DIAMETER OF SPRAY

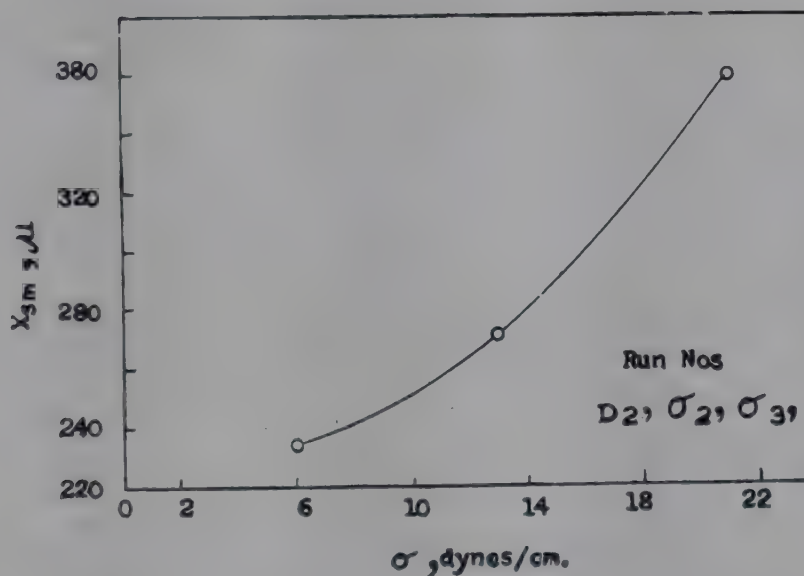
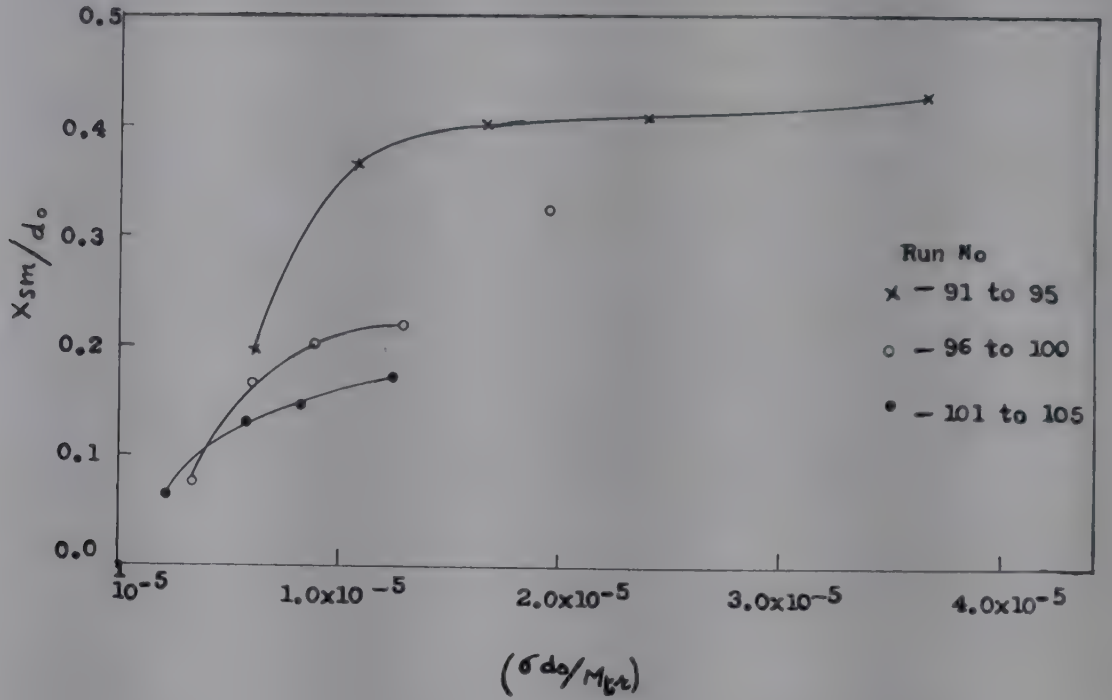
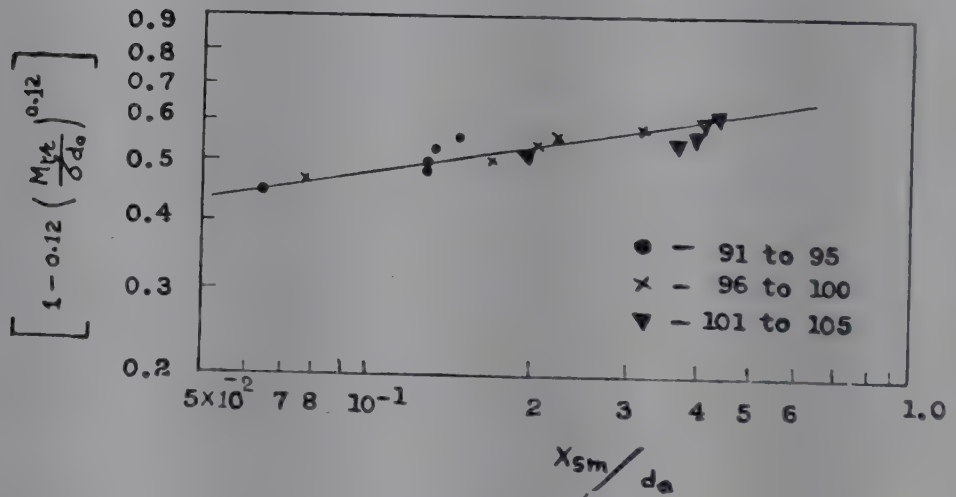


FIG. 11—PLOT OF SÄUTER MEAN DIAMETER VERSUS INTERFACIAL TENSION

The group $\frac{\sigma d_o}{M_v}$ expresses the ratio of the stabilizing forces due to interfacial tension to the disruptive forces acting on the jet. Hence the quantity M_c , the momentum flow rate of continuous phase, can be replaced by the relative momentum between the two streams. As the continuous phase in the present case possesses a tangential velocity component also, a similar group can be introduced to take into account the forces acting in the tangential direction.

FIG. 12—PLOT OF SÄUTER MEAN DIAMETER VERSUS $(\sigma d_o/M_{tr})$ FIG. 13—PLOT OF $1 - 0.12\left(\frac{M_{tr}}{\sigma d_o}\right)^{0.12}$ VERSUS (X_{sm}/d_o)

The groups $\frac{\mu_d}{\sqrt{M_d \rho_d}}$ and $\frac{\mu_c}{\sqrt{M_c \rho_c}}$ are the Reynolds groups for the two streams, where M_d and M_c have been considered to be equal to $W \sqrt{V_a^2 + V_t^2}$. Eq. (3) has been further modified by taking the ratio of the above two groups, and can be written as

$$\frac{X_{sm}}{d_o} = \Psi \left(\frac{\sigma d_o}{M_{ar}}, \frac{\sigma d_o}{M_{tr}}, \frac{M_d}{M_c}, \frac{\rho_d}{\rho_c}, \frac{\mu_c}{\mu_d} \right) \quad (4)$$

The nature of the function for the group has been found to be of the form $\left[1 - C_1 \left(\frac{\sigma d_o}{M_{tr}} \right)^{C_2} \right]$ (Fig. 12 & 13). For the rest of the groups straight

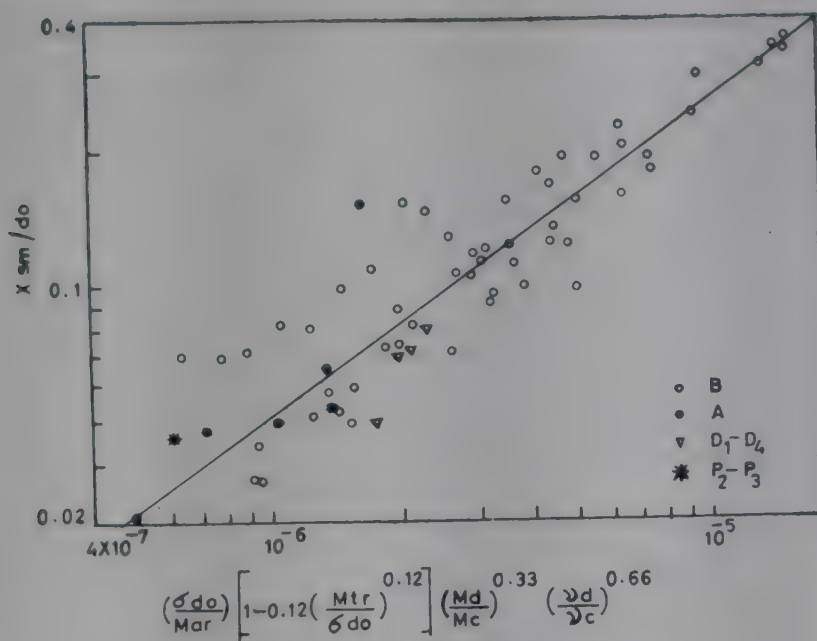


FIG. 14—PLOT OF X_{sm} VERSUS $\frac{\sigma d_o}{M_{ar}} \left[1 - 0.12 \left(\frac{M_{tr}}{\sigma d_o} \right)^{0.12} \right] \left(\frac{M_d}{M_c} \right)^{0.33} \left(\frac{\nu_d}{\nu_c} \right)^{0.66}$

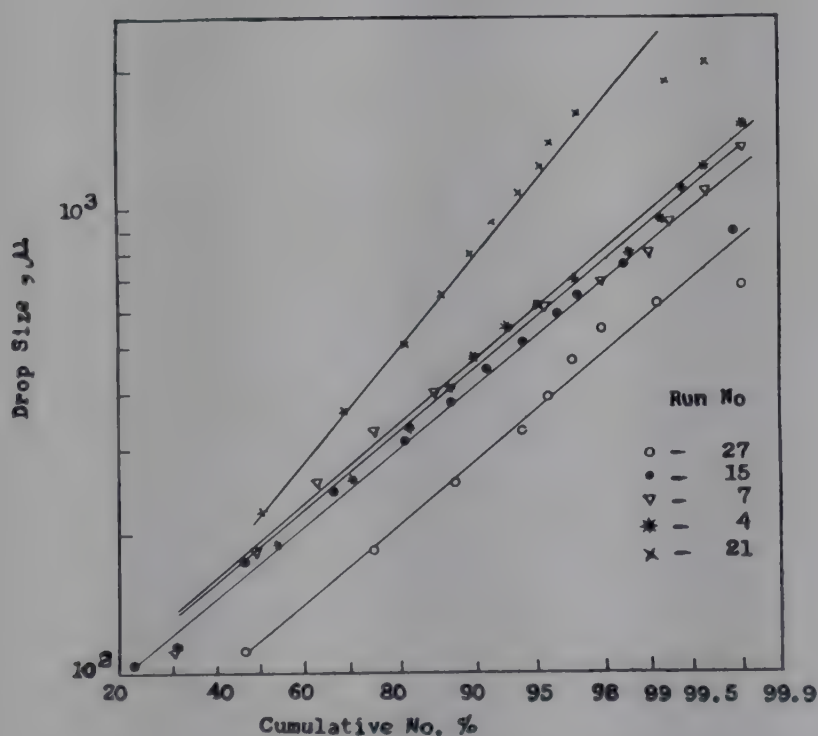


FIG. 15—PLOT OF DROP SIZE VERSUS CUMULATIVE NUMBER

line plots resulted on logarithmic coordinates. Hence the correlation can approximately be written as

$$\frac{X_{sm}}{d_o} = K \left(\frac{\sigma d_o}{M_{ar}} \right) \left[1 - 0.12 \left(\frac{M_{tr}}{\sigma d_o} \right)^{0.12} \right] \left(\frac{M_d}{M_c} \right)^{0.33} \left(\frac{\nu_d}{\nu_c} \right)^{0.66} \quad (5)$$

TABLE 3—COMPARISON OF EXPERIMENTAL AND CALCULATED* VALUES OF SÄUTER MEAN DIAMETER

| RUN No. | X_{sm}, μ | |
|----------------|---------------|-------|
| | Exp. | Calc. |
| 81 | 777 | 719 |
| 82 | 550 | 573 |
| 83 | 373 | 458 |
| 84 | 302 | 407 |
| 85 | 258 | 353 |
| 86 | 185 | 292 |
| D ₁ | 398 | 530 |
| D ₂ | 380 | 507 |
| D ₃ | 346 | 485 |
| D ₄ | 244 | 446 |
| a ₁ | 238 | 249 |
| a ₂ | 245 | 319 |
| a ₃ | 327 | 375 |
| a ₄ | 648 | 427 |

*On the basis of Eq. (5).

Eq. (5) has been plotted in Fig. 14. The equation of the best straight line is found to be

$$\frac{X_{sm}}{d_o} = 1953 \left(\frac{\sigma d_o}{M_{ar}} \right)^{0.7} \left[1 - 0.12 \left(\frac{M_{tr}}{\sigma d_o} \right)^{0.12} \right]^{0.7} \left(\frac{M_d}{M_c} \right)^{0.23} \left(\frac{\nu_a}{\nu_c} \right)^{0.46} \quad (6)$$

A comparison between the values of X_{sm} obtained from Eq. (6) and the experimental values is shown in Table 3.

Sample plots of log-normal probability are shown in Fig. 15. The drop size distribution for all the runs has been found to follow the log-normal distribution.

NOMENCLATURE

- d_o = jet diameter or inside diameter of tube for flow of dispersed phase, *ft*
 M_{ar} = axial momentum difference = $W_o V_{ao} - W_d V_d$, *lb. ft/sec.*²
 M_{tr} = tangential momentum difference = $W_o V_{to} - W_d V_d$, *lb. ft/sec.*²
 M_o = momentum flow rate of continuous phase = $W_o V_{ao}^2 V_{to}^2$, *lb. ft/sec.*²
 M_d = momentum flow rate of dispersed phase, *lb. ft/sec.*²

- V_{ao} = linear axial velocity of continuous phase, $ft/sec.$
 V_{to} = tangential velocity of continuous phase, $ft/sec.$
 V_d = linear axial velocity of dispersed phase, $ft/sec.$
 W_o = mass flow rate of continuous phase, $lb./sec.$
 W_d = mass flow rate of dispersed phase, $lb./sec.$
 X_{sm} = Sauter mean diameter, ft
 σ = interfacial tension, $lb./sec.^2$
 ρ_d = density of dispersed phase, $lb./ft^3$
 ρ_o = density of continuous phase, $lb./ft^3$
 μ_d = viscosity of dispersed phase, $lb./ft-sec.$
 μ_o = viscosity of continuous phase, $lb./ft-sec.$
 ν_o = kinematic viscosity of continuous phase, $ft^2/sec.$
 ν_d = kinematic viscosity of dispersed phase, $ft^2/sec.$
 Q_o = volumetric flow rate of continuous phase, $ft^3/sec.$
 Q_d = volumetric flow rate of dispersed phase, $ft^3/sec.$

REFERENCES

1. SÄUTER, J., *Forsch. Ing. Wes.*, No. 297, (1926).
2. LITTAYE, G., *C. R. Acad. Sci. Paris*, **217** (1943), 99, 340; **218** (1944), 440.
3. SCHEUBEL, F. N., *Jahr. Wiss. Ges. Luftfahrt*, (1927), 140; *National Advisory Committee, Aeronut. Tech. Mem.*, (1931), 644.
4. CASTLEMAN, R. A., Jr, *J. Res. nat. Bur. Stand.*, **6** (1931), 281, 369.
5. NUKIYAMA, S. & TANASAWA, Y., *Trans. Soc. mech. Engrs, Japan*, **4**(14) (1938), 86; **4**(15) (1938), 138; **5**(18) (1939), 63, 68; **6**(22) (1940), II-7; **6**(23) (1940), II-8.
6. LEWIS, H. C., EDWARDS, D. G., GONGLIA, H. J., RICE, R. I. & SMITH, L. W., *Industr. Engng Chem.*, **40** (1948), 67.
7. WETZEL, R. H. & MARSHALL, W. R., Jr, Paper presented at Washington D. C. National Meeting, *Amer. Inst. chem. Engrs*, (March 1954).
8. LANE, W. R., *Industr. Engng Chem.*, **43** (1951), 1312.
9. MARSHALL, W. R., Jr, *Atomization and Spray Drying*, CEP. Monogr. Ser., **50** (2), (1954).
10. HINZE, J. O., *Appl. sci. Res., Hague*, **1A** (1949) 273; *Amer. Inst. chem. Engrs J.*, **1** (1955), 289.
11. KLMOGRAFF, A. N., (cited in Sleicher in 11).
12. SLEICHER, C. A., *Amer. Inst. chem. Engrs J.*, **8**(4) (1962).
13. MUGGLE, R. A., *Amer. Inst. chem. Engrs J.*, **6** (1960), 3.

Dispersed Phase Hold-up in a Pulsed Sieve Plate Extraction Column

P. C. DEB & D. K. DUTT

Chemical Engineering Department, Jadavpur University
Calcutta 32

Dispersed phase hold-up measurements have been done in a pulsed sieve plate liquid-liquid extraction column (internal diam., 7.5 cm. and height, 1.52 m.) for isoamyl alcohol-water system. The isoamyl alcohol phase was dispersed with water as the continuous phase. The effects of dispersed phase flow rates, continuous phase flow rates, pulsed amplitudes and pulsed frequencies on dispersed phase hold-up have been studied. Hold-up is found to increase with increase in dispersed flow rates, other variables remaining constant. Variations of continuous phase flow rates show negligible effect on hold-up. Increase in pulsed amplitudes at constant flow rates and constant frequencies shows a general increase in hold-up.

Variations of frequencies at constant amplitudes and flow rates show a minimum value of hold-up at a particular frequency, known as transition frequency. The transition frequency is found to be practically independent of the dispersed and the continuous phase flow rates, but related to the pulsed amplitude only for a given system and a given column geometry, as determined from the experimental data of the authors as well as the data of other workers on different other systems.

Attempts have also been made to find the 'characteristic velocity', at different pulsed frequencies and amplitudes from the hold-up data. Only in the regions of high amplitudes at a constant frequency and high frequencies at a constant amplitude, determination of characteristic velocities has been possible.

The characteristic velocities thus determined have been shown to increase with decrease in frequency at a constant amplitude, and also to increase with decrease in amplitude at a constant frequency.

Hold-up in the present study is defined as the average per cent of the total effective volume of the column occupied by the dispersed organic phase

at steady-state operation. Dispersed phase hold-up in pulsed sieve plate extraction column is a measure of interfacial contact area and is also necessary for the calculation of residence time in the analysis of mass transfer rates.

Though several workers have reported hold-up data and correlations for unpulsed conventional extraction columns¹⁻⁴, reported data on hold-up for pulsed sieve plate extraction column are rather few. Thornton⁵ has applied hold-up values for correlating characteristic droplet velocity at flooding conditions and mass transfer data in pulsed sieve plate extraction column. Cohen and Beyer⁶ have reported the effect of flow rates and pulse amplitudes on volumetric hold-up ratios in a pulsed sieve plate extraction column. Sehmel and Babb⁷ have recently investigated the effect of pulse amplitude, frequency and phase flow rates on dispersed phase hold-up data for three different organic solvents as the individual dispersed phases and with water as the continuous phase in a pulsed sieve plate extraction column. They have used their results in the analysis of continuous phase longitudinal mixing data.

EXPERIMENTAL SET-UP AND PROCEDURE

The column used for the study (Fig. 1) was constructed of pyrex glass of 7.5 cm. internal diam. and 1.52 m. height. It was built of five individual glass sections joined together by stainless steel flanges. The perforated plates made of 3 mm. thick stainless steel were supported by central stainless steel rods of 3.2 mm. diam. in the top four glass sections, where the plates fitted closely. The average plate spacing used was 5 cm., and there were a total of 25 plates, with 57 perforations on each plate. The diameter of each perforation was 3.17 mm. (1/8 in.) which corresponds to *c.* 10.2 per cent free area. Thus the column and the plate geometry were kept fixed.

The 5-gal. feed vessels and receiving tanks, the 10-gal. overhead tanks, pipelines and regulating cocks were all made of stainless steel. Two glass rotameters were used to meter the flow of liquids into the column proper. The liquids entered the column through two stainless steel distributors.

The liquid in the column was pulsed by a reciprocating mechanism, driven by one 0.5 h.p. electric motor through a reduction gear box and a separate belt driven speed-regulating unit. The amplitude of pulsation was controlled by an eccentric mechanism. A stepwise change in the eccentric position gives different amplitudes varying from 7.9 to 17.5 mm. in five steps. The pulse frequency could be varied from 0 to 180 c./min. in the speed-regulating device.

In the present study, isoamyl alcohol was used as the dispersed phase and water as the continuous phase.

The aqueous phase was fed in a feed vessel C_1 , whence it was pumped into the overhead tank D_1 . Isoamyl alcohol was similarly fed into the other vessel C_2 , and thence into the overhead tank D_2 through the action of com-

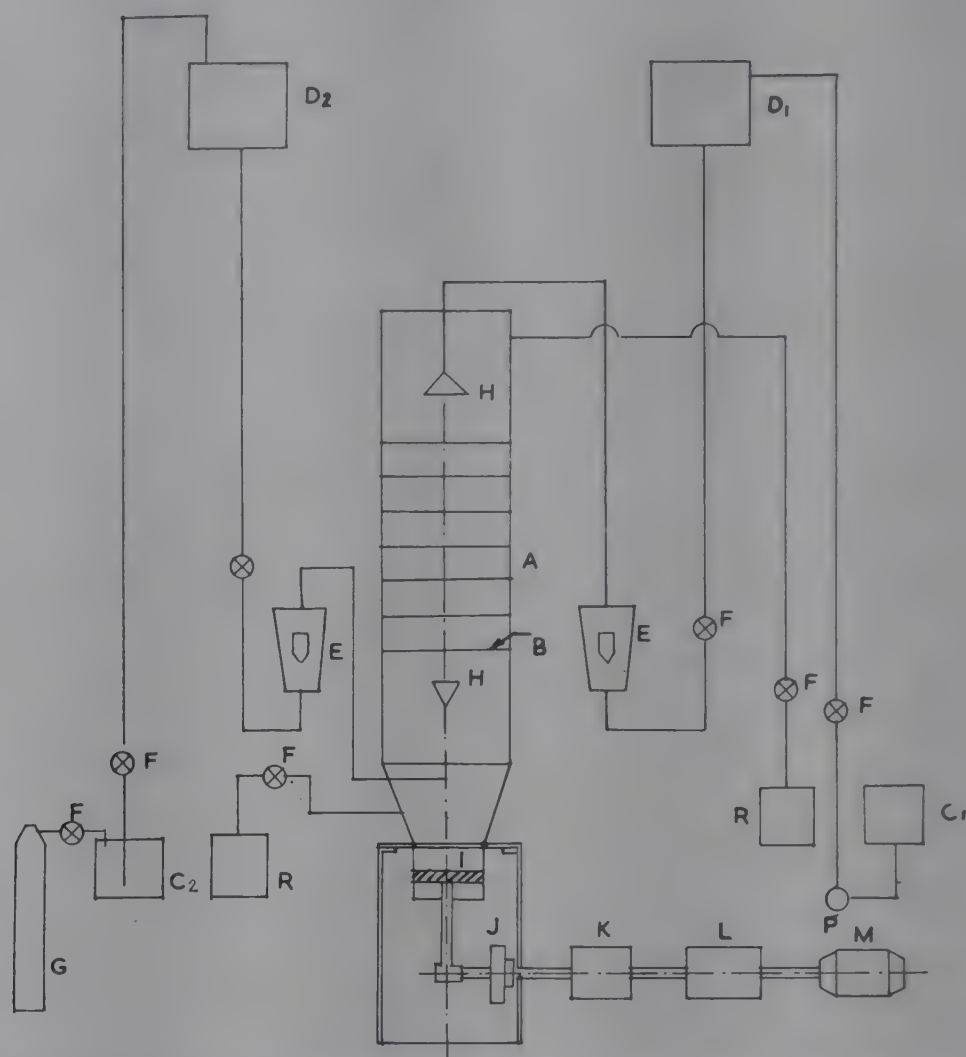


FIG. 1—EXPERIMENTAL SET-UP [A, Tower; B, Plates; C₁, C₂, Feed vessels; D₁, D₂, Overhead tanks; E, Rotameters; F, Regulating cocks; G, Gas cylinder; H, Distributors; I, Piston; J, Cam; K, Speed reduction gear box; L, Belt-driven speed fixation unit; M, Motor; P, Pump; R, Receivers]

pressed nitrogen. The aqueous phase was then allowed to enter the column at a pre-determined rate with the solvent phase outlet cock open, and the water phase outlet cock closed. When the column was almost full of the aqueous phase, the pulsator was started at the desired frequency and amplitude. The dispersed phase was run into the column at the desired rate. The outlet cocks were then regulated to maintain the solvent-water interface at a fixed position very near the water phase inlet. This was noted as the mid-point of the two extreme positions of the interface corresponding to the upward and the downward strokes of the pulse mechanism. The flow rates of the two phases were measured under steady states by collecting the liquids of known volumes in known intervals of time. The hold-up measurement was started by closing the water inlet and outlet valves and the organic phase inlet valve simultaneously after the steady state condition had reached.

As a result the interface between the disengaged organic phase and the two-phase region receded below the initial interface position. The

pulsation was continued till all the solvent droplets had risen to form a continuous phase in the upper part of the column. The pulsation was stopped and the new interface position was noted similarly as for the initial one. The difference in the two positions gives the volume of the dispersed organic phase.

The fractional hold-up was then calculated as the ratio of the volume of the organic phase to the total effective volume of the column.

The experimental measurements were made at ambient room temperature varying from 28° to 32°C.

RESULTS AND DISCUSSION

The effect of the dispersed phase flow rate, V_d , on hold-up at nearly constant continuous phase velocity, constant amplitude, and frequency is shown in Fig. 2. The hold-up is found to be increasing appreciably with increase in V_d .

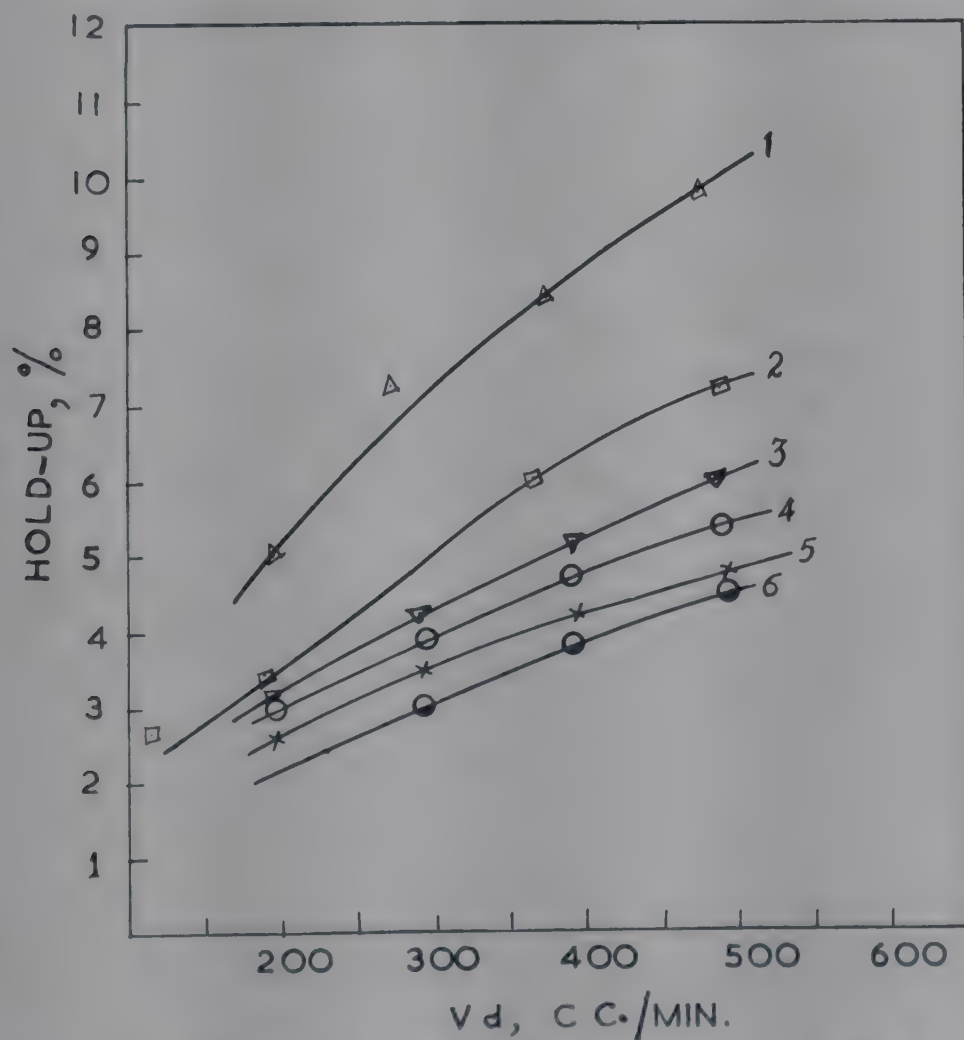


FIG. 2—PLOT OF HOLD-UP VERSUS V_d AT CONSTANT V_c [(1) $a=10.2$ mm. & $f=90$ c./min.; (2) $a=13$ mm. & $f=50$ c./min.; (3) $a=7.9$ mm. & $f=33$ c./min.; (4) $a=9.9$ mm. & $f=31$ c./min.; (5) $a=7.9$ mm. & $f=90$ c./min.; (6) $a=7.9$ mm. & $f=50$ c./min. V_c for all = 365–390 $\text{cm}^3/\text{min.}$]

This observation may be compared with that of Cohen and Beyer⁶, who have shown the effect of dispersed phase flow rate on volumetric hold-up (defined by them as the ratio of the volume of dispersed phase to the volume of continuous phase) at constant pulse frequency, amplitude and different continuous phase flow rates for the system isoamyl alcohol-boric acid-water in 2.54 cm. diam. pulsed sieve plate column. Increase in dispersed phase flow rates is found to increase the hold-up appreciably, similar to the present observation. The effect of the continuous phase flow rate, however, on hold-up at constant pulse frequency, amplitude and nearly constant dispersed phase velocity, is found to be negligible in the present study as shown in Fig. 3. Although this observation very well compares with that of Sehmel and Babb,⁷ it is not similar to that of Cohen and Beyer⁶, who have shown an appreciable increase in the hold-up values with increase in continuous phase flow rates, other factors remaining constant.

The effect of pulsed amplitude on hold-up at constant flow rates and constant frequencies is shown in Fig. 4. It is clear from the figure that hold-up values increase with amplitudes. The effect of pulsed frequency on hold-up at different constant amplitudes and flow rates is represented in Fig. 5 for the constant amplitudes of 7.9 mm. Similar behaviour is shown at three more amplitudes 10, 13.1 and 16 mm.

At low values of frequencies, the hold-up decreases as the frequency is increased, and passes through a minimum value, beyond which the hold-up increases with increase in frequencies at constant amplitudes and flow rates. This observation is very similar to that of Sehmel and Babb⁷, who have published hold-up data for three systems, viz. hexane-water, benzene-water and methyl isobutyl ketone-water for 2 in. pulsed sieve plate column containing 43 plates with 2 in. plate spacing, each plate having 1/8 in. diam. holes, corresponding to 23 per cent free area.

The frequency corresponding to the minimum hold-up has been termed transition frequency, f_H , by Sehmel and Babb, as it represents a transition region between the mixer-settler type of operation in the lower frequency range, and emulsion type operation in the higher frequency range. The two types of operation have been visually observed in the present experimental runs, though the emulsion type operation predominated compared to the mixer-settler types of operation.

The transition frequencies have been determined from Fig. 5, and other amplitudes studied and have been plotted against dispersed phase flow rates V_d at different constant amplitudes and constant continuous phase flow rates V_c , as shown in Fig. 6. This plot shows that the transition frequency is independent of the dispersed phase flow rates, if amplitude is kept constant.

The effect of different continuous phase flow rates V_c on hold-up at different frequencies and constant V_d and amplitude is shown in Fig. 7. The transition frequency, determined from Fig. 7, shows that it is also

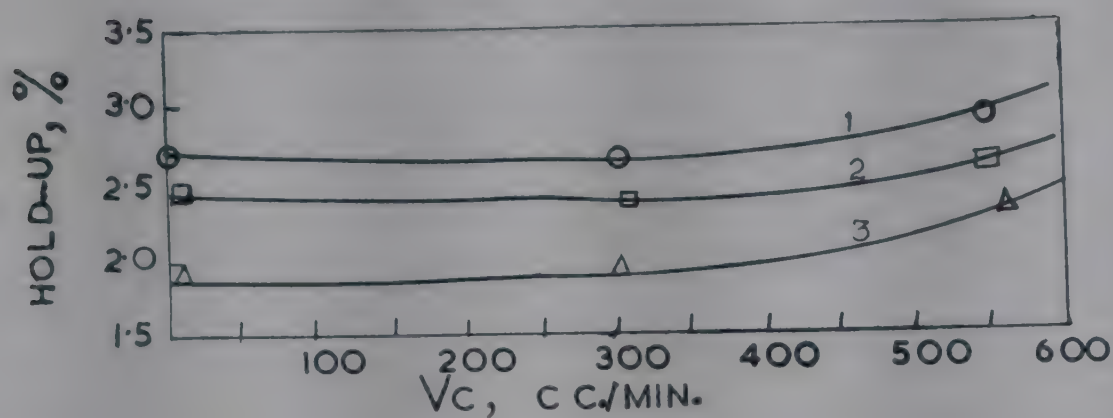


FIG. 3—PLOT OF HOLD-UP VERSUS V_c [$a=7.9$ mm. & $V_d=190-198$ cm.³/min. (1) $f=30$ c./min.; (2) $f=90$ c./min.; (3) $f=72$ c./min.]

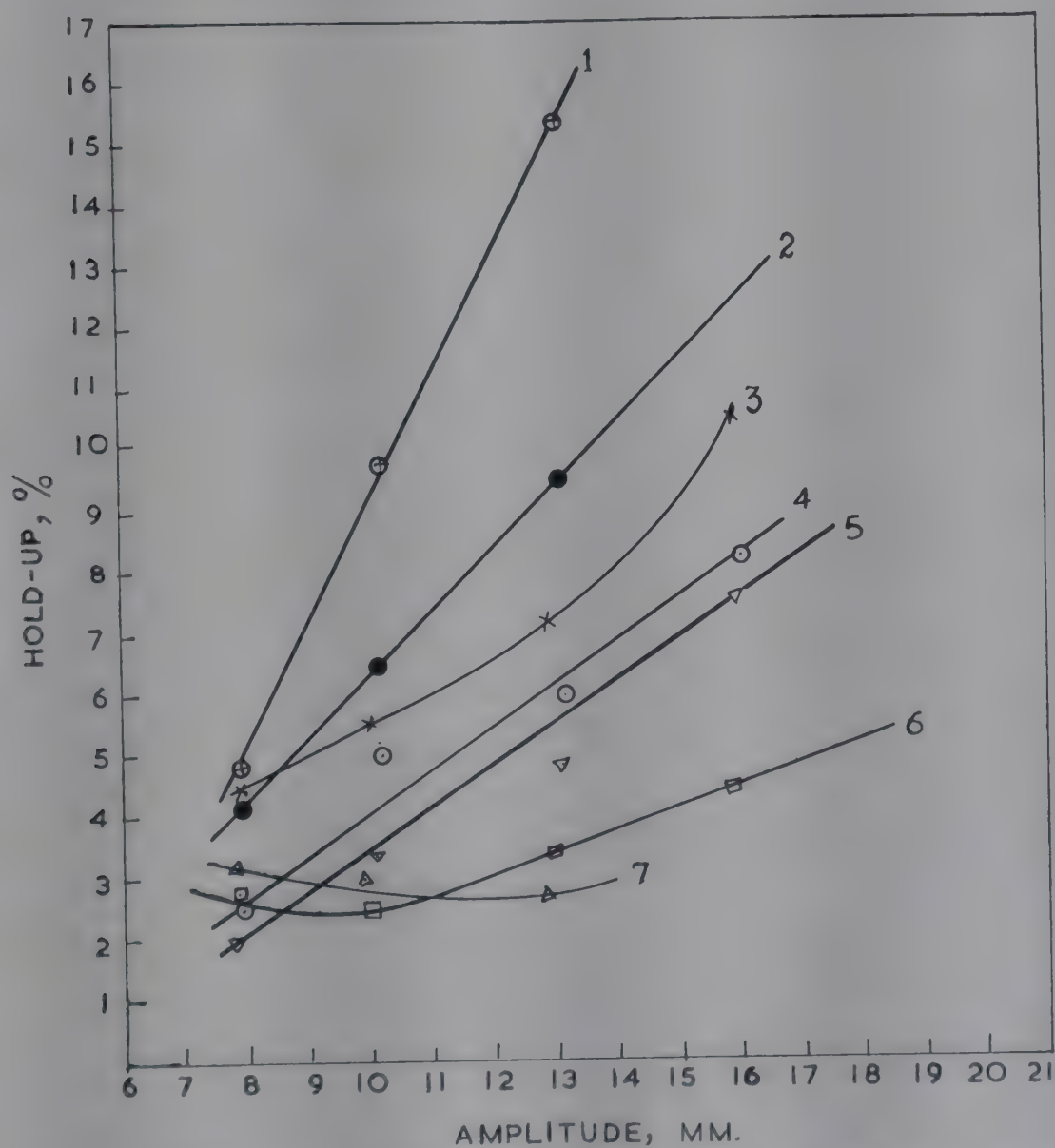


FIG. 4—PLOT OF HOLD-UP VERSUS AMPLITUDE [$V_d=490$ cm.³/min. & $V_c=365$ cm.³/min. (1) $f=90$ c./min.; (2) $f=70$ c./min.; (3) $f=50$ c./min.; $V_d=190$ cm.³/min.; $V_c=365$ cm.³/min.; (4) $f=90$ c./min.; (5) $f=70$ c./min.; (6) $f=50$ c./min.; (7) $f=31$ c./min.]

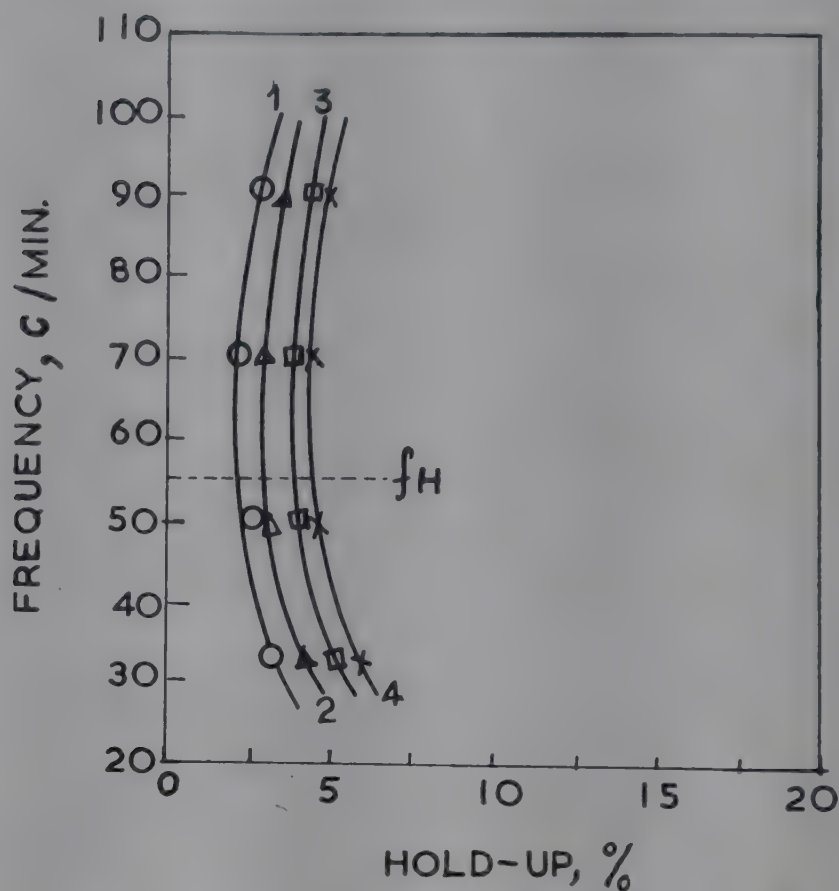


FIG. 5—PLOT OF FREQUENCY VERSUS V_d [$V_c = 360-390 \text{ cm}^3/\text{min.}$ & $a = 7.9 \text{ mm.}$ (1) $V_d = 195 \text{ cm}^3/\text{min.}$; (2) $V_d = 295 \text{ cm}^3/\text{min.}$; (3) $V_d = 390 \text{ cm}^3/\text{min.}$; (4) $V_d = 490 \text{ cm}^3/\text{min.}$]

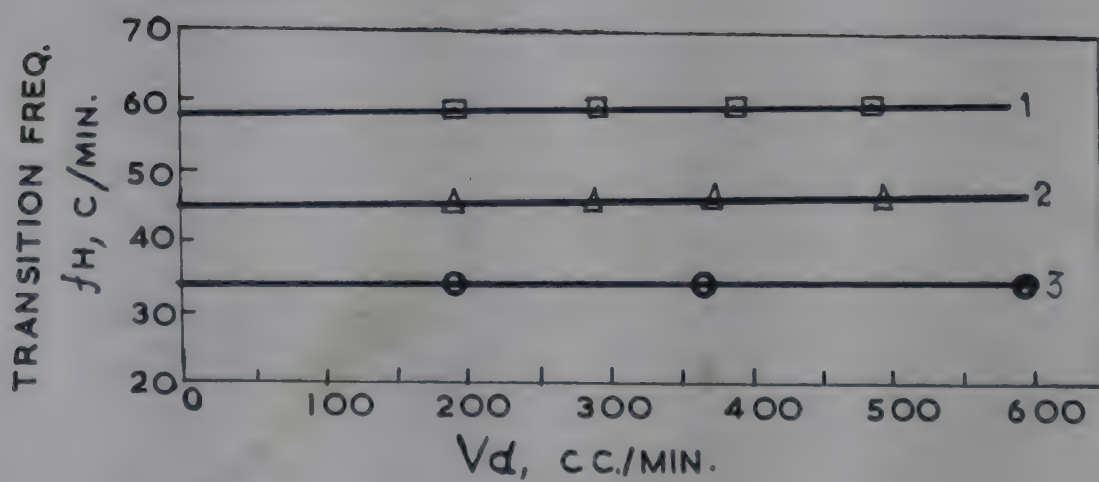


FIG. 6—PLOT OF TRANSITION FREQUENCY VERSUS V_d [$V_c = 365-390 \text{ cm}^3/\text{min.}$ (1) $a = 7.9 \text{ mm.}$; (2) $a = 10.0 \text{ mm.}$; (3) $a = 13.1 \text{ mm.}$]

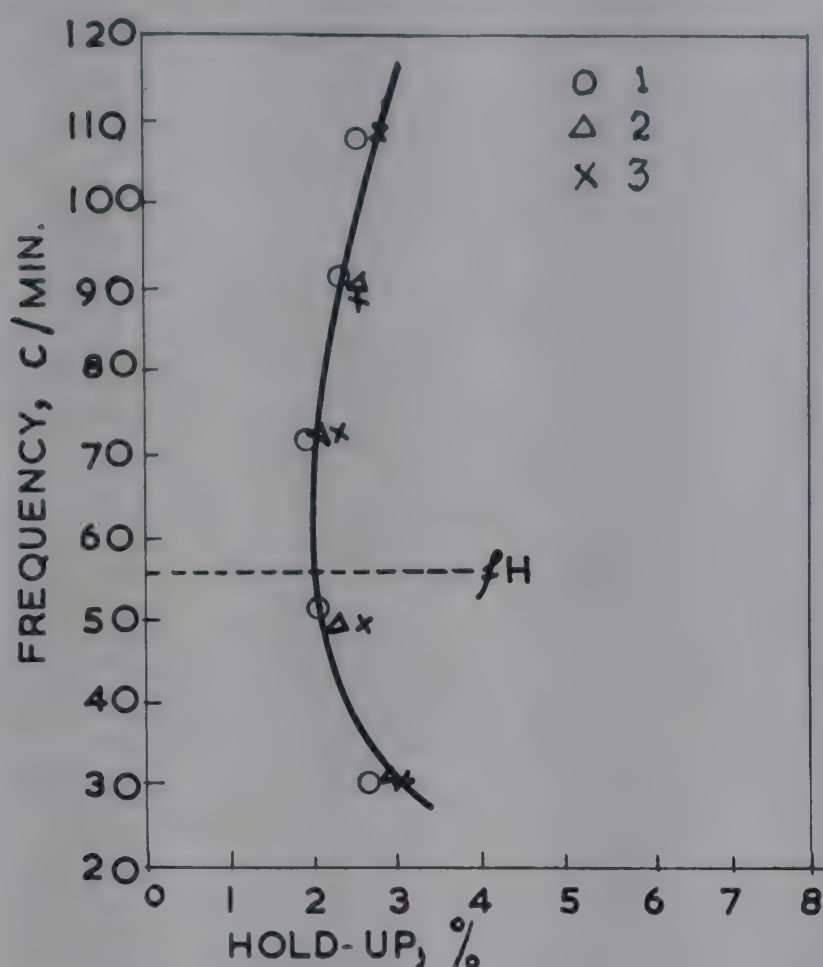


FIG. 7—PLOT OF FREQUENCY VERSUS HOLD-UP [$V_d=190 \text{ cm.}^3/\text{min.}$ & $a=7.9 \text{ mm.}$
(1) $V_o=0 \text{ cm.}^3/\text{min.}$; (2) $V_o=300 \text{ cm.}^3/\text{min.}$; (3) $V_o=550 \text{ cm.}^3/\text{min.}$]

independent of the continuous phase flow rates V_o , if amplitude is kept constant. Similar behaviour has also been reported by Sehmel and Babb⁷.

The values of the transition frequency f_H at different amplitudes have been plotted in Fig. 8, showing a linear relationship with a negative slope in semilog plot. On the same plot, the data of Sehmel and Babb⁷ have also been presented, showing straight lines of the same slope for three other systems.

All these graphs may be represented by the equation

$$\log_{10} a = C - 0.011 f_H \quad (1)$$

where C is the intercept on the Y-axis, and its value is different for the different systems.

Sehmel and Babb have shown from their data that the intercept C is a linear function of the product $\mu_d \gamma \Delta \rho$, for the three different systems studied by them, where μ_d is the viscosity of the dispersed phase, γ is the interfacial tension and $\Delta \rho$ is the difference of the phase density. The value of C calculated for the system under investigation has been plotted against $\mu_d \gamma \Delta \rho$ in Fig. 9, along with the data of Sehmel and Babb, which shows that the

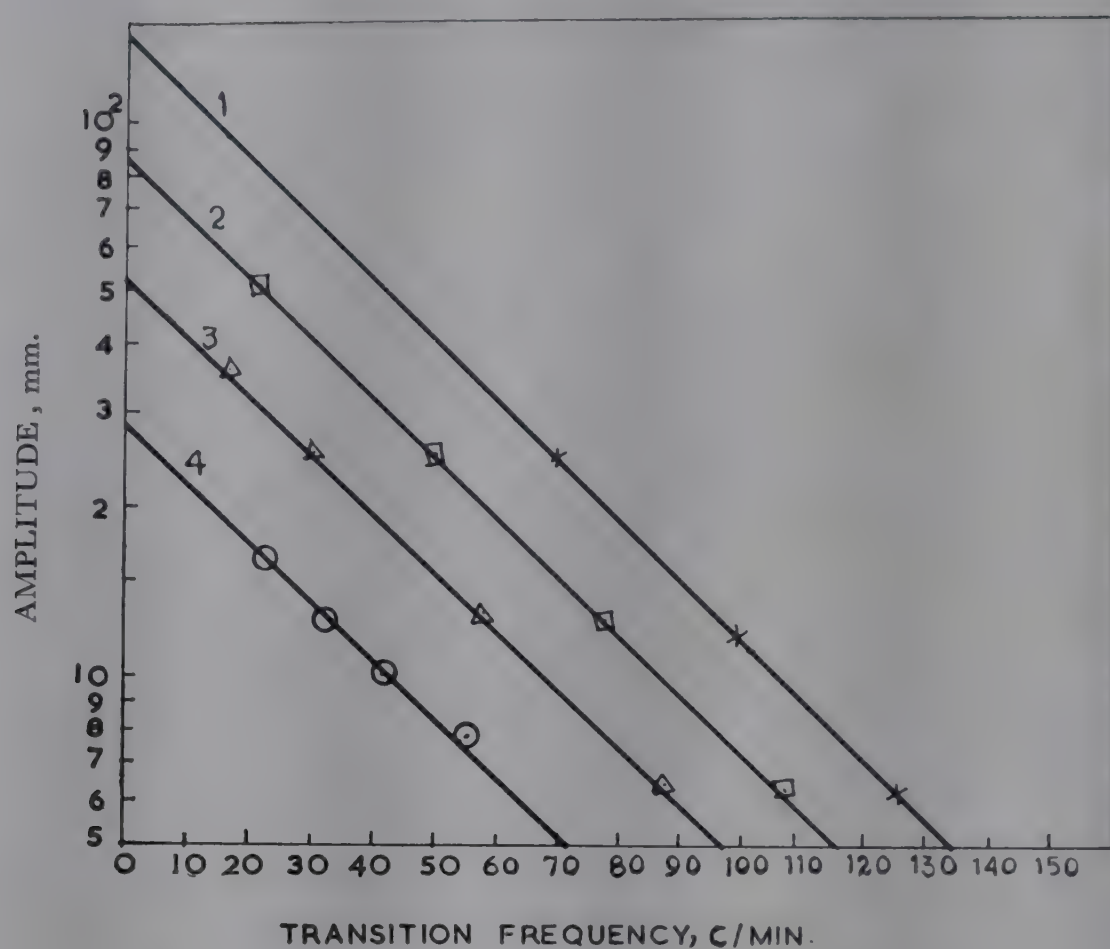


FIG. 8—PLOT OF AMPLITUDE VERSUS TRANSITION FREQUENCY [(1) Hexane-water; (2) Benzene-water; (3) M.I.B.K.-water; (4) Isoamyl alcohol-water]

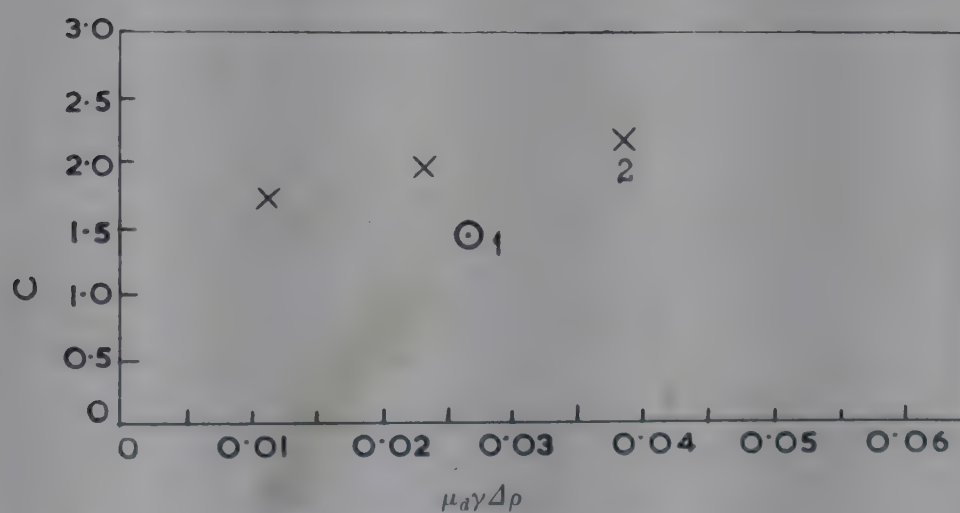


FIG. 9—PLOT OF C VERSUS $\mu_d \gamma \Delta \rho$ [(1) Author's data; (2) Schmel & Babb's data]

linear relationship is not applicable for the present system, studied with column and plate geometry, different from that used by Sehmel and Babb.

An attempt has also been made to find the 'characteristic velocity', i.e. the mean droplet velocity at zero flow rates, as defined by Gayler, Roberts and Pratt², and used by Thornton⁵ for studying flooding and mass transfer rate in pulsed sieve plate column.

As shown by Gayler, Roberts and Pratt² the characteristic velocity \bar{V}_o is related to fractional hold-up X by the equation

$$\frac{V_d'}{X} + \frac{V_c'}{1-X} = \bar{V}_o (1-X) \quad (2)$$

where V_d' and V_c' are linear superficial velocity of the dispersed and the continuous phase respectively, provided droplet coalescence is absent.

Rearranging,

$$V_d' + \frac{X}{1-X} V_c' = \bar{V}_o X (1-X) \quad (3)$$

A plot of experimental values of $\left(V_d' + \frac{X}{1-X} V_c'\right)$ as ordinate and $X(1-X)$ as abscissa should give straight lines passing through the origin of slope equal to \bar{V}_o in absence of droplet coalescence. Such a plot at nearly constant pulsed amplitude of 13 mm. at different frequencies is shown in Fig. 10. Also the same plot at constant frequency of 90 c./min. at different pulsed amplitudes is shown in Fig. 11.

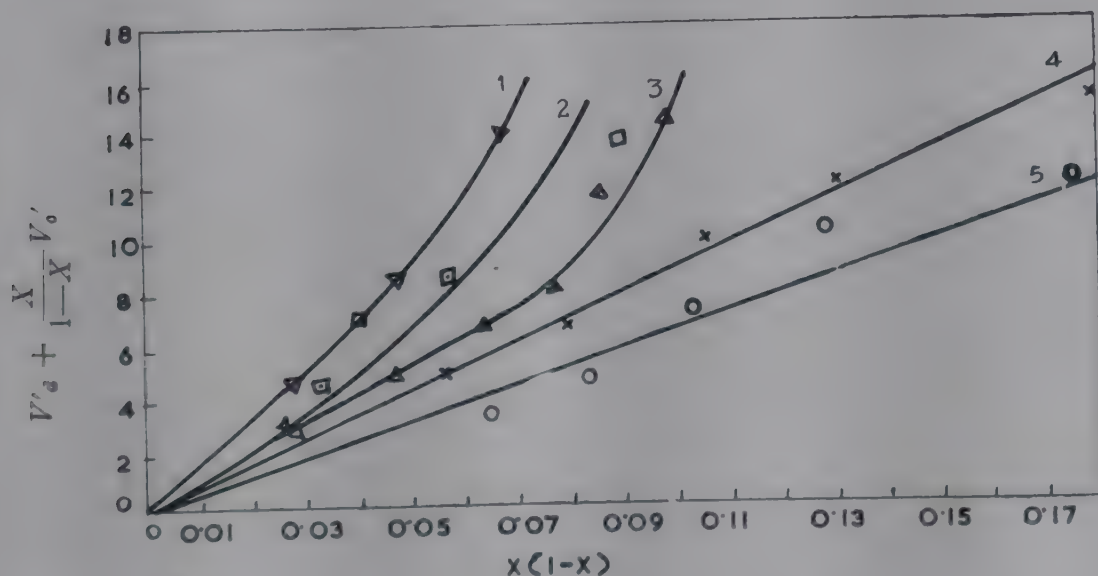


FIG. 10—PLOT OF EXPERIMENTAL VALUES OF $\left[V_d' + \frac{X}{1-X} V_c'\right]$ VERSUS $X(1-X)$ AT CONSTANT PULSED AMPLITUDE AND AT DIFFERENT FREQUENCIES [$a=13$ mm. (1) $f=33$ c./min.; (2) $f=50$ c./min.; (3) $f=70$ c./min.; (4) $f=90$ c./min.; (5) $f=110$ c./min.]

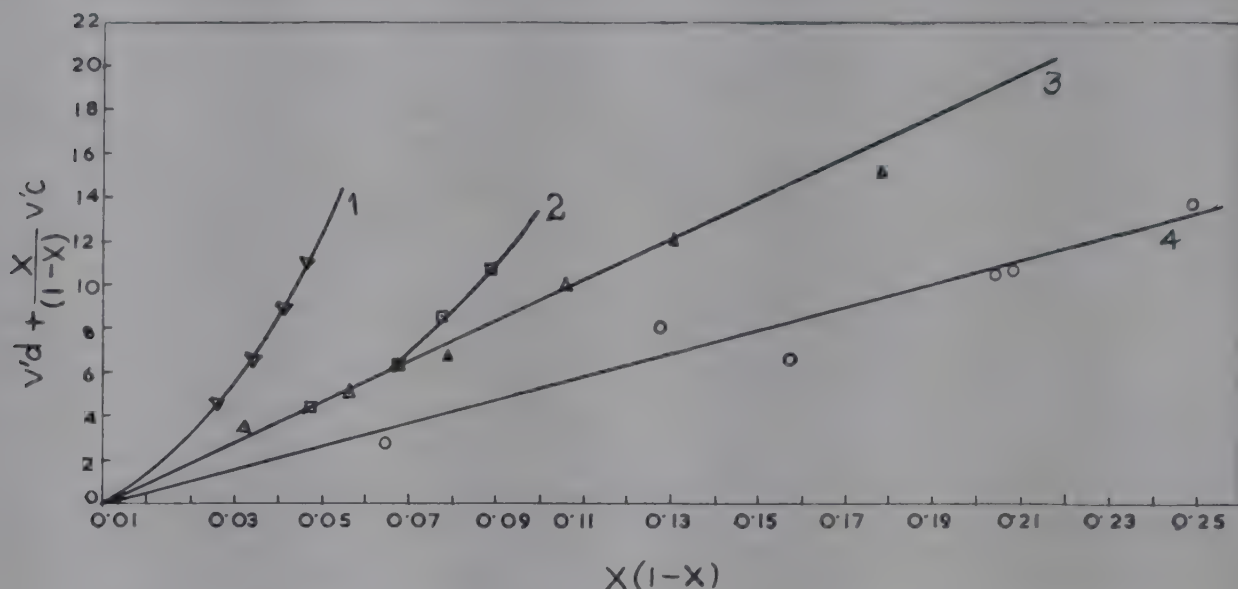


FIG. 11—PLOT OF $(V'_d + \frac{X}{(1-X)} V_o)$ VERSUS $X(1-X)$ AT CONSTANT FREQUENCY AND AT DIFFERENT PULSED AMPLITUDES [$f=90$ c./min. (1) $a=7.9$ mm.; (2) $a=10.2$ mm.; (3) $a=13.0$ mm.; (4) $a=16.0$ mm.]

As is shown in Fig. 10, straight line relationship is only obtained at the higher frequencies for the given amplitude, giving the values of slopes, i.e. the characteristic velocities \bar{V}_o , increasing with decrease in frequency. At lower frequencies, however, the graphs do not give straight line relationship, which indicate that Eq. (2) cannot be applied to give the characteristic velocities, at the conditions involved. Similarly, as shown in Fig. 11, the slopes obtained at a constant frequency of 90 c./min. are constant only at higher amplitudes (16 and 13 mm.), showing an increase in characteristic velocity with decrease in pulse amplitude. At lower amplitudes, again, Eq. (2) fails to give the characteristic velocities at the conditions involved.

These observations may be explained as due to the presence of droplet coalescence at low pulse frequencies and amplitudes.

ACKNOWLEDGEMENT

The authors acknowledge with thanks the grants received from the Union Ministry of Education under the Fundamental Grant-in-aid for equipment and under the Research Training Scheme for the scholarship to carry on the research project.

NOMENCLATURE

- V_c = aqueous phase volumetric flow rate, $\text{cm.}^3/\text{min.}$
- V_d = solvent phase volumetric flow rate, $\text{cm.}^3/\text{min.}$
- V'_c = aqueous phase superficial linear velocity, $\text{cm.}/\text{min.}$
- V'_d = solvent phase superficial linear velocity, $\text{cm.}/\text{min.}$
- \bar{V}_o = characteristic velocity, i.e. mean droplet velocity when $V' = 0$, and $V'_d \rightarrow 0$, $\text{cm.}/\text{min.}$
- a = amplitude of pulsation, mm.
- f = frequency of pulsation, c./min.

- fH = transition frequency, $c./min.$
 γ = interfacial tension, $dynes/cm.$
 μ_d = solvent phase viscosity, $P.$
 $\Delta\rho$ = phase density difference, $g./cc.$
 X = fractional dispersed phase hold-up
 C = constant as defined by Eq. (1)

REFERENCES

1. GAYLER, R. & PRATT, H. R. C., *Trans. Instn chem. Engrs, Lond.*, **29** (1951), 110.
2. GAYLER, R., ROBERTS, N. W. & PRATT, H. R. C., *Trans. Instn chem. Engrs, Lond.*, **31** (1953), 57.
3. WICKS, C. E. & BECKMANN, R. B., *Amer. Inst. chem. Engrs J.*, **1** (1955), 426.
4. GHOSAL, S. R., CHATTERJEE, S. N. & DUTT, D. K., *Trans. Indian Inst. chem. Engrs*, **11** (1958-59), 23.
5. THORNTON, J. D., *Trans. Inst. chem. Engrs, Lond.*, **35** (1957), 316.
6. COHEN, R. M. & BEYER, G. H., *Chem. Engng Progr.*, **49** (1953), 279.
7. SEHMEL, G. A. & BABB, A. L., *Process Design & Developm. (Industr. Engng Chem.)*, **2**(1) (1963), 38.

Studies on Fluidization of Pyrites

A. K. MITRA & S. K. NANDI

Department of Chemical Engineering, Indian Institute of Technology
Kharagpur

Fluidization of Amjhore pyrites has been done in a 4.445 cm. diam. and 57.75 cm. long tube, using air at room temperature. The minimum fluid voidage and minimum mass rate for onset of fluidization have been determined for different particle sizes and bed heights.

Pyrites is available in huge quantities at Amjhore in Bihar and the Government of India have recently established a Pyrites and Chemicals Development Corporation with the object of recovering elemental sulphur and also manufacturing sulphuric acid from pyrites. The composition of Amjhore pyrites is as follows¹: Sulphur, 42.80; iron, 38.20; insolubles, 14.50; copper, 0.01; and arsenic, 0.05 per cent.

Production of sulphur dioxide and elemental sulphur will be most economical if pyrites is treated in fluidized bed. The present investigation has been undertaken with a view to studying some aspects of fluidization of pyrites, e.g. minimum fluid voidage and onset of fluidization for different particle sizes and bed heights. Such data^{2,3} are available for soft brick, coal, coke, glass, etc. but not for pyrites.

EXPERIMENTAL PROCEDURE

Representative samples from 2 tons of pyrites obtained from Amjhore were crushed in a ball mill to obtain three different sizes ranging from 18 to 72 B.S. mesh. The fluidization apparatus (Fig. 1) used is almost similar to the one used by Parent and Steiren⁴. The fluidization tube is made of transparent plastic of 4.445 cm. diam. and 57.75 cm. length. The pyrites were fluidized taking four different bed heights ranging from 9.9 to 24.5 cm. Fluidiza-

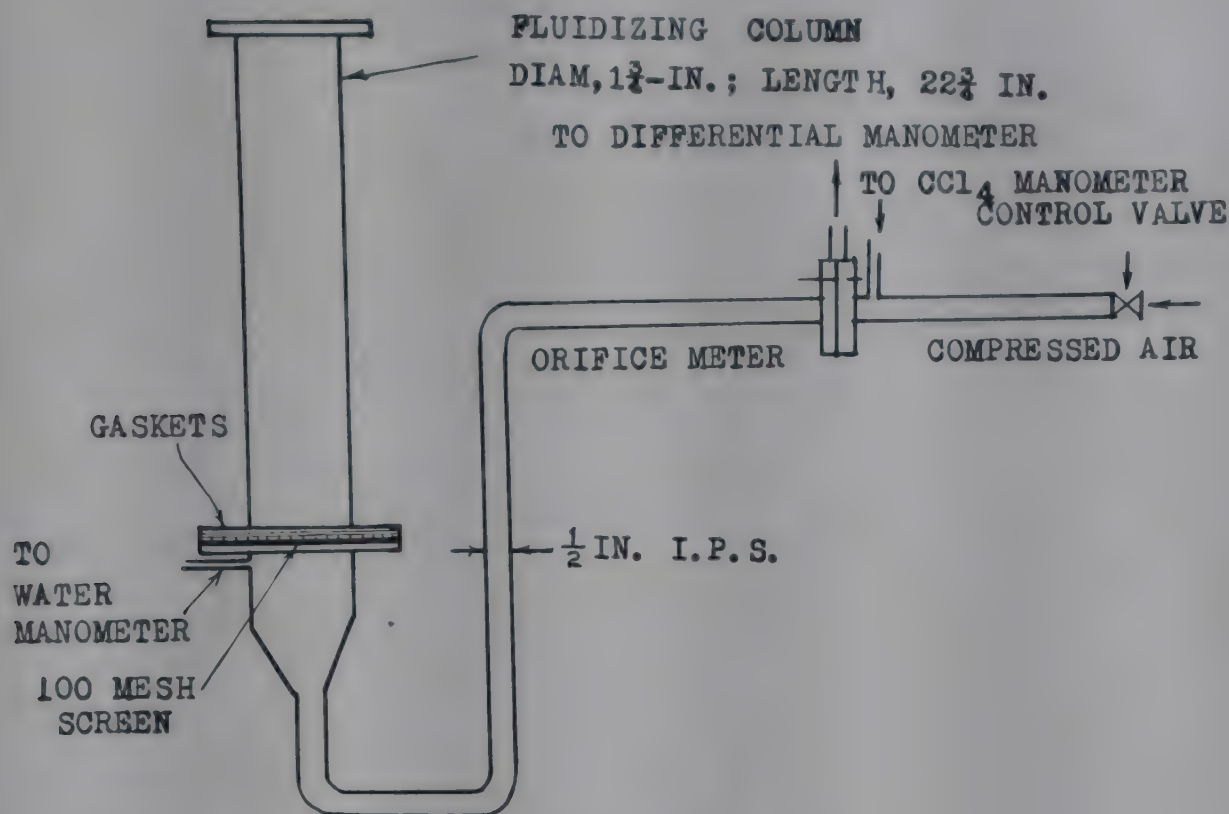


FIG. 1—EXPERIMENTAL SET-UP

tion was done using air at room temperature. A perforated wire screen of 150μ opening was fixed at the bottom of the fluidization tube for uniform distribution of air. Pressure drop across the bed was measured by a manometer with its low pressure arm open to the atmosphere. The rate of air flow was measured by an orifice meter, which was calibrated against a standard gas meter. The static pressure at the orifice inlet was also measured by a manometer.

The minimum fluid voidage and the minimum fluidization mass flow rate were calculated by standard equations⁵:

$$\epsilon_{mf} = 1 - \frac{W}{L_{mf} A (\rho_s - \rho_F)} \quad (1)$$

$$G_{mf} = \frac{0.005 D_p^2 g_0 \rho_F (\rho_s - \rho_F) \Phi_s^2 \epsilon_{mf}^3}{\mu (1 - \epsilon_{mf})} \quad (2)$$

The value of shape factor Φ_s was taken from the data reported by Gross⁶.

RESULTS AND DISCUSSION

The results obtained at different particle sizes and bed heights are given in Table 1.

TABLE 1—MINIMUM FLUID VOIDAGE AND MINIMUM FLUIDIZATION MASS RATE FOR ONSET OF FLUIDIZATION FOR DIFFERENT PARTICLE SIZES AND BED HEIGHTS

| (Density of pyrites, 4.15 g./cc.) | | | | | | | |
|--|-----------------|------------|----------------------|-------------------------------|--|-----------------|--|
| PARTICLE SIZE (B.S.) & AV. DIAM. (μ) | SHAPE FACTOR | RUN No. | BED HEIGHT cm. | WEIGHT OF PYRITES g. | EXPANDED BED HEIGHT AT ONSET OF FLUIDI- ZATION cm. | ϵ_{mf} | G_{mf} g./hr) (cm. ²) |
| -18+25 | 0.312 | 1 | 11.2 | 310 | 12.0 | 0.595 | 150 |
| | | 2 | 11.8 | 350 | 12.8 | 0.574 | 155 |
| | | 3 | 13.6 | 400 | 14.2 | 0.560 | 160 |
| | | 4 | 16.7 | 495 | 17.5 | 0.556 | 160 |
| | | Av. | | | | | 0.571 |
| -30+36 | 0.370 | 1 | 9.9 | 303 | 10.6 | 0.555 | 130 |
| | | 2 | 12.8 | 402 | 13.7 | 0.545 | 120 |
| | | 3 | 16.1 | 500 | 17.7 | 0.560 | 125 |
| | | 4 | 19.2 | 600 | 20.7 | 0.550 | 125 |
| | | Av. | | | | | 0.567 |
| -60+72 | 0.500 | | 11.9 | 300 | 12.6 | 0.630 | 25 |
| | | 2 | 15.5 | 400 | 17.2 | 0.638 | 22 |
| | | 3 | 20.0 | 500 | 21.3 | 0.635 | 25 |
| | | 4 | 24.5 | 625 | 26.8 | 0.638 | 24 |
| | | Av. | | | | | 0.635 |

These results are plotted in Fig. 2, 3 and 4. A plot of ϵ_{mf} versus D_p is shown in Fig. 5 in which the average value of ϵ_{mf} has been taken.

Minimum fluidization mass rate, G_{mf} , was calculated by using Eq. (2). This value for the smallest particle size (0.0231 cm.) is 46.0 g./hr) (cm.^2), for particle size 0.0461 cm., it is 52.6 and for particle size 0.0726 cm., it is 100 g./hr) (cm.^2). The calculated and the experimental values are shown in Fig. 6. Fig. 2, 3 and 4 show that G_{mf} remains practically constant for

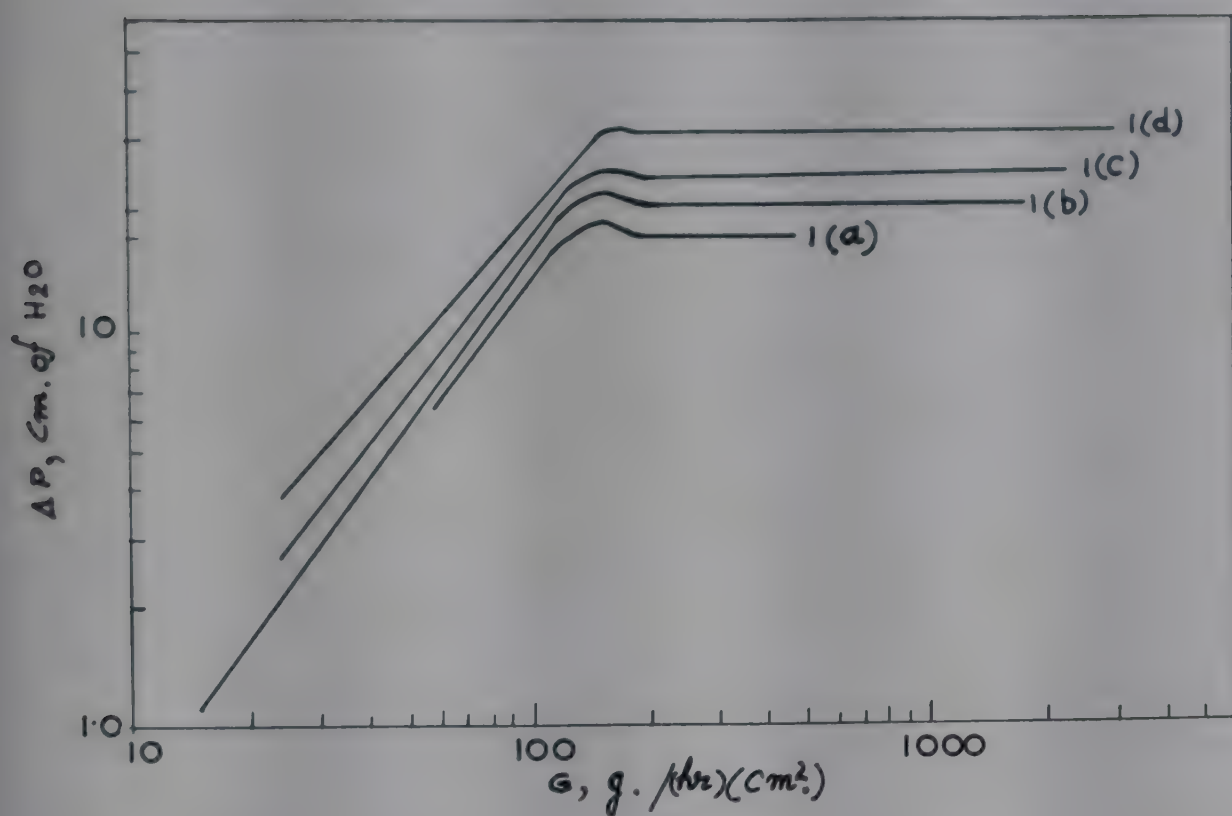


FIG. 2—PLOT OF ΔP VERSUS G [Particle size, $-18+26$ mesh; av. diam., 726μ]

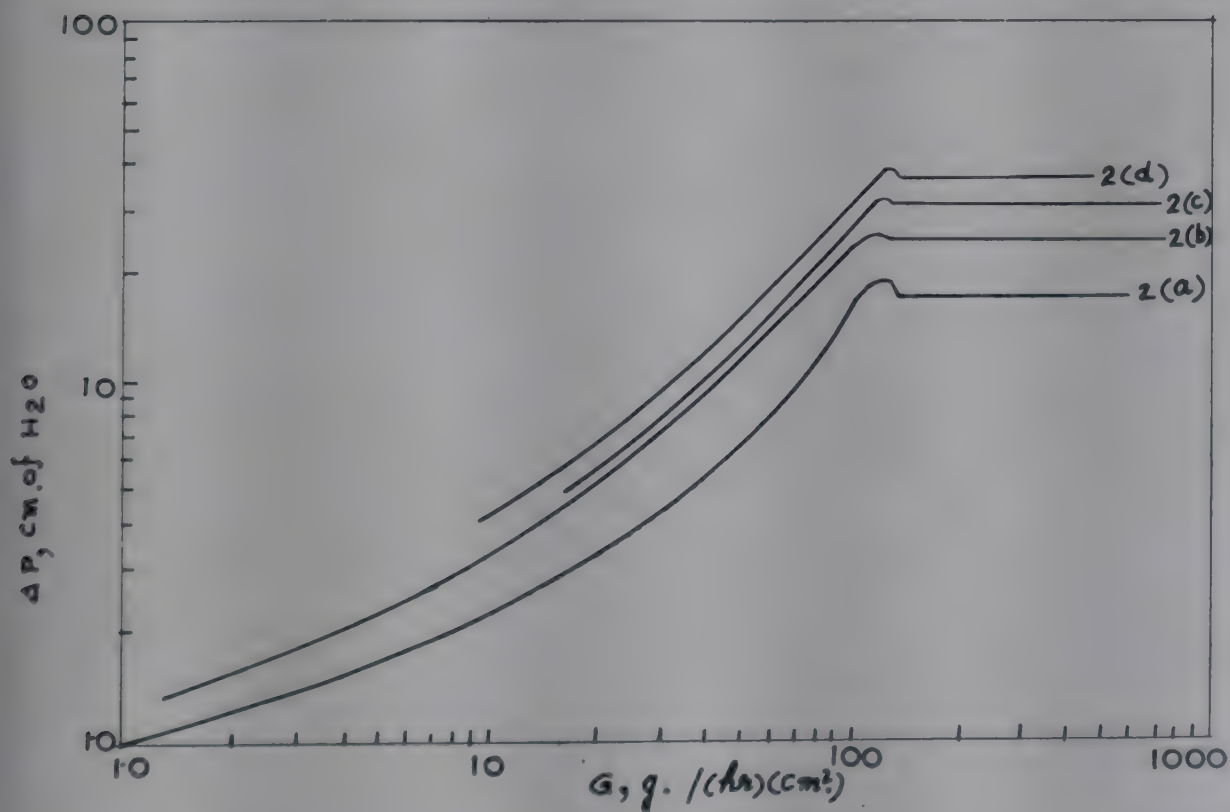


FIG. 3—PLOT OF ΔP VERSUS G [Particle size, $-30+36$ mesh; av. diam., 461μ]

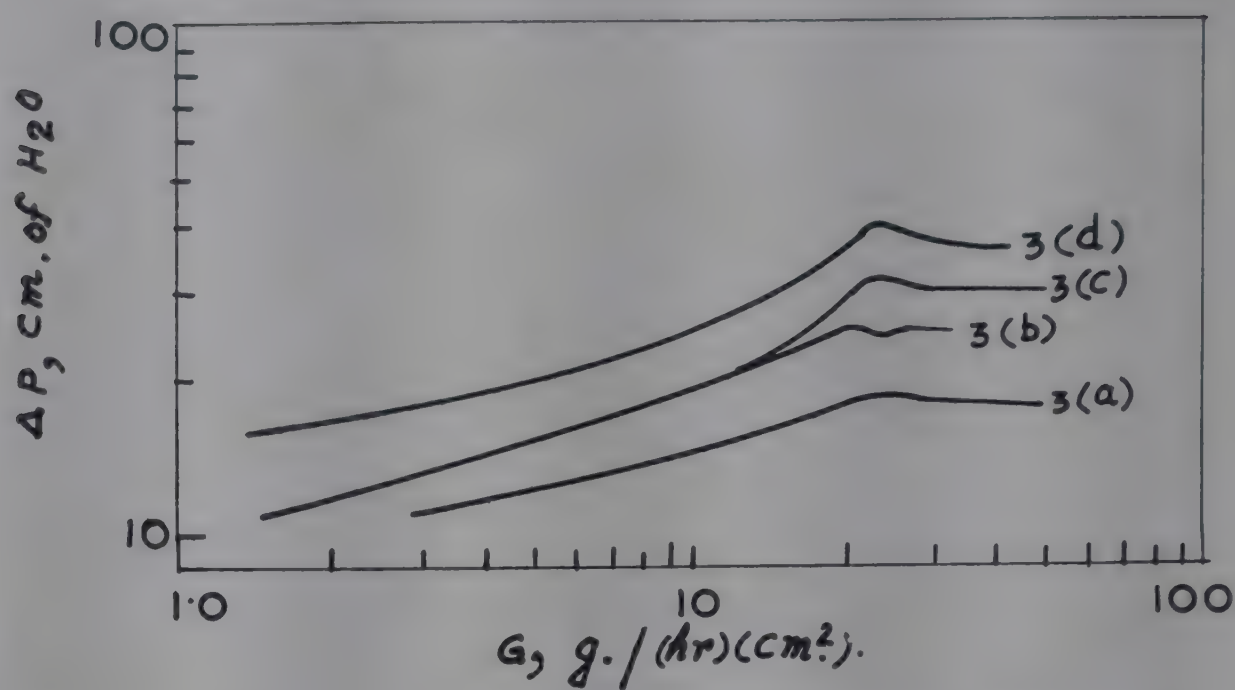


FIG. 4—PLOT OF ΔP VERSUS G [Particle size, $-60+72$ mesh; av. diam., 231μ]

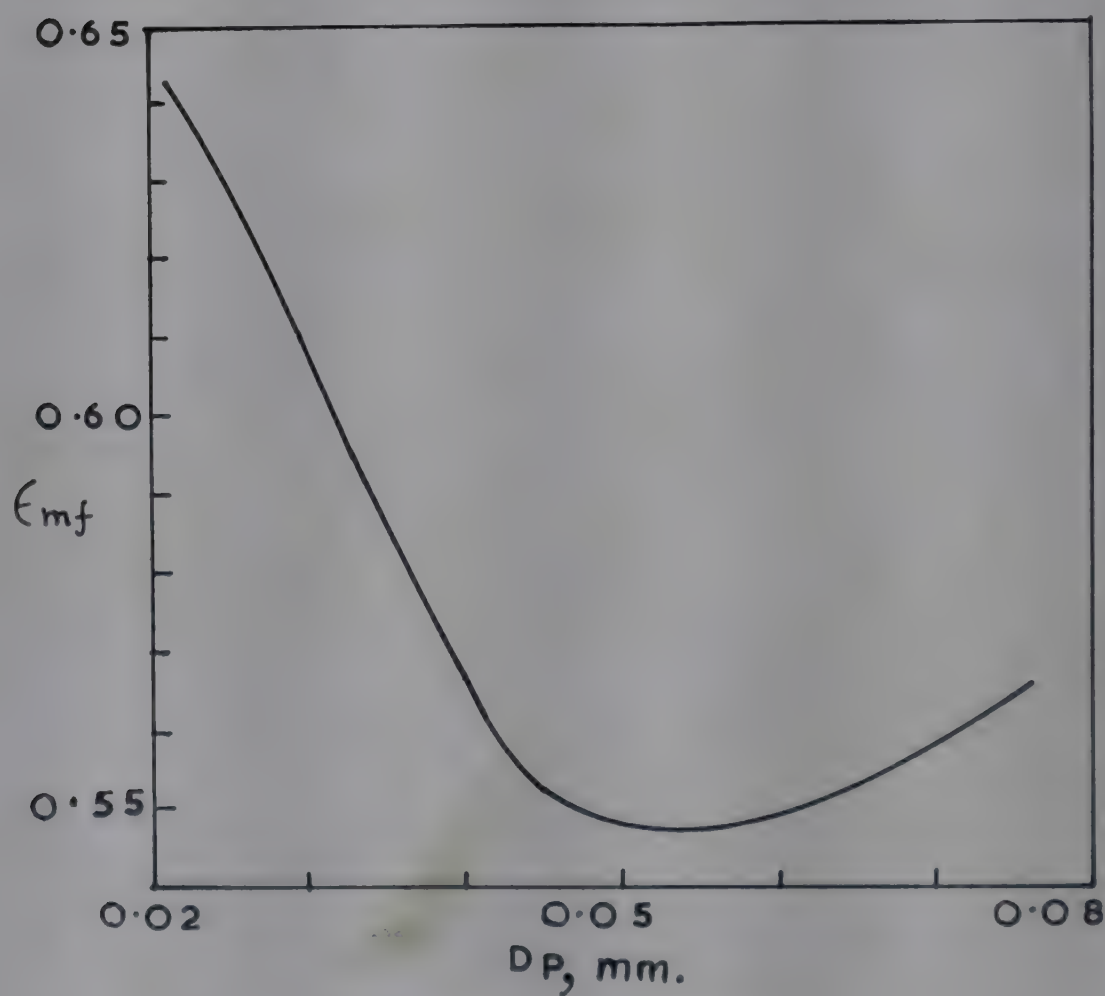
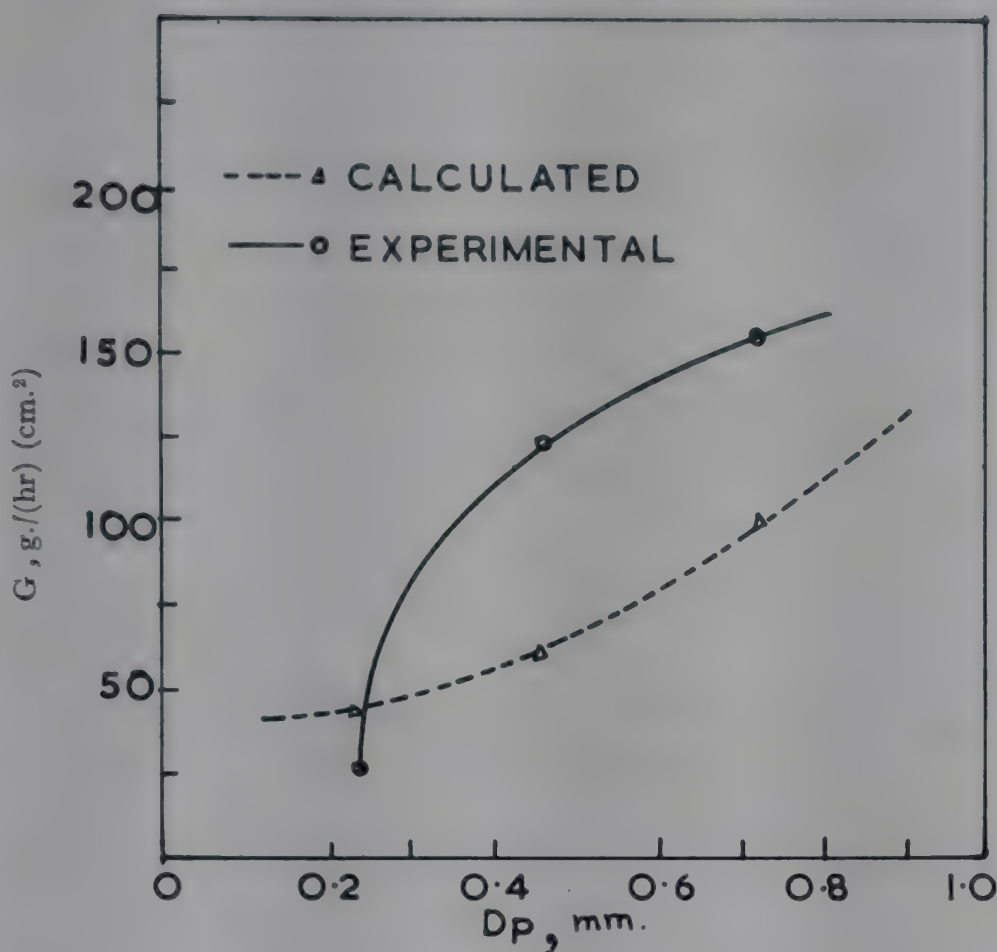


FIG. 5—PLOT OF ϵ_{mf} VERSUS D_p

FIG. 6—PLOTS OF EXPERIMENTAL AND CALCULATED VALUES OF G_{mf}

different bed heights although the pressure drop goes on increasing with increased bed heights. Fig. 6 shows that the observed and calculated values of G_{mf} do not agree, due probably to the fact that pyrites is not a homogeneous compound, but on grinding free sulphur particles are partially set free resulting in change of properties of particles.

NOMENCLATURE

- A = cross-sectional area of bed, cm.^2
- D_p = average particle diameter, cm.
- G_{mf} = minimum fluidization velocity, $\text{g.}/(\text{hr}) (\text{cm.}^2)$
- g_o = conversion factor
- H = height of bed, cm.
- L_{mf} = length of bed at onset of fluidization, cm.
- W = weight of material, g.
- ϵ_{mf} = minimum fluid voidage, dimensionless
- μ = viscosity of air, $P.$
- ρ_g = density of air, g./cc.
- ρ_s = density of solid, g./cc.
- Φ_s = shape factor of particles, dimensionless

REFERENCES

1. KARIM BAZLE, Rep. Pyrites and Chemicals Development Corporation (Pvt.) Ltd, India, 1961, 83.

2. AGARWAL O.P. & ANDERSON STORROW, *Chem. & Ind.*, (1951), 278.
3. HEERDEN, C., NOBEL & KREVELEN, *Chem. Engng Sci.*, **1**(1) (1951), 37.
4. PARENT, J.D. & STEIREN, C.S., *Chem. Engng Progr.*, **43** (1947), 429.
5. LEVA, M., *Fluidization* (McGraw-Hill Book Co. Inc., New York), 1959, 20.
6. GROSS, *Crushing and Grinding*, *U.S. Bur. Mines Bull.*, 1938, 402.

SECTION THREE

Mass Transfer in Fluidized Beds

Mass Transfer Study in Fluidized Bed for Hydrogen Sulphide-Iron Oxide System

S. BANERJEE, R. K. CHAKRAVARTI, B. K. BHATTACHARYA & A. LAHIRI

Central Fuel Research Institute
Dhanbad, Bihar

Mass transfer coefficient and mass transfer factors have been measured in a small fluidized bed in which hydrogen sulphide present in coke oven gas has been chemisorbed on the surface of porous iron oxide catalyst prepared for the purpose, employing a steady flow system. The results indicated that as the modified Reynolds number of the fluidizing gas increased, the mass transfer coefficient increased and the mass transfer factor decreased, a change in modified Reynolds number being effected by changing the gas mass velocity only. The results can be represented by the expressions

$$j_d = 2.62 N_{Re}^{-0.8}$$

$$k_g = 21.0 N_{Re}^{-0.21}$$

A method for determining the quantity of iron oxide mass required for purifying coke oven gas from hydrogen sulphide has also been suggested.

It has been reported in an earlier paper¹ that coke oven gas can be purified from hydrogen sulphide very efficiently in a fluidized bed rather than in the static bed by chemisorption of hydrogen sulphide on the surface of iron oxide catalyst prepared in the Institute². When a steady state (condition being not a function of time) is adopted, the process may be, on the one hand, continuous to any length of time and, on the other, more efficient than the static bed due to higher space velocity and mass transfer coefficient.

To establish the theoretical justification of this statement, attempts were made primarily to determine the mass transfer coefficient and mass transfer factors and their relation to the modified Reynolds number when a

change was effected with the fluidizing gas mass velocity only. Based on the results, a method has also been suggested wherein by knowing the mass transfer coefficient for a specified fluidizing gas mass velocity and an overall material balance of the system, a rough estimate can be made of the quantity of the iron oxide catalyst required for the purification process. Several past investigations and correlations³⁻¹¹ regarding mass transfer studies have been considered, and for calculating the mass transfer coefficient and mass transfer factor, the correlations suggested by Chilton and Colburn¹² and Chu, Kulil and Wetterworth¹³ were used.

EXPERIMENTAL SET-UP AND PROCEDURE

The experimental set-up (Fig. 1) for carrying out the reaction consisted of a 3 in. glass fluidizer column in which the iron oxide mass was maintained in the fluidized state by means of the fluidizing medium such as coke oven gas and hydrogen sulphide mixture. Hydrogen sulphide was generated separately in a Kipp's apparatus and mixed with hydrogen sulphide-free coke oven gas in desired quantity of 150 gr./100 ft³ of coke oven gas. Cyclones and expansion chambers at the outlet gas line removed the entrained iron oxide dust. As the chemisorption of hydrogen sulphide on the iron oxide catalyst is exothermic in nature, cooling arrangements were

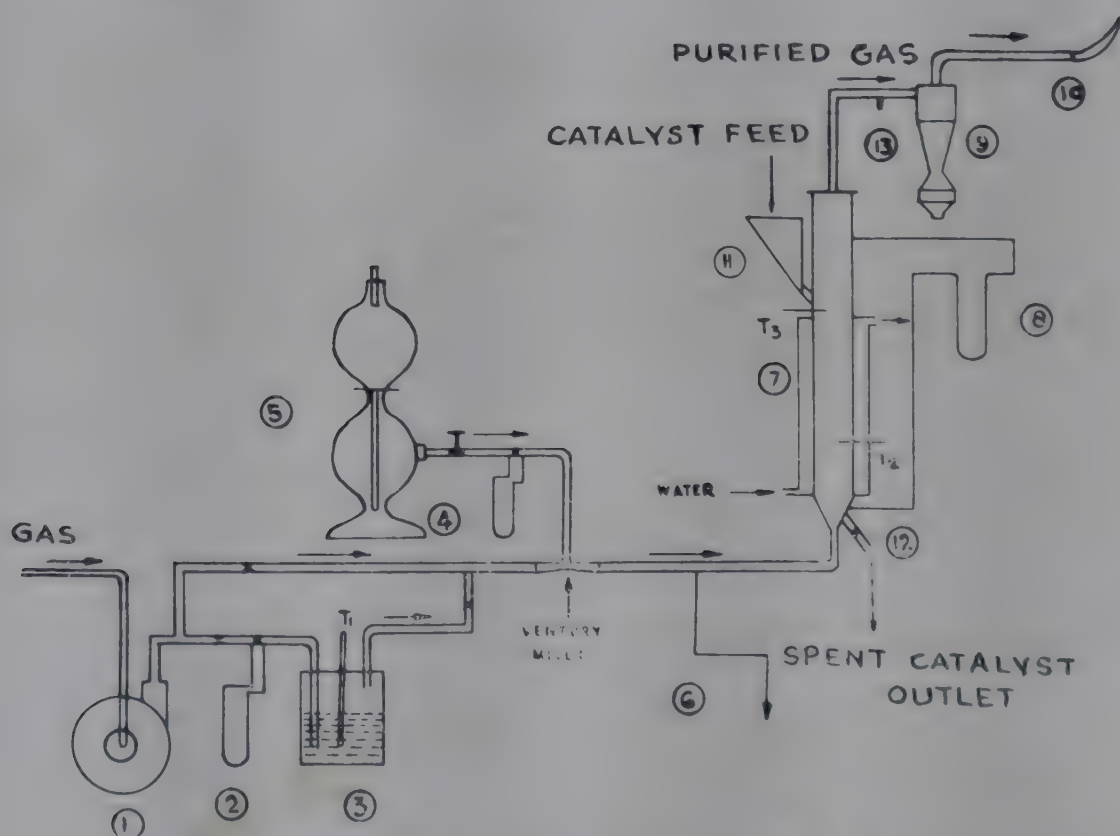


FIG. 1—FLUIDIZED BED GAS PURIFICATION UNIT [(1) Blower; (2) Gas flow meter; (3) Gas humidifier; (4) H₂S flow meter; (5) Kipp's apparatus; (6) Inlet gas sampling point; (7) Fluidized column; (8) Fluidizer pressure-difference indicator; (9) Cyclone separator; (10) Gas burner; (11) Catalyst inlet; (12) Catalyst outlet; (13) Outlet sampling point]

made so as to keep the bed temperature low, about 30°C . The system was operated continuously and a definite quantity of about 50 g./hr of fresh iron oxide was introduced in the reactor from the top of the bed and an equal quantity of heavier spent oxide was withdrawn from its bottom so that the catalyst surface remained always fresh without being saturated with sulphur complexes. Also, continuous operation of the system was necessary to keep the ratio of bed height to diameter or the total bed volume constant. However, in spite of a good amount of back-mixing between the spent and fresh iron oxide mass within the bed, the overall average activity of the fluidized bed was maintained more or less constant throughout the experiment.

Five different sets of experiments were carried out when the mass velocity of the fluidizing medium was gradually increased.

RESULTS AND DISCUSSION

As can be seen from Fig. 2 the fluidized bed can be assumed to be in a stabilized state within the gas flow velocity range, $0.6\text{--}1.6\text{ ft}^3/\text{min}$. ($19\text{--}38.1\text{ lb./hr ft}^2$), where the minimum bed voidage (ϵ_{mf}) is same because there is no appreciable change in the bed pressure drop (ΔP). Conditions beyond that mass velocity range have not been considered because the ideal fluidization characteristics of the bed are then not attainable and there will be

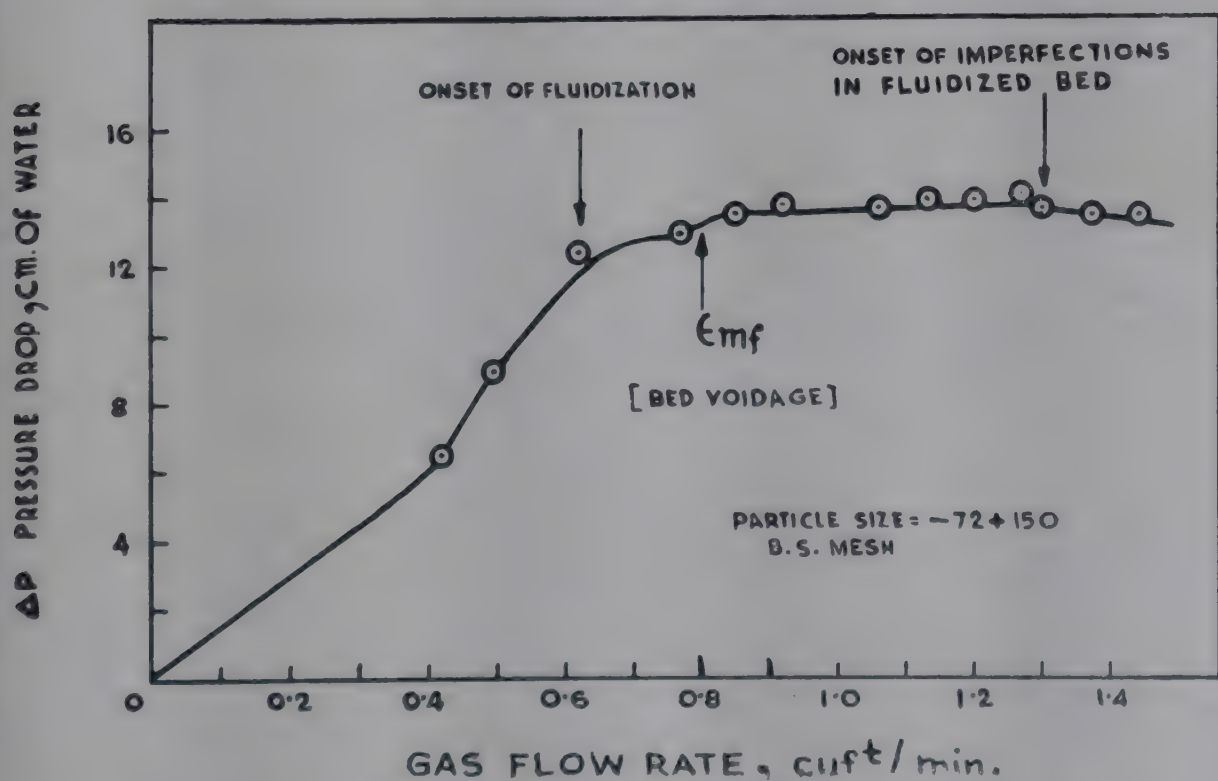


FIG. 2—RELATION BETWEEN BED PRESSURE DROP AND GAS FLOW RATE

appreciable loss of catalyst due to entrainment. The mass transfer coefficient (k_g) and the mass transfer factor (j_d) have been calculated from the correlations suggested by Chilton and Colburn¹² and Chu, Kulil and Wetterworth¹³.

$$j_d = \frac{k_g P_{bm}}{G_m} \left[\frac{\mu}{\rho D_F} \right]^{\frac{2}{3}} \quad (1)$$

$$\frac{k_g P_{bm}}{G_m} \left[\frac{\mu}{\rho D_F} \right]^{\frac{2}{3}} = 5.7 \left[\frac{D_p G}{\mu (1-\epsilon)} \right]^{-0.78} \quad (2)$$

The factor k_g can be correlated with the standard material balance equation^{14,15} of the system which may be represented as follows:

$$-Gdw = k_g A (P_g - P_s) dh \quad (3)$$

Due to the instantaneous chemical reaction between hydrogen sulphide gas and iron oxide, i.e. the rate of chemical reaction on the catalyst surface being much quicker than the rate of hydrogen sulphide gas diffusion, and due to the phase change of the hydrogen sulphide during the reaction, the back pressure of hydrogen sulphide from each particle surface may be assumed for practical purposes not to offer any resistance to the mass transfer and thus only the gas diffusion may be considered as the main controlling factor. However, it may be noted that in case of an unsteady state where a definite quantity of catalyst is allowed to react for a certain length of time in fluidized bed, the condition is entirely different.

Considering the partial pressure of hydrogen sulphide on the gas-solid interface to be negligible, P_s in Eq. (3) may be assumed as zero. Hence, Eq. (3) may be written as

$$-Gdw = k_g AP_g dh \quad (4)$$

A fluidized bed reactor simulates largely a stirred reactor or a back-mix reactor where the composition does not change along the length of the reactor and hence Eq. (4) may be written as

$$G (W_1 - W_2) = k_g AP_2 h$$

$$\text{i.e. } h = \frac{G(W_1 - W_2)}{k_g AP_2} \quad (5)$$

Thus, after knowing h and k_g , the desired quantity of the iron oxide catalyst necessary in fluidized bed for the purification of the coke oven gas containing a certain amount of hydrogen sulphide may be determined.

The void fraction (ϵ) for an idealized condition of the fluidized bed

as mentioned in Eq. (2) is derived from the minimum bed voidage (ϵ_{mf}) according to the correlation^{14,15}:

$$\epsilon = 1 - \frac{1 - \epsilon_{mf}}{N_f} \quad (6)$$

According to Leva¹⁶, in the gas-solid fluidized system where the bed is stabilized, the total average bed voidage (ϵ) is always greater than ϵ_{mf} , i.e. at the state where there is no change of pressure difference (ΔP). This is due to the presence of bubbles and channels in the fluidized bed. Hence, for obtaining the value of ϵ , some corrections are made as shown in Eq. (6). For a maximum fluidization efficiency¹⁶, the value of N_f for the average particle size of 0.0032 in. may be chosen as 1.33.

The difficulties encountered in determining mass transfer coefficient are due to the absence of any precise data of the diffusivity factor (D_F) for hydrogen sulphide in coke oven gas. As in this case coke oven gas may be assumed to behave as an inert gas, the empirical relationship of Gilliland¹⁷ may be used. The correlation is as follows:

$$D_F = 0.0043 \frac{T_z^2}{P [V_A^{\frac{1}{3}} + V_B^{\frac{1}{3}}]^2} \sqrt{\frac{1}{M_A} + \frac{1}{M_B}} \quad (7)$$

As the experiments were carried out at a constant atmospheric pressure, the pressure term (P) may be considered to be unity. The total molar volume of coke oven gas may be calculated from the data mentioned in standard text-books^{18,19}.

The overall particle diameter D_p for the iron oxide catalyst mass used for carrying out the experiments was calculated from the screen analysis data suggested by Leva¹⁶ and was found to be equal to 0.0032 in.

The results of the study as presented in Table 1 and in Fig. 3 and 4 indicate that j_d value decreases with increase of the modified Reynolds

TABLE 1—EXPERIMENTAL DATA AND CALCULATED VALUES FOR k_g AND j_d
[Schmidt No. ($\mu/\rho D_F$) = 1.62]

| FLUIDIZING GAS MASS VELOCITY $lb./hr\ ft^2$ | GAS FLOW RATE $lb./hr$ | N_{Re} | k_g $lb./mol./hr\ ft^2\ atm.$ | j_d |
|---|---------------------------|----------|------------------------------------|-------|
| 19.1 | 0.0077 | 0.16 | 14.33 | 11.40 |
| 22.23 | 0.0090 | 0.19 | 14.81 | 9.00 |
| 27.6 | 0.0110 | 0.23 | 15.38 | 8.50 |
| 33.03 | 0.0131 | 0.28 | 16.11 | 7.28 |
| 38.11 | 0.0155 | 0.32 | 16.66 | 6.50 |

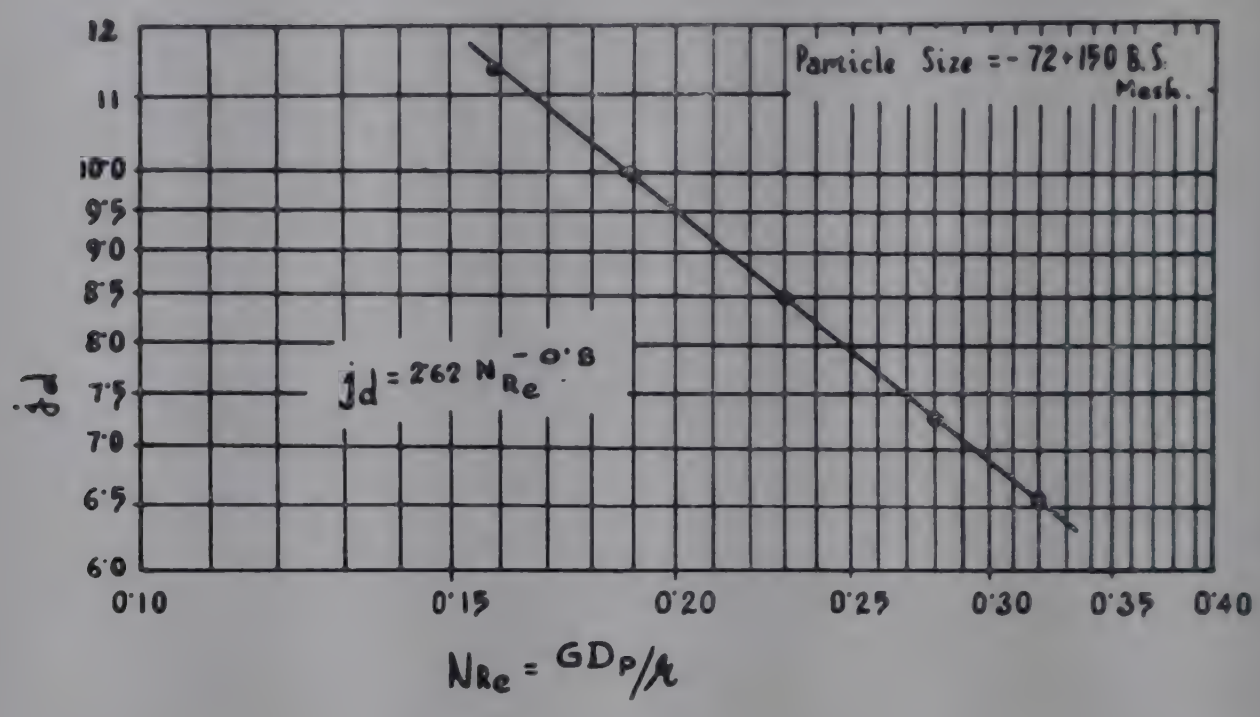


FIG. 3—RELATION BETWEEN MASS TRANSFER FACTOR AND MODIFIED REYNOLDS NUMBER

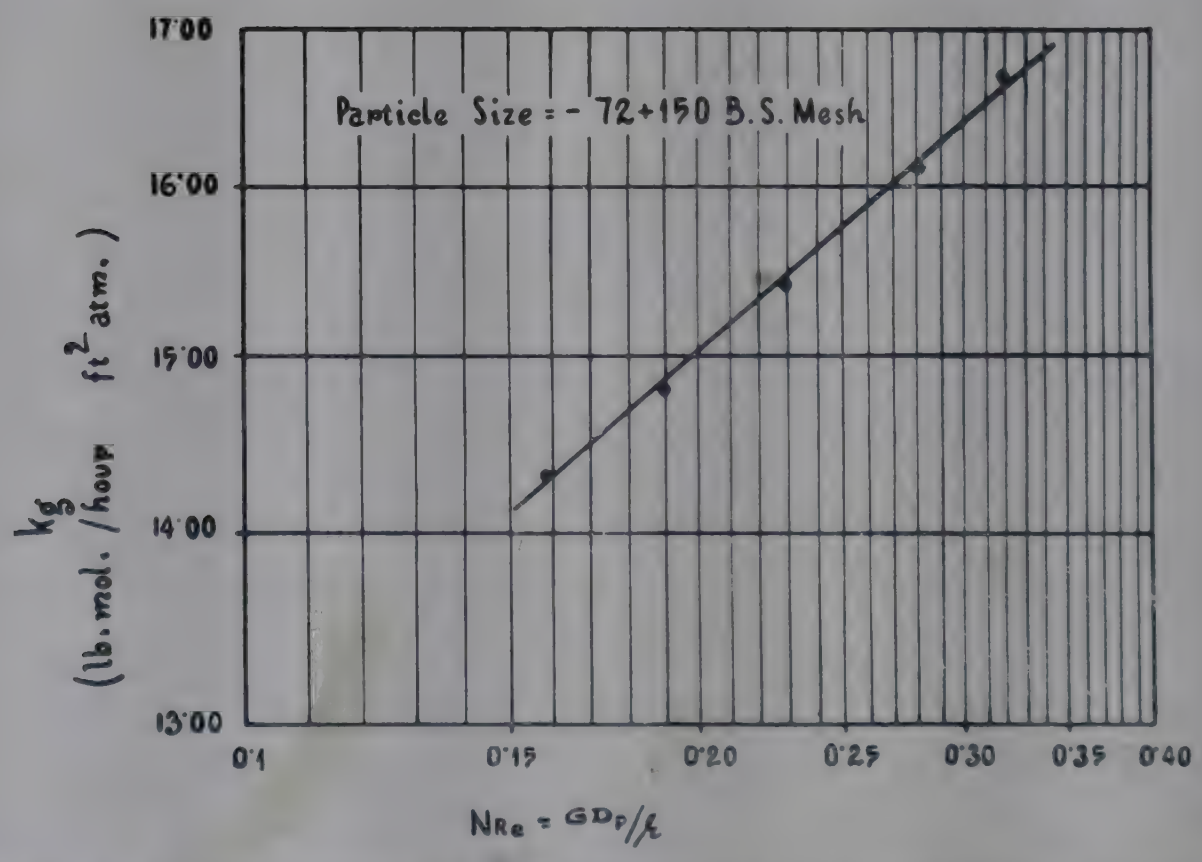


FIG. 4—RELATION BETWEEN MASS TRANSFER COEFFICIENT AND MODIFIED REYNOLDS NUMBER

number whereas k_g value increases. From the trend of the curves as presented in Fig. 3 the relation between j_d factor and modified Reynolds number may be expressed in the form of an equation which is applicable only within the Reynolds number range 0.16–0.32, and particle size range –72+150 B.S. mesh with which the experiments were actually carried out. The equation may be expressed as follows:

$$j_d = 2.62 N_{Re}^{-0.8} \quad (8)$$

Fig. 4 indicates that the mass transfer coefficient increases with increase of modified Reynolds number and the relation may be expressed as

$$k_g = 21.0 N_{Re}^{0.21} \quad (9)$$

It is to be noted that for other conditions having a different hydrogen sulphide concentration and for other particle size fractions of the iron oxide mass, the constant factors for Eq. (8) and (9) may have to be modified.

As shown in Fig. 4, the modified Reynolds number range below 0.15 represents the conditions of static bed, or distended bed when the value of mass transfer coefficient has an appreciably low value. Thus the experimental results indicate that in the steady state condition, the fluidized bed has a much higher mass transfer coefficient than the static bed. Due to the intense agitation in a well-fluidizing dense-phase bed, the state of sub-division and the mass transfer surfaces are so much greater that the gas-solid mass transfer is actually much higher in the fluidized bed than in the static bed. The higher mass transfer coefficient value may also be attributed to the higher mass velocity.

CONCLUSION

Purification of coke oven gas by iron oxide catalyst in fluidized bed is more efficient than in the static bed because increased gas mass velocity through the system increases mass transfer coefficient value. Mass transfer coefficient increases with the increase of gas mass velocity or modified Reynolds number, whereas mass transfer factor decreases correspondingly.

Substituting the k_g factor in the overall material balance equation $-G \Delta w = k_g A P_2 h$, a rough estimate of the quantity of catalyst required for hydrogen sulphide removal from gas can be made. However, for designing large commercial fluidized bed gas purification plants, the applicability of this method for determining the quantity of catalyst will have to be investigated further.

NOMENCLATURE

| | |
|-----------------|---|
| A | = effective surface area of bed, ft^2/ft^3 |
| D_F | = diffusivity constant, ft^2/hr |
| D_p | = average particle diameter, $in.$ |
| G | = mass velocity of hydrogen sulphide-free main gas stream, $lb./ft^2\ hr$ |
| G_m | = superficial mass flow rate, $lb.\ mol./hr\ ft^2$ |
| h | = height of fluidized bed |
| j_d | = mass transfer factor |
| k_g | = mass transfer coefficient, $lb.\ mol./hr\ ft^2\ atm.$ |
| M_A, M_B | = molecular weight of hydrogen sulphide and coke oven gas respectively |
| N_f | = bed expansion ratio |
| P_0 | = partial pressure of hydrogen sulphide at the main gas stream |
| P_1, P_2 | = partial pressure of hydrogen sulphide in the entering and exit gas stream |
| P_s | = back pressure of hydrogen sulphide just on the solid surface |
| P | = pressure, $atm.$ |
| P_{bm} | = partial pressure of nondiffusing component, $atm.$ |
| T | = temperature, $^{\circ}K.$ |
| V_A, V_B | = molar volume of hydrogen sulphide and coke oven gas respectively |
| W | = $lb.\ mol.$ of hydrogen sulphide/ $lb.$ of hydrogen sulphide-free coke oven gas |
| ϵ | = overall bed voidage fraction |
| ϵ_{mf} | = bed voidage at minimum fluidization velocity |
| ρ | = density of fluid, $lb./ft^3$ |
| μ | = viscosity of fluid, $lb./hr\ ft$ |

REFERENCES

1. CHAKRAVARTI, R. K., BANERJEE, S., BASAK, N. G. & LAHIRI, A., *Indian J. Technol.* **1** (1963), 423.
2. LAHIRI, A., BASAK, N. G. & MAJUMDAR, A., *Indian Pat.*, No. 55816, 1957.
3. GAMSON, B. W., *Chem. Engng Progr.*, **47** (1951), 19.
4. WRENSICK, W. & WHITE, R. R. *Chem. Engng Progr.*, **45** (1949), 377.
5. McCUNE, L. K. & WILHELM, R. H., *Industr. Engng Chem.*, **41** (1949), 1124.
6. KETTENRING, K. N., MANDERFIELD, F. L. & SMITH, J. M., *Chem. Engng Progr.*, **46** (1950), 139.
7. THODOS, G. & McCONNACHIE, J. T. L., *Amer. Inst. chem. Engrs J.*, **9** (1963), 60.
8. HSU, C. T. & MOLSTAD, M. C., *Industr. Engng Chem.*, **47** (1955), 1551.
9. HSU, C. T. & MOLSTAD, M. C., *Industr. Engng Chem.*, **47** (1955), 1550.
10. RICCETTI, E. R. & THODOS, G., *Amer. Inst. chem. Engrs J.*, **7** (1961), 442.
11. RICHARDSON, J. F. & SZEKELY, J., *Trans. Instn chem. Engrs, Lond.*, **36** (1961), 212.
12. CHILTON, T. H. & COLBURN, A. P., *Industr. Engng Chem.*, **26** (1934), 1183.
13. CHU, J. C., KULIL, J. & WETTERWORTH, W. A., *Chem. Engng Progr.*, **49** (1953), 141.
14. WALAS, S. M., *Reaction Kinetics for Chemical Engineers* (McGraw-Hill Book Co. Inc., London) 1959, 202, 214.
15. RICHARDSON, J. F. & BAKHTIAR, A. G., *Trans. Instn chem. Engrs, Lond.*, **36** (1959), 283.
16. LEVA, M., *Fluidization* (McGraw-Hill Book Co. Inc., New York), 1959, 67, 102.
17. GILLILAND, E. R., *Industr. Engng Chem.*, **26** (1934), 681.
18. HOUGEN, O. A. & WATSON, K. M., *Chemical Process Principles* (John Wiley & Sons, London), Part III, 1962, 988.
19. McCABE, W. L. & SMITH, J. C., *Unit Operation of Chemical Engineering* (Kogakusha Co. Ltd, Tokyo), Asian Students' Edn, 616.

Drying in Fluidized Beds

P. SEN GUPTA, K. J. R. SARMA* & M. N. RAO

Department of Chemical Engineering, Indian Institute of Technology
Kharagpur

A comprehensive literature survey of the existing fluidized bed drying processes and the types of driers is presented along with the relative merits and demerits of each type. Choice of driers suitable for certain processes is indicated. Design aspects and factors that control the drier operation are discussed.

DIFFERENT TYPES OF DRIERS

Various processes utilize the technique of fluidization. Starting with granular substances, materials like pastes, solutions and sheet materials are being dried by this technique. The advantages of this technique are uniformity in drying, precise control and easy automation; a few disadvantages like heavy losses due to entrainment, erosion of materials of construction, etc. cannot, however, be ignored.

Fluidized bed driers can be classified as shown in Chart 1.

Table 1 shows the various substances that have been dried using fluidized bed technique, their size ranges varying from 0.057 to 20 mm., and moisture contents as high as 140 per cent. Some of the units are gigantic while some are pilot plant units.

Continuous single-stage cocurrent type drier. The most popularly used type is the spouted column drier (Fig. 1). In this, the fluidizing medium entrains the wet material and enters at the bottom of the drier. The fluid velocity is so adjusted as to keep the material in suspension inside the drier till its size is reduced sufficiently to be carried away from the drier.

While this type of drier is very suitable for bigger size material and materials having high moisture content, it is to be noted that the material

*Present address: Department of Chemical Engineering, Regional Engineering College, Rourkela 8.

CHART 1—CLASSIFICATION OF FLUIDIZED BED DRIERS

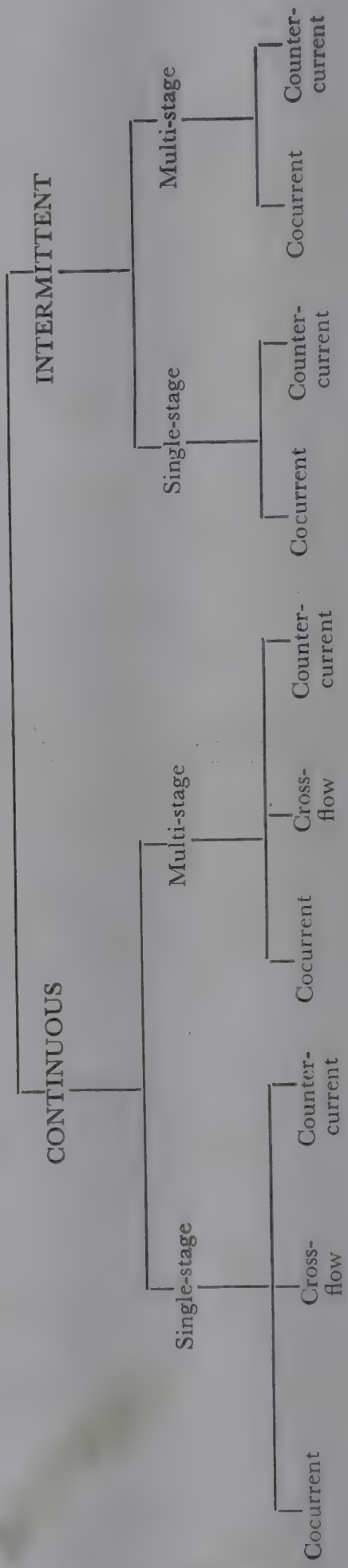


Fig. 1
Fig. 2 with
recirculation

Fig. 3

Fig. 4 with
recirculation
Fig. 5-7

Fig. 8-11

Fig. 12-13

Fig. 14

TABLE 1—DATA ON DRYING IN FLUIDIZED BED

| AUTHOR & REFERENCE | MATERIAL DRIED | SIZE mm. | MOISTURE CONTENT (DRY BASIS), % | | GAS TEMPERATURE, °C. | | GAS VELOCITY m./sec. | CAPACITY kg./hr | DRIER DIMENSIONS mm. | kg. GAS | |
|---|-------------------------|-------------|------------------------------------|-------|-------------------------|---------|----------------------------|--------------------|--------------------------------|--------------|---------|
| | | | Initial | Final | Initial | Final | | | | kg. MOISTURE | kg. GAS |
| Fedorov ¹ | Coal (Moscow region) | 0-10 | 45-55 | 2-40 | 500 | 260-340 | 12-31 | .. | .. | .. | .. |
| Zverev ¹ | do | 0-15 | 40-60 | 27-43 | 200-400 | 100-240 | 17-20 | .. | .. | .. | .. |
| Vinogradov ¹ | do | 0-20 | 47-51 | 26-34 | 400-600 | 150-190 | 30-44 | .. | .. | .. | .. |
| Lebedev ¹ | Anthracite | 0-15 | 8-14 | 3-5 | 240-380 | 150-280 | 16-25 | .. | .. | .. | .. |
| Garpinich ¹ | Peat | 0-10 | 100-140 | 18-57 | 400-700 | 100-320 | 19-33 | .. | .. | .. | .. |
| | Sunflower seeds | 6 | 12-23 | 8-16 | 660-870 | 300-350 | 26-34 | .. | .. | .. | .. |
| Goldstick ² | Magnesium sulphate | 0-8 | 92-97 | 11-25 | 610-720 | 270-350 | 30-42 | .. | .. | .. | .. |
| Walson ¹ | Sunflower seeds | 6 | 15-22 | 6-13 | 370-620 | 130-220 | 24-28 | .. | .. | .. | .. |
| Liberov ¹ | Coal (Moscow region) | 0-20 | 15-40 | 26-29 | 550-760 | 210-340 | 22-28 | .. | .. | .. | .. |
| Institute of Chemical Machinery Bldg, Leningrad ³ | Polysterol | >1 | 10 | 0-7 | 70 | .. | 3-0 | 1310 | 2520(L) × 1300(W) × 3700(H) | .. | .. |
| | do | <1 | 10 | 0-7 | 78 | .. | 2-5 | do | do | .. | .. |
| Morilov <i>et al.</i> ³ | Potassium salt | Up to 2 | 20-2 | .. | 226-547 | .. | 1-13-1-36 | .. | 98(D) × 950(H) | .. | .. |
| Romankov <i>et al.</i> ⁴ | Paints | .. | 70-4 | 0-9 | 235 | 90 | 0-38-35-0 | .. | .. | 37-4 | .. |
| | solution | .. | 81-4 | 4-0 | 300 | 97 | 0-60-40-0 | .. | .. | 26-4 | .. |

TABLE 1—DATA ON DRYING IN FLUIDIZED BED (Contd)

| AUTHOR & REFERENCE | MATERIAL DRIED | SIZE mm. | MOISTURE CONTENT (DRY BASIS), % | | GAS TEMPERATURE, °C. | | GAS VELOCITY m./sec. | CAPACITY kg./hr | DRIER DIMENSIONS mm. | kg./ Gas Moisture |
|---|--|-----------------------|------------------------------------|---------------|-------------------------|---------|----------------------------|--------------------|----------------------------|----------------------|
| | | | Initial | Final | Initial | Final | | | | |
| Romankov <i>et al.</i> ⁵ | Cu-Ni catalyst paste | .. | 80.0 | 8-10 | 350 | .. | 0.40-8.0 | 800* | 600(L) × 20(W) × 350(H) | .. |
| Donom <i>et al.</i> ⁶ | Pyrites froth | 57 × 10 ⁻³ | 8-10 | 2-2.5 | .. | .. | 0.10-0.12 | 816 | 200(L) × 100(W) | 0.58 |
| Shakhova <i>et al.</i> ⁷ | Paints, sugar soln | .. | 79-96 | .. | 177-511 | .. | 0.795-2.44 | 59.6 | 175(D) | 5.19-9.42 |
| Richkov <i>et al.</i> ⁸ | Ammonium phosphate | .. | 20-78.5 | 1.0 | 100-250 | .. | 0.3-0.7 | .. | 250(D) | 35.6-52.7 |
| Richkov <i>et al.</i> ⁹ | NH ₄ HCO ₃ | .. | 4.23-5.80 | 0.41- 0.49 | 74-93 | 36-41 | 0.306-0.363 | 211.8- 541.2 | 245(D) × 1300(H) | 64.5-111.0 |
| Frantz ¹⁰ | Sea water | .. | .. | .. | 703-931 | 149-348 | .. | .. | 102(D) | .. |
| Jonke <i>et al.</i> ¹¹ | UO ₂ (NO ₃) ₂ | .. | .. | .. | 0-850 | 240-450 | .. | .. | 152.4(D) | .. |
| | Al(NO ₃) ₃ | .. | .. | .. | .. | 320-550 | .. | .. | do | .. |
| Philoon ¹² | UO ₂ (NO ₃) ₂ | .. | .. | .. | .. | .. | .. | .. | .. | .. |
| Jackson <i>et al.</i> ¹³ | Al(NO ₃) ₃ | .. | .. | .. | .. | .. | .. | .. | .. | .. |
| Vanecek <i>et al.</i> ¹⁴ | FeSO ₄ 7H ₂ O | .. | .. | .. | .. | .. | .. | .. | .. | .. |
| Australian Pat. ¹⁵ | Na ₂ SO ₄ 10H ₂ O | .. | .. | .. | 450 | 80-100 | .. | .. | .. | .. |
| Kaganovich <i>et al.</i> ¹⁶ | Na ₂ SO ₄ 10H ₂ O | .. | .. | .. | 610-850 | 90-250 | .. | .. | 1350(D) | .. |
| Kaganovich ¹⁷ | KCl | .. | 8-9 | 8.5 | 750-850 | 150-200 | 0.5-0.8 | 1814† | .. | .. |

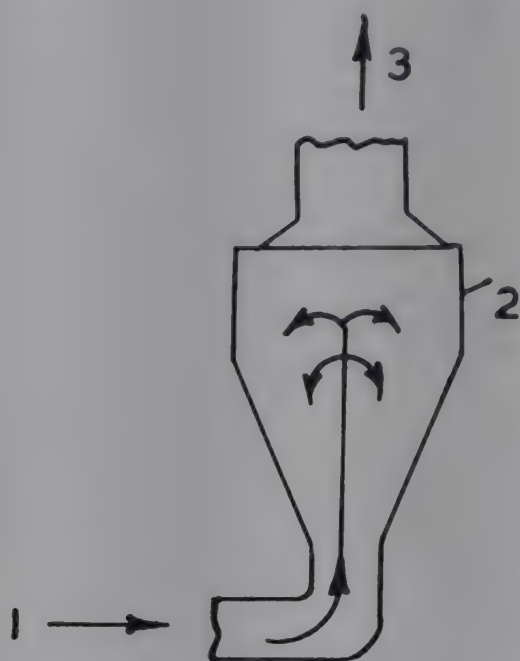


FIG. 1

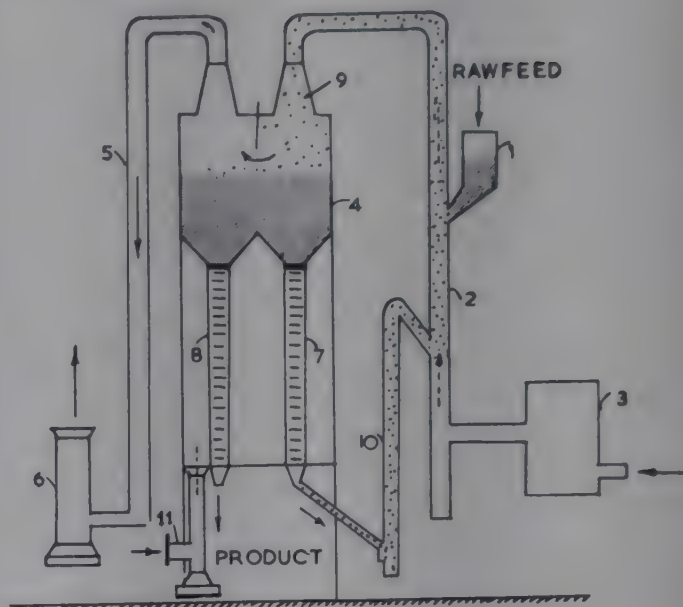


FIG. 2

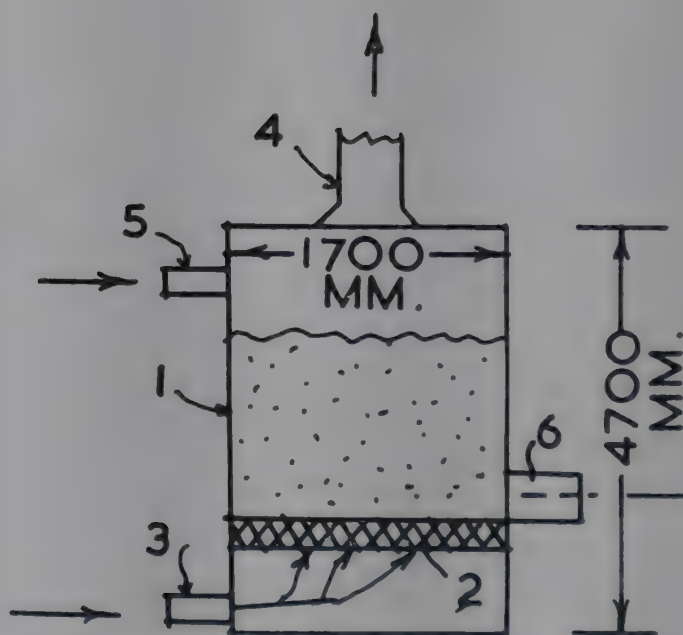


FIG. 3

FIG. 1—SINGLE-STAGE CONTINUOUS COCURRENT SPOUTED COLUMN DRIER [(1) Gas-solid inlet; (2) Drier; (3) Gas-solid exit to cyclone separator]

FIG. 2—SINGLE-STAGE CONTINUOUS COCURRENT RECIRCULATORY TYPE DRIER WITH COOLING ARRANGEMENT FOR PRODUCTS [(1) Bunker; (2) Drying zone; (3) Furnace; (4) Contact zone; (5) Gas outlet; (6) Blower; (7) Intermediate cooling zone; (8) Final cooling zone; (9) Separator; (10) Elevator; (11) Blower for cooling zone]

FIG. 3—SINGLE-STAGE CONTINUOUS CROSS-FLOW DRIER WITH CONSTANT MOVEMENT OF MATERIAL [(1) Fluidized bed; (2) Perforated plate; (3) Gas inlet; (4) Gas outlet, (5) Solid inlet; (6) Product exit]

should be such that its terminal velocity changes sharply during the process of drying; otherwise, there is a possibility of both the dry and the wet material being carried off the drier, resulting in nonuniform drying.

The drier shown in Fig. 2 has been designed by the Power Institute, Byelorussia for cooling simultaneously the dried product. The unit is claimed to have a very high heat economy. Part of the dried material is taken out as product, and the remainder recirculated to prevent agglomeration.

Single-stage continuous cross-flow drier. In this drier (Fig. 3), the movement of the material is made to take place in a definite direction, i.e. from feed end to discharge end, with the help of a mechanical device and thus uniformity in drying is achieved.

Single-stage continuous counter-current drier. The type of drier used by Fedorov for drying of coal is shown in Fig. 4. Raw coal enters the drier (1) through the feeder (2). Air and furnace gas are admitted at the bottom of the drier at a velocity ranging from 15 to 20 kg./m.² sec. The velocity in the cylindrical section ranges from 4 to 5 kg./m.² sec. Coal bigger than 20 mm. falls down, gets crushed in the crusher (3) and is returned through the elevator (5) to the vessel for redrying. Particles smaller than 2 mm. are carried along with the gases, separated in cyclone (4) and recovered. Medium size particles are withdrawn through the overflow pipe after drying. This type of drier is suitable for drying material with high moisture content and wide size ranges but not suitable when uniform drying is required.

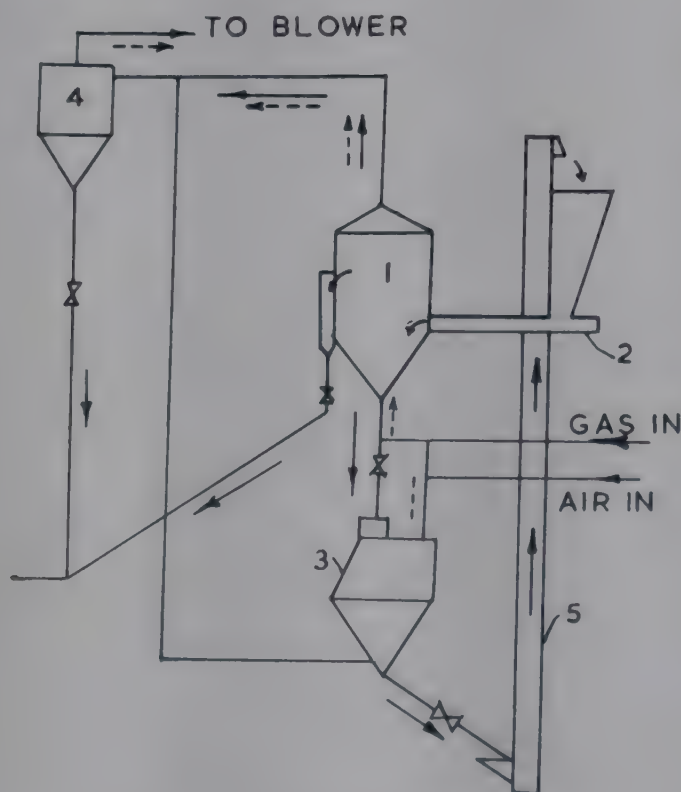


FIG. 4—SINGLE-STAGE CONTINUOUS RECIRCULATORY TYPE DRIER [(1) Drier; (2) Feeder; (3) Crusher; (4) Cyclone; (5) Elevator]

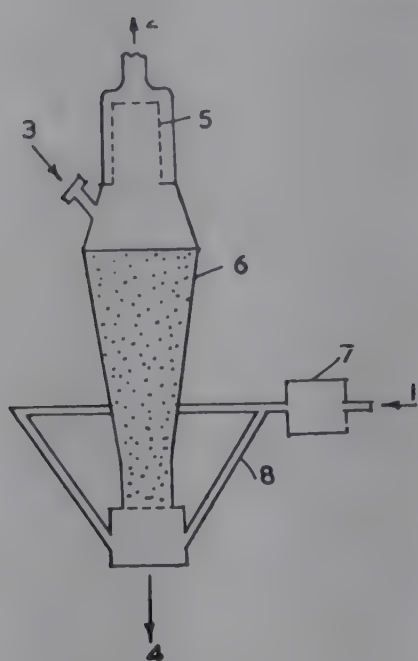


FIG. 5

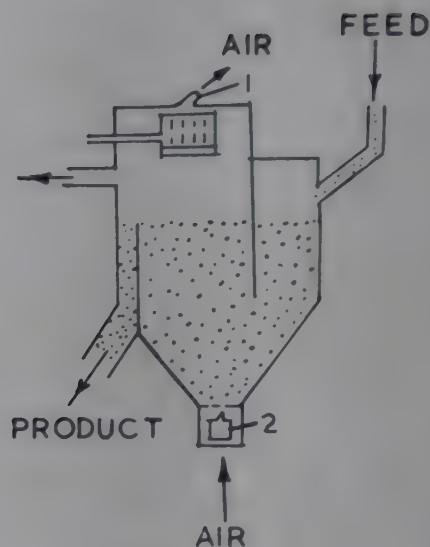


FIG. 6

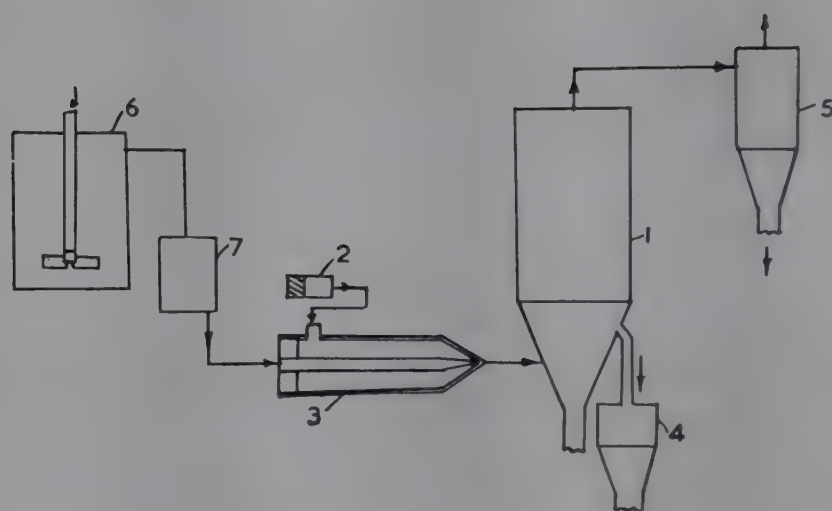


FIG. 7

FIG. 5—SINGLE-STAGE CONTINUOUS COUNTER-CURRENT CYLINDRO-CONICAL DRIER [(1) Gas inlet; (2) Gas exit; (3) Feed inlet; (4) Product exit; (5) Filter; (6) Drier; (7) Heater; (8) Gas distributor; $\cdots \rightarrow$ Gas flow; \rightarrow Material flow]

FIG. 6—SINGLE-STAGE CONTINUOUS COUNTER-CURRENT ULTRASONIC DRIER [(1 & 2) Ultrasonic sirens]

FIG. 7—SINGLE-STAGE CONTINUOUS COUNTER-CURRENT DRIER FOR SOLUTIONS, PASTES, ETC. [(1) Drier; (2) Compressor; (3) Ejector; (4) Product receiver; (5) Cyclone separator; (6) Mixer; (7) Electromagnetic feeding device]

In certain types, pulsating flow of gas is used to prevent channelling and driers having a cylindroconical shape (Fig. 5) are very popular in Rumania, West Germany, etc.

The Institute of Chemical Machinery Building, Moscow, has suggested the use of ultrasonic driers for drying granular materials (Fig. 6.) Air is used as the fluidizing medium which enters the drier through the screen (2).

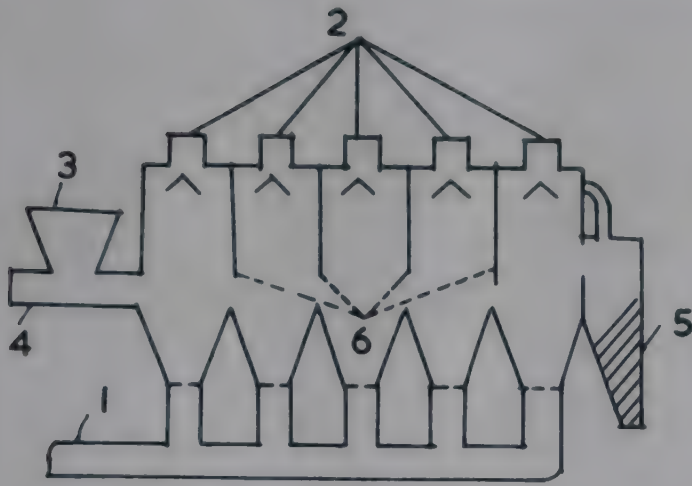


FIG. 8

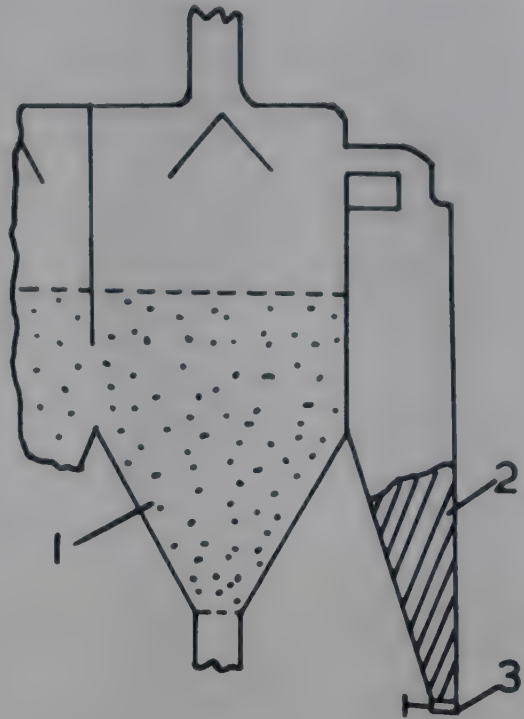


FIG. 9

FIG. 8—MULTI-STAGE CONTINUOUS CROSS-CURRENT DRIER [(1) Gas inlet; (2) Gas exit; (3) Raw feed; (4) Feeder; (5) Product outlet; (6) Orifice]

FIG. 9—MULTI-STAGE CONTINUOUS CROSS-CURRENT TYPE DRIER WITH PROVISION FOR PRODUCT REMOVAL [(1) Fluidized bed; (2) Stationary layer; (3) Product withdrawal mechanism]

At the top of the drier, another screen (1) is kept to minimize the carry-over of fines. The process has been claimed to be much better than vacuum drying. For example, in drying ferments which cannot withstand temperatures higher than $40^{\circ}\text{C}.$, ultrasonic driers require 14 min. whereas vacuum driers require 1 hr.

The next in this series is the spray drier used for drying solutions and pastes (Fig. 7).

Multi-stage cross-flow type drier. To obtain a uniform dried product it is sometimes advantageous to divide the fluidized bed into different zones. One such type of drier is shown in Fig. 8. Material overflows from section to section just as a fluid flows through an orifice. The location of orifice is therefore very important for effective drying and in controlling the height of the bed.

In Fig. 9 is shown another drier in which the bed density in the fluidizer can be controlled by devices like screw conveyors at the feed and discharge ends.

In both these cases the fluidizing medium is led through a common duct and then dispensed to different zones. This system suffers from the drawback that the control of the process is very difficult. For example, if the quantity of material increases in any one of the sections, the resistance to flow of the gas in the section will increase and less gas passes through it.

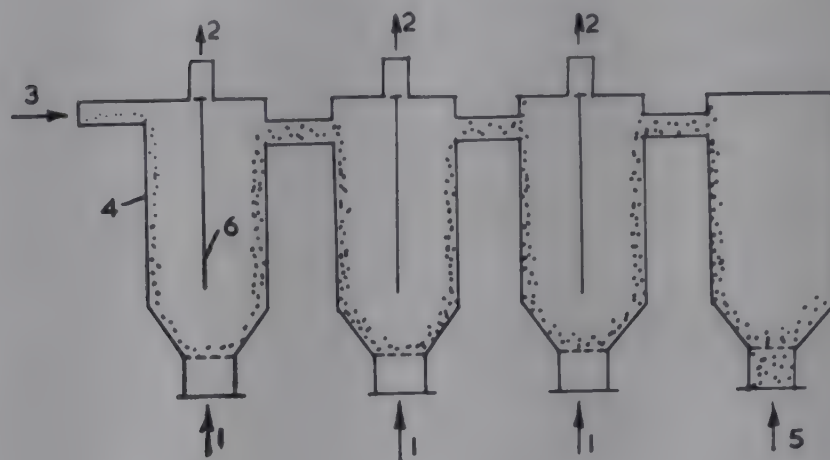


FIG. 10

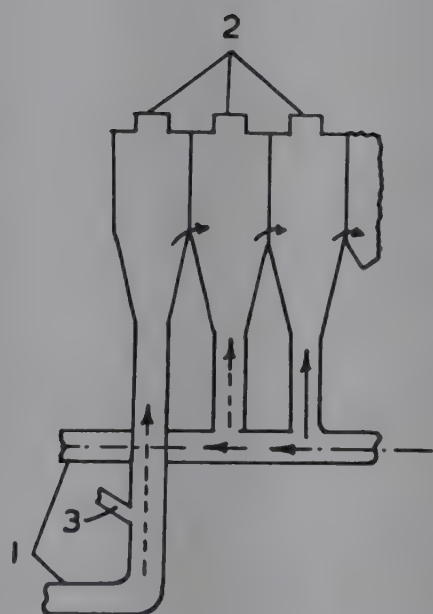


FIG. 11

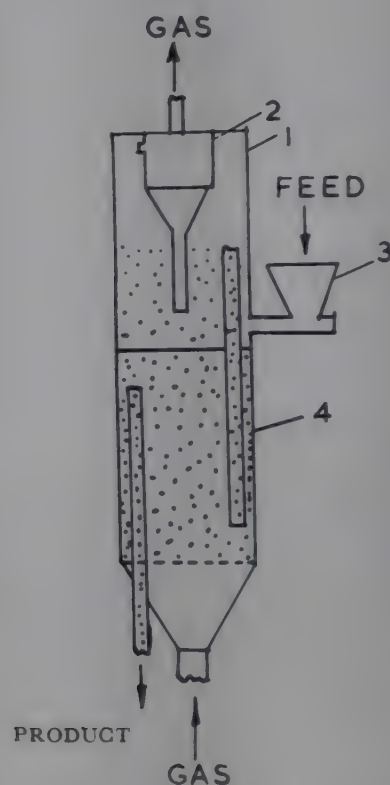


FIG. 12

FIG. 10—MULTI-STAGE CROSS-FLOW TYPE DRIERS IN SERIES [(1) Gas inlet; (2) Gas exit; (3) Raw feed; (4) Fluidizer; (5) Product exit; (6) Overflow device]

FIG. 11—MULTI-STAGE CROSS-FLOW TYPE CONTINUOUS DRIER [(1) Gas inlet; (2) Gas exit; (3) Raw feed]

FIG. 12—MULTI-STAGE CONTINUOUS COUNTER-CURRENT DOUBLE-STAGE DRIER [(1) Drier; (2) Cyclone; (3) Feeder; (4) Overflow pipe]

This in turn helps in accumulation of more material and as a limiting case the fluidizer section may finally choke.

To overcome this drawback, driers have been designed with separate or mixed sources of gas supply. These two types of driers are shown in Fig. 10 and 11 respectively.

Continuous multi-stage counter-current drier. In Fig. 12 is shown a typical multi-stage drier with counterflow of solid and gas, generally



FIG. 13

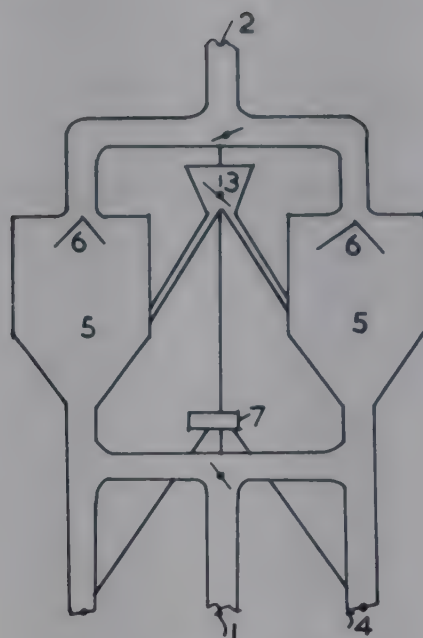


FIG. 14

FIG. 13—MULTI-STAGE COUNTER-CURRENT STAGE DRIER WITH ARRANGEMENT FOR FLUIDIZATION IN CYLINDRICAL ROTOR [(1) Feed inlet; (2) Gas inlet; (3) Gas-solid suspension to cyclone]

FIG. 14—SINGLE-STAGE COUNTER-CURRENT DRIER WITH INTERMITTENT OPERATION [(1) Gas inlet; (2) Gas outlet; (3) Raw feed; (4) Product outlet; (5) Drier; (6) Baffles; (7) Automatic control]

known as Fluosolids drier. The fluidizer is sectioned with horizontal partitions having perforations.

Fig. 13 represents a novel design in which the solid material flows in succession through rotating perforated cylinders of increasing diameter. This type gives very good contact of the gas with the solid.

Single-stage counter-current intermittent drier. Driers shown in Fig. 14 are operated batch-wise in sets of two, while one is under operation the other will be under discharge. The advantages of this type are uniformity in drying and considerably high rates of heating and drying, while the disadvantages are the necessity of stand-by unit and the difficulty in control and operation.

Choice of the drier. Single-compartment drier is recommended for drying granular materials. Conical driers are preferred for semi-dispersive materials, solutions, pastes, etc. Spouted columns of cylindro-conical shape are recommended for drying big granular materials.

DESIGN PRINCIPLES

For designing a drier, the heat requirement for the process and the major dimensions of the drier have to be determined. Methods of calculation have been suggested by Fedorov, Likov, Lebedev, Sazin *et al.* and Romankov *et al.*⁵ In designing a drier, data must be obtained on the capacity of the unit, the initial and final moisture contents of the material, characteris-

tics of the material such as particle size distribution, surface area, density, and the initial temperatures of the drying medium and the material. Other important data include the coefficient of heat transfer between the gas and the material as well as residence time of the material in the drier. Besides, the design depends upon the type of equipment chosen and its method of operation.

In drying, just as in the case of heating of particles in fluidized bed, basic considerations are to be given to the heat transfer problem and the equation of continuity. Thus the following equation can be obtained for the amount of moisture evaporated:

$$\Delta M = G \cdot \frac{W_1 - W_2}{100 + W_1} = \frac{\rho VC (t_1 - t_w)}{\lambda} \cdot Z \quad (1)$$

The heat balance equation assuming no loss to the surroundings gives

$$\begin{aligned} Q &= \rho VC (t_1 - \theta) = Q_v + Q_H \\ &= G \left[\frac{d_w}{dZ} \cdot \frac{\lambda}{100 - W} + C_M \cdot \left(\frac{d\theta}{dZ} \right) \right] \end{aligned} \quad (2)$$

In case heat loss is not negligible, an additional term Q_L should be added up in Eq. (2). The amount of gas necessary can be determined by dividing the total heat requirement with the specific heat of the gas multiplied by its temperature drop during the process of drying.

The final temperature of the material, t_{M_2} depends upon its initial and final moisture contents and the following method was suggested for its determination:

$$\text{If } W_1 > W_2 \geq W_{CN}; t_{M_2} = t_w \quad (3)$$

$$W > W_{CN} > W_2; t_{M_2} = t_w + (t_2 - t_w) \cdot \frac{W_{CN} - W_2}{W_{CN} - W_E} \quad (4)$$

$$W_1 < W_{CN}; t_{M_2} = t_{M_1} + (t_2 - t_{M_1}) \cdot \frac{W_1 - W_2}{W_1 - W_E} \quad (5)$$

Once the volumetric flow rate of the gas is known, the cross-sectional area of the drier is found by dividing this rate with the velocity of the fluid, v_f and so the diameter is known. The fluidizing velocity, v_f is so chosen that $v_f > v_{mf}$.

The bed density β_M is found as follows (by considering the average values for both gas and material):

$$\beta_M = K_1 \cdot K_2 \cdot K_3 \cdot \frac{\frac{G}{Z}}{F(v_f - v_{mf})} \quad (6)$$

The particle velocity can now be determined as

$$v_p = \frac{\frac{G}{Z}}{F \cdot \beta_M} \quad (7)$$

The fluid-to-particle heat transfer coefficient can be determined by using any one of the equations suggested by Ketternig *et al.*²², Heertjes and McKibbons²³, Walton *et al.*²⁴, Federov²⁵, etc.

According to Ketternig *et al.*,

$$Nu = 0.0135 Re^{1.30} \quad (8)$$

Heertjes and McKibbons gave the following equation:

$$h = 6.395 Re^{0.76} \quad (9)$$

The equation given by Walton *et al.* is

$$Nu = 0.0028 Re^{1.7} \left(\frac{D_p}{D_t} \right)^{-0.2} \quad (10)$$

While drying coal in fluidized bed, Federov²⁵ found that the data could be well represented by Eq. (11) and (12).

$$Nu = 0.0151 Ki^{0.74} \cdot Re^{0.65} \left(\frac{H}{D_p} \right)^{-0.34} \quad (11)$$

for Ki value ranging between 30 and 100.

$$Nu = 0.0283 Ki^{0.604} \cdot Re^{0.65} \left(\frac{H}{D_p} \right)^{-0.34} \quad (12)$$

for Ki value ranging between 100 and 200.

Knowing h , the volumetric heat transfer coefficient, h_v can be calculated as follows:

$$h_v = \frac{6 \cdot Nu \cdot K \cdot \beta_M}{D_p^2 \cdot \rho_p} \quad (13)$$

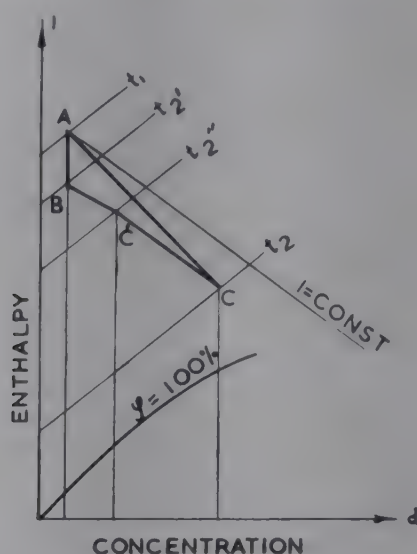


FIG. 15—PLOT OF ENTHALPY VERSUS CONCENTRATION [AB, Heating up to the wet bulb temperature; BC', Drying in the constant rate period; C'C, Drying in the falling rate period; AC, Total drying period]

The height of the drier can now be determined by summing up the total lengths of the drier required for heating the material and for drying both in the constant rate and the falling rate periods, i.e.

$$l = l_H + l_{const} + l_{fall} \quad (14)$$

Each of these individual lengths can be determined as follows:

$$l_{sec} = \frac{\Delta Q_{sec}}{h_v \cdot F \cdot \Delta t_{av.(sec)}} \quad (15)$$

Q_{sec} for each section can be determined from the enthalpy-concentration diagram²⁶ (Fig. 15).

Empirical equations are also available, as suggested by Romankov *et al.*²⁷ for calculating the total drying time and the falling rate period.

Optimum Operating Conditions of Fluidized Driers

The efficient performance of a fluidized drier depends upon a number of factors.

Effect of rate of heating. Rewriting Eq. (2) in the following form, rate of heating of the particles

$$C_M \cdot \frac{d\theta}{dz} = \frac{\rho V C (t_1 - \theta)}{G} - \frac{dW}{dz} \cdot \frac{\lambda}{100 - W} \quad (16)$$

i.e. heating period, ΔZ

$$= \frac{C_M \cdot \Delta\theta}{\frac{\rho VC (t_1 - \theta)}{G} - \frac{dW}{dZ} \cdot \frac{\lambda}{100 - W}} \quad (17)$$

When the rate of heating the particles is equal to zero,

$$\frac{dW}{dZ} \cdot \frac{\lambda}{100 - W} = \frac{\rho VC (t_1 - \theta)}{G} \quad (18)$$

Thus, the higher the value of $\rho VC (t_1 - \theta)/G$ and the lesser the rate of drying, the higher is the rate of heating. With a given temperature and a given rate of drying, the rate of heating is determined only by the quantity $\rho VC (t_1 - \theta)/G$. It is possible to fix any rate of heating by changing any of the factors in the above quantity. Similarly, with a given rate of heating, conditions can be so created as to increase the duration of drying and consequently, by choosing suitable parameters, the material can be dried to a greater degree.

Effect of bed density. In the constant rate period, as it is well known, temperature of the material can be equal to the wet bulb temperature. Hence, if the bed density of the material is sufficiently high, capacity of the drier per unit area increases and the gases will leave the bed fully saturated at a temperature equal to the wet bulb temperature. Further increase in bed density will not be advantageous, because the quantity of heat given by the gas to the material and the amount of moisture evaporated remain unchanged and pressure drop will be more. On the other hand, if the bed density is sufficiently low, there will be much of heat loss with the exit gases. Besides, the material at this high temperature might be superheated, which is detrimental to heat-sensitive materials.

It appears, therefore, that the most suitable bed density should be equal to or greater than the minimum density required for cooling the gas to the temperature of the material.

Effect of gas velocity. Increase in velocity gives rise to higher pressure drop; voidage increases and so the height of the drier has to be increased. Also, higher velocity results in production of more fines and consequently difficulty in separation. As a result, it has been recommended¹ to operate the drier at the medium velocity ensuring good mixing in the bed.

Effect of temperature. It is to be noted from Eq. (16) that at the beginning of drying, when the material is at a lower temperature and the rate of drying is low, heating of the material takes place very fast, and afterwards it falls off. In fact, for rapid rate of heating of the material, very high temperature is employed initially. After the material attains the maximum allowable temperature, the temperature is decreased sharply (especially for heat-sensitive materials) and thereafter it decreases gradually such that the quantity $\rho VC (t_1 - \theta)/G$ changes proportionally with change in the rate of drying (which evidently falls off with the lowering of moisture content).

While drying gelatine in fluidized bed Rosental²⁸ found that for the removal of the same quantity of moisture, lesser drying time is required at a higher temperature.

Effect of humidity. Rosental²⁸ has also shown that drying time increases with increase in humidity of the air. Thus, for the removal of the same quantity of moisture, the greater the humidity of air, the greater is the drying time.

Effect of particle size. With increase in particle size the heat transfer coefficient decreases and consequently, the drying rate decreases. For the same period of drying, finer particles were found²⁸ to have lesser moisture content.

Residence time in drier. Residence time of solid materials in a fluidized drier widely varies and there is a wide distribution. No data are available and normally the 'average' or 'nominal' residence time is determined.

Reboux²⁹ has suggested a method for calculating the probability of period of residence of solid material in a multi-stage reactor. Taking for example, a reactor consisting of two identical sections connected in series, if t_o = av. residence time in each section and if material is introduced into the upper layer at time $t=0$, the probability of stay of the material after a lapse of time, t , will be

$$X_1 = e^{-t/t_o} \quad (19)$$

Let X_2 be the probability of stay of particles in the second section.

During the time interval $t-dt$, let X_2 increase by dX_2 . The probability of the particles falling into the second section during the time interval $(t \sim t+dt)$ is $X_1 \cdot dt/t_o$. But some of the particles may as well leave this section, and let this probability be $X_2 \cdot dt/t_o$. Hence the probability of the particles staying in the second section is

$$X_2 = X_1 \cdot \frac{dt}{t_o} - X_2 \cdot \frac{dt}{t_o} \quad (20)$$

Substituting for X_1 and integrating,

$$X_2 = \frac{t}{t_o} \cdot e^{-t/t_o} \quad (21)$$

Evidently, the probability of particles staying in either of the sections is

$$X = X_1 + X_2 = \left(1 + \frac{t}{t_o}\right) e^{-t/t_o} \quad (22)$$

For a multi-stage drier having n sections, probability is

$$= e^{-t/t_o} \left[1 + \frac{t}{t_o} + (t/t_o)^2 \cdot \frac{1}{2!} + (t/t_o)^3 \cdot \frac{1}{3!} + \dots + (t/t_o)^{n-1} \cdot \frac{1}{(n-1)!} \right] \quad (23)$$

The more the ratio t/t_o approaches unity, the greater the fraction of the material which will have drying period nearing the average residence time; and consequently, the less is the nonuniformity of drying. Nonuniformity in drying, thus sharply decreases with increase in the number of stages in the drier.

Romankov *et al.*³⁰ have recently pointed out that only the kinetic equations and the average residence time of solid materials in a drier do not adequately represent the phenomenon of drying. For example, it was shown that because of the distribution of residence time of particles in a fluidized drier, the actual moisture content of the product varies widely from the calculated values. This is more important when the data for a batch system have to be utilized for the design of a continuous unit. Equations have been developed by these authors for calculating the distribution of residence time both in the constant rate and the falling rate periods.

NOMENCLATURE

| | |
|-----------------|--|
| C | = specific heat of fluid, $kcal./kg. ^\circ C.$ |
| C_M | = specific heat of material, $kcal./kg. ^\circ C.$ |
| D_p | = mean diameter of particles, $m.$ |
| D_t | = diameter of fluidized drier, $m.$ |
| F | = cross-sectional area, $m.^2$ |
| G | = weight of material dried, $kg.$ |
| g | = acceleration due to gravity, $m./sec.^2$ |
| H | = height of bed, $m.$ |
| h | = heat transfer coefficient, $kcal./m.^2 hr ^\circ C.$ |
| h_v | = volumetric heat transfer coefficient, $kcal./m.^3 hr ^\circ C.$ |
| K | = thermal conductivity, $kcal./m. hr ^\circ C.$ |
| Ki | = Kirpichev number, $D_p^3 \sqrt{\frac{4}{3} \cdot \frac{g}{\nu^2} \left(\frac{\rho_p}{\rho} - 1 \right)}$ |
| K_1, K_2, K_3 | = correction factors considering the drag effect on the particles, the effect of inter-particle and particle-to-wall collision, and the effect due to changes in the physical constants of the material and gas respectively |
| l | = length of drier, $m.$ [l_H , length required for heating; l_{const} , the constant rate period; l_{fall} , falling rate period; l_{sec} , any section] |
| Nu | = Nusselt number, $h D_p / K$ |
| Q | = total heat requirement, $kcal./hr$ [subscript V refers to the heat of vaporization, H to that of heating the material, L to that of loss] |
| Q_{sec} | = heat requirement for any section, $kcal./hr$ |
| Re | = Reynolds number, $D_p v_f \rho / \mu$ |
| t_1 | = initial temperature of fluid, $^\circ C.$ |
| t_2 | = final temperature of fluid, $^\circ C.$ |
| t_{M1} | = initial temperature of material, $^\circ C.$ |
| t_{M2} | = final temperature of material, $^\circ C.$ |
| t_w | = wet bulb temperature, $^\circ C.$ |
| Δt_{av} | = average temperature drop, $^\circ C.$ |
| V | = flow rate of fluid, $m.^3/hr$ |
| v_f | = velocity of fluid, $m./hr$ |
| v_{mf} | = minimum fluidization velocity, $m./hr$ |

| | |
|----------------------|--|
| v_p | = particle velocity, $m./hr$ |
| W_1 | = initial moisture content of material, % |
| W_2 | = final moisture content of material, % |
| W_E | = equilibrium moisture content, % |
| W_{CN} | = critical moisture content, % |
| z | = drying time, hr |
| $\frac{dW}{dz}$ | = rate of drying of material, % moisture/ hr |
| $\frac{d\theta}{dz}$ | = rate of heating of material, $^{\circ}C./hr$ |
| β_M | = bed density, $kg./m.^3$ |
| ρ | = density of fluid, $kg./m.^3$ |
| ρ_p | = particle density, $kg./m.^3$ |
| μ | = viscosity of fluid, $kg./m. hr$ |
| λ | = latent heat of vaporization, $kcal./kg.$ |
| ν | = kinematic viscosity of fluid, $m.^2/sec.$ |

REFERENCES

1. LEBEDEV, P. D., *Rach. Proekt. Su Ustan. Gosenergoizdat*, 1963.
2. ROMANKOV, P. G., *Khim. Mash.*, **1** (1963), 7.
3. MORILOV, A. A., RUBTSOV, G. K., SIROMIATNIKOV, N. I. & BACKALOV, A. P., *Khim. Prom.*, **2** (1962), 809.
4. ROMANKOV, P. G. & RASHKOVSKAYA, N. B., *Khim. Prom.*, **2** (1962), 836.
5. ROMANKOV, P. G. *et al.*, *Mas. Jir. Prom.*, **7** (1962), 10.
6. DONOM, E. V. & MOLOKOVA, G. K., *Khim. Prom.*, **2** (1962), 842.
7. SHAKHOVA, N. A. & MASLOVSKY, M. F., *Khim. Mash.*, **6** (1959), 27.
8. RICHKOV, A. I. & SHAKHOVA, N. A., *Khim. Prom.*, **2** (1962), 839.
9. RICHKOV, A. I., SHAKHOVA, N. A., DIMITRENKO, E. V., *Khim. Prom.*, **2** (1961), 783.
10. FRANTZ, J. F., Thesis, Louisiana State University, May 1958.
11. JONKE, A. A., PETKUS, E. J., LEEDING, J. W. & LAWROSKI, S., *Nuclear Sci. & Engng*, **2** (1957), 303.
12. PHILOON, W. C., SANDER, E. F. & TRASK, W. T., *Chem. Engng Progr.*, **56** (1960), 106.
13. JACKSEN, J. D., SORGENTI, H. A., WILCOX, G. A. & ECCOKEY, R. S. *Industr. Engng Chem.*, **52** (1960), 795.
14. VANECEK, V. & LEDERES, E., *Rep. Res. Instrn inorg. Chem. (U.K.)*, No. 234, 1959.
15. *Australian Pat.* No. 279907 (1957).
16. KAGANOVICH, U. I. *et al.*, *Khim. Prom.*, (1960), 389.
17. KAGANOVICH, U. I., *Khim. Nayk. Prom.*, **2**(6) 1957, 764.
18. MARKAVART, M., VANECEK, V. & DRBOHLOV, R., *Brit. chem. Engng*, **7**(7) (1962), 503.
19. *Lit. Proiz.*, **1** (1963), 39.
20. OTHMER, D. F., *Fluidization* (Reinhold Publishing Corp., New York), 1956.
21. WALL, C. J. & ASH, W. J., *Industr. Engng Chem.*, **41** (1949), 1247.
22. KETTERING, K. N., MANDERFIELD, E. L. & SMITH, J. M., *Chem. Engng Progr.*, **46** (1950), 139.
23. HEERTJES, P. M. & MCKIBBONS, S. W., *Chem. Engng Sci.*, **5** (1956), 161.
24. WAITON, J. S., OLSON, R. I. & LEVENSPIEL, O., *Industr. Engng Chem.*, **44** (1952), 1474.
25. FEDOROV, I. M., *Theo. Rach. Proc. Syshki, Gosenergoizdat*, 1955.
26. KASATKIN, A. G. & OSNOV, *Proc. appl. Khim. Tech. Goskhimizdat*, **2** (1961), 658.
27. ROMANKOV, P. G. *et al.*, *J. Pri. Khim.*, **35**(3) (1962), 530.
28. ROSENAL, E. O., *Iss. Proc. Syshki*, Dissertation, Institute of Food Technology, Moscow, 1955.
29. REBOUX, P., *Phénoménés de fluidisation* (Ass. franc. fluidis., Paris), 1954.
30. ROMANKOV, P. G. *et al.*, *J. Pri. Khim.*, **35**(1) 1962, 80.

Inter-phase Mass Transfer during Drop or Bubble Formation: A Re-evaluation

D. VIR* & F. H. GARNER

Department of Chemical Engineering, University of Birmingham
Birmingham 15, U.K.

The assumption that the character of mass transfer during formation is in some way radically different from that of mass transfer during movement through continuous phase has been examined. Since actual calculations of overall coefficients are usually based on ignoring the effect of different initial concentrations in these two stages, an effort has been made to re-evaluate reported results by treating these stages as one composite stage. It has been shown that a satisfactory linear relationship exists between the logarithmic value of the fraction extracted and the logarithmic value of $(0.6 t_f + t_{tr})/r^2$ where t_f represents the time of formation, t_{tr} the time of movement, and r the radius of the drop or bubble. A reference to the authors' work on liquid-liquid systems provides corroboration of these conclusions.

Licht and Conway¹ postulated three distinct stages in mass transfer in a spray column: (i) drop formation at entry to column, (ii) drop movement through the column, and (iii) drop coalescence at the interface at the terminal end of the column.

Studies on mass transfer during formation have hitherto mainly relied on extrapolation procedure. Whitman, Long and Wang² studied absorption of carbon dioxide by water drops falling through a constant height and concluded that the amount of carbon dioxide absorbed per unit drop volume of water was a linear function of the time of formation; by extrapolation to zero time of formation, they obtained results purporting to represent absorption during free fall. In regard to the absorption of ammonia by

*Present address: Department of Chemical Engineering & Technology, Panjab University, Chandigarh 3.

water drops, they found that the mass transfer coefficient was a linear function of the time of formation. Using a similar method, Hatta and Baba³ observed that the extraction of carbon dioxide during formation of water drops was small.

Sherwood, Evans and Longcor⁴ in liquid-liquid extraction studies kept the formation time constant and obtained a linear relationship between column height and the logarithmic value of unextracted fraction. In the extraction of acetic acid from water drops by isopropyl ether, methyl isobutyl ketone and ethyl acetate, Licht and Conway¹ came to a somewhat startling conclusion that, with this extrapolation procedure, the fraction extracted during drop formation was independent of the formation time. However, investigations by Farmer⁵, Katz⁶, and West *et al.*⁷, using the same procedure with other systems, have shown that this is by no means a universal case. Licht and Pansing⁸ have questioned the validity of the extrapolation procedure on the ground that, in general, a plot of the logarithmic value of the unextracted fraction against column height is not a straight line all the way back to zero column height. Their work on liquid-liquid systems confirms the conclusions of Sherwood, Evans and Longcor to the effect that drop diameter as well as drop formation time determines the degree of extraction over varying column heights.

The extrapolation procedure was found to be general in application by Garner and Skelland⁹, Foord¹⁰, Garner, Foord and Tayeban¹¹, Tayeban¹², and Garner and Hale¹³ in a series of extended studies by the Birmingham University chemical engineering group.

Extraction during First and Second Stages

There is an implicit assumption in all these investigations that the character of mass transfer during formation is in some way radically different from that of mass transfer during movement through the continuous phase. It is beyond dispute that certain dissimilarities in the mechanism of mass transfer do exist as between the first and the second stage; in particular, drop motion itself as well as oscillation and internal circulation would tend to differentiate the two.

Actual calculations of mass transfer overall coefficients are based on ignoring the effect of changing concentration on individual film coefficients. The concentration at the start of the second stage is not the same as at the start of the first stage. Accordingly, for a rigorous theoretical treatment of overall coefficients in each stage, these concentration variations need to be taken into account. Conditions for such a rigorous analysis are, however, seldom known and the normal procedure is to evaluate overall coefficients on the basis of initial concentration. With this procedure there appear to be no reasons why the two stages should be distinguished at all, except for the complications that are necessarily introduced by changes in area or shape, by circulation and oscillation phenomena and by formation of a

wake. The exact impact of these complications is uncertain. Wherever it can be estimated, it should be taken into account.

In other cases, it is necessary to re-examine the results to explore the possibility of treating the first two stages as one composite stage. The third stage, being minor, may in this context be treated as negligible, though it undoubtedly contributes to any observed scatter.

Diameter and Area of Drops and Bubbles

The area of mass transfer during growth continuously expands. At any stage of formation, as shown by Licht and Pansing⁸,

$$Q = 0.6 K t S (\Delta C)_{lm}$$

where Q is the amount of solute transferred, $(\Delta C)_{lm}$ is the driving force, K is the overall mass transfer coefficient and S is the area of the sphere after time t , provided the volumetric feed rate to the nozzle is constant.

Since the amount transferred in this stage is proportional to $0.6 t S$, no error will be introduced if S is treated as constant over a period of time $0.6 t$. Therefore, if t_I and t_{II} denote respectively the actual time of formation and the time taken for movement through the continuous phase, the total time of contact may be taken as $0.6 t_I + t_{II}$ with a constant area of exposure S . For unsteady state extraction, Q may similarly be shown as proportional to $(0.6 t_I + t_{II})^{\frac{1}{2}}$. Theoretically, a linear relationship between $\log (0.6 t_I + t_{II})$ and $\log E$ (fraction extracted) is predictable, provided the two separate stages can be treated as a composite stage, and provided the final diameter is uniform for all plotted results.

When different final diameters are involved, there should result a different straight line for each size. Assuming steady state extraction,

$$Q = 4\pi D t \left(\frac{a b}{b-a} \right) (C_2 - C_1)$$

where C_2 is the concentration at a point b units of length away from the centre of the sphere and located in the continuous phase, and C_1 is the concentration at a point a units away and located on the interface. The length a is thus equal to radius r . Taking length b as infinite and Q equal to $4/3 \pi r^3 (C_1 - C_0)$, where C_0 is the initial concentration, we have

$$E = \frac{C_1 - C_0}{C_\infty - C_0} = D t / r^2$$

Barrer¹⁴ has shown that for unsteady state extraction

$$-\ln (1-E) = 0.5\pi^2 D t / r^2$$

Whence

$$E = 6\pi^{\frac{1}{2}} (D t / r^2)^{\frac{1}{2}}$$

Thus, in either case the term t/r^2 may replace the previous t to take into account different final diameters for correlation of experimental results on varying drop sizes.

In the present analysis, data from various sources have been re-evaluated by plotting $\log t/r^2$ (where t represents $0.6 t_I + t_{II}$) against $\log E$ or against some variable analogous to $\log E$.

Data on Time of Contact and Approach to Equilibrium

Fig. 1 shows data of Groothuis and Kramers¹⁵ on absorption of carbon dioxide by water drops. The technique of their work made it possible for them to measure directly absorption during the formation stage. Since the concentration after time t is in this case directly proportional to the fractional approach to equilibrium, their data show the required linear relationship between $\log (0.6 t_I/r^2)$ and $\log E$. The data of Whitman, Long and Wang², plotted in Fig. 2, relate to t_I values ranging between 0.5 and 5.94 sec. and t_{II} (estimated) value of 0.35 sec. for the same system and also indicate a linear relationship.

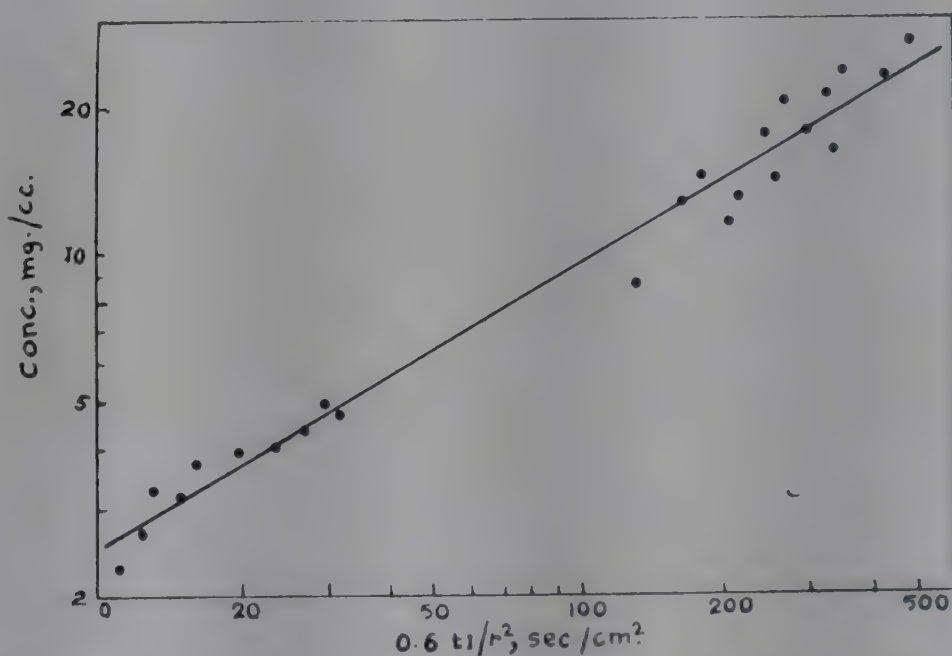


FIG. 1—DATA OF GROOTHUIS AND KRAMERS ON ABSORPTION OF CARBON DIOXIDE BY WATER DROPS [Concentration versus $0.6 t_I/r^2$]

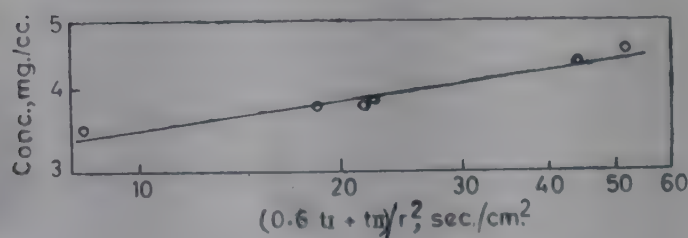


FIG. 2—DATA OF WHITMAN, LONG AND WANG ON ABSORPTION OF CARBON DIOXIDE BY WATER DROPS [Concentration versus $(0.6 t_I + t_{II})/r^2$]

Results of Groothuis and Kramers¹⁵ on absorption of sulphur dioxide by water drops and of Whitman, Long and Wang² on absorption of ammonia by water drops (Fig. 3) do not give very satisfactory plots because of high amounts being absorbed; large changes in concentration introduce a further complication which is examined elsewhere by Garner and Vir (unpublished results).

In the data of Garner, Foord and Tayeban¹¹, and Tayeban¹² on transfer of diol from drops to a continuous column of water, plotted in Fig. 4, t_I is constant at 5.0 sec. and t_{II} varies between 1.8 and 43.8 sec.; there are also large variations in drop diameter, ranging from 0.12 to 0.50 cm. Fig. 5 records Tayeban's data on transfer of diol to water drops with t_I constant at 5.0 sec. and t_{II} having a large range, 0.3–70.0 sec., and shows the plotted points closely clustered along a straight line. In the present context, his work on transfer of benzyl alcohol to water drops does not appear to be significant because of t_I being constant at a comparatively low value of 1.0 sec. These results are plotted in Fig. 6.

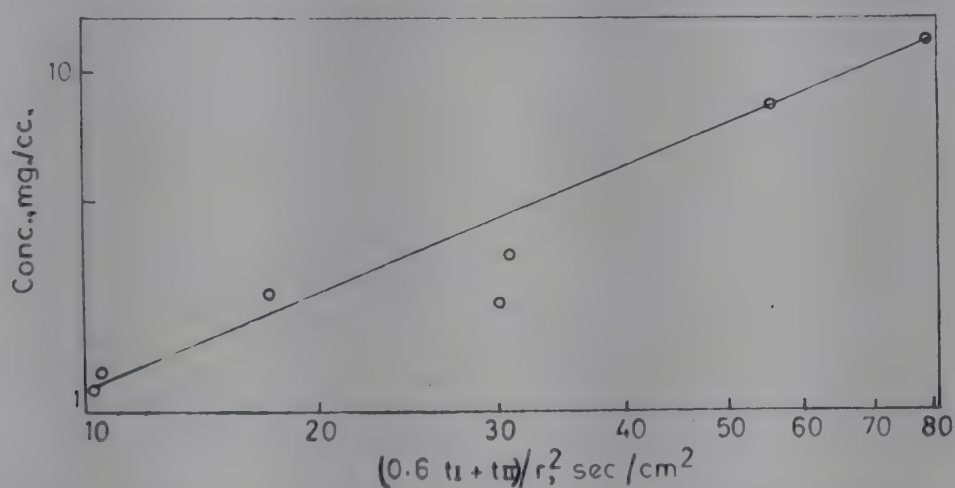


FIG. 3—DATA OF WHITMAN, LONG AND WANG ON ABSORPTION OF AMMONIA BY WATER DROPS [Concentration versus $(0.6 t_I + t_{II})/r^2$]

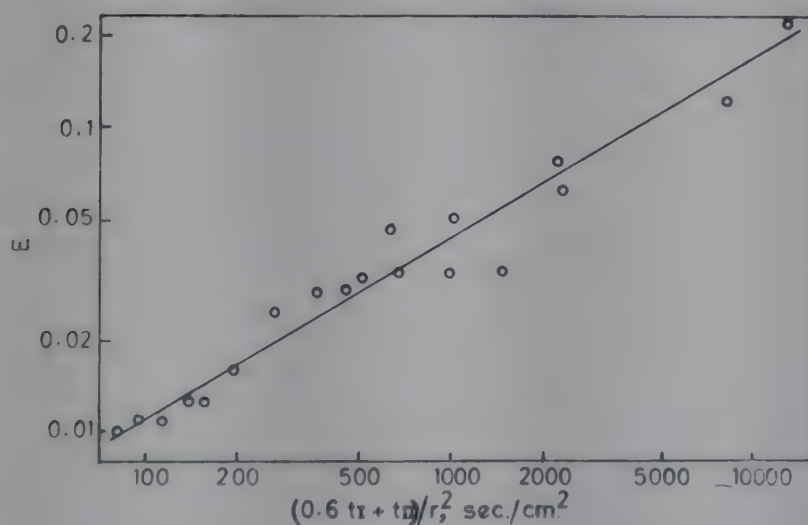


FIG. 4—DATA OF TAYEBAN ON TRANSFER FROM DIOL DROPS TO WATER [E versus $(0.6 t_I + t_{II})/r^2$]

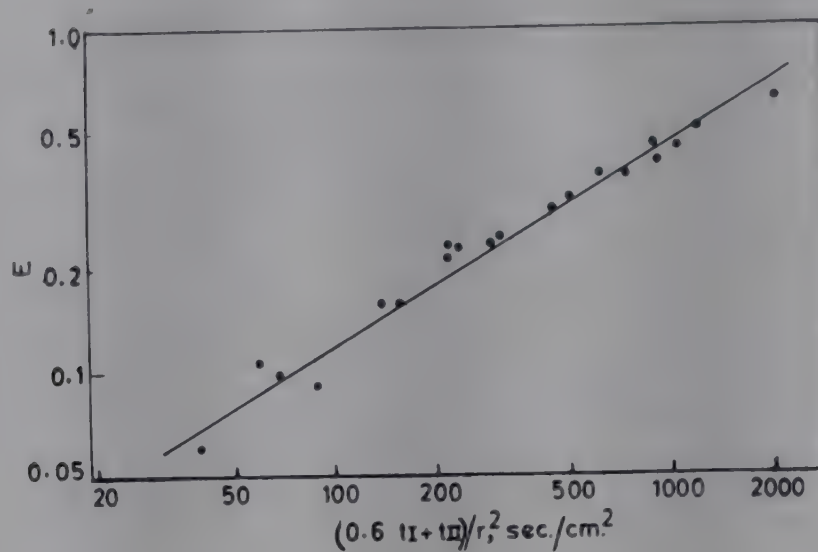


FIG. 5—DATA OF TAYEBAN ON TRANSFER OF DIOL TO WATER DROPS [E versus $(0.6 t_I + t_{II})/r^2$]

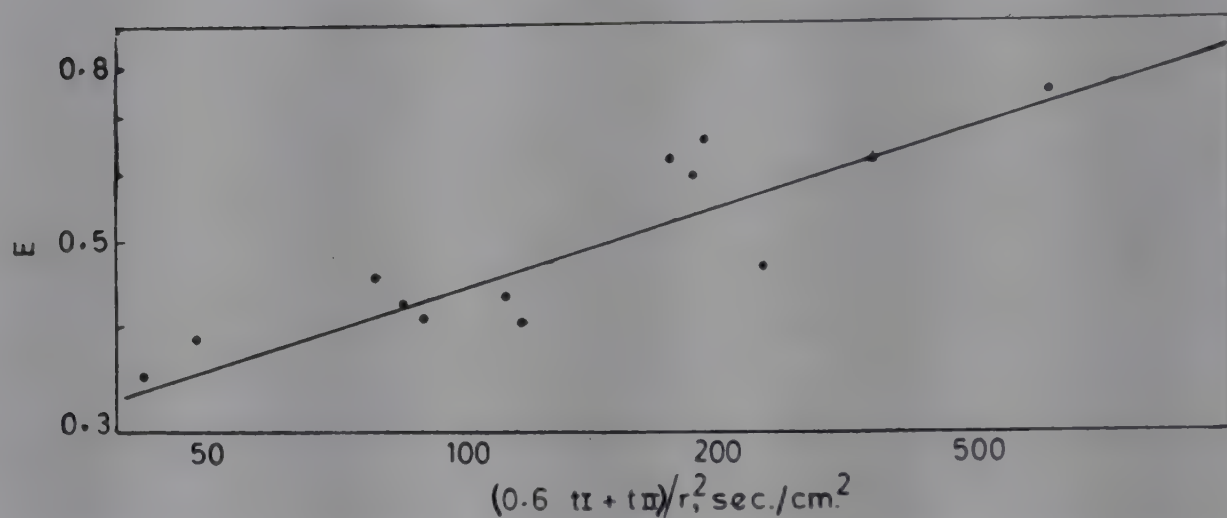


FIG. 6—DATA OF TAYEBAN ON TRANSFER OF BENZYL ALCOHOL TO WATER DROPS [E versus $(0.6 t_I + t_{II})/r^2$]

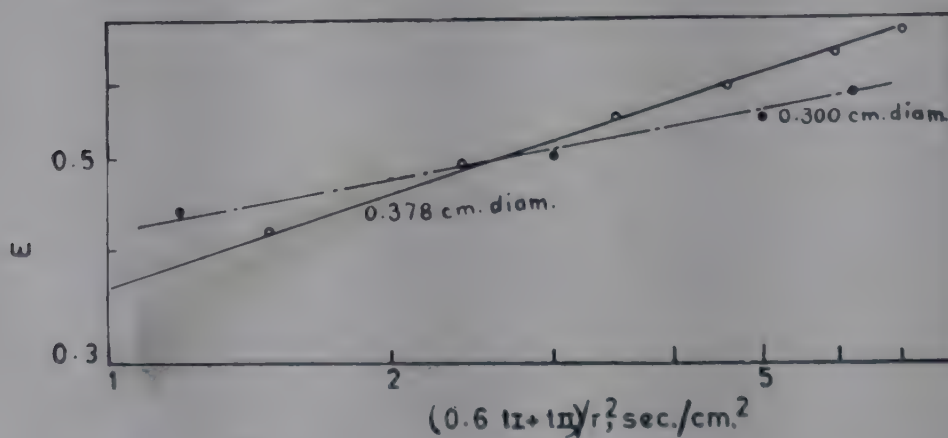


FIG. 7—DATA OF JOHNSON *et al.* ON WATER-*n*-BUTANOL SYSTEM [E versus $(0.6 t_I + t_{II})/r^2$]

Fig. 7, 8 and 9 are based on results obtained by Johnson *et al.*¹⁶ on water-*n*-butanol and water-cyclohexanol systems. Each of these figures confirms the present conclusions. The same is the case with Fig. 10 based on data from Licht and Pansing⁸ on carbon tetrachloride-oil-water system. The work of Garner and Skelland⁹ on the mechanism of extraction of acetic acid from nitrobenzene drops by water shows a similar trend. All points plotted in Fig. 11 had t_I varying within a wide range.

In an intensive study on the extraction of acetic acid and propionic acid from trichloroethylene and pentachloroethane drops by water within wide ranges of t_I and t_{II} and at different temperatures, Garner and Vir (unpublished results) also have shown that the percentage approach to equilibrium is clearly in direct linear correlation with the time of contact, as defined above, when it is adjusted for variations in drop size.

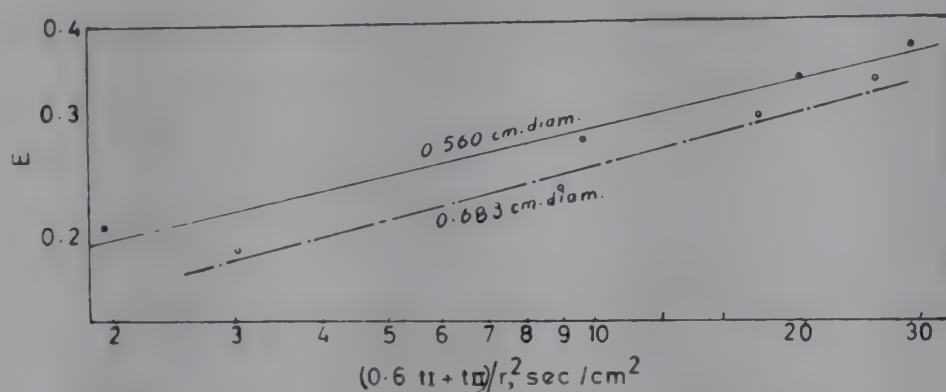


FIG. 8—DATA OF JOHNSON *et al.* ON WATER-CYCLOHEXANOL SYSTEM
[E versus $(0.6 t_I + t_{II})/r^2$]

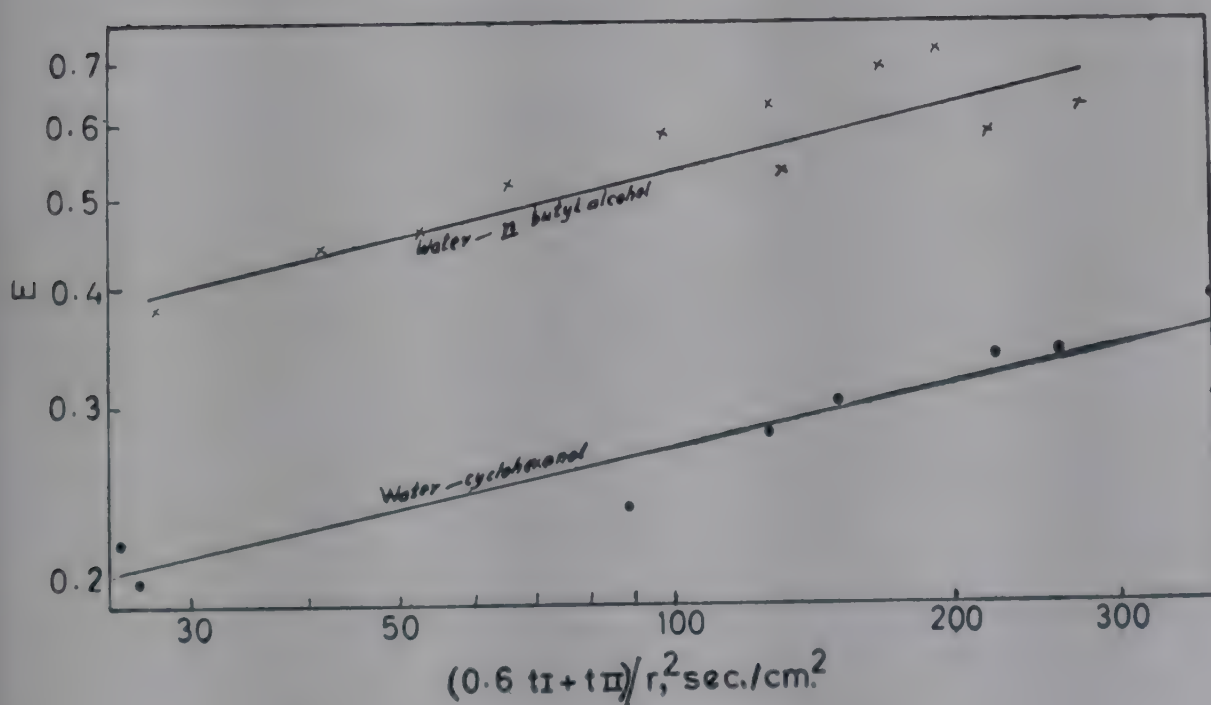


FIG. 9—DATA OF JOHNSON *et al.* ON LIQUID-LIQUID SYSTEMS
[E versus $(0.6 t_I + t_{II})/r^2$]

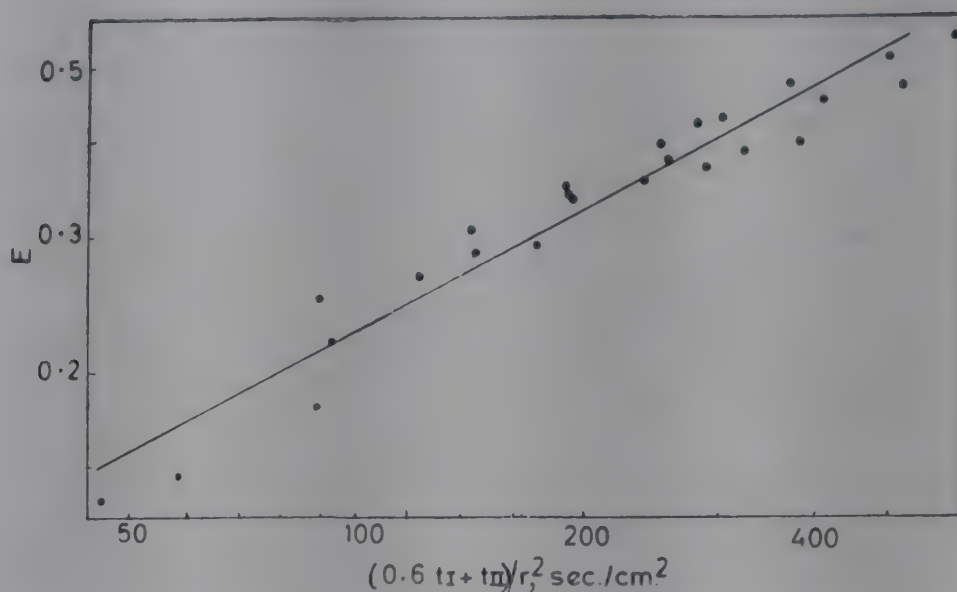


FIG. 10—DATA OF LIGHT AND PANSING ON CARBON TETRACHLORIDE-OIL-WATER SYSTEM
[E versus $(0.6 t_I + t_{II})/r^2$]

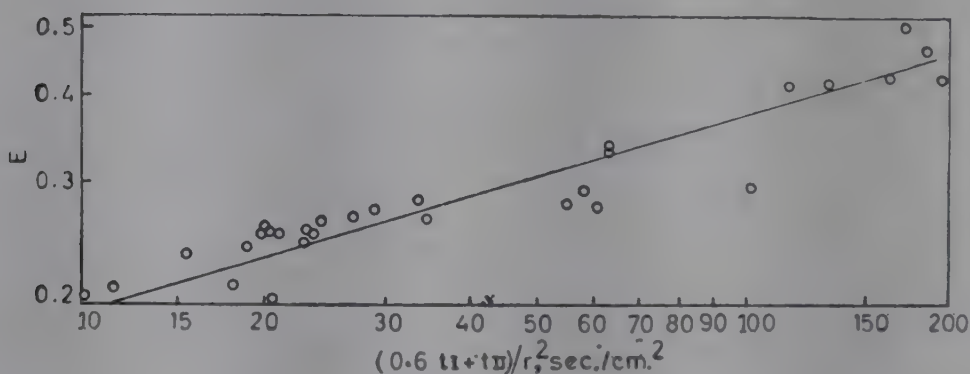


FIG. 11—DATA OF GARNER AND SKELLAND ON EXTRACTION OF ACETIC ACID FROM
NITROBENZENE DROPS BY WATER [E versus $(0.6 t_I + t_{II})/r^2$]

It is thus obvious that, in most cases, the stage of drop or bubble formation and drop movement through the column is one continuous process for all practical purposes.

Reasons for Scatter of Points

It is worthwhile to examine the various factors which lead to deviations from predicted linear character. These may be attributed to: (i) empirical nature of reasoning in using $\log E$ and $\log t/r^2$ as coordinates, (ii) role of oscillation in influencing mass transfer rates, (iii) internal circulation in the second stage, (iv) non-spherical shape of drops or bubbles during formation and movement, (v) distortion at the nozzle tip, (vi) effect of formation of wake during movement, (vii) assumptions inherent in taking 2 as the exponent of r , (viii) equation of concentration gradient with driving force (this being common to all mass transfer calculations), (ix) change in drop or bubble volume as a result of solute transfer, (x) assumption that the solute is uniformly distributed throughout the main body of fluids,

(xi) change in solute concentration in the continuous phase, (xii) variation of diffusivity and distribution ratio with concentration or with changes in physical characteristics of systems as diffusion proceeds, and (xiii) comparatively high degree of inaccuracy in experimental results in spite of some refinements in equipment introduced by successive investigators.

REFERENCES

1. LICHT, W. & CONWAY, J. B., *Industr. Engng Chem.*, **42** (1950), 1151.
2. WHITMAN, W. G., LONG, L. & WANG, H. W., *Industr. Engng Chem.*, **18** (1926), 363.
3. HATTA, S. & BABA, A., *J. Soc. chem. Ind. Japan*, **38** (1935), 544B.
4. SHERWOOD, T. K., EVANS, J. E. & LONGCOR, J. V. A., *Industr. Engng Chem.*, **31** (1939), 1144.
5. FARMER, W. S., *Oak Ridge nat. Lab. Unclassified Rep.* No. ORNL 635, 1950.
6. KATZ, H. M., M.Sc. Thesis, Cincinnati University (U.S.A.), 1950.
7. WEST, F. B. *et al.*, *Industr. Engng Chem.*, **43** (1951), 234.
8. LICHT, W. & PANSING, W. F., *Industr. Engng Chem.*, **45** (1953), 1885.
9. GARNER, F. H. & SKELLAND, A. H. P., *Industr. Engng Chem.*, **46** (1954), 1255; **48** (1956), 51; *Chem. Engng Sci.*, **4** (1955), 149; *Nature, Lond.*, **173** (1954), 1239; *Trans. Instn Chem. Engrs, Lond.*, **29** (1951), 315.
10. FOORD, A., Ph.D. Thesis, Birmingham University (U.K.), 1956.
11. GARNER, F. H., FOORD, A. & TAYEBAN, M., *J. appl. Chem. Lond.*, **9** (1959), 315.
12. TAYEBAN, M., Ph.D. Thesis, Birmingham University (U. K.), 1959.
13. GARNER, F. H. & HALE, A. R., *Chem. Engng Sci.*, **2** (1953), 157; *J. appl. Chem., Lond.*, **5** (1953), 653.
14. BARRER, R. M., *Diffusion in and through Solids* (Cambridge University Press, London), 1941.
15. GROOTHUIS, H. & KRAMERS, H., *Chem. Engng Sci.*, **4** (1955), 17.
16. JOHNSON, A. I., HAMIELEC, A., WARD, D. & GOLDING, A., *Canad. J. chem. Engng*, **36** (1958), 221.

SECTION FOUR

Heat Transfer in Fluidized Beds

Heat Transfer and Pressure Drop in Continuous Fluidization

P. S. LELE*

Department of Chemical Engineering, Panjab University
Chandigarh 3

Continuous aggregative fluidization has been defined and inter-relation between pressure drop, fraction voids, fluid velocity and solid flow rate for continuous aggregative fluidization has been studied. The experimental data have been compared with those of previous workers.

The work was further extended to wall-to-bed heat-transfer. An empirical equation has been proposed to explain the data.

If a batch of solid particles with free upper surface is subjected to counter-gravity flow of a fluid, relative motion of solid particles is obtained without elutriation, over a range of fluid velocities. This range is designated as the fluidization range. Outside this range, there is either elutriation or the bed remains fixed. Since the solids settle in the gravitational field, the fluid flow is always upwards. If solid particles are continuously fed to a fluidized bed at the bottom and removed at the same rate from the top and the fluid velocity is maintained within the fluidization range, there is continuous fluidization. As defined here, it is distinct from pneumatic transport or moving beds.

The object of the present work was to obtain experimental data to investigate the inter-relation between pressure drop, Reynolds number, fraction void and heat-transfer coefficient in continuous fluidization.

EXPERIMENTAL SET-UP AND PROCEDURE

The pressure drop experiments were conducted in a glass apparatus

*Present address: Department of Chemical Engineering, Indian Institute of Technology, New Delhi 16.

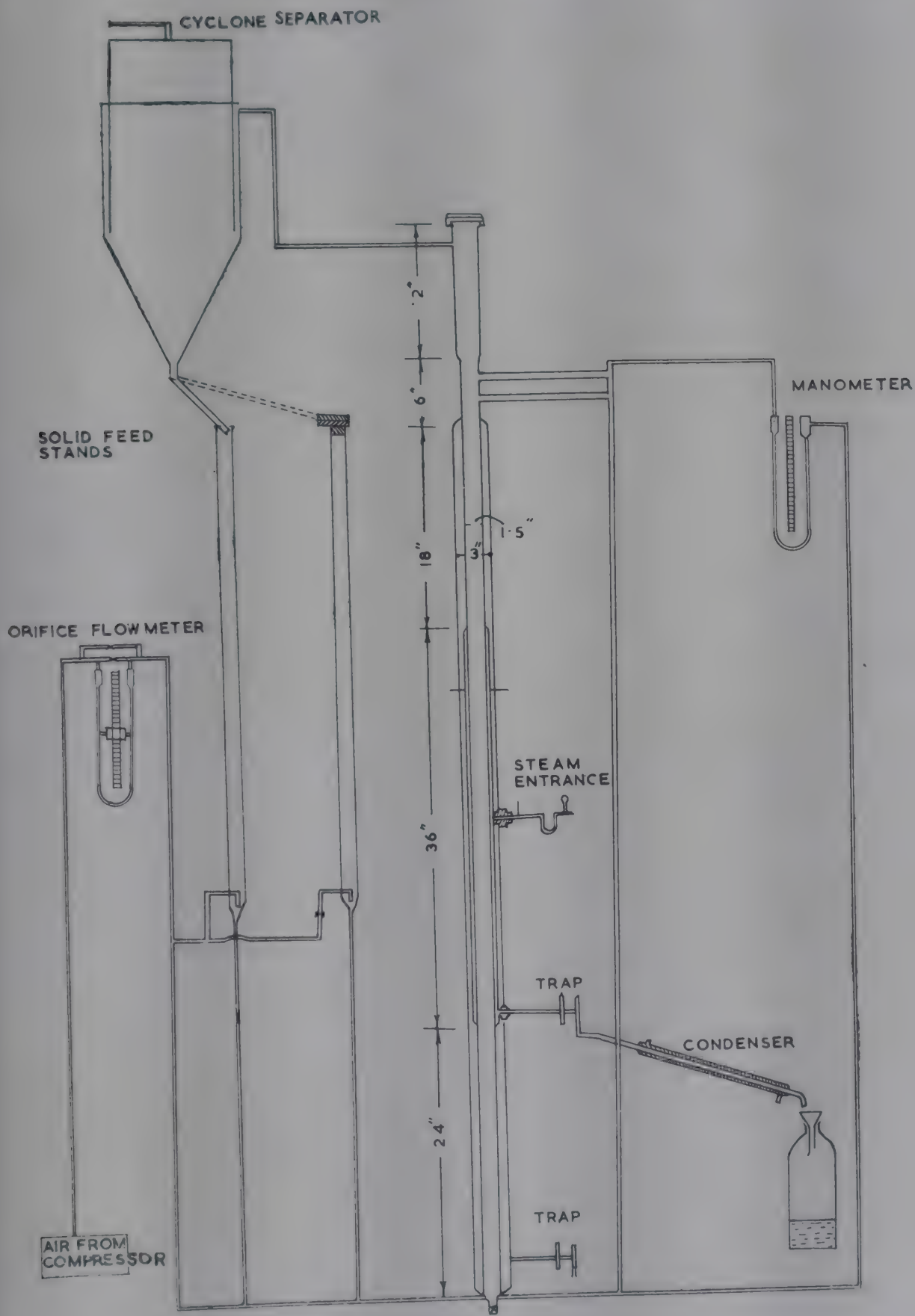


FIG. 2—STEAM-HEATED FLUIDIZATION COLUMN

At a fixed air velocity within the fluidization range, the solid feed was started and continued till solid escape rate was equal to solid feed rate. The average pressure drop across the column was then measured. From this the fraction void or the solid concentration was calculated.

For heat transfer experiments the fluid velocity was fixed within the fluidization range. The solid feed and steam supply were started and continued till a steady bed temperature was indicated by the thermocouple. Continuous solid circulation at varying rates was possible because of the two solid feed stand pipes which were alternately used to feed and collect the solid particles respectively. At steady state the condensate from the central jacket and the solid particles collected over a fixed time interval were measured. The former was used to calculate the amount of heat transferred and latter to measure the solid feed rate. At steady state the temperature of the solid fed was constant at 76°C.

RESULTS AND DISCUSSION

Pressure Drop Data

Graph of solid concentration versus solid feed rate at constant fluid velocity for typical material is shown in Fig. 3 which indicates that the solid concentration is independent of solid feed rate but increases with decrease in the fluid velocity.

Likewise graphs of the pressure drop versus solid feed rate (Fig. 4) show that the pressure drop is a function of the fluid velocity and not of the solid feed rate.

The plot of pressure drop versus Reynolds number on logarithmic scale showed two straight lines intersecting at the point of fluidization. The same value at transition point was obtained in experiments on batch fluidization.

In Fig. 5 solid concentration has been plotted against fluid velocity with solid feed rate as the parameter. These graphs are obtained by cross plotting the previous data.

The above graphs suggest that it should be possible to extend the analysis of batch fluidization to continuous fluidization. To verify this a theoretical bed height was calculated using the values of fraction void obtained from data on batch fluidization, and the values of solid concentrations obtained in the present work. It is seen that a constant value is obtained for a given material, indicating that it is possible to extend the observations in batch fluidization to continuous fluidization provided that the quality of fluidization remains same and provided the Reynolds number is strictly within the fluidization range.

It is evident from the data that the 'slip velocity' is not constant but is a function of the solid feed rate at constant fluid velocity and vice versa.

Theoretical equations on continuous fluidization were not available

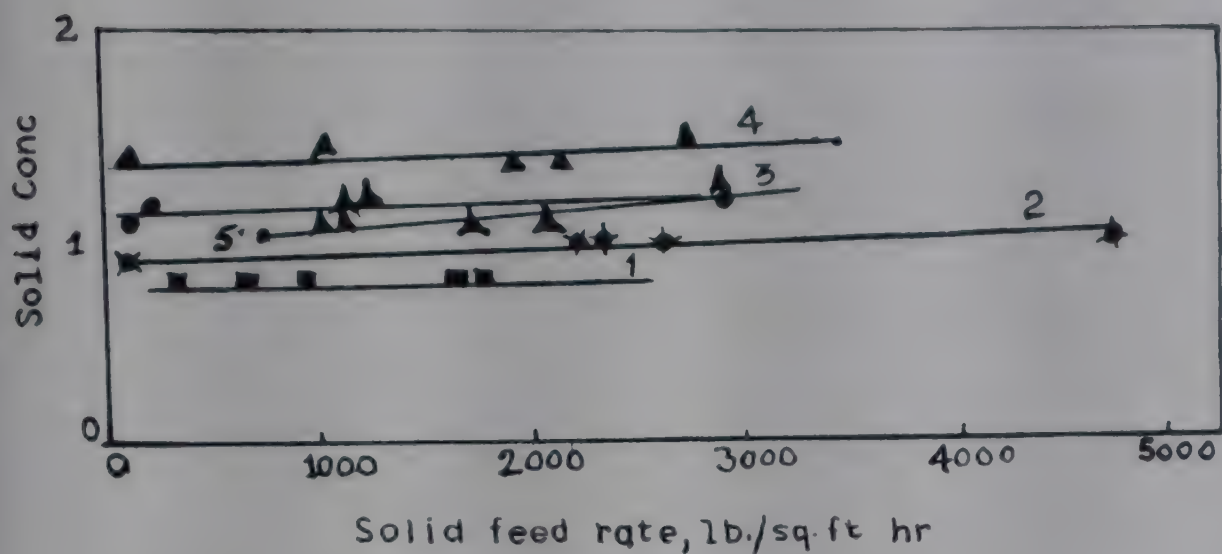


FIG. 3 —PLOT OF SOLID CONCENTRATION VERSUS SOLID FEED RATE [Air-Ganges sand system: air mass velocity (lb./ft² hr) for (1) 1430; (2) 887; (3) 545; (4) 3990]

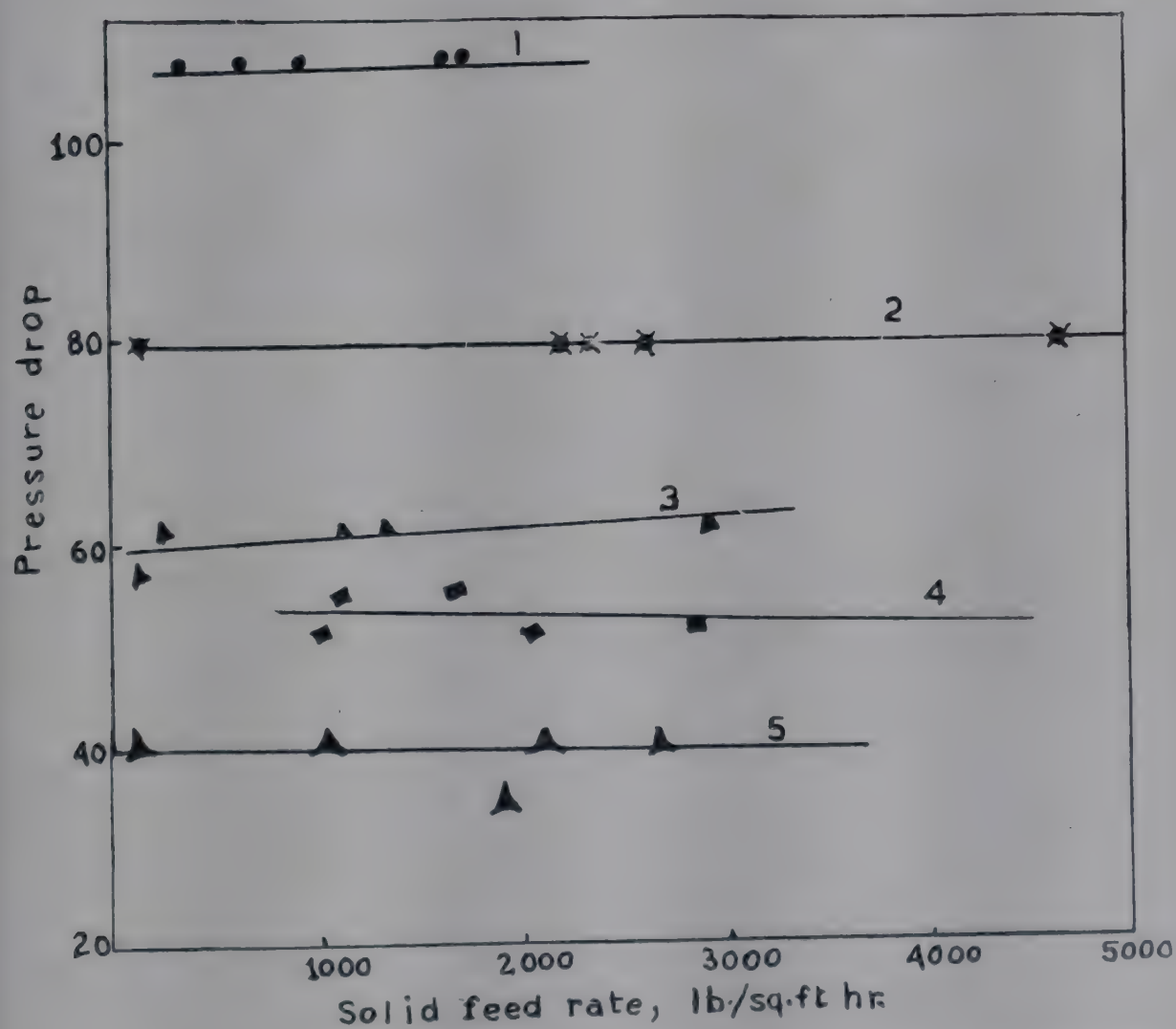


FIG. 4—PLOT OF PRESSURE DROP VERSUS SOLID FEED RATE [Air-Ganges sand system, particle diam., 0.00138 & air mass velocity (lb./ft² hr) for (1) 1439; (2) 887; (3) 545; (4) 786; (5) 390]

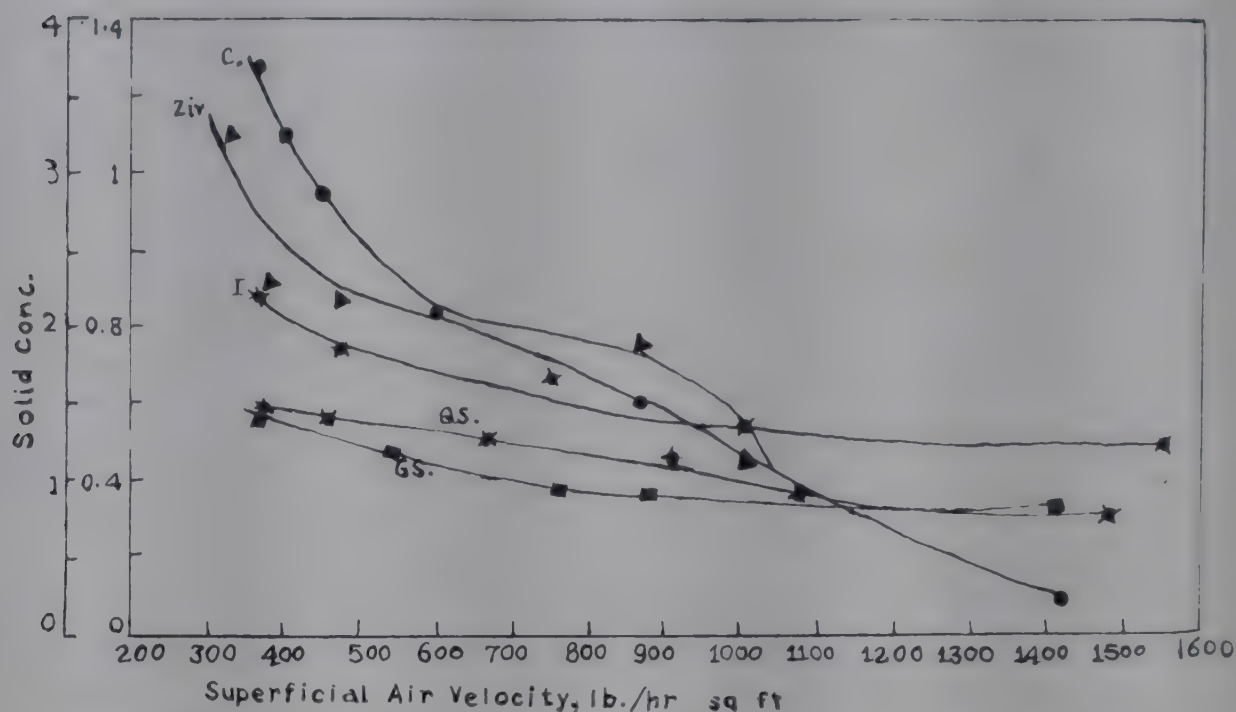


FIG. 5—PLOT OF SOLID CONCENTRATION VERSUS FLUID VELOCITY [Inner scale for calcite (C); Solid feed rate for calcite, 1250 lb./ft² hr; for others, 2530 lb./ft² hr]

to the author for comparison. Therefore, an attempt was made to extend the equations proposed for pneumatic transport to the present data. The equations thus studied are those of Vogt and White¹, Kassel and Belden² and Molstad Haritu³ respectively. But the comparison indicated invalidity of their correlation for the present data. Also, the assumption of Molstad concerning constant slip velocity (=Stoke's velocity) was not applicable to the present data. The particle acceleration reported by Molstad was not studied in the present work.

An attempt to predict the pressure drop from the solid concentration (Table 1) shows that a close agreement between the observed and calculated pressure drops is obtained. This fact suggests that frictional losses for the solid transport are negligible for such systems. It has been already stated that the solid concentration for continuous fluidization can be predicted from the corresponding data on batch fluidization.

It was also observed that up to a solid feed rate equal to about 1.5 times the fluid velocity the quality of fluidization remained unaffected by increase in the solid feed rate.

Heat Transfer Data

Owing to difficulty in obtaining a steady state only limited data on heat transfer were obtained. The data are presented in Table 2.

Kolbe⁴ has proposed that for heat transfer, coefficient h for suspensions is an exponential function of the solid mass velocity. To verify such relation a plot of Nusselt's number and solid feed rate was prepared, which indicated the invalidity of such a correlation.

TABLE 1—COMPARISON OF CALCULATED AND OBSERVED PRESSURE DROPS FOR DIFFERENT MATERIALS

| SOLID | Re_p | PRESSURE DROP | |
|-------------|--------|---------------|-------|
| | | Calc. | Obs. |
| Yellow sand | 27.8 | 22.35 | .. |
| | 18.55 | 39.0 | 36.8 |
| | 17.2 | 50.0 | 47.0 |
| | 12.65 | 55.0 | 52.5 |
| | 7.16 | 39.0 | 50.0 |
| | 8.57 | 50.0 | .. |
| Ilmenite | 17.75 | 47.6 | 50.0 |
| | 11.65 | 47.6 | 50.0 |
| | 8.75 | 63.8 | 65.0 |
| | 5.525 | 73.0 | 106.0 |
| | 4.42 | 90.0 | 106.0 |
| Zircon | 3.98 | 41.0 | 22.0 |
| | 3.28 | 63.0 | 50.8 |
| | 2.681 | 76.0 | 39.0 |
| | 1.49 | 85.0 | 78.0 |
| | 1.341 | 130.0 | 106.0 |
| Calcite | 16.20 | 10.8 | 10.0 |
| | 10.05 | 27.821 | 26.84 |
| | 6.96 | 32.8 | 33.0 |
| | 5.30 | 37.2 | 33.43 |
| | 4.38 | 50.0 | 39.00 |
| Ganges sand | 4.935 | 44.0 | 36.2 |
| | 48.0 | .. | .. |
| | 21.6 | .. | .. |
| | 18.2 | .. | .. |
| | 16.4 | 40.0 | 39.0 |
| | 25.61 | 39.5 | 50.0 |

TABLE 2—DATA ON HEAT TRANSFER IN CONTINUOUS FLUIDIZATION

(Solid, Ganges sand)

| AIR VELOCITY <i>ft/sec.</i> | SOLID FEED RATE <i>lb./hr</i> | HEAT TRANSFER COEFF. |
|--------------------------------|----------------------------------|-------------------------|
| 2.82 | 8.66 | 70.9 |
| 2.82 | 16.30 | 70.9 |
| 2.82 | 19.45 | 82.55 |
| 2.82 | 20.9 | 77.5 |
| 2.82 | 20.9 | 74.5 |
| 2.82 | 21.3 | 100.0 |
| 3.32 | 3.61 | 72.25 |
| 3.32 | 9.95 | 51.75 |
| 3.32 | 14.68 | 71.0 |
| 3.32 | 15.99 | 99.4 |
| 3.32 | 19.35 | 59.7 |
| 3.32 | 20.8 | 102.0 |
| 3.64 | 7.85 | 76.5 |
| 3.64 | 16.18 | 77.9 |
| 3.64 | 17.40 | 63.6 |
| 3.64 | 23.1 | 98.75 |
| 3.84 | 5.64 | 81.0 |
| 3.84 | 13.71 | 106.15 |
| 3.84 | 14.88 | 45.9 |
| 3.84 | 16.6 | 95.75 |
| 3.84 | 18.52 | 26.375 |
| 3.84 | 21.8 | 27.55 |
| 4.07 | 9.14 | 23.55 |
| 4.07 | 9.15 | 23.125 |
| 4.07 | 11.18 | 23.05 |
| 4.07 | 13.70 | 23.45 |
| 4.07 | 21.20 | 30.75 |
| 4.07 | 29.10 | 63.25 |
| 4.34 | 11.30 | 50.50 |
| 4.34 | 11.75 | 26.55 |
| 4.34 | 14.68 | 52.55 |
| 4.34 | 15.65 | 41.74 |
| 4.34 | 16.30 | 71.25 |
| 4.34 | 19.00 | 79.55 |

Plots of h versus solid feed rate indicate linear curves for individual runs, a sample of which is shown in Fig. 6. But since neither the intercepts nor the slopes of different runs coincide, it is not possible to postulate a generalized linear relationship. In Fig. 7, a plot of h versus air velocity at constant solid feed rates is shown. All these curves have similar shape

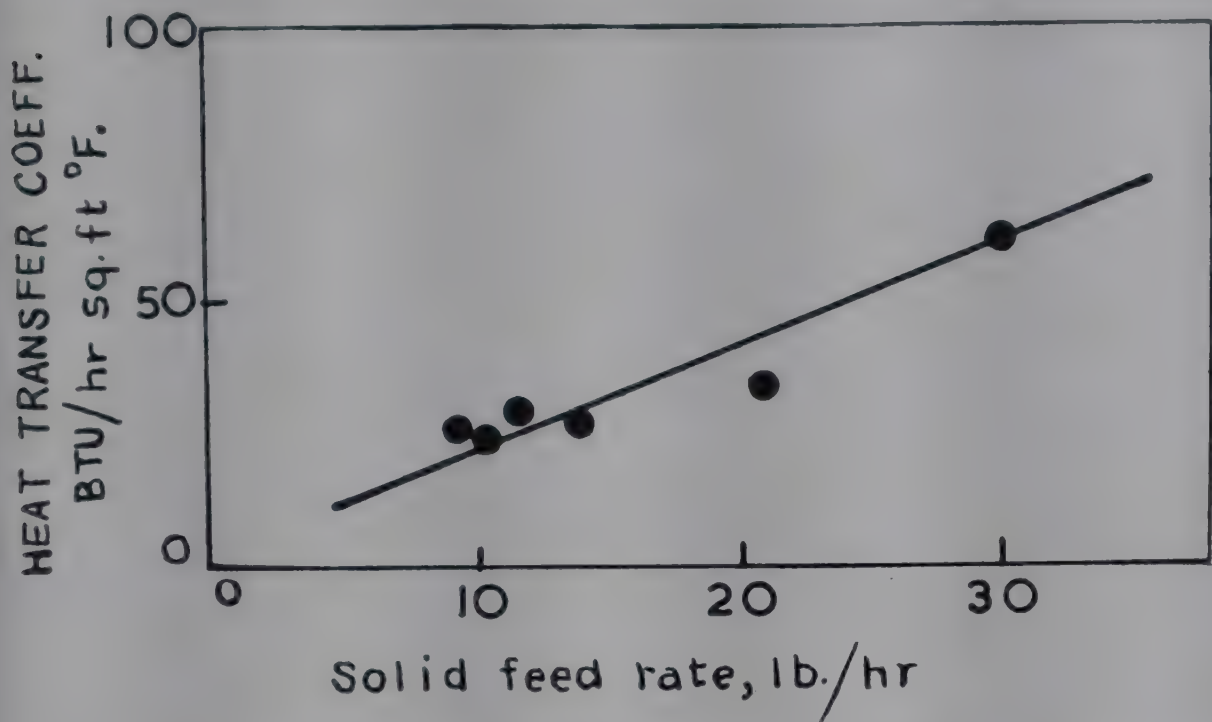


FIG. 6—PLOT OF HEAT TRANSFER COEFFICIENT VERSUS SOLID FEED RATE [Air velocity, 4.34 ft/sec.]

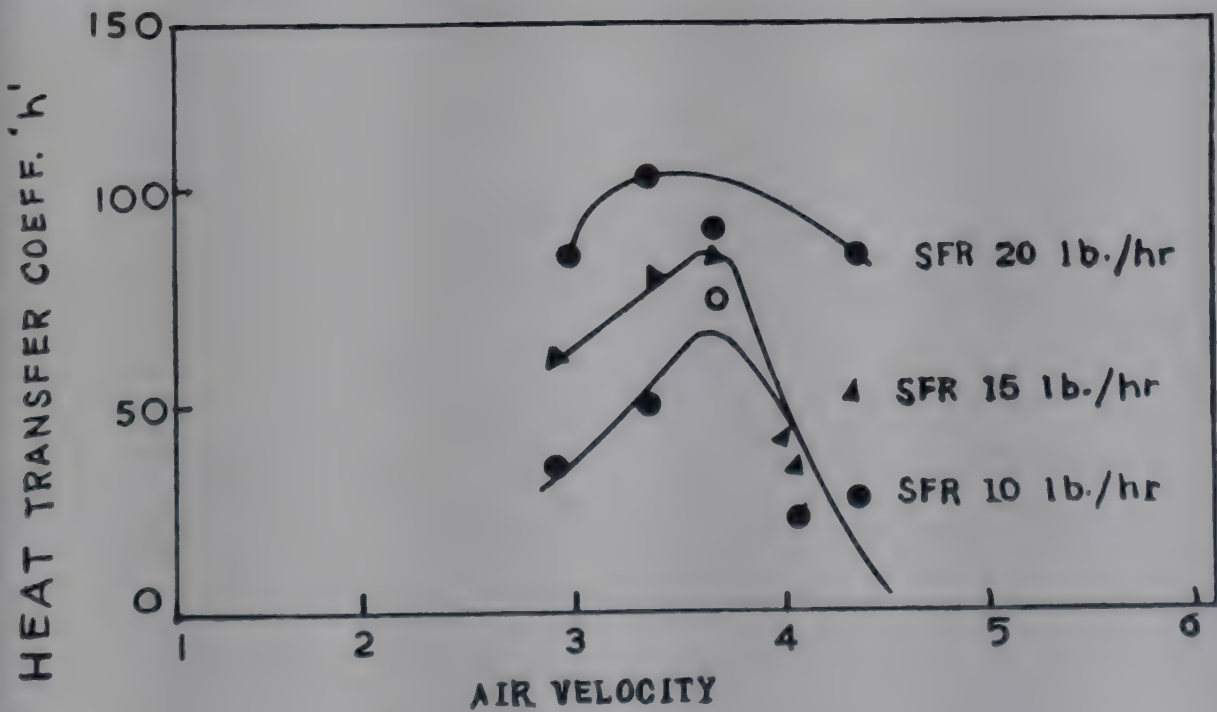


FIG. 7—PLOT OF HEAT TRANSFER COEFFICIENT VERSUS AIR VELOCITY AT DIFFERENT CONSTANT SOLID FEED RATES

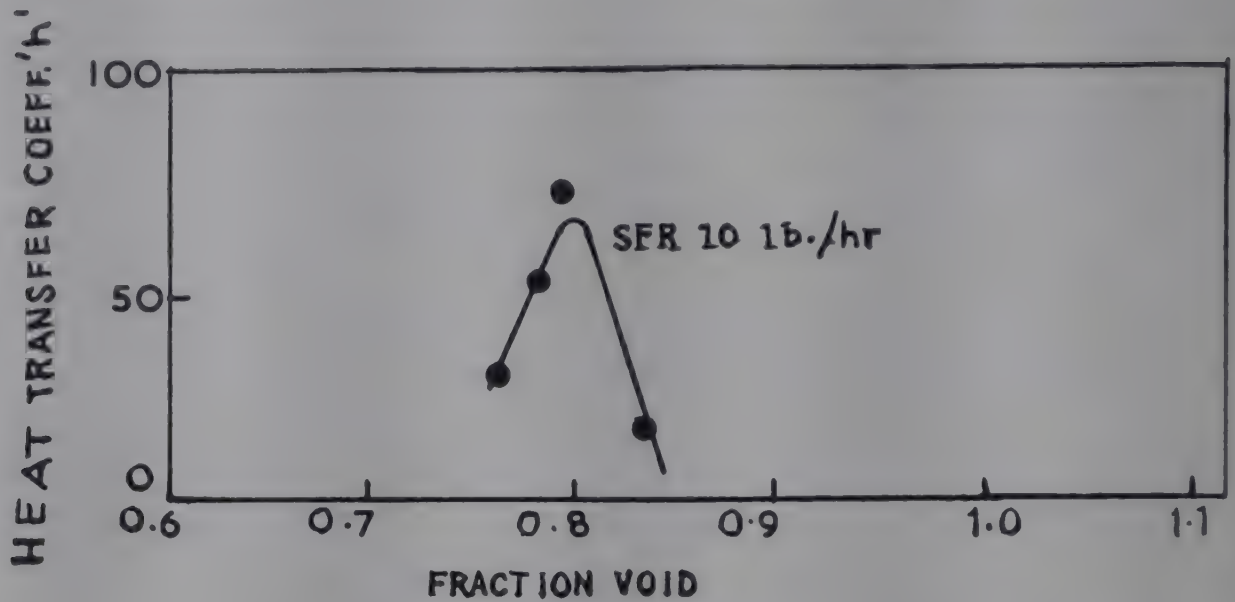


FIG. 8—PLOT OF HEAT TRANSFER COEFFICIENT VERSUS VOID FRACTION

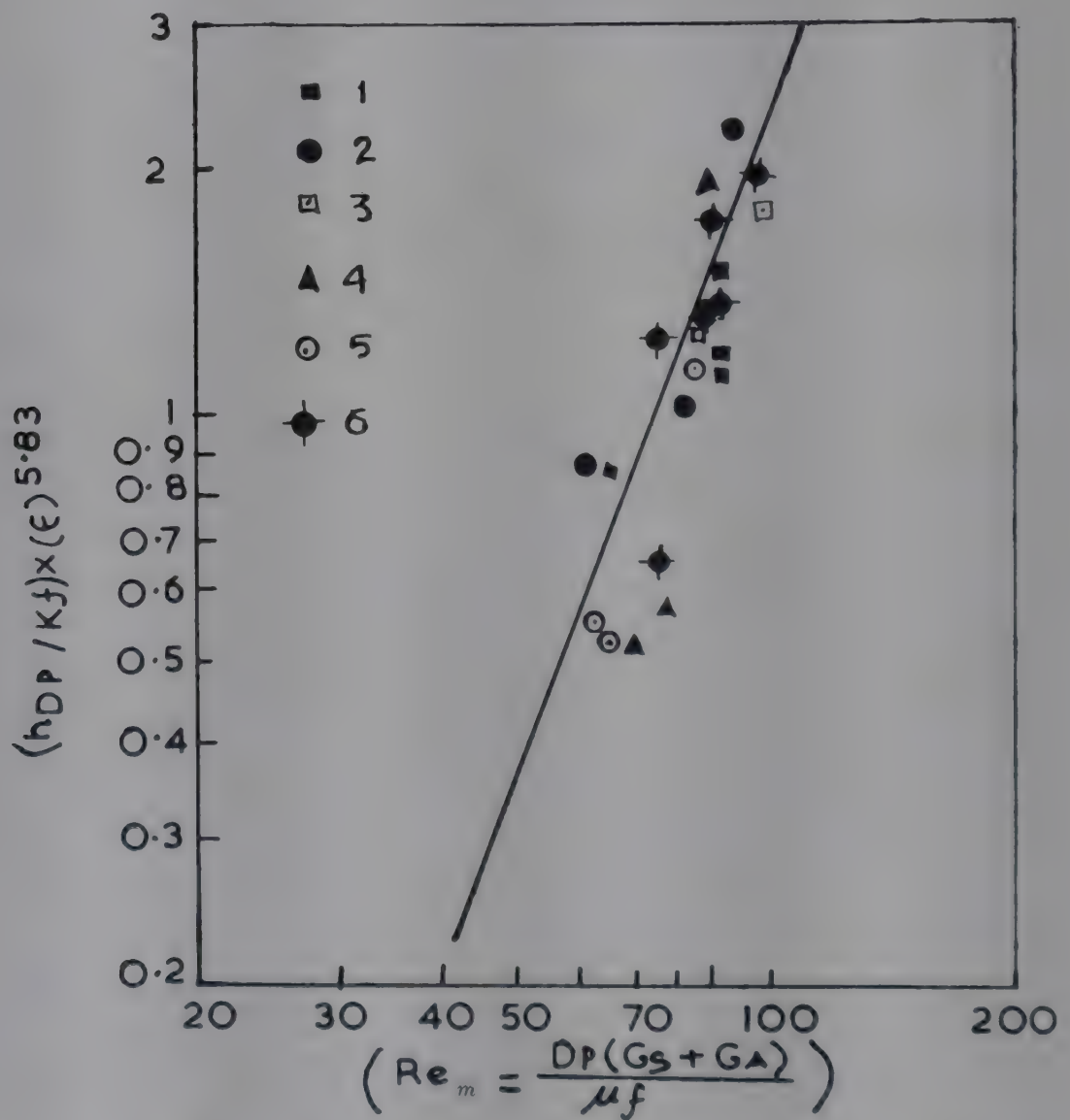


FIG. 9—PLOT OF $(h D_p / k_f) (E)^{5.83}$ VERSUS Re_m FOR DIFFERENT AIR VELOCITIES AND VOID FRACTIONS [Air velocity ($lb./ft^2 hr$) and void fraction for (1) 745 & 0.76; (2) 885 & 0.78; (3) 975 & 0.79; (4) 1025 & 0.80; (5) 1095 & 0.82; (6) 1195 & 0.85]

with a maximum at the point of fluidization. In Fig. 8, the fraction void versus h has been plotted. The fraction void is calculated from the corresponding values in batch fluidization.

These figures indicate that h is a function of all the three variables, viz. fraction void, Reynolds number and the solid feed rate. The last two can be combined in one dimensionless number:

$$Re_m = \frac{D_p (G_s + G_f)}{\mu} \quad (1)$$

In an attempt to extend heat transfer correlations for batch fluidization to continuous fluidization, a plot of $(Nu) (\epsilon)^{5.83}$ versus Re_m on a log-log scale was made (Fig. 9). It is evident that the data can be reasonably represented by the equation

$$hD_p/k_f = 2.15 \times 10^{-5} (Re_m)^{2.65} (1/\epsilon)^{5.83} \quad (2)$$

CONCLUSION

It is possible to extend the results of batch fluidization to continuous fluidization both in the fields of fluid flow and heat transfer, whereas equations for pneumatic transport are not applicable in this case.

The above analysis is based on the limited data presented here and must be used with great caution for other systems and experimental arrangements. Extensive data are needed to establish wider applicability or otherwise of this analysis.

NOMENCLATURE

| | |
|------------|--|
| D_p | = particle diameter |
| G | = mass velocity |
| μ | = fluid viscosity |
| Re_p | = Reynolds number based on particle diameter and fluid density and viscosity |
| Re_m | = modified Reynolds number as defined by Eq. (1) |
| ϵ | = fraction void |
| h | = heat transfer coefficient |
| k | = thermal conductivity |

Subscripts

s = solid

f = fluid

Solid feed rate [$lb./sq. ft.(hr.)$] has been based on column cross-section.

REFERENCES

1. VOGT & WHITE, R. H., *Industr. Engng Chem.*, **40** (1948), 1738.
2. KASSEL, L. S. & BELDEN, D. R., *Industr. Engng Chem.*, **41** (1949), 1174.
3. MOLSTAD & HARITU, O. H., *Industr. Engng Chem.*, **41** (1949), 1148.
4. KOEBE, R. A., *Chem. Engng*, **58**(9) (1951), 174.

Heat Transfer to Flowing Gas-Solid Suspensions in Circular Tubes

V. R. K. RAO & P. S. MURTI*

Department of Chemical Engineering
Indian Institute of Technology
Bombay 76

Heat transfer data have been obtained from condensing steam to a mixture of gas-solid suspension flowing vertically in a 19.0 mm. inner diam. and 1.43 m. long copper tube using spent silica-alumina catalyst (47μ), sand (86μ and 121μ), and iron powder (100μ) as solid material and varying the velocity of carrier gas (air) from 5.15 to 12.2 m./sec. and the loading ratio from zero to a maximum 14.0. The mixture heat transfer coefficients were found to be dependent on the properties and size of the particles, gas velocity and loading ratio. A minimum value was noticed with each of the particles investigated on a plot of h_m versus R . The values beyond this minimum were correlated in terms of dimensionless parameters. Two equations, one for sand and catalyst and the other for iron powder, have been proposed. The equations were found to be in agreement with the data of Farbar and Morley. Agreement with Müller's data was satisfactory only with the highest and the lowest particle sizes.

Transfer line reactors or dilute phase continuous fluidized bed reactors are being viewed with greater interest in chemical processing industries following the developments in such fields as hydrocarbon synthesis, coal gasification and mineral processing. Some of the possible applications of this technique in different chemical and allied industries are given in recent literature¹⁻²².

The problem of heat transfer to gas-solid suspensions flowing in bare tubes has been experimentally investigated by many workers²³⁻³¹. The

*Present address: Regional Research Laboratory, Hyderabad 9.

results of various workers confirm that the film heat transfer coefficients on the suspension side, in general, increase with increased loading ratio and gas velocity and also with decreased particle size. The earlier work of Farbar and Morley²⁶ indicates a constancy in the values of the coefficients up to a loading ratio of about one, while the results of Müller²⁹ and those of Farbar and Depew^{24,25} indicate the existence of a 'critical' loading ratio below which the coefficients are actually less than the particle-free gas values. A mathematical analysis of this problem, seemingly valid at low loading ratios, was made by Tien³² who also extended the isothermal tube-wall case to arbitrary wall temperature variations and wall heat fluxes by the method of Tribus and Klein³³ and Sellars *et al.*³⁴.

The experimental investigations on this subject were started in these laboratories in 1959 and very little information was then available to draw quantitative conclusions. The results on heat transfer employing sand (86μ and 121μ), spent silica-alumina catalyst (47μ) and iron powder (100μ) and air as the carrier gas have been reported in this paper.

EXPERIMENTAL SET-UP AND PROCEDURE

The isometric view of the experimental set-up is shown in Fig. 1. Solids from the storage tank (1) and solids leg (3) enter the mixing nozzle (7) through a slide valve (5). Air from a compressor (25) passes through a set of control valves (27, 28, 29) to a silica-gel drier (30) and from there to a standard orifice meter (32). The metered air meets the down-flowing solids at the mixing nozzle and picks them up, and travels in a horizontal pipe where a metering nozzle (8) to measure the combined flow of gas-solid suspension is located. The mixture travels vertically through a calming section of 19 mm. inner diam., 2.2 m. long copper tube before entering the main heat transfer zone (11). The mixture is heated by condensing steam essentially at atmospheric pressure which is generated in the vaporizer (34) with an adjustable electrical heating source. On either side of the heat transfer section, glass tubes ($3/4$ in. inner diam.) are introduced to minimize heat losses in the axial direction beyond the zone of interest. These also serve to make the visual observations of the flow of the suspension. Two copper-constantan thermocouples are located at the inlet and the outlet to measure the temperature of the gas.

The suspension then passes through a horizontal cooler (15) and enters the twin cyclone separators. The outgoing air is sent through a scrubber (33) before being let out to the atmosphere. The solids separated in the cyclones fall into the solids storage tank, where provision is made to measure the rate of flow of solids by diverting the solids from the cyclones into a receiver. The main heat transfer section described in detail by Rao³⁵, is shown in Fig. 2.

Before starting a run, the solids in the solids leg (3) were fluidized by

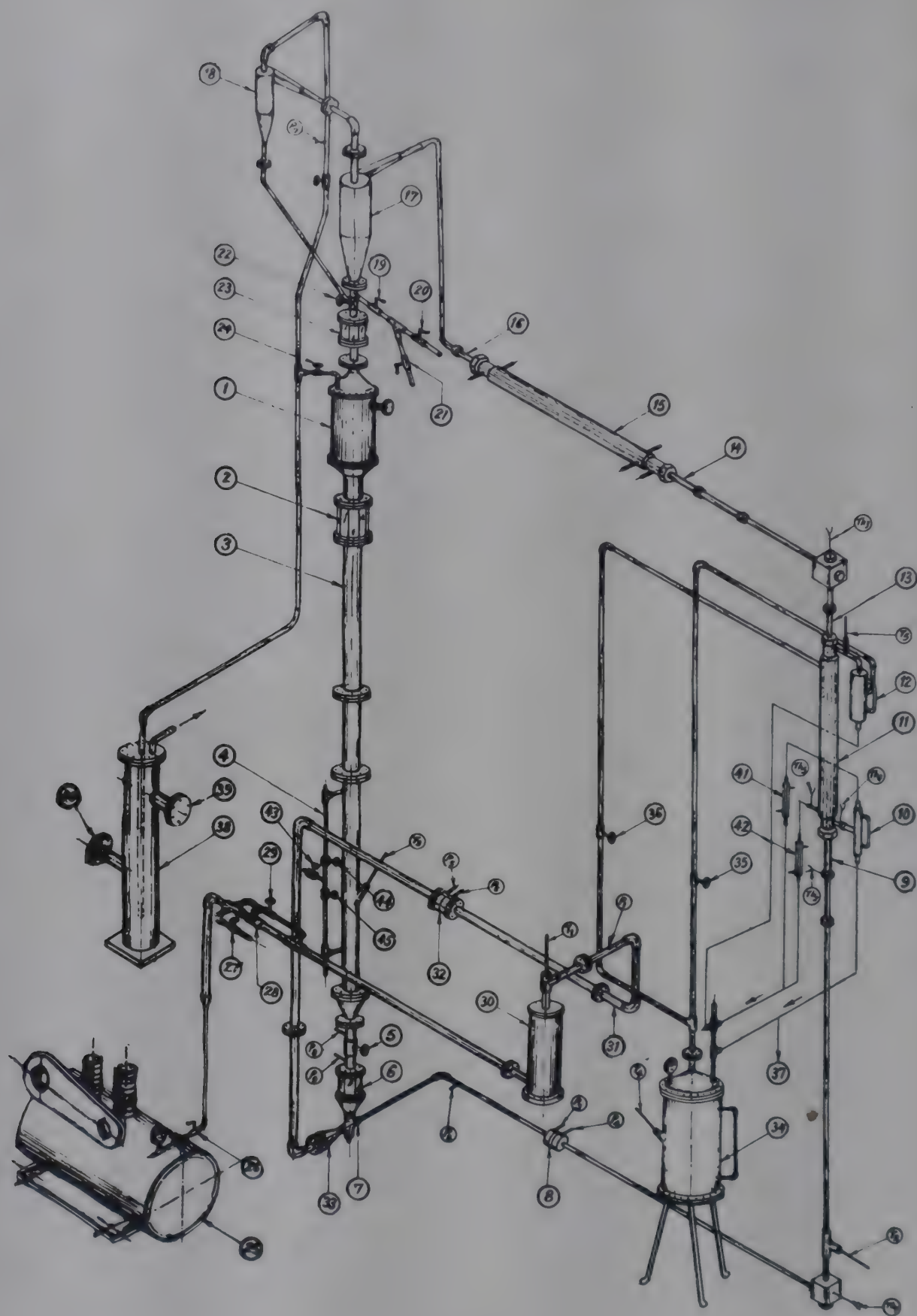


FIG. 1

TABLE 1—PROPERTIES OF SOLID MATERIALS

| MATERIAL | D_p | ρ_s | C_s | u_i^* |
|-------------------------|-------|--------------------|--------|---------|
| Quartz sand 1 | 121 | 2.64×10^3 | 0.195 | 0.75 |
| Quartz sand 2 | 86 | 2.64×10^3 | 0.195 | 0.51 |
| Silica-alumina catalyst | 47 | 2.43×10^3 | 0.256† | 0.24 |
| Iron powder | 100 | 7.2×10^3 | 0.115 | 2.99 |

*Terminal velocities were calculated using the Intermediate law.

†In view of the presence of a small percentage of carbon on silica-alumina catalyst, a value of 0.256 was assigned for its heat capacity.

a controlled admission of air for at least an hour, if the run was made freshly on the day. Air rate was adjusted to a predetermined value by adjusting the valves (27, 28) and noticing the pressure differential across the orifice meter.

Temperatures of the suspensions before and after the heat transfer sections were noted by copper-constantan thermocouples (0.3 mm. enamel coated and cloth covered and supplied by *S.R.E. Huber and Co.*, Switzerland) and the constancy of these values indicated steady state conditions. Observations were recorded when steady state conditions were attained.

Particle diameter determination in the sieve range was done using B.S.S. standard sieves on an Inclino type sieve shaker supplied by *AIML Ltd*, Bombay, following the standard procedure³⁶.

The sub-sieve fraction of the material, particularly catalyst and iron powder, was subjected to sedimentation experiment in an apparatus described by Stairmand²⁰. The results of particle size analysis and other properties are listed in Table 1.

The apparatus was first standardized by running only air into the transfer section.

RESULTS AND DISCUSSION

The data thus obtained during standardization satisfy the familiar Dittus-Boelter equation as shown in Fig. 3.

◀ FIG. 1—EXPERIMENTAL SET-UP [1, Solids storage tank; 2, 90-mm. Glass section; 3, 90-mm. Solids leg; 4, Side pipe; 5, Slide valve; 6, Glass section; 7, Mixing nozzle; 8, Metering nozzle; 9, 19-mm. Glass tube; 10 & 12, Liquid separators; 11 & 15, Heat exchangers; 13, 14 & 16, 19-mm. Glass tubes; 17 & 18, Cyclone separators; 19, 20 & 21, 25.4-mm. Quick opening valves; 22, 38.0-mm. Gate valve; 23, Glass section; 24, 25.4-mm. Gate valve; 25, Air compressor (20 ft³/min.); 26, 13.0-mm. Quick opening valve; 27, 25.4-mm. Exhaust valve; 28, 50.8-mm. Globe valve; 29, 25.4-mm. Needle valve; 30, Silica gel drier; 31, 30.5-mm. Calming section; 32, Orifice meter; 33, Converging nozzle; 34, Vaporizer; 35 & 36, 10-mm. Gate valves; 37, Glass stopcock (3-way); 38, Water scrubber; 39 & 40, Sight glasses; 41 & 42, Condensers; 43, 44 & 45, 13-mm. Control valves; $P_1 \dots P_9$, Pressure tappings; T_1 , T_2 & T_3 , 0–50°C. Thermometers; T_4 & T_5 , 0–110°C. Thermometers; $Th_1 \dots Th_5$, Copper-constantan thermocouples]

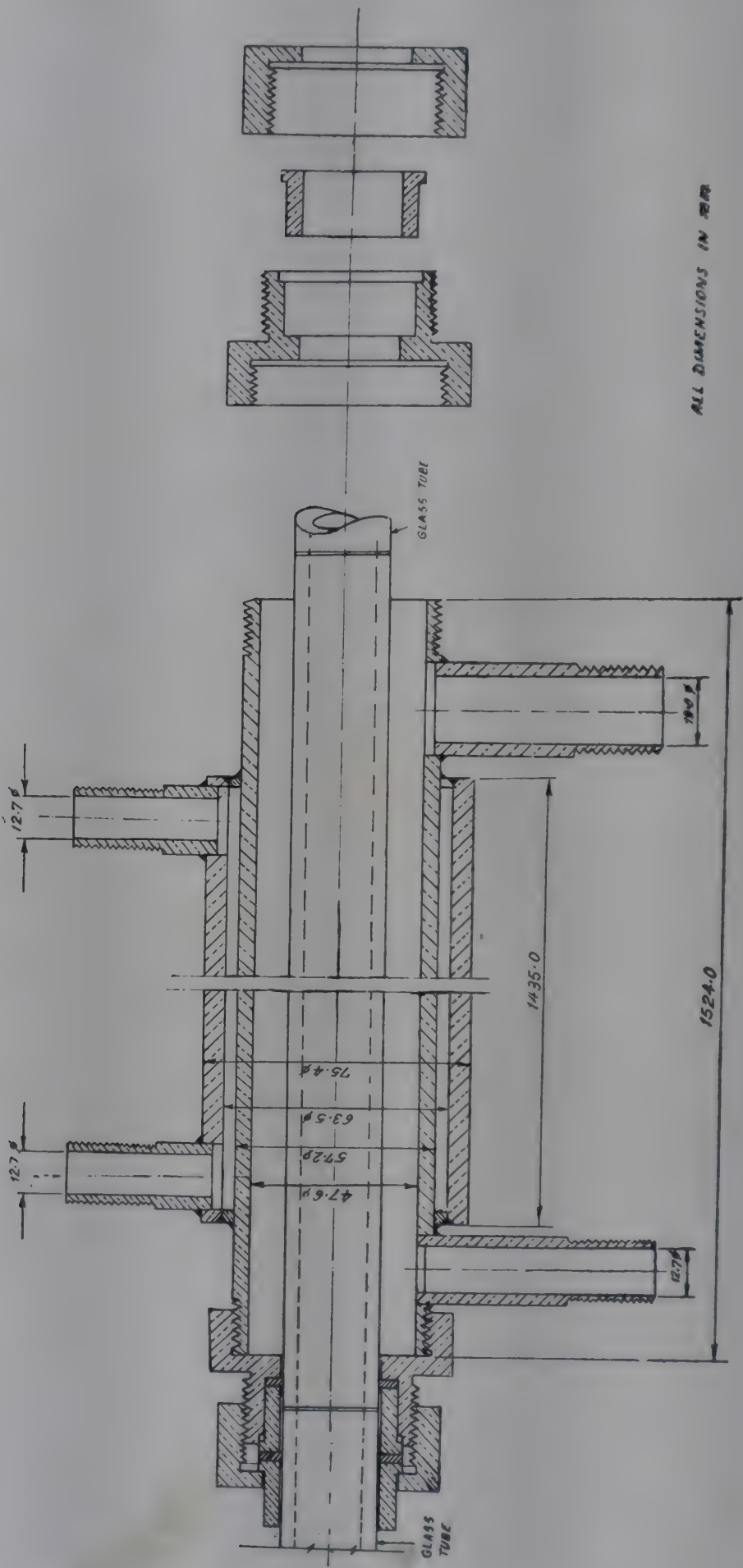


FIG. 2—DETAILS OF HEAT EXCHANGER

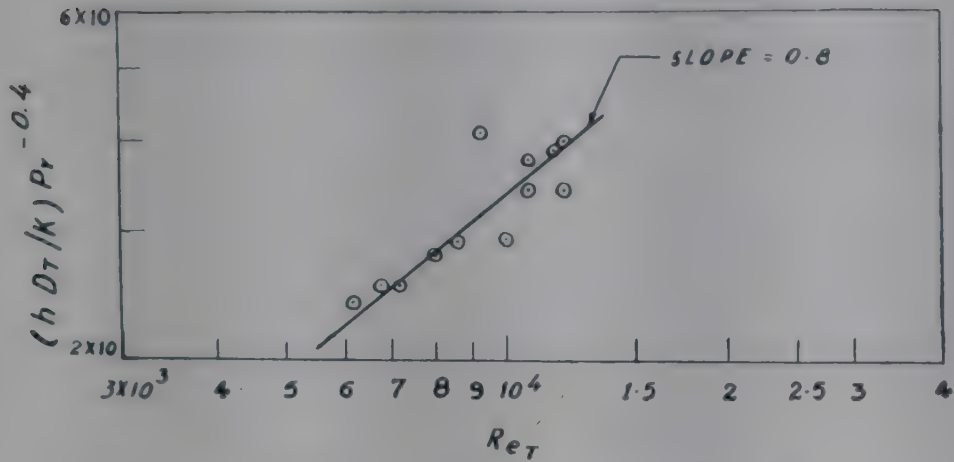


FIG. 3—PLOT OF (NUSSLELT NUMBER) (PRANDTL NUMBER)^{-0.4} VERSUS REYNOLDS NUMBER WITH AIR ALONE IN EMPTY TUBE

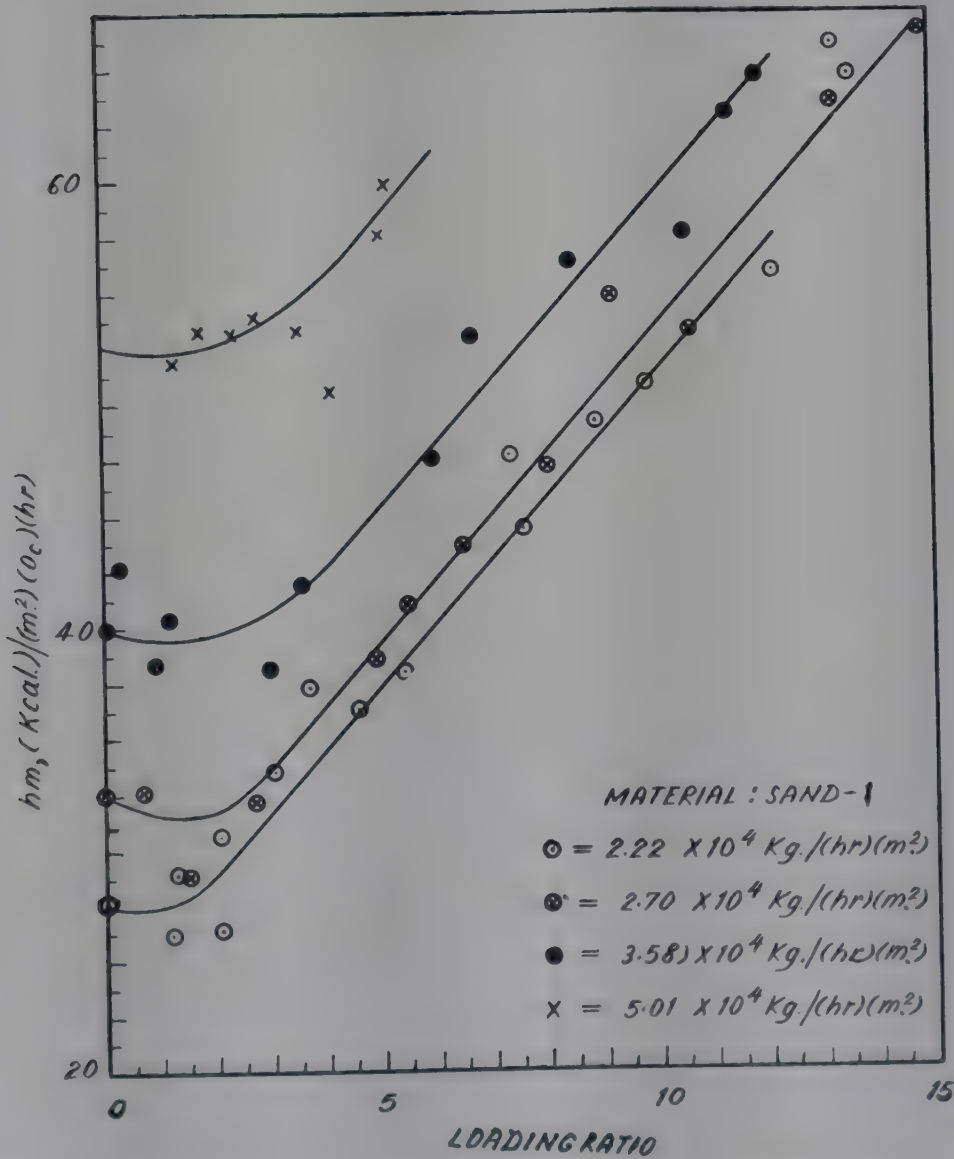


FIG. 4—PLOT OF EXPERIMENTAL MIXTURE HEAT TRANSFER COEFFICIENT VERSUS LOADING RATIO FOR SAND 1

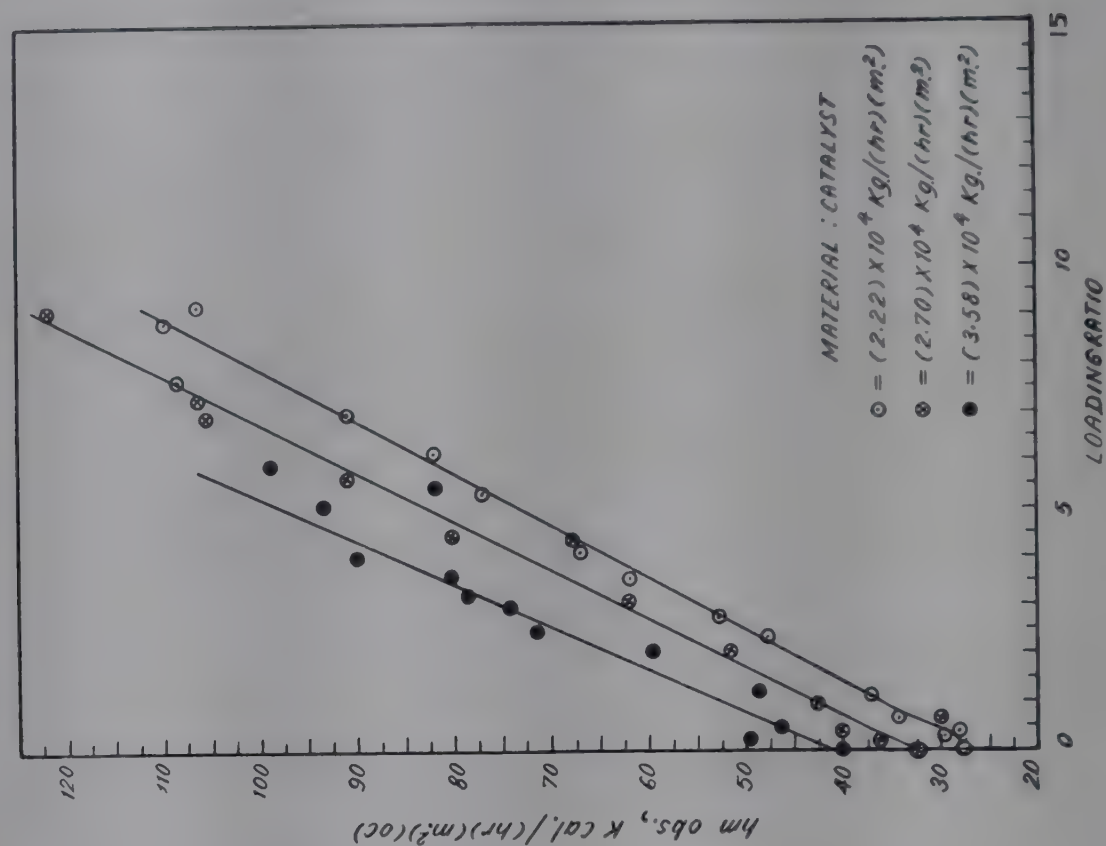


FIG. 5—PLOT OF EXPERIMENTAL MIXTURE HEAT TRANSFER COEFFICIENT
VERSUS LOADING RATIO FOR SAND 2

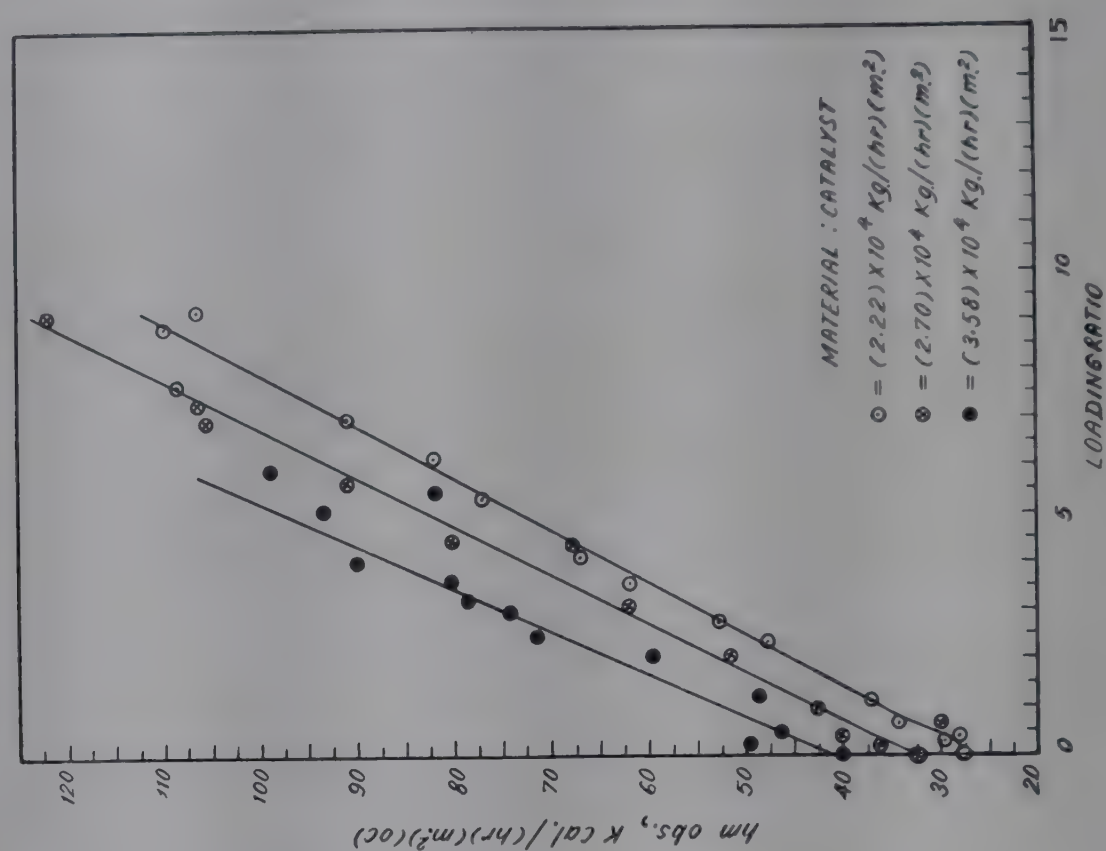


FIG. 6—PLOT OF EXPERIMENTAL MIXTURE HEAT TRANSFER
COEFFICIENT VERSUS LOADING RATIO FOR CATALYST

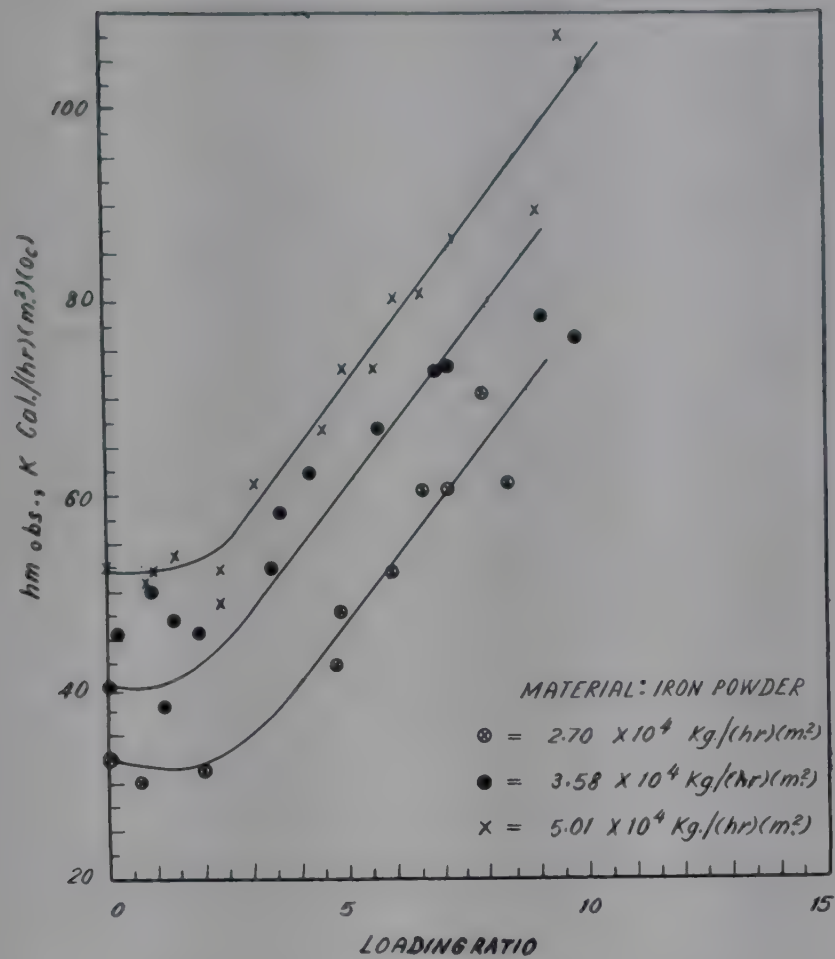


FIG. 7—PLOT OF EXPERIMENTAL MIXTURE HEAT TRANSFER COEFFICIENT VERSUS RATIO FOR IRON POWDER

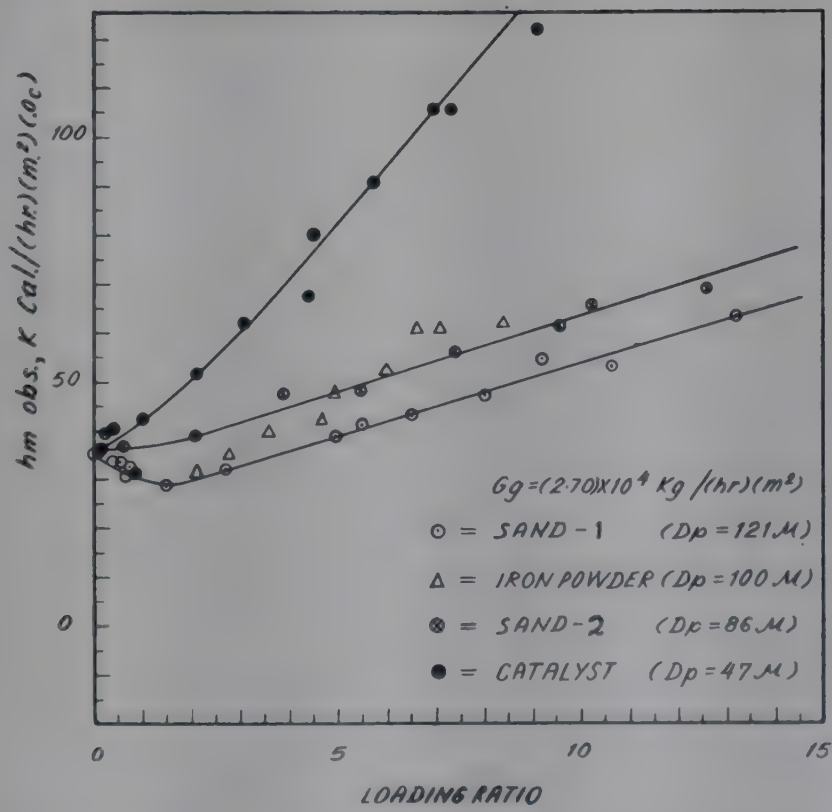


FIG. 8--CROSS-PLOT OF EXPERIMENTAL MIXTURE HEAT TRANSFER COEFFICIENT VERSUS LOADING RATIO FOR ALL THE FOUR MATERIALS

The heat transfer coefficient for the mixture flow was calculated in a similar manner. It was assumed, however, that the combined resistances of the tube wall and steam side remain unaltered even when the suspension was flowing. During the course of this work, the latter value was evaluated five times by stopping the suspension flow and admitting air only. It was observed that the values remained fairly constant throughout the period, with a maximum deviation of ± 5 per cent.

The mixture heat transfer coefficients are plotted against loading ratio for each of the four species of particles (sand 1, sand 2, spent silica-alumina catalyst, iron powder) with gas velocity as the parameter in Fig. 4-7. A cross-plot of mixture heat transfer coefficient versus loading ratio for all the particles at a gas mass velocity of 2.70 kg./hr m^2 is given in Fig. 8 to show more clearly the effect of particle size. These plots indicate that the coefficients, in general, increase with increase in loading ratio and decrease in particle size. However, with sand 1 and sand 2 and to some degree with iron powder, the coefficient at first decreases to a value lower than that of the particle-free gas transfer coefficient value and subsequently increases as the loading ratio increases. It has been observed that the dip increases with particle diameter but decreases with carrier gas velocity; thus the minimum value shifts to lower loading ratio with decrease in particle diameter. This minimum behaviour is nearly absent with silica-alumina catalyst particles, possibly because of their small diameter.

A similar lowering of heat transfer coefficients up to a certain loading ratio for quartz particles of moderate size (up to 600μ) was reported by Müller²⁹ and Brötz, Hiby and Müller²³. Farbar and Morley²⁶, on the other hand, working with fine size particles of silica-alumina catalyst reported that the transfer coefficients are fairly constant up to a loading ratio of 1 in the velocity range $12.5\text{--}25.3 \text{ m./sec}$. Farbar and Depew²⁵ have mentioned that the coefficients are nearly constant up to a loading ratio of 2, although the graphs indicate a decreasing tendency in the region. Jepson, Poll and Smith²⁷ reported the decrease in heat transfer coefficients at low loading ratios, which they suspected as due to the faulty measurement of the temperature of the air. The results of this work also show that the improvement factor (defined as the ratio of mixture heat transfer coefficient to particle-free gas value) is inversely proportional to the carrier gas velocity. This is in agreement with the results of other workers²⁷.

The improvement in the coefficient beyond a critical loading ratio may be explained on the basis of the film model. The film thickness is influenced by the degree of turbulence and the solid population; higher loading ratios lead to frequent bombardments of the particles on the film with a consequent reduction in its thickness.

Farbar and Morley²⁶ ruled out the possibility of direct heat transfer to the solid from the metal wall, purely from geometric and time basis. Under these conditions, the heat transferred to the solids must have been from the

gas only and as such the solids temperature is always lower than the gas temperature. This hypothesis is tenable only when the solids are either dispersed uniformly in the gaseous media or when they are travelling mainly in the central portion. But in actual operating conditions, the particle path is erratic, often hitting the wall with an angle of incidence different from the angle of emergence. This virtually increases the actual residence time of the solid particles in the transfer tube. Zoonen³⁷ recently reported that the solid density across the cross-section of the tube is not uniform but it is four times higher near the wall than in the centre. Therefore, the improvement in heat transfer may be due to reduction in film thickness at higher loading ratio and to increased heat capacity due to the presence of solids. However, no satisfactory explanation can be offered to account for the decrease in heat transfer coefficients up to a critical loading ratio.

CORRELATIONS

Farbar and Morley correlated their data in terms of Nusselt number, Reynolds number and loading ratio. Their correlation is similar in form to Dittus-Boelter equation and the presence of solids is characterized by the loading ratio. Wen and Miller³⁸ correlated the data in terms of Nusselt number, Prandtl number, ρ_m/ρ_s and Froude number. In this work an attempt was made to correlate the data in terms of the dimensionless numbers given by the functional relationship

$$\frac{h_m D_x}{k_g} = A_1 \left(\frac{D_x G_g}{\mu_g} \right)^a \left(\frac{D_x}{d_p} \right)^b \left(\frac{u_t}{u_g} \right)^c \left(\frac{C_s}{C_g} \right)^d R^e \quad (1)$$

In this, the diameter of the particle is taken as the geometric mean of the adjacent screens (in the sieve range) or cuts (in the sub-sieve range). The terminal velocity u_t has been calculated following Leva³⁹. The physical properties of the air are taken at the mean surface temperature of the tube (assumed to be constant for this purpose for all the runs).

At first, the functional relationship is written as

$$\frac{h_m D_x}{k_g} = A_1 \left(\frac{D_x G_g}{\mu_g} \right)^a \left(\frac{D_x}{d_p} \right)^b \left(\frac{u_t}{u_g} \right)^c R^e \quad (2)$$

In order to determine the values of the constants, A_1 , a , b , c , and e , the method proposed by Levenspiel⁴⁰ is adopted. According to this method, logarithms of both sides of Eq. (2) are taken and the constants are evaluated by the method of least squares. This approach does not, however, minimize the square of the deviation. Plots of

$$\left(\frac{h_m D_x}{k_g} \right) \left(\frac{D_x G_g}{\mu_g} \right)^{-0.66} \left(\frac{D_x}{d_p} \right)^{-0.65} \left(\frac{u_t}{u_g} \right)^{0.3} \text{ versus } R$$

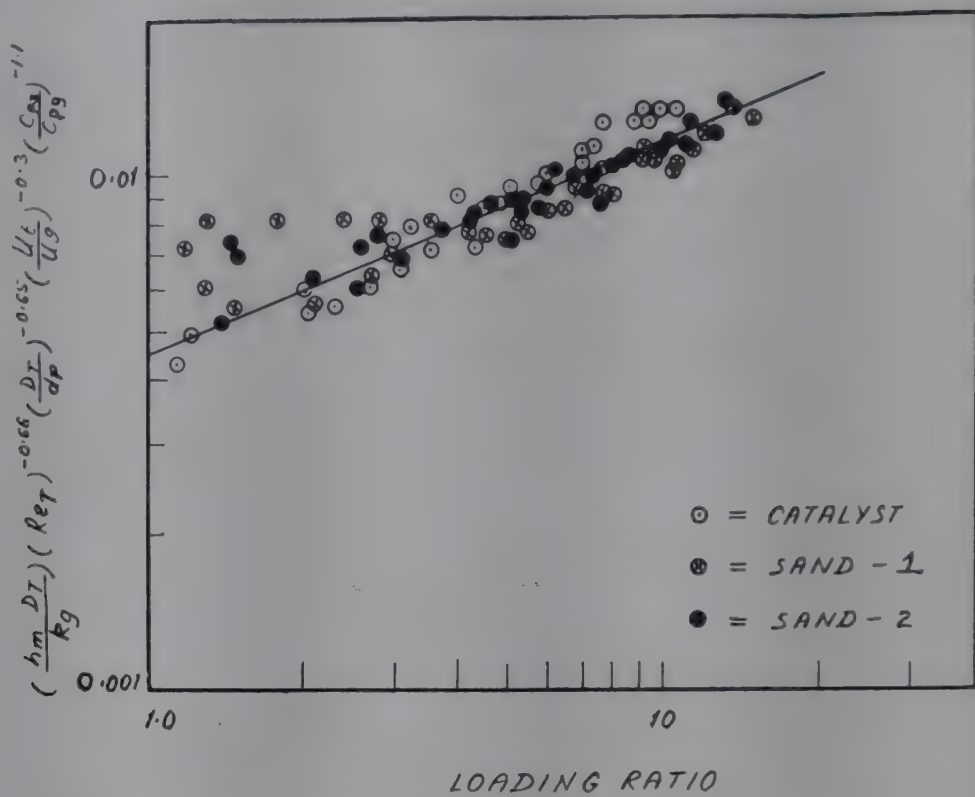


FIG. 9—FINAL CORRELATION FOR HEAT TRANSFER FOR SANDS AND CATALYST

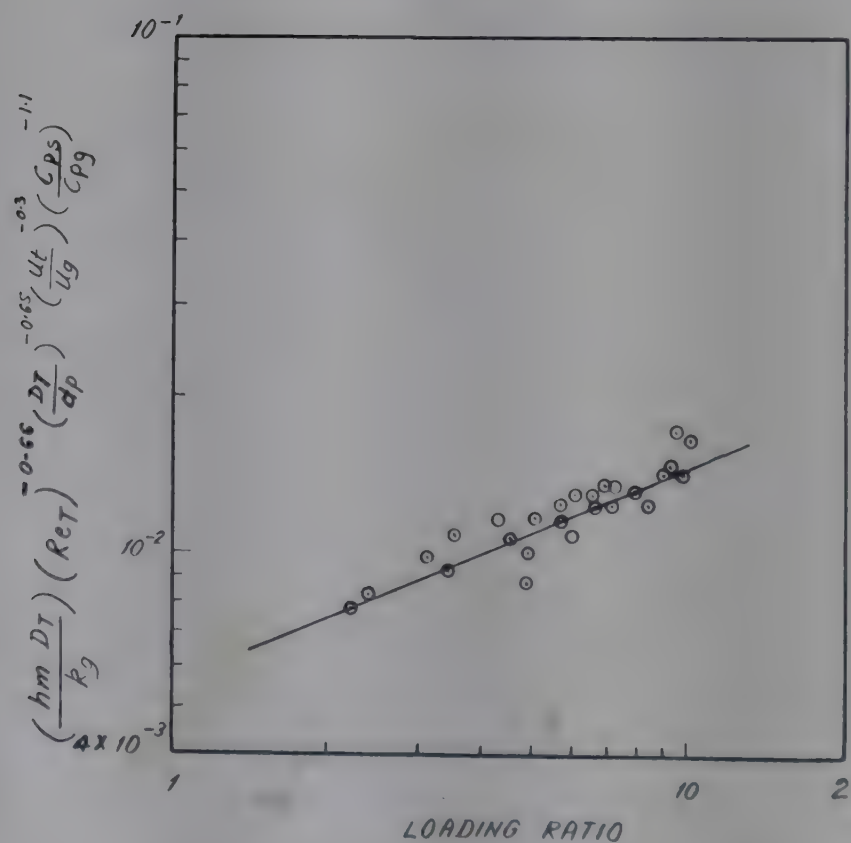


FIG. 10—FINAL CORRELATION FOR HEAT TRANSFER FOR IRON POWDER

on logarithmic coordinates are made and it is observed that the data for the two sands fall on a straight line, while the data for catalyst and iron fall on two other lines which are parallel to the line for the sands. Introduction of the parameter, $\left(\frac{C_s}{C_g}\right)^{1.1}$ satisfactorily merged the data for sands and catalyst. But, the data for iron powder still followed a separate parallel line. Probably, introduction of either $\frac{k_s}{k_g}$ or $\frac{\rho_s}{\rho_g}$ would have merged the data together. Although density or conductivity variation between iron and the rest of the materials is large, the number of points that can be obtained in determining the exponents on either of these simplexes is only two, as the catalyst and sand have very nearly the same physical properties other than heat capacity. Therefore, it is preferred to represent the data by separate correlations, until more data with particles of varying thermal conductivity and density are available. The final correlation graphs are shown in Fig. 9 and 10. The equations satisfying the straight lines are:

$$\frac{h_m D_r}{k} = (4.5 \times 10^{-3}) \left(\frac{D_r G_g}{\mu_g}\right)^{0.66} \left(\frac{D_r}{d_p}\right)^{0.65} \left(\frac{u_t}{u_g}\right)^{0.3} \left(\frac{C_s}{C_g}\right)^{1.1} (R)^{0.42} \quad (3)$$

for catalyst and sands.

$$\frac{h_m D_r}{k_g} = (5.5 \times 10^{-3}) \left(\frac{D_r G_g}{\mu_g}\right)^{0.66} \left(\frac{D_r}{d_p}\right)^{0.65} \left(\frac{u_t}{u_g}\right)^{0.3} \left(\frac{C_s}{C_g}\right)^{1.1} (R)^{0.42} \quad (4)$$

for iron powder.

It is observed that the average deviation of about 104 points is ± 7 per cent and standard deviation is 13.2 per cent. Similarly, the equation for iron powder describes the data with an average deviation of ± 7.1 per cent and with a standard deviation of 12.5 per cent.

Application of the correlation to others' data. The validity of the correlation developed from this work has been tested on the data of Farbar and Morley²⁶, and of Müller²⁹. The mean catalyst diameter of the particles used by Farbar and Morley is evaluated from the sieve analysis results and the cumulative plot given by them, and is found to be 30.7. The calculated and observed data are shown plotted in Fig. 11. These show that the correlation fits the experimental data satisfactorily. The accuracy of this correlation is comparable with that proposed by Farbar and Morley. Considering the range of gas velocities of this work (5.15–12.2 m./sec.) and of Farbar and Morley (12.5–25.3 m./sec.), extrapolation of this correlation to higher gas velocities seems permissible.

Application of this correlation to the data of Müller is shown in Fig. 12. It can be seen that Eq. (6) predicts rather satisfactorily the highest and lowest particle size but the agreement is poor in the intermediate particle

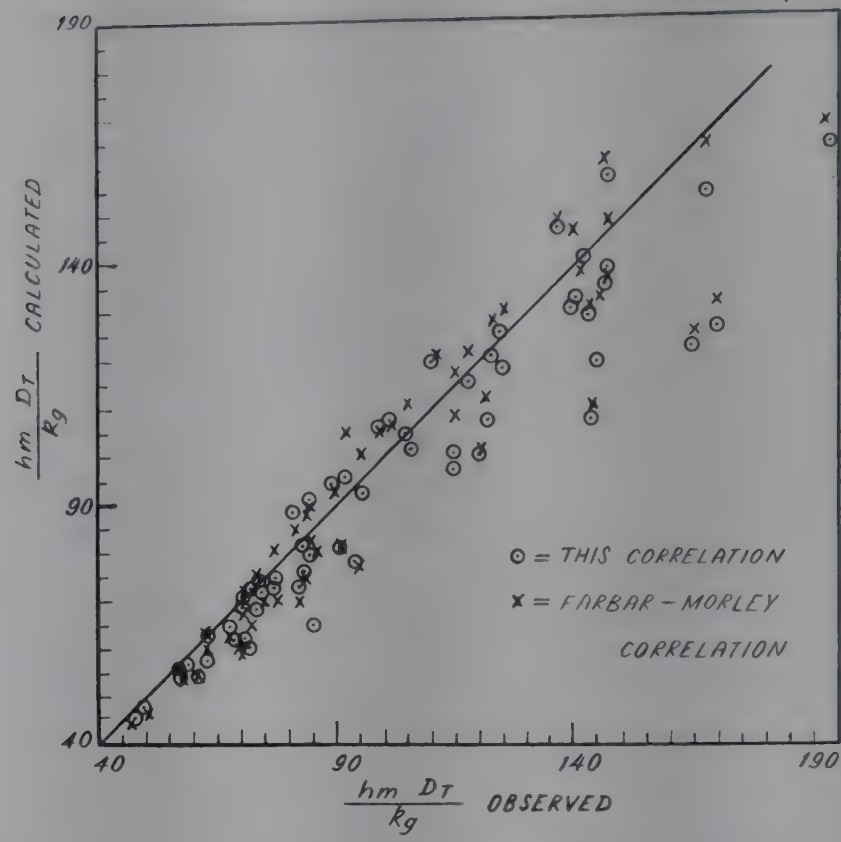


FIG. 11—PLOT OF OBSERVED VERSUS CALCULATED HEAT TRANSFER DATA IN COMPARISON WITH DATA OF FARBAR AND MORLEY

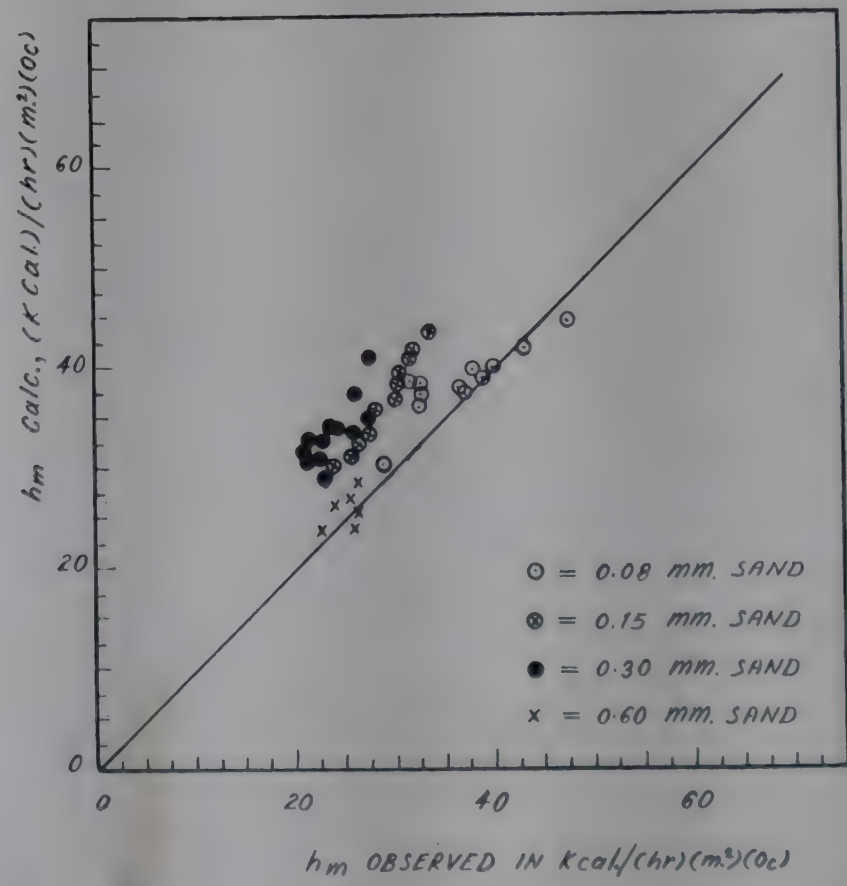


FIG. 12—PLOT OF OBSERVED VERSUS CALCULATED HEAT TRANSFER DATA OF MÜLLER

size. This may be due to: (i) the original degree of scatter that is to be seen from their observed data with these particle sizes, and (ii) the data as reported by them to a great extent are in the region of minimum, while the correlation is based on the points after the minimum.

CONCLUSION

1. Heat transfer rate in general increases with gas-solid mixture at a constant gas velocity loading ratio. Increase of gas velocity, and decrease of particle size increase the heat transfer rate.

2. The mixture heat transfer coefficient increases for solids loading ratios greater than the critical loading. The critical loading increases with increased particle size and increased carrier gas velocity. The improvement factor is higher at lower gas velocities, confirming that the solids affect the thickness of the boundary layer and the heat capacity of the flowing mixture. This may be due to the greater population of solid particles at the wall than at the centre.

3. The mixture heat transfer coefficient may also be influenced by the thermal conductivity of the solid material.

ACKNOWLEDGEMENTS

The authors wish to express their gratitude to Brig. S. K. Bose, Director, and Prof. N. R. Kamath and Dr G. S. R. Narasimhamurty, Department of Chemical Engineering, Indian Institute of Technology, Bombay, for their encouragement during the course of the work. The donation of the spent catalyst by *Esso Standard Eastern Inc.*, Bombay, is gratefully acknowledged.

NOMENCLATURE

- A_1 = constant
- C_g = heat capacity of air, $kcal./kg. ^\circ C$.
- C_s = heat capacity of solids, $kcal./kg. ^\circ C$.
- d_p = diam. of the particle, m .
- D_T = diameter of the tube, m .
- G_g = gas mass velocity, $kg./m.^2 sec$.
- h_m = mixture heat transfer coefficient, $kcal./hr m.^2 ^\circ C$.
- k_s = thermal conductivity of metal wall, $kcal. m./m.^2 hr ^\circ C$.
- k_g = thermal conductivity of carrier gas, $kcal. m. /m.^2 hr ^\circ C$.
- R = loading ratio, dimensionless
- u_g = gas velocity, $m./sec$.
- u_t = terminal velocity of particle, $m./sec$.
- μ_g = viscosity of gas, $kg./hr m$.
- ρ_g = density of air, $kg./m.^3$
- ρ_m = bed density, $kg./m.^3$
- ρ_s = density of solids, $kg./m.^3$

REFERENCES

1. Anon., *Atomics* (Tech. Publ. Co., Barrington, Illinois, U.S.A.)
2. Anon., *Chem. Engng News*, **32** (1954), 2213.
3. Anon., *Petrol. Refin.*, **32** (1953), 135.
4. *Final Rep. Babcock-Wilcox Co.*, Aug. 15, 1959, B.A.W.-1159.
5. BUCKER, H. & LUCKOW, H., *Brit. Pat.* 716, 273, Sept. 29, 1954.
6. CILLINS, R. R. & MARCIER, S. M., *U.S. Pat.* 12, 489, 863, Nov. 29, 1949.
7. DALLA LANA, I. G. & AMUNDSON, N. R., *Industr. Engng Chem.*, **53** (1961), 22.
8. GOODSON, L. B. & GUYER, J. A., *U.S. Pat.* 12, 606, 097, Aug. 5, 1952.
9. HELDMAN, J. D., KURENTHNER, F., MARSHALL, J. A. & REHEIN, C. A., *Petrol. Process.*, **11** (1956).
10. HELDMAN, J. D., KURENTHNER, F., MARSHALL, J. A. & REHEIN, C. A., *Petrol. Refin.*, **35** (1956), 166.
11. HELDMAN, J. D., KURENTHNER, F., MARSHALL, J. A. & REHEIN, C. A., *Petrol. Refin.*, **37** (1958), 240.
12. KASATKIN, A. G., *Basic Processes and Installations for Chemical Technology* (Goskhimizat, Moscow), 1960.
13. KIRKBRIDE, C. G. & DART, J. C., *U.S. Pat.* 12, 628, 188, Feb. 10, 1953.
14. KLEIN, D. X. & GAGE, H. B., *U.S. Pat.* 12, 768, 872, Oct. 1956.
15. KRÖLL, K. Z., *Ver. Deut. Ing.*, **94** (1952), 360.
16. LEWIS, W. K. & GILLILAND, E. R., *U.S. Pat.* 2, 498, 088, Feb. 21, 1950.
17. LLOYD, W. A. & AMUNDSON, N. R., *Industr. Engng Chem.*, **53** (1961), 19.
18. PELZER, H. L. & WATSON, K. M., *U.S. Pat.* 2, 464, 257, March 15, 1959.
19. SOLMS, H. W., TIKKOLA, E. E., COX, R. J., BRANKBY, E. E., COLLINGS, W. G. & MURPHY, W. I. R., *Industr. Engng Chem.*, **47** (1955), 461.
20. STAIRMAND, C. J., *Symp. on particle size analysis, Trans. Instn chem. Engrs, Lond.*, **25** (1947) (Suppl.), 128.
21. VISSAC, G. A., *Min. Engng*, **5** (1953), 1004.
22. ZENZ, F. A. & OTHMER, D. F., *Fluidization and Fluid Particle Systems* (Reinhold Publishing Corp., New York), 1960.
23. BRÖTZ, W., HIBY, J. W. & MÜLLER, K. G., *Chem. Ing. Techn.*, **30** (1958), 139.
24. DEPEW, C. A. & FARBAR, L., *J. Heat Transf.*, **85** (1963), 164.
25. FARBAR, L. & DEPEW, C. A., *Industr. Engng Chem. (Fundamentals)*, **2** (1963), 130.
26. FARBAR, L. & MORLEY, J. J., *Industr. Engng Chem.*, **49** (1957), 1143.
27. JEPSON, G., POLL, A. & SMITH, W., *Trans. Instn chem. Engrs, Lond.*, **41** (1963), 207.
28. KOBLE, R. A., ADEMINO, J. N., BARTHUS, E. P. & CORRIGAN, T. E., *Chem. Engng*, **58** (1951), 174.
29. MÜLLER, K. G., Doktor Ingeneiur Thesis, Technischen Sochschule, Aachen (West Germany), 1958.
30. SARMA, K. J. R., SEN GUPTA, P. & RAO, M. N., *Trans. Indian Inst. chem. Engrs*, **14** (1963).
31. SCHMID, W. E., BARTKUS, E. P. & CORRIGAN, T. E., *Chem. Engng*, **59** (10) (1952), 172.
32. TIEN, C. L., *J. Heat Transf. (Trans. Amer. Soc. mech. Engrs Ser.)*, **83** (1961), 183.
33. TRIBUS, M. & KLEIN, J., *Symp. Heat Transfer* (University of Michigan, U.S.A.), 1952, 211.
34. SELLARS, J. R., TRIBUS, M. & KLEIN, J. S., *Trans. Amer. Soc. mech. Engrs*, **78** (1956), 441.
35. RAO, V. R. K., Doctorate Thesis, Indian Institute of Technology, Bombay, 1963.
36. CADDLE, R. D., *Particle Size Determination* (Interscience Publishers Inc., New York), 1955.
37. ZOONEN, VAN D., *Proc. Symp. Interaction between Fluids and Particles* (European Federation of Chemical Engineers), 1952, A54.
38. WEN, C. Y. & MILLER, E. N., *Industr. Engng Chem.*, **53** (1961), 51.
39. LEVA, M., *Fluidization* (McGraw-Hill Book Co. Inc., New York), 1959.
40. LEVENSPIEL, O., WEINSTEIN, J. J. & JAROME, C. R., *Industr. Engng Chem.*, **48** (1956), 324.

Heat Transfer to Flowing Gas-Solid Suspensions in Circular Conduits Containing Turbulence Promoters

V. R. K. RAO & P. S. MURTI*

Department of Chemical Engineering
Indian Institute of Technology
Bombay 76

Heat and momentum transfer data pertaining to air flowing under turbulent conditions in a tube (length, 1.4 m.; inner diam., 19 mm.) containing spent silica-alumina catalyst particles of average size 47μ and full-width spiral turbulence promoters have been investigated. The effect of varying the pitch distance of the spiral promoter to 15, 10 and 6.5 cm. on the heat and momentum transfer has been studied.

It has been observed that the heat transfer coefficients increased up to 27-fold compared to particle-free gas values when the gas-solid suspension was flowing in tubes containing the spiral promoters. The improvement in heat transfer was dependent on loading ratio and pitch distance. The pressure drop increased in the same manner.

The data for heat transfer have been tentatively correlated in terms of Nusselt number, loading ratio, pitch distance and Reynolds number based on the tube diameter.

The introduction of turbulence promoters was shown to increase the heat transfer coefficient many-fold by Colburn and King¹ who investigated the heat and momentum transfer with heated air flowing in tubes containing turbulence promoters. Their results, however, are restricted to single phase systems. *Babcock and Wilcox Co.*²⁻³ reported data with graphite (less than 5μ) flowing as a suspension in carrier gases like nitrogen, helium and carbon dioxide in circular tubes containing spiral turbulence promoters. Their

*Present address: Regional Research Laboratory, Hyderabad 9.

findings show that heat transfer coefficients on the suspension side attain values as high as $34160 \text{ kcal./hr m.}^2\text{C.}$ depending upon the loading ratio and the carrier gas velocity. These values compare favourably with those obtainable with dropwise condensation of steam. They concluded that a flowing gas-solid suspension can be successfully employed in removing large quantities of heat from a limited area as in the case of a nuclear reactor. Their data, however, are of restricted applicability to transfer line reactors in which the carrier gas velocities are usually in the range, 7–15 m./sec. and the particle sizes well above 20μ . In this paper, results on heat and momentum transfer studies with spent silica-alumina catalyst having a mean particle size of 47μ , in air flowing under turbulent conditions in a 19 mm. inner diameter copper tube containing full-width spiral promoters are reported. The air mass velocity was varied from 2.22×10^4 to $3.58 \times 10^4 \text{ kg./hr m}^2$. Three different pitch distances (15, 10 and 6.5 cm.) of promoters were used to find the influence of this parameter on heat and momentum transfer.

EXPERIMENTAL SET-UP AND PROCEDURE

The apparatus used in this work and the operating procedure are the same as described elsewhere (*see* page 165).

Turbulence promoters. A photograph of the spiral turbulence promoters is shown in Fig. 1. These were made from 1.2 mm. thick, stainless steel strips, nearly 19 mm. wide on a lathe in lengths of 78 cm. and the shorter length pieces were silver-brazed to the required length. The excess silver was carefully removed by filing. The width of the spiral promoter was such that the clearance between the tube wall and the spiral was less than 0.1 mm. Initially, a spiral of the same length as the heat transfer section was inserted and another piece of about 1.20 m. long was placed in the upstream section, leaving a gap of about 2 mm. between the two. The second spiral served as a stabilizer for the flow pattern of the suspension before it entered the heat transfer section and the gap between the two spirals minimized the transmission of heat by conduction along the longitudinal direction beyond the experimental length.

RESULTS AND DISCUSSION

The heat transfer coefficients have been calculated using the relation

$$q = (w_1 - w_2) \lambda = U A (\Delta T)_{lm} \quad (1)$$

In this equation, w_2 , the amount of condensate accountable for radiation losses, was evaluated at intervals and found to be 108 kcal./hr within ± 5 per cent. The overall coefficient calculated from Eq. (1) was then resolved by means of Wilson plot from which the individual coefficient of heat transfer on the tube side was found. It was assumed, however, that the

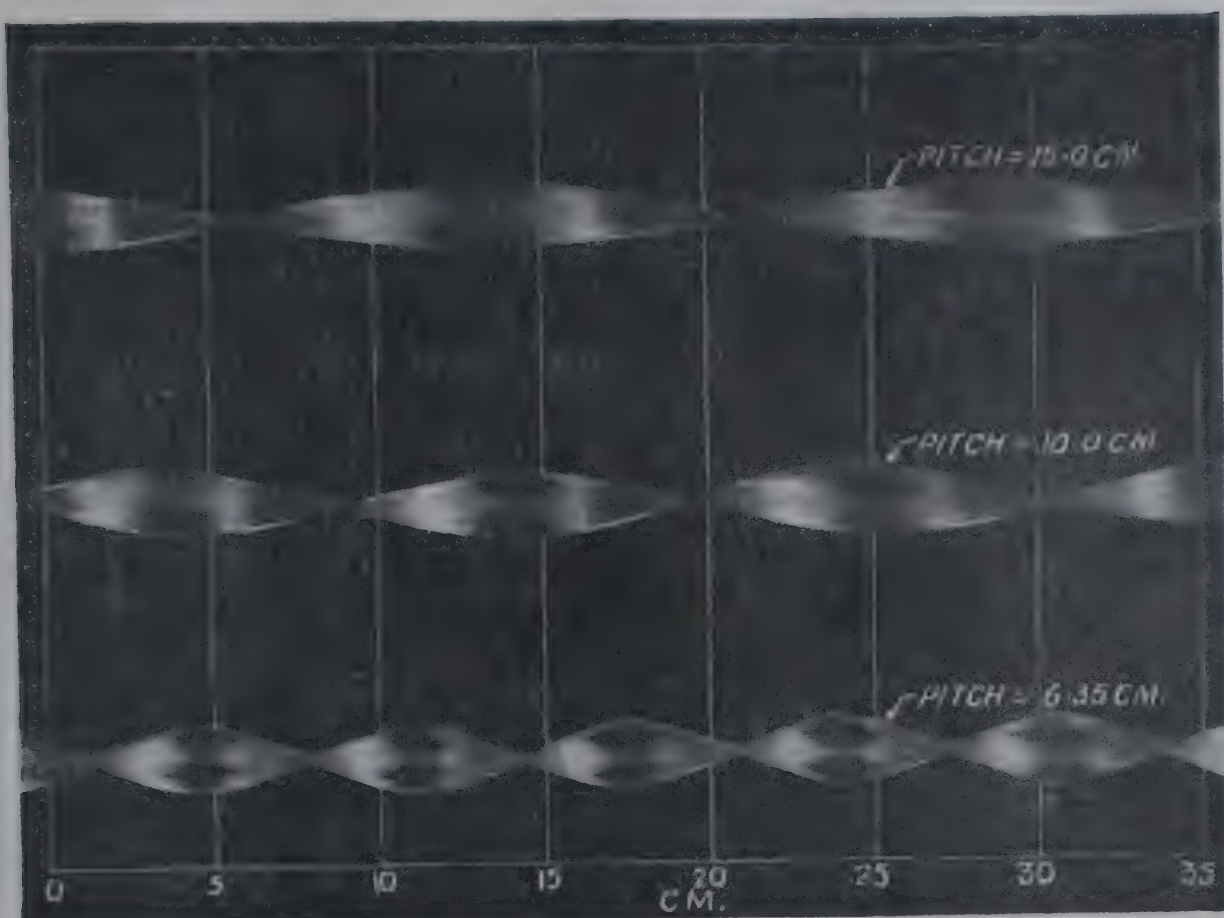


FIG. 1—SPIRAL TURBULENCE PROMOTERS MADE OF STAINLESS STEEL STRIPS

combined resistances of the metal wall and the steam film remain unaltered from run to run. A frequent check on this value made during the course of the work showed it to be fairly constant with a maximum deviation of ± 5 per cent.

Gas flow. At first, the experimental set-up was operated with air only to get the single phase flow heat and pressure drop data. The data are plotted in Fig. 2. The plots show that the data follow closely a modified Dittus-Boelter equation, where the constant seems to be a function of the pitch distance of the turbulence promoter. The data can be represented by the equation.

$$Nu = A_1 Re_r^{0.8} Pr^{0.4} \quad (2)$$

in which A_1 has the values 0.047, 0.042 and 0.037 respectively for the pitch distances, 6.35, 10.0 and 15.0 cm. Fig. 2 reveals that the heat transfer coefficients are always higher with turbulence promoters; thus, a value of 80.2 kcal./hr m.² °C. was obtained with a 6.35 cm. pitch promoter at a velocity of 8.73 m./sec. compared to 40.0 kcal./hr m.² °C. at the same velocity but without a promoter. In order to realize the value of 80.2 in an empty tube, a gas velocity of 21.0 m./sec. has to be employed. However, the pressure drop also correspondingly increases, and the ratio of pressure

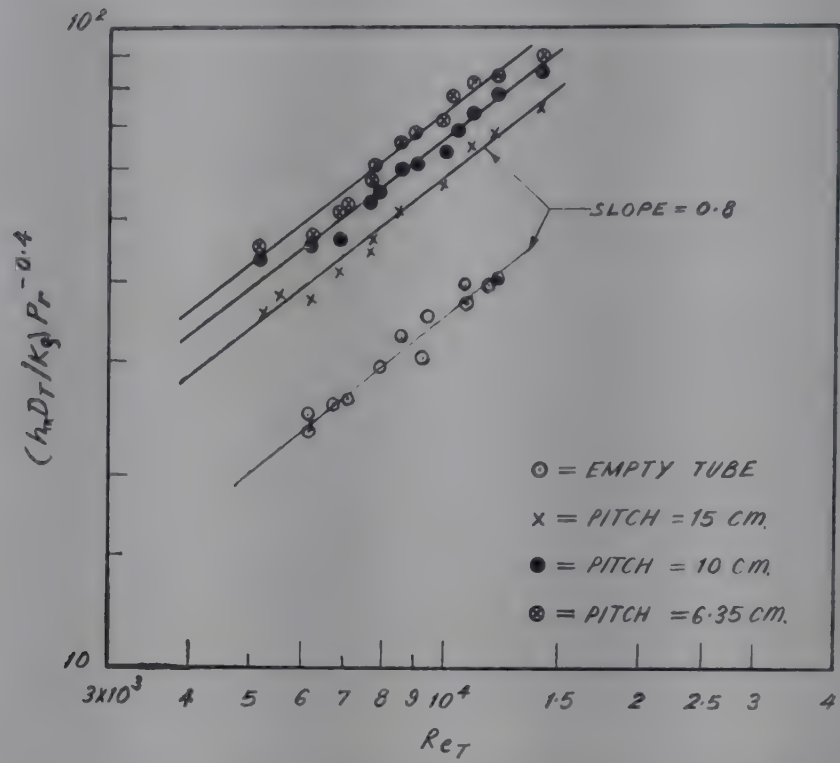


FIG. 2—PLOT OF (NUSELT NUMBER) (PRANDTL NUMBER)^{-0.4} VERSUS REYNOLDS NUMBER BASED ON TUBE FOR AIR FLOW WITH AND WITHOUT TURBULENCE PROMOTERS

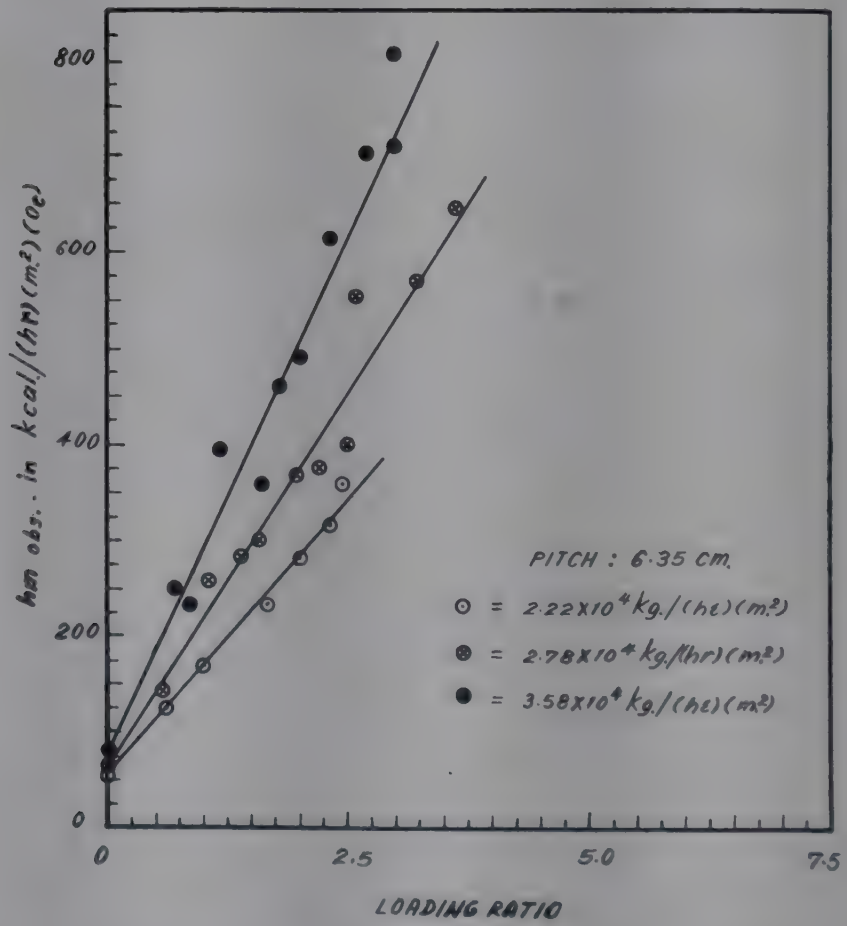


FIG. 3—PLOT OF MIXTURE HEAT TRANSFER COEFFICIENT WITH TURBULENCE PROMOTERS VERSUS LOADING RATIO [Pitch, 6.35 cm.]

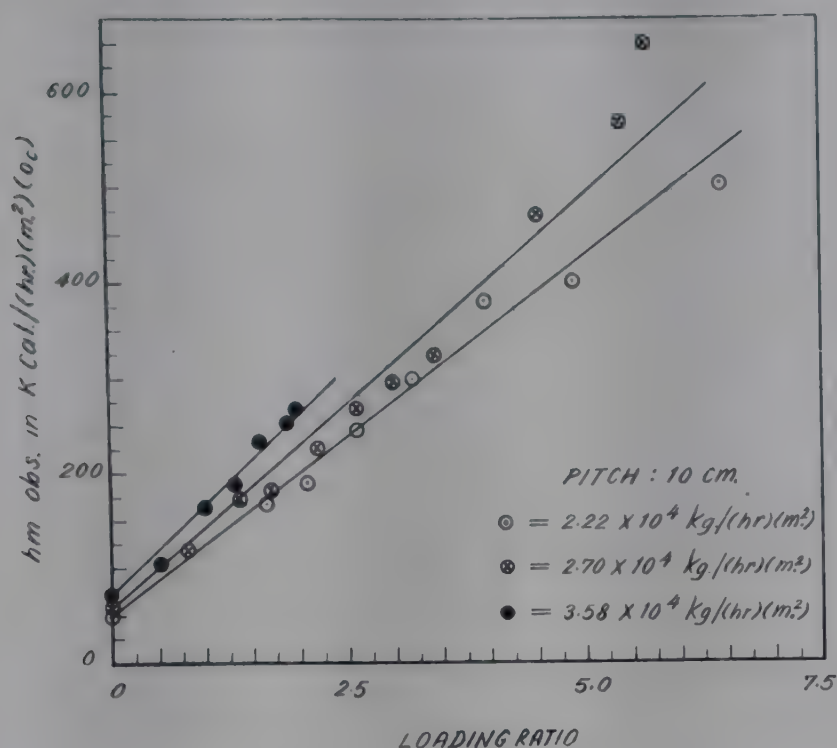


FIG. 4—PLOT OF MIXTURE HEAT TRANSFER COEFFICIENT WITH TURBULENCE PROMOTERS VERSUS LOADING RATIO [Pitch, 10.0 cm.]

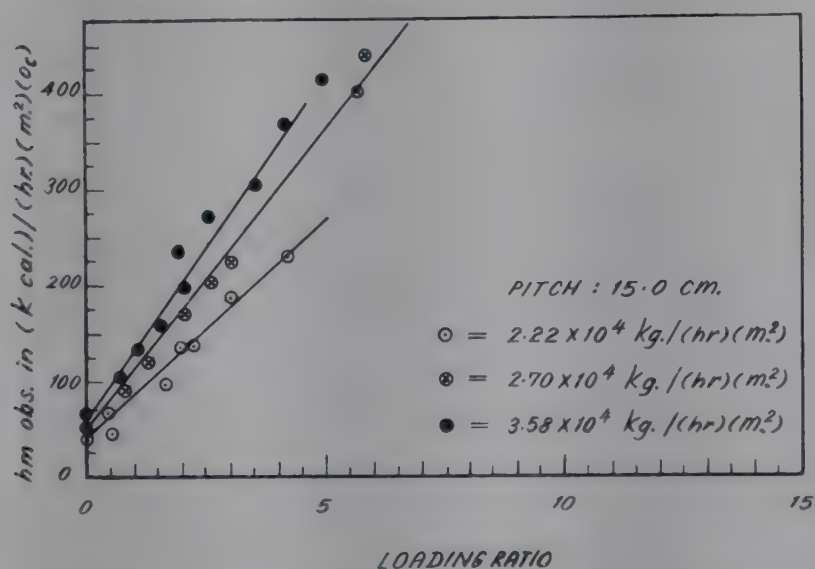


FIG. 5—PLOT OF MIXTURE HEAT TRANSFER COEFFICIENT WITH TURBULENCE PROMOTERS VERSUS LOADING RATIO [Pitch, 15.0 cm.]

drop with the promoter to the pressure drop without promoter is of the order of 4.6 at a gas velocity of 8.73 m./sec., while the ratio of the corresponding heat transfer coefficients is only 2.0. Hence, operating costs will increase with the introduction of a promoter, while the initial investment on equipment is low.

Suspension flow. Some sample data with suspension flow are given in Table 1. The heat transfer coefficients are plotted against loading ratio with gas velocity as the parameter for each of the three promoters used in

TABLE 1—CALCULATED AND OBSERVED MIXTURE HEAT TRANSFER DATA WITH TURBULENCE PROMOTERS

| (Pitch, 6.35 cm.) | | | | | | | | |
|---|------|--------------|--------------|--------------------------|-----------------|-------|-------|----------------|
| ΔH_s | R | t_i °C. | t_o °C. | $(\Delta t)_{lm}$ °C. | q kcal./hr | h_m | | DEVIATION % |
| | | | | | | Obs. | Calc. | |
| $(Gg=2.22 \times 10^4 \text{ kg./hr m.}^2)$ | | | | | | | | |
| 21.0 | 2.48 | 30.4 | 95.2 | 24.2 | 492 | 402.0 | 380.0 | + 5.48 |
| 7.4 | 0.62 | 29.9 | 96.0 | 23.1 | 211 | 128.0 | 117.0 | + 8.6 |
| 16.0 | 2.31 | 30.0 | 94.9 | 24.8 | 437 | 317.0 | 358.0 | - 12.95 |
| 9.4 | 0.99 | 29.9 | 96.0 | 23.1 | 265 | 171.0 | 174.0 | - 1.76 |
| 16.0 | 2.48 | 34.0 | 95.7 | 22.6 | 430 | 360.0 | 380.0 | - 5.55 |
| 15.0 | 2.00 | 34.1 | 95.7 | 22.6 | 379 | 281.0 | 315.0 | - 12.1 |
| 13.4 | 1.68 | 33.6 | 96.0 | 22.2 | 320 | 234.0 | 272.0 | - 16.2 |
| $(Gg=2.7 \times 10^4 \text{ kg./hr m.}^2)$ | | | | | | | | |
| 9.8 | 0.56 | 30.1 | 96.3 | 24.2 | 241.0 | 143.0 | 133.0 | + 7.0 |
| 20.3 | 1.98 | 32.6 | 93.6 | 25.8 | 497.0 | 370.0 | 386.0 | - 4.33 |
| 14.0 | 1.06 | 27.4 | 96.5 | 24.5 | 343.0 | 262.0 | 227.0 | + 13.4 |
| 15.5 | 1.59 | 30.6 | 96.4 | 22.2 | 380.0 | 303.0 | 321.0 | - 2.64 |
| 24.2 | 2.56 | 32.2 | 95.1 | 23.9 | 578.0 | 555.0 | 480.0 | + 13.5 |
| 29.5 | 3.23 | 32.8 | 93.7 | 25.7 | 629.0 | 571.0 | 585.0 | - 2.45 |
| 32.0 | 3.62 | 32.7 | 93.9 | 25.5 | 656.0 | 640.0 | 643.0 | - 0.47 |
| 30.3 | 2.21 | 31.9 | 95.3 | 23.7 | 463.0 | 379.0 | 423.0 | - 11.9 |
| 27.0 | 2.47 | 32.7 | 94.5 | 24.7 | 548.0 | 472.0 | 477.0 | - 1.00 |
| 17.0 | 1.41 | 27.9 | 94.2 | 25.5 | 428.0 | 284.0 | 289.0 | - 1.76 |
| $(Gg=3.58 \times 10^4 \text{ kg./hr m.}^2)$ | | | | | | | | |
| 37.0 | 1.60 | 30.3 | 90.2 | 30.6 | 584.0 | 363.0 | 420.0 | - 15.7 |
| 22.5 | 0.87 | 29.8 | 93.6 | 26.8 | 388.0 | 235.0 | 251.0 | - 6.8 |
| 18.0 | 0.70 | 29.8 | 96.0 | 23.1 | 351.0 | 252.0 | 209.0 | + 17.1 |
| 37.0 | 2.30 | 35.2 | 92.6 | 26.5 | 668.0 | 614.0 | 577.0 | + 6.05 |
| 27.5 | 1.16 | 30.1 | 91.8 | 28.8 | 483.0 | 295.0 | 310.0 | - 5.08 |
| 40.0 | 2.67 | 35.9 | 91.5 | 27.5 | 736.0 | 701.0 | 647.0 | + 7.57 |
| 43.0 | 2.94 | 33.6 | 92.8 | 26.7 | 757.0 | 809.0 | 706.0 | + 12.7 |
| 46.0 | 3.00 | 35.2 | 91.7 | 27.6 | 743.0 | 710.0 | 720.0 | - 1.47 |
| 35.0 | 1.80 | 31.2 | 92.8 | 27.4 | 579.0 | 433.0 | 464.0 | - 7.25 |
| 36.0 | 2.00 | 31.5 | 92.7 | 27.3 | 615.0 | 487.0 | 508.0 | - 2.67 |

this work in Fig. 3-5. The data indicate that the coefficients greatly increase in comparison to either single component flow or with two-component flow without turbulence promoters. The increase is as high as 27 times the former and 6 times the latter at a gas velocity of 6.62 m./sec. The coefficients seem to be directly proportional to solid loading ratio and inversely proportional to pitch distance. It was visually observed that the solid density at the wall was always higher than at the centre, probably due to centrifugal force exerted on the particles during their spiral upward motion. The additional turbulence in the vicinity of the wall caused by the spinning of the particles, the size of which is comparable to the laminar sub-layer effectively scours the layer and thus reduces the film thickness. The scouring action apparently depends upon the solid population near the wall, i.e. loading ratio and pitch distance, as well as carrier gas velocity.

CORRELATIONS

The suspension heat transfer data with turbulence promoters were obtained with only one particle size of silica-alumina catalyst and, therefore, a correlation incorporating the solid properties is not possible at this stage. It was observed from the figures given above that the mixture heat transfer coefficients are dependent on the loading ratio, pitch distance and gas velocity. Hence, a correlation of the form, Eq. (3) was tried.

$$\frac{h_m D_T}{k_g} = A_2 \left(\frac{D_T G_g}{\mu_g} \right)^a (P)^b (R)^c \quad (3)$$

The values of the constants A_2 and a , b and c were determined by the method of least squares. The final correlation graph is shown in Fig. 6, and the equation satisfying the data is

$$(h_m D_T / k_g) = 1.4 \times 10^{-3} (D_T G_g / \mu_g) P^{-1} R^{0.81} \quad (4)$$

In order to express the equation in terms of dimensionless parameters the pitch distance was divided by the inner diameter of the tube and the constant was correspondingly changed. However, it was realized that this may not be an acceptable practice since the tube diameter was not changed during the course of the work. The final form of the equation thus becomes

$$(h_m D_T / k_g) = 7.36 \times 10^{-6} (D_T G_g / \mu_g) (D_T / P) (R)^{0.84} \quad (5)$$

The average and standard deviations within which this equation represents the data are respectively 8.8 and 15.6 per cent.

Colburn and King¹ in their investigations with heated air passing through tubes containing different types of promoters observed that an

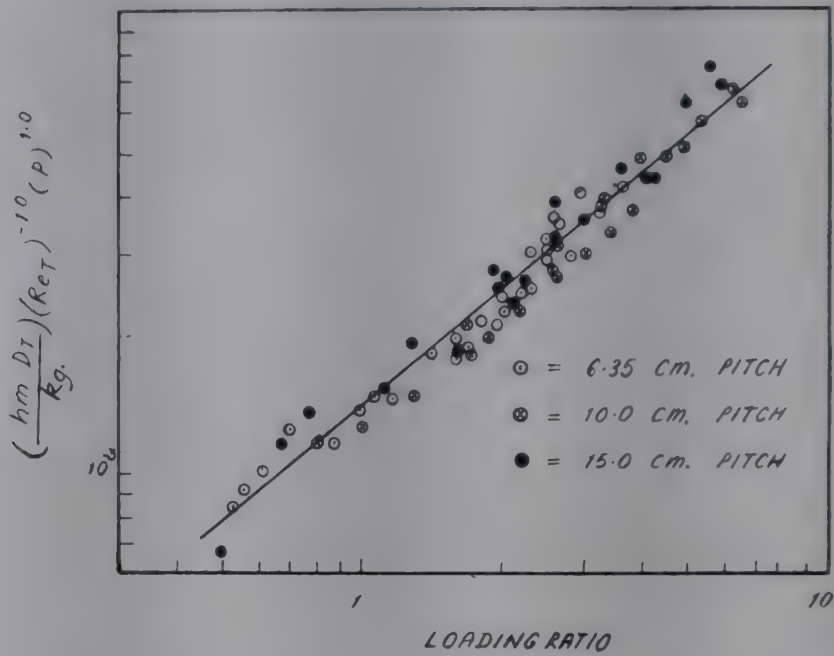


FIG. 6—PLOT OF (NUSSELT NUMBER) (PITCH DISTANCE)/(REYNOLDS NUMBER) VERSUS LOADING RATIO FOR DIFFERENT PITCHES

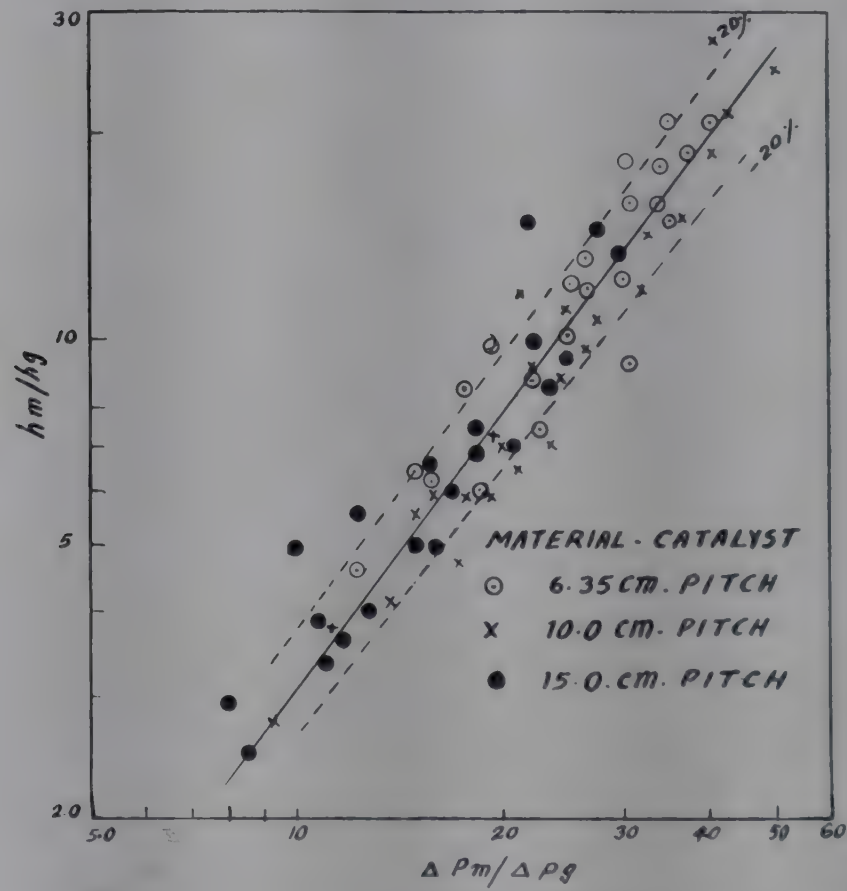


FIG. 7—PLOT OF MIXTURE AND GAS HEAT TRANSFER RATIO VERSUS PRESSURE DROP RATIO FOR DIFFERENT PITCHES

analogy might exist between heat and momentum transfer. An attempt was made during the course of this investigation to see the trend of behaviour by plotting mixture heat transfer coefficient versus pressure drop. Subsequently, it was observed that a plot of h_m/h_g versus $\Delta P_m/\Delta P_g$ (Fig. 7)

nearly brought all the data on to a line with 90 per cent of the data points lying within a band of ± 20 per cent. This is comparable to the standard deviation reported in Eq. (4). The equation governing this straight line plot is

$$\frac{h_m}{h_g} = 0.13 \left(\frac{\Delta P_m}{\Delta P_g} \right)^{1.4} \quad (6)$$

This method permits calculation of the mixture heat transfer coefficients from a knowledge of h_g , ΔP_g (which are obtained from standard correlations), and ΔP_m which is the only quantity to be evaluated experimentally. Further experimental data are needed to prove the existence of the analogy for all types of promoters.

CONCLUSION

The relatively very high heat transfer coefficient in tubes containing spiral promoters is due to the spiral motions of the particles, which in turn create extra turbulence near the solid boundary. Factors like lower pitch distances, increased carrier gas velocity and loading ratio greatly contribute to the increase in the heat transfer rate.

An analogy appears to exist between heat and momentum transfer, although the form is not of the conventional type. Further work is, however, needed to confirm its existence.

ACKNOWLEDGEMENTS

The authors wish to express their gratitude to Brig. S. K. Bose, Director, Prof. N. R. Kamath and Dr G. S. R. Narasimhamurty, Department of Chemical Engineering, Indian Institute of Technology, Bombay, for their encouragement during the course of the work. The donation of the spent catalyst by *Esso Standard Eastern Inc.*, Bombay, is gratefully acknowledged.

NOMENCLATURE

| | |
|---------------------|--|
| A | = area of heat transfer section, m^2 . |
| A_1, A_2, a, b, c | = constants |
| D_i | = inner diameter of tube, m . |
| G_g | = gas mass velocity, $kg./hr\ m.^2$ |
| h_g | = gas heat transfer coefficient without promoters, $kcal./hr\ m.^2\ ^\circ C$. |
| h_m | = mixture heat transfer coefficient with promoters, $kcal./hr\ m.^2\ ^\circ C$. |
| ΔH_1 | = pressure drop across 1.435 m. long vertical test section |
| k_g | = thermal conductivity of gas, $kcal./m.\ hr\ ^\circ C$. |
| Nu | = Nusselt number, dimensionless |
| P | = pitch distance, m . |

| | |
|-------------------|--|
| ΔP_g | = gas pressure drop without promoters |
| ΔP_m | = mixture pressure drop with promoters |
| Pr | = Prandtl number, dimensionless |
| q | = amount of heat transferred, $kcal./hr$ |
| R | = loading ratio, dimensionless |
| Re_T | = Reynolds number based on the inner diameter of tube, dimensionless |
| t_i | = temperature at the inlet, $^{\circ}C$. |
| t_o | = temperature at the outlet, $^{\circ}C$. |
| $(\Delta T)_{lm}$ | = log mean temperature difference, $^{\circ}C$. |
| U | = overall coefficient of heat transfer, $kcal./hr\ m.^2\ ^{\circ}C$. |
| w_1 | = total quantity of condensate collected, $kg./hr$ |
| w_2 | = condensate equivalent of the radiation and convection losses, $kg./hr$ |
| λ | = latent heat of vaporization, $kcal./kg$. |
| μ_g | = viscosity of gas, $kg./hr\ m$. |

REFERENCES

1. COLBURN, A. P. & KING, W. J., *Trans. Amer. Inst. chem. Engrs*, **26** (1931), 166.
2. Babcock and Wilcox Co., *Gas Suspension Coolant Project, Final Rep.*, Aug. 1959, B.A.W. 1159.
3. Babcock and Wilcox Co., *Gas Suspension Task II, Final Rep.*, Nov. 1959, B.A.W. 1181.

Heat Transfer Studies in Batch-Fluidized Beds: Liquid-Solid Systems

G. J. V. JAGANNADHA RAJU, M. S. KRISHNA
& C. VENKATA RAO

Department of Chemical Technology, Andhra University
Waltair

Experiments have been conducted to determine the rate of heat transfer from an external wall to liquid-solid batch-fluidized beds employing different sizes of steel balls and glass spheres, Raschig rings and Berl saddles fluidized by water and water-glycerol mixtures. The experiments covered a modified Reynolds number values from 1000 to 70,000 and Prandtl number from 4 to 20. A study of the effect of variables such as diameter and concentration of solids, mass velocity of fluid, has shown that heat transfer coefficients increased with solid concentration up to 20-30 per cent solids and remained nearly constant thereafter. For a given concentration of solids, an increase of particle size resulted in an increase of heat transfer coefficients.

The experimental heat transfer coefficients and the reported data on gas-solid system have been correlated with modified *J*-factor as a function of modified Reynolds number.

During recent years much effort has been made in the application of fluid-solid technique to heat transfer problems; but most of it has been directed towards the study of gas-solid systems and comparatively less work has been reported on liquid-solid systems¹⁻⁷.

Lemlich and Caldas² experimented with six closely sized groups of scotchlite glass beads fluidized by water and reported that operations at Reynolds numbers less than that at which the maximum heat transfer coefficient was obtained resulted in a dense phase fluidization and that operations at higher Reynolds numbers resulted in a lean phase fluidization.

Richardson and Mitson³ fluidized various sizes of solids like glass, lead, gravel, iron and copper with water and water-glycerol mixtures and found that at volumetric concentrations in excess of 7 per cent solids the heat transfer coefficient reached a constant maximum value for each system. In a later paper Richardson and Smith⁴ reported that in the earlier work (i) the temperatures were not measured sufficiently close to the tube walls and insufficient allowance was made for the heat flow in the laminar sub-layer, and (ii) the equation used for the prediction of solid concentration was unreliable under conditions where uniform fluidization is not obtained⁵. Using the experimentally determined solid concentration, Richardson and Smith reported with the aid of new data that the heat transfer coefficient increased with volumetric concentration until a concentration between 0.2 and 0.35 was reached, and began to decrease slightly.

Ananda Rao and Kaparathi¹ employing different sizes of granite and quartz fluidized by water reported that the heat transfer coefficient attained a maximum value at a solid concentration between 14 and 16 per cent.

Most of the workers^{1,4,6} investigating on the liquid-solid fluidized beds reported that the heat transfer coefficient depended on the particle size and for a given mass velocity it increased with increasing particle size. Lemlich and Caldas reported, however, that in the dense phase region the particle size had no effect on the heat transfer coefficient.

These significant deviations in the results of various investigators resulted in widely different correlations for the heat transfer in liquid-solid fluidized beds.

In view of these disagreements among the findings of the previous investigators, the study on heat transfer from a confining wall to liquid-solid batch-fluidized beds was undertaken for the purpose of evaluating the effect of physical properties of fluids and solids, the effect of mass velocity and solid concentration and, if possible, for offering improved correlations.

EXPERIMENTAL SET-UP AND PROCEDURE

The flow diagram of the apparatus is given in Fig. 1. The liquid from the feed tank (1) is circulated by a centrifugal pump (2) through a rotameter (3), fluidization unit (4, 5, 6), and a heat exchanger (7).

The fluidization unit comprised a heat transfer section (5) and calming sections (4, 6). The heat transfer section is a 1/4 in. thick brass tube of inner diam. 2 in. and length 1 ft. Three 1/16 in. holes, 3 in. deep, were drilled 120° apart on either side of the heat transfer section (Fig. 2) to facilitate the introduction of thermocouples to measure the mid-wall temperatures. The insulated thermocouple leads were drawn out through the flanges provided on either end to connect the heat transfer section to the calming sections. Three independent heating elements made of nichrome

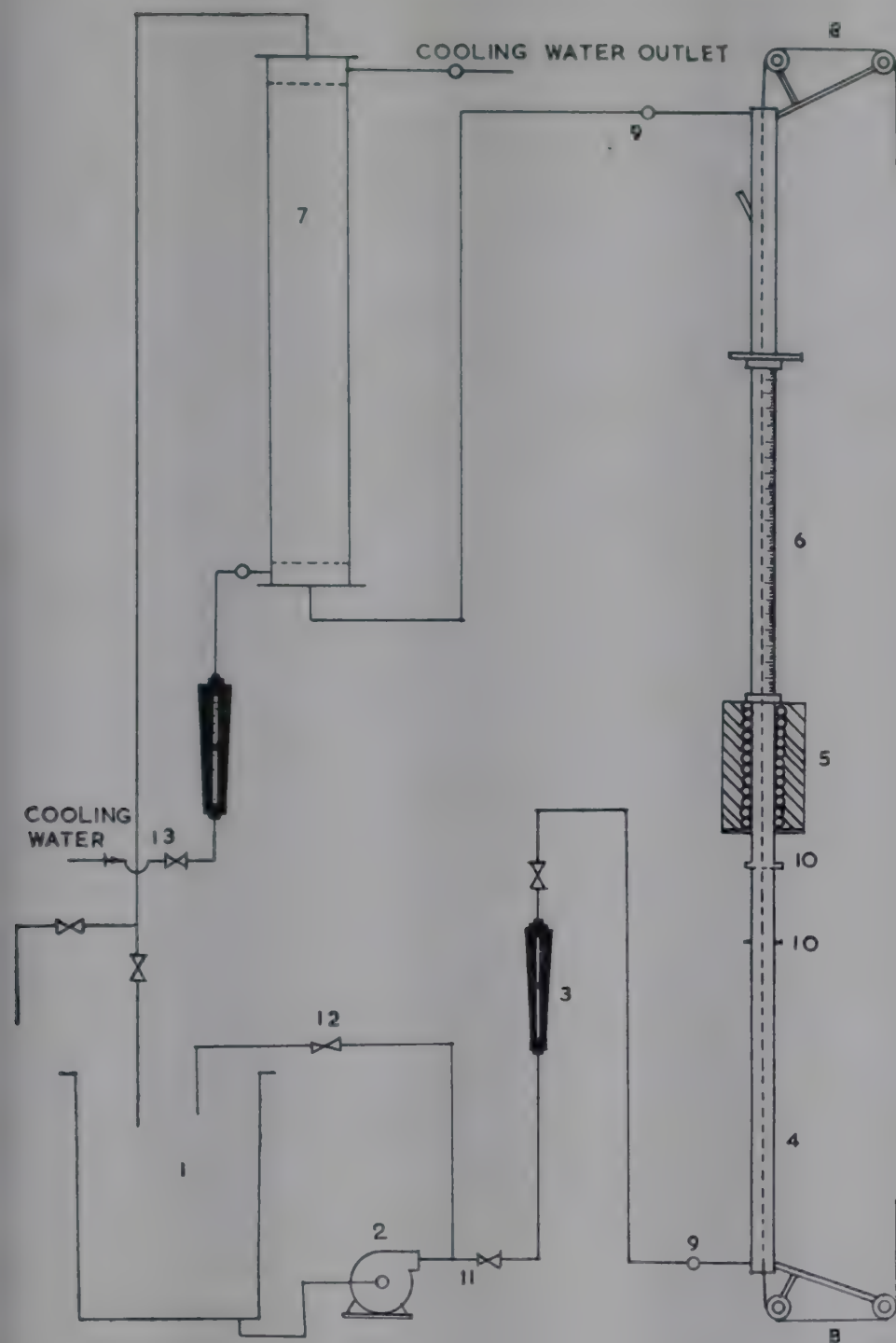


FIG. 1

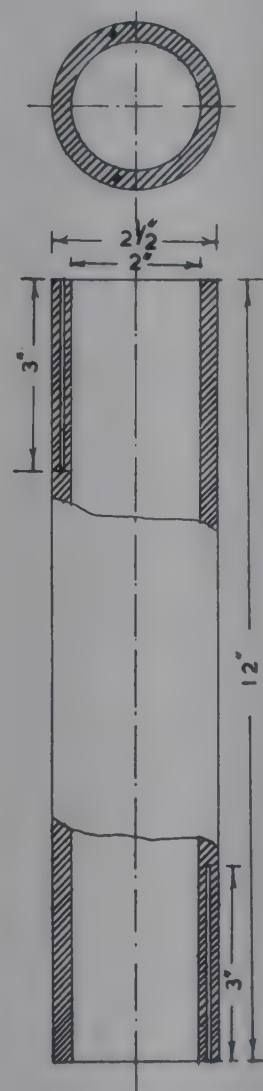


FIG. 2

FIG. 1—APPARATUS FOR HEAT TRANSFER STUDIES IN BATCH FLUIDIZED BEDS [(1) Feed tank; (2) Centrifugal pump; (3) Rotameter; (4, 5 & 6) Fluidization unit; (7) Heat exchanger; (8) Travelling thermocouple; (9) Thermocouple pockets; (10) Grid; (11, 12 & 13) Flow control valves]

FIG. 2—HEAT TRANSFER SECTION

wire covered with porcelain beads were wound round the heating section. The heaters were insulated from the end flanges by asbestos sheet and were thoroughly lagged to minimize the heat loss to the surroundings. An auto-transformer supplied power to the heaters.

The bottom calming section was a 3 ft long G.I. pipe of inner diam. 2 in. The top calming section was made of a $2\frac{1}{2}$ ft glass column of inner diam. 2 in. (to observe the bed expansion) followed by a 2 ft long G.I. pipe.

All the connecting units were of G.I. pipes of 1 in. inner diam. which were lagged with asbestos rope and powder, and felt. Provision was made for the introduction of travelling thermocouple (8) to measure the longitudinal temperature profiles. Two thermocouple pockets (9) just before and after the bottom and top calming sections facilitated the measurement of inlet and outlet temperatures. All the thermocouples employed were of copper-constantan and were brought out through a selector switch to a potentiometer. The thermo E.M.F.'s with reference to a cold junction in melting ice were measured by a Leeds-Northrup potentiometer (having an accuracy of $0.1 \mu\text{V.}$) coupled with a multiflex galvanometer.

Provision was also made to introduce grid (10), 6 in. and 1 ft below the heat transfer section. A 50-mesh brass screen was employed as the grid.

Standardization runs conducted with distilled water in the absence of solids resulted in heat transfer coefficients very close to those predicted from Dittus-Boelter equation.

After placing a weighed quantity of bed material into the column the flow was allowed. The flow rate necessary for a given bed expansion was adjusted by control valves (11, 12). Potential was gradually applied to the heating element to get the required heat flux. The desired flow of the cooling water was then turned on through the heat exchanger by operating the valve (13).

After steady conditions were reached at each flow rate, usually after 3 hr, readings were taken of the mid-metal wall thermocouples, travelling thermocouple, liquid and cooling water thermocouples. Flow rates of the liquid and cooling water were recorded. Since the bed expansion increases with liquid velocity, the runs were carried out by progressively increasing the weight of the solids present thereby reducing the liquid velocity.

Heat transferred to the system at the heat transfer section was found to be within 3 per cent of the heat removed by the cooling water in the heat exchanger. Due to inherent heat losses to surroundings from heating elements, the electrical heat input was found to be 10-15 per cent higher than the heat transferred into the systems. Hence, these values were not used in the calculations.

Calculation of heat transfer coefficient. Sensible heat gained by the liquid was calculated by Eq. (1).

$$q = W_L C_p (t_2 - t_1) \times 1.8 \times 3600 \quad (1)$$

Mid-metal wall temperature representing the temperature at a distance of 1/8 in. from the inside surface was taken as the average of the readings of the six thermocouples. The temperature drop, Δt_s , across this distance was then calculated by using Eq. (2) and (3).

$$\Delta t_s = \frac{q \times b}{k_M A_M \times 1.8} \quad (2)$$

$$t_s = t_M - (\Delta t_s) \quad (3)$$

Using the surface temperature t_s , the transfer coefficient h , was evaluated by Eq. (4).

$$h = \frac{q}{A (t_s - t_{av.}) \times 1.8} \quad (4)$$

RESULTS

The systems studied are summarized in Table 1. In all the figures the legends are given by series numbers corresponding to the systems indicated in Table 1.

The fluidization was observed to be particulate for all runs with glass spheres while in case of steel balls slugging was observed at higher initial bed heights. In case of nonspherical bed materials in general and Berl

TABLE 1—SYSTEMS INVESTIGATED

*SERIES
No.

| | |
|-----|--|
| | Position of the grid: 6 in. upstream of the heat transfer section |
| H-1 | 0.01041 ft glass spheres—water |
| H-2 | 0.013 ft steel balls—20 wt per cent glycerol |
| H-3 | 0.01968 ft glass spheres—20 wt per cent glycerol |
| | Position of the grid: 12 in. upstream of the heat transfer section |
| H-4 | 0.01041 ft steel balls—water |
| H-5 | 0.01041 ft steel balls—50 wt per cent glycerol |
| H-6 | 0.0130 ft steel balls—water |
| H-7 | 0.01666 ft steel balls—water |
| H-8 | 0.01417 ft Raschig rings—water |
| H-9 | 0.01750 ft Berl saddles—water |

*The tables containing the data are available with the authors.

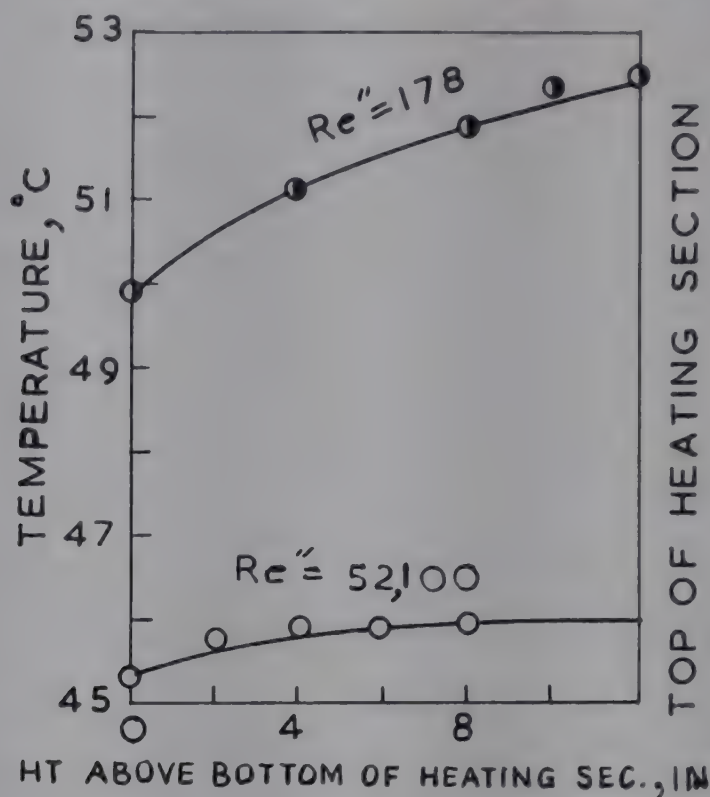


FIG. 3—LONGITUDINAL TEMPERATURE PROFILES FOR TWO FLOW RATES

saddles in particular the phenomenon of channelling was also observed at higher initial bed heights.

Typical longitudinal temperature profiles for two flow rates are shown in Fig. 3. They indicate negligible amount of back mixing. Similar observations were reported by Richardson and Mitson³ and Lemlich and Caldas².

Effect of solid concentration. The heat transfer coefficients are shown in Fig. 4 and 5 as a function of solid concentration. The heat transfer coefficients increase with solid concentration up to 20-30 per cent solids, above which they remain nearly constant. The effect of solid concentration as it approaches the concentration of the fixed bed is not clear. At lower concentrations, the heat transfer coefficients fall off linearly to reach the value for pure liquids as the concentration of solids approaches zero. Similar observations were reported⁹ with bed characteristic studies.

Effect of particle diameter. In Fig. 5 heat transfer coefficients are plotted as a function of solid concentration for two sizes of steel balls. For the same solid concentration, an increase in particle size results in an increase in heat transfer coefficient; since to obtain comparable concentration of larger particle, higher liquid velocity is needed. This consequently increases turbulence and hence the heat transfer rate.

CORRELATION

Colburn^{10,11} developed the heat and momentum transfer analogy for flow of fluids through circular conduits by utilizing the dimensionless J -factor to relate the significant variables of the transfer process.

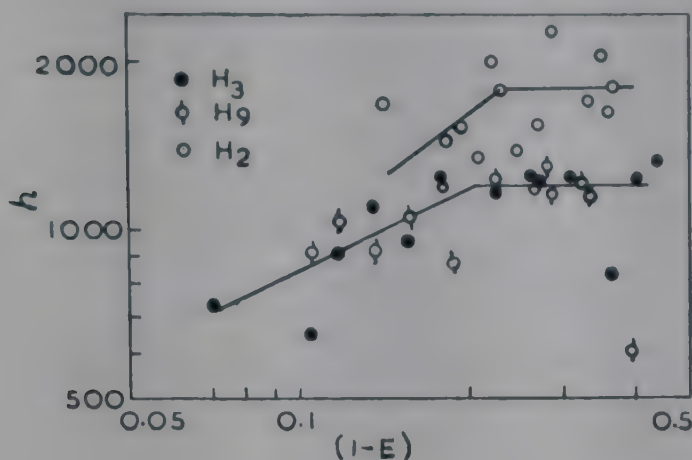


FIG. 4

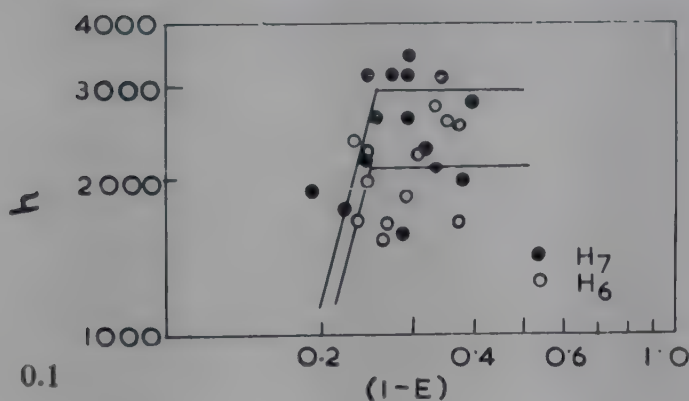


FIG. 5

FIG. 4—PLOT OF HEAT TRANSFER COEFFICIENT VERSUS $(1-E)$ FOR SYSTEMS H2, H3 & H9FIG. 5—PLOT OF HEAT TRANSFER COEFFICIENT VERSUS $(1-E)$ FOR SYSTEMS H6 & H7

The \mathcal{J} -factor was related to the Reynolds number which defines the flow conditions. The relation in its general form is given by Eq. (5).

$$\mathcal{J}_H = \left(\frac{h}{C_p G} \right) \left(\frac{C_p \mu}{k} \right)^{2/3} = C \left(\frac{DG}{\mu} \right)^n \quad (5)$$

By applying correction of V/E for V to account for interstitial velocities and considering $\left(\frac{D_p E}{1-E} \right)$ as equivalent diameter available for fluid flow in a fluidized bed, Eq. (5) takes the form

$$\mathcal{J}_H E = \left(\frac{h E}{C_p G} \right) \left(\frac{C_p \mu}{k} \right)^{2/3} = C \left(\frac{D_p G}{\mu(1-E)} \right)^n \quad (6)$$

The data, with the grid positioned 6 in. upstream of the heat transfer section, are plotted in Fig. 6, which shows modified \mathcal{J} -factor as a function of modified Reynolds number. This resulted in a satisfactory correlation of the data by Eq. (7).

$$\mathcal{J}_H E = 0.53 (Re'')^{-0.38} \quad (7)$$

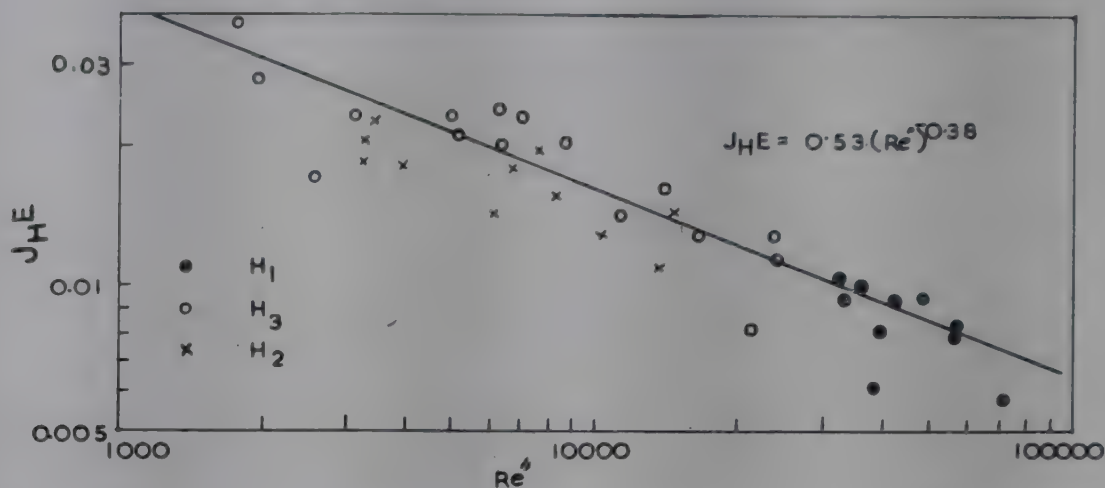


FIG. 6—PLOT OF MODIFIED J -FACTOR VERSUS MODIFIED REYNOLDS NUMBER FOR SYSTEMS H1, H2 & H3 (Grid position, 6 in. upstream)

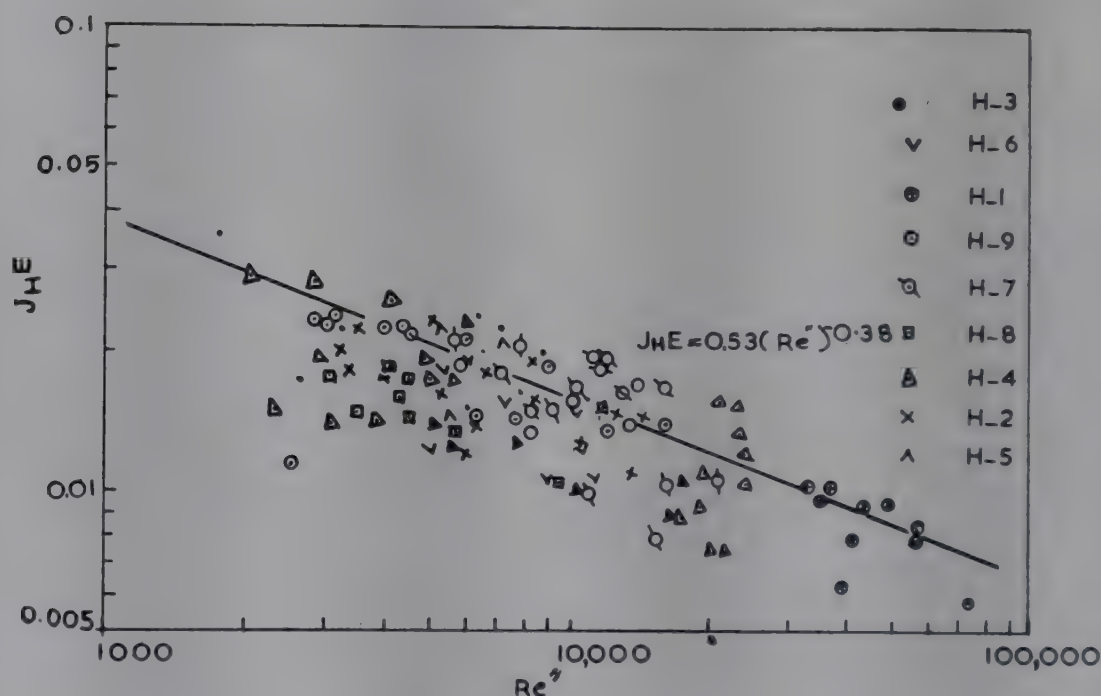


FIG. 7—PLOT OF MODIFIED J -FACTOR VERSUS MODIFIED REYNOLDS NUMBER FOR SYSTEMS H1-H9 (Grid position, 1 ft upstream)

The equation represents the experimental data with an average deviation of ± 15 per cent.

Fig. 7 shows the entire experimental data, wherein the data obtained with the grid positioned 1 ft upstream of the heat transfer section show a greater scatter. This may be due to the existence of longitudinal variation of solid concentration in the expanded bed as observed in the light intensity measurements⁹. The solid concentration used for calculating the correlation factors is an average value based on the uniform bed density distribution and is, therefore, not representative of that portion of the fluidized bed covered by the heat transfer section. Some scatter may be attributable also to slugging.

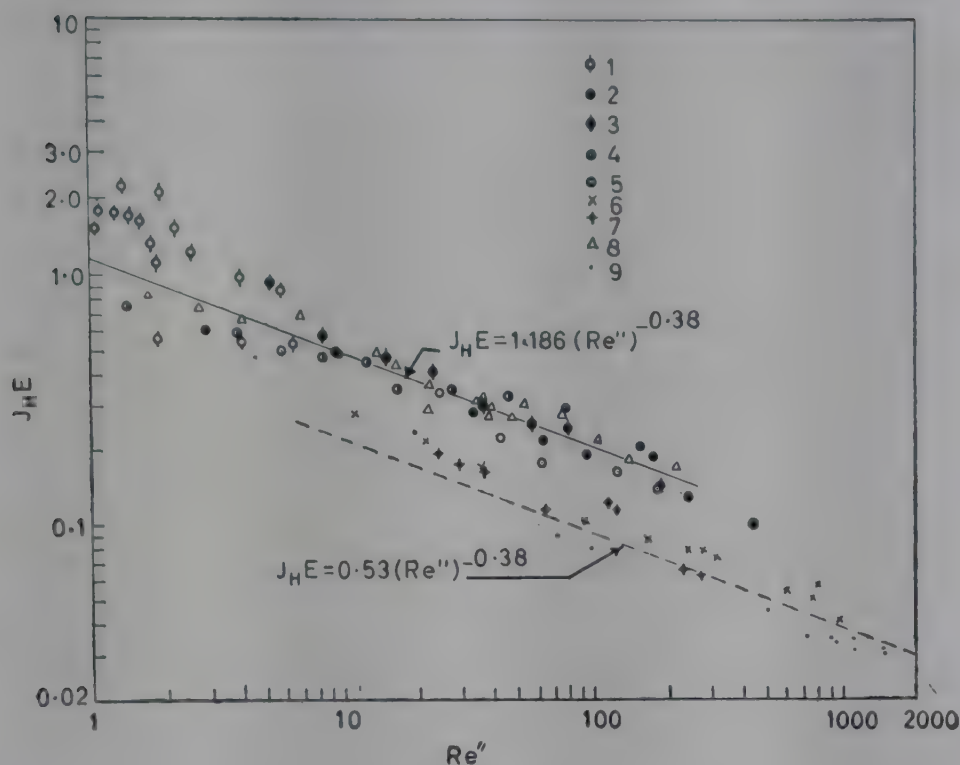


FIG. 8—PLOT OF MODIFIED \mathcal{J} -FACTOR VERSUS MODIFIED REYNOLDS NUMBER [(1) Dow & Jakob's data; (2-9) Mickley & Trillings data; (2) $Dp = 5.08 \times 10^{-4}$ ft & 4 in. column; (3) $Dp = 3.33 \times 10^{-4}$ ft & 1 in. column; (4) $Dp = 2.29 \times 10^{-4}$ ft & 4 in. column; (5) $Dp = 5.08 \times 10^{-4}$ ft. & 1 in. column; (6) $Dp = 8.83 \times 10^{-4}$ ft & 4 in. column; (7) $Dp = 9.33 \times 10^{-4}$ ft & 4 in. column; (8) $Dp = 3.33 \times 10^{-4}$ ft & 4 in. column; (9) $Dp = 14.8 \times 10^{-4}$ ft & 4 in. column]

Since Eq. (6) for the fluidized beds is developed from the \mathcal{J} -factor Reynolds number relation for flow of fluids through circular conduits, it may be capable of extension to other fluid-solid systems.

In order to test the applicability of Eq. (6) to gas-solid systems, the data of Mickley and Trilling¹² and Dow and Jakob¹³ for externally heated fluidized beds were considered.

The calculated data of Mickley and Trilling for externally heated fluidized bed in 4 in. and 1 in. columns in terms of modified \mathcal{J} -factor and modified Reynolds number are plotted in Fig. 8, which also shows the line representing Eq. (7). The calculated values of Dow and Jakob are also shown in the figure. The data for the Reynolds number ($Re_p = D_p G/\mu$) greater than 20 have shown good agreement with the proposed correlation. For the values of Re_p lower than 10, the data are correlated with the same functional relationship between the modified \mathcal{J} -factor and the modified Reynolds number but with a higher constant.

In the light of these studies the following equations are suggested for heat transfer between confining wall and a fluidized bed:

$$\mathcal{J}_H E = 0.53 (Re'')^{-0.38}, \text{ for } Re_p > 20 \quad (7)$$

$$\mathcal{J}_H E = 1.186 (Re'')^{-0.38}, \text{ for } Re_p < 10 \quad (8)$$

The applicability of the correlation to both the experimental data on liquid-solid systems and the calculated data on gas-solid systems reveals that the applied corrections reasonably represent the conditions in fluidized bed.

CONCLUSION

1. The presence of fluidized solids can increase the rate of heat transfer from a retaining wall to liquid considerably.

2. The heat transfer coefficients increase with the solid concentration up to a value of 20-30 per cent solids and nearly remain constant thereafter.

3. For any given concentration of solids an increase of particle size results in an increase in heat transfer coefficient.

4. The experimental data on heat transfer in liquid-solid batch fluidized beds are correlated by the equation:

$$\mathcal{J}_H E = 0.53 (Re'')^{-0.38}$$

5. The thermal conductivity and the specific heat of the particle have no significant effect on the heat transfer coefficient.

6. The increase in heat transfer coefficients is attributable to the increase in turbulence due to higher interstitial velocities and the convective movement of the particles.

7. The correlation for the heat transfer for externally heated fluidized bed is given by the following equations:

$$\mathcal{J}_H E = 0.53 (Re'')^{-0.38}, \text{ for } Re_p > 20$$

$$\mathcal{J}_H E = 1.186 (Re'')^{-0.38}, \text{ for } Re_p < 10$$

NOMENCLATURE

| | |
|-----------------|---|
| A | = heat transfer surface, ft^2 |
| A_M | = average heat transfer surface, ft^2 |
| b | = half of the metal wall thickness, ft |
| C | = constant |
| C_p | = specific heat of fluid, $B.t.u./lb. ^\circ F.$ |
| D | = diameter of tube, ft |
| D_p | = diameter of particle, ft |
| E | = bed voidage, dimensionless |
| G | = fluid mass velocity based on empty cross-section of tube, $lb./ft^2 hr$ |
| h | = heat transfer film coefficient, $B.t.u./hr ft^2 ^\circ F.$ |
| \mathcal{J}_H | = heat transfer factor, dimensionless |
| k | = thermal conductivity of fluid, $B.t.u./hr ft^2 (^\circ F./ft)$ |
| k_M | = thermal conductivity of metal, $B.t.u./hr ft^2 (^\circ F./ft)$ |
| q | = heat transferred to liquid, $B.t.u./hr$ |
| Re_p | = particle Reynolds number, $D_p G/\mu$, dimensionless |
| Re'' | = modified Reynolds number, $D_p G/\mu (1-E)$, dimensionless |
| t_1 | = inlet temperature of liquid, $^\circ C.$ |
| t_2 | = outlet temperature of liquid, $^\circ C.$ |
| $t_{av.}$ | = average temperature of liquid, $(t_1 + t_2)/2$, $^\circ C.$ |

t_m = mid-metal wall temperature, °C.

t_s = liquid-metal surface temperature, °C.

V = velocity of fluid based on empty cross-section of tube, ft/hr

W_L = liquid flow rates, lb./sec.

Δt_s = temperature drop across half of the metal wall thickness, °C.

μ = fluid viscosity, lb./hr/ft

REFERENCES

1. ANANDA RAO, M. & KAPARTHI, R., *J. sci. industr. Res.*, **20D** (1961), 261.
2. LEMLICH, R. & CALDAS, I. (Jr), *Amer. Inst. chem. Engrs. J.*, **4** (1958), 376.
3. RICHARDSON, J. F. & MITSON, A. E., *Trans. Instn chem. Engrs, Lond.*, **36** (1958), 270.
4. RICHARDSON, J. F. & SMITH, J. W., *Trans. Instn chem. Engrs, Lond.*, **40** (1962), 13.
5. SUNKOORI, N. R. & KAPARTHI, R., *Chem. Engng Sci.*, **12** (1960), 166.
6. WESSER, U. & MARDUS, G., *Chem. Ing. Tech.*, **29** (1957), 332.
7. WICKE, E. & HEDDEN, K., *Chem. Ing. Tech.*, **24** (1952), 82.
8. RICHARDSON, J. F. & ZAKI, W. N., *Trans. Instn chem. Engrs, Lond.*, **32** (1954), 35.
9. JAGANNADHA RAJU, G. J. V., D.Sc. Thesis, Andhra University, 1959.
10. COLBURN, A. P., *Trans. Amer. Inst. chem. Engrs*, **29** (1933), 174.
11. CHILTON, T. H. & COLBURN, A. P., *Industr. Engng Chem.*, **26** (1934), 1183.
12. MICKLEY, H. S. & TRILLING, C. A., *Industr. Engng Chem.*, **41** (1949), 1135.
13. DOW, W. M. & JAKOB, M., *Chem. Engng Progr.*, **47** (1951), 637.

Heat Transfer Studies in Continuous Fluidized Beds: Part III—Prediction of Heat Transfer Coefficients from Simple Fluid Flow Considerations applying Momentum Heat-Transfer Analogies

P. SEN GUPTA, K. J. R. SARMA* & M. N. RAO

Department of Chemical Engineering, Indian Institute of Technology
Kharagpur

The film coefficient of heat transfer in fluidized bed containing low concentrations of solid can be fairly predicted from simple fluid flow considerations and by applying analogies, such as those of Reynolds and Colburn. For higher solid concentrations, the suspension characteristics of the bed are taken into account and the properties evaluated. The deviations observed are of smaller magnitude and the experimental results have been found to agree fairly well with those of Colburn's analogy.

As far back as 1874, Reynolds¹ anticipated that transfer processes of heat and momentum might be closely related, in view of the fact that each of these transfer processes depends on molecular properties and the motion of eddies in the turbulent stream. For fluids flowing through conduits,

$$\frac{h}{C_f G} = \frac{f}{2} \quad (1)$$

*Present address: Regional Engineering College, Rourkela 8.

It has been shown later by Prandtl² and Taylor³ that the entire cross-section of a fluid in turbulent flow is not turbulent. Instead, a laminar layer is found to exist near the pipe wall through which conduction occurs. Reynolds' analogy, as such, had ignored the differences in heat transfer mechanisms existing in the laminar film, turbulent core and intervening buffer zone. For both gases and low viscosity liquids, for which the value of Prandtl number is not far from unity, this correlation stands good. Various extensions of these analogies have been proposed and have been reviewed by Sherwood⁴.

An important and useful modification of these analogies presented by Colburn⁵ is

$$\left(\frac{h}{C_f G}\right) \left(\frac{C_f \mu_f}{k_f}\right)^{2/3} = \frac{f}{2} = \mathcal{J}_h \quad (2)$$

where \mathcal{J}_h is termed as the heat transfer factor; and f , fanning friction factor, is based on shear friction rather than on total drag.

The validity of this equation in the case of packed beds has been shown by various workers.

Gamson⁶ has derived the following relationships by using the results reported by Mickley and Trilling⁷.

$$\mathcal{J}_h = 2.0 \left(\frac{DG}{\mu_f}\right)^{-0.69} (1-\epsilon)^{-0.3} \quad (3)$$

for heat transfer between fluidized bed and containing wall; and

$$\mathcal{J}_h = 2.82 \left(\frac{DG}{\mu_f}\right)^{-0.8} (1-\epsilon)^{-0.3} \quad (4)$$

for heat transfer between fluidized bed and axial heater.

Combining the analogy between heat and mass transfer proposed by Wamsley and Johanson⁸ on the basis of their recalculations of the data of Kettenring *et al.*⁹, and the analogy between mass and momentum transfer proposed by Chu *et al.*¹⁰, Chu¹¹ considers the following relationships to hold good for fluidized system:

$$\mathcal{J}_h = 1.77 \left[\frac{DG}{\mu_f (1-\epsilon)} \right]^{-0.44} \quad \text{for} \quad \frac{DG}{\mu_f (1-\epsilon)} > 30 \quad (5)$$

$$\mathcal{J}_h = 5.70 \left[\frac{DG}{\mu_f (1-\epsilon)} \right]^{-0.98} \quad \text{for} \quad \frac{DG}{\mu_f (1-\epsilon)} < 30 \quad (6)$$

EXPERIMENTAL WORK

The present investigations were undertaken with a view to determine the heat transfer coefficient from a metal wall to a dilute-phase fluidized bed,

using coal particles as the solid and air as the fluidizing medium. The experimental set-up and the procedure are essentially the same as described in earlier papers^{12,13}. The steam coal having a volatile matter content of 23.46 per cent and ash content of 28.92 per cent (dry basis) was used in the study. The variables studied have been reported earlier¹².

The densities of the bed in all these cases were very low (maximum up to 20 per cent) and the observed values of the heat transfer coefficients were also low. It was, therefore, thought proper to compare these flow conditions with those of a pure fluid. Assuming that solid particles were absent and instead an equivalent amount of gas was flowing along with the main stream, the heat transfer coefficients were calculated on the basis of either Reynolds' or Colburn's¹³ analogies. The calculated values as well as their percentage deviations from the measured coefficients are given in Table 1. It is seen that the maximum deviation of the experimental value from the calculated value based on Colburn's analogy is of the order of 57-40 per cent.

TABLE 1—COMPARISON OF EXPERIMENTAL AND CALCULATED HEAT TRANSFER FILM COEFFICIENTS FOR LEAN BED ZONES

(Fluidizer of 5 $\frac{7}{8}$ in. inner diam. with 3 in. outer diam. baffle; Heat transfer coefficient values are in *B.t.u./hr/ft²/°F.*)

| RUN No. | CALCULATION BASED ON SIMPLE FLUID FLOW | | | | | CALCULATION BASED ON FLOW OF SUSPENSION | | | |
|---------------------------------|---|-------|-------|------------------------------------|---------|--|-----------|------------------------------------|-----------|
| | h_{exp} | h_R | h_e | Deviation (%) of h_{exp} from | | h_R (s) | h_e (s) | Deviation (%) of h_{exp} from | |
| | | | | h_R | h_e | | | h_R (s) | h_e (s) |
| | | | | | | | | | |
| | | | | | | | | | |
| CoAL, $D_p=0.0008301\text{ ft}$ | | | | | | | | | |
| 69 | 6.736 | 3.311 | 4.572 | + 103.30 | + 47.35 | 3.585 | 4.785 | + 87.90 | + 40.80 |
| 70 | 7.667 | 3.700 | 5.125 | + 107.30 | + 49.65 | 4.068 | 5.420 | + 88.40 | + 41.50 |
| 71 | 7.749 | 4.392 | 6.198 | + 76.40 | + 25.00 | 4.882 | 6.520 | + 58.80 | + 18.87 |
| 72 | 8.680 | 4.764 | 6.598 | + 82.30 | + 31.55 | 5.315 | 6.985 | + 63.30 | + 24.26 |
| 74 | 8.896 | 4.916 | 7.096 | + 81.10 | + 25.35 | 5.487 | 7.540 | + 62.20 | + 17.97 |
| 73 | 9.020 | 5.325 | 7.515 | + 69.45 | + 20.05 | 5.907 | 7.840 | + 52.70 | + 15.05 |
| 75 | 8.339 | 4.442 | 6.191 | + 37.70 | + 35.00 | 4.861 | 6.470 | + 71.70 | + 28.90 |
| 76 | 8.489 | 4.843 | 6.790 | + 75.30 | + 25.00 | 5.346 | 7.142 | + 58.80 | + 18.86 |
| 77 | 8.706 | 5.207 | 7.324 | + 67.30 | + 18.84 | 5.789 | 7.730 | + 50.20 | + 12.62 |
| CoAL, $D_p=0.001304\text{ ft}$ | | | | | | | | | |
| 21 | 3.89 | 3.070 | 4.007 | + 26.70 | - 2.92 | 3.227 | 4.140 | + 20.60 | - 6.04 |
| 22 | 4.11 | 3.136 | 4.095 | + 31.10 | + 0.37 | 3.266 | 4.175 | + 27.60 | - 1.56 |

TABLE 1—COMPARISON OF EXPERIMENTAL AND CALCULATED HEAT TRANSFER FILM COEFFICIENTS FOR LEAN BED ZONES—(Contd)

(Fluidizer of 5 $\frac{7}{8}$ in. inner diam. with 3 in. outer diam. baffle;Heat transfer coefficient values are in $B.t.u.^2/hr/ft/^{\circ}F.$)

| RUN No. | CALCULATION BASED ON SIMPLE FLUID FLOW | | | | | CALCULATION BASED ON FLOW OF SUSPENSION | | | |
|-------------------------|---|-------|-------|------------------------------------|---------|--|-----------|------------------------------------|-----------|
| | h_{exp} | h_R | h_c | Deviation (%) of h_{exp} from | | h_R (s) | h_c (s) | Deviation (%) of h_{exp} from | |
| | | | | h_R | h_c | | | h_R (s) | h_c (s) |
| 20 | 4.44 | 3.174 | 4.143 | + 39.90 | + 7.17 | 3.373 | 4.280 | + 34.20 | + 3.74 |
| 18 | 3.97 | 3.213 | 4.409 | + 23.60 | − 9.98 | 3.534 | 4.470 | + 12.30 | − 11.20 |
| 23 | 5.43 | 3.106 | 4.288 | + 74.90 | + 26.60 | 3.314 | 4.430 | + 67.40 | + 22.60 |
| 24 | 4.64 | 3.203 | 4.383 | + 44.85 | + 58.70 | 3.395 | 4.800 | + 36.70 | − 3.34 |
| 25 | 5.74 | 3.487 | 4.848 | + 64.55 | + 18.40 | 3.706 | 4.850 | + 56.60 | + 18.35 |
| 28 | 7.26 | 4.207 | 5.825 | + 72.50 | + 24.63 | 4.570 | 5.920 | + 58.90 | + 22.60 |
| 26 | 7.80 | 3.837 | 5.009 | + 103.20 | + 55.80 | 4.085 | 5.120 | + 91.10 | + 52.40 |
| 27 | 8.55 | 4.231 | 5.859 | + 102.30 | + 45.90 | 4.680 | 5.970 | + 82.60 | + 43.20 |
| 33 | 6.22 | 3.183 | 4.408 | + 95.00 | + 41.10 | 3.404 | 4.610 | + 82.80 | + 34.90 |
| 32 | 4.95 | 3.323 | 4.765 | + 49.10 | + 3.78 | 3.568 | 4.980 | + 38.70 | − 0.62 |
| 30 | 6.27 | 3.517 | 5.043 | + 78.10 | + 24.40 | 3.852 | 5.270 | + 62.80 | + 19.00 |
| COAL, $D_p=0.001304$ ft | | | | | | | | | |
| 31 | 7.100 | 3.808 | 5.273 | + 86.40 | + 34.70 | 4.120 | 5.470 | + 72.30 | + 29.80 |
| 29 | 9.310 | 4.703 | 6.616 | + 98.10 | + 40.70 | 5.325 | 7.220 | + 73.00 | + 28.90 |
| 34 | 7.20 | 3.506 | 4.856 | + 105.20 | + 48.20 | .. | .. | .. | .. |
| 37 | 7.05 | 3.934 | 5.535 | + 79.40 | + 27.20 | 4.270 | 5.805 | + 65.00 | + 21.30 |
| 35 | 7.05 | 4.100 | 5.880 | + 71.90 | + 19.90 | 4.405 | 6.095 | + 59.80 | + 15.70 |
| 38 | 7.21 | 4.578 | 6.566 | + 57.40 | + 9.74 | 5.005 | 6.830 | + 44.10 | + 5.55 |
| 36 | 8.11 | 5.063 | 7.214 | + 60.00 | + 12.50 | 5.662 | 7.810 | + 43.30 | + 3.84 |
| 42 | 6.85 | 3.690 | 5.258 | + 85.70 | + 30.25 | 3.900 | 5.390 | + 75.60 | + 27.10 |
| 41 | 8.15 | 4.472 | 6.351 | + 82.30 | + 28.35 | 4.862 | 6.670 | + 67.60 | + 22.10 |
| 39 | 8.35 | 4.864 | 6.996 | + 71.90 | + 19.60 | 5.360 | 7.280 | + 55.70 | + 14.70 |
| 40 | 9.70 | 5.351 | 7.802 | + 81.30 | + 24.35 | 6.140 | 8.295 | + 58.00 | + 16.90 |
| 43 | 5.624 | 3.138 | 4.670 | + 79.00 | + 20.30 | 3.270 | 4.730 | + 71.80 | + 18.80 |
| 44 | 6.567 | 3.607 | 5.367 | + 81.70 | + 22.15 | 3.728 | 5.620 | + 76.10 | + 16.84 |

TABLE 1—COMPARISON OF EXPERIMENTAL AND CALCULATED HEAT TRANSFER FILM COEFFICIENTS FOR LEAN BED ZONES—(Contd)

(Fluidizer of 5 $\frac{7}{8}$ in. inner diam. with 3 in. outer diam. baffle
Heat transfer coefficient values are in *B.t.u./hr/ft.²/°F.*)

| RUN No. | CALCULATION BASED ON SIMPLE FLUID FLOW | | | | | CALCULATION BASED ON FLOW OF SUSPENSION | | | | |
|-------------------------|---|-------|-------|------------------------------------|---------|--|-----------|------------------------------------|-----------|--|
| | h_{exp} | h_R | h_c | Deviation (%) of h_{exp} from | | h_R (s) | h_c (s) | Deviation (%) of h_{exp} from | | |
| | | | | h_R | h_c | | | h_R (s) | h_c (s) | |
| | | | | | | | | | | |
| | | | | | | | | | | |
| COAL, $D_p=0.001304$ ft | | | | | | | | | | |
| 45 | 7.166 | 4.083 | 6.075 | + 75.80 | + 17.93 | 4.670 | 7.810 | + 53.50 | — 8.32 | |
| 46 | 7.800 | 4.220 | 6.279 | + 84.80 | + 24.20 | 4.750 | 7.850 | + 64.30 | — 0.64 | |
| 47 | 6.836 | 4.726 | 7.061 | + 44.40 | — 3.10 | 5.260 | 7.450 | + 30.00 | — 8.25 | |
| 48 | 8.555 | 4.878 | 7.176 | + 75.40 | + 19.20 | 5.485 | 7.720 | + 55.00 | + 10.80 | |
| 59 | 10.300 | 5.141 | 7.650 | + 81.10 | + 34.60 | 6.850 | 7.920 | + 50.40 | + 30.30 | |
| 49 | 14.140 | 5.610 | 8.322 | + 157.20 | + 70.00 | 6.430 | 8.880 | + 120.00 | + 59.20 | |
| 50 | 8.450 | 4.273 | 6.357 | + 97.60 | + 32.80 | 5.035 | 6.030 | + 67.70 | + 40.10 | |
| 51 | 9.281 | 4.876 | 7.233 | + 90.20 | + 28.40 | 5.865 | 6.900 | + 58.20 | + 34.50 | |
| 52 | 9.380 | 5.220 | 7.767 | + 79.70 | + 20.70 | 6.428 | 7.480 | + 45.90 | + 25.40 | |
| 53 | 10.400 | 5.450 | 8.166 | + 90.80 | + 27.30 | 6.845 | 7.870 | + 52.00 | + 32.10 | |
| 54 | 4.535 | 2.975 | 4.395 | + 52.40 | + 3.18 | 3.620 | 4.415 | + 25.30 | + 2.72 | |
| 55 | 5.299 | 3.436 | 5.095 | + 54.20 | + 4.00 | 4.135 | 4.963 | + 28.20 | + 6.76 | |
| 57 | 6.525 | .. | .. | .. | .. | 5.280 | 6.215 | + 23.60 | + 5.00 | |
| 58 | 6.488 | 4.108 | 6.099 | + 58.00 | + 6.38 | 4.946 | 5.820 | + 31.20 | + 11.50 | |
| COAL, $D_p=0.001969$ ft | | | | | | | | | | |
| 60 | 5.053 | 3.254 | 4.521 | + 55.35 | + 11.76 | 3.531 | 4.680 | + 43.10 | + 7.34 | |
| 61 | 5.170 | 3.672 | 5.199 | + 40.80 | — 0.56 | 4.234 | 5.320 | + 22.11 | — 2.90 | |
| 62 | 5.378 | 4.044 | .. | + 32.85 | .. | 4.657 | 5.750 | + 15.47 | — 6.70 | |
| 63 | 5.689 | 3.613 | 5.182 | + 57.40 | + 9.78 | 4.343 | 5.850 | + 30.98 | — 3.00 | |
| 64 | 6.440 | 4.285 | 6.017 | + 50.30 | + 7.03 | 4.864 | 6.190 | + 32.41 | + 3.27 | |
| 65 | 6.191 | 4.719 | 6.723 | + 31.15 | — 7.92 | 5.261 | 7.120 | + 17.68 | — 12.90 | |
| 66 | 5.991 | 4.772 | .. | + 25.54 | .. | 4.582 | 6.220 | + 30.75 | — 3.55 | |
| 67 | 6.958 | 5.338 | .. | + 30.34 | .. | 6.039 | 7.800 | + 15.22 | — 12.00 | |
| 68 | 7.238 | 5.160 | .. | + 40.30 | .. | 6.074 | 7.280 | + 19.16 | — 0.50 | |

Calculated values of the heat transfer coefficients that could be predicted by assuming that the mixture of air and coal particles behaves as a pseudo-fluid are also given. The density and specific heat of this pseudo-fluid were evaluated on the weighted average basis. The viscosity was calculated by the equation suggested by Einstein¹⁴ for suspensions, and the thermal conductivity was evaluated by the equation given by Tareef¹⁵. All the above properties were evaluated at the mean of the inlet and exit temperatures of the air-solid mixture. The calculated values of h as well as their deviations from the experimental values are given in the table. It will be seen that the values calculated by Reynolds' analogy are less than the experimental values by 15-43 per cent and the values calculated by Colburn's analogy are higher by about 13 per cent (maximum).

CONCLUSION

The film coefficient of heat transfer from wall to bed for a dilute gas-solid fluidized bed can be predicted within fair accuracy by considering the fluidized bed as a suspension of solid particles in a fluid and using these properties of the suspension, the experimental film coefficient of heat transfer can be calculated.

NOMENCLATURE

| | |
|------------|---|
| C_f | = specific heat of fluid, $B.t.u./lb. ^\circ F.$ |
| D | = diameter of tube, ft |
| f | = fanning friction factor |
| G | = superficial fluid mass velocity, $lb./hr ft^2$ |
| h | = experimental film coefficient of heat transfer, $B.t.u./hr ft^2 ^\circ F.$ |
| h_R | = predicted film coefficient of heat transfer based on Reynolds' analogy, $B.t.u./hr ft^2 ^\circ F.$ |
| h_c | = predicted film coefficient of heat transfer based on Colburn's analogy, $B.t.u./hr ft^2 ^\circ F.$ |
| $h_{R(s)}$ | = predicted film coefficient of heat transfer based on Reynold's analogy (suspension properties), $B.t.u./hr ft^2 ^\circ F.$ |
| $h_{c(s)}$ | = predicted film coefficient of heat transfer based on Colburn's analogy (suspensions properties), $B.t.u./hr ft^2 ^\circ F.$ |
| J_h | = heat transfer factor |
| K_f | = thermal conductivity of fluid, $B.t.u./hr ft^2 ^\circ F./ft$ |
| μ_f | = viscosity of fluid, $lb./ft hr$ |
| ϵ | = void fraction in the bed |

REFERENCES

1. REYNOLDS, O., *Scientific Papers of Osborne Reynolds* (Cambridge University, London), Vol. 1 (1901), 81.
2. PRANDTL, L., *Z. Phys.*, **11** (1910), 1072; **29** (1928), 487.

3. TAYLOR, G. I., *Brit. adv. Comm. Aeronaut., Rep.* **272** (1916-17), 423.
4. SHERWOOD, T. K., *Chem. Engng (Symp. Ser.)*, **55** (25) (1959), 71.
5. COLBURN, A. P., *Trans. Amer. Inst. chem. Engrs*, **28** (1932), 105.
6. GAMSON, B. W., *Chem. Engng Progr.*, **47** (1951), 19.
7. MICKLEY, H. S. & TRILLING, C. A., *Industr. Engng Chem.*, **41** (1949), 1135.
8. WAMSLEY, W. W. & JOHANSON, L. N., *Chem. Engng Progr.*, **50** (1954), 347.
9. KETTENRING, K. N., MANDERFIELD, E. L. & SMITH, J. M., *Chem. Engng Progr.*, **46** (1950), 139.
10. CHU, J. C., KALIL, J. & WETTERTH, W. A., *Chem. Engng Progr.*, **49** (1953), 141.
11. CHU, J. C., *Fluidization* (Reinhold Publishing Corp., New York), 1956, 72.
12. SARMA, K. J. R., SEN GUPTA, P. & RAO, M. N., *Trans. Indian Inst. chem. Engrs*, **14** (1961-62), 14.
13. COLBURN, A. P., *Trans. Amer. Inst. chem. Engrs*, **29** (1933), 174.
14. EINSTEIN, A., *Ann. Phys., Lpz.*, **19** (1906), 289.
15. TAREEF, B. M., *Colloid J., Voronezh (U.S.S.R.)*, **6** (1940), 545.

SECTION FIVE

Chemical Reactions in Fluidized Beds

Scaling up of Fluidized Bed Process for Production of Fertilizers by Reaction of Ammonia-Air Mixture on Coal

S. BANERJEE, R. K. CHAKRAVARTI, B. K. BHATTACHARYA
D. K. BANERJEE & N. G. BASAK

Central Fuel Research Institute
Jealgora, Bihar

The reaction of ammonia and air mixture on solid carbon surfaces has been studied in fluidized bed in a 7 in. reactor column with the object of preparing coal fertilizers as developed and patented by this Institute. The results obtained were compared with the data regarding process variables from a previous study for the same reaction in a 3 in. reactor column. A definite improvement in the performance has been observed in the case of the 7 in. column over that in the 3 in. column, because of the lower space velocity of the gases and a more efficient utilization of ammonia.

The thermodynamics of the system has also been studied and the data obtained are being utilized for designing a larger semi-scale plant for the production of coal fertilizers.

Experiments were conducted in an intermediate pilot plant (Fig. 1 and 2) of a capacity of 30 lb. per charge, designed and fabricated in the Institute with a view to scaling up of a process for producing coal fertilizer by reacting coal with ammonia and air from the laboratory model equipment to a large scale plant. The data of the laboratory model equipment were utilized for studying the process variables on the pilot plant. Using the data obtained from this pilot plant operation, attempts are being made to design and fabricate at the Institute a bigger plant of capacity 500 lb. per charge.

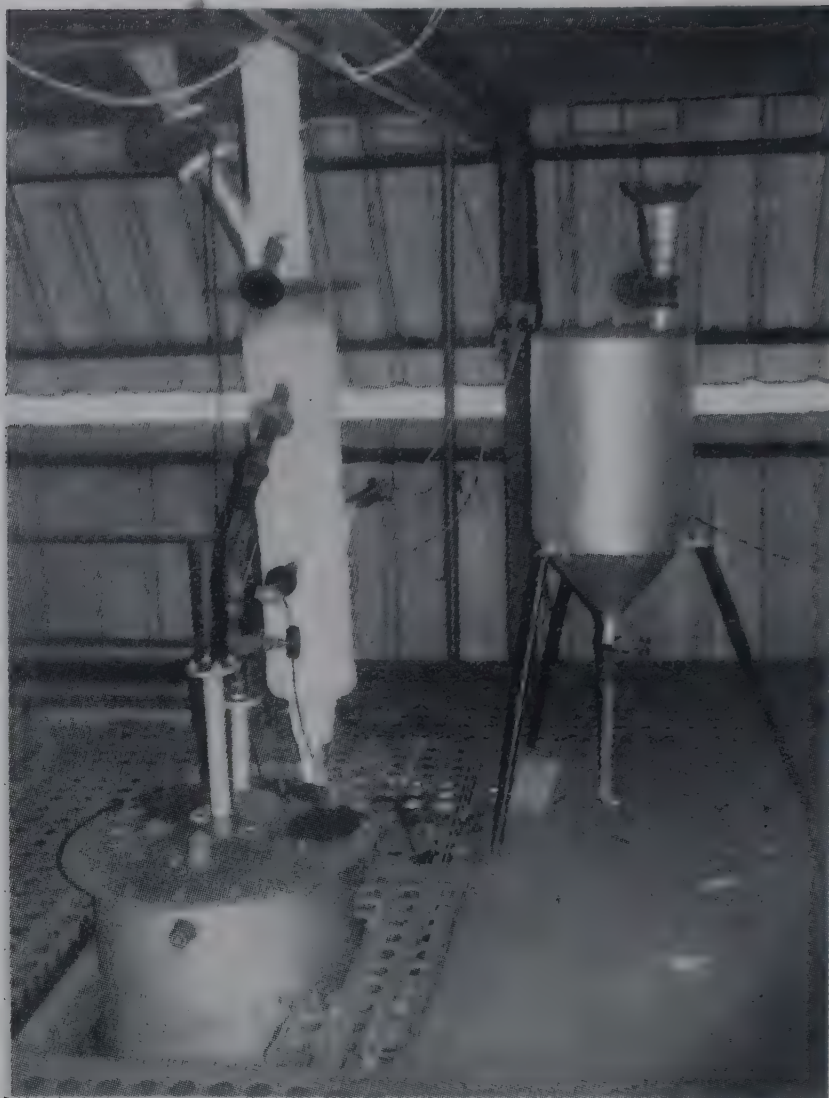


FIG. 1—PILOT PLANT FOR PRODUCING COAL FERTILIZER [Reactor and Storage bunker]



FIG. 2—PILOT PLANT FOR PRODUCING COAL FERTILIZER [Disengaging chamber, Cyclone dust separator and Gas coolers]

EXPERIMENTAL SET-UP AND PROCEDURE

The pilot plant (Fig. 3) consists of a 7 in. fluidizing reactor column (6) electrically heated, into which 30 lb. of coal sample of particle size, $-36+150$ B.S. mesh were allowed to react with ammonia-air mixture in requisite proportions under optimum conditions of reaction time and temperature, determined in a small scale laboratory unit. The required quantity of fluidizing air was supplied by a compressor (1) and ammonia gas was supplied from ammonia cylinder (2). Both air and ammonia gas were measured by means of orifice meters (3, 4). Thermocouples T_2 and T_3 indicated the bed temperatures which were recorded on a 6-point temperature recorder. The mixture of out-going gas and ammonia laden with entrained coal dust and moisture was allowed to pass through cyclone dust collector (9), expansion chamber (10) and finally through indirect cooling tower (11). The coal feed and product were stored in bunkers (5) and (13) respectively. Coal charge was fed pneumatically to the fluidizing reactor column, the conveying medium being the same ammonia-air mixture used for fluidizing the coal mass.

The temperature of the reactor was first raised to about 212°F . and thereafter 30 lb. of noncaking coal were charged and the whole mass was kept in a state of fluidization. The ratio of ammonia to air in the fluidizing medium was kept low, *c.* 1:9.75, at the beginning of the reaction and was later increased to the desired value (1:3.6) as soon as the reactor temperature reached 617°F . As the reaction between coal and ammonia-air mixture is exothermic in the beginning and endothermic towards the end, the reactor temperature was maintained at the desired value of about 617°F . by adjusting the current input through variable resistance (8).

RESULTS AND DISCUSSION

Before starting the experiments, a minimum fluidization velocity for the 30 lb. of coal charge having the size fractions $-36+150$ B.S. mesh was determined and then the effects of the process variables, (i) ammonia-air ratio, (ii) time of reaction, (iii) bed height to diameter ratio (L/D), and (iv) space velocities were studied in the 7 in. reactor column.

Ammonia-air ratio. Experiments for determining the effect of variation of the ammonia-air ratio in the fluidizing medium on the nitrogen content of the product were repeated in the 7 in. reactor column. The results are shown in Fig. 4. It can be seen that an average value of the ratio of about 1:4 (on volume basis) gives the best performance. It is to be noted that although the ratio 1:4 both in the 3 in. and 7 in. column reactors indicates the best results, the quantity of ammonia used in the latter case is comparatively much less than that in the 3 in. column. As can be seen from Table 1, that for 1 lb. of coal, optimum quantities of ammonia needed

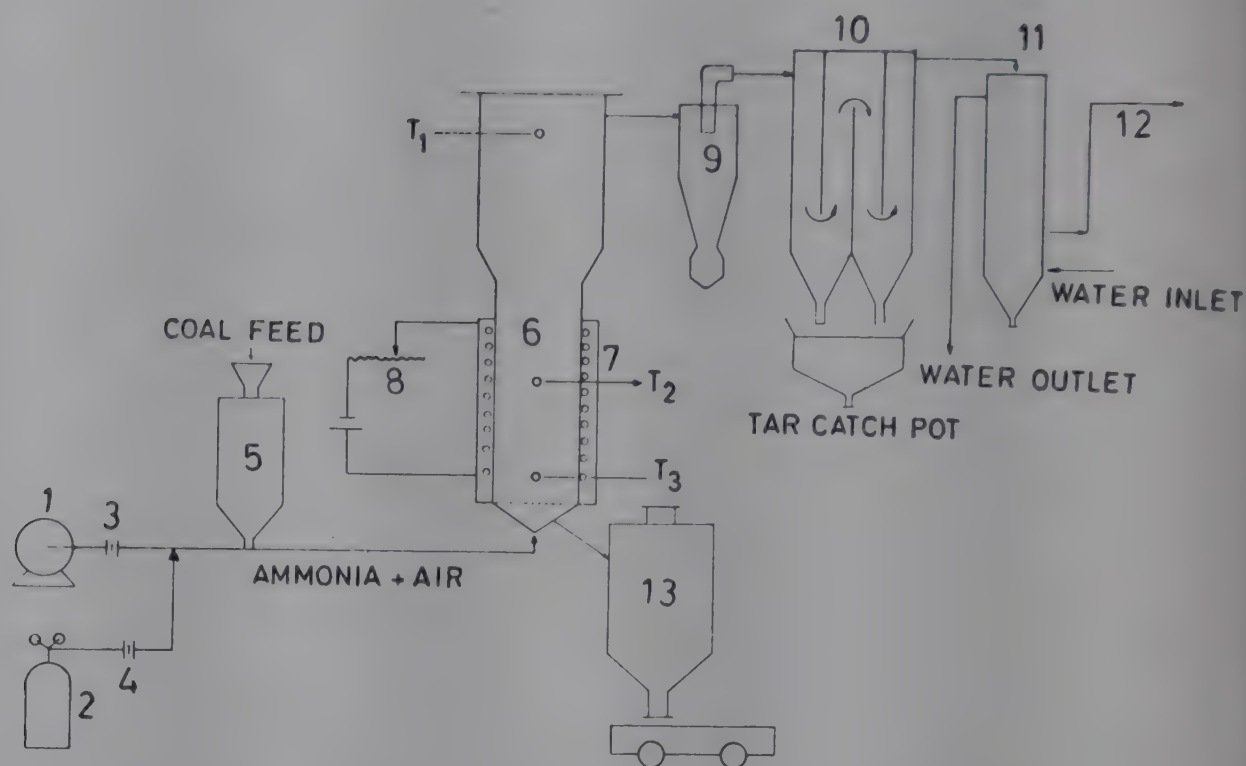


FIG. 3—FLOW DIAGRAM OF FLUIDIZED BED COAL FERTILIZER PLANT [(1) Positive displacement type air blower; (2) Ammonia cylinder; (3,4) Orifice meters; (5) Coal charge bunker; (6) Reactor column; (7) Electrical heating coil; (8) Variable resistance; (9) Cyclone dust catcher; (10) Expansion chamber; (11) Indirect cooler; (12) Outlet gas line (13) Coal fertilizer storage; T_2 , T_3 , Thermocouples]

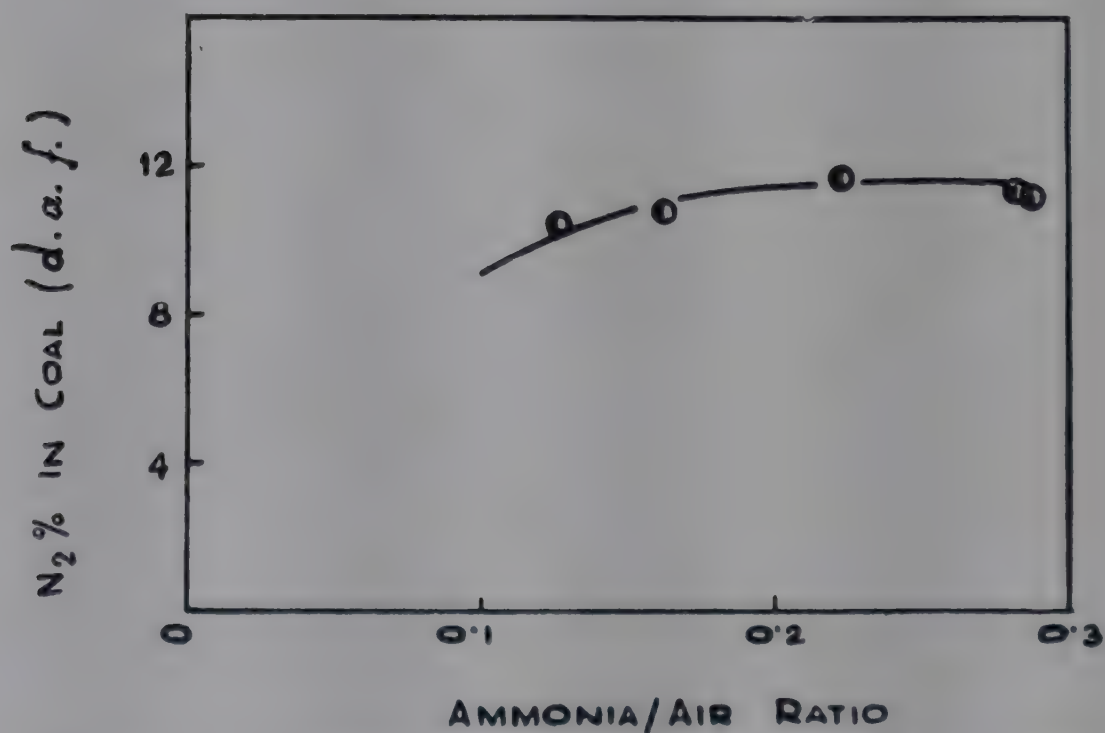


FIG. 4—RELATION BETWEEN AMMONIA-AIR RATIO AND TOTAL NITROGEN (on volume basis)

for the reaction in 3 in. and 7 in. reactor columns are 2.2 and 1 lb. respectively. The lower requirement of ammonia gas for the reaction in the 7 in. reactor column might be due to better gas distribution in the fluidized bed, resulting in a uniform gas-solid contact.

TABLE 1—COMPARATIVE PERFORMANCES OF 3 in. AND 7 in. FLUIDIZED COLUMNS

| PARTICULARS | 3 IN. COLUMN | 7 IN. COLUMN |
|---|--------------|--------------|
| Coal charge (size $-36+150$ B.S.S.), <i>lb.</i> | 1.5 | 30 |
| Quantity of air at S.T.P., <i>ft³/min.</i> | 0.92 | 7.0 |
| Quantity of ammonia gas at S.T.P., <i>ft³/min.</i> | 0.25 | 1.95 |
| Ammonia-air ratio | 1 : 3.7 | 1 : 3.6 |
| Theoretical amount of ammonia required for 15% nitrogen fixation, <i>ft³/min.</i> | 0.0133 | 0.26 |
| Excess ammonia introduced | 20 | 7.5 |
| Space velocity, volume of gas/vol. of coal/hr | 1450 | 552 |
| Modified Reynolds number (N_{Rg}) | 2.00 | 2.7 |
| Percentage (av.) ammonia escaping with outlet gas | 45 | 39 |
| Quantity of ammonia introduced per lb. of coal for 5 hr at 617°F. for 15% nitrogen fixation, <i>lb.</i> | 2.2 | 1.0 |
| Height-diameter (L/D) ratio | 4 : 1 | 4.6 : 1 |

Time of reaction. The variation of nitrogen content of coal during the course of its reaction with ammonia-air mixture, was studied using 30 lb. of coal charge and maintaining the ammonia-air ratio at 1:4 (on volume basis) and the reaction temperature at 617°F. throughout the experiment. At regular intervals of 1.5, 2.5, 3.5, 5 and 5.5 hr after the experiment was started, samples of about 50 g. of the product were withdrawn from the reactor and their nitrogen contents were determined. The results are shown in Fig. 5. It can be seen from the figure that the nitrogen content increases gradually in the beginning and remains steady after 5 hr. Hence, it may be assumed that for this batch type reaction a period of 5 hr is optimum.

Bed height-diameter ratio. Fluidization performance is influenced not only by the bed height but also by the reactor diameter, and as observed by Leva and others¹⁻³ the ratio of bed height to diameter (L/D) affects the fluidization efficiency. Experiments were conducted to examine this effect on nitrogen fixation on coal. The ratios were altered only by changing the weight of coal charge (20, 30 and 40 lb.), so that the bed heights were different in different cases but the diameter was the same for all the cases. A bed temperature of 617°F., reaction time of 5 hr and the minimum fluidization mass velocity used for 30 lb. of coal charge were maintained constant in all the experiments. The results (Table 2) indicate a maximum nitrogen content of the product for the bed height-diameter ratio of 4.6 : 1. Thus increasing the ratio L/D beyond

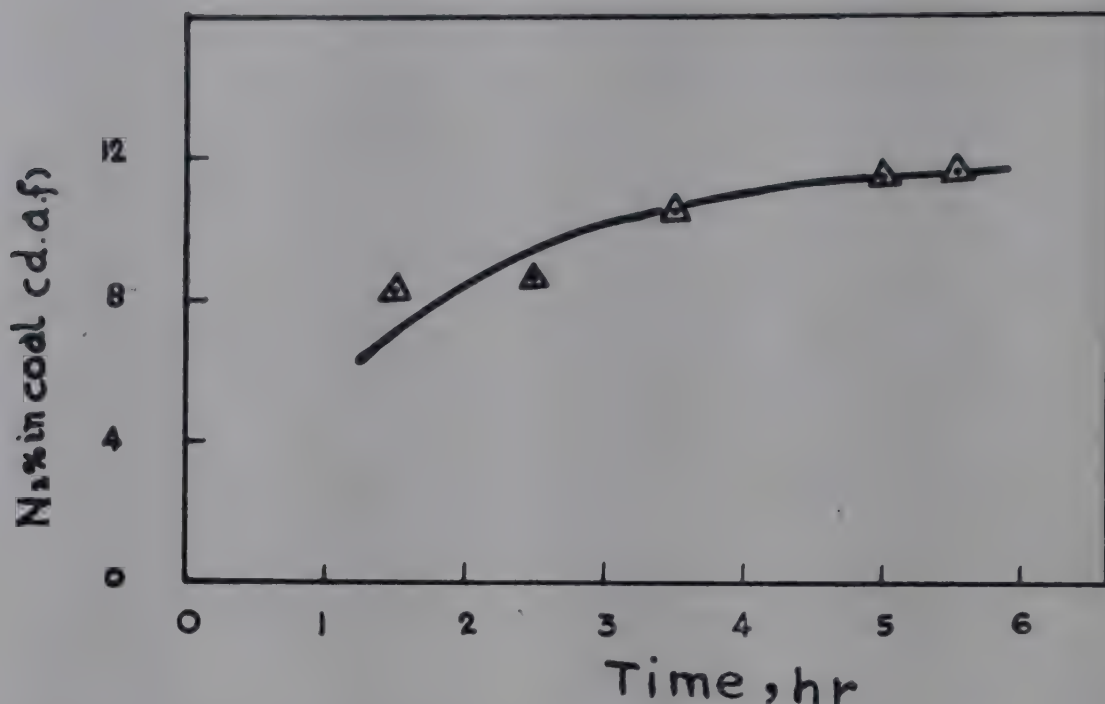


FIG. 5—RELATION BETWEEN TOTAL NITROGEN IN COAL AND REACTION TIME

TABLE 2—NITROGEN CONTENT OF PRODUCT AT DIFFERENT BED HEIGHT-DIAMETER RATIOS

(Reaction time, 5 hr; temp., 617°F.; fluidizing gas velocity at S.T.P., 9 ft³/min.)

| CHARGE WEIGHT | PRODUCT WEIGHT | L/D | NITROGEN CONTENT (d.a.f.) % |
|---------------|----------------|---------|-----------------------------|
| lb. | lb. | | |
| 20 | 18.5 | 3.2 : 1 | 10.9 |
| 30 | 26.0 | 4.6 : 1 | 13.2 |
| 40 | 34.0 | 6.4 : 1 | 11.45 |

this optimum limit of 4.6:1, a piston type movement of the bed in the reactor is assumed to predominate⁴ and hence the back-mixing is lessened. On the other hand, the ratio below this limit affects the fluidization efficiency due to excessive channelling and bubbling⁵.

Effect of space velocity. The effect of changing the space velocity, i.e. volume of gas/volume of coal charge/hr, on the total nitrogen content of the product is represented graphically in Fig. 6. In these experiments, keeping the weight of charge constant, only the mass velocity of the fluidizing medium was altered. As regards other variables, such as reaction time, temperature and ammonia-air ratio, optimum conditions determined in previous experiments were maintained. As can be observed from Fig. 6, lower space velocities indicate higher nitrogen fixation on the product. Hence, it may be assumed that for lower space velocities, an

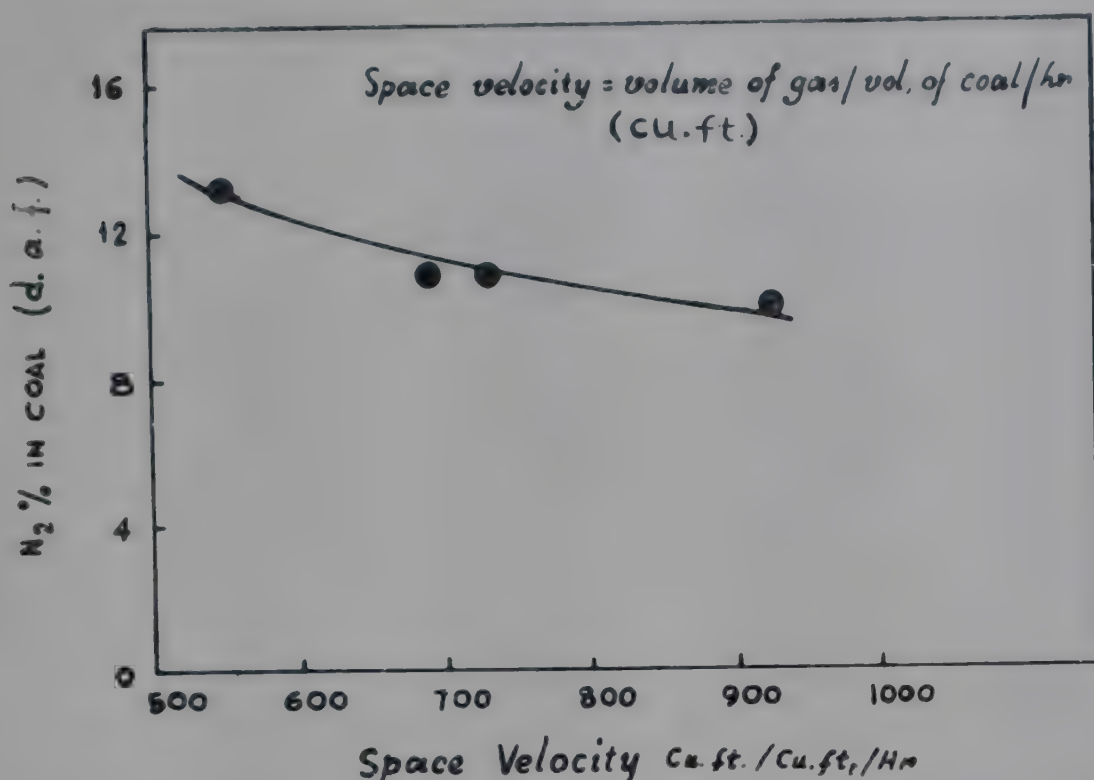


FIG. 6—RELATION BETWEEN TOTAL NITROGEN IN COAL AND SPACE VELOCITY OF FLUIDIZING GAS

increased retention time of ammonia in the fluidized bed as well as a higher fluidization efficiency in comparison to higher space velocities is responsible for the improved result. Further, lower space velocities perhaps, result in better mixing between the reacting substances⁶. A space velocity below 550 ft³/ft³ of coal/hr could not be considered because fluidization of the bed was not effected, whereas, above the value of 950 ft³/ft³ of coal/hr fluidization efficiency deteriorated due to the formation of spouting channelling and slugging action. A high entrainment loss of product at higher space velocities was another disadvantage.

Energy and material balance. Application of the laws of thermodynamics is helpful in evaluating the performance of a system. A consideration of the energy balance in conjunction with inventory changes, i.e. the material balance, is of paramount importance in problems of process, design and operation. Fig. 7-9 indicate a rough account of the energy⁷, and material balances of the whole operation in the fluidized bed. It may, however, be noted that an exact energy balance including the consideration of the exothermic and endothermic reactions taking place between the individual components participating in the process is not possible, because the nature of the reaction products is not yet thoroughly understood. The energy and material balances for the pilot plant were calculated on the basis of 13 per cent nitrogen fixation on the product, wherein for plant operation optimum conditions were maintained.

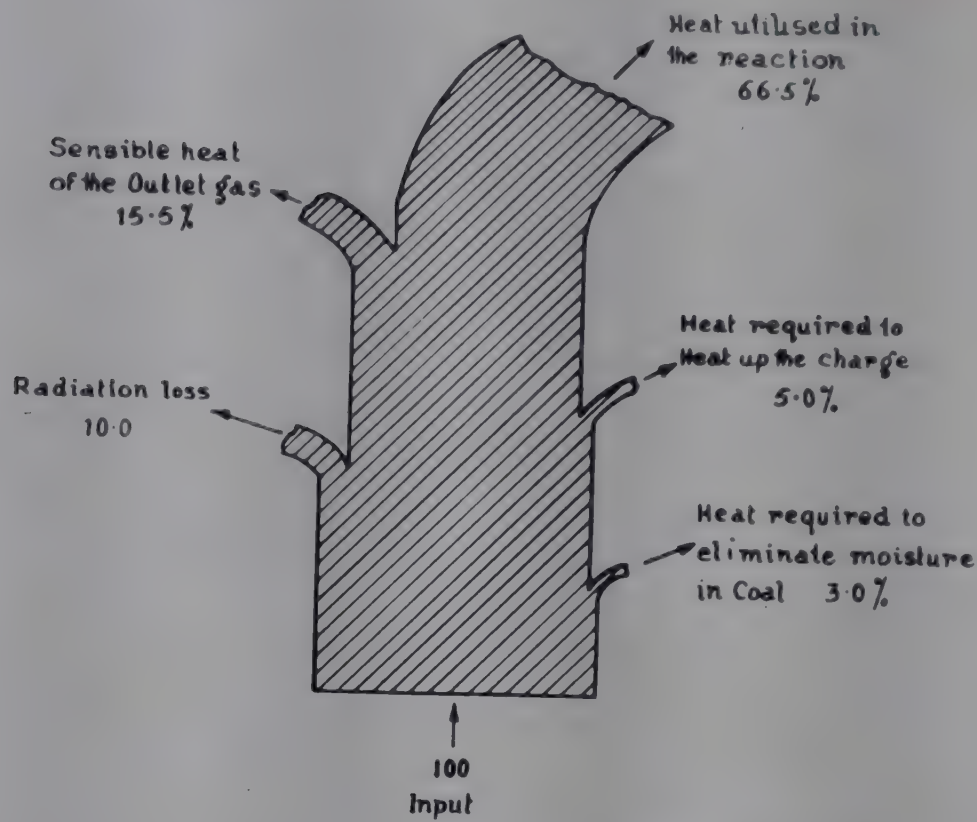


FIG 7—ENERGY BALANCE (SANKEY DIAGRAM) FOR THE REACTION OF COAL WITH AMMONIA AND AIR

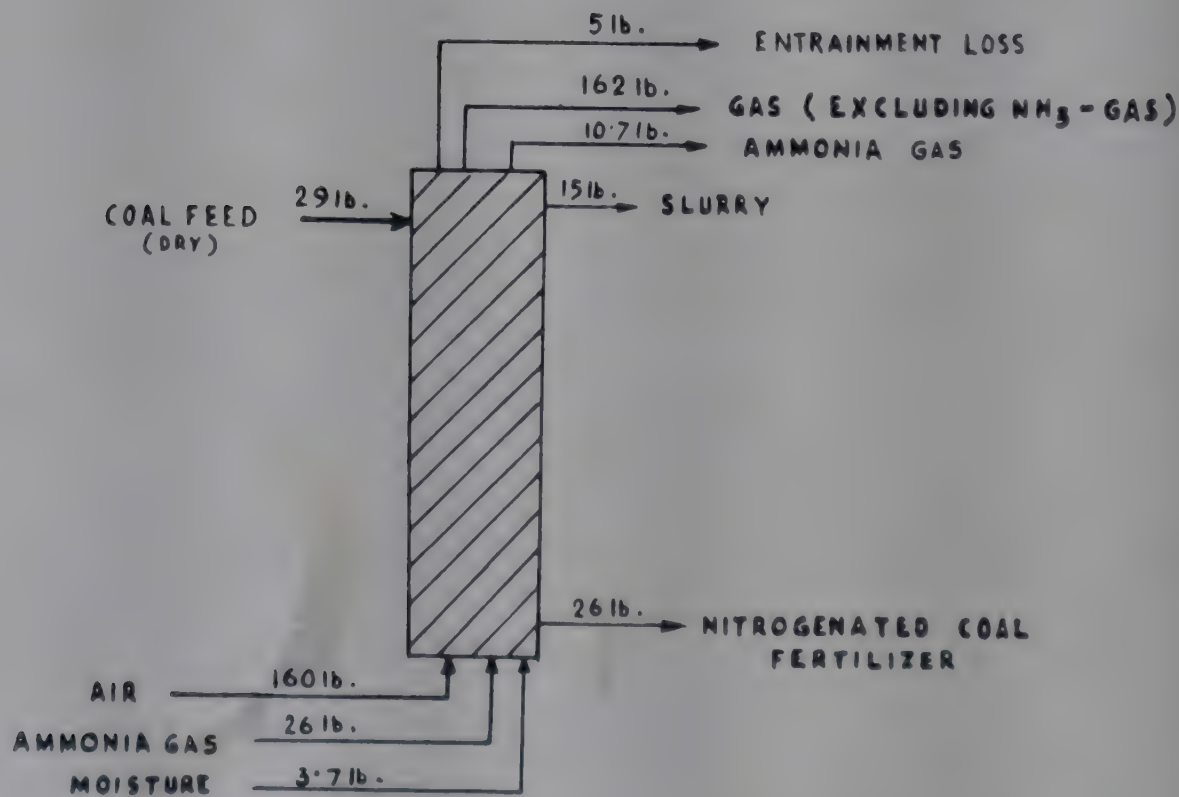


FIG. 8—MATERIAL BALANCE OF THE PROCESS FOR PRODUCING COAL FERTILIZER

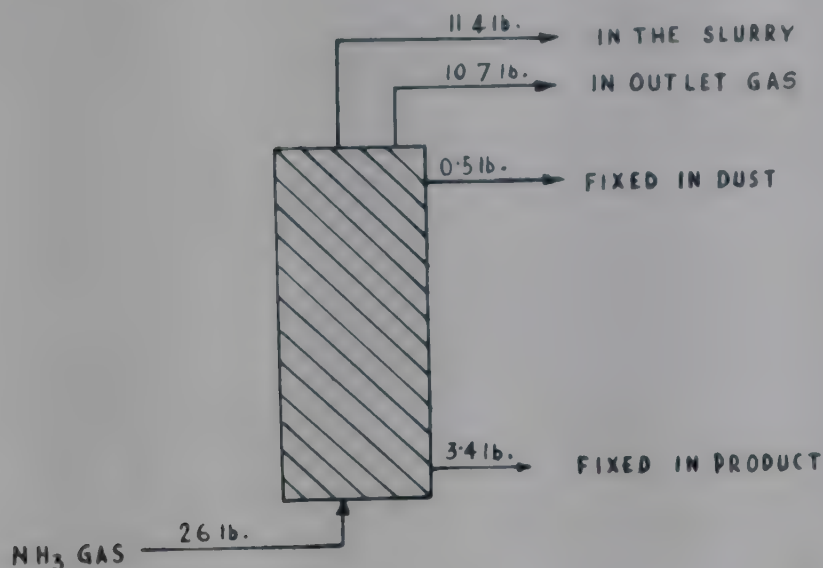


FIG. 9—AMMONIA BALANCE OF THE PROCESS FOR PRODUCING COAL FERTILIZER

Comparative performances of model equipment and pilot plant. In order to assess the reaction performances of the 3 in. and 7 in. reactor columns, a comparative statement from typical test runs was prepared as in Table 1 which indicates that the total ammonia requirement per lb. of product in the 7 in. column is comparatively less. It may be noted that in 7 in. column, for a reaction time of 5 hr and at a temperature of about 617°F., only 13 per cent fixation of nitrogen on coal could be attained; however, the fixation could be increased to 15 per cent by improving the process and choosing suitable raw material and hence the calculations in Table 1 are made on this basis.

CONCLUSION

The quantity of ammonia required for carrying out the reaction in the pilot plant is lower than that in the model equipment. For designing a large commercial plant, the height-diameter ratio of the fluidized coal bed should not exceed the limit, 4.5-5.1. A reaction time of 5 hr, a temperature of 617°F. and the ammonia-air ratio of 1:4 (on volume basis) in the fluidizing medium should be maintained during the course of reaction. An average coal particle size within the range of $-36+150$ B.S. mesh should be used for the charge. A space velocity of the range, 500-600 volume of fluid/volume of coal/hr helps maximum nitrogen fixation in the product.

ACKNOWLEDGEMENT

The authors are grateful to the Director, Central Fuel Research Institute for giving permission to present this paper at the symposium. Thanks are

also due to the analytical section for estimating the nitrogen content in the product samples.

REFERENCES

1. LEVA, M., *Fluidization* (McGraw-Hill Book Co. Inc., New York), 1959, 30.
2. SHUSTER, W. W. & KISLIAK, P., *Chem. Engng Progr.*, **48** (1952), 455.
3. LEWIS, W. K., GILLILAND, E. R. & BAUER, W. C., *Industr. Engng Chem.*, **41** (1949), 1104.
4. PARENT, J. D. *et al.*, *Chem. Engng Progr.*, **43** (1947), 429.
5. JOLLOY, L. J. & STANTON, J. E., *J. appl. Chem. Lond.*, **2** (Suppl. to 1) (1952), 62.
6. ZENZ, F. A. & OTHMER, D. F., *Fluidization and Fluid-particle System* (Reinhold Publishing Corp., New York), 1960, 464.
7. THRING, M. W., *The Science of Flames & Furnaces* (Chapman & Hall Ltd, London), 1952, 57.
8. *Efficient Use of Fuel* (Her Majesty's Stationery Office, London), 1958, 696.

Fluidization Studies in an Operating Fluidized Bed Reactor

C. M. LAKSHMANAN*, B. CHENNAKESAVAN
& H. E. HOELSCHER†

Department of Chemical Engineering, Alagappa Chettiar College of
Technology, University of Madras
Madras 25

The design of a fluidized bed reactor for kinetic studies and the interpretation of the results from such studies depend upon predictions of and detailed data on the quality of fluidization. Most studies of fluidization have been in non-reacting systems at low temperatures and the results from such studies (correlations permitting predictions of the minimum fluidization velocity, etc.) are therefore of questionable value when application to an operating high-temperature reactor is necessary. This present study illustrates the data required for interpretation of kinetic results from an operating fluidized bed reactor. The applicability of correlations from non-reacting, low-temperature beds is discussed.

Fluidized bed chemical reactors have gained great importance in processes involving reactions between gases and solids, since their introduction for catalytic cracking some years ago. None the less, they continue to present a large number of challenging research and development problems, mostly concerned with the dynamics of both particle and fluid motion. Industrial and university research studies have yielded useful correlations of particle-to-fluid heat¹⁻⁴ and mass^{2,5,6} transfer rates as a function of operating conditions and more recently an understanding of both the particle and fluid dynamics within the bed seems to be developing⁷⁻¹⁴. However, such work has been done in non-reacting systems at low temperatures and few studies have been specifically pointed toward the conditions within an operating fluidized bed reactor.

*Present address: Regional Research Laboratory, Bhubaneswar (Orissa).

†Present address: School of Mines & Engineering, University of Pittsburgh, Pittsburgh, Pennsylvania, U.S.A.

It is evident that the fluid/particle heat and mass transfer rates in a fluidized bed must play an important role in the determination of local reaction rates at or on the solid surface and the gross or large-scale structure of the bed (the 'bubble volume' to 'emulsion volume' ratio) must be of significance in determining the residence time as well as the residence time distribution. Hence, it would be desirable to be able to predict the quality of fluidization in a reactor proposed for reaction kinetic studies and it is surely necessary to know the 'quality' of fluidization under operating conditions in a reactor used for kinetic studies before meaningful interpretations of the results can be made. The word 'quality' denotes both the gross fluid and particle motions, and the 'bubble volume' to 'emulsion volume' ratios.

This paper presents some observations made during a preliminary study of the fluidization characteristics of ilmenite in a reactor to be used in a kinetic investigation of the beneficiation (by chlorination) of ilmenite. The fluidized bed technique was adopted for reasons of heat transfer and to ensure continuous removal of the ferrous and ferric chloride formed during reaction. Two types of fluidization studies were made to obtain a better understanding of the quality of fluidization under actual reaction conditions. The first was a 'classical' type of study in a pyrex glass column, thus permitting visual observation of the quality of fluidization. Air was used as the fluidizing medium. The effect of operating variables, solid particle size and bed weight for the particular solid system of interest was thus determined. The second study was made in the chlorination reactor itself to observe the effect of the gas distributor (the distributor used in the reactor was different from that used in the glass column) and to study the quality of fluidization at operating temperatures. Residence time distribution studies were also made to examine the flow forms of the reactant gases under operating conditions in the fluidized bed reactor.

EXPERIMENTAL SET-UP AND PROCEDURE

A schematic diagram of the experimental set-up used for fluidization studies is shown in Fig. 1. The glass fluidization column used in the experiments had an inner diam. of 2.69 cm. and the gas distributor was a porous plate fused to the body of the column. The reactor used for chlorination experiments was made out of a mullite tube of 2.46 cm. inner diam. The gas distributor in the reactor was porcelain disc having 42 orifices of 0.2 mm. diam. The gas used as fluidizing medium was dried in a silica gel drying system and the gas flow rate was measured by a capillary flow meter.

A weighed quantity of ilmenite of a particular sieve fraction was charged into the fluidization column and the dry gas introduced into the column at a measured flow rate. The combined pressure drop across the bed and the gas distributor was noted for various gas flow rates. The actual

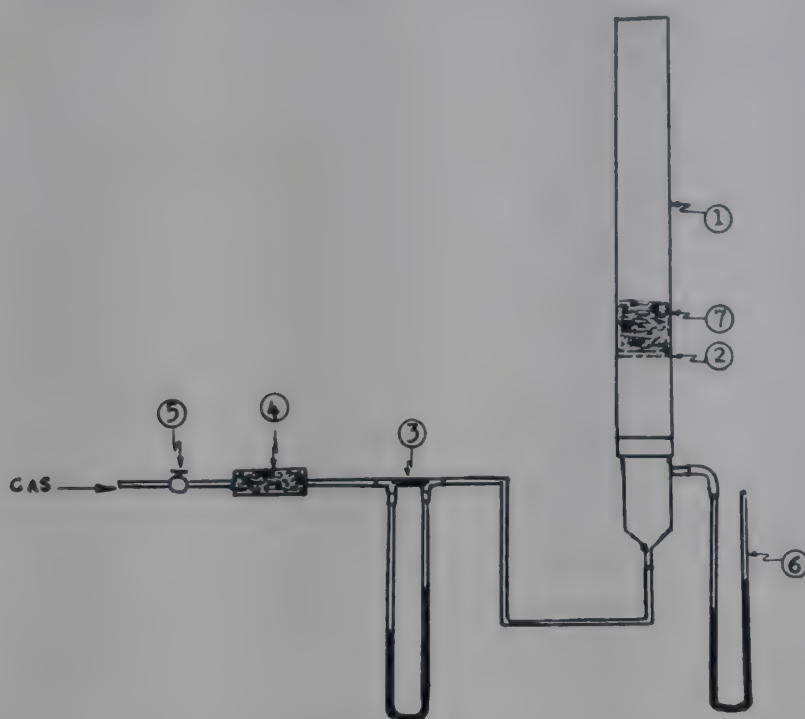


FIG. 1—EXPERIMENTAL SET-UP [(1) Fluidization column; (2) Bed support; (3) Flow meter; (4) Silica gel; (5) Valve; (6) Pressure drop manometer; (7) Ilmenite bed]

pressure drop through the bed alone was then calculated by subtracting the pressure drop through the bed support determined previously in a similar manner.

RESULTS AND DISCUSSION

Low Temperature Studies in Glass Column

The size and amount of solid particles present in the reactor influence both the fluidization characteristics and the reaction rate. Thus, a careful selection of the range of particle sizes and the amount of solid yielding good fluidization was of interest in the later reaction kinetic studies. This was determined by conducting fluidization experiments in the glass column using different sieve fractions and different weights of ilmenite. Air was used as fluidizing medium.

Effect of particle size. The physical characteristics of the different sieve fractions used for fluidization experiments are presented in Table 1. The shape factor was calculated from fixed bed data using the equation suggested by Leva¹⁵

$$\frac{\Delta P D_p \phi_s^2 g_c \epsilon^3}{2 U_o^2 L \rho_f (1 - \epsilon)^2} = 100 \left(\frac{D_p U_o \rho_f}{\mu} \right)^{-1.0}$$

where ΔP is the pressure drop across the bed, D_p is the particle diameter, ϕ_s is shape factor, ϵ is the overall fixed bed voidage fraction, U_o is the superficial gas velocity, L is the height of the bed, ρ_f is the density of fluid and μ is the viscosity of the fluid.

TABLE 1—PHYSICAL CHARACTERISTICS OF DIFFERENT SIEVE FRACTIONS

| CHARACTERISTICS | SIEVE FRACTIONS | | |
|---|-----------------|------------|-------------|
| | (-48 +65) | (-65 +100) | (-100 +150) |
| Av. particle size (D_p), cm. | 0.0252 | 0.0178 | 0.0126 |
| Density (ρ_s), g./cc. | 4.234 | 4.344 | 4.251 |
| Shape factor (ϕ_s) | 0.845 | 0.842 | 1.080 |
| Minimum fluidization voidage (ϵ_{mf}) | 0.437 | 0.414 | 0.438 |
| Minimum fluidization velocity (U_{mf}) at 30°C., cm./sec. | 7.39 | 3.15 | 3.10 |

The minimum fluidization velocity U_{mf} was also calculated using the correlation suggested by Leva¹⁵

$$U_{mf} = \frac{D_p^2 g_c \phi_s^2 (\rho_s - \rho_f) \epsilon_{mf}^3}{200 \mu (1 - \epsilon_{mf})}$$

The pressure drop-flow diagram for different sizes of ilmenite is shown in Fig. 2. It is observed that the calculated and observed values of U_{mf} are in very good agreement. The minimum fluidization velocity required for both -65+100 mesh fraction and -100+150 mesh fraction is almost the same. Very high velocity is required for -48+65 mesh fraction for fluidization. From these observations and from the fact that the orifice diameter on the gas distributor plate on the chlorinator was 0.02 cm., it was decided that -65+100 mesh size fraction of ilmenite could be conveniently used for the kinetic studies in the reactor.

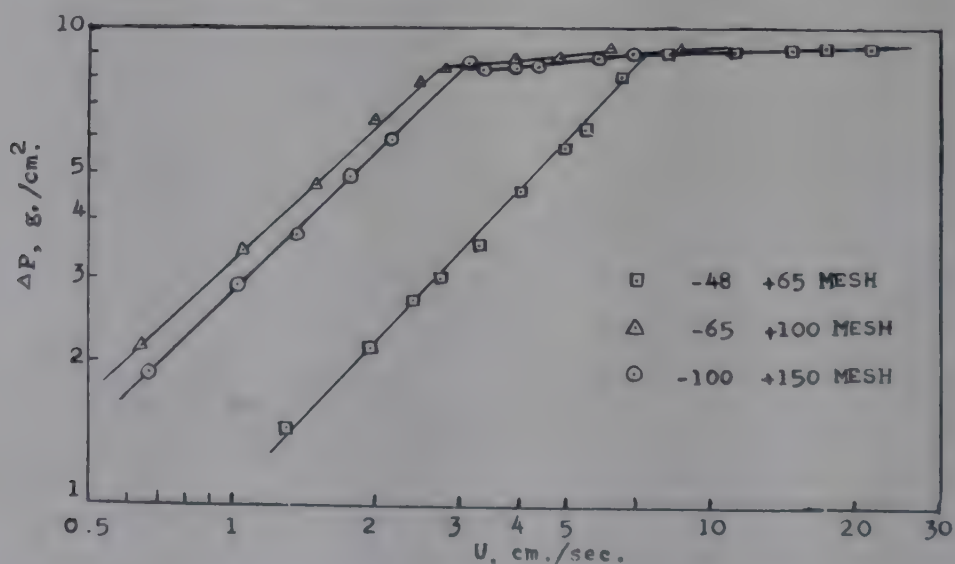


FIG. 2—PRESSURE DROP-FLOW DIAGRAM: EFFECT OF PARTICLE SIZE

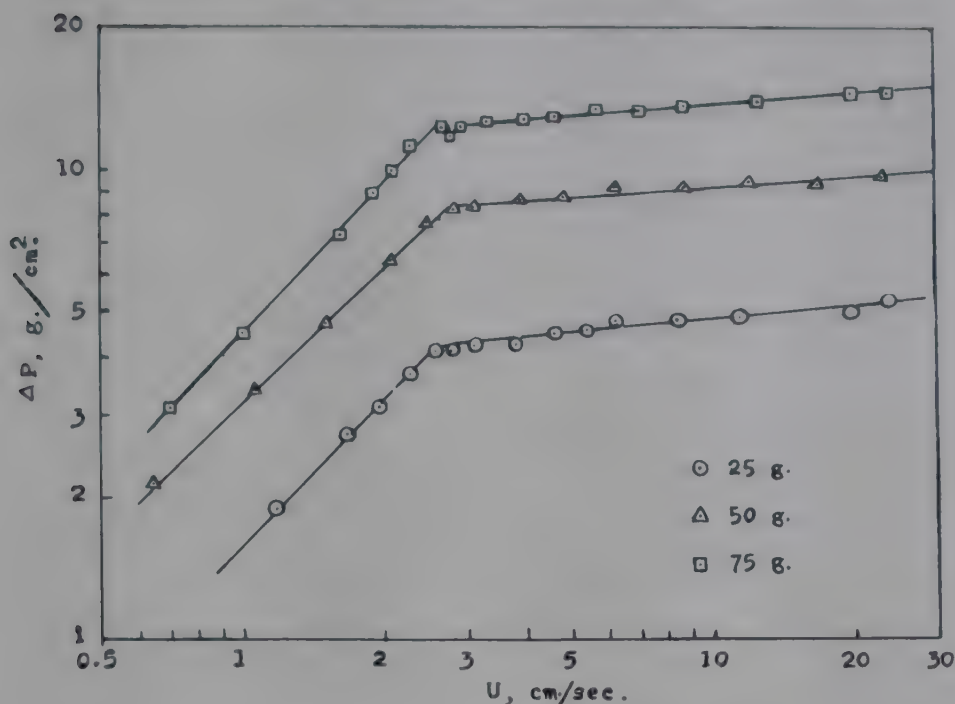


FIG. 3—PRESSURE DROP-FLOW DIAGRAM: EFFECT OF BED WEIGHT

Effect of bed weight. The pressure drop-flow diagram for three weights, viz. 25, 50 and 75 g. of $-65+100$ mesh fraction of ilmenite is shown in Fig. 3. It was observed that the bed weight did not alter the fluidization characteristics.

Visual observation. Visual observation of the fluidization indicated the following: (i) there was no slugging over the range of variables studied; (ii) there was noticeable circulation of the solid particles upwards through the centre and down along the wall of the column; and (iii) bubbles were observed to be small by comparison to the tube diameter even when the flow rate was very much greater than the minimum fluidization velocity.

This last observation could be expected when a porous plate is used as gas distributor but chances of larger bubbles and channels are greater in the case of multi-orifice plate¹⁶.

Studies in the Reactor

Effect of gas distributor. As the gas distributor in the reactor was a multi-orifice plate, a comparison of fluidization characteristics was made by conducting fluidization experiments in the chlorination reactor using 50 g. of $-65+100$ mesh fraction of ilmenite and air as fluidizing medium at room temperature. The pressure drop-flow diagram for the experiments in the glass column and the reactor is shown in Fig. 4. The pressure drop for fixed bed region in the reactor was found to be less than that in the glass column. This might be due to less uniform gas distribution in the reactor because of channelling resulting from the multi-orifice plate gas distributor. The distributor in the glass column (porous disc) would be expected to yield better gas distribution. The U_{mf} observed in the reactor

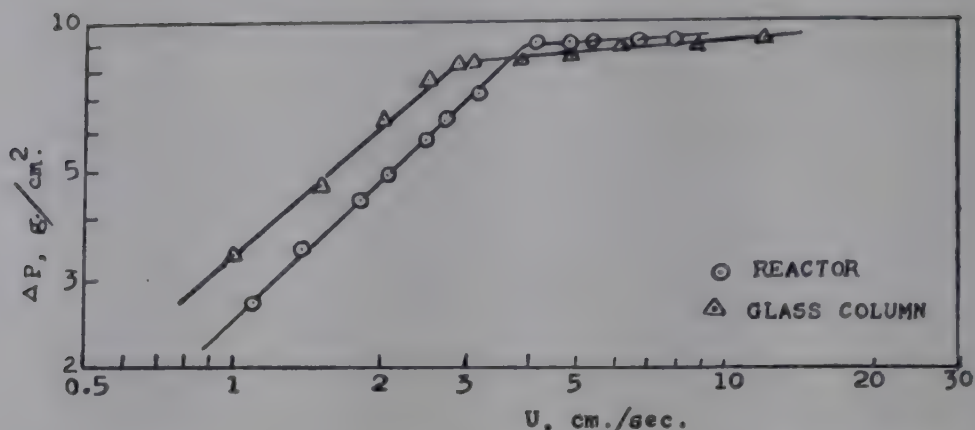


FIG. 4—PRESSURE DROP-FLOW DIAGRAM: EFFECT OF GAS DISTRIBUTOR

was higher than the calculated value, 3.15 cm./sec. This higher value of U_{mf} could be due to the effect of wall frictional drag on the particles. An additional force (over that required in a smooth wall tube) is required to lift the particles. The theoretical pressure drop (calculated by dividing the weight of the bed by cross-sectional area of the column) in the chlorination reactor is 10.5 g./cm.² The pressure drop experimentally observed at incipient fluidization in the reactor is 9.3 g./cm.² Lewis *et al.*¹⁷ indicated that this decrease may be due to channelling which is quite likely to occur when a multi-orifice plate gas distributor is used. But channelling tendency might be reduced considerably at higher flow rates due to higher solid circulation. This effect can also be observed from Fig. 4 as the pressure drop seems to increase with the increase in fluidization velocity.

Studies at High Temperature

The chlorination of ilmenite using a gas mixture of carbon monoxide and chlorine was to be conducted at high temperature. Hence, fluidization of ilmenite particles of -65+100 mesh size fraction was studied in the reactor at the operating temperature range, 700–950°C., using nitrogen as the fluidizing medium. The pressure drop-flow diagrams in these experiments are shown in Fig. 5. In Table 2, the observed minimum fluidization velocity and U_{mf} calculated using Leva's correlation¹⁵ for nitrogen, as well as the U_{mf} calculated for the reactant gas mixture (composition CO: Cl₂=1.5:1) and the actual operating velocity used are presented.

The experimentally observed value of U_{mf} is found to increase with the increase in temperature but the calculated value of U_{mf} is found to decrease with the increase in temperature. The decrease in the calculated value of U_{mf} results from the increase in gas viscosity with temperature. The observed value of U_{mf} is about 2–5 times more than the calculated value of U_{mf} and the difference in values increases with temperature. This phenomenon is of considerable importance in predicting the quality of fluidization at the operating conditions.

A similar observation was made by Harrison *et al.*¹⁸ while studying the bubble diameters in a fluidized column at high temperatures. They noted

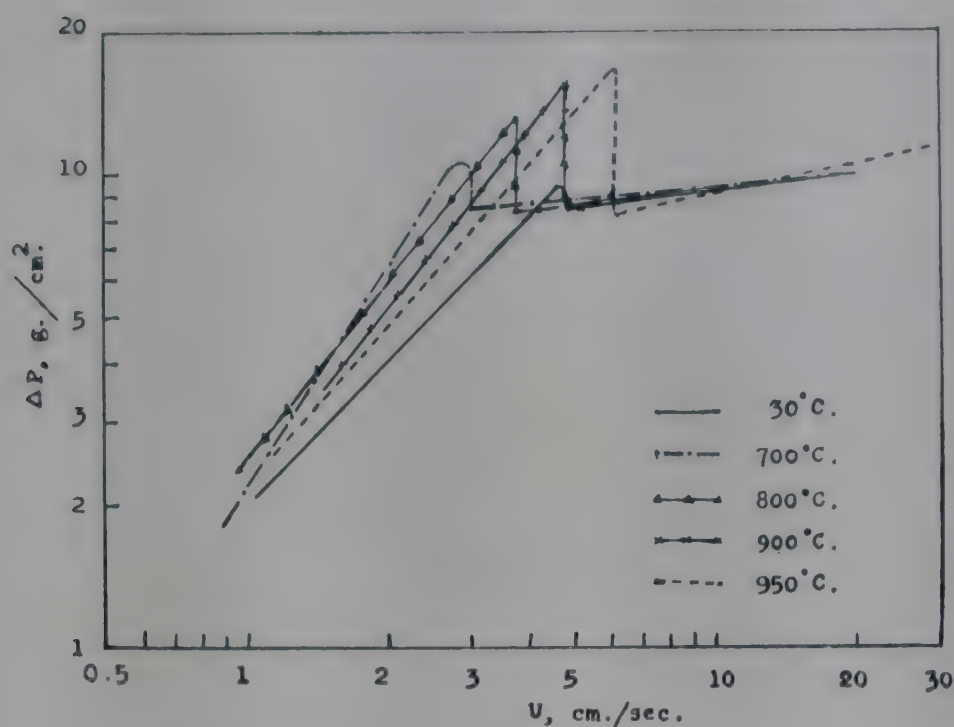


FIG. 5—PRESSURE DROP-FLOW DIAGRAM: EFFECT OF TEMPERATURE

TABLE 2—MINIMUM FLUIDIZATION VELOCITY (CALCULATED & OBSERVED) AT DIFFERENT TEMPERATURES

| TEMPERATURE °C. | U_{mf} CALC. FOR N ₂ cm./sec. | U_{mf} OBS. FOR N ₂ cm./sec. | U_{mf} CALC. FOR REACTANT GASES cm./sec. | OPERATING VELOCITY OF REACTANT GASES cm./sec. |
|--------------------|---|--|---|--|
| 30 | 3.14 | 4.2 | 3.33 | 3.88 |
| 700 | 1.41 | 3.0 | 1.43 | 12.48 |
| 800 | 1.30 | 3.8 | 1.32 | 13.78 |
| 900 | 1.20 | 4.8 | 1.24 | 15.07 |
| 950 | 1.18 | 6.2 | 1.19 | 15.70 |

that the ratio of bubble diameter to solid particle diameter decreased as the temperature increased. According to the two-phase fluidization theory, first postulated by Toomey and Johnstone¹⁹, all gas in excess of the minimum fluidization requirement passes through the column as bubbles. Hence, it can be concluded that the decrease in bubble volume at higher temperatures could be due to this observed increase in minimum fluidization velocity with temperature.

This increase in U_{mf} over the value predicted by the correlation might be attributed to an increase in an effective size of the particle. For example, the change in dielectric property of the material with increasing temperature

could lead to agglomeration due to electrostatic forces. For many ceramic materials, e.g. ilmenite, the temperature coefficient of the dielectric constant seems to be positive. In addition, Whitehead²⁰ pointed out that agglomeration and sintering may start several hundred degrees below the usually reported melting point. The melting point of ilmenite is reported to be 1367°C.²¹

Another possible explanation for the increase in U_{mf} might arise from purely fluid-dynamical considerations. The weight of an individual particle does not increase with the temperature, and therefore, the drag force required to lift the particle does not increase with the temperature. However, the viscosity of the gas increases with temperatures and therefore the velocity gradient at the particle surface must decrease. Hence, the boundary layer thickness increases which in turn may be considered to increase the effective diameter of the particle. It is quite likely, all of these three possible effects might occur at the same time.

It is also observed from Fig. 5 that the difference between the maximum pressure drop and the pressure drop at U_{mf} increases with temperature. This increase in the instability of the bed at incipient fluidization could be due to the increase in the gas viscosity with temperature which in turn causes the bed to behave like an artificially stabilized expanded bed in that region, thereby delaying the onset of (collapse to) the stable fluidized state.

Residence Time Distribution Studies in Reactor

A knowledge of the history of the reacting fluid in the reactor is essential in a kinetic study. The technique usually adopted for this purpose is a residence time distribution study on the fluid. Hence, such a study was conducted in the chlorination reactor. The mean residence time and the mean dispersion of the reactant gases which are of particular significance, were determined.

The standard step input technique was adopted using chlorine as the tracer gas and nitrogen as the fluidizing medium. The experiments were conducted at room temperature in the empty reactor and in reactor in which 50 g. of ilmenite of $-65+100$ mesh size fraction were fluidized. When the nitrogen gas flow rate was adjusted to steady rate (approximately equal to the operating conditions at 900°C. given in Table 2) chlorine gas as introduced into the system at a flow rate of 1 cc./sec. and a stop watch was simultaneously started to note the injection time of the tracer gas. The concentration of chlorine in the exit gas at 1 sec. intervals was determined by passing the gas through potassium iodide solution and subsequently estimating the liberated iodine with thiosulphate until the concentration of chlorine in the exit gas became constant.

The step function response curves for both fluidized bed and empty reactor were drawn using the tracer gas concentration data. The first, second and third moments which represent the mean residence time, degree

TABLE 3—FIRST, SECOND AND THIRD MOMENTS FOR BOTH THE FLUIDIZED BED AND THE EMPTY REACTOR

| REACTOR | FIRST MOMENT (τ) | SECOND MOMENT (σ_t^2) | THIRD MOMENT (μ^3) |
|---------------|----------------------------|-----------------------------------|-----------------------------|
| Fluidized bed | 11.7 | 5.4 | 18.0 |
| | 12.3 | 5.3 | 12.1 |
| Empty | 12.35 | 2.8 | 0 |

TABLE 4—CALCULATED REACTOR DISPERSION NUMBERS FOR CLOSED-CLOSED VESSEL AND OPEN-CLOSED VESSEL DISPERSION MODELS

| MODEL | D/UL FOR | |
|----------------------|---------------|-----------------------|
| | Empty reactor | Fluidized bed reactor |
| Closed-closed vessel | 0.025 | 0.11 |
| Open-closed vessel | 0.023 | 0.10 |

of dispersion and the degree of skewness respectively were calculated and the values are presented in Table 3.

The reactor dispersion number D/UL , where D is the dispersion coefficient, U is the superficial gas velocity and L is the length of reactor, calculated for closed-closed vessel and open-closed vessel dispersion models are presented in Table 4²².

The results are interesting. The agreement of the values for the first moment (mean residence time) for both empty column and the fluidized bed is surprising. The deviation in values of σ_t^2 is in the expected direction. All these observations seem to force the conclusion that the gas flow pattern is essentially plug flow in the reactor, as expected in a small diameter fluidized bed. However, it has to be pointed out that the values of the third moment are unexplained, and this may be due to error in the data. Errors tend to magnify greatly in passing from the first to third moments.

CONCLUSION

On operating the reactor at gas velocities approximately 3–5 times the minimum fluidization velocity actually required at operating temperatures, good quality fluidization could be expected in the reactor. The pressure drop values observed under such conditions are very nearly equal to the theoretical value (10.5 g./cm.²). Hence, channelling in the bed is expected to be negligible. The chances of large bubble by passing must also be small considering the operating velocities in relation to the minimum fluidization

velocity. The gas flow pattern in the reactor must essentially be plug flow under operating conditions.

ACKNOWLEDGEMENTS

The authors are extremely grateful for the generous support of this project afforded by the University Grants Commission.

REFERENCES

1. HEERTJES, P. M. & MCKIBBINS, S. W., *Chem. Engng Sci.*, **5** (1956), 161.
2. KETTENRING, K. N., MANDERFIELD, E. L. & SMITH, J. M., *Chem. Engng Progr.*, **46** (1950), 139.
3. RICHARDSON, J. F. & AYERS, P., *Trans. Instn chem. Engrs, Lond.*, **37** (1959), 314.
4. WAMSLEY, W. W. & JOHNSON, *Chem. Engng Progr.*, **50** (1954), 347.
5. CHU, J. C., KALIL, J. & WETTEROTH, W. A., *Chem. Engng Progr.*, **49** (1953), 141.
6. RICHARDSON, J. F. & SZEKELY, J., *Trans. Instn chem. Engrs, Lond.*, **39** (1961), 212.
7. GILLIAND, E. R. & MASON, E. A., *Industr. Engng Chem.*, **44** (1952), 218.
8. JACKSON, R., *Trans. Instn chem. Engrs, Lond.*, **41** (1963), 13.
9. JACKSON, R., *Trans. Instn chem. Engrs, Lond.*, **41** (1963), 22.
10. MAY, W. G., *Chem. Engng Progr.*, **55** (1959), 49.
11. ROWE, P. N. & HENWOOD, G. A., *Trans. Instn chem. Engrs, Lond.*, **39** (1961), 43.
12. ROWE, P. N., *Trans. Instn chem. Engrs, Lond.*, **39** (1961), 175.
13. ROWE, P. N., *Chem. Engng Progr. (Symp. Ser.)*, **58** (No. 38) (1962).
14. SHEN, C. Y. & JOHNSTONE, H. F., *Amer. Inst. chem. Engrs J.*, **1** (1955), 349.
15. LEVA, M., *Fluidization* (McGraw-Hill Book Co. Inc., New York), 1959.
16. GROHSE, E. W., *Amer. Inst. chem. Engrs J.*, **1** (1955), 358.
17. LEWIS, W. K., GILLILAND, E. R. & BAWER, W. C., *Industr. Engng Chem.*, **41** (1949), 1104.
18. HARRISON, D., DAVIDSON, J. F. & DE KOCK, J. W., *Trans. Instn chem. Engrs, Lond.*, **39** (1961), 202.
19. TOOMEY, R. D. & JOHNSTONE, H. F., *Chem. Engng Progr.*, **48** (5) (1952), 220.
20. WHITEHEAD, A. B., *Brit. chem. Engng*, **6** (1961), 259.
21. SHOMATE, C. H., NAYLOR, B. F. & BOERICKE, F. S., *U.S. Bur. Mines, Rep. Invest.*, No. 3864 (1946).
22. LEVENSPIEL, O., *Chemical Reaction Engineering* (John Wiley & Sons Inc., New York), 1962.

Kinetics of Fluidized Bed Vapour Phase Oxidation of Toluene

R. N. KUMAR, G. N. BHAT & N. R. KULLOOR

Department of Chemical Engineering, Indian Institute of Science
Bangalore 12

The kinetics of fluidized bed vapour phase oxidation of toluene has been studied in the temperature range 325–370°C. at atmospheric pressure using vanadia catalyst supported on $-65 + 100$ mesh silica gel under varying space velocities (15–23 g./g. mol./hr) and at a constant feed ratio (1 mole of toluene: 42.5 moles of air).

The specific reaction rates and the apparent energies of activation based on the assumed mechanism of consecutive reaction steps have been evaluated. An attempt has been made to elucidate the probable rate-controlling step and the rate-determining reaction. The rate-determining reaction appears to be the conversion of toluene to benzaldehyde, as this reaction step has relatively the lowest specific reaction rate.

As a result of recent commercial development in the field of oxidation, industry is quick to take advantage of novel results with economic promise in today's increasingly competitive market. An example is the commercialization by the California Research Corporation of Dow process for phenol based on the currently less expensive toluene rather than the more conventional benzene as raw material. Two catalytic air oxidation steps are involved in this process. The first step yields benzoic acid; the second step using copper catalyst converts the acid to phenyl benzoate which is hydrolyzed to phenol. Benzoic acid manufacture by the toluene oxidation process has a great scope for expansion, for not only is benzoic acid an important intermediate in phenol manufacture but it is a potential source of terephthalic acid by the Henkel process.

The following methods¹ are at present employed for the manufacture of benzoic acid: (i) decarboxylation of phthalic acid (in solution and in vapour phase); (ii) hydrolysis of benzotrichloride; and (iii) oxidation of

toluene in liquid phase with nitric acid, sodium dichromate, etc. Attempts have also been made to prepare benzoic acid by the vapour phase oxidation of toluene and a detailed review on the subject has been given by Dixon and Longfield².

The kinetics of the oxidation of toluene with vanadia catalyst in a fixed bed has been studied recently by Downie *et al.*³ Pargal¹ studied the reaction in a fluidized bed; but no kinetic data were presented.

THERMODYNAMICS

Free energy changes occurring in the different vapour phase reactions of the toluene oxidation process were calculated^{5,6} on the basis of heat of formation and entropy data obtained from literature⁶ for the different compounds. The specific heat data of toluene, water and carbon dioxide were available from Hougen and Watson⁷ and those of other compounds were calculated by the group contribution method⁸.

Using the concerned thermodynamic relationship⁵ and the data presented in Table 1, standard free energy changes at different temperatures for different reactions were obtained and the corresponding equilibrium constant values were calculated. The values are given in Table 2.

On the basis of the thermodynamic considerations, it is evident that the catalytic vapour phase oxidation of toluene not only results in benzoic acid, but yields benzaldehyde, benzoquinone, maleic acid and carbon dioxide, the relative amounts of various products depending upon the operating conditions. It is also evident that all the reactions are highly exothermic. Thus, it is necessary to maintain the temperature of the catalyst at a constant and uniform condition in order that any desired reaction may preferentially take place. The use of catalyst in a fluidized bed shows promise of yielding the desired isothermal conditions and also may facilitate efficient heat removal from the bed, if necessary. As the thermodynamic equilibrium

TABLE 1—CONSTANTS FOR ELUCIDATING FREE ENERGY CHANGE OCCURRING DURING DIFFERENT REACTION STEPS

| REACTION: CONVERSION OF TOLUENE TO | Δa | $\Delta b \times 10^3$ | $\Delta c \times 10^6$ | I_H kcal./g. mol. | I_S cal./g. mol. (°K.) |
|--|------------|------------------------|------------------------|------------------------|--------------------------------|
| 1. Benzaldehyde | 9.288 | -81.47 | 64.28 | -48.27 | -59.69 |
| 2. Benzoic acid | 6.340 | -15.99 | 10.35 | -149.14 | -46.60 |
| 3. Benzoquinone | 18.720 | -138.04 | 97.92 | -240.24 | -97.65 |
| 4. Maleic acid | 35.930 | -69.53 | 62.78 | -114.44 | -179.70 |
| 5. Carbon dioxide | 21.502 | -64.30 | 49.60 | -915.60 | -91.41 |

TABLE 2—FREE ENERGY CHANGES AND EQUILIBRIUM CONSTANTS AT DIFFERENT TEMPERATURES

| REACTION | $-\Delta G, \text{kcal./g. mo.}^1$ | | | | $\log K$ | | | |
|--------------------------------|------------------------------------|--------|--------|--------|----------|--------|--------|--------|
| | 573°K. | 673°K. | 773°K. | 873°K. | 573°K. | 673°K. | 773°K. | 873°K. |
| 1. Toluene→ Benzaldehyde | 27.8 | 27.36 | 23.32 | 21.6 | 10.53 | 8.83 | 6.55 | 5.38 |
| 2. Toluene→ Benzoic acid | 108.32 | 101.32 | 94.3 | 86.83 | 41.02 | 32.71 | 26.49 | 21.6 |
| 3. Toluene→ Benzoquinone | 235.5 | 236.9 | 238.05 | 239.28 | 89.23 | 76.42 | 66.85 | 59.53 |
| 4. Toluene→ Maleic acid | 214.8 | 223.4 | 231.9 | 246.9 | 81.37 | 72.07 | 65.13 | 61.41 |
| 5. Toluene→ CO ₂ | 920.18 | 921.8 | 897.8 | 895.6 | 348.3 | 297.5 | 252.2 | 222.7 |

constants of all the reactions are high, the fluidized condition may not affect the conversion adversely owing to the possible back-mixing of the products in the fluidized beds.

In view of these considerations, investigations were taken up to study the kinetics of the catalytic vapour phase oxidation of toluene in a fluidized bed. This paper presents the results obtained using vanadia catalyst of $-65 + 100$ Tyler mesh size fraction. On the basis of the results, an attempt has been made to elucidate the rate controlling step of the various reactions.

EQUIPMENT, MATERIALS AND METHODS

Equipment

The equipment consisted of the following: (i) arrangement for the supply of air at constant pressure by the method reported by Venkitakrishnan and Bhat⁹; (ii) a calcium chloride tower for drying the constant pressure air available from the arrangement; (iii) arrangement for supply of toluene by pressurizing the toluene reservoir with the constant pressure air supply; (iv) toluene vaporizer; (v) preheater for heating toluene vapour and air to the desired temperature; (vi) reactor for containing the desired amounts of catalyst and for effecting toluene oxidation; and (vii) condensers for condensing the products. The details of the flow diagram are given in Fig. 1.

The preheater was made of stainless steel tube (length, 6 ft, and inner diam., $\frac{3}{8}$ in.) and was heated by 24 S.W.G. nichrome wire. The reactor was made of stainless steel tube (length, 2 ft and outer diam., 2 in.) and heated by 20 S.W.G. wire. The reactants, toluene vapour and air mixture, entered the reactor through a conical bottom containing coarse solids which were earlier found not to affect the reaction and which acted as the distributor for

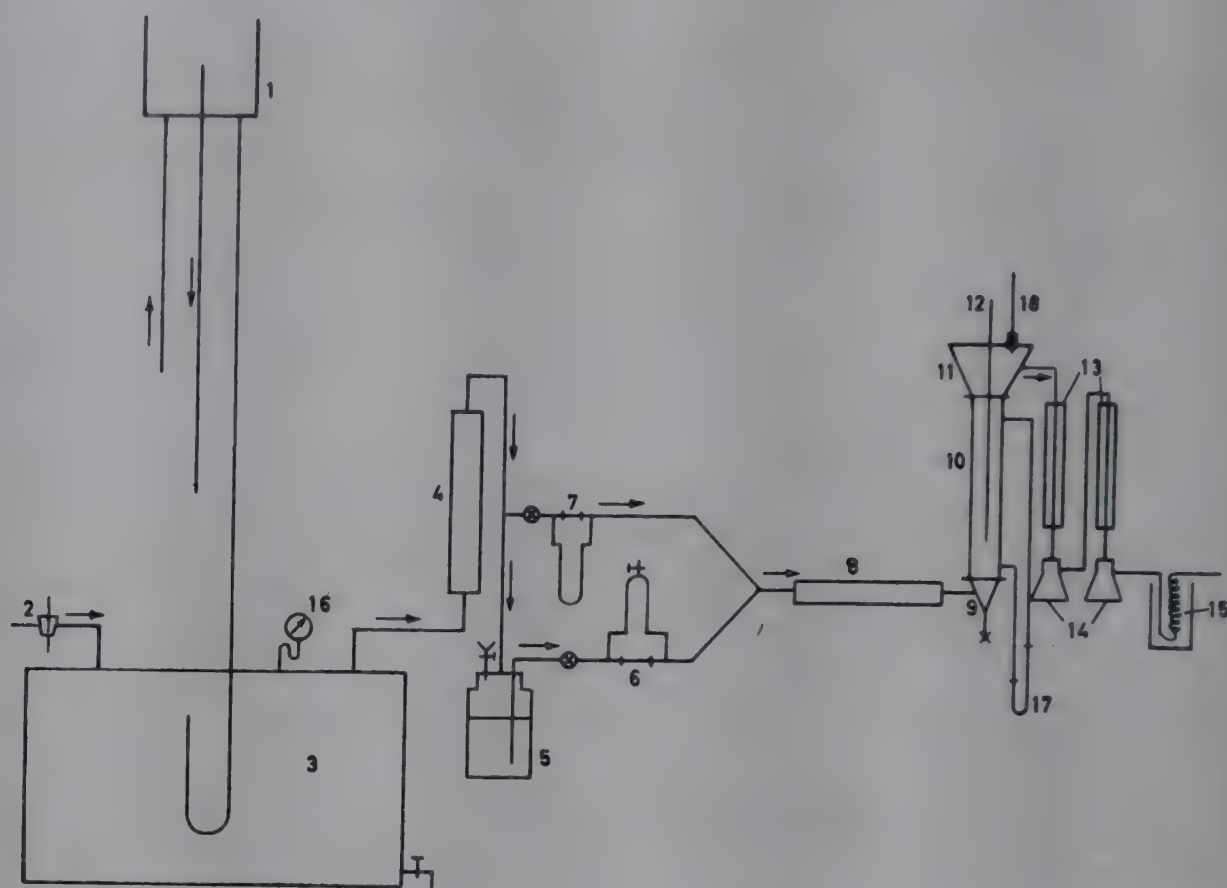


FIG. 1—FLOW DIAGRAM OF THE PROCESS [(1) Overhead water tank; (2) Needle valve for compressed air inlet; (3) Constant pressure drum; (4) Calcium chloride drying tower; (5) Toluene; (6) Liquid flow meter; (7) Air flow meter; (8) Preheater; (9) Conical bottom; (10) Reactor; (11) Disengaging section; (12) Thermocouple; (13) Condensers; (14) Product; (15) Ice bath; (16) Pressure gauge; (17) Manometer; (18) Thermometer]

air-toluene vapour mixture. The temperature of the reactor was controlled by a Dimmerstat and that of the preheaters by Simmerstats.

Materials

Vanadia catalyst impregnated on silica gel ($-65 + 100$ Tyler mesh size) was prepared as follows:

About 168 g. of ammonium metavanadate were dissolved in hot water and the solution was added to about 200 g. of chromatographic grade silica gel. The resulting mixture was evaporated on a water bath. The residue was dried in an electric oven at about 105°C . and was finally kept in a furnace at about 600°C . for 24 hr. The resulting solid was sieved to get the $-65 + 100$ mesh size catalyst.

Commercial toluene obtained was distilled and the distillate having the refractive index (n_{D}^{20}), 1.4969, was used in the toluene oxidation runs.

Methods

Experimental procedure of a run. A known quantity of the catalyst was charged to the reactor to obtain about 15 cm. of the bed. Air at constant pressure and at a rate calculated to obtain a chosen reactant mixture

composition and the time factor, was fed to the reactor through the preheaters and the power supply to the preheater and reactor was switched on and adjusted to obtain the required reaction temperature.

When the fluidized bed attained the desired temperature, toluene at a rate calculated to yield the desired composition and time factor was fed into the preheater and thence to the reactor. At this stage the fluidized bed temperature tended to increase slightly and the power supply to the reactor was suitably adjusted to obtain the desired isothermal conditions. Products formed under these conditions were condensed by cooling with water condensers and ice baths in series.

Analysis of products. The uncondensed gaseous products were collected over brine. The overall analysis of the solid and liquid products was carried out by the method of Kumar, Bhat and Kuloor¹⁰ with the modifications: (i) Benzaldehyde was determined by the bisulphite method instead of the oxime method; and (ii) maleic acid in solution was determined by adding a known excess of standard potassium permanganate solution, neutralizing the excess of permanganate by a standard solution of oxalic acid and back-titrating the excess oxalic acid by standard potassium permanganate.

Gaseous products were analysed for carbon dioxide by Orsat analysis. Material balance checked within -15 per cent. The errors in flow rate measurements were of the order of ± 3 per cent in the case of liquids and ± 4 per cent in the case of gases.

Runs were carried out at a constant toluene-air feed composition and at the operating conditions: (i) Reaction temperature, 325°C ., 350°C . and 370°C .; (ii) Time-factor (W/F), g./g.mol./hr, 13.9, 15.9, 20.5 and 23.

RESULTS AND DISCUSSION

Selectivity is the percentage ratio of the moles of the desired product per mole of converted toluene to the number of moles which would have resulted if there were no undesired side reactions.

Time-factor is the ratio of the weight of the catalyst (g.) to the gram moles of the total feed per hour.

Selectivity of Catalyst

The effect of total conversion on the selectivity of the catalyst with regard to the formation of different products is shown in Fig. 2. It is evident that as the total conversion increases, the selectivity decreases in the case of every one of the products. This is due to the fact that as the total conversion increases, there is a greater tendency for the complete oxidation of the hydrocarbon to carbon dioxide. Extrapolation of these curves to zero conversion fixes the product distribution of the primary reactions,

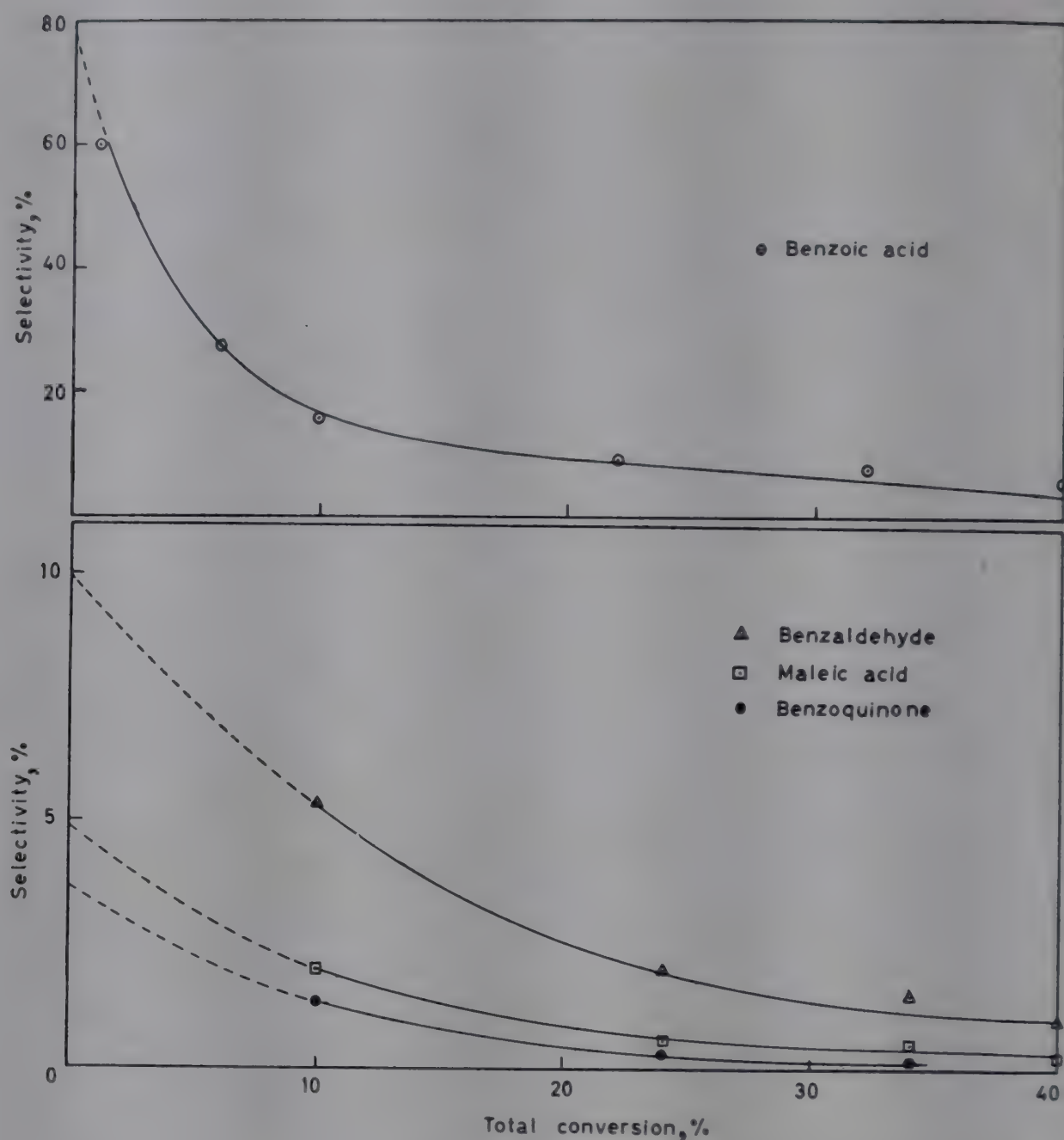


FIG. 2—EFFECT OF TOTAL CONVERSION ON THE SELECTIVITY OF BENZOIC AND BENZALDEHYDE. MALEIC ACID AND BENZOQUINONE

and shows that the catalyst has better selectivity for benzoic acid than for other products of reaction.

Conversion of Toluene into Products

In order to determine if reactions other than those catalysed by the vanadia occurred, a simulated run was conducted at 370°C. without catalyst. In this run no conversion occurred as confirmed by the refractive index of the liquid product and the analysis of the gaseous products.

Effect of time factor. As W/F increases, the total conversion and the conversion to carbon dioxide continuously increase, while conversion to other products increases at first, reaches a maximum and then decreases (Fig. 3-7).

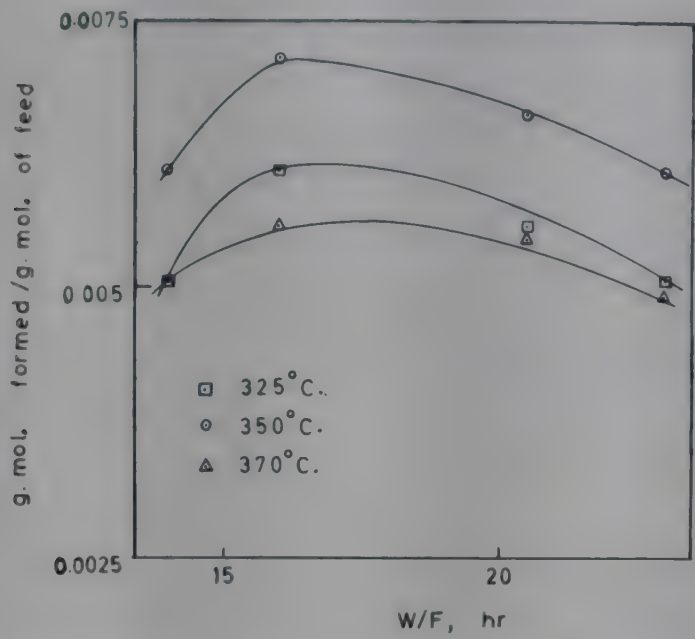


FIG. 3—EFFECT OF W/F ON CONVERSION TO BENZALDEHYDE

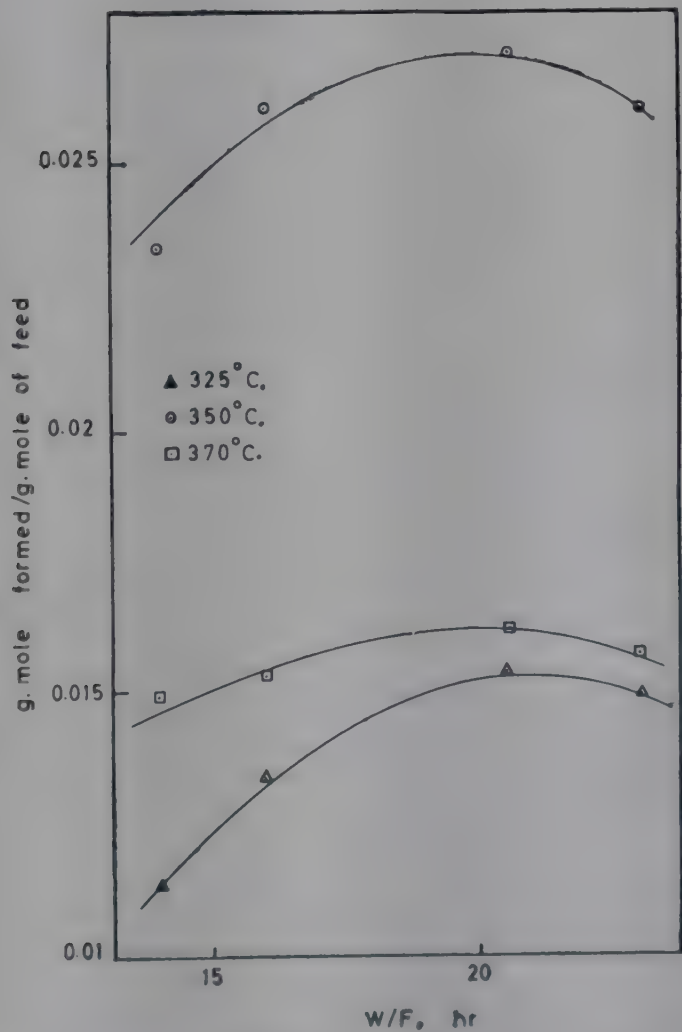
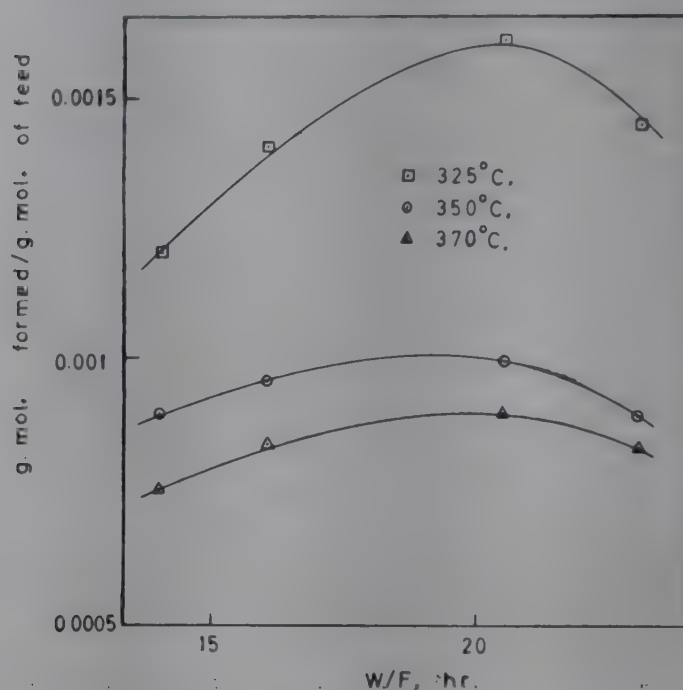
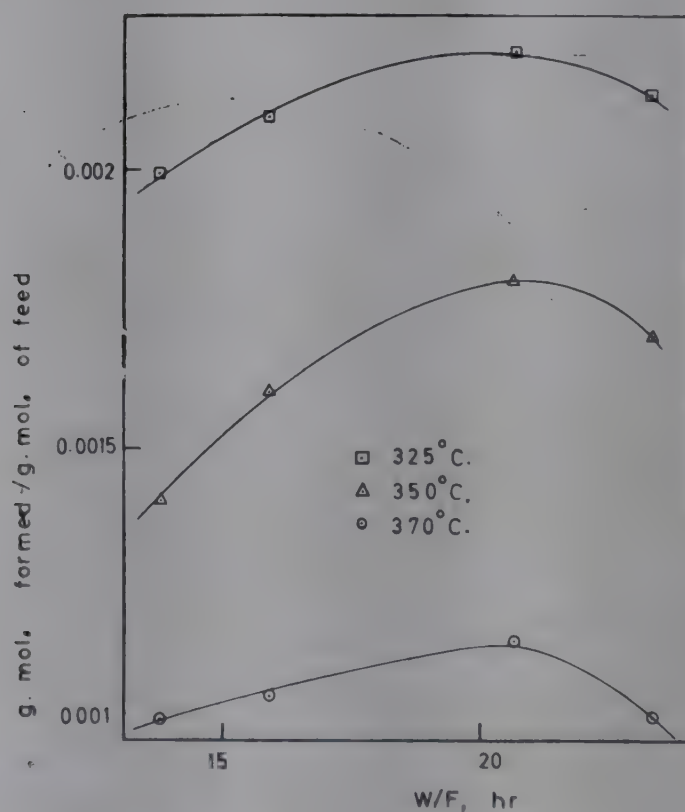
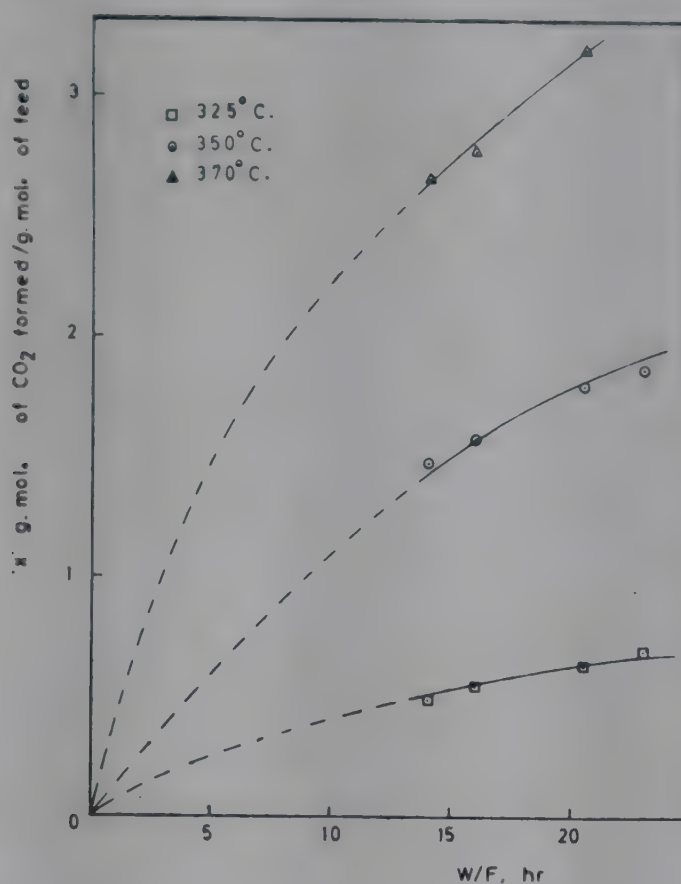


FIG. 4—EFFECT OF W/F ON CONVERSION TO BENZOIC ACID

FIG. 5—EFFECT OF W/F ON CONVERSION TO BENZOQUINONEFIG. 6—EFFECT OF W/F ON CONVERSION TO MALEIC ACID

Effect of temperature. As the temperature increases, the total conversion and conversion to carbon dioxide increase, while the conversion to other products increases with increasing temperature, reaches a maximum at a certain temperature and then falls off with further increase in temperature (Fig. 3-7).

FIG. 7—EFFECT OF W/F ON CONVERSION TO CARBON DIOXIDE

Yield of Products

Fig. 8 and 9 show the effect of variation of W/F on the yield of various products with temperature as the parameter. It is observed that the yield of benzoic acid is maximum at a W/F value of about 18 and at a temperature of 325°C. These conditions are also found to be favourable for the formation of other products. As the time factor or the temperature increases, the yield decreases due to the conversion of toluene and other intermediate products to subsequent products of oxidation and finally to carbon dioxide.

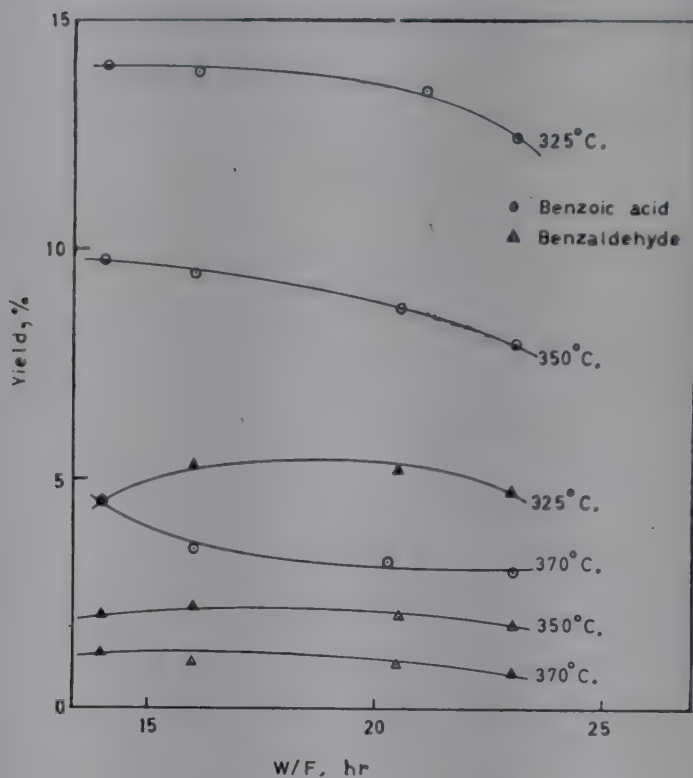
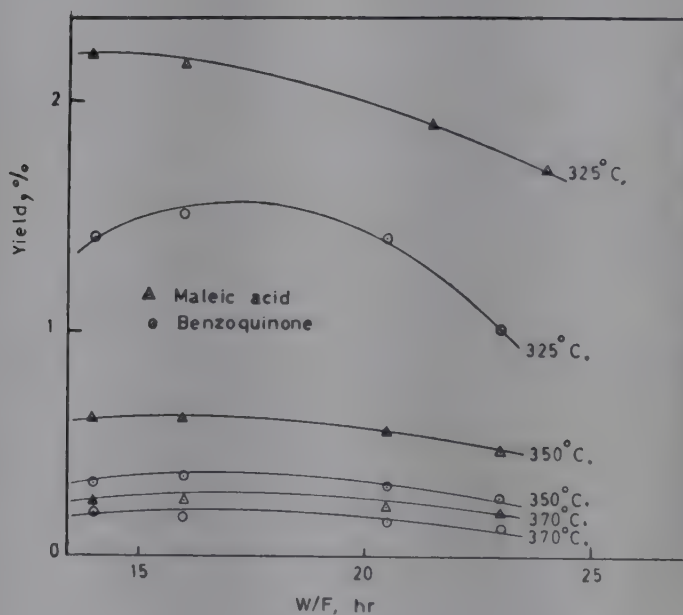
Overall Order of Reaction

Attempts have been made by various workers¹¹⁻¹³ to determine the order of reaction occurring in fluidized beds and in flow reactors. In a steady state flow system, the relation between the space velocity (W/F) and the conversion is obtained by consideration of an elementary section of reactor containing a mass of catalyst dW in which the conversion dx is produced. Assuming the occurrence of piston flow in the bed, the material balance is given by

$$F_T dx = r dW \quad (1)$$

Therefore,

$$W/F_T = \int_0^x \frac{dx}{r} \quad (2)$$

FIG. 8—EFFECT OF W/F AND TEMPERATURE ON YIELD OF BENZOIC ACID AND BENZALDEHYDEFIG. 9—EFFECT OF W/F AND TEMPERATURE ON YIELD OF MALEIC ACID AND BENZOQUINONE

The term r can also be written as follows assuming the reaction to be pseudo-first order:

$$r = k_1 \left[\frac{1-x}{n_t} \right] P \quad (3)$$

Substituting Eq. (3) in (2)

$$W/F_T = \int_0^x \frac{dx}{k_1 \left[\frac{1-x}{n_t} \right] P} \quad (4)$$

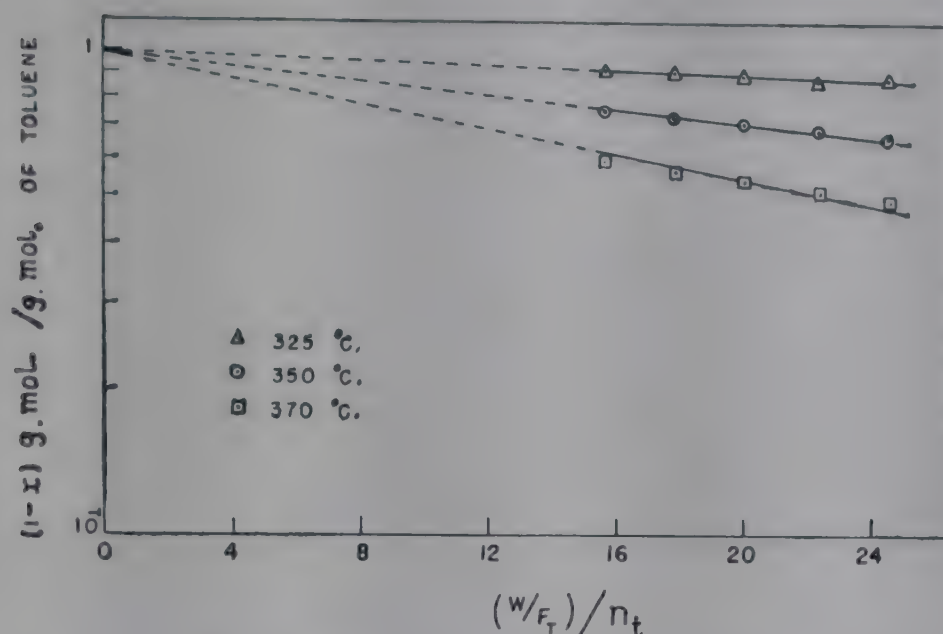
FIG. 10—PLOT OF $(1-x)$ VERSUS $(W/F_T)/n_t$

TABLE 3—PSEUDO-FIRST ORDER RATE CONSTANTS AT DIFFERENT TEMPERATURES

[Values in g. mol./ (hr) (g. catalyst) (atm.)]

| TEMP. °C. | k_1 | k_2 | k_3 | k_4 | k_5 |
|--------------|------------------------|--------|--------|--------|--------|
| 325 | 4.198×10^{-3} | 0.7530 | 0.2689 | 2.588 | 1.953 |
| 350 | 1.673×10^{-2} | 1.7440 | 0.4261 | 11.500 | 6.392 |
| 370 | 2.845×10^{-2} | 2.9270 | 1.0420 | 17.610 | 13.660 |

Experimental results indicated that n_t remains almost constant and is independent of W/F_T under the conditions studied. Hence, carrying out the integration of Eq. (4), we get

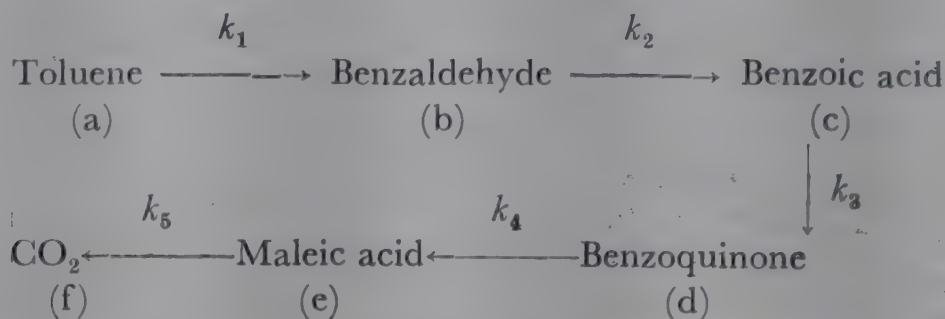
$$-\log (1-x) = k_1 P (W/F_T)/n_t \quad (5)$$

The results obtained in the present investigations at the operating pressure of almost 1 atm. showed that the $\log (1-x)$ versus $[(W/F_T)/n_t]$ relationship yielded straight line plots as shown in Fig. 10 from the slope of which k_1 was obtained. This observation points to the fact that (i) the reaction is pseudo-first order, and (ii) the piston flow occurs in the bed. The values of k_i thus obtained at three different temperatures are given in Table 3.

Determination of Probable Rate-controlling Step and Rate-determining Reaction

The results presented in the Fig. 3-9 showing the effect of variations of W/F on yields and conversions of various products support the observation that various reactions occur in a consecutive or consecutive and

parallel manner. Assuming the simpler case of consecutive mechanism, the following reactions appear to be possible during the oxidation reaction under study:



Assuming the above scheme of reactions, the following rate equations can be written when the operating pressure is 1 atm.:

(a) The rate of disappearance of toluene

$$\frac{-dn_a}{d(W/F_T)} = k_1 (n_a/n_t) \quad (A)$$

or $-\frac{d(1-x)}{d(W/F_T)} = k_1 \left[\frac{1-x}{n_t} \right]$, which on integration yields Eq. (5).

(b) The rate of formation of benzaldehyde

$$\frac{dn_b}{d(W/F_T)} = k_1 \frac{n_a}{n_t} - k_2 \frac{n_b}{n_t} \quad (B)$$

(c) The rate of formation of benzoic acid

$$\frac{dn_c}{d(W/F_T)} = k_2 \frac{n_b}{n_t} - k_3 \frac{n_c}{n_t} \quad (C)$$

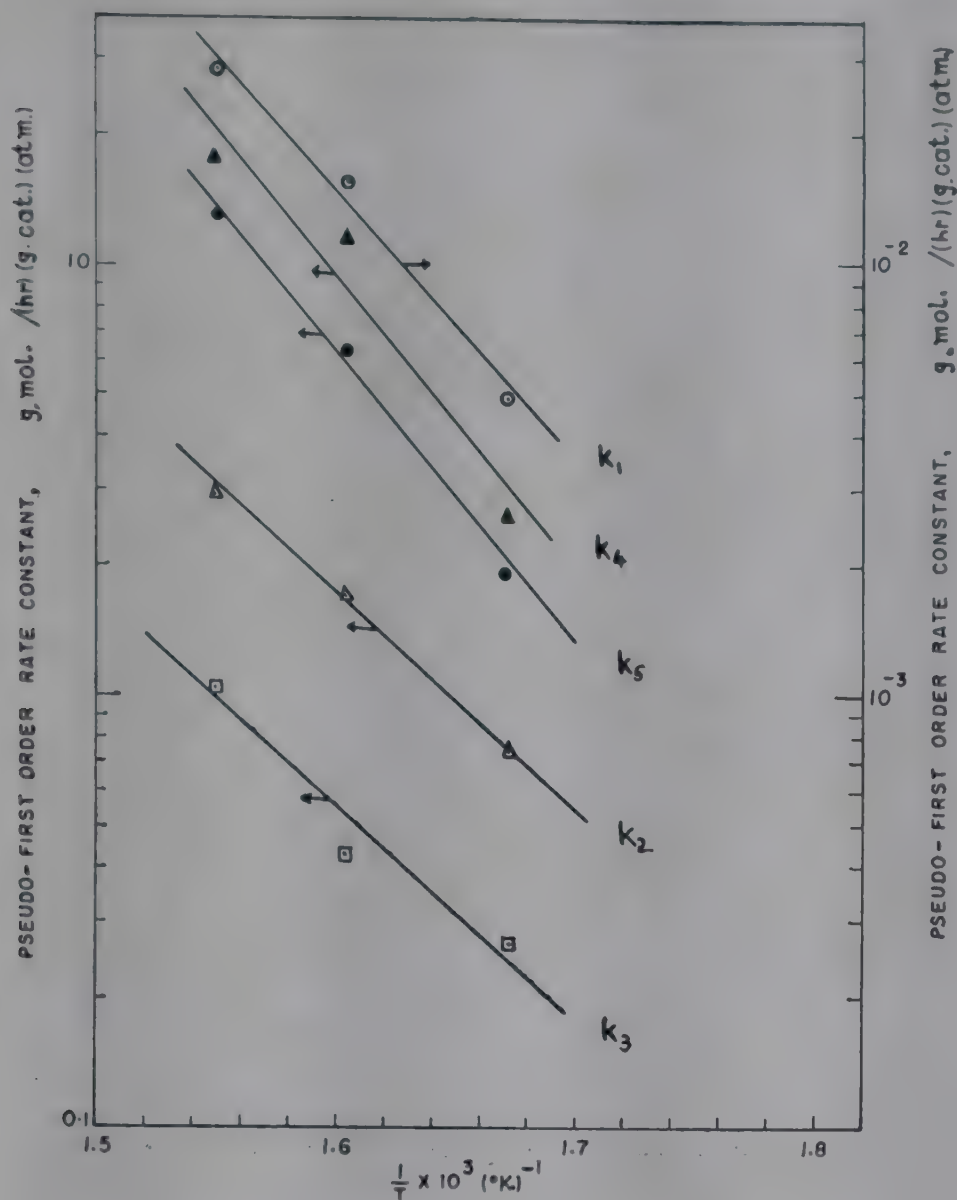
(d) The rate of formation of benzoquinone

$$\frac{dn_d}{d(W/F_T)} = k_3 \frac{n_c}{n_t} - k_4 \frac{n_d}{n_t} \quad (D)$$

(e) The rate of formation of maleic acid

$$\frac{dn_e}{d(W/F_T)} = k_4 \frac{n_d}{n_t} - k_5 \frac{n_e}{n_t} \quad (E)$$

As already pointed out, the value of k_1 is calculated from Eq. (5) at different temperatures. As the left hand side of Eq. (B) becomes zero when n_b is a maximum, the knowledge of n_a at the W/F_T value at which n_b is a maximum is enough to define the value of k_1/k_2 and since k_1 is known, k_2 can be calculated. Similarly, k_3 to k_5 can be evaluated for different temperatures. The calculated values are given in Table 3. The Arrhenius plots, viz. the plots of $\log k$ versus $1/T$ are shown in Fig. 11. From these, the apparent energies of activation (E) of the various reactions have been calculated. They are 29.24, 23.20, 23.40, 29.00 and 26.55 kcal./g. mole respectively for reactions 1, 2, 3, 4 and 5.

FIG. 11—ARRHENIUS PLOT OF $\log k$ VERSUS $1/T$

In general, the magnitude of the energy of activation is related to the rate-controlling step. The magnitudes of the energy of activation obtained during the present studies are consistent with those of a surface-reaction controlled mechanism^{14,15}. In other words, the present results suggest that the rate-controlling step is possibly a surface reaction. The rate-determining reaction appears to be the conversion of toluene to benzaldehyde, as this reaction step has the lowest specific reaction rate relative to such constants of the other reaction steps.

NOMENCLATURE

| | |
|--------------------------------|---|
| K | = thermodynamic equilibrium constant |
| $k_1, k_2, k_3,$ k_4, k_5 | = pseudo-first order rate constants for reactions 1, 2, 3, 4 & 5 respectively, $\text{g. mol. / hr g. catalyst atm.}$ |
| n_a | = mole of toluene converted/mole of toluene fed |
| n_b | = mole of benzaldehyde formed/mole of toluene fed |
| n_c | = mole of benzoic acid formed/mole of toluene fed |

| | |
|--------------------------------------|--|
| n_d | = mole of benzoquinone formed/mole of toluene fed |
| n_e | = mole of maleic acid formed/mole of toluene fed |
| n_t | = total number of moles in the exit gas stream/mole of toluene fed |
| W | = weight of the catalyst, g. |
| F | = total feed rate of air and toluene, g. mol./hr |
| F_T | = molal flow rate of toluene, g. mol./hr |
| $\frac{W}{F}$, W/F_T | = time-factor, g./g. mol./hr |
| ΔG | = free energy change, kcal./g. mol. |
| ΔH | = heat of reaction, kcal./g. mol. |
| ΔS | = entropy change, cal./g. mol. °K. |
| ΔC_p | = change in heat capacity, cal./g. mol. °K. |
| r | = rate of reaction, g. mol./hr g. catalyst |
| x | = conversion of toluene = g. mol. of toluene converted/g. mol. of toluene fed |
| P | = total pressure, atm. |
| T | = temperature, °K. |
| Δa , Δb , Δc | = constants of equation of Ref. 5 |
| I_H , I_S | = constants of equation relating the heat of reaction and entropy change with temperature respectively |

REFERENCES

1. KIRK, R. E. & OTHMER, D. F., *Encyclopedia of Chemical Technology* (Interscience Publishers Inc., New York), Vol. 2, 1960, 262.
2. DIXON, J. K. & LONGFIELD, J. E., *Catalysis* (Reinhold Publishing Corp., New York), Vol. 7, 1960, 207.
3. DOWNIE, J., SHELSTAD, K. A. & GRAYDON, W. F., *Canad. J. chem. Engng.* **39** (5) (1961), 201.
4. PARGAL, H. K., Ph.D. Thesis, University of Colorado, U.S.A. (1954).
5. HOUGEN, O. A., WATSON, K. M. & RAGATZ, R. A., *Chemical Process Principles* (Asia Publishing House, Bombay), 1st Indian Edition, Part II, 1960, 986, Eqn 14.
6. LANGE, N. A., *Handbook of Chemistry* (McGraw-Hill Book Co. Inc., New York), 8th edn, 1672.
7. HOUGEN, O. A., WATSON, K. M. & RAGATZ, R. A., *Chemical Process Principles* (Asia Publishing House, Bombay), 1st Indian Edition, Part II, 1960, Appx XXVI, Table D.
8. HOUGEN, O. A., WATSON, K. M. & RAGATZ, R. A., *Chemical Process Principles* (Asia Publishing House, Bombay), 1st Indian Edition, Part II, 1960, 1005.
9. VENKITAKRISHNAN, G. R. & BHAT, G. N., *Brit. chem. Engng.* **7** (1962), 549.
10. KUMAR, R. N., BHAT, G. N. & KULLOOR, N. R., *Curr. Sci.*, **31** (1962), 491.
11. COSTA NOVELLA, E. & ESCARDINO BENLLOCH, A., *An. Soc. esp. Fis. Quim.*, **59B**(11) (1963), 669.
12. JOHNSTONE, H. F., BATCHELOR, J. D. & SHEN, C. Y., *Amer. Inst. chem. Engrs J.*, **1**(3) (1955), 320.
13. SHEN, C. Y. & JOHNSTONE, H. F., *Amer. Inst. chem. Engrs J.*, **1**(3) (1955), 349.
14. CALDERBANK, P. H., *Industr. Chem.*, **29** (1952), 291.
15. FRYE, C. G., LAKE, W. C. & ECKS, H. C., *Proc. annu. Meeting Amer. Inst. chem. Engrs*, Chicago, III, Dec. 11, 1957.

Studies on Some Catalytic Reactions of Industrial Importance in Fixed as well as Fluidized Bed

S. K. BHATTACHARYYA, N. D. GANGULY
B. N. AVASTHI, A. K. KAR & VIJAY SHANKAR

Department of Applied Chemistry, Indian Institute of Technology
Kharagpur

A number of catalytic reactions of industrial importance have been thoroughly studied both in the fixed and in the fluidized bed reactors in order to assess the comparative performance of the two reactors. The process data of the following reactions have been discussed in the paper: (i) oxidation of *o*-, *m*- and *p*-xylenes to phthalic anhydride, isophthalic and terephthalic acids respectively; (ii) oxidation of 2-, 3- and 4-picolines to picolinic, nicotinic and isonicotinic acids respectively; (iii) oxidation of crotonaldehyde to maleic acid; and (iv) one-step conversion of ethanol to butadiene by composite dehydration-dehydrogenation reaction.

Using fused vanadium pentoxide, the best catalyst, a maximum conversion of 67.8 per cent of *o*-xylene to phthalic anhydride is obtained in the fluidized bed, as against 61.7 per cent in the fixed bed, under optimum conditions. Oxidation of *m*- and *p*-xylenes leads to some interesting results.

2-Picoline undergoes almost complete degradation under the reaction condition. With the best catalyst, the maximum conversions of 4-picoline to isonicotinic acid are 48.94 and 37.43 per cent in the fixed and fluidized beds respectively. The conversions of 3-picoline to nicotinic acid are 29.60 and 19.61 per cent in the fixed and fluidized beds respectively.

Under optimum conditions and using the best catalyst, the maximum yields of maleic acid are 46.20 and 66.87 per cent respectively in the fixed and fluidized beds. But the fixed bed operation requires more drastic reaction conditions.

Using Al_2O_3 -ZnO (60:40) as catalyst and under optimum conditions, a maximum conversion of 72.8 per cent of ethanol to butadiene is obtained in the fluidized bed as against 55.8 per cent in the fixed bed. In all cases, space-time yields (S.T.Y.) have been found to be higher in the fluidized bed reactor.

The application of fluidized bed technique in the field of chemical technology has been often found to be remarkably advantageous compared to the fixed bed operations, particularly for reactions having high values of equilibrium constants and involving large thermal effects, either exothermic or endothermic. This paper discusses the performance characteristics of fixed as well as fluidized bed operations for a few industrially important catalytic reactions.

The following reactions have been studied exhaustively in the vapour phase under wide ranges of operating variables using fixed as well as fluidized bed catalytic reactor: (i) oxidation of *o*-, *m*- and *p*-xylenes to phthalic anhydride, isophthalic and terephthalic acids respectively; (ii) oxidation of 2-, 3-, and 4-picolines to picolinic, nicotinic and isonicotinic acids respectively; (iii) oxidation of crotonaldehyde to maleic anhydride; and (iv) one-step conversion of ethanol to butadiene by composite dehydration-dehydrogenation reaction.

EXPERIMENTAL SET-UP AND PROCEDURE

For the first three oxidation reactions, air, purified and dried, was used as the oxidizing agent. The other necessary reactants were used after proper purification. In the case of one-step catalytic conversion of ethanol to butadiene in fluidized bed, a regulated stream of nitrogen was passed along with ethanol vapour to maintain the catalyst bed in the fluidized state. The experimental arrangements and procedures are the same as described by Bhattacharyya and coworkers¹⁻¹¹.

RESULTS AND DISCUSSION

Oxidation of Xylenes

Of the three xylenes, *o*-, *m*-, and *p*-, the catalytic vapour phase oxidation of *o*-xylene has been studied most exhaustively since it produces phthalic acid which is commercially the most important of the three benzene dicarboxylic acids.

The catalytic vapour phase oxidation of xylenes in the fluidized bed differs from the fixed bed operation in various points, though the most active catalyst in both the cases is fused vanadium pentoxide. A comparative assessment of the two methods using vanadium pentoxide catalysts is recorded in Table 1. Only the important differences between the fixed and fluidized bed operations which are not included in Table 1 are discussed here.

The most remarkable deviation exists in the product distribution. As reported by Bhattacharyya and Gulati¹, oxidation of *o*-xylene in the fixed bed did not yield even traces of *o*-toluic aldehyde, whereas oxidation of *o*-xylene in the fluidized bed reactor gave appreciable quantities

TABLE 1—PERFORMANCE OF CATALYSTS FOR VAPOUR PHASE OXIDATION OF *o*-XYLENE, 3- & 4- PICOLINES AND CROTONALDEHYDE IN FLUIDIZED (A) AND FIXED (B) BEDS

| CATALYST | TYPE OF BED | VOLUME OF CATALYST cc. | SPACE VELOCITY <i>litre/</i> <i>litre cat./</i> <i>hr</i> | MOLAR RATIO (air/ reactant) | TEMP. °C. | CONVERSION % | |
|--|-------------|---------------------------|--|-----------------------------------|--------------|-----------------|--------|
| OXIDATION OF <i>o</i> -XYLENE | | | | | | | |
| Fused V ₂ O ₅ | A | 17.3 | 10030 | 95.1 | 490 | 67.8* | .. |
| | B | 20 | 5740 | 275 | 490 | 61.7* | 9.6† |
| OXIDATION OF 3-PICOLINE | | | | | | | |
| V ₂ O ₅ : MoO ₃ : Pumice= 33.06 : 5.83 : 100 | A | 60 | 2300 | 230 | 400 | 19.61‡ | 19.10§ |
| | B | 20 | 1800 | 116 | 400 | 29.60‡ | 16.05§ |
| OXIDATION OF 4-PICOLINE | | | | | | | |
| V ₂ O ₅ : MoO ₃ : Pumice= 33.06 : 5.83 : 100 | A | 40 | 2096 | 142 | 360 | 35.67● | 11.68§ |
| | B | 20 | 2436 | 171 | 360 | 47.36● | 6.80§ |
| V ₂ O ₅ : Fe ₂ O ₃ : Pumice= 33.06 : 10.64 : 100 | A | 40 | 1766 | 210 | 360 | 37.43● | 11.14§ |
| | B | 20 | 2414 | 154 | 320 | 48.94● | 7.96§ |
| OXIDATION OF CROTONALDEHYDE | | | | | | | |
| V ₂ O ₅ : Pumice=51.84 : 100 | A | 20 | 9092 | 300 | 325 | .. | 46.19▲ |
| V ₂ O ₅ : Kieselguhr=51.84:100 | B | 10 | 11800 | 145-165 | 425 | .. | 36.40▲ |
| V ₂ O ₅ : MoO ₃ : Pumice= 33.06 : 5.83 : 100 | A | 20 | 9057 | 286 | 325 | .. | 66.87▲ |
| V ₂ O ₅ : MoO ₃ : Kieselguhr= 38.9 : 6.86 : 100 | B | 19 | 11800 | 145-165 | 400 | .. | 46.20▲ |
| *Phthalic anhydride †Maleic anhydride ‡Nicotinic acid §Carbon dioxide ● Isonicotinic acid ▲ Maleic acid | | | | | | | |

*Phthalic anhydride

†Maleic anhydride

‡Nicotinic acid

§Carbon dioxide

● Isonicotinic acid

▲ Maleic acid

of *o*-toluic aldehyde (3.6%). Moreover, in the fluidized bed, maleic anhydride was formed only with the unfused catalyst, while in the fixed bed oxidation, it was one of the primary products for all the catalysts.

Oxidation of *m*-xylene in the fluidized bed did not produce isophthalic acid which was formed in the fixed bed.

Oxidation of *p*-xylene in the fluidized bed led to the formation of

terephthalaldehyde and terephthalaldehydic acid in addition to the products obtained in the fixed bed.

The characteristic product distribution, as obtained in the fluidized bed operation, speaks for its advantages over the fixed catalyst bed. The oxidation of *o*-xylene in the fluidized bed resulted in higher conversion to phthalic anhydride, greater space-time yield (467 g. / litre / hr as against 85.6 for fixed bed) and also higher purity of the product; the selectivity of the catalyst for the fluidized bed was also higher, 95 per cent as compared to 86.6 per cent for the fixed bed. Further, it is easier to separate phthalic anhydride, the desired product, from the liquid products, rather than from maleic anhydride which is formed in the fixed bed.

The maximum conversion of *m*-xylene to maleic anhydride in the fluidized bed was found to be 32.7 per cent as against 21.0 per cent in the fixed bed.

Terephthalaldehyde and terephthalaldehydic acid which were obtained only in the fluidized bed can either be converted to terephthalic acid (an intermediate for synthetic fibres) or can be used as such in the dyestuff industry¹².

The optimum temperatures for oxidation of *m*- and *p*-xylenes were found to be lower in the fluidized bed. For the *o*-xylene oxidation, the optimum temperature was the same both in fixed and fluidized catalyst beds. Further, so far as the oxidation of *o*-xylene was concerned, there was no reaction below 440°C. in the fixed bed, while in the fluidized bed appreciable conversion was obtained at 430°C.

It was reported by Bhattacharyya and Gulati¹ that in the fixed bed, by using pure oxygen for the oxidation of *o*-xylene, the space-time yield of phthalic anhydride could be doubled. But in the fluidized bed, even with air, higher space-time yields and higher conversions to phthalic anhydride could be obtained.

It may be concluded that on account of such advantages as better control on the conditions and course of reaction, higher yields and purity of the desirable products, absence of explosion hazard and greater throughput (per unit volume of the catalyst), the fluidized catalyst bed holds greater promise than the fixed bed.

Oxidation of Picolines

Of the three different picolines (α -, β -, and γ - or 2-, 3- and 4-), 2-picoline was found to undergo severe degradative reactions under the operating conditions and led to the formation of mainly carbon dioxide, nitrogen, water, pyridine and very little picolinic acid. Hence, detailed studies on its oxidation were not pursued. Moreover, picolinic acid does not have any commercial importance, whereas the other two isomeric pyridine carboxylic acids (i.e. nicotinic and isonicotinic acids) are extensively used in the preparation of pharmaceuticals. Hence, an exhaustive investigation

on the catalytic vapour phase oxidation of 3- and 4-picolines has been carried out.

The results obtained for the catalytic oxidation of 3-picoline to nicotinic acid with some of the active catalysts (under the respective optimum conditions) in the fixed and fluidized bed operations are recorded in Table 1. The optimum temperatures in both the cases (for highest conversion of 3-picoline) were nearly identical. In the fluidized bed, the optimum space velocities were slightly higher and resulted in higher space-time yields. For each catalyst, the conversion of 3-picoline to nicotinic acid was always higher in the fixed bed. Conversion to carbon dioxide was almost the same in both the cases.

The optimum performance data for the oxidation of 4-picoline to isonicotinic acid with a number of comparatively active catalysts in the fixed as well as in the fluidized bed, under the respective optimum conditions, are given in Table 1.

Since the oxidation of 3- and 4-picolines is highly exothermic, it was anticipated that fluidized bed operation would be advantageous. But from the experimental data obtained, it is clear that the fixed bed operation gives much better yields of nicotinic and isonicotinic acids than the fluidized bed operation. This may be due to the progressive oxidation of the acids in the fluidized bed, caused by the back-mixing of the products, which leads to the formation of more carbon dioxide in the fluidized bed.

Oxidation of Crotonaldehyde

The vapour phase oxidation of crotonaldehyde to maleic acid or anhydride, a very important raw material for synthetic plastics, has been quite popular in recent years for various practical reasons. This important oxidation reaction has been thoroughly studied in the presence of a large number of catalyst compositions consisting of the oxides of vanadium, molybdenum, tungsten, uranium, cobalt, titanium, etc. both in the fixed and fluidized reactors.

The comparative performances of the different active catalysts for the conversion of crotonaldehyde to maleic acid are also recorded in Table 1.

It is clear from the table that V_2O_5 - MoO_3 -pumice is the most active catalyst system both in the fixed and in the fluidized bed operations. But with almost all the catalysts, fluidized bed operation was found to be more advantageous than the fixed bed not only in leading to higher yield of maleic acid but also in promoting higher conversions at comparatively lower temperatures.

Conversion of Ethanol to Butadiene

The comparative performances (under optimum conditions) of the active catalysts used in the fluidized as well as the fixed bed are recorded in Table 2. It is worth noting that catalysts like Fe_2O_3 , ZrO_2 , ThO_2 ,

TABLE 2—COMPARATIVE PERFORMANCES OF ACTIVE CATALYST SYSTEMS IN FIXED AND FLUIDIZED BEDS FOR CATALYTIC CONVERSION OF ETHANOL TO BUTADIENE

(Temp. 425°C.; Wt % of ethanol in feed, 99.36)

| CATALYST SYSTEM | FIXED BED | | | FLUIDIZED BED | | |
|--|--------------------------------------|----------------------|---------------------------|--------------------------------------|----------------------|---------------------------|
| | Ethanol feed rate ml./hr g. | Conver- sion % | S.T.Y. g./litre/ hr | Ethanol feed rate ml./hr g. | Conver- sion % | S.T.Y. g./litre/ hr |
| Al_2O_3 | 1.25 | 23.9 | 101.4 | 5.82 | 25.9 | 506.6 |
| Fe_2O_3 | 0.93 | 29.7 | 114.0 | 3.89 | 25.6 | 406.2 |
| ZrO_2 | 1.25 | 35.4 | 250.0 | 3.32 | 34.2 | 655.8 |
| ThO_2 | 1.25 | 26.7 | 276.4 | 2.05 | 25.4 | 267.0 |
| Al_2O_3 -ZnO (60 : 40) | 1.875 | 55.8 | 420.6 | 2.58 | 72.8 | 769.1 |
| Al_2O_3 -CaO (60 : 40) | 1.875 | 28.6 | 160.8 | 5.66 | 28.8 | 394.3 |
| Al_2O_3 -MgO (80 : 20) | 1.875 | 47.7 | 322.1 | 5.69 | 35.2 | 362.1 |
| Al_2O_3 -Cr ₂ O ₃ (60 : 40)* | 1.875 | 47.2 | 206.9 | 4.96 | 34.7 | 474.3 |

*Temperature in fixed bed, 450°C.

Al_2O_3 -MgO (80 : 20), Al_2O_3 -Cr₂O₃ (60 : 40) give higher percentage conversions of ethanol to butadiene in the fixed bed than in the fluidized bed. This may be due to the slower rates of one or more of the processes occurring on the surface of these catalysts. The fluidized bed operating at higher space velocities naturally allows little time for the reactant to undergo the desirable chemical changes and hence causing the lower yield of butadiene.

But with all the catalysts, except ThO_2 , the space-time yield (S.T.Y.) values were very high in the fluidized bed evidently because of the higher feed rate of ethanol. Increase in the value of S.T.Y. at the cost of percentage conversion to some extent is of great industrial significance.

The application of fluidized catalyst bed brings about a phenomenal improvement of the butadiene yield. Al_2O_3 -ZnO (60 : 40) is the best catalyst for the fixed as well as fluidized bed operation. Under the optimum conditions, a maximum conversion of 72.8 per cent of ethanol to butadiene is obtained in the fluidized bed as against 55.8 per cent in the fixed bed operation. In both the reactors, 425°C. is the optimum temperature, but the conversion in the fluidized bed is affected by temperature to a greater extent.

The optimum ethanol flow rate in the fixed bed is not sufficient to bring about the effective fluidization of the catalyst bed. The increase in

the flow rate beyond the optimum value affects the yield of butadiene much more adversely in the fixed bed than in the fluidized bed operation.

The optimum weight of the catalyst in the fluidized bed (52.0 g.) operation was much higher than that used in the fixed bed (20.0 g.). Hence, the increased catalyst surface area, resulting from the increased weight of catalyst, might indirectly be responsible for the increased yield of butadiene. But that the intrinsic property of the fluidized catalyst bed rather than the increased surface area was mainly conducive for this endothermic reaction was evident from the fact that in the low ethanol feed rate range, the fixed bed operation was more effective than the fluidized bed synthesis, though the optimum weights of the catalysts were used in both the cases (i.e. 20 g. for the fixed bed and 52.0 g. for the fluidized bed). The yield of butadiene in the fixed bed decreased when the weight of the catalyst was more than 20 g. In the fluidized bed, at the lower feed rate, the adverse effect, due to back-mixing, more than counteracted the otherwise beneficial influence of the fluidized catalyst bed.

The conversion of ethanol to butadiene in the fluidized bed fell down appreciably when the ethanol content in the feed was less than 95 per cent, while in contrast, the fixed catalyst bed could tolerate up to 90 per cent ethanol feed.

A striking contrast between the fixed and the fluidized bed operation lies in the product distribution. In the fixed bed synthesis of butadiene from ethanol, considerable liquid product containing a little unconverted ethanol, was obtained; the fluidized bed operation, on the other hand, was generally characterized by the complete absence of liquid product. The volume of the gas produced was comparatively higher in the fluidized bed synthesis.

REFERENCES

1. BHATTACHARYYA, S. K. & GULATI, I. B., *Industr. Engng Chem.*, **50** (1958), 1719.
2. BHATTACHARYYA, S. K. & KRISHNAMURTHY, R., *J. appl. Chem., Lond.*, **13** (1963), 547.
3. KĀR, A. K., Ph.D. Thesis, Indian Inst. Tech., Karagpur, 1962.
4. VIJAY SHANKAR, Ph.D. Thesis, Indian Inst. Tech., Karagpur, 1963.
5. BHATTACHARYYA, S. K. & VENKATARAMAN, N., *J. appl. Chem., Lond.*, **8** (1958), 728.
6. BHATTACHARYYA, S. K. & KĀR, A. K., *J. Catalysis*, **1** (3) (1962), 293.
7. BHATTACHARYYA, S. K. & GANGULY, N. D., *J. Indian chem. Soc.*, **38** (1961), 463.
8. BHATTACHARYYA, S. K. & GANGULY, N. D., *J. appl. Chem., Lond.*, **12** (1962), 97.
9. BHATTACHARYYA, S. K. & GANGULY, N. D., *J. appl. Chem., Lond.*, **12** (1962), 105.
10. BHATTACHARYYA, S. K. & GANGULY, N. D., *Proc. Second int. Congr. on Catalysis, Paris*, July 1960.
11. BHATTACHARYYA, S. K. & AVASTHI, B. N., *Industr. Engng Chem. (Process Design & Developm.)*, **2** (1963), 45.
12. VENKATARAMAN, K., *Chemistry of Synthetic Dyes* (Academic Press Inc., New York), Vol. 2, 1952, 722, 944, 1207.

Particle Distribution of a Heterogeneous Mixture of Ilmenite and Carbon in Fluidized Bed Reactors*

M. N. KRISHNAMURTHI

National Chemical Laboratory

Poona 8

When Indian beach sand ilmenite of particle size 250–300 μ is fluidized with petroleum coke particles of 500–800 μ as a reducing agent, the latter segregate and start floating on the bed due to a large difference in their relative densities. Also, at high temperature reaction conditions the mixtures of carbon and ilmenite undergo changes in density with changes in chemical composition, particle size and shape. It is, therefore, difficult to determine how the basic reactions could be utilized in the system. In an endeavour to bring about a closer contact of the component particles during the reaction conditions, an improved reactor has been designed using $\frac{1}{2}$ in. lumps of charcoal as a fixed perforated packing in the reactor bed. The mechanism of the system provides increased bed depths in narrow-tube reactors and allows a greater range of contact time and area between the ilmenite and the carbon surface.

In the chlorination of beach sand ilmenite either carbon or carbon monoxide is used as the reducing agent. With carbon monoxide, reduction is slow; while in the presence of carbon, the reaction velocity is much higher particularly if the distance between the ore and the carbon surface is less than 200 μ ¹. When ilmenite is chlorinated in the presence of carbon, the following exothermic reactions may be assumed to take place under ideal conditions:

*Communication No. 659 from the National Chemical Laboratory, Poona 8.



or



The difficulty with the fluidization of the heterogeneous mixture has been segregation of the component particles due to a large difference in their relative densities, thus aggravating the distance between the ilmenite and carbon particles. Therefore, preliminary studies were undertaken to determine the fluidizing characteristics of the material, nature and extent of segregation in glass reactor models.

EXPERIMENTAL SET-UP AND PROCEDURE

The fluidization apparatus used in the experiment is of the standard type. It consists of a vertical cylindrical glass vessel (diam., 7.5 cm. and height, 57.5 cm.) open at the top and a graphite porous plate of 0.016 in. holes is fixed above the 60° inlet cone at the base. The assembly is provided with discharge ports on the sides for taking out samples, and with two lateral taps for measuring the pressure drop.

Travancore beach sand ilmenite used in this work has a particle size of about 250-300 μ , sp. gr., 4.17, bulk density, 2.55 g./cc. and the chemical composition, TiO_2 , 59.52; Fe_2O_3 , 25.21; FeO , 10.80 per cent and impurities (mainly SiO_2 and Al_2O_3), 4.47 per cent. The carbon chosen is calcined petroleum coke of particle size, 500-800 μ ; sp. gr., 1.4; and bulk density, 0.92 g./cc.

A well stirred heterogeneous mixture of 500 g. of ilmenite and 150 g. of coke in stoichiometric proportions based on reaction (2) was fluidized with air pressure at about 10 lb./sq. in. A series of runs with 20, 25 and 30 l.p.m. air flow in the system for periods of 30, 45 and 60 min. were made with the following operating data: tube diam., 2.8 in.; void fraction as determined, 0.4; density of air at fluidizing temperature of 95°F., 0.072 lb./cu. ft; bulk density of the mixture, 1.8 g./cc.; and column depth, 10.8 cm. Samples were withdrawn after definite periods of fluidization and the percentage of coke particles was determined at the top, middle and bottom of the bed. Table 1 shows the percentage of coke particles in the top, middle and bottom layers of the bed in relation to air flow rate and fluidizing time at these velocities.

DISCUSSION OF RESULTS AND CORRELATIONS

The particle size of petroleum coke was based on the individual value of a particle weight of carbon that should exceed the individual value of a particle of ilmenite. The limiting lower value of carbon which should

TABLE 1—SEGREGATION OF A MIXTURE OF COKE AND ILMENITE PARTICLES AT DIFFERENT AIR VELOCITIES AND FLUIDIZING PERIODS

(Values are expressed in percentages)

| AIR FLOW RATE l.p.m. | SEGREGATION OF COKE PARTICLES OF SIZE 500-800 μ FOR FLUIDIZING PERIODS | | |
|-------------------------|---|---------|---------|
| | 30 min. | 45 min. | 60 min. |
| TOP LAYER | | | |
| 20 | 43 | 45 | 45 |
| 25 | 32 | 34 | 35 |
| 30 | 28 | 30 | 37 |
| MIDDLE LAYER | | | |
| 20 | 27 | 28 | 29 |
| 25 | 29 | 30 | 31 |
| 30 | 27 | 28 | 30 |
| BOTTOM LAYER | | | |
| 20 | 13 | 14 | 14 |
| 25 | 20 | 21 | 22 |
| 30 | 20 | 23 | 24 |

correspond to 250–300 μ particle size ilmenite would be around 350 μ . Therefore, coke particles of 500–800 μ size would serve as the most reasonable particle size that should enter into the system, taking into consideration the possible attrition of the carbon particle which normally does not exceed 3 per cent limit.

Table 1 illustrates the particle distribution in a column of mixture of ilmenite and carbon after fluidization at different air velocities over different periods. The minimum air flow rate chosen is at the minimum fluidization velocity and it was found to be 20 l.p.m. Under this condition, the entire solid bed is supported by the rising air stream, the pressure drop across the bed is nearly constant at increasing air rates. Studies on the particle distribution show that the light particles of coke start floating on the bed at the minimum fluidization velocity within the first half an hour and if the particle density of a component exceeds the bed density of the mixture the segregated particle will deposit on the bottom of the bed and this behaviour is in accordance with the observations of Van Heerden².

Particle variation in bed layer in relation to fluidization period from the experimental data in Table 1 is given in Fig. 1. At the minimum fluidization velocity the bed will have expanded to such a state that the indi-

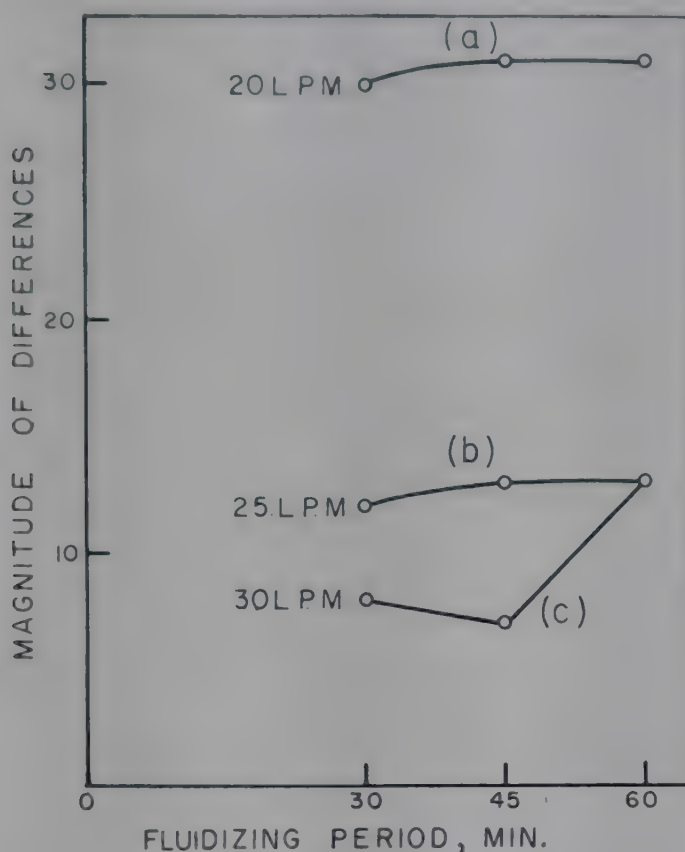


FIG. 1—PARTICLE VARIATION IN BED LAYER IN RELATION TO FLUIDIZATION PERIOD

vidual particles will become disengaged sufficiently from each other to permit internal motion of the particles in the bed. The internal motion is induced by the fluid moving through the interstices of the bed and indicates the beginning of fluidization. This condition is illustrated by graph (a) in Fig. 1. It can be seen that segregation takes place even with very low air velocities and during relatively short periods of fluidization. When the fluid rate is increased the bed expands further and intensifies the motion of the particles. The magnitude of differences in the bed begins to diminish progressively. Graph (b) in Fig. 1 shows these convection currents. For much higher rates of fluid flow, the state of agitation increases still further and the position of the top of the bed fluctuates considerably. Segregation becomes less evident at the highest air velocity of 30 l.p.m., but the results show that the movement of individual particles becomes disorganized and irregular. This condition is illustrated by graph (c) in Fig. 1. Apart from the considerations of random movement, the reaction cannot be carried out at such high fluid rates.

Again at high temperature reaction conditions, owing to the formation of titanium tetrachloride, ferric chloride and oxides of carbon, the heterogeneous mixture undergoes changes in particle shape, size and density and it is rather difficult to investigate how the basic reactions could be utilized in this system.

In an endeavour to bring about closer contact of the carbon with the ilmenite which segregates in the bottom layer, the design of the reactor

is modified by the use of $\frac{1}{2}$ in. lumps of carbon as a fixed perforated packing in the column. The lumps of carbon are supported on fixed quartz lump of appropriate size to facilitate better gas distribution. When ilmenite charge is fed, it distributes itself evenly all over the channels of the bed and during fluidization the carbon lumps remain static excepting some notable expansion in the bed of the reactor. The best fluid conditions can only be attained if the proportion of the void be sufficiently large. This property fits well with practical requirements with a rising velocity of air sufficiently high to fluidize and this bed retains the heterogeneous mixture of ilmenite and carbon and delays their segregation by entanglement in the interstices. Here, attrition effects are insignificant since the individual particles are surrounded by bed of pockets and they have few chances to jostle one another on the walls and the carbon cushion saves the wall surface from wear. During the course of reaction when the carbon gets consumed, the particles constantly undergo redistribution with change in the void proportion. Thus the mechanism of the system provides increased bed depths manifold in narrow tube reactors and allows a greater range of contact time and area between the ilmenite and the carbon surface.

As it is necessary to have means of predicting the fluid flow rate to begin fluidization, the correlations developed by Leva *et al.*³, which permit calculations of the minimum fluidizing velocity and the percentage expansion for a given velocity when the physical properties of solid and gas are known, are applicable equally well in this design.

Quantitative data on the working of this type of reactor in actual chlorination work will be reported later.

ACKNOWLEDGEMENT

The author is grateful to Dr J. Gupta and Dr L. K. Doraiswamy for their helpful criticism. Thanks are also due to Dr V. V. Dadape and Shri S. H. Iqbal for advice and help rendered in the experimental work.

REFERENCES

1. BERGLEOLM, *Trans. Amer. Inst. min. (metall.) Engrs*, **221** (1961), 1123.
2. VAN HEERDEN, C., *J. appl. Chem., Lond.*, **2** (1952) (Suppl. 1), S 11.
3. LEVA, M., GRUMMER, M., WEINTRAUB, M. & POLICHNIK, H., *Chem. Engng Progr.*, **44** (1948), 511.

Catalytic Upgrading of Water Gas in Fluidized Bed

R. K. S. MEHTA*

Indian Institute of Petroleum
Dehra Dun

Attempts were made to reduce the carbon monoxide content of town gas by incorporating the steam/iron oxide reaction in the fluidized bed coke/steam reactor at atmospheric pressure to generate self-propagating hydrogenation process. The effect of pretreatment of coke with iron oxide promoted by nickel oxide was investigated in this context to determine the conditions for increased yields of methane and hydrogen. The results indicate that a gas containing as much as 7 per cent methane and a H_2/CO ratio of 5, compared to 1.86 in Lurgi gas, could be obtained.

For several years, Dent *et al.*¹⁻⁴ in U.K. have been engaged in developing processes for the production of nontoxic town gas via methane synthesis. A similar attempt to improve the reactivity of coke/coal in such a way that an increase in hydrogen and methane could be obtained by a single step process, which would not involve any major modification of the conventional gas plant, was taken up.

The iron oxide/steam reaction in conjunction with coke/steam reaction was chosen for the purpose. The object was to utilize steam cracking on iron oxide deposited on porous coke in a fluidized bed to generate self-propagating hydrogenation process. The effect of pretreatment of the coke with relatively less expensive material, such as FeO promoted by nickel oxide, was investigated and the conditions which are conducive to increased yield of methane and hydrogen were studied. The results of the study are presented in this paper.

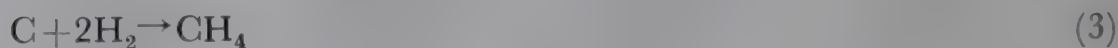
*Present address : Department of Chemical Engineering & Chemical Technology, Imperial College of Science & Technology, London S. W. 7

GENERAL FEATURES OF THE REACTION

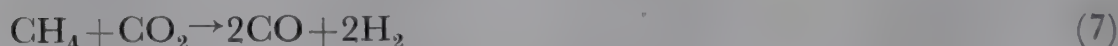
Various reaction possibilities involved in the process are detailed below, as they help in the understanding of the high temperature synthesis using steam as carrier gas:



For methane synthesis:

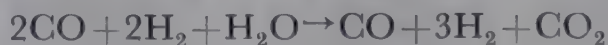


At 1000°C.



The gasification of coal in fixed bed at normal pressure differs fundamentally from that at high pressure. Earlier work on steam/coal reaction under pressure indicated that the difference of reactivities of fuels becomes insignificant as the pressure increases, and at 20 atm. or more, the advantages of using the more reactive fuel such as lignite may not be as great as might be supposed. At atmospheric pressure, the gas produced consists mainly of CO, H₂, CO₂ and N₂. At higher pressure, the thermodynamic change results in methane synthesis. But it is not economical to employ pressures above 50 atm., for an increase of pressure from 25 to 50 atm. yields 11.1 additional therms of methane/ton and a further increase to 100 atm. gives only 7.0 additional therms of methane/ton.

Many workers³⁻⁶ have reported that from the point of view of detoxification of gasified coal, it is important to reduce the CO content. They have reported the use of water gas shift system⁷, $\text{CO} + \text{H}_2\text{O} \rightarrow \text{CO}_2 + \text{H}_2$, or removal of CO partially by the use of steam treatment of water gas as



whereby an ideal synthesis mixture is obtained without an increase in the total thermal value. But by employing the decomposition reaction of steam on iron oxide along with this, it was hoped that the 'active' or 'atomic' hydrogen could be made, which could be utilized for hydrogenation of coke. Since the ideal gas composition of gas (H₂:CO=3:1) was desired, it was expected to provide a basis for increase in hydrogen value.

Another factor to be taken into account in this context is temperature. Catalytic synthesis of methane is adversely affected by high temperature.

The synthesis reaction is exothermic and for getting good yield of methane the heat of synthesis has to be dissipated. This cannot be effectively carried out by steam or nitrogen/air. A temperature range of 900-950°C. is optimum, but at 1000°C. and above, methane decomposition results with consequent lowering of the yield. The fact that catalytic decomposition of methane starts even at 400°C. sets a limit to the production of methane-rich gas.

EXPERIMENTAL SET-UP AND PROCEDURE

The modified coke reactivity apparatus employed for the investigation is shown in Fig. 1. The following are the important modifications:

The lagged copper tubing from the boiler entering the reaction tube was provided with an electrically heated jacket of quartz tube (length, 4 ft; inside diam., 1.3 in.); the heat input was controlled by maintaining the temperature at $100^{\circ} \pm 2^{\circ}\text{C}$. by means of a variac. Asbestos corks for the reaction tube were made of compressed asbestos string. Since the packing in the furnace tube was found to choke up the gas flow, the lower cork was provided with three 0.5 in. nails at the top to support a perforated fire-clay disc (aperture $< 1/16$ in.). Fire-clay beads (*c.* 1/8 in.) were used as support and found to give uniform fluidization. The emerging gases after passing through a silica tube at room temperature entered a condenser followed by a graduated carboy. This permitted wet gas to be measured accurately using the constant head float valve. Also, 'spot' samples were picked up by inserting the gas sampling tube between the condenser and the bottle, overall samples for analyses being drawn from the carboy when desired.

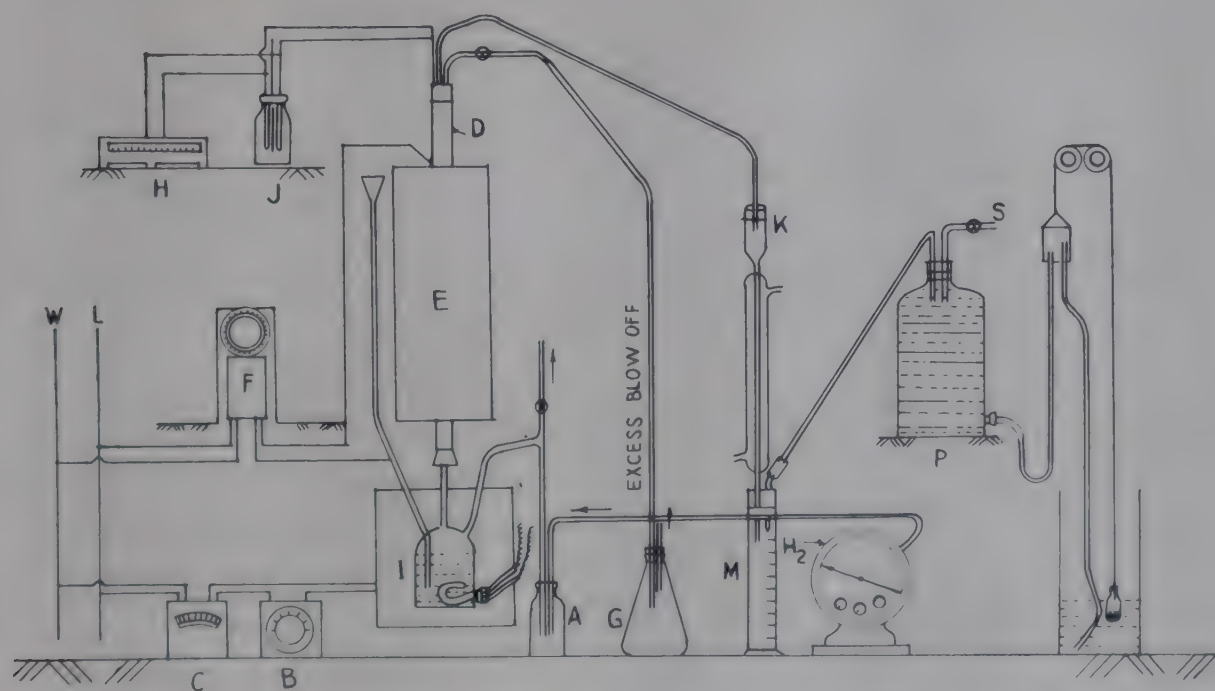


FIG. 1—EXPERIMENTAL SET-UP [A, Bubbler; G, Blow-off; B, F, Regulators; C, H, Potentiometers; D, Silica tube reactor; E, Furnace; I, Steam generator; K, Condenser; M, Graduated cylinder; P, Reservoir bottle]

In the first part of the work, nitrogen as an inert carrier gas was used to fluidize the coke bed with steam. Later on, steam itself was generated to a pressure required for good fluidization. The pressure head at which a known height of charge fluidized was determined separately by observation and it was found that the funnel-topped tube attached to the boiler acted as a good indicator of inlet pressure. By regulating the current input to the boiler, a somewhat steady head of pressure was easily maintained.

The quartz tube was mounted in an electrically heated furnace (inside diam., 2 in.; length, 2 ft) whose temperature was controlled by Sunvic relay to $\pm 50^{\circ}\text{C}$. Asbestos corks were used to seal the two ends of the tube, and the copper tubing from the boiler passed through the bottom cork. The fire-clay disc supported a length of fire-clay beads (1/16 in. size) standing 6 in. high. This was covered by 0.5 in. of silica chips (1/16–1/32 in. size). About 40 g. of coke (30–60 mesh) were usually charged for each run.

At the top of the silica tube, an asbestos cork carrying the bent silica tube leading to the condenser was fitted. Air from the system was displaced by blowing nitrogen through the boiler tube rejecting it at the condenser end. The furnace was then heated to the required temperature and the boiler allowed to 'prime'. The jacket water around the steam generator was kept at boiling point to reduce radiation losses. The tube leading into the furnace was kept at $\pm 100^{\circ}\text{C}$. (to prevent condensation of steam) by the use of an electrically heated element whose temperature could be controlled by the use of the variac.

Tests showed that a flow rate of 0.12 ft^3 of N_2 /sec. gave adequate fluidization of coke powder. Pressure was controlled using open tube bubblers to let off the excess of carrier gas. When only steam was used, the funnel-topped tube (height, 5 ft) was used as an indicator of the steam pressure and acted as a safety device when the line got choked with carried over coke or when the pressure became excessive. From time to time hot water was added in small doses through this tube to replenish the water loss from boiler during steam generation.

Experiments were conducted at a temperature range of $800\text{--}1000^{\circ}\text{C}$. as measured by a nickel-chromal thermocouple. For about 30 min. the temperature was allowed to remain steady before passing the steam, while the products coming through for the first 15 min. were rejected. A pre-evacuated gas sampling tube (100 ml.) provided with three-way stopcocks at ends was kept in the line. It could be easily manipulated to collect spot samples. After collecting about 1500 ml. of gas in the carboy, the power supply to the boiler was cut off, and the stoppers were closed. This was taken as a representative sample of gas at the operating temperature of the furnace. Gas analysis was carried out using 21 ml. Haldane apparatus whose accuracy was checked to be within ± 0.02 per cent.

The basis of hydrogen production by the steam-iron reaction involves reversible oxidation-reduction reactions of iron and its oxides. Although the

oxidation of FeO is about 15 kcal. endothermic and its reduction about 4 kcal. exothermic, these do not cause any appreciable effect on fluidized bed temperature. This is particularly the case since not only is the concentration of catalysts small but the actual amount of iron oxide undergoing this oxidation/reduction reaction may be a fraction of the lot. It is, however, necessary to employ iron in the reduced state for the following reactions to occur:



The reduction step involves the presence of reducing gas ($\text{CO} + \text{H}_2$) formed from the steam-coke reaction.

The steam-coke reaction is largely dependent upon the reactivity of the coke, a higher reactivity giving higher decomposition at lower temperature. Improvement in reactivity is brought about by the presence of hydrogen during coking as has been shown by Dent and coworkers^{1, 8-10}. This has been interpreted as reflecting a competition between hydrogenation reactions and reactions leading to graphitization of the carbon residue. Graphitized carbon surfaces resist the restoration of the reactivity by hydrogen.

RESULTS AND DISCUSSION

The proximate analysis of proven coke used in the experiments is given in Table 1.

Studies in the glass reactor of similar dimensions gave data regarding loss of fines in fluid bed effluent bases, effect of bed depth, steam rate, etc. on fluidization, while data on gasification of fine size coal in a fluidized bed at elevated pressures are available from the work of Squires⁵. Coke power (36-60 mesh) was found to give good performance in the reactor. On the other hand, steam-nitrogen gasification of coke at atmospheric pressure^{4, 6, 11} has shown that anthracite gasified at somewhat higher rate than soft coke.

Some experiments using Fe^{++} state catalyst in the presence of promoters like nickel nitrate were tried. Addition of small doses of 2 per cent solution of

TABLE 1—PROXIMATE ANALYSIS OF PROVEN COKE

(Values in percentage)

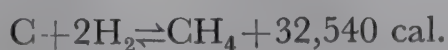
| | AS RECEIVED | MOISTURE-FREE BASIS |
|-----------------|-------------|---------------------|
| Moisture | 0.8 | .. |
| Ash | 8.3 | 8.4 |
| Volatile matter | 1.6 | 1.6 |
| Fixed carbon | 89.3 | 90.0 |

nickel nitrate showed that the increase was 50 per cent over the normal value with ferrous sulphate. Higher temperature gave increased CO_2 but on CO_2 -free basis the methane value showed a rise with temperature, contrary to the results obtained in experiments in which promoters were not used. Similar increase in methane value was found in experiments in which ferric chloride was used as source for FeO .

Effect of carrier gas on methane yield. In view of the observation that when nitrogen was used as a carrier gas for steam relatively higher values of methane (on $\text{CO}_2 + \text{N}_2$ -free basis) were obtained, as also higher hydrogen values, it was considered that methane decomposition actually occurs. The exothermic nature of the synthesis would certainly give rise to such a decomposition unless the contact time is low. With steam as carrier gas, the values under similar conditions fell off. This proves an important aspect of the reaction that the synthesis of methane actually occurs.

With air, the kinetics of reaction changed considerably but not in favour of methane increase. The methane value (on $\text{N}_2 + \text{CO}_2$ -free basis) did not show an increase but the ratio H_2/CO fell for runs at about the same temperature. Only on recirculating the gas into the system and employing it as carrier for steam, an increase in methane and H_2/CO ratio was found.

Yield of methane in fluid-bed gasification. The production of methane is basically a hydrogenation process where the reaction is reversible and exothermic



The yield of methane depends upon the reactivity of the carbonaceous material. From the calculation based on free energy data for the reaction one could expect 15.8 per cent methane, although methane may also be formed by carbon-steam reaction. There is evidence from low-pressure studies⁶ that methane yield can be increased up to 80 per cent by condensing H_2O in liquid air trap. Moreover, in fluidized bed, the conditions are well removed from equilibrium. It has been found that the trend of $\log (\text{CH}_4)/(\text{H}_2)^2$ versus $1/T$ for the coke used followed a pattern similar to the one noticed for coal char, bituminous coal¹² and peat⁵. In the case of untreated coke methane production has been reported to be higher than with peat, but never more than attained by depositing iron oxide as in the present work.

With precipitated iron oxide on coke, the yields of methane showed a wide variation with temperature, lower values being common at 960 C. With the increment of reduced iron oxide, methane plot showed a distinct rise. At the same time the ratio H_2/CO improved greatly and was as high as 6–7 in several experiments, compared to values around 2 with untreated coke. The methane value on N_2 -free basis is comparable to that of unpurified gas from Westfield Lurgi plant. But the high nitrogen values are undesirable.

The iron precipitated from ferrous sulphate in the presence of nickel

oxide used as promoter, resulted in the increased yield of methane. Also, use of FeO precipitated in the presence of sodium carbonate increased the yield of methane (about 9%).

TABLE 2—COMPARISON OF THE COMPOSITION OF RAW GASES OBTAINED IN THE LURGI PLANT WITH THAT OBTAINED IN THE PRESENT INVESTIGATION AT TWO FLUIDIZATION TEMPERATURES

(Values in percentage)

| | LURGI PLANT GAS | GAS (PRESENT STUDY) OBTAINED AT TEMP. | |
|-------------------------------|-----------------|--|---------|
| | | 1010°C. | 1100°C. |
| CO ₂ | 27.7 | 22.2 | 15.8 |
| O ₂ | .. | 0.4 | 0.6 |
| CO | 21.1 | 11.2 | 24.8 |
| H ₂ | 39.0 | 57.0 | 50.0 |
| CH ₄ | 10.1 | 6.5 | 7.0 |
| N ₂ | 1.0 | 2.7 | 1.6 |
| C _n H _m | 0.9* | .. | .. |
| H ₂ /CO | 1.86 | 5.1 | .. |

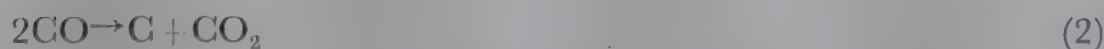
*Enriched

A comparison of the gases obtained in the present study with those of Westfield Lurgi plant is shown in Table 2. It is encouraging to see that not only does the methane value reach 7 per cent but the ratio H₂/CO is as high as 5, compared to the value of 1.86 in Lurgi gas.

Equilibrium ratios CO₂/(CO)². It has already been seen that CO₂ may come from various steps:



or



The second reaction can occur in the absence of a catalyst. Work on synthesis of methane³ and on the catalytic dissociation of carbon monoxide¹⁰ has shown that although below 400 C. the reaction is far too slow for any perceptible change to be observed in the absence of a catalyst, yet in the presence of nickel catalyst an equilibrium is established fairly rapidly. Thus the ratio of the gases will be expected to vary under the influence of catalyst.

The equilibrium ratio $\text{CO}_2/(\text{CO})^2$ can be considered from the thermodynamic standpoint. This ratio should be a constant if the solid phase (coke) is of constant thermodynamic activity, i.e. is in equilibrium with a constant vapour pressure of carbon in gas phase. Actually, the coke contains some hydrogen that is given off at the higher temperature of the reactor and imparts to the carbonaceous material increased reactivity. Only in the case of pure crystalline graphite, the ideal conditions represented by

$K = (\text{CO}_2 \times C)/(\text{CO})^2$ (where C is the fugacity or vapour pressure of the solid carbon), are obtained.

It is interesting to see the variation of K as a function of temperature. Fig. 2 shows that the effect of the pretreatment of coke on these values is of

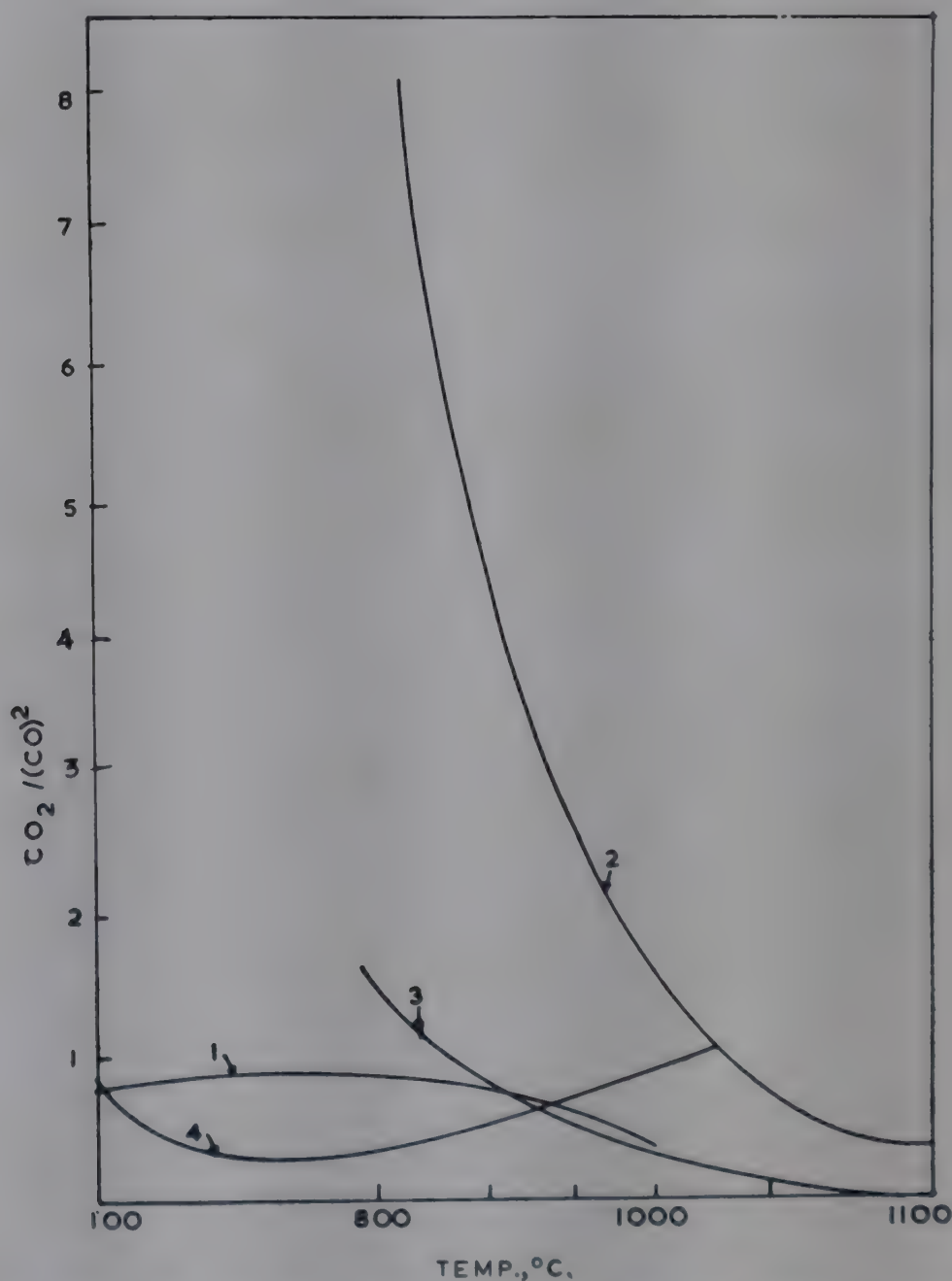


FIG. 2—VARIATION OF $\text{CO}_2/(\text{CO})^2$ WITH TEMPERATURE FOR GASIFICATION OF RAW COKE AND PRETREATED COKE [(1) Raw coke; (2) Coke + ferric chloride + nickel nitrate; (3) Coke + ferric chloride (50 ml.); (4) Coke + ferrous sulphate + nickel nitrate]

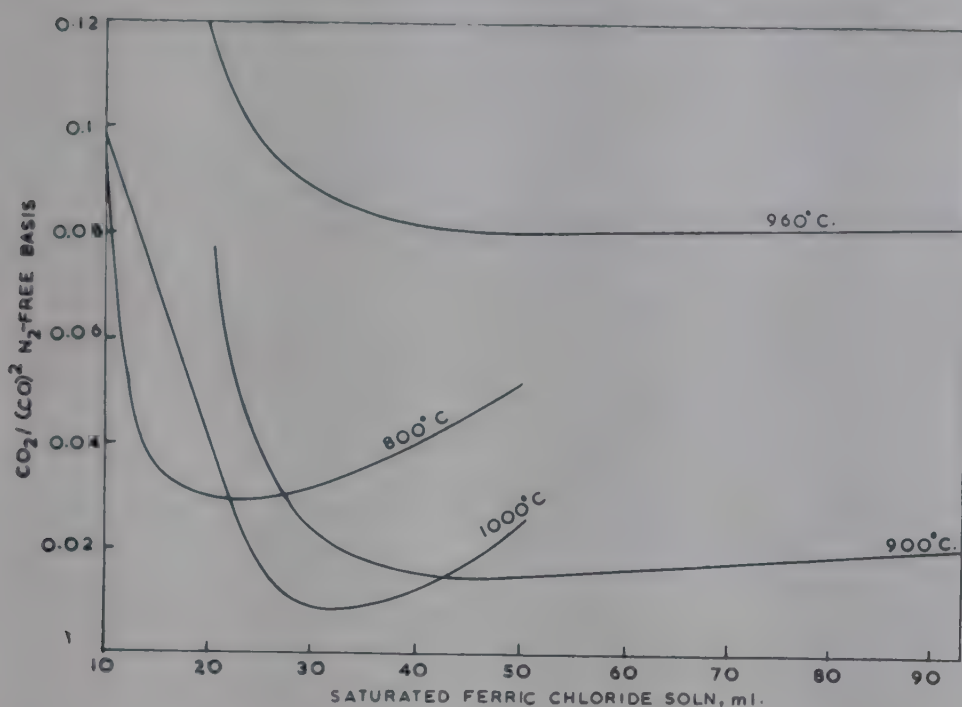


FIG. 3—RELATIONSHIP BETWEEN $\text{CO}_2/(\text{CO})^2$ AND CONCENTRATION OF FERRIC CHLORIDE USED FOR PRETREATMENT OF COKE AT DIFFERENT TEMPERATURES

special significance, for treatment with ferric chloride in the presence of a promoter showed a clear trend of rise or fall entirely dependent on the pretreatment. The presence of nickel in ferric chloride or ferric sulphate caused a reverse trend on these values. A plot of $\text{CO}_2/(\text{CO})^2$ against the amount of ferric chloride used shows a sharp fall as the amount of the latter increases from 10 to 30 ml. (Fig. 3). The curves corresponding to temperatures 900 and 960°C. showed no further rise, whereas those corresponding to 800 and 1000°C. showed a further rise.

At higher concentrations of FeO, precipitated from ferric chloride, it is interesting to see the gaseous distribution.

An interesting pattern emerges from Fig. 4. The curve corresponding to CO_2 percentage is the exact mirror image of the curve corresponding to CO percentage, i.e. CO_2 percentage increases as the concentration of ferric chloride rises from 10 ml. to 20 ml. and thereafter shows only a slight fall, whereas the CO value shows exactly the opposite trend. Though the oxygen percentage shows a steady rise, the methane percentage falls as the concentration of ferric chloride increases. Thus, there is no advantage in adding unduly large amounts of ferric chloride for methane synthesis.

Fig. 5 shows a plot of the percentages of gases obtained when ferric chloride was precipitated with ammonium oxalate, which on decomposition to iron oxide in the reactor was supposed to furnish iron in its lower oxide state. The patterns of CO and CO_2 percentages are again the mirror image of each other; so also are the values of hydrogen and methane.

Fig. 6 shows the composition of gases formed from coke treated with iron oxide precipitated from ferrous sulphate with nickel oxide as promoter.

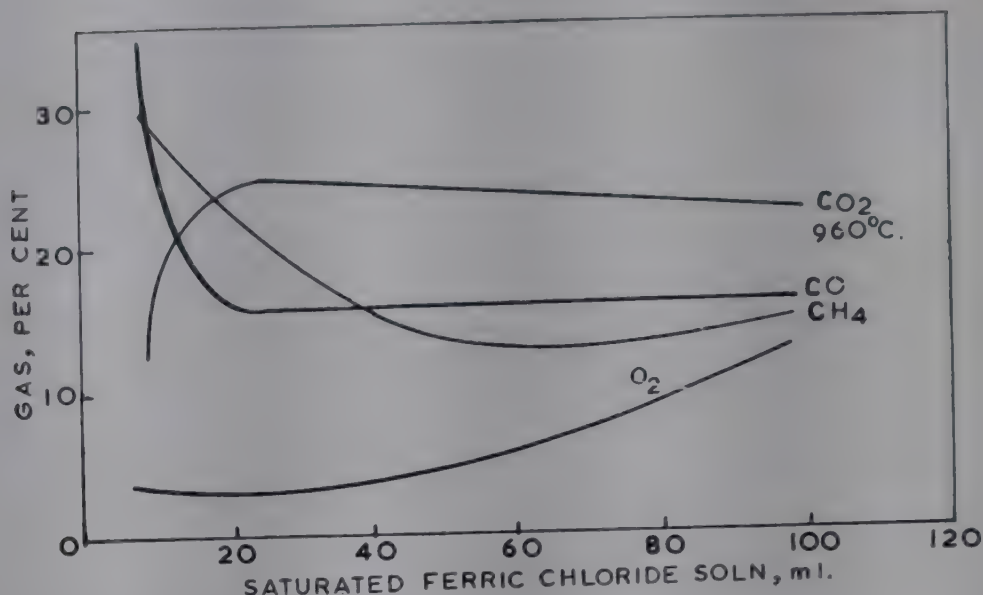


FIG. 4—VARIATION OF GAS DISTRIBUTION IN GASIFICATION OF COKE PRETREATED WITH DIFFERENT CONCENTRATIONS OF FERRIC CHLORIDE

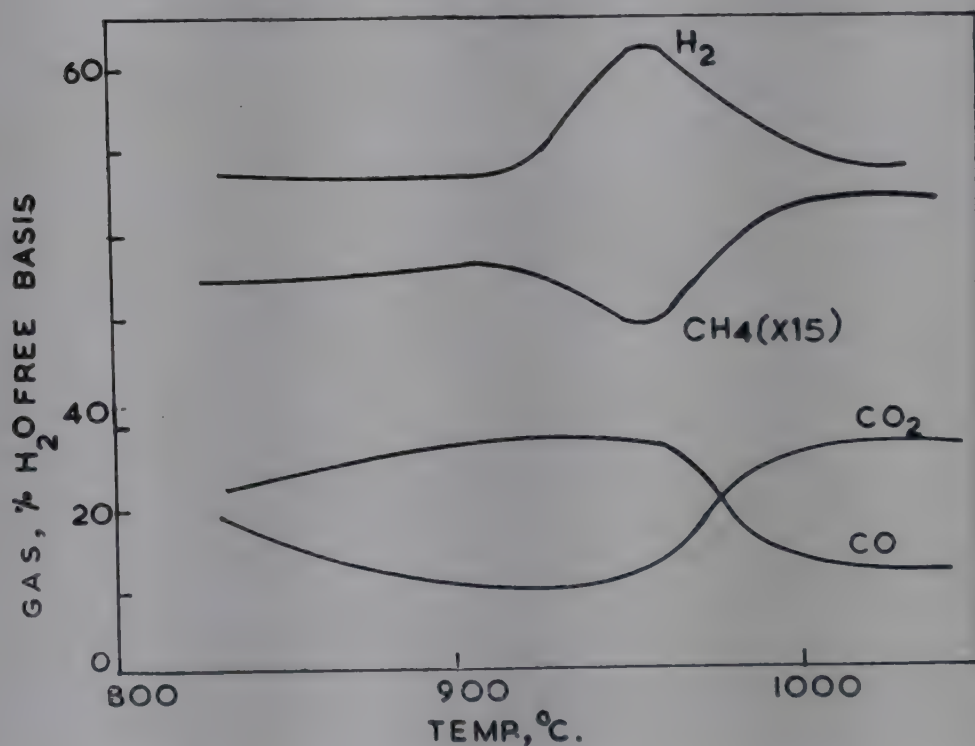


FIG. 5—RELATIONSHIP BETWEEN GAS COMPOSITION AND TEMPERATURE IN GASIFICATION OF COKE TREATED WITH FERRIC CHLORIDE PRECIPITATED WITH AMMONIUM OXALATE

The values of CO_2 and CO again vary with temperature in a manner similar to that in Fig. 4. But the divergence is large. Below 925°C . as the temperature decreases, the percentage of CO_2 decreases and that of CO increases; above 925°C . the sequence is reversed. The methane and hydrogen values show a gradual increase between 880°C . and 930°C .

Effect on H_2/CO ratio. The H_2/CO ratio is a good index of detoxification of gas. Experiments were therefore conducted to improve this ratio to

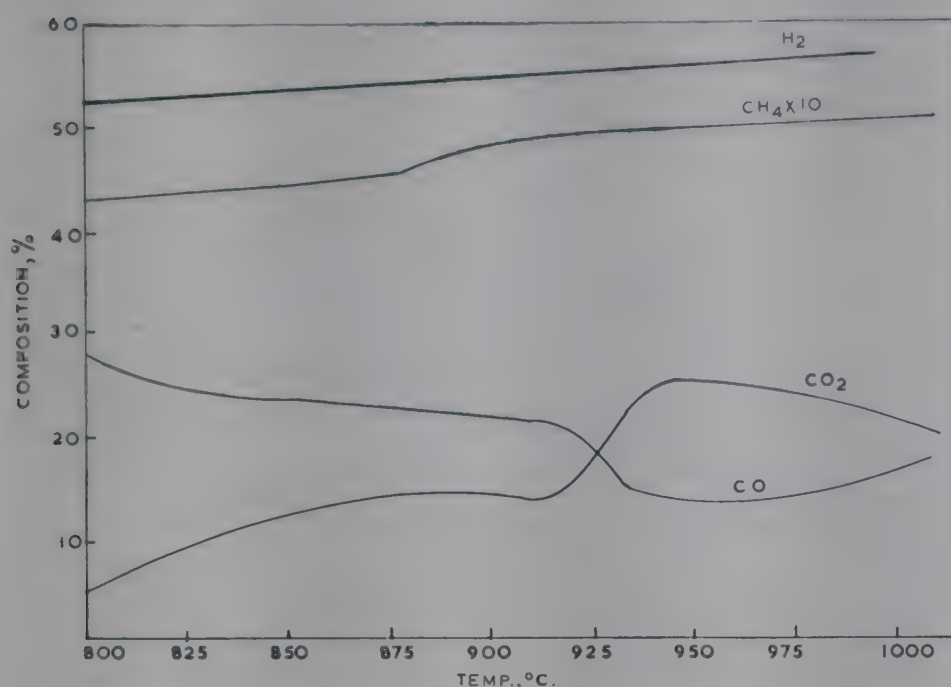


FIG. 6—RELATIONSHIP BETWEEN GAS COMPOSITION AND TEMPERATURE IN GASIFICATION OF COKE TREATED WITH IRON OXIDE PRECIPITATED FROM FERROUS SULPHATE AND PROMOTED BY NICKEL OXIDE

higher than 3.0 sought for synthesis reaction. In several experiments carried out with treated coke, this ratio was too often found to lie below 3. When the coke was pretreated with anthracene oil, the H_2/CO value increased to 4.7. Similarly, on placing the spathic iron ore below the charge or above it, remarkable increase (up to 6.9) in the H_2/CO ratio was obtained.

The quartz tube was filled with fire clay bead to the length as usual, and 0.2 in. layer of spathic iron ore freshly calcined to remove organic impurities was placed at (i) the bottom of the charge, (ii) the top of it, and (iii) in admixture after powdering it. As the ore was in granular form, the conditions of fluidization did not alter much with such an operation. Mixing the coke with reduced iron oxide gave higher yield of methane (9%) as well as higher H_2/CO ratio (6.9). Spathic iron ore as such gave H_2/CO ratio lower than 3 at 900–1080°C. Results showed higher value of methane than usual though the H_2/CO ratio remained low. Also, reduced iron filing, due to the constant agitation with the coke, enabled oxidation/reduction sequence to occur adequately thus allowing better yield of methane as well as H_2 with a higher H_2/CO ratio.

ACKNOWLEDGEMENT

The author acknowledges with thanks the facilities and help given to him by the Scottish Gas Board, Glasgow, and in particular Mr Burman.

REFERENCES

1. DENT, F. J., *Gas Research Board Publication GRB 13/3*, 1944.
2. DENT, F. J., *Int. Conf. on Complete Gasification of Mined Coal, Liege*, 1954, Pap. B 1, 113.
3. DENT, F. J., MOIGNARD, L. A., EASTWOOD, A. H., BLACKBURN, W. H. & HEBDEN, D., *49th Rep. of GRB and University of Leeds, GRB 20*, 1945.
4. DENT, F. J., *Institute of Gas Engineering Joint Research Committee Rep. No. 43*, 1938.
5. SQUIRES, A. M., *Trans. Inst. chem. Engrs, Lond.*, **39** (1961), 10.
6. Strickland-Constable, *Gas Research Board, GRB 46*.
7. MAY, W. G., MUELLER, R. H. & SWEETSER, S. B., *Industr. Engng Chem.*, **50** (1958), 1289.
8. *Institute of Gas Engineering Joint Research Committee Rep. 41*, 1937.
9. *Institute of Gas Engineering Joint Research Committee Rep. 43*, 1938.
10. McCORMACK, K. E., *Equilibria and adsorption involved in the catalytic dissociation of CO*, Thesis, University of Leeds, 1946.
11. GRAHAM, H. S., D.Sc. Thesis, M.I.T., Cambridge, Mass., 1947.
12. JOLLEY, L. J. *et al.*, *Int. Conf. on Complete Gasification of Mined Coal, Liege*, 1954, Pap. D 3, 245.

Reactivation of Clays in Fluidized Beds

D. K. GUPTA, R. SATAPATHY*
& B. C. BANERJEE†

Shri Ram Institute for Industrial Research
Delhi 6

Pozzolanic materials are available in abundance in this country and can replace a part of cement after proper heat activation. Selection of suitable clay and calcination under controlled conditions are the prerequisites for producing good quality pozzolana cement with high reactivity.

Conventional methods of heat treatment of clays in down-draft and rotary kilns are considered briefly, and the possibility of using fluidized bed technique for reactivation of clays for manufacturing *surkhi* pozzolana has been discussed.

There has been considerable expansion in cement production in the last decade, the production has increased from 3.1 million tonnes in 1951 to 9.6 million tonnes in 1964. It is estimated that by the end of third Five-Year Plan production may total 11.1 million tonnes. Still, the *per capita* production of cement is only about 0.02 tonnes in India as compared to 0.35 tonnes in advanced countries¹. Efforts are being made to install new cement factories and to maximize production in the existing ones by ensuring adequate supplies of coal, transport and power. Even then the production would fall short of the demand. With a view to meeting this demand, avenues are being explored to substitute portland cement with hydraulic cement, like pozzolanas manufactured from various clays and shale found in abundance in different parts of the country.

Pozzolonic Materials in India and their Scope

Pozzolanas may be defined as silicious or aluminous materials which in themselves possess little or no cementitious value but when in finely divided form and in the presence of moisture will react chemically with calcium hydroxide at ordinary temperatures to form compounds

*Present address: Indian Organic Chemicals Ltd, Khopoli, Dist. Kolaba, Maharashtra.

†Present address: Directorate General of Technical Development (Cement Section), Udyog Bhawan, New Delhi 1.

possessing cementitious properties². Most pozzolanas when blended with portland cement in requisite amounts produce concrete having some desirable characteristics such as increased plasticity and workability, reduced bleeding and segregation of the aggregates, and reduced heat of hydration. The pozzolanas also possess additional advantages like increased resistance to freezing and sulphate-bearing water and reduced expansion to alkali aggregate reaction.

Some of the commonly known pozzolanas in India are reactive *surkhi*, fly ash, calcined shale, and crushed conglomerates. Some of the clays and shale, which in their normal state cannot be classed as pozzolanas, may be rendered pozzolanic by pyroprocessing. In India burnt clay is the pozzolana that is most commonly used and most of the manufacturers usually prefer to powder bricks to make *surkhi*. Clays of high reactivity suitable for pozzolana have been found in different parts of the country. The production of active pozzolana by evaluation on a small scale industry basis will go a long way in solving the acute shortage of cementitious materials. Also, in places where cement is either not available or is difficult and uneconomical to procure, it could be used with lime.

A good deal of work has been done in this country on the reactivation of *surkhi* derived from various Indian clays, and the degree of reactivity of most of them is well established³. The experimental investigations that have been so far accomplished on degree of burning were confined to heating in muffle furnaces, down-draft kilns, and rotary kilns. The mode of burning, particle size and residence time are as important as the composition of the clay mineral. The economics of manufacture of *surkhi* pozzolana would mainly depend on the method of burning and reactivation.

Methods of Manufacture and Present Trend

Surkhi pozzolana is manufactured mostly by burning clays in muffle furnaces, country kilns, down-draft kilns and rotary kilns. In all these processes, the clay material is burnt to suitable temperature in the furnace, discharged, cooled and pulverized to proper fineness. The country kilns and down-draft kilns are difficult to operate scientifically and it is doubtful whether they could be made to work economically as an independent unit to produce standard quality *surkhi* pozzolana. On the other hand, the rotary kiln process is a continuous one wherein considerable amount of work has been done to improve the thermal efficiency and product quality. Still, this would not prove as economical as other continuous processes, in which the efficiency of heat application is beyond 80 per cent and the fuel economy is effected by exposing larger surface area of the clay to the flame.

Greater economy in continuous gas-solid contacting processes is achieved by the use of fluidized bed technique. This technique has been lately employed in the calcination of the limestone, drying of granular materials⁴ and mixing of solid particles⁵. It also finds application in the production of other types

of building materials, such as gypsum plaster by calcination of gypsum, cement clinkers by the cintering of cement raw materials, and separation of lime from the core^{6,7}.

The advantages of the technique are its adaptability to continuous operation, high thermal efficiency and close control of conditions of operation as a result of which there is definite reduction in the cost of manufacture.

Prospects of Fluid Bed

Recently, the Shri Ram Institute for Industrial Research has developed a new method for heat treatment in counter-current fluidized beds, in which solid particles fall under gravity into a chamber containing fins or rods protruding from the periphery of the column and extending up to the centre of the chamber⁸. Gas is blown through nozzles or burners from the bottom, by which solid particles moving downwards are kept in suspension. This system has the added advantage over fluidized beds in that the bubbling and slugging in the bed are eliminated, thus ensuring uniformity of fluidization. The fins also provide greater surface area giving higher heat transfer coefficients between wall and bed. The friction due to fins is found to contribute negligible pressure drop over the beds without fins.

The application of this technique to reactivate clay for the manufacture of *surkhi* pozzolana is of recent development. In fluid bed, since the material is pulverized and calcined in powder form and there is no chance of agglomeration due to continuous agitation of the material, further pulverization or processing of the material is not necessary. This leads to low energy requirements for grinding and low capital outlay for the plant. Apart from this, fluidized bed systems have thermal efficiency as high as 80 per cent⁴. Even after introducing crosses, segments, flights and baffles, the thermal efficiency of rotary kilns does not go beyond 25–30 per cent⁹. Hold-up in the rotary kiln is about 10 per cent with the result that major portion of heat goes waste without being utilized for heat transfer and also large surface area of the equipment is exposed for radiation losses. In the fluid bed the equipment size is small and hold-up is at least three times that of rotary kilns with the result that heat losses are minimized. Rotary kilns require about 800 kcal. per kg. of pozzolana produced, whereas the fluidized beds require less 400 kcal. per kg. of pozzolana. In addition, the fluidized bed plant is compact, the mechanical parts involved are fewer in number, labour requirement is low, and operational and maintenance cost is lower.

The reactivation of clays in fluidized beds for the manufacture of *surkhi* pozzolana will, therefore, be of commercial importance.

In the present context of shortage of cement in the country and in view of availability of suitable clays in different parts of the country, the National Buildings Organisation of the Ministry of Works, Housing and Rehabilitation has sponsored a scheme on design data for a fluidized bed to manufacture *surkhi* pozzolana.

REFERENCES

1. Anon., *J. nat. Build. Org.*, **8** (1963), 1.
2. NORDMEYER, R. L., *Pozzolanas—Their Properties and Manufacture*, 55th Annual Meeting of Amer. ceram. Soc., New York, April 1953.
3. SRINIVASAN, N.R., *Surkhi as a pozzolana*, Road Res. Pap. No. 1 (1956)
4. ZENZ, F. A. & OTHMER, D. F., *Fluidization and Fluid Particle Systems* (Reinhold Publishing Corp., New York), 1960, 421.
5. LEVA, M., *Proc. Symp. on the Interaction between Fluids and Particles* (Institution of Chemical Engineers, London), 1962, 143.
6. Anon., *Cement & Lime Manuf.*, **35** (1962), 55.
7. Anon., *Cement & Lime Manuf.*, **23** (1950), 33.
8. MAHALINGAM, M.S., SATAPATHY, R. & CHIPALKATTI, V.B., *Trans. Indian Inst. chem. Engrs*, (1964), Trans-31.
9. PERRY J. H., *Chemical Engineers' Handbook* (McGraw-Hill Book Co. Inc., New York), 3rd edn, 1950, 1608.

Conversion of Barytes to Barium Chloride in Fluidized Bed

M. V. CHANDORIKAR, D. J. MEHTA
& B. K. SHUKLA

Central Salt & Marine Chemicals Research Institute
Bhavnagar

Simultaneous reduction and chlorination of barytes were carried out under both static bed and fluidized bed conditions. Conversion of barytes to barium chloride was about 85 per cent at 600°C. in fluidized bed, and only 38 per cent in static bed condition. A static bed temperature of about 1000°C. was required to attain 85 per cent conversion. Essential data on fluidizing velocity, time and temperature of reaction, amounts of reactants and their effects on the extent of conversion have been obtained.

Bhatnagar, Parthasarathy and Sundara Rao¹ prepared barium chloride from barytes by passing hydrochloric acid or chlorine gas over a mixture of barytes and coke at 600°C. Strokov² studied chlorination of barium sulphide and found that conversion to barium chloride at 200°C. was complete in about 3 hr. Iqbal, Lobo and Gupta³ obtained 95 per cent conversion by chlorinating briquettes of powdered barytes and carbon ($\text{BaSO}_4:\text{C}=1:16$) with a suitable binder at 700°C. The quantity of chlorine gas passed was 30 per cent over that theoretically required and sulphur was largely removed in the form of volatiles.

The object of the present investigation was to prepare barium chloride from barytes by chlorination in a fluidized bed and to compare the extent of reaction with that obtained under static bed conditions.

Static Bed Chlorination

Briquettes were prepared from a mixture of barytes and carbon ($\text{BaSO}_4:\text{C}=1:6-8$), using neutralized, concentrated tamarind extract as a binder and containing 1-2 per cent Al_2O_3 catalyst. The briquettes were charged

into a furnace, the temperature was raised to 600°C . and dry chlorine gas was passed through the furnace for 2.5 hr. The product was leached with hot water, and barium sulphide and barium chloride in solution were estimated.

It was observed that with briquettes prepared from BaSO_4 and carbon in the ratio 1:8 and 2 per cent catalyst, and 40 per cent excess of chlorine over that required theoretically, the conversion of barium sulphate to barium chloride was 38 per cent only. The product contained 50 per cent barium as barium sulphide. However, when the briquettes were heated at 1000°C . for 1.5 hr, cooled to 200°C . and calculated volume of dry chlorine gas was admitted from the bottom of the furnace, the recovery of barium chloride was 87.4 per cent.

Fluidized Bed Chlorination

An intimate mixture of barytes (-120 B.S.S., 115 g.) and powdered charcoal (-150 B.S.S.) in the molar ratio, $\text{BaSO}_4:\text{C}=1:19$ was fed into a vertical furnace made of pyrex tube and wound with kanthal wire. The tube furnace was provided with an inlet tube for chlorine and an outlet for exhaust gases, as shown in Fig. 1. Dry chlorine gas was fed through the

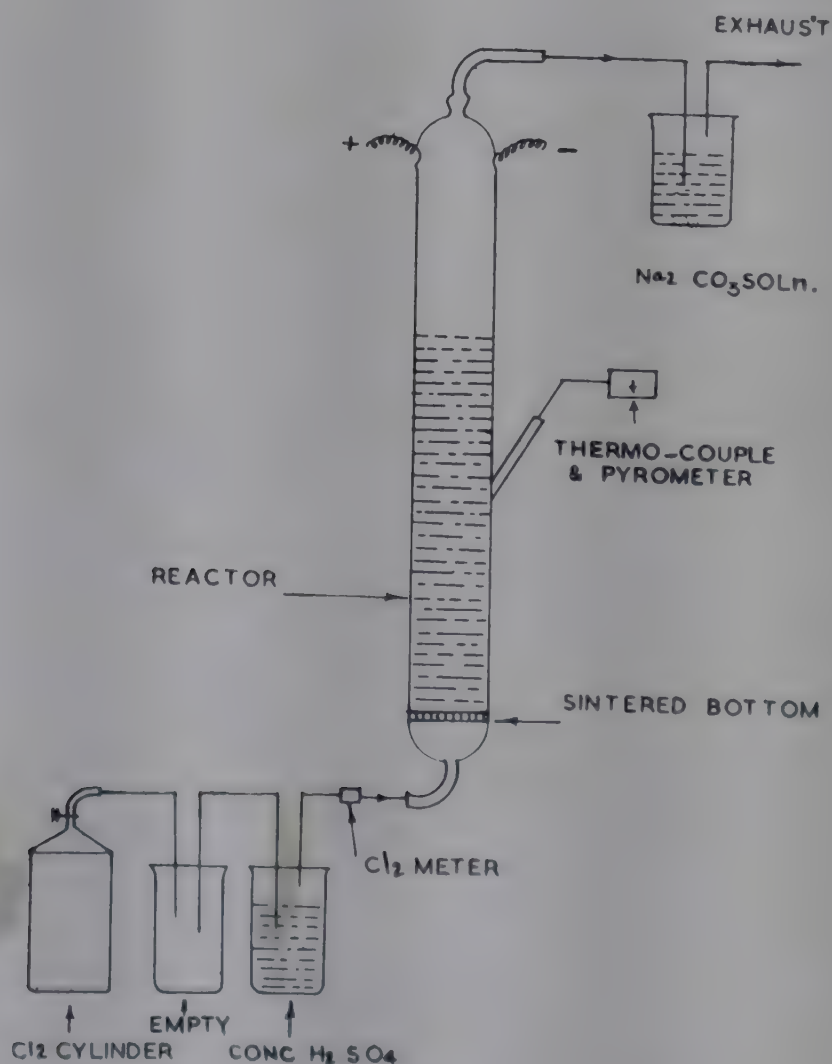


FIG. 1—FLUIDIZATION APPARATUS FOR CHLORINATION OF BARYTE

TABLE 1—CHLORINATION OF BARYTES TO BARIUM CHLORIDE

| CHLORINE EXCESS OVER THEORETICAL % | TIME hr | CONVERSION TO BaCl ₂ % |
|--|------------|--------------------------------------|
| Nil | [2] | 65.9 |
| 50 | [2] | 84.0 |
| 100 | [2] | 85.1 |
| 50 | [1.5] | 64.3 |
| 50 | [2] | 85.8 |
| 50 | 2.5 | 85.7 |

bed, when the temperature of the furnace was 600°C. The rate of gas was so controlled as to maintain the bed in a fluidized stage. The effects of the amount of chlorine and the time of chlorination on the conversion efficiency were studied at 600°C. The results (Table 1) show that maximum conversion of barium sulphate to barium chloride (85 per cent) can be obtained when the amount of chlorine used is 50 per cent more than the theoretical value and chlorination is continued for 2 hr. In this method, there is no trace of barium sulphide in the product.

REFERENCES

1. BHATNAGAR, S. S., PARTHASARATHY, S. & SUNDARA RAO, A. L., *J. sci. industr. Res.*, **3** (1944), 108.
2. STROKOV, F. N., *Trans. State Inst. appl. Chem. (Moscow)*, (No. 10) (1928), 36.
3. IQBAL, S. H., LOBO, J. & GUPTA, J., *Proc. Symp. on Mineral Industries in Andhra Pradesh*. Feb. 1962, 33.

AUTHOR INDEX

| | | | | | | | |
|---------------------------|-----|-----|-----------|------------------------|-----|-----|------------|
| Avasthi, B. N. | ... | ... | 241 | Lahiri, A. | ... | ... | 117 |
| Banerjee, B. C. | ... | ... | 265 | Lakshmanan, C. M. | ... | ... | 217 |
| Banerjee, D. K. | ... | ... | 207 | Lele, P. S. | ... | ... | 153 |
| Banerjee, S. | ... | ... | 117,207 | Mahalingam, M. S. | ... | ... | 46 |
| Bagai, S. K. | ... | ... | 1 | Manchanda, K. D. | ... | ... | 33 |
| Basak, N. G. | ... | ... | 207 | Mehta, D. J. | ... | ... | 269 |
| Bhat, G. N. | ... | ... | 65,72,227 | Mehta, R. K. S. | ... | ... | 253 |
| Bhattacharya, B. K. | ... | ... | 117,207 | Misra, G. B. | ... | ... | 51 |
| Bhattacharyya, S. K. | ... | ... | 241 | Mitra, A. K. | ... | ... | 110 |
| Chakravarti, R. K. | ... | ... | 117,207 | Murti, P. S. | ... | ... | 164,179 |
| Chandorikar, M. V. | ... | ... | 269 | Nandi, S. K. | ... | ... | 110 |
| Channakesavan, B. | ... | ... | 217 | Narasimhachar, V. S. | ... | ... | 9 |
| Deb, P. C. | ... | ... | 98 | Rao, M. N. | ... | ... | 83,125,200 |
| Dutt, D. K. | ... | ... | 98 | Rao, V. R. K. | ... | ... | 164,179 |
| Ganguly, N. D. | ... | ... | 241 | Sarma, K. J. R. | ... | ... | 125,200 |
| Garner, F. H. | ... | ... | 143 | Satapathy, R. | ... | ... | 46,265 |
| Gopal Krishna, N. | ... | ... | 33 | Sen Gupta, P. | ... | ... | 125,200 |
| Gupta, D. K. | ... | ... | 265 | Shukla, B. K. | ... | ... | 269 |
| Guruswamy, S. | ... | ... | 1,9 | Srimathi, (Miss) C. R. | ... | ... | 65 |
| Hoelscher, H. E. | ... | ... | 217 | Varma, S. K. | ... | ... | 83 |
| Jagannadha Raju, G. J. V. | ... | ... | 189 | Venkata Rao, C. | ... | ... | 189 |
| Kar, A. K. | ... | ... | 241 | Venkitakrishnan, G. R. | ... | ... | 72 |
| Kaura, N. N. | ... | ... | 83 | Vijay Shankar | ... | ... | 241 |
| Krishna, M. S. | ... | ... | 189 | Vir, D. | ... | ... | 143 |
| Krishnamurthi, M. N. | ... | ... | 248 | Zenz, Frederic A. | ... | ... | 17 |
| Kuloor, N. R. | ... | ... | 227 | | | | |
| Kumar, R. N. | ... | ... | 227 | | | | |

